PHYSICAL AND NUMERICAL INVESTIGATION OF CONGLOMERATIC ROCKS

By

Mian Sohail Akram

A THESIS SUBMITTED IN FULFILMENT OF THE REQUIREMENTS FOR THE DEGREE OF

DOCTOR OF PHILOSOPHY

THE UNIVERSITY OF
NEW SOUTH WALES

SCIENTIA

MANU ET MENTE

SYDNEY·AUSTRALIA

School of Mining Engineering
The University of New South Wales
Sydney, Australia
September 2010

ORIGINALITY STATEMENT

'I hereby declare that this submission is my own work and to the best of my knowledge it contains no materials previously published or written by another person, or substantial proportions of material which have been accepted for the award of any other degree or diploma at UNSW or any other educational institution, except where due acknowledgement is made in the thesis. Any contribution made to the research by others, with whom I have worked at UNSW or elsewhere, is explicitly acknowledged in the thesis. I also declare that the intellectual content of this thesis is the product of my own work, except to the extent that assistance from others in the project's design and conception or in style, presentation and linguistic expression is acknowledged.'

Signed ....

Date ....07/02/2011..............

COPYRIGHT STATEMENT

'I hereby grant the University of New South Wales or its agents the right to archive and to make available my thesis or dissertation in whole or part in the University libraries in all forms of media, now or here after known, subject to the provisions of the Copyright Act 1968. I retain all proprietary rights, such as patent rights. I also retain the right to use in future works (such as articles or books) all or part of this thesis or dissertation.
I also authorise University Microfilms to use the 350 word abstract of my thesis in Dissertation Abstract International (this is applicable to doctoral theses only).
I have either used no substantial portions of copyright material in my thesis or I have obtained permission to use copyright material; where permission has not been granted I have applied/will apply for a partial restriction of the digital copy of my thesis or dissertation.'

Signed ....

Date ....07/02/2011..

AUTHENTICITY STATEMENT

'I certify that the Library deposit digital copy is a direct equivalent of the final officially approved version of my thesis. No emendation of content has occurred and if there are any minor variations in formatting, they are the result of the conversion to digital format.'

Signed ....

Date ....07/02/2011..

DEDICATION

To
my devoted mother for her endless love and prayers,
&
my wife for her understanding and the love she demonstrated over and over.

You are the loves of my life.

ABSTRACT

This research addressed idealised clast-supported conglomerates, composed of high strength and stiffness spherical clasts, cemented with a weak, homogeneous cement matrix. Very few studies have directly measured the mechanical properties of intact conglomeratic rock at a valid scale. This is because very large samples are necessary to meet the ISRM testing standard, which requires a minimum ratio of 10 between specimen diameter and clast size. In addition, the collection of undisturbed samples of conglomerates with weak cement matrices is very difficult. For these reasons the strength and deformations properties of intact conglomerates remain largely unknown.

An increased understanding of the intact conglomerate strength and deformation parameters was gained by applying physical and numerical modelling techniques. In the physical experiments synthetic conglomerate specimens were prepared from steel spheres as clasts and Portland cement paste as the cement matrix. ISRM testing methods such as uniaxial, triaxial, Brazilian tensile and shear box tests were used to measure the mechanical properties of the specimens. Similarly, numerical specimens were prepared in PFC3D using measured and known micro parameters rather than estimated by inverse modelling.

Numerical specimens were tested in conditions approximating the physical experiments as close as possible. The response of numerical conglomerate was compared with the synthetic conglomerate in each testing method, to validate the numerical simulations against the physical experiments. The numerical conglomerate reproduced peak strength, progressive damage, and failure mechanisms during uniaxial testing, peak strengths in triaxial and Brazilian tensile tests, and cohesion and the angle of friction in the shear box tests. However, for numerical conglomerates, the following tests did not correspond with physical test results: the Young's modulus and Poisson's ratio in uniaxial and triaxial tests; the angle of dilation in shear box tests, and the failure mechanism in the Brazilian tests.

The differences between the mechanical behaviour of the numerical and synthetic conglomerates were explained by the presence of the cement matrix. Due to cement only being present in the synthetic conglomerates, a high degree of interlocking and dilation between clasts was induced. Both of these factors affected the failure mechanism.

After establishing a reasonable agreement between the physical and numerical experiments, the numerical simulations were extended to investigate multiple factors including: sensitivity of the cement matrix; the clasts' properties; effect of specimen size, and size distribution of the clasts in controlling the mechanical response of a clast supported conglomerate. Results provided evidence that, in uniaxial stress states, the peak strength and elastic response is sensitive to the strength and stiffness of the cement matrix, whereas negligible sensitivity was observed in triaxial stress states. However, the strength and stiffness of the clast significantly affects the peak strength and elastic response in triaxial loading, whereas no effect was observed in uniaxial loading.

The specimen size was found to influence the strength and elastic response of the conglomerates, similar to natural rocks. The strength and stiffness of the conglomerate decreased as specimen size increased. In the clast size distribution study, conglomerate peak strength and stiffness decreased as the maximum to minimum clast size ratio was increased.

Clast-cement interaction was explored by modelling the cement matrix as an aggregate of micro particles. The results demonstrated that the clast-cement interface properties significantly influence the failure mechanism and peak strength through the various modes of micro deformation. Similarly, the role of the cement matrix was also investigated to gauge its influence on the mechanical response of the cemented clasts. It was found that the cement matrix acted as a stress riser and a relation was proposed to estimate the cement induced stress effect, named, the Cement Wedge Effect (*CWE*).

LIST OF ABBREVIATIONS

3DEC	Three Dimensional Distinct Element Code
AE	Acoustic Emission
ARG	Argillaceous
ARN	Arrenaceous
BEM	Boundary Element Method
BPM	Bonded Particle Model
CPM	Clumped Particle Model
CBM	Composite Bond Model
CWE	Cement Wedge Effect
DDA	Discontinuous Deformation Analysis
DEM	Discrete Element Method
FDM	Finite Difference Method
FEM	Finite Element Method
FVM	Finite Volume Method
GR	Granite
HB	Hoek-Brown
ISRM	International Society for Rock Mechanics
MC	Mohr-Coulomb
PBM	Parallel Bond Model
PFC	Particle Flow Code
PFC2D	Particle Flow Code in Two Dimensions
PFC3D	Particle Flow Code in Three Dimensions
RBM	Rock Block Model
REV	Representative Elementary Volume
SST	Sandstone
STL	Steel
T	Tensile Strength
UCS	Uniaxial Compressive Strength
UDEC	Universal Distinct Element Code
UNSW	University of New South Wales

ACKNOWLEDGEMENTS

I would like to extend sincere thanks to following persons and organisations for providing assistance and guidance during the process of the research and writing of this thesis:

Dr. **Glenn Sharrock**, my supervisor, for his guidance and technical support throughout the research, and his feedback and encouragement in the completion of this dissertation.

Dr. **Rudrajit Mitra**, my co-supervisor, for providing valuable comments and suggestions on my work.

Dr. **Paul Hagan,** Dr. **Yuejun Cai** and Mr. **Paul Gwynne**, for their assistance in the experimental design and testing.

Prof. **Bruce Hebblewhite** being Head of the School, and Dr. **Serkan Saydam** being Postgraduate Research Coordinator for their constructive feedback being Progress Review Meetings Panel to keep me on track, and also providing resources during my research.

Ms **Bronwen Phillips,** Mr. **Arif Sadiq** and Mr. **Barryland**, for editing this thesis and providing comments during the write-up.

University of the Punjab, Pakistan, for awarding me a Faculty Development Programme Scholarship for this research.

Staff members and research fellows of the School of Mining Engineering, for their individual help and encouragement and for providing both resources and friendship during my time with the school.

My cousins, **Khurram Nawaz, Javed Chaudhry** and family members, for their support and encouragement throughout my stay in Australia.

Finally, to my family back home, for their endless love and support, and for encouraging me to pursue this research.

The deepest appreciation is reserved for my mother and my wife whose love, understanding and caring sustained me throughout my study.

TABLE OF CONTENTS

LIST OF TABLES

LIST OF FIGURES

Introduction

1.1 Background

Granular rocks, such as conglomerates, breccia, and agglomerates are composite materials consisting of *rock fragments* embedded in a *fine grained cement matrix*. Rock fragments are generally the detritus of pre-existing rocks and vary in sizes from gravels (equivalent diameter >2mm) to boulders (equivalent diameter >264 mm) with angular to rounded shapes, depending on the degree of transportation prior to deposition. Various terminologies have been used in literature to denote these rock fragments, for example, granules, clasts, gravels, cobbles and boulders as per their sizes (equivalent diameters) and geological background. However, in the present research the term *clasts*[1] is used to denote rock fragments of all sizes greater than 2mm. Similarly, the terms *matrix* or *cement matrix*[2] are used to denote the intergranular or interparticle fine-grained materials having a grain size less than 2mm. Hence, in the present research, an equivalent diameter of 2mm represents the division line between the clasts and cement matrix of a granular rock. Conglomerates are principally divided into two classes: *clast supported*, in which clasts are in contact with each other and a cement matrix fills the intergranular gaps, and *matrix supported*, in which clasts are embedded in the cement matrix. The former class of conglomerates, clast supported, is the main focus of the present research.

The intact strength, in situ strength and deformability of clast supported conglomerates are thought to be controlled by the characteristics of the cement matrix as well as the clasts. Generally, the strength and stiffness of the clasts are high compared to the cement matrix which is frequently argillaceous or siliceous.

[1] Clasts are rock fragments having equivalent diameter > 2mm and comprise gravels (2-64mm), cobbles (64-264mm) and boulders (>264mm).
[2] Cement matrix consists of particles or crystals having equivalent diameter <2mm and can be of sand (2.0-0.06mm), silt (0.06-0.002mm) or clay (<0.002mm) size with varying degree of cementation as per mineral composition and geological history.

Thus the failure in such conglomerates is understood to be governed principally by the distribution and characteristics of the cement matrix, and generally occurs through the cement or along the clast boundaries, that is, the clast-matrix interface.

The measurement of intact strength and deformation parameters for conglomerates by laboratory testing is constrained by the practical difficulties associated with the extraction of undisturbed samples and their inherent heterogeneities. The disturbed samples may have a lower strength compared to in situ conditions. Furthermore, laboratory testing can only be completed on a specific size of cored samples (generally 76-150mm). Firstly, rocks containing clast sizes greater than the core size or even half of the core size with a weak cementing matrix, will pose practical uncertainties in extracting undisturbed samples. And, secondly, if the samples are extracted by sophisticated means, such as a triple tube core barrel, the test results may be highly unreliable, because of the heterogeneous proportions of the clasts and cement matrix, or invalid if the sample to clast diameter ratio is less than the minimum required value (i.e., 10) as recommended by International Society of Rock Mechanics (ISRM) testing standards. In the case that both these conditions are met, the position of the clasts will influence the stress distribution across the sample owing to the discrete nature of the material and the contrast in the strength and stiffness of the clasts and matrix. As a result, laboratory test results do not return a good approximation of the in situ strength, characterised by the localised failure through the cement and influenced by the distribution and position of the clasts and cement matrix. Hence, the measurement of intact strength and deformation of conglomerates is largely constrained by the extraction of representative and valid samples that meet the recommended testing requirements. These requirements state that the minimum specimen diameter should be ten times the size of the clast, to qualify any specimen for intact strength measurement, and, hence, the term “intact sample” for conglomerates, varies corresponding to clast size. Generally, these requirements can be met for conglomerates with gravel sized clasts, however for cobbles or boulders, the required core size (for an intact sample) would be 640 mm to greater than 2640 mm, which cannot be routinely collected using conventional diamond drill rigs.

The estimation of rock mass strength and deformation parameters for conglomerates can only be addressed properly when laboratory testing is valid and representative of the in situ conditions. Further, it is not yet known to what extent the empirical downgrading of intact strength and deformation, as suggested by Hoek-Brown criterion, is applicable to conglomerates. In situ testing, being the direct measurement of rock mass parameters, is always expensive and time consuming, and is not even routinely available in most large projects such as dams, tunnels and mines.

Laboratory testing on the cored samples is typically considered an efficient and economical way to evaluate strength and deformation parameters in rock mechanics. Nevertheless, as mentioned above, laboratory testing of conglomerates is constrained by the selection of a suitable and valid specimen size. In addition, various factors have been found to influence the mechanical response of clastic rocks in laboratory testing, which include:

- geometry or shape of the clasts,
- clast size and size distribution,
- composition and mechanical characteristics of the clasts and cement matrix,
- proportion of clasts and cement in a given specimen,
- packing characteristics, such as preferred orientations of the clasts,
- clast-cement interface characteristics and properties.

Hence, the laboratory measured strength and deformation parameters of conglomerates are thought to be a function of all these factors. In natural conglomeratic rocks, the relative sensitivity of a specific factor can not be examined due to the inherent heterogeneities and anisotropies. The interplay of all these factors generally, results in a high co-efficent of variation in the results even for valid and representative samples. Therefore, even at a laboratory scale, to understand and predict the behaviour of such rocks has been an ongoing challenge for researchers and professionals in the discipline of rock engineering. Consequently, at large scale, the design parameters for these rocks remain unknown, except through back analysis of excavation failures.

Two indirect approaches have been used to understand and predict the behaviour of natural rocks in rock engineering. Firstly, the preparation of idealised physical models equivalent to natural rocks, generally called *synthetic*[3] *rocks*, to study basic mechanics and failure mechanisms. The advantage of this approach is to obtain the reproducibility of the test results for a definite degree of the model's homogeneity and isotropy. Moreover, the dependence of a particular parameter can also be studied by varying the selected parameters. In the past, this approach has been utilised extensively as an aid in understanding the mechanics of relatively fine-grained rocks such as sandstones, but the approach has not been applied to conglomerates.

[3] The term synthetic, in this thesis, refers to the physical models prepared in the laboratory by using granular materials and cementing agents.

Secondly, numerical models, based on experimental and theoretical knowledge of the mechanics of the materials, have been used to study and model the behaviour of natural rocks. Both continuum and discontinuum approaches have been applied in rock mechanics to model the behaviour of natural rocks. There are key assumptions and constraints associated with each approach. Existing continuum methods are not efficient enough to model the behaviour of a granular material based on the micro-mechanics of particle motion and interparticle contacts and cement, especially when dealing with the particle shape which is an important parameter in controlling the mechanical response of granular materials. In contrast, discontinuum methods, such as discrete element methods (DEM), incorporate the motion and interaction of discrete bodies of any shape efficiently to yield a macroscopic response of a particulate assembly. Also, recent research has shown that under certain conditions, a cemented granular assembly can be simulated by binding discrete particles with bonds of definite characteristics, so that the interparticle bonds represent the interparticle cement. The macroscopic behaviour of such a cemented granular assembly is controlled by the properties of both the particles and the interparticle cement, named the *micro parameters,* and the packing of the assembly (e.g., particle size, size distribution and porosity).

Given the DEM's capability in simulating the movements and interactions of discrete bodies and representing the interparticle cement matrix, it is quite relevant to utilise DEM for research into granular rocks, such as conglomerates. The main idea, behind the DEM simulations presented in this thesis, is to build and test intact numerical conglomerate specimens in accordance with ISRM testing requirements, as a step towards the estimation of rock mass strength. The structure of such conglomerates should necessarily be based on the information collected from the cored samples about the clast and matrix. However, the real challenge in modelling intact conglomeratic rock is to estimate the micro parameters specifying the particle (clast) system and to adequately represent the mechanics of the interparticle cement.

In recent DEM studies on fine grained intact rock, the input parameters defining the interparticle contacts and cements were mostly estimated by the trial and error method, that is, the inverse modelling approach. These studies, although reproducing the many features of intact rock, did not recover the mechanical behaviour of the sample in all tensile and compressive stress states. Various parameters have been studied, such as, the modelling of complex shaped particles to obtain realistic results; however, this made the numerical simulation even more complex rather than achieving a simplification in solving the problems. Moreover, as the knowledge of the geological factors controlling the mechanical response of a natural rock can never be complete, a blind comparison between the numerical simulation with estimated parameters and natural rocks can not guarantee an accurate prediction of a realistic mechanical response for a specific rock. However, successful efforts have been made for relatively less heterogeneous rocks with simplified microstructures, but the modelling of heterogeneous rocks with a complex microstructure will include many assumptions (that may or may not be realistic) to yield a mechanical response which itself may or may not be realistic.

Therefore, in modelling the behaviour of natural conglomerates which are highly heterogeneous, the micro structure and the micro parameters for the clasts and cement matrix should be as close as possible to that of natural conglomerates, so that the numerical simulations can represent the behaviour of natural conglomerates. In such numerical simulations, the sensitivity of various parameters can be studied straightforwardly by changing the selected parameters and observing the mechanical response of the assembly.

However, given the heterogeneous nature of natural conglomerates, it is hardly possible to obtain a simplified and homogeneous micro structure that can be rigorously modelled in numerical simulations. In view of this limitation, it is imperative to prepare an idealised conglomerate (a synthetic conglomerate, using physical modelling technique) with a simplified micro structure, instead of a natural conglomerate with a complex structure, which can be rigorously replicated in numerical simulations. All the properties of such a conglomerate should be determined experimentally rather than estimated. Then an equivalent numerical conglomerate should be prepared by using measured input parameters and tested in a manner as equivalent as possible to the physical testing conditions. If both the numerical and physical test results are similar, then the numerical approach can be extended to examine the dependence of various factors governing the mechanical response in natural conglomerates incorporating more complexities.

Solely applying numerical methods is not sufficient, as no means are available to verify the predicted behaviour of the numerical methods unless monitoring the dependence of all factors that can affect the mechanical response of a conglomerate. Hence, it is more reasonable to prepare physical models and equivalent numerical models which can provide a basic understanding of the behaviour of such idealised rocks at a laboratory scale and then apply the findings to estimate the in situ strength and deformation parameters of conglomeratic rock masses.

For this reason, the present study is focused on the application of both approaches, physical modelling and discrete element numerical simulation, to investigate the behaviour of idealised conglomerates.

1.2 Research Hypothesis

The present research is based on the premise that by using an *idealised*[4] synthetic conglomerate (with spherical and uniformly sized clasts, and homogeneous cement matrix) and DEM simulations, the role of the cement matrix in controlling the strength, deformation and the failure mechanisms of natural clast supported conglomerates can be understood. An added premise is to use the DEM simulations in investigating the sensitivity of an idealised conglomerate for the clast size and size distribution (packing), the strength and stiffness of the clasts and cement matrix, and the clast-cement interface properties in controlling mechanical behaviour.

1.3 Study Objectives

The broad aim is to use physical and numerical ISRM tests to explore the factors controlling the failure mechanisms, and the intact strength and deformation properties of clast-supported conglomerates. In addition, the extension of this work is to investigate the impact of clast and cement properties of commonly occurring natural conglomerates.

The objectives set to obtain the research aim are given below:

1. To prepare and test an idealised synthetic conglomerate (by physical modelling) comprised of spherical uniformly sized clasts having sufficient *similitude credibility*[5] with a natural conglomerate in ISRM recommended laboratory tests.
2. Use DEM simulation to prepare and test an equivalent numerical conglomerate similar to the synthetic conglomerate.
3. To determine correlations between the macroscopic responses of both the synthetic and numerical conglomerates to validate the response of DEM simulations.
4. To investigate the sensitivity of the clasts and matrix properties on the mechanical behaviour of commonly occurring natural conglomerates in DEM simulation.

[4] The term idealised conglomerates in this thesis, refers to the conglomerates having spherical and uniformly sized clasts with a fine grained homogeneous cement matrix.

[5] The term similitude creditability refers to the degree of similarity of the two systems having similitude and is properly defined in Chapter 2.

5. To conduct a micro-mechanical investigation to explore the clast-cement interaction and the role of the cement matrix on the macroscopic response in conglomerate rocks.

1.4 Research Outline

The present research involves the preparation and testing of synthetic conglomerates (i.e., physical models) and numerical conglomerates (PFC3D models) having similarity in their micro structures together with the correlation of their mechanical behaviours in the same tests. The first part of the research focuses on the preparation and testing of a physical system (synthetic conglomerate) that is then modelled in numerical simulations using PFC3D.

The synthetic conglomerate is representative of a natural conglomerate and is composed of clasts and a cement matrix. The clasts are in contact, and the cement matrix fills the interparticle gaps. It long been known that clast shape influences the overall response of the clastic rocks; therefore, to simplify the procedure and remove the effect of variation in the particle shape, initially, a spherical shape of clasts was considered in the present research. After considering the stiffness and strength contrast of the clasts and cement matrix in real conglomerates, steel spheres and Portland cement were selected to replicate the clasts and matrix of natural conglomerates. It was anticipated that the contrast of the stiffness of the steel balls and Portland cement would represent the stiffness contrast of the hard rock and argillaceous cement. The synthetic conglomerate after fabrication was subjected to laboratory testing to record its mechanical response under various loading states.

The second part of the research sought to fabricate the equivalent synthetic conglomerate in a numerical simulation, that is, a numerical conglomerate. Particle Flow Code in 3 dimensions (PFC3D) was used to construct the numerical conglomerate specimens, equivalent to the synthetic conglomerate in physical parameters (i.e., size and density of particles, particle size distribution, porosity and specimen’s dimensions). In PFC3D, interparticle cement was provided using a parallel bond which simulates the cement as a cylinder among the bonded particles. The properties of the parallel bond were derived from testing on Portland cement paste. The Hertz-Mindlin contact model was used to replicate the elastic deformation of the particles and, accordingly, elastic parameters were specified. The numerical specimens were then subjected to the same laboratory tests as the physical samples. Afterwards, test results of the synthetic and numerical conglomerates were compared. PFC3D was used to assess the sensitivity of the clasts and matrix material, together with the effect of specimen dimensions and particle size distribution. The conceptual of the present research is illustrated in Figure 1-1.

Finally, a micro-mechanical investigation using PFC2D was conducted to explore the clast-cement interaction by modelling cement as an aggregate of micro particles. It was observed that the interface properties have a significant role in controlling the failure mechanism and peak strength in various modes of deformation at a micro level. Similarly, the presence of cement among the particles was also shown to influence the overall mechanical response of the cemented particles.

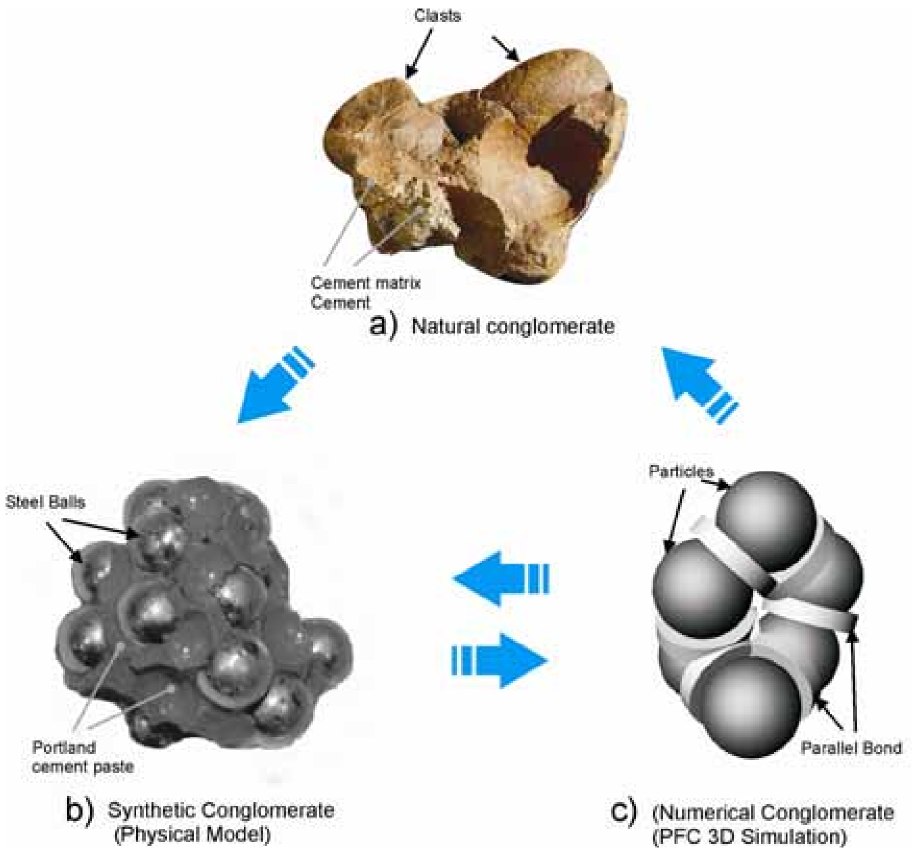

Figure 1-1: Conceptual illustration of the present research: a) micro structure of natural conglomerate, b) physical model (steel balls bounded by Portland cement) representing the synthetic conglomerate and, c) numerical simulation of particles and interparticle cementing material (parallel bonds) in PFC3D, representing the numerical conglomerate.

1.5 Organisation of the Thesis

This thesis is organised into 8 chapters. A brief summary covering the contents of each chapter is given below:

This chapter (Chapter-1) gives a brief overview of the background, hypothesis and the objectives of the present research. Following this introductory chapter, a review of the literature pertaining to this research is presented in Chapter 2.

Chapter 2 (Literature Review), firstly presents the broad picture of granular rocks with special emphasis on the types, compositions and mechanics of conglomerates. This is followed by a review of discrete element methods (DEM) with reference to their applications, formulations and limitations for the simulation of granular materials. Then, a brief historical background as well as the applications of physical modelling techniques is presented in order to understand the behaviour of granular rocks. Previous studies involving physical modelling and discrete simulations in rock engineering are reviewed. At the end of the chapter, a summary of the literature review, together with an outline of the methodology adopted in the present research for the experimental stage is provided.

Chapter 3 (Experimentation: Techniques, Testing and Analyses) describes in detail all the experimental work undertaken in this study. Firstly, the preparation of synthetic conglomerate and Portland cement samples is discussed, and then a description of the tests undertaken (uniaxial, triaxial, Brazilian tensile and shear box) on synthetic conglomerates and cement samples is presented together with the test results. Afterwards, analyses on the test results of the synthetic conglomerate and the cement paste are presented. Finally, a summary of the micro parameters used in the numerical simulations is presented based on derived and known parameters.

Chapter 4 (Numerical Simulation: Diagenesis, Testing and Analyses) explains the preparation of numerical conglomerates (using PFC3D) for known and laboratory measured micro parameters. Following this is a discussion on the numerical simulation of uniaxial, triaxial, Brazilian tensile and shear box testing along with the test results. Parametric sensitivity studies conducted in each testing are also described. Finally, the analyses of the numerical test results are presented.

Chapter 5 (Comparison of Synthetic and Numerical Conglomerates) presents the correlations in the mechanical responses of the synthetic and numerical conglomerates in uniaxial, triaxial, Brazilian tensile and shear box tests. Finally, a summary of the conclusions of these comparisons is provided.

Chapter 6 (Numerical Investigation of Idealised Natural Conglomerates) discusses the results of the sensitivity studies conducted on numerical conglomerates for particle size distribution, specimen dimensions (scaling) and particle and cementing materials.

Chapter 7 (Micro-mechanical Investigation of Particle-Cement Interaction) is aimed at the micro mechanical investigation of clast-cement interaction using PFC2D. Initially, discussion on the calibration process for the cement matrix (in PFC2D) is presented.

Then, the results of a microscopic investigation of two and three ball tests are presented together with a discussion of the results and findings.

Chapter 8 (Summary, Conclusions and Recommendations for Future Research) presents a discussion on the findings, summarises the major conclusions of this study and recommends the direction of future work in this area.

1.6 Published Papers

The following papers containing extracts of this thesis were published during the period of research:

- Akram, M. S. and Sharrock, G. (2009). Physical and numerical investigation of a cemented granular assembly under uniaxial and triaxial compression. *The 43rd US Rock Mechanics Symposium and 4th U.S.-Canada Rock Mechanics Symposium June 28 – July 1, 2009*, Asheville, ARMA09-024 (CD-ROM), Paper No. 24.

- Akram, M. S. and Sharrock, G. (2010). Physical and numerical investigation of a cemented granular assembly of steel spheres. *Int. J. Numer. Anal. Meth. Geomech.* 34 (18): 1896-1934. DOI: 10.1002/nag.885.

- Akram, M. S., Sharrock, G. and Mitra, R. (2011). Physical and numerical investigation of conglomeratic rocks. *2nd international FLAC/DEM Symposium, February 14-16, 2011,* Melbourne, Australia (Paper No. 102).

- Akram, M. S., Sharrock, G. and Mitra, R. (2011). The role of interstitial cement in synthetic conglomeratic rocks. *2nd international FLAC/DEM Symposium, February 14-16, 2011,* Melbourne, Australia (Paper No. 103).

Literature Review

2.1 Introduction

The strength and deformation of natural granular rocks is a complex combination and there is an interplay of both particle and interparticle cement properties. Naturally, the mineral composition, the physical and mechanical properties of particles and cementing materials vary extensively, as per the geologic origin and depositional history of the granular rocks. To analyse the sensitivity of the clasts or cementing matrix discretely is very difficult, if not impossible, due to the inherent heterogeneities and complex phenomena occurring at both the micro and macro scale. Hence, the first section of the literature review discusses the types of natural granular rocks, with particular reference to conglomeratic rocks, their types and associated challenges for the determination of their mechanical response at laboratory and field scales. Subsequently, numerical methods and physical modelling, a useful technique to prepare and test a synthetic rock in the laboratory, are discussed in view of understanding and investigating the mechanics of granular rocks. Of the numerical methods, Discrete Element Methods (DEM) show potential in modelling the behaviour of granular rocks, and are discussed in detail along with their applications, strengths and limitations for modelling a granular rock. Likewise, the effectiveness and efficiency of physical modelling is presented in the context of understanding the mechanics of natural materials. Finally, a discussion on previous research conducted in these areas is presented and the research gaps in this area are highlighted. A review on each area is presented as a separate section and is followed by a section summary. The logical flow of these sections is illustrated in Figure 2-1.

Literature on the significance, effectiveness, and application of Acoustic Emission (AE) monitoring of rocks is also reviewed, with reference to laboratory testing and is presented in Appendix A.

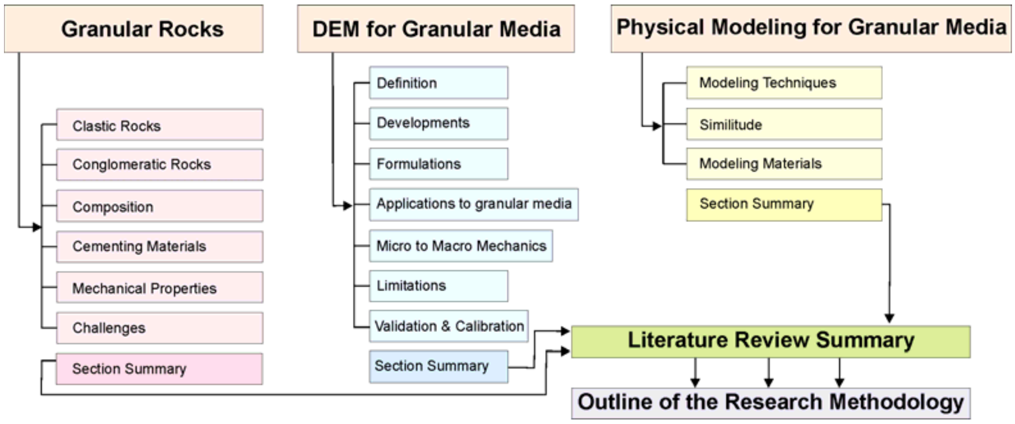

Figure 2-1: Structure and flow of the literature review sections discussed in Chapter 2.

2.2 Granular Rocks

There are no criteria to define granular rocks. Natural rocks are principally divided into three main classes; sedimentary, metamorphic and igneous rocks based on their mode of formation. In engineering geology, however, rock texture is the primary parameter that affects the mechanical behaviour and characteristics in a specific mode of deformation. Therefore, rocks are categorised into granular and non-granular rocks. Here, the term non-granular rocks refer to a rock class having a glassy texture or consisting of very fine grains, that is, less than silt size. By contrast, granular rocks consist of crystals or grains joined together with some cementing materials. Regardless of geologic origin and mineral composition, both granular and non-granular rocks belong to all three basic geologic classes. For example, granular rocks can be sedimentary rocks (sandstones, conglomerates etc.), metamorphic rocks (slates, phyllites, quartzite etc.) and igneous (granite, diorite etc.). Similarly, non-granular rocks consist of sedimentary (mudstones, limestone, shales, cherts etc.), metamorphic (schists, marble etc.) or igneous (obsidian, basalts etc.) rocks. In laboratory testing, non-granular rocks are treated as a single phase material consisting of homogeneous micro structure. However, granular rocks are normally considered as composite or two phase materials consisting of rock fragments or clasts and a cementing matrix. The mechanical response of such materials or rocks is governed by the characteristics of both the clasts and cement matrix. In mechanical testing, dilation of the materials basically draws a line between the granular and non-granular materials and provides a rationale to this differentiation in natural rocks (Stimpson 1970).

Granular rocks are a broad class of natural rocks and can be further classified based on grain size and geologic origin (Figure 2-2) (Clark & Walker 1977; AS 1993).

Granular rocks with mainly sedimentary origins are the primary focus of the present research.

The fine grained sedimentary rocks are also called argillaceous rocks and have a grain size less than 0.06mm. The grain size cannot be viewed with the naked eye, for example, shales, mudstones, siltstone and claystone. The medium to coarse grained rocks are also called arrenaceous rocks having sand sized grains (i.e. >0.06 and <2mm), for example, sandstones. The process by which arrenaceous rocks form is partly mechanical and involves the breaking and deformation of parent rocks into re-lithified sand sized grains. The other important mechanism is chemical activity which includes chemical decomposition and the solutioning of grains, the precipitation of material from pore fluids and intergranular reactions. Silica is the most common cementing agent in sandstones with the less common calcite, ferruginous and gypsiferous cements (Bell 2007).

The rocks having a grain size greater than 2mm are classified as very coarse grained rocks and termed as rudaceous or pebbly. They are made up of clasts having a size greater than 2mm up to a boulder size (>20mm) embedded in a fine grained matrix with particle size less than 2mm.

Extensive studies are reported on arrenaceous and argillaceous rocks such as, mudstones, shales, siltstones and sandstones. Conversely, very few studies on rudaceous rocks have been documented in the literature. Since rudaceous rocks are of particular interest and are relevant to the present research, these are discussed in detail in the following sections.

2.2.1 Rudaceous Rocks

Rudaceous is a sedimentological term to define coarse grained rocks and rudaceous rocks are defined as "sediments in which at least quarter of whose volume is made up of particles larger than 2mm in diameter" (Richard 2000).

Rudaceous rocks are a class of granular rock which are formed by the transportation, sedimentation and cementation of the grains of the existing rocks. This definition excludes crystalline granular rocks which are the result of the solidification of magma and/ or of metamorphic activity. Simplistically, it refers to sediments with a particle size greater than 2mm deposited by the action of transportation agents. Traditionally rudaceous rocks are divided into breccias, whose particles are angular, and conglomerates whose particles are rounded due to the action of transportation. Breccias are rocks that usually occur in fault zones and termed as tectonic breccias, and also in some screes. Hence, the majority of rudaceous rocks on the earth's surface are conglomeratic (Koster & Steel 1984).

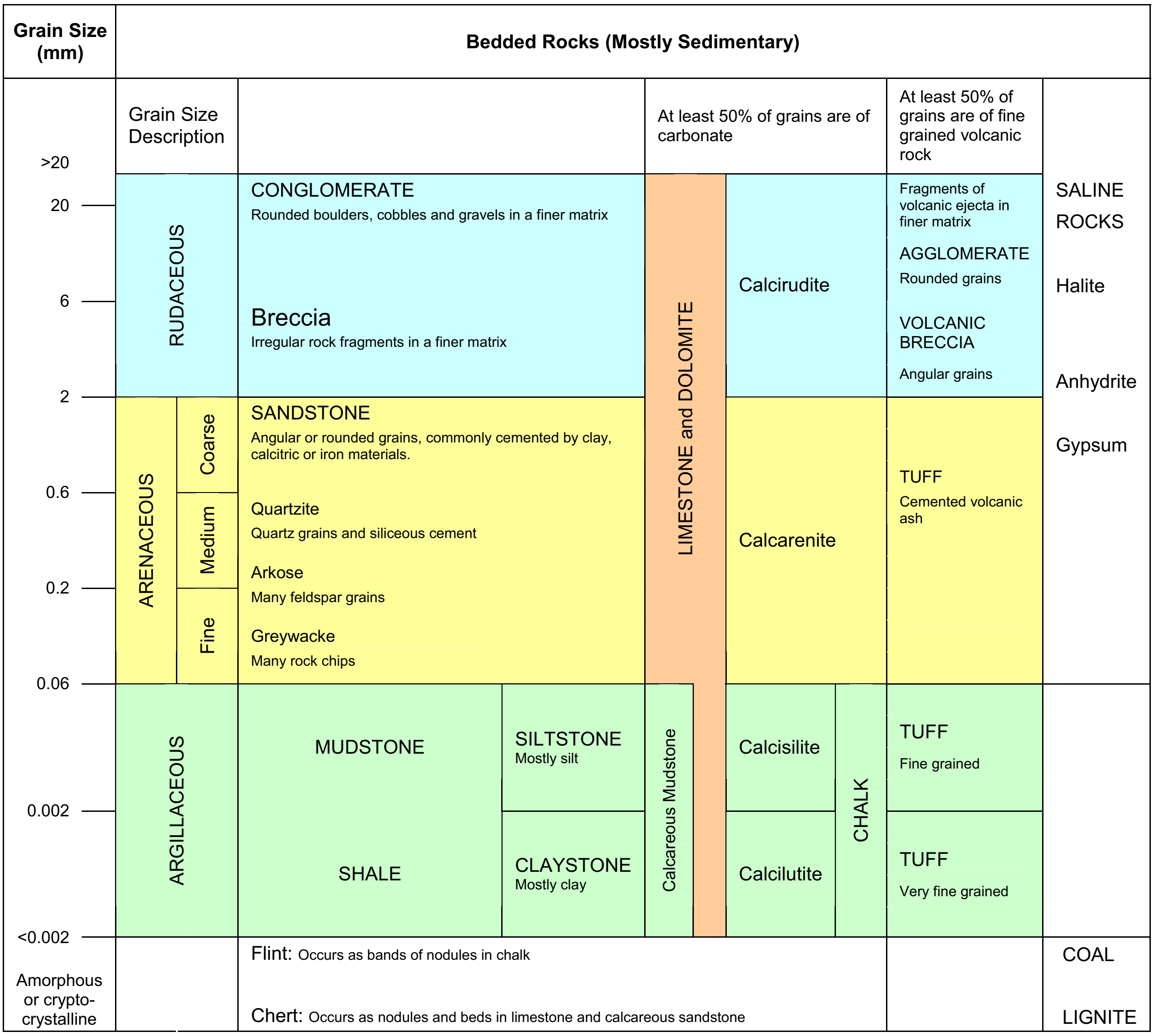

Figure 2-2: Classification of sedimentary rocks based on grain size and mineral composition (after AS 1993).

2.2.2 Conglomeratic Rocks

Conglomerate is a terragenous sedimentary rock type containing large, usually rounded rock fragments (Shafiei & Dusseault 2008). In engineering geology, conglomerate refers to a sedimentary rock containing more than 50% of gravels, cobbles or boulders embedded in a cementing matrix. If rock fragments are less than 50%, the rock is described as very coarse grained or pebbly sandstone (Berkman 2001). The composition of the conglomerates is highly variable depending on their depositional environment and the origin of the clasts. Conglomerates can be divided into the following three main groups based on their compositions (Richard 2000):

2.2.2.1 Volcaniclastic Conglomerates (Agglomerates)

The volcaniclastic conglomerates are commonly known as agglomerate in engineering geology and rock mechanics. These are generally formed both by explosive eruptions and by the scree movement of volcanic detritus derived from volcanic activity (Richard 2000). Generally, these are preserved and embedded in the lava flows and usually are associated with volcanic terrains. The coarse rock fragments in agglomerates are “volcanic bombs” and eroded basaltic detritus, whereas the cementing material is normally the volcanic sand (tuff) or volcanic dust (ashes). A typical specimen of an agglomerate is shown in Figure 2-3a.

2.2.2.2 Carbonate Conglomerates (Calcirudites)

The carbonate conglomerates are also termed Calcirudites in geologic and sedimentologic literature. The best known examples of carbonate conglomerates are “coral rocks”, the boulder beds that form submarine screes around reef fronts (Richard 2000). Their origin is submarine and rare continental carbonate conglomerates are present due to their solubility in the acidic groundwaters.

A typical specimen of a carbonate conglomerate is shown in Figure 2-3b.

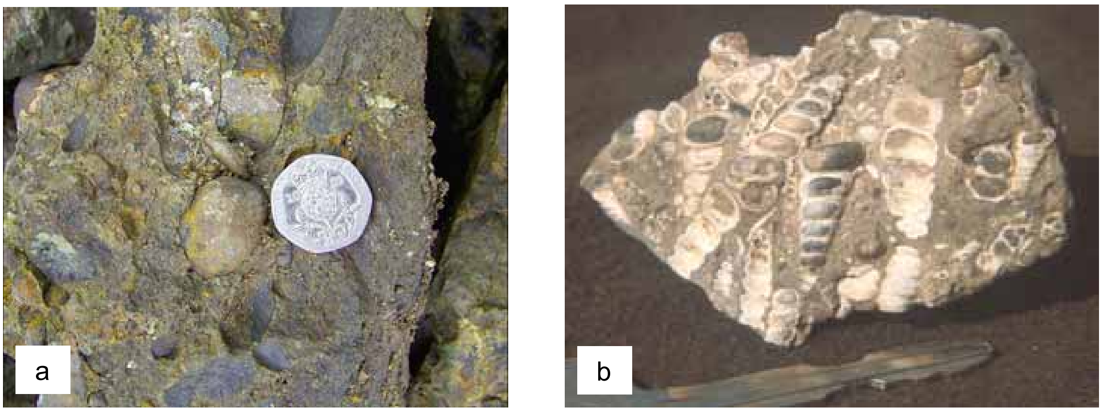

Figure 2-3: a) Volcaniclastic Conglomerate (Agglomerate), b) Carbonate Conglomerate (Calcirudite).

2.2.2.3 Terrigenous Conglomerates (Silicirudites)

Terrigenous conglomerates are the most common conglomerates on the earth’s surface. Their origin is normally fluvial (along fan deposits) or glacial. During their primary deposition, they contain high porosities and permeabilities, which can reduce quickly by matrix infilling. The term “conglomerate” is generally used to represent a terrigenous conglomerate in the engineering geological literature. Therefore, hereafter in this thesis, this term has been used instead of terrigenous conglomerates.

Conglomerates are broadly divided into two main groups as per the percentage of clast and cement matrix, namely grain (or clast) supported and matrix supported.

In matrix supported conglomerates, rock fragments are suspended in the matrix and have no intergranular contacts (Figure 2-4a). The origin of this type can be attributed to the flow and deposition of thick mudflows containing rock fragments or clasts (Richard 2000). In grain supported conglomerates, clasts are interconnected to each other so that the matrix fills the intergranular gaps (Figure 2-4b). These conglomerates are considered to originate in fan deposits and high-current river flows. Grain supported conglomerates are in abundance, compared to matrix supported conglomerates, on the earth (Richard 2000) and hence are the focus of the present research.

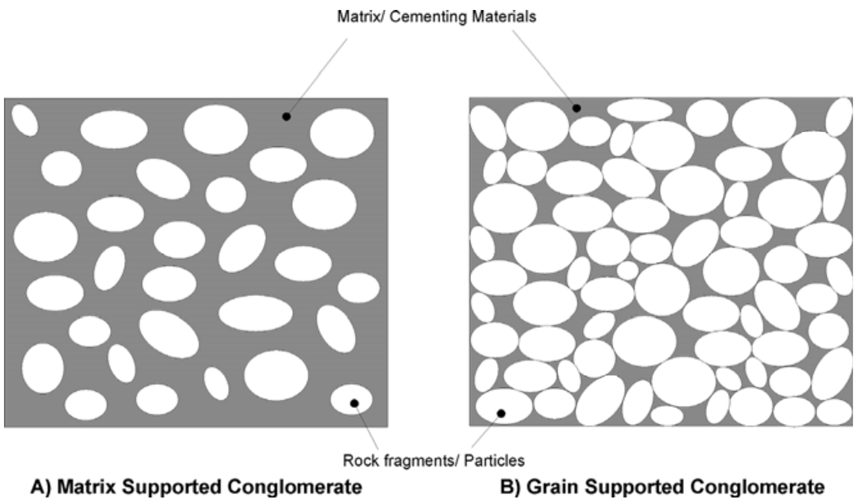

Figure 2-4: A schematic section of conglomerates a) matrix supported, b) grain supported.

Walker (1975; 1978) identified four properties of conglomerates that are useful for diagnosing their origin (Figure 2-5);

- Grain size distribution, and whether the deposit is clast-supported (grain supported) or matrix supported.
- Long-axis preferred orientation or random orientations.
- Stratified (cemented) or not; stratification horizontal or inclined layers; layers with well defined boundaries or gradational boundaries.
- Normal grading, reverse grading or no size grading at all.

The above mentioned criteria are suggested to differentiate the well graded (organised) and poorly graded (disorganised) conglomerate (McLane 1995).

The composition of the clasts and types of cement matrices are discussed in the following sections.

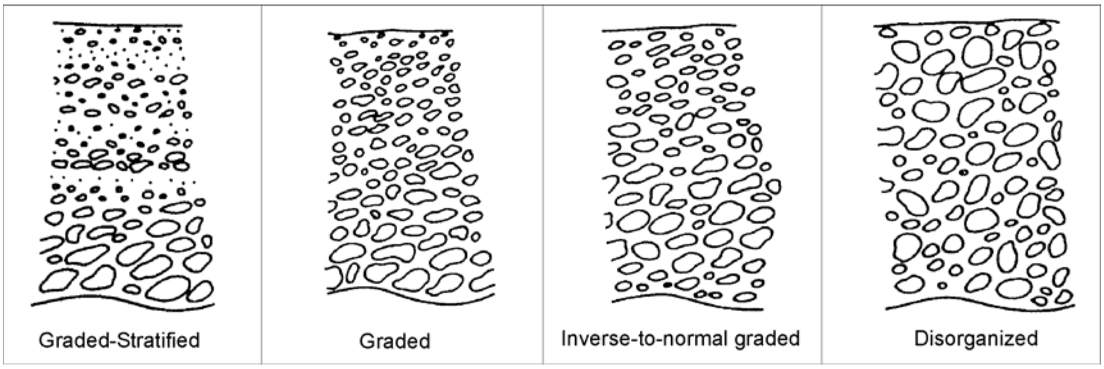

Figure 2-5: Four kinds of conglomerates (after Walker 1978).

- **Composition of Clasts**

Conglomerates are further divided based on the composition of clasts. Polymictic conglomerates with rock fragments having an origin from more than one parent rock, while oligomictic conglomerates are comprised of fragments that are derived only from one rock. The polymictic conglomerates are of diverse composition, while the oligomictic conglomerates are primarily quartzose because of the chemical stability of the silica. Thus the conglomerates of polycyclic sediments are commonly made up of fragments of vein quartz, quartzite, and chert. Polymictic conglomerates are mainly the product of aggradations where tectonically active source areas shed wedges of fanglomerates. Oligomictic conglomerates, by contrast, are generally the product of degradation where tectonic stability allows extensive reworking to produce the laterally extensive basal conglomerates along unconformities (Richard 2000).

In view of the above classifications, the determination of the mineral composition of conglomerates is difficult and is specific to certain depositional environments. Traditional petrographic study is insufficient for determining the mineral composition of clastic rocks as each rock fragment is variable due to being outsourced from different parent rock (Blatt et al. 1980). The typical varieties of conglomerates are presented in Figure 2-6.

- **Composition of Cements**

Conglomerates are cemented by various agents, including calcite, quartz (silica), clay and gypsum. During the first deposition of sediment, there are many open spaces or pores that are later filled by the deposition of a matrix. The matrix can affect the amount of pore space that remains in a rock as it lithifies. Conglomerates normally have significant voids and therefore, are usually good reservoir rocks for ground water, natural gas and petroleum.

In the conglomerates, the infill matrix can be classified based on its texture and chemical compositions. Texturally, matrices are classified as argillaceous and arrenaceous. The chemical cements are mostly siliceous (quartzitic), calcitic and gypsum cements which are introduced with the increase of temperature and pressure conditions at various burial depths. A brief description of these cements is discussed below.

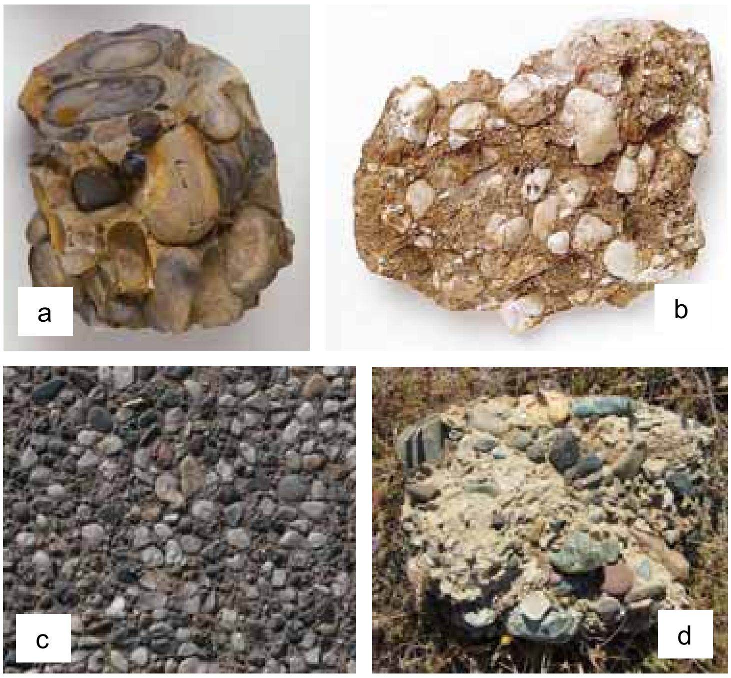

Figure 2-6: Typical varieties of the conglomerates: a) grain supported conglomerate with calcitic cement, b) matrix supported conglomerate with arrenaceous cement, c) well graded polymictic conglomerate, and d) disorganised conglomerate with argillaceous matrix.

Argillaceous Cements

Argillaceous cements are fine grained materials, for example, clays or silts deposited among inter-granular voids, and, with time and depth, these are consolidated to various degrees of cementation. The strength of the argillaceous cements depends on the history of deposition and diagenesis, that is, the post depositional processes. Their strength may vary from the strength of consolidated clays at shallow depths to typical, well cemented claystones at greater depths where secondary mineralization occurs. Generally, the degree of consolidation of argillaceous cements determines their depositional history, that is, the types and abundance of minerals, and the post depositional environment, that is, secondary mineralisation and weathering.

Arrenaceous Cements

Arrenaceous cements are the sandy particles deposited and cemented among the gravels, cobbles and boulders at various depths. In arrenaceous cements, the principal cementing agent is silica (quartz) which is the basic constituent mineral of sands. Quartz is usually a stable mineral at high temperature and pressure conditions compared to gypsum, calcite and clay minerals. However, at greater depths (>1000m), quartz undergoes crystal changes and cements the gravelly particles together (Richard 2000). The degree of the cementation in siliceous cements is also the function of the depositional depth, and post depositional changes in mineralogy and weathering effects. Therefore, the strength of arrenaceous cements range from unconsolidated/ friable sands to well cemented quartz sandstone.

2.2.3 Mechanical Properties of Conglomerates

The mechanical properties of conglomerates refer to their pre and post failure strength and deformation parameters. These are possibly the rocks about which the least amount of information is available in literature (Shafiei & Dusseault 2008). The main reason for this is their composite nature and practical difficulty of sampling and testing them in the laboratory. The in situ testing is prohibitively expensive and is typically only conducted as part of large projects such as dams, tunnels and mines. Therefore, very few test results have been documented in the literature. (see e.g., Lama & Vutukuri 1978; Shafiei & Dusseault 2008; Yasir & Tolgay 2010). A summary of the mechanical properties of conglomerates is provided in Table 2-1.

Given the summary of the test results, it is clear that the mechanical properties of the conglomerates vary widely, subject to their heterogeneous nature and the mineral composition of the clasts and interparticle cement. Similarly, it can be seen that the strength of a conglomerate is a function of the properties of the clasts and matrix, and may range from 1.2 MPa (Shafiei & Dusseault 2008), corresponding to a very weak clayey cement matrix, to 239 MPa (Boyum 1961), with a very high strength quartzitic cement.

Much research has been conducted to investigate the factors influencing the mechanical behaviour of clastic rocks., Dhakal et al. (1993) found that mineral composition and textural features affect the mechanical behaviour in argillaceous clastic rocks. The influence of grain or clast size in sandstones and crystalline rocks has also been observed on peak strength in uniaxial testing (e.g., Olsson 1974; Onodera & Kumara 1980; Prikryl 2001; Meng & Pan 2007). Lindquist (1994) observed that the mechanical behaviour of heterogeneous material is significantly influenced by the proportion of larger clasts. Similarly, an increase in the clast-cement contact area (Dobereiner & De Freitas 1986), the strength of the cement, that is, the quartz content (Bell & Lindsay 1999; Sabatakakis et al. 2008), and the clast packing density (Bell 1978) are additional factors responsible for increasing the strength of clastic rocks. Andriani and Walsh (2002) also found that the mechanical and petrophysical properties of clastic rocks are influenced by the size, shape and packing of grains, the cementing matrix and porosity, all of which are controlled by the rock's depositional and post depositional history. Hence, failure in such rocks is dominated by the presence of clasts as these provide the zones of stress concentration (Farmer 1983) at the clast-matrix interfaces due to the stiffness contrast and therefore, cracks generally initiate and propagate away from such zones (Pollard & Aydin 1988).

Table 2-1: Summary of mechanical parameters of conglomerates (updated after Lama & Vutukuri 1978).

Location	Rock Type	Test	Parameter description*	Value	References
Agri River, Italy	Conglomerate	Jack pressure chamber	*E (GPa)*	11.03 - 11.44	(Lotti & Beamonte 1964)
Abda Donthnala Tunnel, Morocco	Conglomerate (medium compacted)	Plate load	*E (GPa)*	0.40-2.60	(Muller 1960)
Bor Copper Mine, Yugoslavia	Conglomerate	Shear test	*c* (MPa) ϕ *(deg.)*	0.40 70 Peak 63 Res.	(Radosavljevic et al. 1970)
Dez Dam, Iran	Conglomerate	Pressure chamber	*E (GPa)*	6.70 1.80 horiz. 5.70 vert.	(Oberti & Fumagalli 1964)
Dez Dam, Iran	Conglomerate	Plate load	*E (GPa)*	1.40-57 horiz. 2.80-50 vert.	(Muller 1960)
Dez Dam, Iran	Conglomerate	Plate load	*E (GPa)*	9.60-21.37	(Muller 1960)
Dez Dam, Iran	Conglomerate	Pressure chamber	*E (GPa)*	4.89-6.65	(Dodds 1965)
Inferno Dam, Italy	Conglomerate	Not known	*E (GPa)*	14.00	(D.E.H. 1966)
Nagase Dam, Japan	Conglomerate with fissures	Jack loading 25cm Ø	*E (GPa)*	2.30	(J.N.C.L.D. 1958)
Nagase Dam, Japan	Conglomerate	Jack loading 25cm Ø	*E (GPa)*	9.40	(J.N.C.L.D. 1958)
Pietra del Pertusillo, Italy	Conglomerate	Seismic & Hydraulic chamber	*E (GPa)*	2.00	(Link 1964)
Trona Dam, Italy	Conglomerate	Hydraulic chamber	*E (GPa)*	13.30	(D.E.H. 1966)
Not Known	Conglomerate	Hydraulic chamber	*E (GPa)*	2.80-3.00	(Lotti & Beamonte 1964)
Nuclear Power Plant, Japan	Conglomerate	Jack (repeated)	*E (GPa)*	3.67-4.39	(Hayashi et al. 1974)

Location	Rock Type	Test	Parameter description*	Value	References
Estania, New Mexico, USA	Conglomerate	Uniaxial compression and Brazilian tensile	*UCS(MPa)* *E (GPa)* υ	66.9 21.58 0.06	(Bratton & Pratt 1968)
Pamour Mine, Timmins, Canada	Conglomerate	Uniaxial compression and Brazilian tensile	*UCS(MPa)* σ_t *(MPa)* *E (GPa)* υ	144.28 18.97 64.41 0.25	(Jackson et al. 1995)
Estania, New Mexico, USA	Conglomerate	Uniaxial compression and Brazilian tensile	*UCS(MPa)* *E (GPa)* υ	66.9 21.58 0.06	(Bratton & Pratt 1968)
Cliffs mines, Michigan, USA	Conglomerate	Uniaxial compression	*UCS(MPa)* *E (GPa)* υ	238.56 106.86 0.22	(Boyum 1961)
Denison Mine, Canada	Conglomerate	Uniaxial compression	*UCS(MPa)* *E (GPa)*	222 76	(Coates & Parson 1966)
Denison Mine, Elliot Lake, Ontario, Canada	Conglomerate	Uniaxial compression and Brazilian tensile	*UCS(MPa)* σ_t *(MPa)* *E (GPa)* υ	185.4 7.52 71.06 0.13	(Morrison 1970)
Flaming Gorge Dam, Utah, USA	Conglomerate	Unknown	*UCS(MPa)* σ_t *(MPa)* *E (GPa)* υ	88.5 2.96 14.13 0.03	(Lama & Vutukuri 1978)
Mc Dowel Dam North Dakota, USA	Conglomerate	Unknown	*UCS(MPa)* *E (GPa)* υ	30.34 1.26 0.12	(Lama & Vutukuri 1978)
Bhakra Dam, India	Conglomerate	Unknown	*UCS(MPa)* *E (GPa)* υ	105.49 46.19 0.15	(Lama & Vutukuri 1978)
Manitoba, Canada	Conglomerate	Unknown	*UCS(MPa)* σ_t *(MPa)* *E (GPa)* υ	185.4 7.52 71.06 0.13	(Lama & Vutukuri 1978)
Bhakra Dam, India	Conglomerate	Unknown	*UCS(MPa)* *E (GPa)* υ	107.76 51.6 0.13	(Lama & Vutukuri 1978)
Qomroud long Tunnel - 6, Iran	Conglomerate	Uniaxial compression and Brazilian tensile	*UCS(MPa)* σ_t *(MPa)* *E (GPa)* υ	1.2-0-5.00 0.24-0.37 0.70-3.0 0.24-0.37	(Shafiei & Dusseault 2008)
Kayranlik Mountains, Turkey	Conglomerate	Uniaxial compression	*UCS(MPa)*	50.99-64.72	(Yasir & Tolgay 2010)
Unknown	Conglomerate	Large shear box (0.4mX0.4mx0.2m)	ϕ (Deg.) *c (MPa)*	35 0.23	(Krsmanovic 1967)

* *UCS*- Uniaxial Compressive Strength, σ_t - Tensile strength, *E*- Young's Modulus, υ - Poisson's ratio

ϕ - Angle of Friction, *c*- Cohesion, Besides the physical and mechanical properties of the clasts, their arrangement, distribution and proportion in the matrix are also important factors that have been investigated to influence the mechanical response of a conglomerate (Hawkes & Mellor 1970) and contribute to the anisotropy of the rocks (Lisle 1985; Chen & Wan 2004). For example, the loading axis has been investigated to influence the compressive and tensile strengths of such rocks in relation to the orientation of the clasts present in the matrix (Moon 1993). Moon's results agree with the recent findings of Ozbek (2009) who investigated conglomerates with the Schmidt rebound hammer and found that the hammer rebound values (HR) vary along, and perpendicular to, the preferred orientation of the embedded clasts. This variation is due to the variation of the clast-covered area and the random distribution or preferred orientation of the clast and matrix ratio (Johansson 1976; Ozbek 2009).

In addition, laboratory testing on natural (Cecconi et al. 1998) and synthetic conglomeratic rocks (Kobayashi & Yoshinaka 1994; Kobayashi et al. 1994; Kobayashi et al. 1995) revealed that the overall strength and deformation properties of a composite heterogeneous rock, such as a conglomerate, can be estimated by the strength and deformation characteristics of the infill matrices and clasts together with the volumetric proportion of the clasts (Kobayashi & Yoshinaka 1994). It is impractical to completely disaggregate the clasts for the estimation of the particle size distribution and volumetric proportion of the clasts in well-cemented rock and it also depends on the scale used for testing. However, Saotomea et al. (2002) have numerically studied the surface areas of the clasts that form the cylindrical surface of a core sample in relation to their volumetric proportions in the matrix, and found that the coefficient of variation for the volumetric proportion of the clasts depends on the sample size and increases inversely with the sample size. In this case, only low value of coefficient of variation can be determined at any scale by putting a restriction of the maximum clast size to the sample size ratio, as suggested by ISRM (1983).

At the clast scale in Calumet conglomerates, Savanick and Johnson (1974) conducted an investigation to find the tensile strength of interface boundaries between the clast and infill matrix. According to their findings, the interface bond only occurs on a portion of the contact area and the strength of the bond is often significantly lower than the strength of the adjacent materials. Within a conglomerate, the strength of each interface between the clast and matrix varies significantly, suggesting a non-uniform distribution of flaws in the rock.

In view of the above discussion, it is clear that the mechanical response of a conglomeratic rock is a result of a complex combination of composition and mechanical properties of the clasts and matrix, the size distribution and arrangement of the clasts and the micro mechanisms occurring at clast scale. Hence, in natural conditions, the dependence of a specific parameter on the macroscopic behaviour of a conglomerate cannot be examined discretely due to many contributing factors and parameters.

2.2.3.1 Challenges

This section discusses the challenges in determining the geomechanical characteristics of conglomeratic rocks in laboratory testing (intact rock) and the estimation of the strength and deformation parameters on a large scale (rock mass). It has already been discovered that rocks show differences in the strength and deformation at laboratory and field scale owing to their heterogeneous and discontinuous nature. Even at laboratory scale, the strength and deformation parameters were found to vary with the tested specimen sizes (Hoek & Brown 1980b). These differences become more pronounced at rock mass scale in view of the effect of the discontinuities. Various empirical relations have been proposed to estimate the field strength and deformation from the laboratory strength and deformation incorporating the effect of discontinuities and rock structures (see e.g., Hoek & Brown 1980a; Hoek & Brown 1997; Hoek et al. 2002; Hoek & Diederichs 2006).

However, in conglomeratic rocks, the determination of laboratory strength and deformation is not straightforward when compared to other fine grained rocks. It involves practical difficulties in both sampling and testing to determine intact rock parameters, and subsequently the estimation of rock mass strength and deformation is even more challenging.

- **Laboratory Testing**

The main technique to determine intact rock strength parameters is laboratory testing, typically conducted on cored specimens. In laboratory testing, uniaxial and Brazilian tensile tests are the most common tests used on rock specimens to find their strength and deformation characteristics (Hawkes & Mellor 1970; West et al. 1981). These tests are conducted on the rock core samples with standard recommended procedures (e.g., Hoek 1977; Brown 1981; ISRM 1983). Cored samples are usually collected from boreholes as continuous core sampling. It is usually believed that the core samples are undisturbed and laboratory testing will represnt the mechanical properties of the in situ rock conditions. This is true in the case of monolithic or fine grained rocks, or clastic rocks in which clasts are cemented with a very high strength cementing material, for example, quartz. For the clastic rocks with weak cementing material, sampling is always challenging if using conventional coring methods, and it is nearly impossible to extract the samples in an undisturbed condition. In most cases, samples are disturbed by the formation of micro cracks induced by the drilling operation or stress release. Habimana et al. (2002) have discussed sampling techniques and the laboratory testing of cataclastic (tectonically disturbed) rocks with associated difficulties. In some research, cubical sampling is used for uniaxial testing instead of cored samples (e.g., Moon 1993). However, testing cubical samples introduces the effect of sample edges that may make the determined strength misleading.

In case, samples are extracted from the boreholes using sophisticated techniques, for example, by using a triple tube core barrel with diamond bits, assuming no disturbance, the selection of the samples for laboratory testing is another challenge. Samples with more cementing material (discussed in the previous section) will give different results from those with abundant clasts. Moreover, for uniaxial and Brazilian tensile testing of granular rock, the diameter of the sample should be a minimum 10 times the largest grain or clast (ISRM 1983) which restricts the sample selection.

After the selection of the samples, specimen end preparation for UCS testing is again a challenging job when dealing with poorly consolidated rock specimens. It is particularly difficult to obtain uniform stress distribution across the samples so as to avoid tensile splitting or barrelling of the specimen, which is normally caused by the mismatch of the strains on the platen/ rock interface (Hoek 1977). Moreover, the number of tests varies from 3 to 10 as per the various standards used to estimate the uniaxial compressive strength (Ruffolo & Shakoor 2009).

In view of the sampling and testing constraints (e.g., ISRM 1983), the maximum diameter of the sample that can be tested is approximately 100 mm, using conventional compression rigs which corresponds to maximum grain size of 10~11 mm. Whereas, the real life challenge is to evaluate the strength and deformation of a rock having clasts comparable to cobbles and boulders greater than 20 mm with weak cement matrix. It is also not clear whether these large samples are sufficiently representative to determine the mechanical properties of such rocks in laboratory tests.

- **Large Scale Strength and Deformation Evaluation**

In conglomeratic rocks, in situ testing is generally considered more reliable than laboratory testing, as it records mechanical behaviour in natural conditions. In situ testing has been used mainly to determine the in situ deformation of conglomerates by plate load or pressure chamber testing (Lama & Vutukuri 1978). From Table 2-1, it is clear that mostly in situ testing has been conducted as part of large projects, for example, dams, tunnels and mines.

In the absence of in situ testing, laboratory testing data together with field observations and mapping are used to empirically estimate field strength and deformation. Various empirical approaches have been suggested in this regard using intact rock parameters and rock characterization (structure and texture) (e.g., Hoek & Brown 1980a; Hoek & Brown 1997; Hoek et al. 2002; Hoek & Diederichs 2006). These approaches are generally based on past experience and qualitative observations, and may or may not have scientific meaning in relation to the intact rock and rock mass parameters for a composite rock, such as conglomerate. Also, it is unknown so far, the extent to which the empirical downgrading of the intact strength and deformation, based on these techniques, is applicable to conglomerates. In addition, the laboratory testing on conglomeratic specimens is not easy and straightforward as discussed in the previous section. Consequently, intact rock parameters of conglomerates show wide scatter owing to their composite and heterogeneous nature, which casts doubts on the reliability of the data and subsequent estimation of field strength and deformation.

Further, the presence of geologic discontinuities in such rocks make the rock mass evaluation an even more complex exercise. It is obvious that unrealistic strength and deformation evaluation could result due to too many assumptions regarding the material’s behaviour.

2.2.4 Mechanics of Conglomerates

The mechanics of conglomerates can be idealised by considering an assembly of discrete clasts bonded with a cement matrix. In the case where no cement matrix is present among the clasts, the clast assembly will be treated as frictional granular materials in which forces are transmitted among the clasts through the contact points. Microstructure or fabric is now a general term to understand the mechanics of granular materials. The term microstructure denotes the physical constitution of the clasts that can be expressed by the size, shape and nature of bond between them, the internal stresses, the arrangement of clasts, and the voids, whereas fabric refers to the arrangement of the discrete clasts and associated voids (Tobita & Oda 1999). The resistance against the sliding and rolling of the clasts at the contact points defines the interparticle friction, without which clasts cannot resist shear forces. This shearing force, according to Coulomb's frictional law, can be determined as:

$$F_\tau = \mu F_\sigma = F_\sigma \tan\phi_c \qquad (2\text{-}1)$$

Where

F_τ - frictional force,

F_σ - normal force,

μ - frictional constant, and

ϕ_c - interparticle friction angle or micro friction.

Equation (2-1) can be rewritten in terms of stresses at particle contact as;

$$\tau_c = \sigma_n \tan\phi_c \qquad (2\text{-}2)$$

Where

τ_c - contact shear stress (F_τ/A),

σ_n - contact normal stress (F_σ/A) acting on sliding plane with area "A", and

ϕ_c - interparticle contact friction angle or micro friction

Similarly, the strength of an assembly of clasts can be related to its angle of internal friction (bulk friction) as:

$$\tau_b = \sigma_n \tan\phi_b \qquad (2\text{-}3)$$

Where

τ_b - shear strength of the assembly,

ϕ_b - friction angle of the assembly or bulk friction,

σ_n - normal stress

Both equations (2-2) and (2-3) look similar but have different meanings. Micro friction (ϕ_c) in equation (2-2) is the friction between the two interacting particles or clasts only and is a physical parameter depending on the surface roughness of the particles, while bulk friction (ϕ_b) in equation (2-3) is not a physical constant but depends on the void ratio, clast geometry, fabric, stress states etc.

The overall resistance, owing to geometry and the surface roughness of the clasts offered by the assembly against shearing, is termed an interlocking effect (Tobita & Oda 1999). This interlocking effect governs the macroscopic behaviour (deformation and strength) of the frictional granular assemblies. Thus, for the granular materials, the interlocking is not only interparticle friction but also includes a component arising from shearing against the interlocked particles (Bishop 1954). This was named dilatancy by Reynolds (1885) and can be related to the shear strength of a frictional assembly as (Tobita & Oda 1999):

$$\tau = \sigma_n \tan(\phi_b + i) \qquad (2\text{-}4)$$

Where

τ - shear strength of the assembly,

ϕ_b - interparticle friction angle or micro friction,

σ_n - normal stress,

i - dilatancy angle

Hence, a rough quantitative relation of micro to macro friction can be made as:

$$\phi = \phi_b + i \qquad (2\text{-}5)$$

This relation can also be visualized by the following figure:

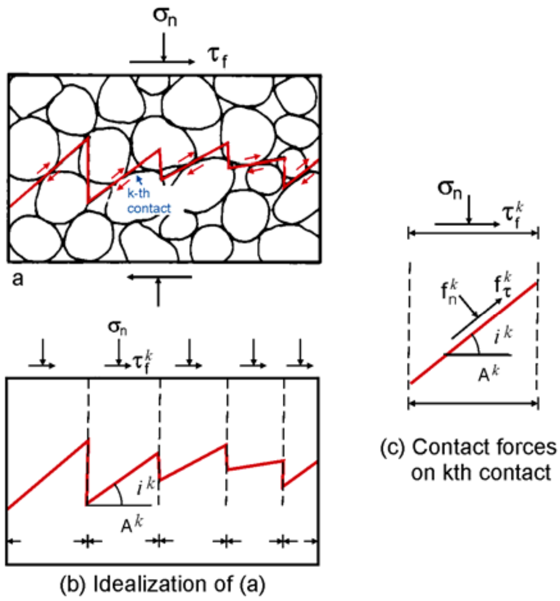

Figure 2-7: Micromechanism of shearing in granular materials (modified after Newland & Allely 1957).

Hence, (i) in equations (2-4) and (2-5) is the dilation which incorporates the factors influencing the assembly's response other than micro friction, such as the particle packing, porosity or void ratio and particle shape.

Moreover, previous studies on frictional granular media reflected that interparticle friction to bulk (assembly) friction does not relate linearly. There is experimental evidence that particles rotate excessively during shearing of granular media (e.g., Skinner 1969; Oda & Konishi 1974). Skinner (1969), after conducting experiments on glass balls, observed that interparticle friction has only a slight, if any, effect on the assembly of the granulates.

Conversely, if the granular media is cemented, that is, cohesive-frictional as in case of conglomerates, the overall response of the material will be governed by the characteristics of the cementing materials in addition to the properties of clasts and voids. It has been long established that the composition and amount of the cement is very important for the strength of granular rocks. Even more important than its amount is the position of the cement deposited among the clasts, which prevents the sliding and rotation of clasts (Bernabe et al. 1992).

In view of the above discussions, conglomerates are a type of cohesive-frictional material whose mechanical behaviour is a function of their microstructure, including cementation and fibre. The properties of both the clasts and cement matrix are important in controlling the strength and stiffness of a conglomeratic rock and need to be investigated for their sensitivity on mechanical response.

2.2.5 Section Summary

There are clear difficulties in evaluating the strength and deformation of the clastic rocks, such as conglomerates. Both clast and cementing materials are highly variable in physical and mechanical properties subject to their geologic origin. Sampling and laboratory testing on such rocks present real life challenges when investigating the degree of dependencies of the mechanical properties of clasts and cement matrix. As a result, the mechanical behaviour of a conglomeratic rock is poorly understood even on a laboratory scale. Instead of direct laboratory testing, other techniques need to be considered for evaluating the strength and deformation characteristics, together with the understanding of the mechanics of such rocks.

2.3 Discrete Element Methods (DEM)

This section presents an overview of an alternative technique that is considered to have potential for modelling the mechanics of granular rocks, such as conglomerates. Numerous numerical techniques have been applied in rock and soil mechanics to solve the problems (Jing & Hudson 2002; Jing 2003). These techniques are based on continuum mechanics, for example, Finite Difference Methods (FDM), Finite Element Methods (FEM), Boundary Element Methods (BEM) and discontinuum mechanics, which are mainly comprised of Discrete Element Methods (DEM). Both continuum and discontinuum methods have associated advantages and disadvantages and their applications mainly depend on the characteristics of the material to be modelled.

In the mechanics of granular materials, microstructure and fibre (force chain through the interparticle contacts) are two interrelated key factors that control the behaviour of a granular material (Tobita & Oda 1999). Any change in the microstructure of a granular material influences the fibre, and consequently affects the overall macroscopic response. Hence, any numerical technique which yields a macroscopic response of granular materials based on microstructure and fibre is capable of simulating the behaviour of granular materials. The methods based on the continuum mechanics generally model the granular materials with the assumption of a homogeneous and isotropic microstructure. These methods can be applied to granular materials whose mechanics is already known but for the research into rocks like conglomerates, these were not considered suitable.

Unlike continuum methods, DEM is an approach to numerical simulation where statistical measures of the global behaviour of a phenomenon are computed from the individual motion and mutual interactions of a large population of elements. It is commonly used in situations where state-of-the-art theoretical knowledge has not yet provided complete understanding and mathematical equations to model the physical system. The method has been implemented in various forms, based on the geometry of discrete bodies and the mode of deformation representation. The most significant advantage of DEM is to model granular media with particle shapes and rock mass incorporating discontinuities which was not effectively possible using FDM, FEM and FBM. Since DEM evolves macro behaviour of a granular system based on the interaction and movement of the discrete particles, it is quite relevant to utilise it for the studies of conglomeratic rocks. A detailed discussion of the DEM is provided in the following sections.

2.3.1 Introduction and Overview

Rock mechanics is one of the disciplines from which the DEM originated (Burman 1971; Cundall 1971; Chappel 1972; Byrne 1974; Cundall 1974). The formulation of the method is based on the solution of equations of motion of rigid and/or deformable bodies using implicit (FEM discretisation) and explicit (FVM discretisation) formulations (Jing 2003). Since its origin, the method has been extensively applied in soil and rock mechanics and in other disciplines, like structural analysis, granular materials, material processing, fluid mechanics, multi-body systems, robot simulation and computer animation. (Jing & Hudson 2002; Jing 2003; Bobet et al. 2009). It is one of the most rapidly developing areas of computational mechanics and is still in the development phase.

The main idea behind DEM is to circumvent the complexity of a large assembly by considering many simple elements, the behaviour of which can be simulated accurately (Ferrez 2001). In the beginning, after Cundall (1971), various theoretical formulations were developed to simulate discontinuous media and these became known as discrete element methods. Cundall and Hart (1993) proposed a formal definition for discrete element methods: "the numerical schemes which can allow finite displacement and rotation of discrete bodies including complete detachment and can recognize new contacts automatically as calculation progresses". Both these conditions need to be fulfilled to qualify any computational scheme as discrete element methods (DEM) because these conditions produce the important mechanisms of the discontinuous medium for numerous discrete particles.

Cundall and Hart (1993) proposed three important aspects of DEM which can help in their classification, as described in next three sub-sections.

2.3.1.1 Representation of Contact

The main difference between continuum and discontinuum is the representation of a contact or interface between the discrete bodies that comprise a system. This interface may be soft, allowing deformation along the interface/ contact, or rigid, with no deformation along the contacts. The selection of contact type mainly depends on the physics of the system (Cundall & Hart 1993).

2.3.1.2 Representation of Solid Material

The material of the discrete bodies in discrete element methods can be grouped into two main categories: rigid or non-deformable and deformable. In discontinuous systems where most of the deformation is along the discrete bodies/ particle contacts, the assumption of rigid material can be used to model this system. Early developments in discrete element methods were based on the use of rigid particles as building blocks. There are two approaches to obtain deformable particles. Firstly by the direct subdivision of discrete body into elements of definite deformation zones (e.g., Cundall 1980; Lemos et al. 1985). The second approach is used to obtain a complex deformation pattern by the superposition of several mode shapes for the whole discrete body (e.g., Willian & Mustoe 1987; Shi 1988).

2.3.1.3 Detection and Review of Contacts

There are two tasks to be performed before the start of calculations, firstly, to identify all pairs of bodies that can interact, and secondly, to determine the type of interaction, that is, the edges, vertices, faces etc. of one particle that are touching the corresponding entities of the other. Various schemes have been formulated to perform these tasks in two and three dimensions with varying computational time (e.g., Cundall 1980; 1988).

On the basis of these aspects, Cundall and Hart (1993) divided the existing discrete element methods into four main classes:

- Class-1 Distinct Element Methods
- Class-2 Modal Methods
- Class-3 Discontinuous Deformation analysis (DDA)
- Class-4 Momentum Exchange methods

The capability of each class of discrete element methods in response to various attributes is given in Table 2-2.

Table 2-2: Attributes of the four classes of Discrete Element Methods and the Limit Equilibrium Method (after Cundall & Hart 1993).

Attributes		Class-1 Distinct element methods	Class-2 Modal methods	Class-3 Discontinuous methods	Class-4 Momentum exchange methods	Limit equilibrium, Limit analysis
Contacts	Rigid	---	---	xxx	xxx	xxx
	Deformable	xxx	xxx	---	---	---
Bodies	Rigid	xxx	xxx	xxx	xxx	xxx
	Deformable	xxx	xxx	xxx	---	---
Displacement	Small	xxx	xxx	xxx	---	xxx
	Large	xxx	xxx	xxx	xxx	---
Strain	Small	xxx	xxx	xxx	---	---
	Large	xxx	xxx	xxx	---	---
Bodies	Fewer	xxx	xxx	xxx	xxx	xxx
	Many	xxx	xxx	x	xxx	x
Material	Linear	xxx	xxx	xxx	---	---
	Non-linear	xxx	x	---	---	---
No fracture		xxx	xxx	xxx	---	---
Fracture		x	xxx	---	---	---
Packing	Loose	xxx	xxx	---	xxx	---
	Dense	xxx	x	xxx	x	xxx
Static		xxx	xxx	xxx	---	xxx
Dynamic		xxx	xxx	x	xxx	---
Forces only		---	---	---	---	xxx
Forces and displacement		xxx	xxx	xxx	xxx	---

--- does not allow, or not pplicable. x can model it, but may be insufficient or not well suited.
xxx can model it well.

Table 2-2 suggests that the distinct element methods can allow maximum modelling strengths against the given attributes, and hence, provide a more rigorous scheme to solve the problems in relation to a wide range of materials.

Discontinuous Deformation Analysis (DDA) is an example of implicit DEM which can be obtained by upgrading FEM or FDM, whereas the distinct element method is an example of explicit DEM which yield a macroscopic response of media based on the interaction of discrete bodies (Jing 2003). The term “Distinct Element Methods” is mainly used when DEM is applied in rock mechanics while, in the literature, the term “Discrete Element Methods” (DEM) is used in other areas (Jing 2003). Therefore, hereafter, the broader term “Discrete Element Methods” (DEM) will be used to denote all formulations of DEM that represent an explicit mode of deformation, including “Distinct Element Methods”.

This section focuses on the formulations of DEM that explicitly show deformation in the models irrespective of the particle geometry which is relevant to the present research.

2.3.2 Previous Developments in DEM

Numerous researches have been conducted in the last four decades in the formulations of the DEM and the development of computer codes depending on particle geometry, contact detection schemes and interparticle cement. A summary of DEM developments is given in Table 2-3. These developments are discussed wherever applicable in the following sections.

2.3.3 Formulations

Various formulations of DEM have been documented in the literature (e.g., Jing 2003; Bobet et al. 2009) based on particle geometry (i.e., polygonal blocks, circular discs or spheres, ovals and arbitrary shaped particles by overlapping clusters or clumped particles of spheres). The choice of adopting a particular formulation for a given problem is influenced by factors such as the level of theoretical knowledge of the micromechanics of discrete or granular media, the nature of the application, or the computational resources available.

However, the theoretical understanding of DEM for all shaped particles is based on the formulation and solution of equations of the motion of rigid or deformable particles (Jing 2003). In deformable particles, particles are further discretised into finite elements using FEM or FDM formulations which also give deformation (implicit) of particles in addition to explicit deformation along the particles’ contacts, for example, UDEC (after Cundall 1980).

Table 2-3: Examples of DEM computer codes (updated after Akram & Sharrock 2009).

Date	Author/s	Computer code	Dim.
1978	Cundall (Cundall 1974)	RBM	2D
1978	Cundall (Cundall 1978)	BALL	2D
1979	Cundall and Strack (Cundall & Strack 1979b)	TRUBALL	2D
1985	Cundall-Itasca	UDEC	2D
1985	Bagster and Kirk (Bagster & Kirk 1985)	Model Heap	2D
1986	Corkum (Ting et al. 1989)	DISC	2D
1987	Cundall	PFC2D/PFC3D	2D/3D
1988	Cundall (Cundall 1988)	3DEC	3D
1988	Walton (Walton et al. 1988)	3DSHEAR	3D
1989	Bathurst and Rothenburg (Bathurst & Rothenburg 1989)	GLUE	2D
1989	Williams and Pentland (Williams & Pentland 1989)	Unnamed code	3D
1989	Taylor and Preece (Taylor & Preece 1989)	DMC	2D
1989	Ng (Ng 1989)	CONBALL	2D
1990	Ghaboussi and Barbosa (Ghaboussi 1990)	BLOCKS3D	3D
1991	Ng and Dobry (Ng & Dobry 1991)	CONBALL	3D
1991	Hakuno and Yamamoto (Hakuno & Yamamoto 1991)	Unnamed code	2D
1992	Rothenburg and Bathurst (Rothenburg & Bathurst 1991)	ELLIPSE2D	2D
1992	Mishra and Rajmani (Mishra & Rajmani 1992)	2DMILL	2D
1993	Cleary (Cleary 1993)	Unnamed code	2D
1994	Hill and Zheng (Hill & Zheng 1994)	Granular.f	2D
1995	Donz´e and Magnier	YADE	3D
1996	Muller (Muller 1996)	Discs-Polyhedra	2D
1996	Kovestsky	Unnamed code	3D
1997	Xu and Yu (Xu & YU 1997)	ELLIPSE3D	3D
1997	Lin and Ng (Lin & Ng 1997)	Unnamed code	3D
1997	Hustrulid and Brown (Hustrulid & Brown 1997)	Parallel DEM	2D
1999	Sharrock (Sharrock 2003)	3DFLOW Distributed DEM	3D
2000	CSIRO – Muhlhaus	FASTDISC	2D
2001	ELFIN	Coupled FEM – DEM	3D
2002	CSIRO - Cleary	Parallel code–spheres, discs	3D
2006	ACcESS MNRF	ESYS_Particle	3D
2007	DEM Solutions Ltd.	EDEM	3D
2008	(Weatherley 2009)	ESYS, High performance parallel code - spheres	3D

A changing contact pattern is the main constituent of DEM formulations that differentiate them from continuum methods. A general formulation of DEM is comprised of the following requirements (Jing 2003):

- Distribution of particles within the defined domain (i.e., area in 2D or volume in 3D).
- Assumptions about the particle material, e.g., rigid or deformable.
- Development of algorithms for contact detection scheme, e.g., Penalty function, Lagrange multiplier, or augmented Lagrange multiplier.

- Development of constitutive equations for the particles/ blocks/ fracture system.
- Solution of the integral equations of the motion of the particles.

Generally, these requirements remain almost the same irrespective of particle shape or geometry. The formulations of DEM, based on particle geometry are discussed in the following sections.

2.3.3.1 Polygonal Blocks

In rock mechanics, DEM was pioneered using a two dimensional polygonal rock block system (Cundall 1971) which was then used in the development of computer code RBM (Cundall 1974). The RBM then progressed to SDEM to model the deformation of a complex 2D geometry of blocks. A parallel version (CRACK) was developed incorporating the fracturing, cracking and splitting of intact blocks under loading, based on a tensile failure criterion (Jing 2003). Later in 1980, UDEC (Cundall 1980) was developed which had the capability to overcome the incompatibility caused in the SDEM when dealing with deformable blocks with complex geometries of blocks. UDEC was extended to 3D problems with the development of 3DEC (Cundall 1988; Hart et al. 1988). In the DEM with blocks, it is assumed that the medium is divided into a finite number of blocks by the intersection of the discontinuities (Figure 2-8). The technique of the explicit DEM for a blocky system is presented comprehensively in Cundall and Hart (1992; 1993). Hart (Hart 1993)

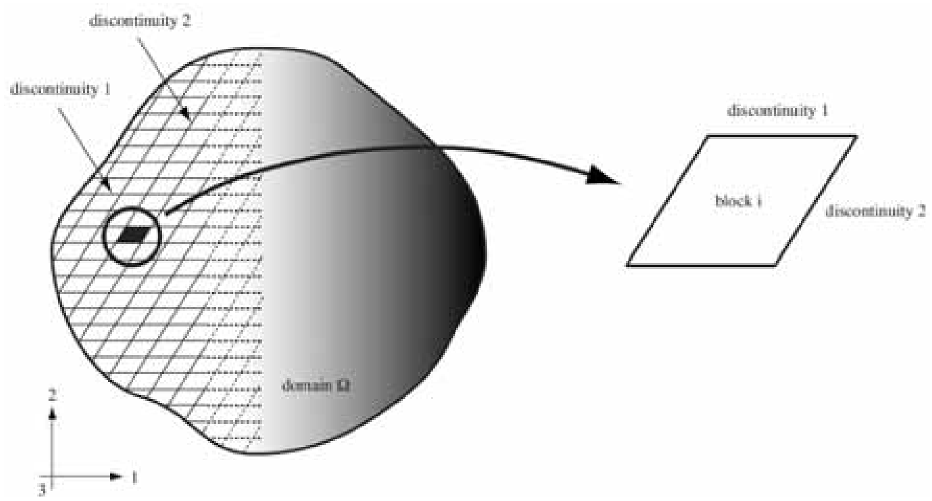

Figure 2-8: A typical discontinuum model with blocks (after Bobet et al. 2009).

The deformation formulation of large scaled blocks was based on the principle of simulating large-scale deformations of elasto-plastic materials using finite difference/volume schemes and dynamic relaxation principles (Jing & Hudson 2002;

Jing 2003), as shown in Figure 2-9. The concept of “contact overlap” provides the basis for contact detection.

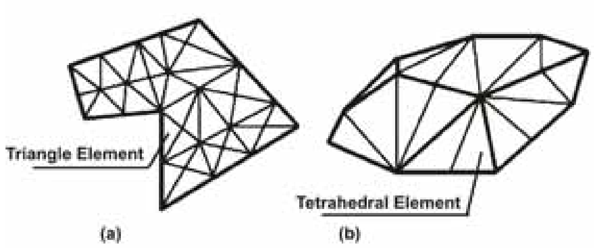

Figure 2-9: Discretization of blocks; a) constant strain triangles in 2D, b) constant strain in tetrahedral in 3D (modified after Jing 2003).

The methods and codes were then extended further to incorporate heat conduction and viscous fluid flow through fractures by establishing interfaces between block boundaries (Jing 2003).

Due to explicit representation of the deformation of the discrete blocks, the method was applied in numerous applications in rock mechanics such as tunnelling, underground excavations, slope stability, reservoir simulations, laboratory testing simulations, rock support design, acoustic emissions in rocks, rock dynamics and the stability of well and borehole (Jing & Hudson 2002; Jing 2003; Bobet et al. 2009).

Despite the above mentioned attraction of DEM with blocks and its application in the rock engineering discipline, it has limited applications in the field of rock mechanics especially in granular rocks and in soft rocks where deformation along the fractures is not as significant when compared to deformation through the rock mass. On the other hand, simulation of hard rocks with fractures is constrained by limited data of the in situ fracture distribution. In most cases, an estimation of fracture frequency and distribution is undertaken by boreholes or mapping which can not portray the exact picture of the in situ fracture distribution and their persistence in three dimensions, hence the reliability of the simulation depends highly on the accuracy of the available data.

2.3.3.2 Circular Discs and Spherical Particles

DEM was implemented on circular discs in the late 1970s with the development of the computer program “Ball” (Cundall 1978; Cundall & Strack 1978; 1979b). Looking into its potential to model many features comparable to physical granular material, the method was applied to model natural granular materials, that is, soils (Cundall & Strack 1979a). Initial work concentrated on granular assemblies of circular discs in 2D and spheres in 3D. The key motivation for circular discs and spheres was fast contact detection, which increases the number of particles that can be simulated in a reasonable time.

Subsequently, this method was applied to many problems across a range of scientific disciplines. Key relevant applications include the fundamental investigation and application in cohesive and frictional granular soils and powders; rock mechanics; the experimental validation of DEM; modelling different shapes of granules; developing improved contact models; in coupled modelling methods; incorporating smooth joints to simulate discontinuities at laboratory and large scale, and industrial applications of DEM (Sallam et al. 2004; Potyondy 2008).

In DEM with circular or spherical particles, the medium can be represented by the assembly of circular discs (2D) or spheres (3D) with a set of micro mechanical properties that specifies the contact and bond conditions. The simplified form of a domain consisting of circular discs and the definition of micro parameters are shown in Figure 2-10.

The frictional materials can be simulated by grouping circular discs and spheres with micro mechanical parameters, that is, contact normal stiffness (k_n), contact shear stiffness (k_s) and friction (μ) along the particle contacts. The macroscopic response of the granular assemblies is governed by the interaction of circular or spherical particles.

Similarly, the cohesive- frictional materials can be simulated by gluing the particles together with a definite set of normal and shear bond strengths (σ_b, τ_b) at particles contacts in addition to contact stiffness (k_n, k_s) and interparticle friction (μ). Different constitutive laws have been proposed for the interaction between particles. The typical computer codes being increasingly applied to model circular discs in 2D and spheres in 3D are Particle flow Codes (PFC2D & PFC3D) (Itasca 1987; 2004; 2005), ESYS-Particle (ACcESS MNRF) and EDEM (DEM Solutions Ltd.).

Among the DEM computer codes, PFC is an increasingly applied and documented code used to solve problems across various disciplines (Konietzky 2002; Shimizu et al. 2004). A detailed description of the PFC formulation is provided in the following sections.

The idea of modelling geomaterials as a collection of discrete circular or spherical particles initially introduced by Cundall and Strack (1979a; 1979b), was extended and implemented in PFC (Potyondy & Cundall 2004) using a Bonded Particle Model (BPM). In a BPM, the rocks can be approximated by an agglomerate of cemented particles (Figure 2-10a). The particles are assumed to be rigid with circular (2D) or spherical (3D) shape with a non-uniform particle size distribution. The particles interact with each other through their contacts so that deformation is produced at the particle contacts or by relative displacements between particles (Figure 2-10b).

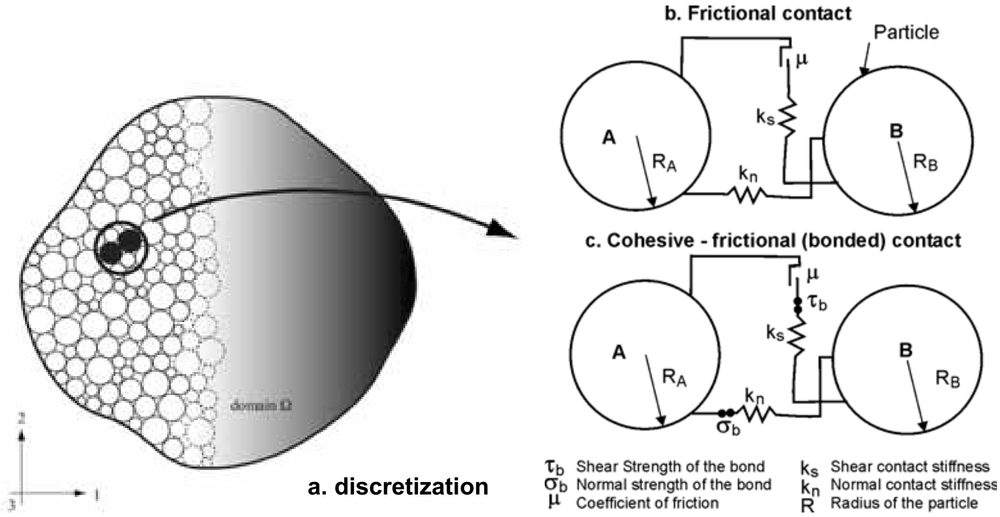

Figure 2-10: a) Representation of a medium with circular discs, b) representation of micro mechanical parameters at frictional contact, c) for cohesive-frictional contact of two circular discs (modified after Bobet et al. 2009).

The main advantage of using circular or spherical particles in the modelling of geomaterials is that the computational speed and efficiency of ordinary personal computers is sufficient as the contact detection scheme is computationally straightforward. However, a key limitation of discs and spheres is to obtain the interlocking effect of the polygonal particles which can allow excessive rotation of particles (Potyondy & Cundall 2004).

2.3.3.3 Elliptical or Ellipsoidal Particles

As discussed above, the use of circular or spherical particles allows excessive rotation of particles mainly due to the particles' geometry and the point friction at their contacts. As a result, the true peak strength and the angle of internal friction of the assembly can not be achieved. In order to eliminate or minimise this rotation, elliptical and ellipsoidal particles were modelled in DEM formulations. Using this philosophy, numerous studies were conducted using elliptical particles in two dimensions e.g. (e.g., Rothenburg & Bathurst 1991; Ting 1991; Wei et al. 1991; Pradhan & Swada 1992; Rothenburg & Bathurst 1992; Ting & Corkum 1992; Ting 1993; Ting et al. 1993; Ng & Lin 1993a; 1993b; Ng 1994; Swada & Pradhan 1994). A conceptual nomenclature of elliptical particle and granular assembly is shown in Figure 2-11. In three dimensions, ellipsoidal elements were also utilised to investigate the mechanics of granular materials (e.g., Lin & Ng 1995; Lin & Ng 1997).

The studies using elliptical or ellipsoidal particles concluded that although elliptical particles show a relatively small tendency to rotate (when compared to discs or spheres), even then particle interlocking and angularity-induced dilation can not be gained using elliptical particles, which is a characteristic feature of natural granular materials with non-spherical particles.

2.3.3.4 Polygonal Particles

In order to obtain the interlocking of natural granular materials, polygonal shaped particles were also studied to simulate the complexities of natural granular materials in both soils and rocks. Particles of arbitrary shapes were constructed joining circular or spherical particles (Potapov & Campbell 1998; Favier et al. 1999; Jensen et al. 1999; Thomas & Bray 1999; Matsushima & Konagai 2001; O' Sullivan & Bray 2002; Ashmawy et al. 2003; Matsushima 2004; Nakata et al. 2004; Sallam et al. 2004). A recent formulation “Clump Logic”, similar to overlapping clusters, has been proposed in PFC (Itasca 2004; 2005) to model rocks or granular materials to get true interlocking of the particles and consequently high bulk friction of the assembly (Fu 2005; Cho et al. 2007; 2008). In the clumped model rotation of individual particles is restricted, as the rotation of the clumped particle is low as compared to the rotation of individual circular or spherical particles (Figure 2-12a & b).

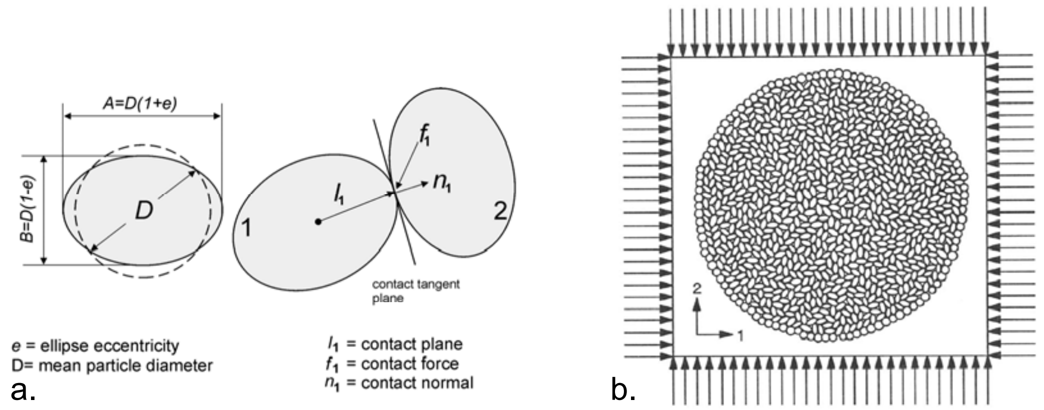

Figure 2-11: a) Nomenclature of elliptical particles, b) isotropic assembly of elliptical particles with particle eccentricity =0.30 (modified after Rothenburg & Bathurst 1992).

These studies showed that macroscopic properties (i.e. peak strength and angle of friction) are greatly influenced by particle shape, and the assemblies with polygonal or angular particles can simulate much higher strength and friction compared to assemblies with circular or spherical particles. However, polygonal or polyhedral particles (Sallam et al. 2004) have complexities, such as the generation of angularity, complex contact detection schemes (along nodes and surfaces), and increased computational cost.

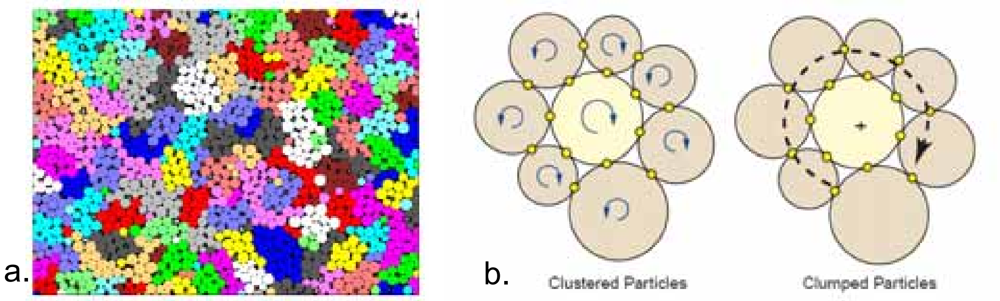

Figure 2-12: a) Clustered particle assembly, obtained by gluing circular particles to produce polygonal particles, b) Particle rotation mechanisms in clustered and clumped particles (after Cho et al. 2007).

2.3.4 DEM Simulation for Granular Materials

Simulating the mechanical behaviour of the granular materials is an important application area of the DEM. Following the early application of DEM to granular materials in the late 1970s (e.g., Cundall 1978; Cundall & Strack 1978; 1979a; 1979b), various studies were conducted to simulate the behaviour of natural granular materials by using different shaped particles (i.e., circular, elliptical, irregular and polygonal). Initially, the behaviour of frictional granular material was studied extensively and then DEM was extended to cohesive-frictional materials by incorporating interparticle bonds of specific strengths. Therefore, DEM's area of application is mainly comprised of two classes; first for "frictional materials" (i.e. granular assemblies having no interparticle bonds which comprise natural materials like sands, gravels, assemblies of steel balls or glass beads), second for "cohesive-frictional materials" which are simulated by gluing the particles with specific cementing materials so that the failure is always allowed to occur through the cementing material (i.e. along the contacts) and not through the particles, assuming the particles are rigid or deformable bodies. The class of cohesive-frictional granular materials is comprised of natural materials such as cohesive soils, granular rocks and concrete, artificially cemented assemblies (synthetic materials) of irregularly shaped particles, like sands, gravels etc., and uniformly shaped particles, like glass beads, steel balls, circular discs etc. Conglomerates are rocks consisting of discrete clasts bonded together with a cement matrix, and hence are also categorised as cohesive-frictional materials.

Besides cohesive-frictional materials, DEM's application to simulate crystalline rocks/ materials using a Bonded Particle Model (BPM) after Potyondy and Cundall (2004) or Clumped Particle Model (CPM) after Cho et al. (2007) is also a form of cohesive-frictional materials such that the interparticle bonds specify the strength of cementing material.

2.3.4.1 Particle Flow Code (PFC)

Particle Flow Code (PFC) from the Itasca consulting group is a well known DEM computer code which has been used extensively across various disciplines (Konietzky 2002; Shimizu et al. 2004) for over two decades. PFC is available for 2D and 3D simulation. The formulation of the method is explained by Cundall (1988) and Hart et al. (1988) and can also be found in PFC manuals (Itasca 1987; 2004; 2005). PFC is based on the simplified implementation of DEM that allows finite displacements and rotations of discrete rigid bodies (Cundall & Hart 1992). It also includes complete detachment and automatic detection of new contacts of the particles with the progress of calculations.

In PFC, the interaction of the particles is treated as a dynamic process with states of equilibrium developing whenever the internal forces balance. The contact forces and displacements of the particle assembly are traced by the movement of the individual particles. Movements of the particles result from the propagation of disturbances due to wall and particle motion, externally applied forces and body forces (Potyondy & Cundall 2004). This is a dynamic process in which the speed of propagation depends on the physical properties of the discrete particle system. The calculations in the PFC alternate between the application of Newton's second law (for the particles) and a force–displacement law (for the contacts). Newton's second law determines the translational and rotational motion of each particle resulting from the contact/ applied/ body forces acting on it, while the force–displacement law updates the contact forces resulting from the relative motion at each contact (Figure 2-13).

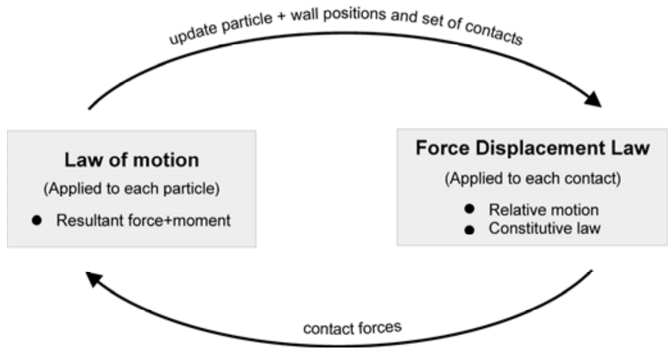

Figure 2-13: Calculation cycle in PFC3D (after Itasca 2005).

This dynamic behaviour is represented numerically by a time-stepping algorithm in which the velocities and accelerations are assumed to be constant within each time step. Each time step is so small that, during a single time step, disturbances cannot propagate from any particle further away than its immediate neighbours. Then, at all times, the forces acting on any particle are determined exclusively by its interaction with the particles with which it is in contact. As the propagation of a disturbance is the function of physical properties of the discrete system (namely, the distribution of mass and stiffness), the time step can be chosen to satisfy the above constraint.

- **Simulation of Frictional Granular Materials**

In the simulation of the frictional materials, the contact properties of the particles are specified, that is, normal and shear contact stiffnesses and interparticle contact friction. The stiffness can be linear, assuming particles as either rigid bodies or as the Hertz-Mindlin (Mindlin 1949; Mindlin & Deresiewicz 1953) treating the particles as elastic bodies. In the simulation of frictional assemblies, it is preferable to use Hertzian contact theory to define interparticle contacts (Itasca 2004; 2005). Besides the linear and Hertz-Mindlin contact theory, some user defined contact models can also be implemented in PFC.

- **Simulation of Cohesive-Frictional Granular Materials**

In the simulation of the cohesive-frictional materials, particles are cemented together with bonds at particle contacts. There are two types of bonding models; the “contact bond” and the “parallel bond”. The contact bond behaves like a point of cementing material between two particles and is defined by normal and shear strengths only. The other bonding model is the parallel bond model that is specified by normal and shear strengths and stiffnesses alongwith its extent. The “parallel bond” acts like a cementing material (Figure 2-14) between the two particles that can transmit forces and moments among the particles compared to contact bond model which can only transmit forces. The properties of the bonding models are specified in addition to the contact model’s properties so that after the breakage of the bonds, forces on the particles can be specified by the contact models.

A detailed discussion of the contact models, bonding models, particle-particle and particle-cement behaviours and associated parameters and simulation assumptions in PFC is provided in Chapter 4.

- **Calibration Process - Inverse Modelling Approach**

In PFC, for the simulation of granular frictional and cohesive-frictional materials, micro parameters are estimated to match the macroscopic behaviour with that of the actual physical materials. For this purpose, numerical tests, including uniaxial, triaxial and Brazilian tensile tests are conducted in PFC simulating the actual laboratory testing. During testing, the PFC’s input parameters are varied until the behaviour of the numerical sample matches that of the physical sample. The corresponding parameters may then be used in a PFC2D or PFC3D simulation of a larger problem containing the same solid material as the sample. This approach has been named inverse modelling approach which includes the following steps (Itasca 1987; 2004; 2005):

1. First, the matching of Young's modulus is achieved by setting material strengths to a large value and varying the stiffness of the contacts and bonds. Then Poisson's ratio is calibrated by varying the ratio of normal to shear contact and bond stiffness ratio.
2. After obtaining the desired elastic response, peak strength in uniaxial testing is matched by varying the strengths (both normal and shear) of the bonds.
3. Post-peak behaviour is matched by varying the interparticle friction.
4. A complete strength envelope is obtained by performing a set of triaxial tests at different confinements and Brazilian tensile strength test.

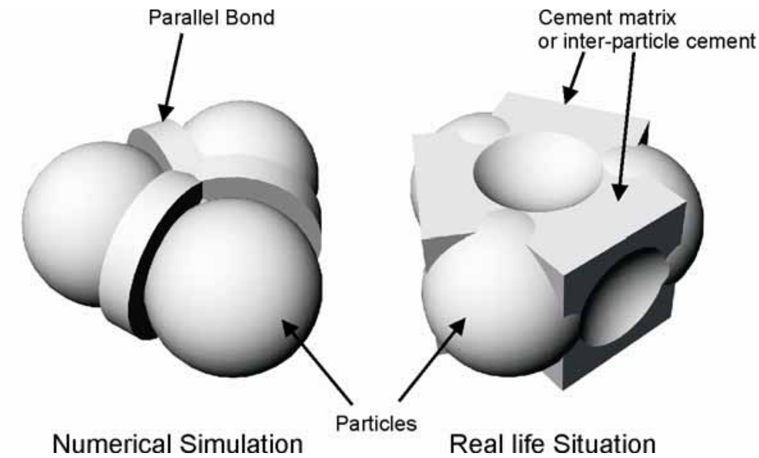

Figure 2-14: Conceptual illustration of: a) parallel bond, b) real life situation represented by parallel bond.

A detailed description of the calibration process by the inverse modelling approach can be found elsewhere (e.g., Itasca 2004; Potyondy & Cundall 2004; Itasca 2005).

This procedure is somewhat based on a "hit-and-miss," approach and includes test iterations to obtain a similar macroscopic response of the numerical assembly in terms of peak strength, Young's modulus, tensile strength, cohesion and bulk friction. Once a reasonable calibration in the assembly response is achieved against a set of micro parameters, these parameters can be used for subsequent large scale modelling. Following the inverse modelling approach, numerous studies have been conducted in the field of rock mechanics and geotechnical engineering (e.g., Konietzky 2002; Shimizu et al. 2004). However, it has been observed that in both PFC2D and PFC3D, 100% calibration can not be achieved using circular or spherical particles (Potyondy & Cundall 2004; Cho et al. 2007) especially the angle of friction of the assembly (bulk friction) over certain values. In addition, tensile strength in the simulation of Brazilian tensile strength is often over-estimated during the calibration process (e.g., Sharrock et al. 2009).

2.3.5 Previous Studies on DEM Simulation for Granular Materials

Previous studies involving DEM for the simulation of granular materials can be broadly classified into frictional materials, that is, unconsolidated materials and cohesive-frictional materials, that is, assembly of cemented particles or granules. These studies are quite relevant to the present research as a conglomerate is a granular rock having clasts cemented with matrix. The research conducted in both areas is discussed in the next two sections and a summary of these studies is provided in Table 2-4.

Table 2-4: Summary of studies conducted previously involving DEM's application and validation using various types of physical materials (after Akram & Sharrock 2009).

Physical material	Material type	Previous studies
Frictional material	Natural (i.e., sands, gravels etc.)	(Sitharam 1999; Sallam et al. 2004; Fu 2005)
	Artificial (i.e., using circular, spherical, angular particles etc.)	(Cundall & Strack 1979b; Strack & Cundall 1979; O' Sullivan & Bray 2002; O' Sullivan et al. 2004; Holt et al. 2005)
Cohesive-frictional materials	Natural (i.e., rocks, cohesive soils	(Tomiczek 2002; Wanne 2002; Potyondy & Cundall 2004; Gil et al. 2005)
	Synthetic/ artificially cemented (i.e., particles joined with cementing materials)	(Holt 2001; Kulatilake et al. 2001b; Holt et al. 2005)

2.3.5.1 Frictional Materials

The studies conducted involving DEM for frictional materials were mainly focused on two objectives:

1. To simulate and understand the behaviour of frictional assemblies using DEM, and
2. To validate the behaviour of the DEM simulation for frictional materials.

However, later on this scope was expanded to various horizons such as the simulation of cohesive frictional material, natural heterogeneous and discontinuous materials, that is, natural rocks and rock masses, understanding of the micromechanics of geologic materials, formulation of various constitutive relations based on various assumptions and similitude. This area is still under development and continuing research is being conducted.

The pioneering validation of DEM was conducted by Strack and Cundall (1979) comparing the stress-strain behaviour of DEM simulation with that of physical experiments on frictional materials. Later, Cundall and Strack (1979a) compared the stress-strain behaviour of a numerical simulation by using computer code “Ball” with the corresponding response of 400 metal cylinders, normally loaded in a frame (Oda & Konishi 1974). Both the numerical and physical responses showed a reasonable correspondence with some minor differences. These differences were considered to be due to errors in the estimation of assumed parameters including density, friction between particles and walls, and contact stiffness, which were unknown in physical tests at that time.

Similarly, further attempts were made to validate DEM using a 16 disc static test and 1000 disc test with varying diameters (Sitharam 1999). The DEM simulations were compared with experimental work on uniform sand for stress-strain plots at various confining pressures of both models, an increase in load carrying capacity and the compressibility of the assembly with confining pressure. Numerical biaxial and hydrostatic tests were conducted on an assembly of 1000 particles and results were compared with the published results of sand (Hakuno & Tarumi 1988). A good qualitative correspondence was noted in DEM simulations and experimental investigations on sand.

To account for the effect of particle shape in granular materials, an assembly of chrome balls was tested physically in shear box and triaxial testing (O' Sullivan & Bray 2002; O' Sullivan et al. 2004). The DEM simulations for the triaxial test were performed by using spherical particles and overlapping sphere clusters based on Fourier shape analysis techniques. The stress ratios (major to minor and intermediate to minor) were plotted against the axial strain for physical tests on spheres, DEM simulations on spheres and overlapping clusters. Physical and numerical simulations for spheres showed good correspondence in minor to major principal ratio plots while in the intermediate to major principal ratio plots, physical tests yielded slightly higher values than numerical tests. The overlapping sphere clusters exhibited significantly higher values in major and minor principal stress ratios with a stiffer response than the sphere responses (O' Sullivan & Bray 2002). DEM simulations were also conducted for a shear box test in comparison with physical shear box tests. Physical tests were undertaken on ~1.0 mm diameter steel balls under 54.5, 109 and 163.5 KPa normal load. DEM simulations were performed using known elastic parameters and the known friction of the steel balls following the physical test conditions. The numerical test results exhibited differences in responses in comparison to physical test, that is, a stiffer response, stress dependency, no compression prior to dilation and an underestimation of overall assembly friction.

An experimental validation of PFC2D was conducted in tracking translations and rotations of angular grains of Fraser river sand as a result of external disturbances in a simple test (Sallam et al. 2004). The wooden pieces were produced in the shapes of sand particles to scale up the model. In PFC2D, angular particles were created using Overlapping Rigid Clusters (ORC) (Ashmawy et al. 2003) to replicate the sand particles. The results of numerical simulations were observed to fall within the variation range of the physical tests and hence were considered reasonable.

Another PFC3D validation study examining wave propagation and the distribution of stress around the hole in sand material (representing the borehole in cohesive material) was undertaken by Narayanasamy (2004). The medium was artificially cemented (using rounded grains) sand, named “Hickory sand”. The micro mechanical properties were estimated by inverse modelling. Both the numerical simulation and experimental results showed almost identical particle displacements and rotations at small displacement, while large differences were noted at high displacement.

Recently, further work was carried out in this area by Holt et al. (2005) who argued that numerical modelling can be used as a virtual laboratory that is essentially identical to the physical laboratory. In order to implement this hypothesis, several tests were conducted on unconsolidated granular assemblies in a physical laboratory under controlled conditions and corresponding simulations were produced in PFC3D. The physical models were comprised of glass beads to represent a frictional assembly. Stress dependent wave velocities were computed in the frictional assembly of glass beads in which particle contact stiffness was kept non-linear using the Hertzian contact model (Mindlin 1949). PFC simulations reproduced the same response without the use of any fitting parameters.

Fu (2005) has conducted a study by undertaking shear and compressions tests on rock crush and simulated the same in PFC3D by modelling the spherical and polygonal particles. The microstructures of the rock crush particles were acquired by x-ray tomography imaging technique and employed in the simulations. The results showed that polygonal particles induced higher friction and dilation angles, and similarly, higher shear and compressive strengths, comparable to experimental results, than with spherical particles.

In summary, DEM simulations have been carried out to investigate and validate the response of frictional materials by using circular, spherical, elliptical, ellipsoidal and polygonal particles. These studies showed a reasonable achievement in understanding and modelling the mechanics of frictional materials. DEM simulation using circular or spherical particles showed less bulk friction owing to the excessive rotation of particles in the absence of interlocking, which is a characteristic feature of natural frictional materials. Using elliptical or ellipsoidal particles can produce a degree of interlocking and limit the rotation of particles, but still the bulk friction is less than that of physical materials. Polygonal particles, however, can yield high bulk friction providing interlocking at particle-particle contacts comparable to the micro structure of natural materials. However, the real challenge in simulation with polygonal particles is the complex contact detection scheme which results in a very high computation cost on a normal personal computer. In addition, to obtain the true angularity of natural grains is not possible as every grain is different in natural material and this affects the force chain or fibre.

2.3.5.2 Cohesive-Frictional Materials

In contrast to DEM's application on frictional materials, less work has been reported in literature with DEM's application and validation for cohesive-frictional materials. After the early DEM simulation for granular media (e.g., Cundall & Strack 1979a), the researchers started looking into the cohesive-frictional materials using DEM. Like frictional materials, again the initial objectives in the DEM's simulation of cohesive-frictional materials were to understand, investigate and validate the behaviour of cohesive-frictional materials with that of the numerical simulation. Later this work was extended to cohesive solids, concrete and natural rocks, and across various disciplines.

In the early eighties, initial theoretical understanding about the normal (Hertz 1882) or oblique (Mindlin 1949) deformation of elastic grains was used to investigate the particle assembly cemented at small areas (Digby 1981). This work led the researchers towards the low and high strain deformations, including sliding along the grains.

Afterwards, in the early nineties, many researchers focused on the effect of the cementation on the elastic and inelastic behaviour of the granular solids. For example, Bruno and Nelson (1991) used a discrete element formulation in 2D to look into the rock failure in tension, uniaxial compression and biaxial loading. Contact stiffness was assumed to be a linear function of the Young's and shear modulii of the cement, and the thickness and width of cementation bonds in the elastic domain.

An experimental study was conducted using synthetic cemented granular materials (Ottawa sand with halite and silica glass cement) in triaxial compression tests

(Bernabe et al. 1992). It was observed that a small amount of cement can significantly increase the strength of granular material if it is precisely deposited at previously formed grain-to-grain contacts.

Numerically, the behaviour of cemented granular materials was studied under low- and high-strain loads using circular particles glued together with elastic bonds (Trent 1989; Trent & Margolin 1992). The results showed that the macroscopic properties of the granular solids are governed by the properties and distribution of individual intergranular bonds or the cementing material.

Dvorkin et al. (1991) examined the normal interaction of two spherical elastic grains and an elastic cementation layer between them for two and three dimensional cases. The results showed that a thin cement layer subject to normal and shear load can be approximately treated as an elastic strip. By this approximation, the problem of grain-cement deformation (where the grains are deformable) was reduced to an ordinary integral equation for the normal stresses at the cemented interface, assuming the deformable grains and the width of the cemented zone was smaller when compared to the grain radius. It was noted that the elastic response of the cemented system increased with the radius and stiffness of the cement layer. The contribution of the increase in the cement layer radius significantly increases the macroscopic stiffness of the bonded assembly. Further, the response of a numerical model comprising random identical spheres bonded with thin layers of cementing material, as in Dvorkin et al. (1991), was investigated for compressional-wave velocity measurements (Dvorkin et al. 1994). The wave velocities were compared for varying amounts of cement along the particle contacts (Figure 2-15). The results were compared to experimental results of compressional-wave velocities determined on 0.4~0.5mm identical glass beads glued together with epoxy. The experimental results were within the numerically predicted results range obtained using two theoretical arrangements.

Holt (2001) conducted a study to address the main discrepancies associated with laboratory measured and in situ virgin compaction using synthetic sandstone and PFC2D and PFC3D modelling. Synthetic sandstone samples were created under stress with an injection of CO_2 in the solution of sand and sodium silicate contained in the triaxial cell to replicate the in situ virgin compaction and to produce a stress released core by the removal of the sample from its container. The samples were tested in uniaxial compression for in situ virgin compaction and stress released core conditions. Acoustic emissions were monitored for numerical and synthetic sandstones. The numerical test results showed good agreement in the stress-strain response with that of physical tests, but with a deviation in microseismic activity.

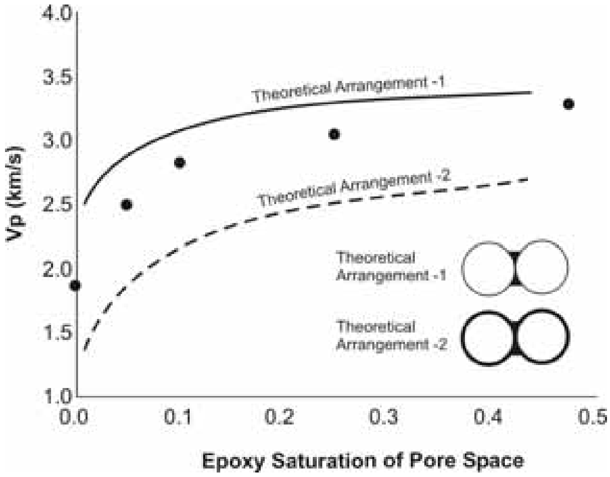

Figure 2-15: Compressional wave velocity (Vp) measured in epoxy-cemented glass beads at varying cement at hydrostatic confining pressure of 30 MPa. The experimental data (dots) lies within lower and upper bound theoretical predictions (modified after Dvorkin et al. 1994).

Kulatilake et al. (2001b) created jointed blocks from a mixture of plaster, sand and water and investigated their response under uniaxial loading. Numerical simulations were conducted in PFC3D incorporating joints in cylindrical samples. The intact material's micro properties were adopted by the inverse modelling approach comparing the macroscopic responses of numerical and physical samples. The numerical simulations were found to be consistent with the findings of laboratory testing in categorising the failure modes against same joint geometry configurations.

Another calibration study using PFC3D was conducted by examining the wave propagation and distribution of stress around the hole in sand material (representing the borehole in cohesive material) (Narayanasamy 2004). The medium was artificially cemented (round grained) sand named "Hickory sand". The micro mechanical properties were estimated by inverse modelling. Both the numerical simulation and experimental results showed almost identical particle displacements and rotations at small displacement, while large differences were noted at high displacement.

PFC3D was used to study the behaviour of Antler Sandstone by selecting the micromechanical properties by the inverse modelling approach (Gil et al. 2005). Young's modulus and Poisson's ratio of numerical simulations and published results (Wang et al. 1995) were found in reasonable agreement. The adopted micro parameters (normal and shear strength and stiffness of cementing material) were validated with the peak strengths and elastic modulus of constituting minerals. The parameters were found to lie within the variation range of mineral properties.

In the DEM validation area, further work was carried out in an effort to use numerical modelling as a virtual laboratory essentially identical to the physical laboratory (Holt et al. 2005). In order to implement this hypothesis, several tests were conducted on unconsolidated and cemented granular assemblies in a physical laboratory under controlled conditions and corresponding simulations were produced in PFC3D. Rock-like material was created by gluing the glass beads with epoxy for UCS and a core scratch test. In the assembly, particle contact stiffness were kept non-linear using the Hertzian contact model (Mindlin 1949). The experimentally observed increase in peak strength and Young's modulus (E) during UCS tests were reproduced in PFC simulations. In order to measure interparticle bond strength, core scratch tests were undertaken on cemented glass beads. The test results exhibited similar force distributions, as resulting from the events when material was released from the specimen. The estimation of the bond breakage force was made by counting the number of released particles in each event. The analysis showed higher force estimation than that simulated in PFC.

Cho et al. (2008) conducted a series of direct shear laboratory tests using a synthetic brittle rock to investigate shear zones. The numerical simulations were conducted using clumped particles in PFC2D. The results showed a reasonable correlation between the laboratory and PFC simulations, even at different stress paths.

The review of studies on the behaviour of cohesive-frictional materials has revealed DEM's capability to reproduce many features of the granular solids and rocks. No effort as such was made to model the behaviour of conglomerates using DEM simulation. However, studies for simulation of fine grained rocks, that is, granite, sandstone etc., highlight DEM's potential for coarse grained rocks, such as conglomerates. The simulation of clast supported conglomerates can be conducted in DEM by gluing the discrete particles with bonds such that DEM's discrete particles represent the conglomeratic clasts, while interparticle bonds represent the cement matrix.

2.3.6 Micro to Macro Mechanics

In the micro to macro mechanics of cohesive-frictional materials, various theoretical formulations have been developed to depict the macroscopic response of the granular solids based on the interaction of the properties of the particles and the interparticle cement. Two types of approaches have been followed to derive the macroscopic response of granular solids or cohesive frictional materials. Firstly, there are homogenization theories in which strength and elastic properties have been extensively studied within the frame work of composite mechanics. These theories were historically developed for a matrix-inclusion system and have been applied to porous media by considering voids as inclusions in a solid matrix. However, the application of homogenization theories has been found inadequate for a densely packed granular material (Chang et al. 1999).

The second approach based on micromechanics was used to derive the elastic response of granular materials based on the behaviour of two particles in direct contact. In this area, work has been done by Digby (1981) for porous rock and by Walton (1987), Chang et al. (1989), and Cambou et al. (1995) for the modulii of granular media that consist of unbounded particles.

On the particle side, mainly theories of the elastic interparticle deformation (e.g., Mindlin 1949; Mindlin & Deresiewicz 1953) or those considering particles as rigid bodies (distinct element methods) and the contact laws for frictional granular materials have been extended towards cohesive-frictional materials. In numerical simulation of the cohesive-frictional materials, most existing DEM formulations incorporate a piece of cementing material between the two particles which is called a bond or a bonding model. This bond glues together the particles and transfer forces and moments across the particles. In DEM, various bonding models have been implemented to obtain a representative cohesive-frictional material, such as rocks, concrete, granular solids, etc.

For example, Chang et al. (1999) formulated mathematical relations to establish the elastic modulus of a granular solids for two phase materials comprising solids, (assuming the particles and binder or interparticle cement have the same properties) and voids, and three phase materials comprising particles, binder and voids. They proposed a particle and binder (cementing material) model in which particles were considered elastic, following theories of the elastic deformation of particles (e.g., Mindlin 1949; Mindlin & Deresiewicz 1953) and incorporating a layer of elastic cement (termed as a binder) of specific thickness (h) and radius (a). The model parameters include the stiffness of particles and the binder, particle size, the binder thickness and width (Figure 2-16), assembly coordination number, the binder content and porosity.

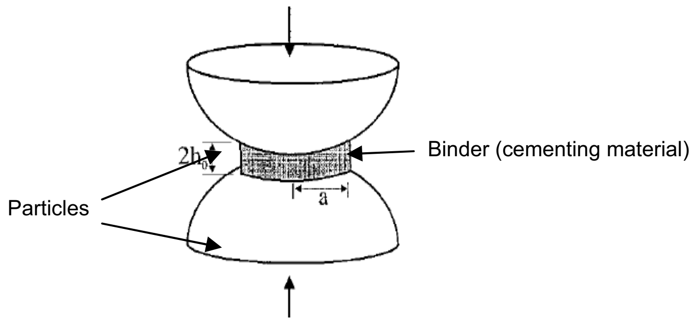

Figure 2-16: Schematic diagram of a particle-binder micro model (after Chang et al. 1999).

According to their proposed relations for determining the elastic and shear modulii, both modulii were determined for a concrete having an aggregate and binder (Portland cement). The results showed a reasonable correlation of the modulii with that of the experimental experience. However, interplay of interparticle friction and the effect of interface properties were not determined.

Jiang et al. (2006) investigated the effect of bond rolling resistance by incorporating surface resistance in the bond model, not only on the interparticle contacts but also on the surfaces. Using the developed DEM computer code (NS2D), a total of 86 (at constant stress ratio) biaxial compression tests were conducted on the bonded granular samples with different densities, bonding strengths and rolling resistances. The numerical test results indicated, firstly, a larger internal friction angle, a larger yielding stress, more brittle behaviour and a larger final broken contact ratio than the original bond model. Secondly, the yielding stress increases nonlinearly by increasing the area of rolling resistance. Thirdly, the first-yield curve (initiation of bond breakage), which defines a zone of no bond breakage and whose shape and size are affected by the material's density, was amplified by the bond rolling resistance and is analogous to that predicted by the original bond model.

2.3.7 Limitations

The Discrete Element Methods (DEM) is an approach of numerical simulation where the macroscopic behaviour of a particle assembly is computed from the individual motions and mutual interactions of the particles. It has been applied in situations where state-of-the-art theoretical knowledge has not yet provided complete understanding and mathematical equations to model the physical systems, such as the mechanics of natural granular materials and rock masses (Ferrez 2001).

Since our understanding about the complex and heterogeneous nature of these materials is incomplete, DEM is considered a very good aid to simulate, understand and investigate the factors and mechanisms controlling the mechanical behaviour of such materials including conglomerates. Nevertheless, DEM simulation is always based on assumptions that limit the accuracy of the model outputs. Among the various assumptions, are those commonly made regarding the geometry and material type of the particles.

DEM with circular or spherical particles is the most common and frequently applied simulation technique for rocks or granular materials because of the attractive computational cost. In contrast, polygonal particles take much longer to simulate, even in laboratory scale models with a limited number of particles. Such large-scale simulations are even more computationally demanding along with memory, online storage, pre and post-processing, etc. (Ferrez 2001).

The particle material is treated as rigid and deformation is allowed to occur at the interparticle contacts. In crystalline and hard rocks, this assumption has produced similar behaviour if there are a reasonable amount of contacts, that is, if large number of particles is used in comparison to sample dimension (e.g., Potyondy & Cundall 2004). In this scenario, deformation along the contacts can result in a reasonable behavioural similarity as per natural rock. This assumption also holds for the simulation of real granular materials with very weak cementing materials (compared to particle materials) in which deformation always occurs through the cement or cement-particle interface.

However, for granular solids with more or less the same strength and elastic characteristics of particles and cement, the net mechanical response of the system will be contributed by the characteristics of both particles and cement. Hence, the use of rigid particles with a linear contact model will result in the response of such materials being misleading. This problem can be resolved by implementing Hertzian contact models (Mindlin 1949) where particles contacts are treated as elastic bodies and can only undergo elastic deformation. Nevertheless, simulation of particle breakage or its plastic deformation cannot be achieved using this contact model.

Other techniques, exist, such as the use of arbitrary shaped particles (super particles) obtained by joining the spheres together with bonds of definite strength. The super particles are then joined with certain cementing materials so that if the forces acting on a super particle exceed the strength of the bonds joining the spheres, the particle will break into spheres, consequently simulating a particle crushing phenomenon. However, the use of a super particle in a model is not practical for large models in view of the high computation cost.

Further, as pointed out by Koyama and Jing (2007) in DEM even with circular or spherical particles, the selection of micro mechanical parameters, model dimensions for the calibration process and particle size and size distributions are the basic constraints for rigorous use of DEM in rock mechanics. Some recent studies have been conducted to overcome these problems especially using the statistical approach to determine a set of mechanical parameters and a representative volume of the model with suitable particle size and size distribution (e.g., Koyama & Jing 2007; Esmaieli et al. 2009; 2010). These studies, although helped in achieving a model representative of a rock or rock mass (by incorporating joints) based on representative elementary volume (REV) that estimates the relative effect of model dimensions, particle size and size distribution, the relation of DEM's parameters with that of real life physical models still remains a challenge that limits DEM's successful and rigorous use in predicting the response of natural materials whose mechanics is not well-understood such as conglomerates. Therefore, DEM requires a careful calibration and validation with real experiments to better understand and overcome its limitations.

2.3.8 Calibration and Validation

In DEM's field of applications, calibration and validation are two separate terms often confused with each other. Validation refers to the macroscopic behaviour of simulation, which is similar to physical systems having a similar microstructure. Calibration is purely a mechanical macroscopic response, which can be gained from a simulation, such as that of a physical system that may or may not have the same microstructure.

In the calibration area, concrete, crystalline rocks or brittle materials can be modelled using DEM with the inverse modelling approach. The Bonded Particle Model (BPM) (after Potyondy & Cundall 2004) or Clumped Particle Model (CPM) (after Cho et al. 2007) are typical examples. The net behaviour is the interplay of micro mechanical parameters, which are normally assumed or estimated rather than measured. It has been observed that by using the inverse modelling approach, a similar mechanical response of a model can be gained with more than one combination of various micro parameters. Hence, there is a possibility that these estimated mechanical parameters can give a good calibration of a specific material in a particular loading and boundary conditions, but may or may not reproduce the response of that material when the loading conditions are changed.

For example, the calibration of peak strength and elastic modulus in uniaxial testing does not mean that the simulation is calibrated with that of the physical material. Over estimation of the tensile strength in the Brazilian test and underestimation of the angle of friction in uniaxial and triaxial testing are inherent problems observed by many authors (e.g., Potyondy & Cundall 2004; Cho et al. 2007; Sharrock et al. 2009). These problems cast doubt on the calibration process and the validity of the adopted micro parameters for subsequent problem-solving simulations.

In contrast, validation refers to a forward modelling approach that determines how much quantitatively realistic behaviour can be obtained using physical or measured parameters. Although DEM has been validated to yield many features of physical materials (Potyondy & Cundall 2004), to what extent real behaviour can be achieved using DEM simulation, is still a question.

Hence, to obtain a test for successful validation, either the DEM simulations should be microstructurally equivalent to the physical materials or the physical materials should be simpler so that an equivalence of microstructure can be obtained in DEM simulations. The geological materials are naturally very non-uniform and there are practical constraints that limit the amount of information that can be determined about the geology and the behavioural properties of the materials. Hence, to simulate or validate the behaviour of such materials will pose difficulties in obtaining microstructural equivalence in simulations and determining micro mechanical parameters.

Alternatively, a physical system can be constructed whose simulation can be obtained in the DEM simulation with an equivalence in microstructure, physical properties and model dimensions. All the physical and mechanical properties of such a system, for example, particle and cement based parameters, should be measured and used in DEM simulations. The comparison of the macroscopic responses of both systems in equivalent loading would validate the DEM simulation against a real physical system.

2.3.9 Section Summary

Discrete element methods have been increasingly applied to model and investigate the behaviour of natural materials comprising soils and rocks. The advanced formulation of DEM can model various particle geometries in 2D and 3D, including rectangular and parallelepiped, circular discs and spheres, elliptical and ellipsoidal particles and polygonal particles. Circular or spherical particles are more efficient in modelling due to their straightforward contact detection schemes and hence require less computation time. However, the disadvantage is not obtaining true interlocking when compared to natural particles due to excessive rotation in shearing and the consequent lesser value of bulk friction. Non-circular or non-spherical shaped particles have the advantage of inducing higher dilation and interlocking at the particle, scale, and accordingly, yield high bulk friction. However, the associated disadvantage is the high computational cost and time required to run the model.

Due to attractive formulation of DEM, they have been used extensively to model and predict the behaviour of granular materials. The use of circular or spherical particles is an efficient option to model and investigate the behaviour of natural granular rocks with rounded particles, such as conglomerates. The dependence of various factors affecting the mechanical response of conglomerate is the real life challenge in such rocks and can be investigated using DEM simulations.

The limitations of the DEM are its assumptions of the rigidity of the particles and its validation against an equivalent physical system. Using the Hertzian contact model in DEM can overcome the assumption of rigid particles when investigating the conglomeratic rocks having weak cementing material and high strength particles.

However, the validation of the DEM is a real life challenge and can be gained by constructing and testing a physical model microstructurally equivalent to the numerical simulation. For such simulations, micro parameters should be measured in laboratory testing rather than estimated by the inverse modelling approach. It is hypothesised that the comparison of the macroscopic responses of both equivalent systems in identical loading would validate the DEM simulation.

2.4 Physical Modelling - Preparation and Testing of Synthetic Materials

Physical modelling is another popular and useful option for understanding the basic mechanics of natural granular materials, such as conglomerates. Natural materials are non-uniform, anisotropic and heterogeneous. If one wishes to understand the behaviour of these materials experimentally, results will be an interplay of various factors for example, particle shape, size distribution, packing, elastic properties, characteristics, composition and distribution of cementing materials and, most importantly the void ratio and natural heterogeneities.

To obtain an understanding of the influence of a specific parameter on the overall results is very difficult. For example, two samples collected and tested from one location in different loading directions will vary in results and hence limit the accuracy of the results. Although the laboratory testing of the rock specimens under various loadings leads towards the basic understanding of the mechanics of the rocks, the net failure and peak strength seem to be governed by above-mentioned factors whose dependence can not be investigated without keeping other parameters constant. In addition, practical considerations limit the amount of information that can be determined about the geology and behavioural properties of the materials (Wiles 2005).

In order to overcome these limitations and obtain an understanding of the mechanisms occurring in the natural materials comprising rocks and soils, an approach of physical modelling has been adopted in rock mechanics, which includes the preparation and testing of artificial materials that are similar to natural rocks. Two main advantages of this approach are the controlling of the heterogeneities that occur in natural materials and obtaining the reproducibility of the test results. This is very difficult in testing natural materials, such as rocks.

Moreover, the texture and structure of the material, that is, the grain size, porosity and cementation, can be controlled (Sebastianus et al. 1997). This approach has lead to the understanding of the various characteristics and mechanics of the rocks such as stress-strain behaviour, pre and post peak dilation, fracture propagation, role of cementing materials and dependence of the particle size. This approach was specifically considered in the laboratory investigation of conglomerates, which are naturally very heterogeneous and anisotropic rocks. The mechanical behaviour of conglomerates is controlled and influenced by many factors discussed earlier in Section 2.2.3. The Laboratory study of natural conglomerates is very difficult because of the practical problems (discussed in Section 2.2.3.1) associated with the sampling and testing of such rocks. Hence, it is more appropriate to understand and investigate such rocks using a physical modelling technique. However, an important factor in the physical modelling of conglomerates is to obtain similitude in the prepared physical model with that of the natural conglomerate both in behaviour and structure. Various modelling materials, both natural and artificial have been used in the past for understating and investigating the mechanics of rocks and soils. A detailed discussion on similitude and modelling materials is provided in the following sections.

2.4.1 Similitude

In rock mechanics, similitude refers to the physical or behavioural similarity of a rock system with that of another system which could be a physical (synthetic rock) or an analytical or numerical model. In other words, two systems that have the same physical characteristics (features, parameters) and have the same reaction in response to some action, for example, loading, are said to have similitude. The similitude can be defined as:

"The similitude of two objects always means that they belong to a common set of well-specified common characteristics, it is an equivalence relation between two systems which is reflexive, symmetric and transitive" (Szucs 1980).

There are two basic conditions of similitude:

1. Geometric Similitude: geometric similarity between two systems; it could be on a macro scale, that is, dimensions of the model and scaling and micro structural equivalence. However, it should be remembered that it is not the only necessary condition of similitude (Szucs 1980).
2. Phenomenon Similitude: two systems are similar if their corresponding characteristics (features, parameters) are connected by bi-unique (one-to-one) mapping (representations). It mainly encompasses the responses of two models, that is, their strength and elastic characteristics.

The similitude is based on the mathematics. Hence, the sufficient and necessary condition of similitude between two systems is that the mathematical model of one is related by a bi-unique transformation to that of the other.

Similitude is measured in terms of its credibility (Sargent 2004), a degree of similarity. The credibility of similitude defines the limit of the acceptance of a system showing simulation as that of the actual system. The detailed discussion on the similitude, its conditions and necessary parameters can be found elsewhere e.g. (Szucs 1980).

The similitude studies in rock mechanics can be categorised in to two main classes: similitude between synthetic rocks (physical models) and natural rocks, and similitude between numerical models and natural rocks (Figure 2-17).

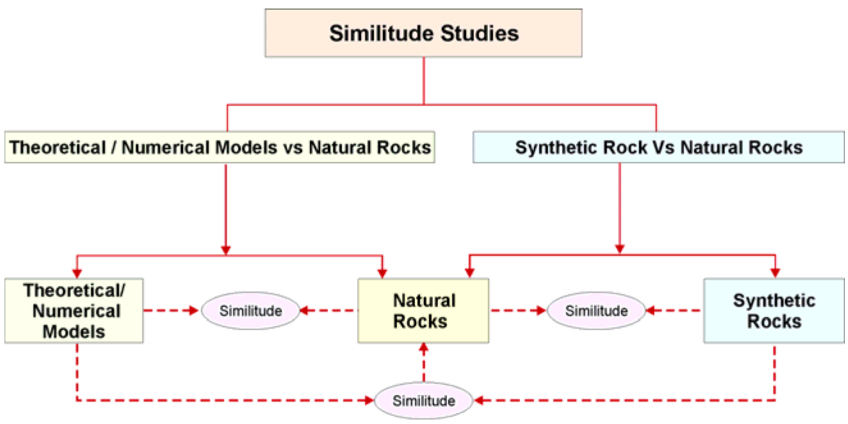

Figure 2-17: Chart showing the main areas of the similitude studies in rock mechanics.

In the study of rock mechanics, physical modelling has been an important technique to understand the dependency of various parameters that are nearly impossible to examine in natural rocks owing to their inherent heterogeneities. Numerous research has been conducted to study and understand the mechanics of the natural materials involving the preparation and testing of synthetic rocks having similitude with natural rocks. In this class of studies, the similitude credibility represents the level of acceptance of the similiarity between the elements of the two systems (i.e., physical materials and the natural rocks). For example, similarity in behaviour (e.g., mechanical parameters), micro texture and/ or structure, model scaling and dimensions.

Numerical methods have also been increasingly applied in rock mechanics to understand and predict the behaviour of natural materials. In the application of the numerical methods, theoretical knowledge of the mechanics of the materials has been introduced to simulate the behaviour of the rocks. Both continuum and discontinuum approaches have been utilised in this respect in rock engineering. The discontinuum approach where rock can be simulated as the assemblage of discrete bodies (after Cundall 1971) has become increasingly popular with the advances in computer technology and computation speeds. It is a rigorous aid in understanding the mechanics of granular media where the macroscopic response of the system is obtained from the movement and interaction of individual particles. However, numerical models are always based on theoretical formulations and simulate behaviour of material based on averaged input parameters and assumptions, which may or may not be true in natural materials. Therefore, to make numerical modelling an effective and rigorous tool, it must be calibrated and validated with the physical model for reasonable similitude credibility (Ferrez 2001). Hence, similitude studies involving numerical modelling should focus firstly on obtaining sufficient similitude (in behaviour, structure, dimensions etc.) with that of simple physical models rather than with natural rocks. Afterwards, if numerical models and simple physical models obtain similarity in behaviour and structure, these can be used for natural rocks. This approach is outlined in Figure 2-17.

2.4.2 Modelling Materials

The preparation and testing of various artificial materials to model natural soils, rocks and granular materials has been reported in the literature (e.g., Stimpson 1970). The artificial materials being studied in the modelling of rocks can be divided into two main classes: granular materials and non-granular materials (Stimpson 1970). Dilation was considered the first parameter which differentiates granular rocks from rocks with a glassy texture (Brace et al. 1966). The physical models prepared from non-granular materials can not induce dilation and hence, are not suitable for modelling the exact behaviour of the rocks. Therefore, the literature concerning the preparation and testing of non-granular materials is not discussed here.

Granular materials can be further classified into uncemented and cemented materials. Since uncemented materials exhibit the response of frictional material such as granular rock, a brief discussion is included especially in relation to early experiments for the calibration and validation of discrete element methods (DEM). Cemented physical material is further categorised based on the origin of the granular materials, that is, whether they are natural or artificial, and on the type of cementing agent it contains, that is, plaster, plastic, resin, cement, silica, glass, etc. (Figure 2-18).

The constituents, important characteristics and study objectives of modelling granular materials, that have been used in the past, are summarised in Table 2-5 followed by a brief discussion.

All these materials (Table 2-5) have associated advantages and disadvantages in modelling a rock which mainly depend on the particular objectives set for the modelling. A detailed discussion of these factors is considered outside the scope of this research and has been discussed elsewhere (e.g., Stimpson 1970; Wang et al. 1995; David et al. 1998).

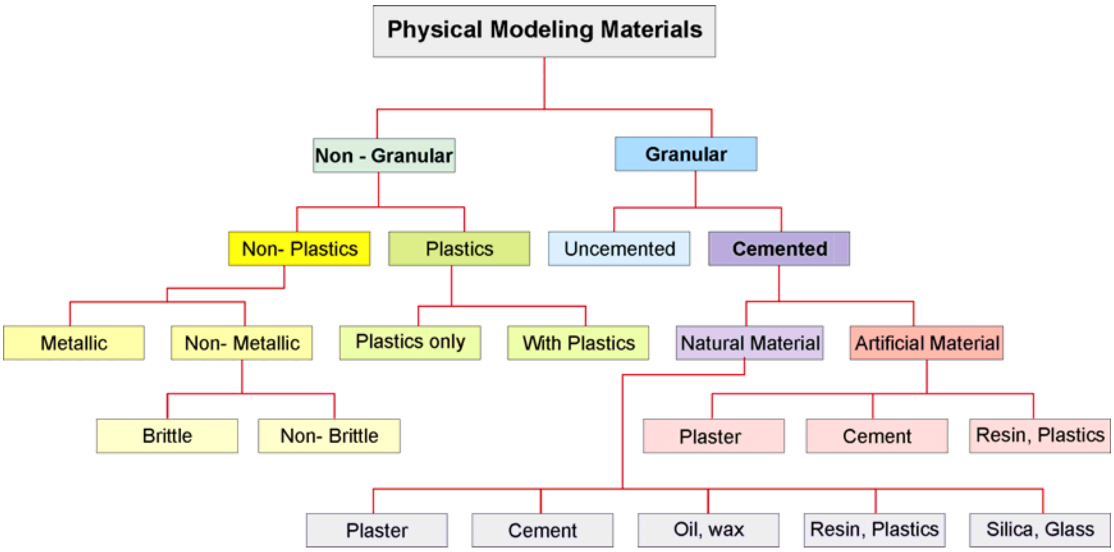

Figure 2-18: Classification of physical modelling materials used in rock engineering to study the behaviour of rocks (updated after Stimpson 1970).

However, in all the modelling studies, a key objective was to achieve the similitude between the models and the rocks, that is, the models should have similarities with the rock that could be at micro level (at laboratory scale) - the micro structure and texture, or have a macroscopic mechanical response - strength and deformation characteristics.

Table 2-5: Summary of physical granular materials used in the past to model and study the behaviour of rocks.

Material Type	Constituents		Application/ Comments	References
	Cementing materials	**Granular materials**		
Unconsolidated Granular	-	Quartz sand and glass beads	Fluid flow studies in models of oil and reservoir gas.	(Leverett et al. 1942)
	-	Slightly tempered sawdust	Model study of thermal effects on concrete dams.	(Massimilla et al. 1958)
	-	Quartz sand	Model studied of rock movements caused by caving in mine.	(Bodonyi & Szabo 1962)
	-	Steel cylinders	Deformation study of granular material in simple shear.	(Oda & Konishi 1974)
	-	Quartz sand	Liquefaction of sand	(Hakuno & Tarumi 1988)
	-	Sand, steel balls	Laboratory testing on sand and steel ball	(O' Sullivan & Bray 2002)
	-	Steel balls	Testing of steel balls in shear	(Deluzarche et al. 2002; O' Sullivan et al. 2004)
	-	Glass beads	Testing for shear wave velocities.	(Winkler 1983; Holt et al. 2005)
Cemented Granular	Plaster	Sand, chalk, clay etc.	Used mainly to model and study sedimentary rocks. Plaster has been used largely because of cheapness, textural similarities, simplicity in construction, low strength and greater deformation.	(Patton 1966; Hobbs 1967; Kulatilake et al. 2001a; Kulatilake et al. 2001b)
		Sawdust		(Roberts 1966)
	Cement	Sand, rock crush etc.	For modelling of sedimentary clastic rocks. Use of Portland cement has the same advantages and limitations as that of plaster, in addition, high strength can be gained in the modelling materials.	(Mogi 1962; 1963; Clegg 1965; Kobayashi & Yoshinaka 1994; Kobayashi et al. 1994; Kobayashi et al. 1995; Wang et al. 1995; David et al. 1998; Holt 2001)
		Cork		(Beshir 1967)
	Oil, Wax	Sand	Simulation of reservoir rocks. Oil/ wax glued models give low strength (no cumbersome loading required), cheapness, easily fabrication etc.	(Benito 1960; Garner & Gatun 1963)
	Resin, Plastics, Epoxy	Sand	Modelling of composite materials to simulate synthetic rocks. Easily available in liquid form, long potable life, low shrinkage, perfect bond.	(Neville 1966; Beshir 1967)
		Cork, Glass beads		(Neville 1966; Beshir 1967; Almossawi 1988; Holt et al. 2005)
	Silica	Sand	Modelling of synthetic sandstone close to real sandstone in studying the role of cementing material on strength and stiffness.	(Clough et al. 1981; Bernabe et al. 1992; Sebastianus et al. 1997; David et al. 1998)

To satisfy all the conditions of similitude is not practically possible as the knowledge of mechanisms involved at the micro level of a particular rock can never be complete (Stimpson 1970). Therefore, the preference for the fulfilment of the conditions of similitude varied with the target objectives of the model. For example, in some laboratory studies the microstructure gained similitude with natural rock while strength and other parameters were given second priority. Similarly, for the modelling of an underground opening, microstructure was not given priority as the stress field and the rock strength and deformation characteristics were considered more important.

In the modelling of granular (sedimentary) rocks, such as sandstones, various efforts have been made to obtain a synthetic rock which produces the same behaviour as that of natural sandstones. Initial work was conducted using the sands and plaster of Paris, Portland cement (Table 2-5). In these efforts, the main purpose was to obtain similitude in the macroscopic behaviour of the synthetic rock, that is, a stress-strain response under mainly uniaxial and triaxial loading.

In these efforts, mainly the fabrication of synthetic rocks was simplified and the reproducibility of the results and the macroscopic response were given priority. Concurrently, researchers also considered various cementing agents, (e.g., resin, epoxy, clay, silica) to study the change in behaviour of the synthetic material with the change in composition of the cementing agents. Together with use of sands, artificial materials such as corks, glass beads and sawdust having uniform grain geometry were used to study and control the impact of granules on the macroscopic response. With the advances of the technology (e.g., Fredrich et al. 1995) in observing the microscopic image of the grain size and cementing material among the grains, numerous researchers focused on studying the texture, microstructure and the distribution and composition of cementing material in the 1990s (e.g., Wang et al. 1995; Wong & Wu 1995; Zhang & Wong 1995; Sebastianus et al. 1997; David et al. 1998). These studies improved the methodology of the fabrication of synthetic rocks using high temperatures and pressures for sample diagenesis. Silica and glass were used as cementing material with quartz sands to control grain sizes, cementing agents and porosity. These efforts reproduced the microstructure, porosities and strength of the natural sandstones (e.g., Clough et al. 1981; Bernabe et al. 1992; Sebastianus et al. 1997; David et al. 1998).

In the modelling of conglomeratic rocks, physical models were constructed by using cement and gravels (e.g., Kobayashi & Yoshinaka 1994; Kobayashi et al. 1994;

1995). These models were tested for mechanical parameters in the context of foundation engineering and reasonable reproducibility of test results was obtained by controlling the properties of the cement matrix. However, the sensitivity of particle shape and size was not determined.

A synthetic conglomerate comprised of spherical clasts (rather than natural gravels) with a controlled proportion of cement as a cement matrix is a good option to understand the mechanics of conglomeratic rocks in simple laboratory testing. Moreover, the equivalent microstructure of such conglomerates can also be constructed using DEM simulations for further investigation and similitude. The use of spherical clasts in the synthetic conglomerates will rule out the effect of particle shape and will provide better understanding of the mechanics of conglomeratic rocks. The behavioural similitude of a synthetic conglomerate can be obtained by comparing its mechanical response with that of natural conglomerates.

2.4.3 Section Summary

In summary, the use of physical models has always been considered a good aid to simplify and understand the complex mechanisms occurring in rocks on a micro to macro scale. However, the time and cost involved to prepare, cure and test a model that can fulfil the specific conditions of similitude for a specific rock or scenario is challenging. Often even after many efforts, similitude can not be gained as it is subject to availability of the modelling materials. In some cases, readily available modelling materials are not sufficient to gain the required macroscopic response of the designed model. In this situation, time and budget constraints further limit the construction of a model using expensive and scarcely available modelling materials. However, despite all the challenges, physical modelling has been an important technique for investigating the behaviour of natural occurring materials. Together with acoustic emission (AE) monitoring (a literature review on AE monitoring is presented in Appendix A), physical modelling can be turned into a very useful tool to study and predict the behaviour of conglomerates that are very difficult, if not impossible to study in natural conditions even on a laboratory scale.

2.5 Literature Review Summary and Conclusions

Conglomerates are rudaceous rocks comprised of gravels, cobbles and boulders embedded in a fine matrix or cementing material and they have been rarely studied in laboratory testing due to their inherent heterogeneities and the practical difficulties in sampling and testing. However, these rocks can be studied using indirect techniques such as physical and numerical modelling.

Physical modelling involves the preparation and testing of synthetic rock which has similitude with natural rock. This technique has been beneficial in controlling the definite parameters in synthetic rocks, which is impossible in natural rock, and to get reproducibility of laboratory testing. However, the key limitation associated with the physical modelling in order to understanding the mechanics of natural rocks, such as conglomerates, is to meet the conditions of similitude in both textureal similarity and mechanical responses.

In laboratory modelling for conglomerates, geometric similarity can be gained by developing the microstructure of granular rocks using various modelling materials and cement, and by controlling the model's dimensions. Similarly, behavioural similitude can be obtained by validating the synthetic model's mechanical response against natural rocks. In physical modelling it is seldom possible to obtain perfect similitude, however, sufficient accuracy can be achieved to greatly contribute in a quantitative sense, to studying the mechanics of natural rocks.

Conversely, numerical modelling has developed into a rigorous technique for solving problems in rock mechanics. Both continuum and discontinuum approaches have been applied in rock and soil mechanics, however, discrete element methods seem more efficient and relevant for modelling the behaviour of granular materials because, in DEM, an overall assembly response is achieved by the interaction and relative movement of discrete particles. Sandstones and granites are the most common granular rocks that have been studied using DEM. These studies indicate DEM's potential for research into conglomeratic rocks.

Although DEM has been used effectively to predict many features of granular materials, its calibration and validation is required against the physical system. Many modelling techniques, such as bonded particle model (BPM) and the clumped particle model (CPM) have been proposed which, to some extent, reproduce the features of natural granular materials using simple circular, spherical or polygonal particles. However, DEM's validation and calibration remain a challenge for researchers and modelling professionals. In this area, work conducted both for frictional granular materials and cohesive-frictional granular materials (cemented assemblies) were reviewed. The work on cohesive-frictional material is of particular importance as granular rocks, such as conglomerate can be viewed as cohesive-frictional materials. The review of previous work on the DEM validation for cohesive-frictional materials can be categorised as:

1. Modelling the macroscopic response of natural materials, such as rocks and soils, in various loading conditions without taking into account the microstructure of the materials. Natural heterogeneities, anisotropy and scaling make it more complex to develop a rigorous correlation between DEM simulations and real materials. Efforts have been focused on the development of complex shaped particles to achieve a similarity of the macroscopic response of the numerical simulation and natural materials, whereas DEM's calibration for a simple model with simple geometric particles (spheres), is still in question.

   It is logical to validate DEM simulation first against a rock like synthetic material, which has an identical or equivalent microstructure to the natural rock and then extend its scope to model complex shaped particles.

2. Validations with synthetic materials were also found to focus on comparing the macroscopic responses of the physical models and numerical simulations. Although synthetic materials controlled the material's heterogeneity and yielded reproducibility of the test results, similitude was not obtained at the micro level. As a result, no correspondence was developed between the micro parameters used in DEM simulations and the microstructure of the synthetic materials. Only macroscopic responses in simple loading were considered sufficient when it is clear that the material's macro response is governed by the grain-cement interaction at micro level.

   The significance of the microstructure and associated micro parameters for DEM simulations becomes more obvious when modelling the coarse-grained rocks, such as conglomerates. In such materials, numerical and physical microstructures have a one-to-one correspondence with each other and should produce similar macroscopic responses.

3. If microstructural equivalence has been gained, micro parameters specifying the grain-cement interaction were either estimated or assumed by the inverse modelling approach rather than through measurements. Furthermore, very few studies focused on the micro level interaction of particle-particle and particle-cement interactions. Yet the effect of particle size and size distribution, the effect of interparticle cement and micro to assembly friction for simple particles are still unsolved questions which need to be studied in relation to physical materials. The simulation of rock masses involving discontinuities, heterogeneities and scaling are the next challenges in this

area that they can only be adequately addressed when DEM simulations are validated for simple laboratory models and comprehensively tested.

It is important and necessary to extend the scope of validation for DEM simulation from simple frictional material to more complex cohesive-frictional materials in order to understand their mechanics. Additionally, the numerical conditions, on which a validation study is to be carried out, should be identical to the physical conditions so as to obtain true representation of the physical conditions. Consequently, a comprehensive validation study is proposed as part of the present research, which will include:

1. The construction of numerical assemblies which are equivalent to physical assemblies, through the measurement of micro mechanical parameters, and
2. Boundary and initial conditions for numerical tests should be varied within the known range of properties of the physical assemblies measured at high confidence.

A comparison of the response of such numerical and physical materials will help to better understand the corresponding similitude characteristics (features and parameters) of the two systems that control the material's response. It will also lead to the calibration and redefining of the physical laws in simulations, that is, the refinement of the contact laws, bonding models, parameters and assumptions. It would also enhance simulation credibility and bring rigor to the modelling of complex materials such as natural rocks.

In summary, it is hypothesised that conglomerates can be studied rigorously through the following steps:

1. Preparation of a synthetic granular rock (synthetic conglomerate) having similitude in microstructure as that of a natural conglomerate and subsequently testing this in the laboratory to record the mechanical responses using conventional tests and AE monitoring;
2. Using DEM, simulation of an equivalent numerical synthetic rock having similitude in microstructure as that of a physical synthetic rock and the determination of micro parameters such as the strength and elastic properties of the cementing material in separate laboratory testing;
3. Quantitative and qualitative comparison of the behaviours of the synthetic and numerical conglomerates to validate the response of numerical simulations.

4. After a reasonable validation of numerical simulation in a comparative study, further investigations of the sensitivity of various parameters affecting the mechanical response in relation to natural rock.

Consequently, the present research consists of four components

1. Physical Modelling of Conglomerates
2. DEM Simulation of Conglomerates
3. Comparison of the output from both modelling techniques, and,
4. Using the validation of DEM and the understanding of the mechanisms from 1, and 2, take steps towards an improved understanding of the strength and deformation properties of natural conglomeratic rocks.

2.6 Outline of the Research Methodology

The research methodology is ordered into the following components and is briefly discussed below:

2.6.1 Physical Modelling for Synthetic Conglomerates

Physical Modelling is the experimental section of the present research and involves the preparation and testing of the synthetic conglomeratic rock that is equivalent to a conglomerate consisting of spherical clasts with a cement matrix. Selection of the modelling materials was established to obtain geometric and behavioural similitude in the synthetic material (Figure 2-19a & b) with that of the natural conglomerate. This necessitated controlling the particle geometry, composition and characteristics so as to obtain reproducibility of the test results. The main objective of the physical modelling was to understand the failure mechanisms, and to obtain the strength and deformation parameters of the synthetic conglomerate under different loading conditions.

Various materials were considered to represent the clasts (i.e., gravels, cobbles) of the conglomerate and matrix. The selection of spherical particles to model the conglomerate was in order to evaluate the capability of the DEM code (PFC) to build the same geometry of the particles in the DEM simulations. Spherical particles were chosen instead of oval or polygonal particles to represent the conglomeratic clasts. ISRM recommended laboratory tests were undertaken to record the response of the synthetic rock, including uniaxial, triaxial, Brazilian tensile and shear box tests. After looking in to various materials to model the synthetic conglomerate, steel balls (as conglomerate clasts) and Portland cement (as the cement matrix) were selected to fabricate the test specimens. The selection criterion was based on the stiffness contrast of the particle and cementing materials as per natural conglomerates, extensive available studies on their behaviour, ready availability and the similitude features of the natural conglomerate. The cement paste specimens were also planned for laboratory testing to determine the matrix properties. The key assumptions regarding the synthetic conglomerates were:

- The use of spherical particles to rule out the effect of non-spherical particle shapes on the mechanical behaviour;
- The initial use of uniform sized particles to rule out the effect of particle size distribution

With these assumptions, the prepared synthetic rock would represent the clast-supported and uniformly graded conglomerate, having perfect rounded clasts. The prepared synthetic granular rock was termed a "synthetic conglomerate" for consistency.

The details of the experimentation are discussed in Chapter 3 together with the analyses of the test results.

2.6.2 DEM Modelling of Conglomerates

DEM simulations of the conglomerates were planned using PFC for 3D. Since, in PFC, particles are cemented together using parallel bonds necessarily representing the interstices' cement, it was considered suitable for the simulation of conglomeratic rock having uniform sized particles. The numerical assemblies prepared to simulate synthetic conglomerate, were termed "numerical conglomerates" for consistency.

The numerical simulations were aimed to construct and test assemblies that are similar to synthetic conglomerates to understand the failure mechanisms, and strength and deformation parameters in loading identical to physical laboratory testing on synthetic conglomerates. Physical properties such as model dimensions, porosities, densities etc. were planned to be same as that of the physical models. Micro parameters defining the particles, interparticle cement and particle-cement interaction were to be derived from laboratory testing on cement material and from known properties of the balls, that is, density and elastic parameters. Equivalent to laboratory testing on physical models, numerical simulations were planned for uniaxial, triaxial, Brazilian tensile and shear box testing. The details of the DEM simulations are provided in Chapter 4.

2.6.3 Comparison of Physical and DEM Modelling

The third component of the present research is to validate the response of the numerical conglomerates against the physical synthetic conglomerates and to develop a correlation between the responses of both conglomerates. A one-to-one correlation was anticipated in the mechanical responses of synthetic and numerical conglomerates with the use of known and derived micro parameters. In numerical simulations, sensitivity studies were also planned to achieve an equivalence with the physical laboratory conditions (i.e., loading rates). The details of the correlation between the numerical and physical synthetic rocks are provided in the Chapter 5. It was hypothesised that the validation of DEM against physical models would give deep insight into the mechanics of the conglomerates and would be applied to the modelling of natural conglomeratic rocks (Figure 2-19).

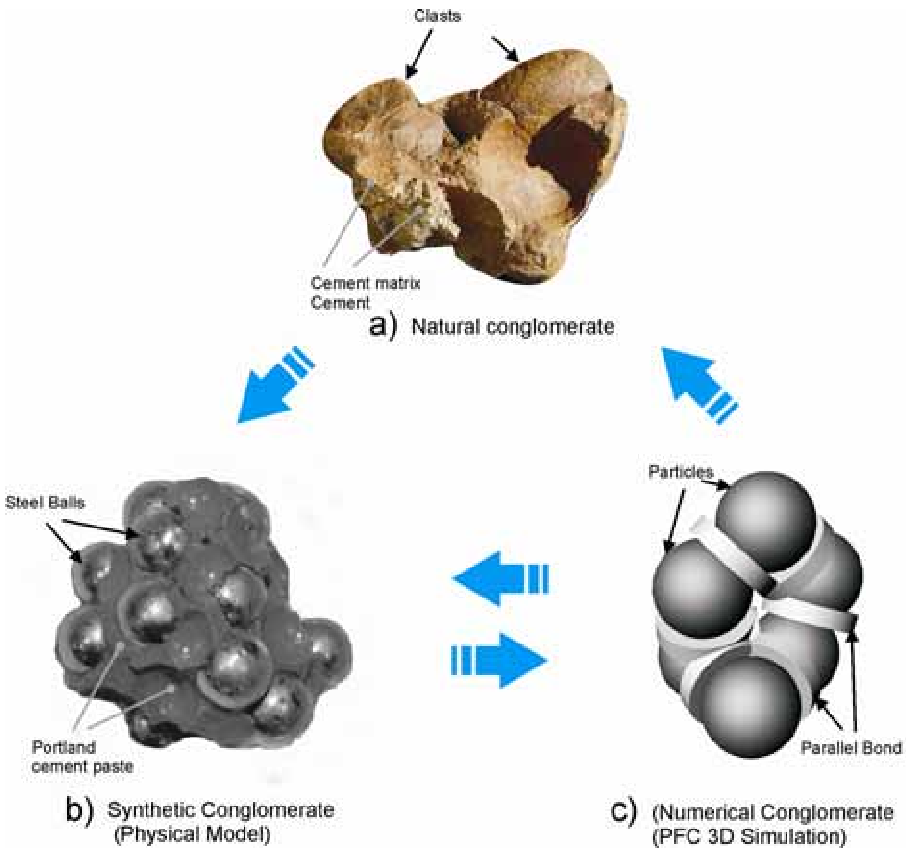

Figure 2-19: Conceptual illustration of the present research: a) micro structure of natural conglomerate, b) physical model (steel balls bounded by Portland cement) representing the synthetic conglomerate and, c) numerical simulation of particles and interparticle cementing material (parallel bonds) in PFC3D, representing the numerical conglomerate.

2.6.4 Investigations on Numerical Conglomerates

Further investigations were planned to study the response of numerical conglomerates with the sensitivity of various parameters that includes:

- Particle size distributions

- Scaling
- Particle material
- Cementing material (cement matrix)

In the comparative studies, the synthetic and numerical conglomerates were constructed in equivalence (i.e., the uniform distribution of particles was considered in both models with same specimen dimensions. The particle material was steel with Portland cement as a cementing matrix in synthetic conglomerates, and the same materials were reproduced in numerical conglomerates.) However, the behaviour of the numerical conglomerate was further analysed by varying these factors to understand and investigate their role in synthetic, and consequently in natural, conglomerates. The details of these investigations are discussed in Chapter 6.

2.6.5 Micro-mechanical Investigations

Micro-mechanical investigations were planned mainly to relate the particle-cement interaction of a physical system and numerical simulations. In a numerical simulation, a parallel bond represents the interparticle cement of a physical system. The response of the parallel bond was investigated in simple tests and correlated with the corresponding response of a physical system, which was also constructed in PFC by creating particles and Interparticle cement comprised of micro particles, The cement was deposited among the particles (macro particles) to represent a real physical system comprised of steel balls with Portland cement. These micro investigations were anticipated to provide an understanding of the particle-cement interaction and its effect on macro level. The micro investigations are discussed in Chapter 7.

Experimentation: Techniques, Testing and Analyses

3.1 Introduction

This chapter is aimed at providing details of the experimental work carried out as part of the present research. The experimental work was aimed at meeting the following two main objectives:

- Preparation of an idealised synthetic conglomeratic rock that is equivalent to a natural conglomerate consisting of spherical or spheroids particles within an homogeneous cement matrix, then record and analyse its mechanical response in various laboratory testing situations.
- Derivation of strength and elastic parameters for the cement matrix (to be used later in the numerical simulations) in laboratory testing on Portland cement.

The chapter is divided into four sections; the first section explains the experimental techniques adopted to prepare a synthetic conglomerate and discusses the laboratory testing planned to determine its mechanical response. The second section discusses the outcome of the laboratory testing and explores the response of the synthetic conglomerate in each testing scenario. The third section elucidates the analyses conducted on laboratory data for the various strength and elastic parameters of synthetic conglomerates. Section four clarifies the derivation of micro mechanical parameters for numerical simulations.

3.2 Experimental Techniques

The experimental techniques were devised in the context of the research hypothesis and research objectives to prepare an idealised synthetic conglomeratic rock that is equivalent to conglomerate consisting of spherical clasts within a homogeneous cement matrix. The modelling materials were chosen to obtain similitude in synthetic material as that of natural conglomerate by controlling the particle geometry, composition and characteristics and subsequently to obtain reproducibility of the test results. Additionally, spherical particles are readily modelled in PFC to obtain the same microstructure in numerical simulations.

Steel balls (as clasts) and Portland cement (as cement matrix) were selected to prepare the test specimens for various testing. The key assumptions regarding the synthetic conglomerates are:

- Use of spherical particles to eliminate the effect of particle shape on the mechanical behaviour;
- Use of uniform size of the particles initially to eliminate the effect of particle size distribution

With the above-mentioned assumptions, the prepared synthetic conglomerate was anticipated to represent the grain-supported and uniformly-graded conglomerate with spherical clasts.

ISRM recommended laboratory tests including uniaxial, triaxial, Brazilian tensile and direct shear tests were planned to record the mechanical response of the synthetic conglomerates. Similarly, uniaxial, triaxial and Brazilian tensile tests were planned on Portland cement paste to record its strength and elastic parameters for the derivation of micromechanical parameters. The required parameters of the cementing material and synthetic conglomerates are summarised in Table 3-1 and correspond to the planned tests.

Table 3-1: Summary of parameters to be determined corresponding to the planned laboratory tests on cement paste and synthetic conglomerate.

Portland cement paste		**Synthetic conglomerate**	
Parameters	**Laboratory tests**	**Parameters**	**Laboratory tests**
Normal and shear strength of cement	UCS, triaxial & Brazilian	Peak and residual strengths	UCS and triaxial
Normal and shear stiffness of cement	UCS and triaxial	Cohesion and angle of friction	UCS, triaxial and shear box
Angle of friction	UCS and triaxial	Young’s modulus	UCS
		Poisson’s ratio	UCS
		Acoustic emission	UCS
		Tensile strength	Brazilian test

Details of the sample preparation and laboratory testing are given in the following sections.

3.2.1 Preparation of Samples

The preparation of synthetic conglomeratic samples was intended to meet the geometrical and microstructural requirements of the similitude study (Szucs 1980). The sizes of all the synthetic conglomeratic specimens in relation to the ball size were selected to overcome the ball size's effect on the granular fibres in laboratory testing. In this regard, ISRM (1983) recommends that the sample to clast diameter (equivalent) ratio should be equal or greater to 10 in uniaxial and triaxial testing. The same recommendation has been proposed for numerical simulations for a granular rock in PFC (Itasca 2005). Hence, considering these constraints, all the synthetic conglomeratic specimens were planned with the sample to diameter ratio of 15~21. Specimens of cement paste were, however, prepared in two sizes due to the limitations of the available laboratory apparatus.

Cylindrical, circular and rectangular disc shaped samples were prepared for uniaxial and triaxial, Brazilian, and shear box tests respectively. The details of the specimen dimensions of synthetic conglomerates and cement paste specimens are summarised in Table 3-2.

Table 3-2: Dimension of the specimens of cement paste and synthetic conglomerate for laboratory testing.

<table>
<tr><th>Synthetic conglomerate samples</th><th>Diameter/ length or thickness (mm)</th><th>Cement paste samples</th><th>Diameter/ length or thickness (mm)</th></tr>
<tr><td rowspan="2">Uniaxial and triaxial</td><td rowspan="2">94/188</td><td rowspan="2">Uniaxial and triaxial</td><td>94/ 188</td></tr>
<tr><td>43/108</td></tr>
<tr><td>Brazilian</td><td>94/47</td><td>Brazilian</td><td>94/47</td></tr>
<tr><td>Shear box</td><td>100X100/36</td><td></td><td></td></tr>
</table>

A detailed discussion regarding the specimen fabrication is provided in the following sections.

3.2.1.1 Synthetic Conglomerate Samples

The synthetic conglomerate samples had three components: Portland cement, steel balls, and water. All the samples for uniaxial, triaxial, Brazilian and shear box testing were prepared using steel balls (diameter 4.75 mm), cement and water. Additionally, uniaxial samples were prepared with a ball diameter of 6.34 mm. Steel balls were placed randomly under gravity in moulds. Special care was taken to have the same number of balls in all samples for any specific test to obtain the reproducibility of the results. The moulds were weighed before and after being filled with balls to ensure the exact number of balls needed to fill the mould to the required depth were used. The porosity of the particle assemblies was determined using the mould volume and the volume occupied by the balls.

The next step was to prepare the water cement paste or solution to bond the balls. For this purpose, cement was sieved using the ASTM sieve #200 to avoid any mixing of coarse cement lumps or grains. The standard practice ASTM C305-99$^{\epsilon 1}$ (ASTM 2005) for the mixing of water and Portland cement was followed to prepare the cement paste using an electrical mixer. Various water to cement ratios (w/c) of cement paste were trialled to allow free movement through the interparticle voids. A final water to cement ratio (w/c) of 0.6 was selected to allow the complete filling of the cement solution into the interstices. The moulds were slotted with a 1.0 mm diameter holes on the cylindrical surface to liberate the enclosed air while pouring in and filling with the cement paste. These tiny holes were closed as cement started coming out of the holes after freeing of the enclosed air. Mixing of the water and cement was carried out at room temperature (25°±2°C) using an electric mixer for a definite period of time for each sample. To ensure the maximum possible homogeneity and isotropy of the cement paste after mixing, it was poured quickly into the ball assemblies in the mould. The moulds were provided with 30% extra sockets at the top and the cement solution was filled to the top of sockets to ensure the settling of cement with uniform concentration throughout the sample lengths (Figure 3-1). The top edges of the samples can not be flattened as balls were arbitrarily filled to the top of the moulds to achieve randomness. As a result, a thin layer of uniform thickness ~3mm of a cement paste was left on each sample to flatten its top edges and facilitate the uniform loading on the sample.

The mixing, casting, and curing of the specimens were carefully controlled to obtain reproducible properties. The dimensions of the samples are given in Table 3-2.

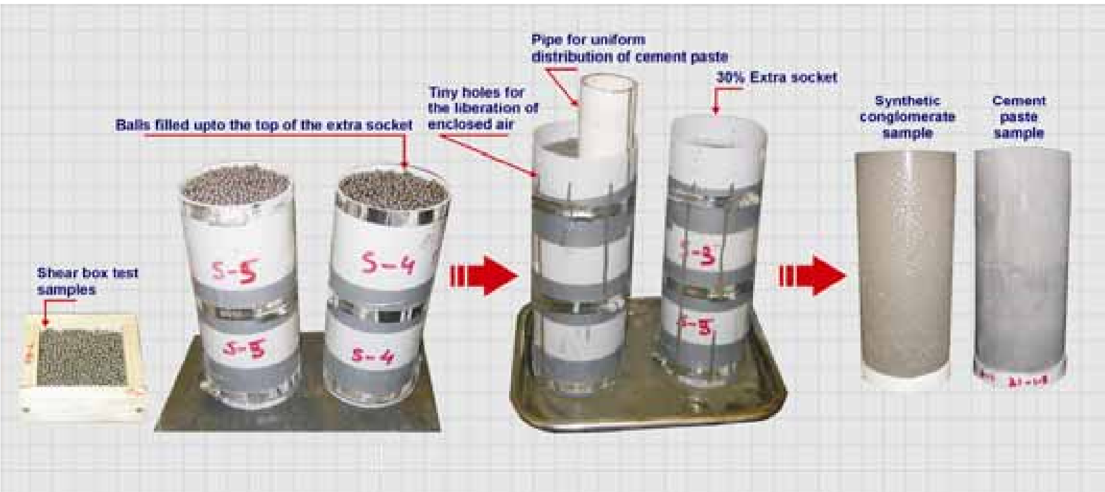

Figure 3-1: Sample preparation steps.

3.2.1.2 Cement Paste Samples

The cement paste samples were prepared for Uniaxial, Triaxial and Brazilian tests to determine the elastic and strength properties of cement paste with the same w/c ratio. The mixing and moulding of the samples was carefully controlled to ensure homogeneity. The cement samples were prepared in two sizes for the above-mentioned testing. The specimen dimensions are given in Table 3-2.

3.2.2 Curing of Samples

All the prepared samples were kept in a geomechanics laboratory at a room temperature of 25°±2°C for 24 hours. The samples were then extracted from the moulds and the top edges were smoothed to obtain planar surfaces. The samples were then placed for a fixed duration of 28 days in a curing chamber where relatively humidity was controlled to 100% at temperature 25°±2°C.

After retrieval from the humidity room, the samples were dried in the geomechanics laboratory room for two days at a controlled temperature of 25°±2°C.

The steps of the sample preparation have been illustrated in Figure 3-1 for cement paste and synthetic conglomeratic samples. The microstructure of the synthetic conglomerate is shown in Figure 3-2.

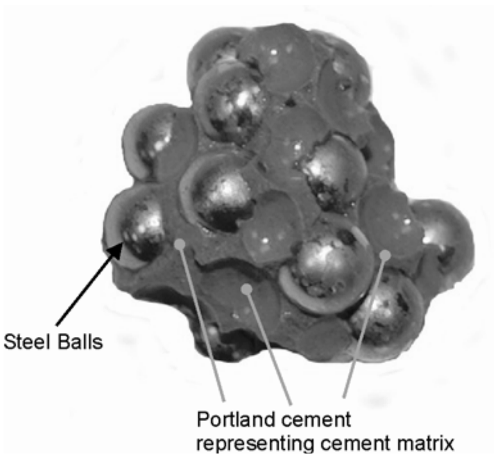

Figure 3-2: Microstructure of the synthetic conglomerate; steel balls embedded in Portland cement matrix.

3.2.3 Laboratory Testing Methodology

The scope of the laboratory testing includes the testing of cement paste samples and synthetic conglomerate samples to determine their strength and elasticity. In testing on cement paste samples, the main focus was to determine tensile and shear strength as well as Young's modulus of the cement paste for onward derivation of micromechanical parameters for numerical simulations.

The main objective behind the laboratory testing on the synthetic conglomerate was to understand the failure mechanisms and to determine its macroscopic response in terms of peak strengths (compressive, tensile and shear), elastic parameters (Young's modulus and Poisson's ratio), and acoustic emissions (AE).

Uniaxial, triaxial and Brazilian tensile tests were performed by using an Instron-Schenk 500 kN testing machine in the geomechanics laboratory at the School of Mining Engineering, UNSW. The shear box tests were conducted in the School of Civil and Environmental Engineering, UNSW. The details of the testing are given in the following section for the cement paste and synthetic conglomerate samples.

3.2.3.1 Testing on Cement Paste

Uniaxial and triaxial tests were conducted on cement samples to record the peak compressive strength and Young's modulus following standard ISRM procedures (Brown 1981). A constant displacement rate of 0.005 mm/s was applied to crush the samples in uniaxial tests and 0.01 mm/s was adopted in triaxial loading. The confining pressure was applied using a Hoek cell (Figure 3-3).

The compression machine is provided with an automatic data logger up to a maximum of 1000 points which records the platens displacement and the load on sample per second. The data was processed for strain measurement using a simple arithmetic calculation and plotted in a stress-stain field. Young's modulus (E) was estimated using the tangent modulus at 50% failure stress level of the stress-strain curve.

Brazilian tensile tests were conducted on the cement paste samples in compression following ISRM standard procedures. Axial loading on each sample disc was continued until the sample fails in axial splitting giving a well defined crack through the middle of the disc. The applied load (force) was monitored to get peak load at failure (Figure 3-3).

The indirect tensile strength was obtained using the following relation (after Goodman 1980):

$$\sigma_t = \frac{F_f}{\pi R t_B} \qquad (3\text{-}1)$$

Where

σ_t - Brazilian tensile strength (MPa)

F_f - Peak force acting on the platens (MN)

R - Radius of the sample (mm)

t_B - Thickness of the sample (mm)

Figure 3-3: Uniaxial, triaxial and Brazilian testing on cement paste samples.

3.2.3.2 Testing on Synthetic Conglomerate

- **Uniaxial and Triaxial Testing**

Uniaxial and Triaxial tests were performed on the granular cement samples to determine the mechanical response of synthetic rock. Young's modulus was estimated using the tangent modulus at a 50% failure stress level of the stress-strain curve. Samples were loaded at a constant displacement rate of 0.001 mm/s in uniaxial and 0.003 mm/s in triaxial testing. The reason for adopting the lower displacement rate was to avoid any vibration in the system due to the steel balls.

Strain Measurements using Strain Gauges

Various techniques can be used to measure the strain of a material in compression, tension and bending. In rock mechanics, strain gauges have been used to measure circumferential and axial strain of a rock specimen under loading. A section of a typical strain gauge is shown in Figure 3-4a with associated details. The sensitivity of a strain gauge is expressed quantitatively as the gauge factor (GF). Gauge factor is defined as the ratio of fractional change in electrical resistance to the fractional change in length (strain):

$$GF = \frac{\Delta R / R}{\Delta L / L} = \frac{\Delta R / R}{\varepsilon} \qquad (3\text{-}2)$$

Where

GF - Gauge factor
ΔR - Change in resistance
R - Initial resistance of strain gauge
ΔL - Change in Length of strain gauge
L - Initial Length of the Strain gauge
ε - Strain

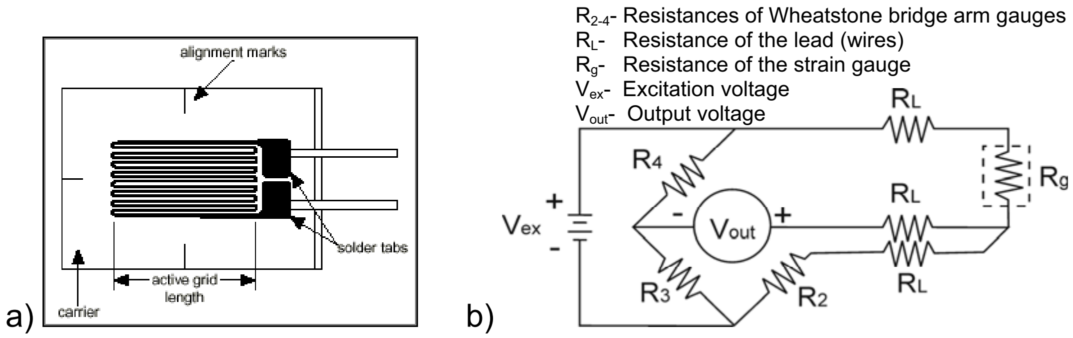

Figure 3-4: a) Section and details of a typical strain gauge; b) Quarter Wheatstone bridge with three wire configuration.

HBM Australia strain gauges (Model No. 1–LY41-20/120 , *R*=120± 0.3Ω) with lengths of 20 mm were used to monitor axial and circumferential strains using a quarter Wheatstone bridge circuit with three wire configuration (Figure 3-4b).

A quarter Wheatstone bridge for every strain gauge was preferred to a half or full Wheatstone bridge to ensure that any variations in strain between gauges was captured. Using a 3-wire connection can eliminate the effects of variable lead wire resistance because the lead resistance affects the adjacent legs of the bridge. Therefore, using three wires cancels out any changes in resistance due to temperature, and the net strain can be determined by the following relation:

$$Strain(\varepsilon) = \frac{-4V_r}{GF(1+2V_r)} \bullet \left(1 + \frac{R_L}{R_g}\right) \qquad (3\text{-}3)$$

Where

R_L - Resistance of lead (wire)

R_g - Resistance of strain gauge

V_r - Ratio of voltage (i.e., $V_r = V_{out}/V_{ex}$)

Considering the heterogeneous and composite nature of the sample, a 20 mm length of strain gauge was selected. Four strain gauges were used on each sample; two in the axial direction and two in the transverse direction at the centre of the sample (Figure 3-5a). All gauges were attached with super glue (X60 SK from HBM Australia) on the sample surfaces.

A National Instruments (NI) data acquisition system (SC-2043-SG) was used to measure the strains directly against time (Appendix A). DaisyLab 6.0 was used to record the data at a sampling rate of 100 readings per second which were then averaged to one reading per second by a built-in module. The circuit diagram of the Daisylab module configured for this purpose is shown in Appendix A. The strains determined from strain gauges were correlated with the uniaxial test data and plotted against the corresponding applied load.

Averaged plots of the axial and circumferential strains were drawn and Poisson's ratio (ν) was determined at 50% of peak stress (linear part of the curve) for each specimen. In the experiments, axial and circumferential strains were determined in uniaxial testing on the synthetic conglomerate for selected samples (i.e., S-41 to S-47). A typical plot of the axial and circumferential strains against axial stress is shown in Figure 3-6.

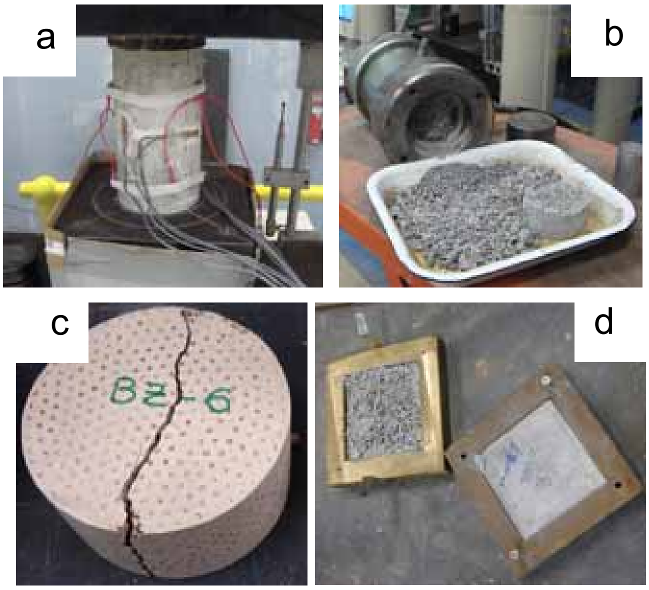

Figure 3-5: a) Uniaxial test in progress with strain measurement and acoustic emission monitoring, b) extraction of specimen after triaxial test, c) Brazilian tensile test sample after the failure, d) after the execution of the shear box test.

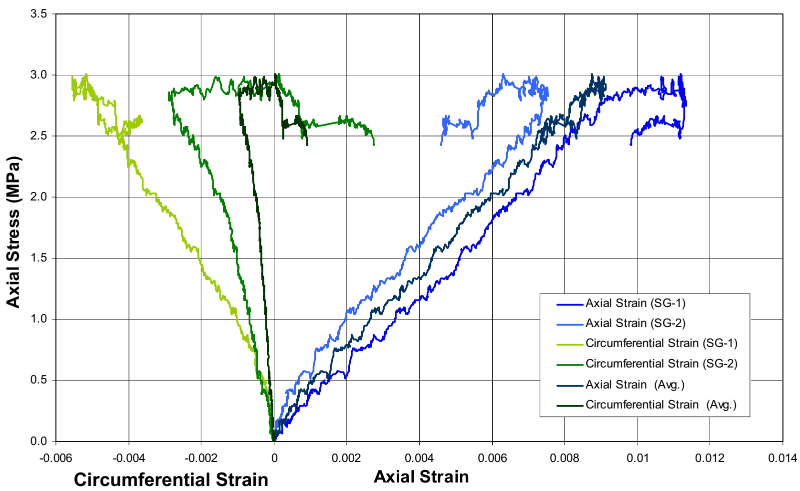

Figure 3-6: Plotting of axial and circumferential strains versus axial stress recorded in the uniaxial test.

Acoustic Emission (AE) Monitoring

Acoustic emission, or microseismicity, is a characteristic feature of a material under loading. This is an indication and function of a material's internal damage/ dislocation or failure. Laboratory studies involving AE are comprised of the recording and processing of acoustic signals in a rock specimen under specific loading conditions. By definition, a true AE study involves only the recording of self-generated events as a result of a material's failure and is hence termed a passive technique (Hardy 2003).

The main objective of AE studies in the present research is to record acoustic events in uniaxial testing to quantify damage thresholds (Diederichs et al. 2004) in a synthetic conglomerate and its onward comparison to numerical simulations. A comprehensive review of the acoustic emission monitoring in laboratory testing has been presented in Appendix A.

A total of seven samples were loaded in uniaxial compression for the recording of acoustic emissions. Numbers of events as a result of axial loading were monitored throughout the tests against time.

Prior to testing on synthetic conglomerates, the maximum value of the triggering level of machine background noise was determined during calibration testing. It was noted that most machine background noise has a trigger level below 0.08mV and very few events lie between 0.0 mV and 0.11 mV. So it was decided to adopt two different triggering levels (i.e., 0.08 mV and 0.11 mV) for this monitoring to differentiate the events caused by sample damage and by machine noise (Figure 3-7a).

a) 

b) 

Figure 3-7: Acoustic emission monitoring; a) Signal of machine background noise during the calibration process, b) National Instruments' data acquisition system (NI-PXI-1045) used in the experimental technique.

For this purpose, four transducers (Nano-30 from Physical Acoustic Corporation) were attached to the sample (two near top and two near bottom) with elastic bands (Figure 3-5a). A high velocity couplant was used between the transducer face and sample surface to ensure full contact devoid of an air gap to record the events. One transducer from the top and one from the bottom were set to high trigger level of 0.11

mV and remaining two to 0.08 mV, to record events having trigger level higher than 0.11 mV and between 0.08 mV and 0.11 mV.

All the transducers were attached to preamplifiers to amplify the signals and then to the PCI card. The NI data acquisition system (Figure 3-7b) was used to record the number of events. The system was configured in LabView8 to record data in Excel format. The circuit diagram configured in Labview 8.0 for this experimental technique is shown in Appendix A.

The laboratory set up for uniaxial testing is illustrated in Figure 3-8. All the events during uniaxial loading were recorded against time units (i.e. milliseconds) and analysed in relation to loading. A typical plot of the measured events in the stress-strain field is shown in Figure 3-9.

Figure 3-8: Complete set up ready to go for uniaxial testing on synthetic conglomerate samples under AE monitoring and strain measurements.

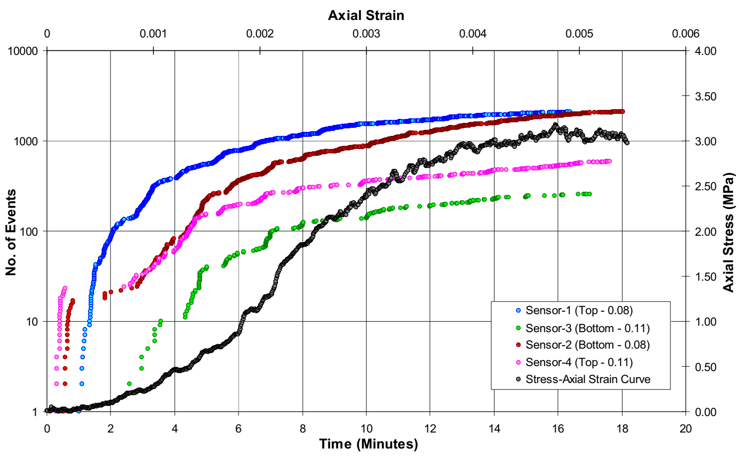

Figure 3-9: Plot showing recorded acoustic emissions near the top and bottom of the sample at thresholds 0.08 mV and 0.11mV in the stress-strain field.

- **Brazilian Tensile Testing**

Brazilian tensile test gives the indirect tensile strength in uniaxial loading (Brown 1981) for a regular geometry, that is, circular discs. A total of six samples were tested to determine the tensile strength of the synthetic conglomerate. ISRM recommended procedures were followed to execute the test. Samples were axially loaded in compression at a constant displacement rate of 0.005 mm/s until the failure. A discrete crack surface parallel to loading axis (Figure 3-5c) was achieved in all the samples loaded for testing. The applied load (force) was monitored with vertical displacement of platens to obtain peak load at the failure. The tensile strength of the material was calculated by putting peak loads at failure and sample dimensions in Equation 3.2 (after Goodman 1980).

- **Shear Box Testing**

Shear Box testing was undertaken on rectangular synthetic rock samples using a heavy duty shear box (Figure 3-10). The maximum load capacity of the shear proving ring is termed as 50 MPa. The apparatus' calibration was confirmed by running initial trial tests on a specimen of known parameters. In all the testing on synthetic conglomerate samples, a low shear displacement rate (i.e. 0.001 mm/s) was adopted for shearing.

A normal load was applied by putting dead weights on the free hanger as per the apparatus's calibration sheet. All the samples were tested by applying lower values of normal stresses (i.e. 0.5~2.0 MPa) so that the applied shear stress may not exceed the apparatus's limit. Shear displacement, vertical dilation and shear force were monitored throughout the test for an applied normal stress using dial gauges. Readings on all gauges were recorded at intervals of 15, 30, and 60 seconds for a maximum shear displacement of 4.5 mm.

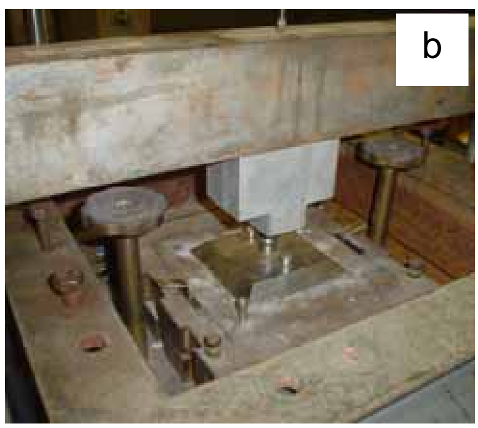

Figure 3-10: a) Shear Box testing in progress, b) Vertical loading on sample by loading hanger.

The recoded vertical and shear loads (force) were transferred to normal and shear stresses as per the equipment's calibration data sheet. Similarly, shear and vertical displacements were calculated from dial gauge readings.

3.3 Laboratory Test Results

This section presents the laboratory test data of synthetic conglomerates and cement paste samples. The results of the uniaxial, triaxial, Brazilian tensile and shear box tests are summarised in tables and illustrated as figures in the following sections.

3.3.1 Cement Paste

Uniaxial, triaxial and Brazilian tensile strength tests were conducted on cement paste samples to record peak strengths and Young's modulus. A total of 11 samples were tested in uniaxial loading, 7 in triaxial loading and 3 in Brazilian tensile testing. The results are provided in Table 3-3 and the stress-strain curves for the uniaxial and triaxial tests are plotted in Figure 3-11.

Table 3-3: Results of uniaxial, triaxial and Brazilian tensile tests on cement paste samples.

Sample no.	Sample dimensions diameter/ length	Confining pressure (MPa)	Peak strength (MPa)	Young's modulus E (GPa)
S-1C	94mm/ 188mm	0	12.12	2.77
S-2C		0	10.32	4.12
S-4C		0	11.75	2.19
S-5C		0	17.30	4.35
S-6C		0	12.10	2.90
S-7C		0	14.80	3.15
S-7C		0	14.80	2.86
S-9C		0	9.80	2.17
SC-1	42.5mm/ 100mm	0	14.59	3.58
SC-6		0	17.04	3.65
SC-10		0	16.94	3.19
SC-5		2	26.48	3.84
SC-9		2	22.70	3.61
SC-2		5	33.36	4.20
SC-4		5	32.85	4.42
SC-8		5	32.73	4.03
SC-3		10	43.65	4.77
SC-7		10	44.09	3.88
BZ-1C	94mm/ 47mm	Tensile strength	-1.33	-
BZ-2C			-1.39	-
BZ-3C			-1.36	-

Uniaxial testing showed a relatively big scatter in peak strength, ranging from 10.32 MPa to 17.30 regardless of the sample's dimensions. Young's modulus was found to vary from 2.17 GPa to 4.12 GPa in uniaxial testing. However, triaxial testing showed less scatter in peak strength, that is, 22.70 - 26.48 MPa, 32.73 - 33.36 MPa and 43.65 - 44.09 MPa at confining pressures of 2.0, 5.0 and 10.0 MPa respectively. Generally, a rising trend of Young's modulus was observed with an increase in confining pressure.

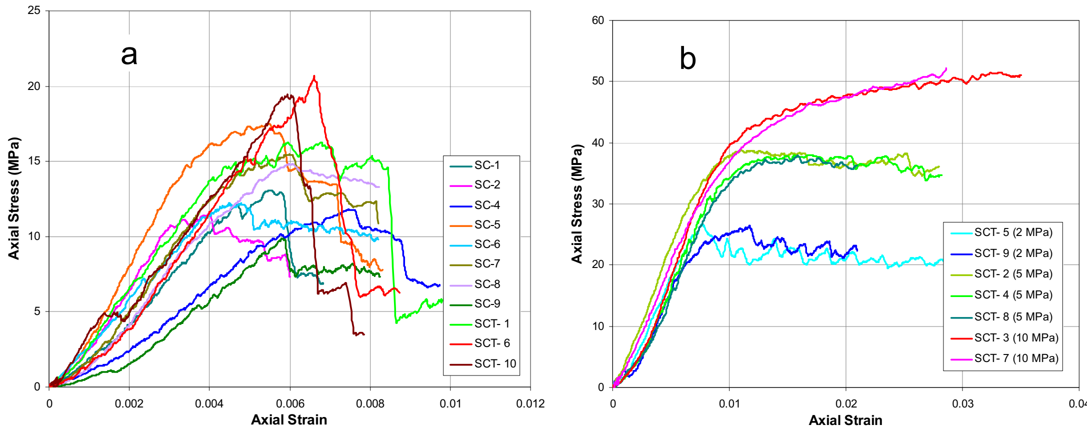

Figure 3-11: Stress-strain plots of Portland cement paste samples in: a) uniaxial tests, b) triaxial tests at confining pressure of 2.0, 5.0 and 10.MPa. See Table 3-3 for details of samples.

The load-displacement curves of cement paste samples in Brazilian tensile testing are shown in Figure 3-12 and the measured tensile strengths are presented in Table 3-3.

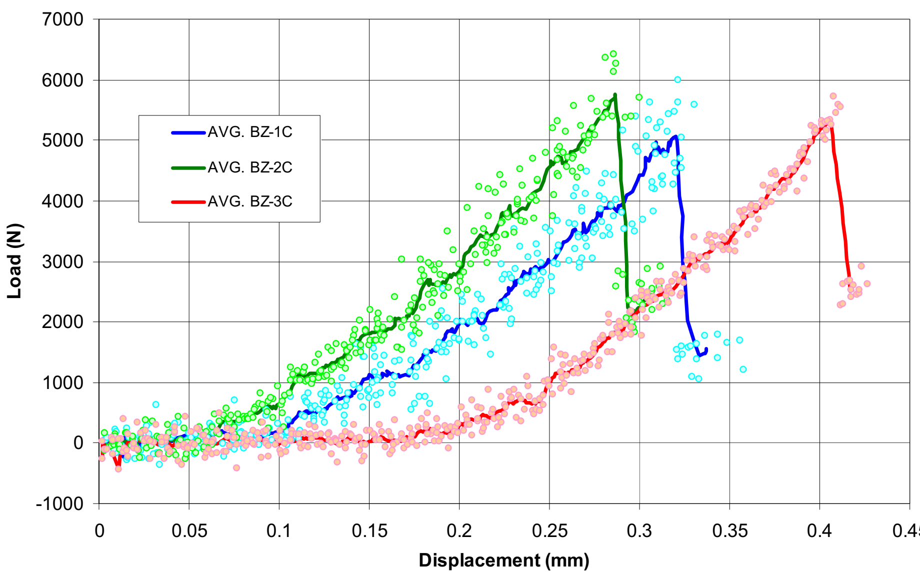

Figure 3-12: Force-displacement plot of Brazilian tensile tests on cement past for peak loads.

All the laboratory test results were statistically analysed for mean values and the variability of the test results. Results' variability was determined in percent standard deviation. The summary of the statistical analysis is provided in Table 3-4.

Table 3-4: Summary of statistical analysis on uniaxial, triaxial and Brazilian tensile tests' data of cement paste samples.

Laboratory test	Peak strength Mean (MPa)	Peak strength Standard deviation (%)	Young's modulus Mean (GPa)	Young's modulus Standard deviation (%)
Uniaxial	12.76	22.1	3.18	22.1
Triaxial (2MPa)	24.59	10.87	3.73	4.47
Triaxial (5MPa)	32.98	1.01	4.22	4.62
Triaxial (10MPa)	43.87	0.71	4.32	14.63
Brazilian Tensile	1.36	2.20	-	-

3.3.2 Synthetic Conglomerate Samples

3.3.2.1 Uniaxial and Triaxial Testing

Uniaxial and triaxial tests were conducted on synthetic conglomerate samples. In uniaxial testing two types of synthetic conglomerates having steel balls with diameters 4.75 mm and 6.34 mm were tested to observe the sensitivity of the particle size. However, triaxial tests were conducted only on the samples with ball diameter of 4.75 mm. The test results are summarised in Table 3-5 and shown in Figure 3-13.

A total of 14 samples were tested in uniaxial testing with a ball diameter of 4.75mm. The peak strength measured ranged from 1.50 to 4.88MPa and Young's modulus varied from 0.83 GPa to 3.00 GPa. Seven (7) samples were monitored for radial strains to determine Poisson's ratio of synthetic conglomerates and AE. The measured values of Poisson's ratio ranged from 0.25 to 0.35. Six samples were loaded for triaxial testing at 5.0MPa and 10.MPa confining pressures which yielded peak strengths of 21.3 - 25.8 MPa and 42.50 - 43.04 MPa, and Young's modulii of 2.50 - 2.80 GPa and 3.20 - 3.27 GPa respectively. Additionally, five (5) synthetic conglomerate samples with a ball diameter of 6.34mm were tested in uniaxial testing. The peak strengths and modulii were observed to vary from 1.35 to 2.64 MPa and 0.87 to 1.13 GPa respectively.

Uniaxial and triaxial test results were statistically analysed to examine the scatter in the data. The output of the analysis is given in Table 3-6.

Table 3-5: Test results of uniaxial, triaxial and Brazilian tensile testing for synthetic conglomerates.

Sample no.	Sample dimension (Average)	Ball diameter (mm)	Confining pressure (MPa)	Peak strength (MPa)	Young's modulus E (GPa)	Poisson's ratio
S-21	Diameter= 94mm Length=188mm	4.75	0	2.11	0.95	-
S-04			0	4.88	2.39	-
S-10			0	2.04	2.60	-
-S-13			0	3.20	3.00	-
S-14			0	1.50	2.40	-
S-15			0	3.60	3.00	-
S-16			0	4.30	3.20	-
S-31		6.34	0	2.64	1.13	-
S-32			0	2.24	0.97	-
S-33			0	1.80	0.95	-
S-34			0	1.89	0.90	-
S-35			0	1.35	0.87	-
S-41		4.75	0	3.37	1.13	0.25
S-42			0	3.11	1.34	0.26
S-43			0	2.35	1.00	0.25
S-44			0	2.70	0.83	0.33
S-45			0	2.66	1.30	0.27
S-46			0	3.70	1.30	0.28
S-47			0	2.97	0.87	0.35
TS-1			5	25.80	2.50	-
TS-2			5	21.3	2.60	-
TS-3			5	25.01	2.80	-
TS-4			10	42.60	3.22	-
TS-5			10	43.04	3.20	-
TS-6			10	42.50	3.27	-
BZ-1	Diameter= 94mm Thickness=47mm	4.75	-	-0.22	-	-
BZ-2			-	-0.12	-	-
BZ-3			-	-0.19	-	-
BZ-4			-	-0.12	-	-
BZ-5			-	-0.23	-	-
BZ-6			-	-0.11	-	-

Table 3-6: Summary of statistical analysis on uniaxial, triaxial and Brazilian tensile tests' data of synthetic conglomerates.

Laboratory tests	Ball diameter (mm)	Peak strength		Young's modulus (E)		Poisson's ratio	
		Mean (MPa)	Standard deviation (%)	Mean (GPa)	Standard deviation (%)	Mean	Standard deviation (%)
Uniaxial	6.34	1.98	24.4	0.96	10.39	-	-
Uniaxial	4.75	2.98	18.30	1.08	19.60	0.32	33.20
Triaxial (5 MPa)		25.48	1.70	2.63	5.80	-	-
Triaxial (10 MPa)		42.70	0.62	3.23	1.12	-	-
Brazilian Tensile		0.16	34.00	-	-	-	-

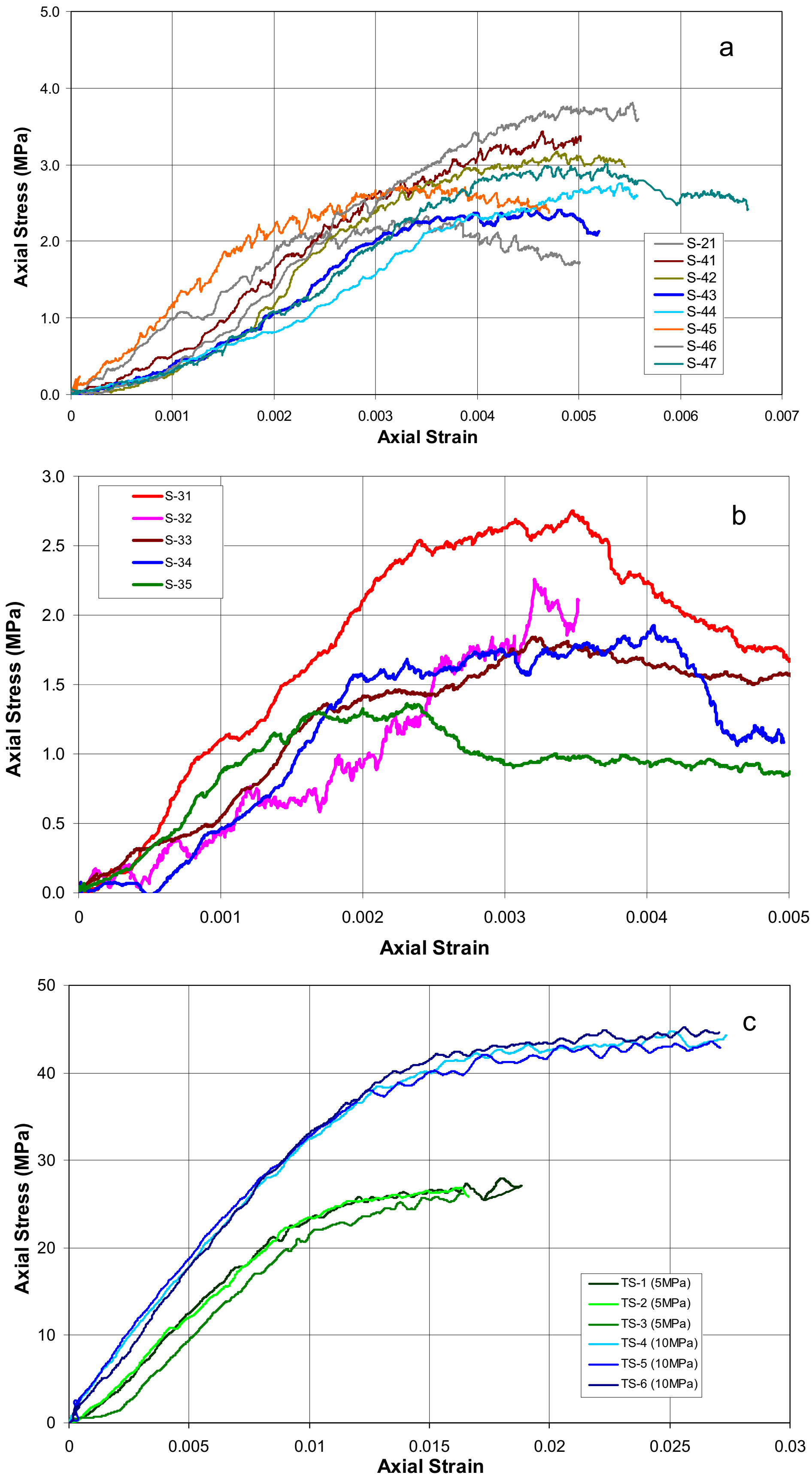

Figure 3-13: Stress-strain plots of synthetic conglomerates: a) Uniaxial tests with ball diameter 4.75 mm, b) uniaxial tests with ball diameter 6.34 mm, c) triaxial tests with ball diameter 4.75mm at confinement of 5.0 and 10.0 MPa. See Table 3-5 for sample details.

3.3.2.2 Brazilian Tensile Testing

A total of six Brazilian tests were conducted on the synthetic conglomerate samples. The determined indirect tensile strength values are summarised in Table 3-5 and load-displacement curves are plotted in Figure 3-14. A large scatter of the tensile strength was observed in Brazilian testing, varying from 0.11 MPa to 0.23 MPa. The variability of the tensile strength is given in Table 3-6 in terms of standard deviation.

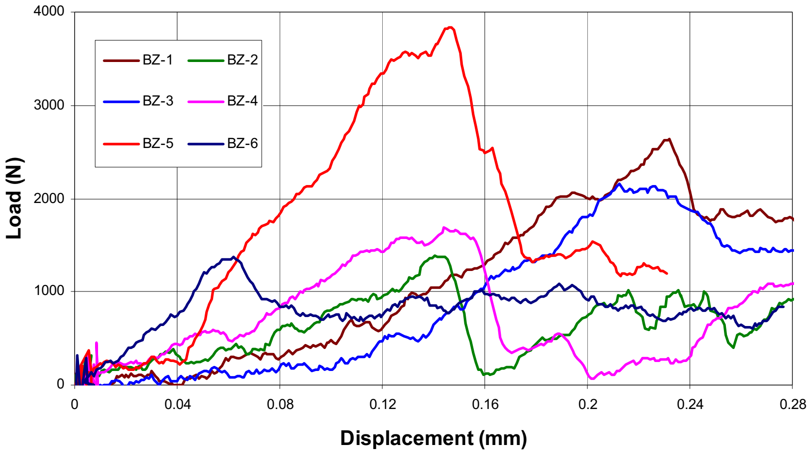

Figure 3-14: Plot of Brazilian tensile tests in load-displacement space.

3.3.2.3 Shear Box Testing

A total of six shear box samples of synthetic conglomerate were tested in direct shear at normal stresses of 0.5, 1.0 and 2.0 MPa. Shear stresses, horizontal or shear displacements and vertical dilations were monitored against each value of normal stress. The shear stresses plotted against shear displacement are shown in Figure 3-15a and vertical dilations with horizontal displacement are shown in Figure 3-15b. Shear strength and the angle of dilations were measured from Figure 3-15a and b for each value of normal stress, and are summarised in Table 3-7. Shear strength was observed as 7.56 - 8.21 MPa, 12.15 - 12.99 MPa and 20.70 - 21.71 MPa, corresponding to normal stress of 0.5, 1.0 and 2.0 MPa respectively. In all shear tests, the dilation angle was found to vary from 45.0 to 47.89 degrees (Table 3-7) and seems to be insensitive to normal stress. The increase in normal stress only suppresses or delays the onset of dilation but does not affect its magnitude (Figure 3-15b).

The results of the shear box tests were statically analysed for mean values and test variability (Table 3-8). Peak shear strengths of the samples were plotted against normal stresses (Figure 3-16) to determine Mohr-Coulomb's strength parameters (i.e. cohesion and apparent angle of friction).

Table 3-7: Results of shear box testing.

sample no.	Normal stress (MPa)	Shear strength (MPa)	Angle of dilation
SB-4	0.5	7.54	47.89°
SB-2	0.5	8.21	45.13°
SB-1	1	12.15	45.00°
SB-3	1	12.99	47.90°
SB-6	2	21.71	45.59°
SB-5	2	20.70	45.00°

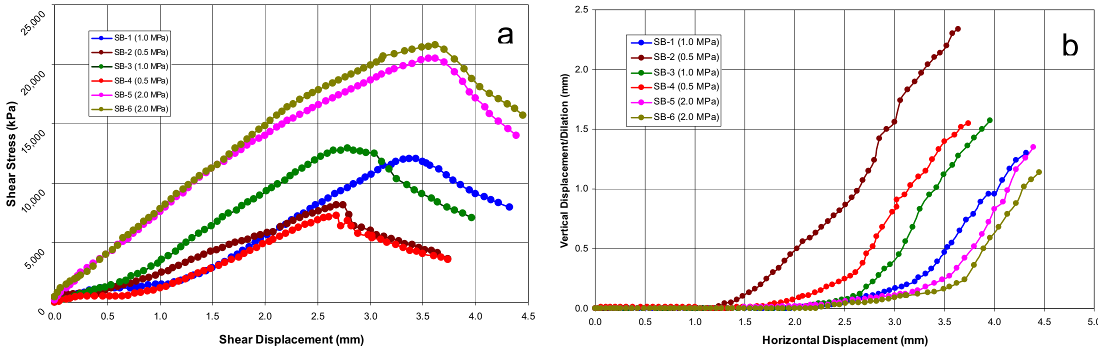

Figure 3-15: Shear box tests results; a) shear stress versus shear displacement for different values of normal stress, b) vertical dilation versus horizontal/ shear displacement for the calculation of dilation angles.

The apparent angle of friction represents the sum of the angle of internal friction (ϕ) and the angle of dilation (i), that is, ($\phi + i$) as per the following relation:

$$\frac{\tau - c}{\sigma_n} = \tan(\phi + i) \qquad (3\text{-}4)$$

Where

τ - shear strength, and

σ_n - normal stress.

c - cohesion

The mean value of the dilation angle (i.e. 46.08°) was then subtracted from the apparent angle of friction (83.9°) to get true angle of friction (37.82°).

Table 3-8: Summary on shear box test results.

Normal stress (MPa)	Shear strength		Angle of dilation	
	Mean (MPa)	Standard deviation (%)	Mean	Standard deviation (%)
0.5	7.88	6.01	46.08°	3.08
1	12.57	4.72		
2	21.21	3.37		
Cohesion (MPa)	3.56	**Mean angle of dilation *(i)***	46.08°	
Apparent angle of friction (ϕ+*i*)	83.9°	**Angle of friction (ϕ)**	37.82°	

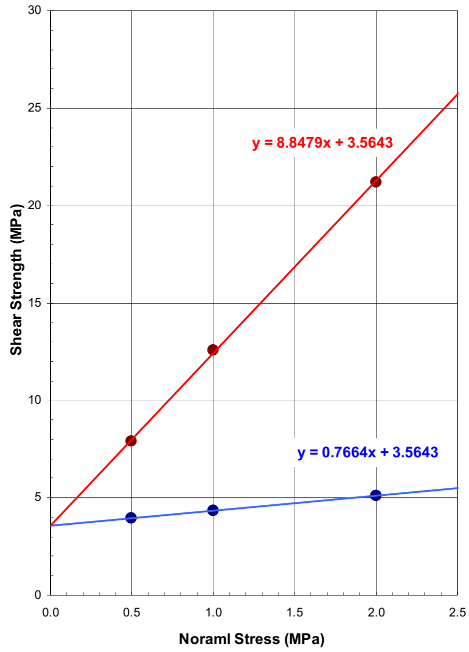

Figure 3-16: Shear strength of the synthetic rock versus normal stress to get a cohesion intercept of 3.56MPa, the apparent angle of friction (ϕ+*i*) 83.90° and the angle of friction (ϕ) 37.82°, subtracting angle of dilation *(i)* of 46.08° from the apparent angle of friction.

3.3.3 Comparison of Synthetic and Natural Conglomerates

The laboratory test results of the synthetic conglomerates were compared to natural conglomerates to validate their response. Synthetic conglomerates are a representation of grain supported conglomerates having weak cementing material, that is, cement paste. Hence, their response was correlated to a natural conglomerate of the Bakhtiari Formation (Iran) (after Shafiei & Dusseault 2008). The correlation of the mechanical response was made in terms of the mechanical parameters and is presented in Table 3-9. The objective of this correlation was to obtain a mechanical behaviour of natural conglomerate having correlation with that of synthetic conglomerate for onward numerical parametric sensitivity studies.

Table 3-9: Correlation of synthetic conglomerates and natural conglomerates.

Mechanical response	Natural conglomerate Bakhtiari Formation (after Shafiei & Dusseault 2008)	Synthetic conglomerate
Uniaxial compressive strength (MPa)	1.20 – 5.0	1.35 – 4.88
Brazilian tensile strength (MPa)	0.25 – 0.51	0.11 – 0.22
Young's modulus (GPa)	0.70 – 3.0	0.83 – 3.0
Poisson's ratio	0.24 – 0.37	0.25 – 0.35

The comparison of the mechanical parameters of both the conglomerates showed a very good correspondence in uniaxial compressive strength, Young's modulus and Poisson's ratio. However, the range of Brazilian tensile strength of synthetic conglomerates was observed slightly lower than that of natural conglomerates. As a whole, the mechanical response of an idealised conglomerate (synthetic conglomerate) was considered to have sufficient credibility of behavioural similitude with that of the natural conglomerate.

3.4 Data analyses for Synthetic Conglomerates

This section presents the analyses conducted on experimental data to explain and understand the behaviour of an idealised synthetic conglomerate by the application of existing strength criteria on laboratory data (presented in section 3.3). The synthetic conglomeratic samples tested showed a good reproducibility of the results and yielded a meaningful and representative value for each parameter (Table 3-6), reflecting a peculiar response in each loading condition. Mohr-Coulomb and Hoek-Brown criteria were applied for strength and the material's parameters to further investigate the response of synthetic conglomerate. Progressive damage in the synthetic conglomerate was characterised in terms of stress stages by AE monitoring and strain data measured in uniaxial testing. Modes of failures of conglomeratic samples were also determined qualitatively in each laboratory testing.

3.4.1 Strength Criteria for Synthetic Conglomerates

A peak strength criterion is defined as a relation between stress components that permits the peak strength developed under various stress conditions. In the same way, a residual strength criterion can be used for the prediction of residual strengths under varying stress conditions. Similarly, a yield criterion is a relation between stress components which predicts the onset of permanent deformation (Brady & Brown 2005).

Synthetic conglomerates were subjected to two well documented strength criteria, Mohr-Coulomb and Hoek-Brown, to characterise their behaviour. According to Mohr-Coulomb criteria, the shear strength (τ) of a material is made up of two parts, a constant cohesion (c), and a normal stress-dependent frictional component (ϕ) and can be expressed as;

$$\tau = c + \sigma_n \tan\phi \qquad (3\text{-}5)$$

Hence, for constant values of the cohesion and internal friction of a material, shear strength can be predicted with a value of normal stress on a failure plane.

Mohr's circles are drawn corresponding to peak strengths and to confining pressures to find Mohr-Coulomb parameters. Cohesion (c) is the y-axis intercept and the slope of the line gives the internal angle of friction (ϕ). This criterion gives a linear relation of shear strength with normal stress. The backward extension of this line (beyond y-intercept) intercepts the negative x-axis at a point indicating the predicted tensile strength of the material. It was noted that the predicted tensile strength overestimates the values as the rocks and rock like materials are weak in tension and give a shear to tensile strength ratio of greater than 2 and usually around 10-15. To overcome this overestimation a tension cut off line was introduced as per actual tensile strength measured in the laboratory (Figure 3-17).

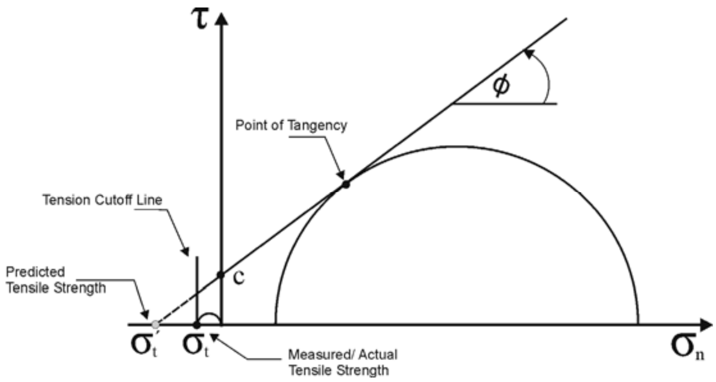

Figure 3-17: Coulomb strength envelopes in terms of shear and normal stresses.

Mohr's circles were plotted for synthetic conglomerates inputting mean values of uniaxial, triaxial and Brazilian test results in shear strength-normal stress space to obtain strength parameters of *c*, ϕ. The plot is shown in Figure 3-18.

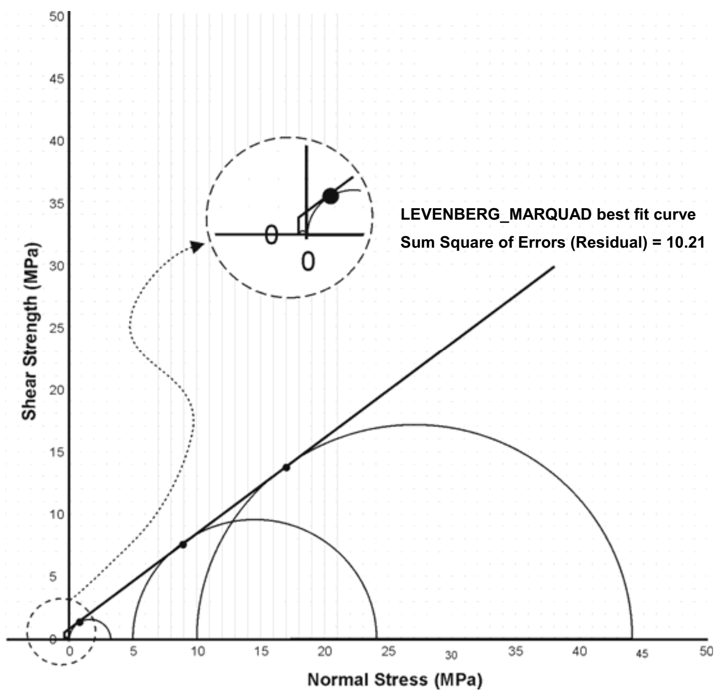

Figure 3-18: Plotting of uniaxial, triaxial and Brazilian results in shear strength - normal stress field to yield Mohr-Coulomb strength parameters i.e. angle of internal friction of 37.3°, cohesion of 0.75 MPa and tensile strength cut-off at 0.16 MPa.

Hoek and Brown (1980a) introduced their failure criterion in an attempt to provide input data for designing underground excavations in hard rock. This criterion incorporates the non-linearity associated with natural rocks in contrast to Mohr-Coulomb criterion, which is applicable to soils and other granulates. The history of the development of Hoek-Brown criterion is found in Hoek et al. (2002) and Hoek and Marinos (2007).

The criterion firstly considers the properties of intact rock and then introduces reduction factors to yield rock mass parameters with the use of the GSI (Geological Strength Index). The values of GSI correspond to the degree of the jointing/ fracturing of rock mass and range from 1 for highly jointed and crushed rock to 100 for intact rock devoid of discontinuities (Hoek et al. 2002).

The generalized form of Hoek-Brown criterion for rock masses is given by Equation (3-6).

$$\sigma_1' = \sigma_3' + \sigma_c \left(m_b \frac{\sigma_3'}{\sigma_c} + s \right)^a \quad (3\text{-}6)$$

Where

σ_1' - major principal stress

σ_3' - minor principal stress

σ_c - uniaxial compressive strength (UCS) of the intact material, and

m_b - reduced value of material constant m_i, and is given by the following relation:

$$m_b = m_i \exp\left(\frac{GSI - 100}{28 - 14D} \right) \quad (3\text{-}7)$$

Where

D - disturbance factor

(*s, a*)- rock mass constants, given by the Equations (3-8) and (3-9);

$$s = \exp\left(\frac{GSI - 100}{9 - 3D} \right) \quad (3\text{-}8)$$

$$a = \frac{1}{2} + \frac{1}{6}\left(e^{-GSI/15} . - e^{-20/3} \right) \quad (3\text{-}9)$$

The uniaxial compressive strength of the rock mass is obtained by setting $\sigma_3'=0$ in Equation (3-6), and is:

$$\sigma_{cm} = \sigma_c s^a \quad (3\text{-}10)$$

The tensile strength can be determined as:

$$\sigma_t = -\frac{s\sigma_c}{m_b} \quad (3\text{-}11)$$

Since, in our case, this criterion was applied to a material equivalent to intact rock, that is, synthetic conglomerate, a GSI value of 100 was adopted along with the UCS and and intact rock E_i. The computer program RocLab1 (Rocscience 2008) was used to apply the Hoek-Brown criterion using uniaxial and triaxial testing data (given in Section 3.3). The criterion was applied using the lab data of the synthetic conglomerate and a value of material constant m_i = 24.14 was chosen as per material's characteristics. This value lies close within the value range of 21±4 for a natural conglomerate, as proposed by Rocscience 2008. However, the m_i value for conglomerates and breccias is variable and sensitive to the type of cementing material and degree of cementation (Brady & Brown 2005). At this value, Hoek-Brown parameters were determined together with the Mohr-Coulomb parameters. The results are given in Table 3-10 and curves are plotted in Figure 3-19a & b.

Table 3-10: Summary of Hoek-Brown and fitted Mohr-Coulomb parameters determined applying Hoek-Brown criterion at m_i=24.14.

Hoek-Brown classification	**Parameters**	**Lab Data (m_i=9.15)**	**Units**
Uniaxial compressive strength	σ_c	3.98	MPa
Geological strength index	*GSI*	100	
Material constant	m_i	24.14	
Disturbance factor	D	0	
Intact rock Young's modulus	E_i	1080	MPa
Hoek-Brown criterion			
Material constant	m_b	24.14	
HB constant	*s*	1.0	
HB constant	*a*	0.5	
Failure envelope range			
	Application	General	
Maximum minor principal stress	σ_3^{Max}	10	MPa
Mohr-Coulomb fit			
Cohesion	c	2.35	MPa
Angle of friction	ϕ	33.48	degrees
Rock mass parameters			
Tensile strength	σ_t	-0.16	MPa
Compressive strength	σ_c	3.98	MPa
Rock mass compressive strength	σ_{cm}	4.02	MPa
Rock mass modulus	E_{rm}	1074	MPa
	Sum square of errors[6]	6.33 (LEVENBERG-MARQUARDT 'best-fit' curve)	

[6] *"The value of sum square of errors is a measure of how well a strength criterion fits a given data set. It is equal to the sum of the square of the vertical distances of the given data points from the fitted curve. The goal of the curve fitting computation is to determine the strength envelope which minimizes the value of the Residuals"* (Rocscience 2010).

The curve of Mohr-Coulomb criterion, applied directly to suit the laboratory data, is also plotted in Figure 3-19 to show its deviation from the fitted Mohr-Coulomb curve. Both the actual laboratory data and mean values determined by statistical analyses of the data are also overlaid on the strength criteria curves.

The values of cohesion, angle of friction and tensile strength are 2.32 MPa, 33.48° and 0.16 MPa respectively. The fitted Mohr-Coulomb parameters for the synthetic conglomerate at a maximum confining pressure of 10 MPa are not the same as determined by directly applying Mohr-Coulomb criterion.

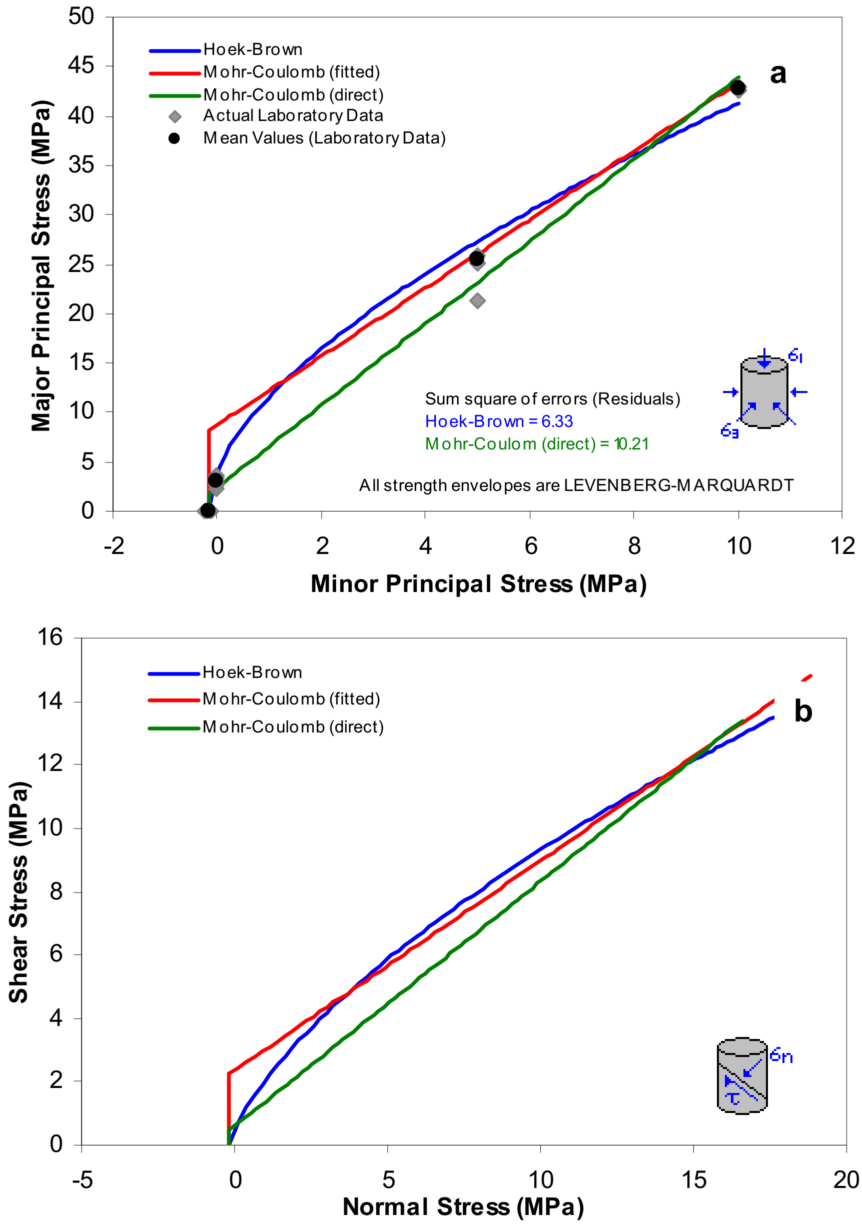

Figure 3-19: Plots showing Hoek-Brown and fitted Mohr-Coulomb criteria curves derived directly based on laboratory data (m_i =24.14); a) in major and principal stress space, b) in normal-shear stress field.

A sensitivity study was undertaken to gauge the variation of the cohesion and angle of friction from 0 to 15 MPa confining pressures. The outcome of the sensitivity study is illustrated in Figure 3-20. The sensitivity study showed that none of the confining pressures could produce the cohesion and angle of friction comparable to those obtained by directly applying Mohr-Coulomb criterion.

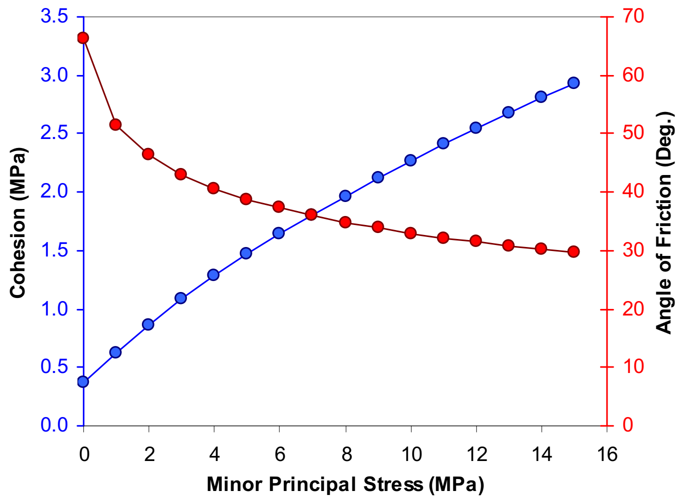

Figure 3-20: Sensitivity of cohesion and angle of friction with minor principal stress (σ_3).

3.4.2 Characterising the Progressive Damage in Uniaxial Testing

Progressive damage in uniaxial testing is indicative of deformation occurring at a microscopic scale and controls the macroscopic failure in a specimen. Micro deformation is associated with the distribution of micro cracks and the movement and interaction of mineral grains. In a conglomeratic rock consisting of macro clasts with interparticle cement, progressive damage is associated with the interaction and movement of the clasts, distribution of cement and clast-cement interface characteristics. Consequently, progressive failure in conglomerates is controlled by these factors.

Understanding the damage thresholds is important for understanding the mechanical response of a specific rock or a material. No attempt was made in the past to identify these damage stages in conglomerates. However, as part of the present research, it was planned to characterise the complete failure envelop from crack initiation to failure (exhibiting peak strength) of the synthetic conglomerate in uniaxial testing by AE monitoring and axial, radial and volumetric strains. And then to compare these stages with that of numerical simulations for a rigorous behavioural similarity.

Numerous researchers (e.g., Martin 1994; Eberhardt et al. 1998; Diederichs et al. 2004) have described the crack initiation parallel to axial loading in uniaxial and confined tests on hard rocks. These cracks initiate at a level of deviatoric stress of 1/4 to 1/2 of the rock rupture strength. At low stress levels, the cracks initiate within or at the boundary of the grains and propagate parallel to the principal stress to the nearest grain boundary. At higher stress levels, these cracks extend beyond the grain boundaries and coalesce to form long axial cracks at low confinements or a through-going shear rupture at high confining pressures (Diederichs 2000). The conceptual damage of a multi-crystalline rock under uniaxial conditions is shown in Figure 3-21, after Martin (1994).

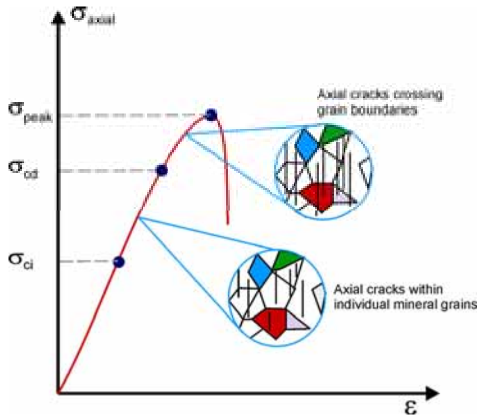

Figure 3-21: Progressive axial crack damage under uniaxial testing (modified after Martin 1994).

This progressive initiation and growth of cracks in a laboratory sample has been studied by numerous researchers (e.g., Eberhardt et al. 1998; Diederichs et al. 2004) who delineated the damage stages into definite stress stages whereby every stress stage corresponds to a definite damage threshold. Eberhardt et al. (1998) explained the methodology to identify these stages by the analysis of axial, radial and volumetric strains and acoustic emission monitoring. Later Diederichs et al. (2004) further explored this area using numerical modelling and provided a typical framework (Figure 3-22) of crack damage thresholds in uniaxial testing as being the function of axial, radial and volumetric strains and acoustic emissions.

3.4.2.1 Crack Closure (σ_{cc})

Crack closure is the point at which most existing, open and appropriately oriented fractures are effectively closed by the increasing axial stress. This is indicated by the change in the axial stress–strain curve from an incremental rate increase to a constant rate increase (linear elastic behaviour), that is, the stress-strain response is nonlinear and exhibits an increase in axial stiffness (deformation modulus). It is also often reflected in a cessation in initial acoustic emissions. The extent of this nonlinear region is dependent on the initial crack density and geometrical characteristics of the crack population. There is often an initial flurry of emissions due to seating and sample adjustment, as well as crack closure. Once the majority of pre-existing cracks have closed, linear elastic deformation takes place. The elastic constants (Young's modulus, Poisson's ratio) of the rock are calculated from this linear portion of the stress-strain curve.

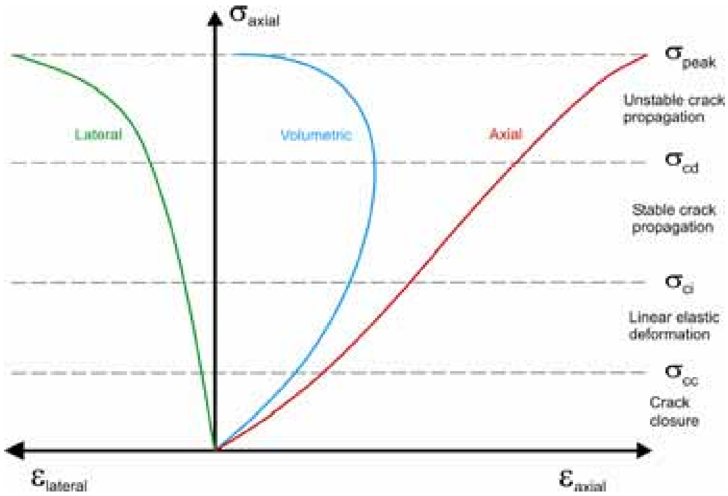

Figure 3-22: Damage thresholds corresponding to stages of stress-strains and acoustic response in uniaxial testing (modified after Diederichs et al. 2004).

3.4.2.2 Crack Initiation (σ_{ci})

Crack initiation represents the stress level where microfracturing begins and acoustic events rise above the background noise. This point can be marked as the point where the lateral and volumetric strain curves depart from linearity (Eberhardt et al. 1998). This point can be further categorised into two crack initiation stages (Figure 3-23): first crack and systematic crack initiation. "First crack" represents the first onset of distributed cracks in the sample that are not associated with the loading platens, while the "systematic initiation" of cracks represents the limit of new damage in a sample. This marks the onset of the ''continuous detection'' of AE and is reflected in a constant increased rate of cumulative acoustic counts with respect to applied axial stress (Diederichs et al. 2004).

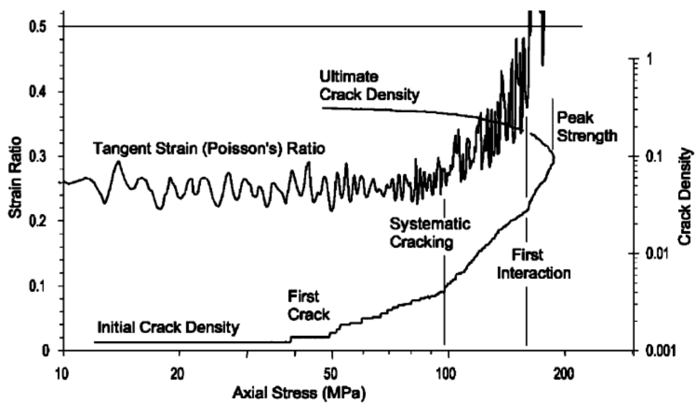

Figure 3-23: Change in axial to lateral strain ratio and crack density for a numerical simulation (after Diederichs et al. 2004).

3.4.2.3 Crack Coalescence (σ_{cs})

According to Diederichs et al. (2004) systematic crack initiation is followed by the crack coalescence or crack interaction; a point at which the stress-strain response becomes non-linear. This point can be schematically illustrated on a log (crack intensity)- log (stress) plot (Figure 3-24).

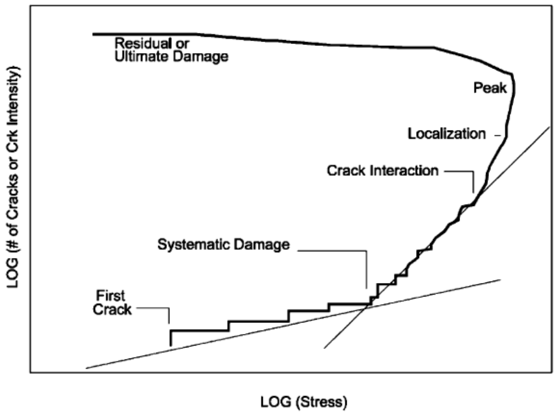

Figure 3-24: Schematic illustration of damage thresholds in crack density-stress space for a uniaxial test with AE monitoring (after Diederichs et al. 2004).

3.4.2.4 Crack damage (σ_{cd})

Crack damage is the final threshold prior to peak strength and can be identified by the reversal in the volumetric strain. Crack propagation can be either stable or unstable. Under stable conditions, crack growth can be stopped by controlling the applied load while unstable crack growth occurs at the point of reversal in the volumetric strain curve (crack damage) and is also known as the point of critical energy release (Martin 1993). Unstable crack growth continues to the point where the numerous micro cracks have coalesced and the rock can no longer support an increase in load. Martin (1993) noted that the peak strength of granite (including the uniaxial compressive strength in unconfined tests) is not a unique material property but is dependent on the loading rate. The localisation at this point can be viewed in Figure 3-24.

However, this threshold was not clearly identified by some researchers (e.g., Diederichs et al. 2004) in numerical simulations.

3.4.2.5 Peak Strength (σ_{Peak})

This is the point followed by crack damage threshold which exhibits the highest value along the stress-strain curve (Figure 3-22). In uniaxial compressive testing, this is referred to as the UCS (uniaxial compressive strength).

3.4.3 Damage Thresholds of Synthetic Conglomerates

Damage thresholds in uniaxial testing on synthetic conglomerate samples were identified with the help of strain gauge data and a number of acoustic events following the standard methodological steps for natural rocks (Eberhardt et al. 1998). It is not always straightforward to detect damage stages. Some of the challenges in this area have been discussed by Diederichs et al. (2004).

Radial strain (ε_{Radial}) and axial strain (ε_{Axial}) measured on each of the samples were averaged and volumetric strain (ε_{Vol}) was determined as per the following relation:

$$\varepsilon_{vol} = \varepsilon_{Axial} + 2\varepsilon_{Radial} \qquad (3\text{-}12)$$

The measured volumetric, radial and axial strains were plotted against the axial stress. Since acoustic events were monitored in time space and were plotted in the same graph using time as a second x-axis. Care was taken in identifying the tests' starting time and they were correlated with initial loads on the samples.

Acoustic events were measured using four sensors set two at 0.08 mV and two at 0.1 mV. Two sensors (each from both the thresholds) were attached near the top and the remaining two near the bottom of the samples with elastic bands. The recorded events with the sensor set at 0.08 mV were 2~10 times greater than those recorded with the sensor set at 0.1 mV. For uniformity in the plots, the events (from sensor 0.1 mV) were multiplied with a factor 2~10 that produced the events comparable to that of the sensor set at 0.08 mV.

The crack closure (σ_{cc}) was then identified as the point where the stress-strain curve becomes linearly elastic, that is, the first point of non-linearity in axial and radial strains (Figure 3-25). Since the samples' ends were made smooth, no major flurry in the acoustic events was recorded at this point. Some of the events recorded could be the sample-platens adjustment induced at this point.

After crack closure, a point of crack initiation (σ_{ci}) was identified where a significant number of initial events were recorded exhibiting new damage in the sample. As per the analyses of AE monitoring on all samples, 10-15 events on a sensor set at 0.08 mV, and 1-5 at a sensor set at 0.1 mV, were set as base line for this threshold in all the samples. In view of this criterion, together with the trend of axial and volumetric strains, a point of crack initiation was identified on a stress-strain curve (Figure 3-25).

In laboratory samples, stages of 'first crack" and "systematic crack growth" could not be separated as per Eberhardt et al. (1998) and Diederichs et al. (2004), but identified as a cumulative stage of crack initiation.

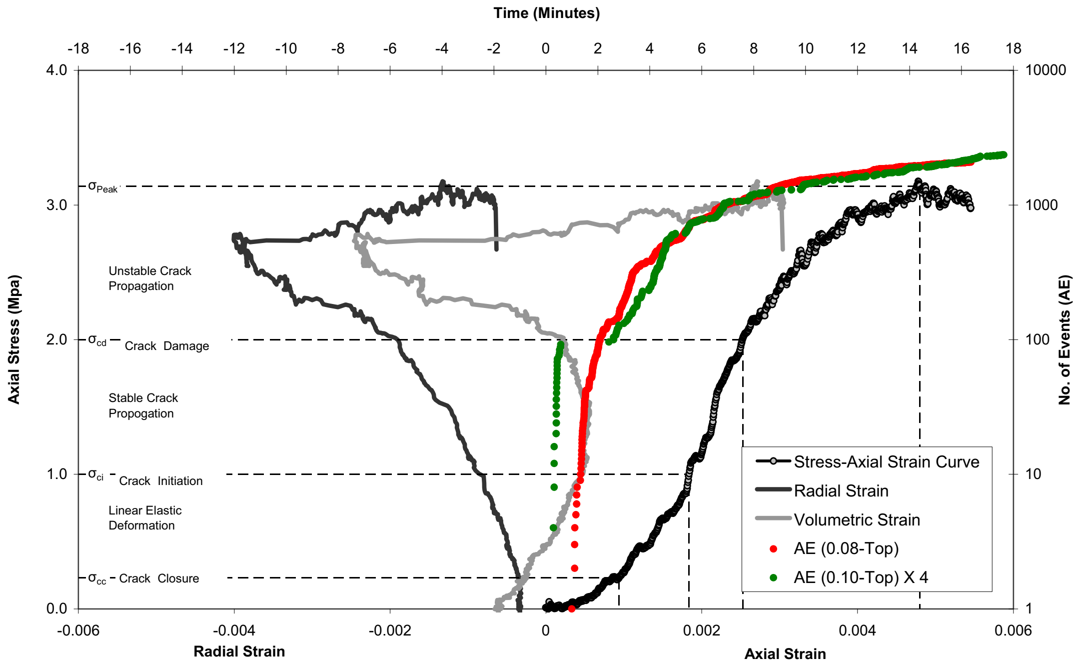

Figure 3-25: Stages of damage in synthetic conglomerate samples with the help of strain data and acoustic emission monitoring (modified after Akram & Sharrock 2009; 2010).

Crack initiation is followed by the systematic damage in a sample indicated as a progressive increase in the AE events. It was analysed as a stable and systematic growth of cracks along with the coalescence of cracks (σ_{cs}). Crack coalescence or crack interaction was not separately identified on the stress-strain curve but considered part of the systematic crack growth.

Crack damage (σ_{cd}) is an important stress threshold which is followed by unstable crack growth (Figure 3-25). At this point, the coalescence of the cracks turns into a macroscopic fracture initiation with a progressive incremental trend in AE events. The reverse trend in volumetric strain is another important indication at this point, together with the change of slope in axial and radial strain curves (Figure 3-25).

Crack damage is followed by an unstable growth of cracks resulting into macroscopic fracture propagation which extends to the sample surface showing maximum strength as peak strength (σ_{Peak}); the highest point on the stress-axial strain curve. Localised damage on the sample surface was observed to occur even before the peak strength, that is, fracture propagation through the strain gauge areas resulted into an abnormal increase in the radial strains (Figure 3-25).

A summary of stress stages corresponding to damage thresholds is given in Table 3-11 for all synthetic conglomerate samples loaded in uniaxial testing. The variability of these stages is also provided and expressed in standard deviation. It was observed that the closure of the micro cracks shows more variation and moves from 8% to 20% of peak strength in the synthetic conglomerate. Cracks initiate at 28-35% of peak strength which is followed by crack coalescence and interaction in the elastic deformation domain.

At approximately 65-70% of peak strength, synthetic conglomerate samples showed a crack damage stage which was followed by the unstable growth of cracks resulting in the plastic deformation in the samples. The crack damage stage gradually promoted the growth of the macroscopic cracks in the sample and ended into sample failure after showing the highest point (peak strength) along the stress-strain curve.

Table 3-11: Summary of stress stages corresponding to damage thresholds in synthetic conglomerate samples in uniaxial testing.

Stress states corresponding to damage thresholds	σ_{cc}	σ_{ci}	σ_{cd}	σ_{Peak}
Mean (MPa)	0.31	1.05	2.03	2.98
Standard deviation (%)	32.50	10.16	7.47	15.41
Mean % of Peak	11.07	32.84	68.31	100

3.4.4 Post Peak Behaviour

Post peak behaviour in all the uniaxial samples was observed as strain softening and ductile. This can be attributed to the presence of cementing material among the steel balls and the undulating fracture surface due to the steel balls. Post peak behaviour in shear box testing also resembles the uniaxial samples because of dilation and cement crushing.

Triaxial samples, in contrast, showed strain hardening behaviour due to presence of steel balls of higher stiffness and the crushing of the cement in the interstices. These responses can be observed in the test result curves for respective testing in Section 3.3.

3.4.5 Failure Modes

The failure mode of the synthetic conglomerate samples in the uniaxial testing was mainly axial splitting, that is, crack propagation from top to bottom and parallel to sub-parallel to the loading axis. This is a feature of some weak and ductile rock owing to very high dilation along the possible shearing plane. Post peak behaviour is also consistent with the determined mode of failure. This could be attributed to high dilation because of the steel balls and very weak cement paste. Generally Portland cement composites with fine grained materials, such as sands at a high water to cement ratio behave like semi brittle material (i.e., a material between soils and rocks) (Alonso et al. 2008).

The fracture traces on the uniaxial synthetic conglomerate samples were highlighted as colour lines and are shown in Figure 3-26.

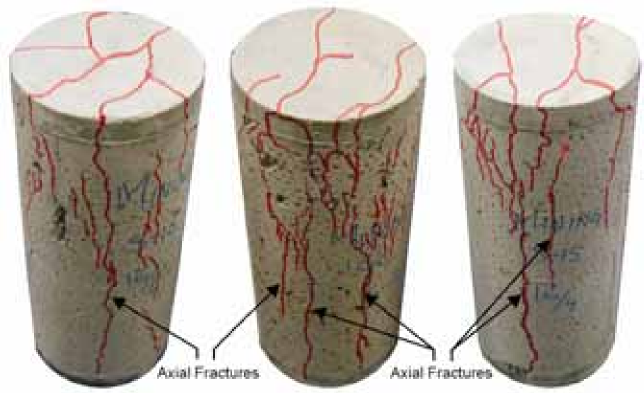

Figure 3-26: Failure modes (axial splitting parallel to loading axis) observed in uniaxial samples. Fracture traces are highlighted with colour lines.

In triaxial testing, the exact estimation of the samples' failure mechanism could not be made as samples lost complete cohesion during extraction from the Hoek cell. But a judgement of the failure mode was made by observing the extracted intact part of the synthetic conglomerate specimens. These remains did not show any axial crack through the sample or on the sample surface (Figure 3-27). Hence, it could be suggested that the sample under confinement showed a shift of failure mode from axial splitting to shear failure, or possibly the combination of the two. In the triaxial specimens, cement powder was also observed indicating cement crushing in confined loading.

In all Brazilian tensile tests on synthetic conglomerate, a well developed axial crack was observed through the specimen extending from top to bottom. This is the characteristic failure mode of a disc shaped specimen indicating, its tensile splitting (Figure 3-28).

In shear box tests, the samples showed a well developed failure surface through the samples dividing into two halves. But along this failure surface the presence of micro fractures and cohesion loss was also observed extending obliquely into the sample halves, indicating stress chains during the testing. A mechanism of cement crushing was also observed along the shearing surfaces of the samples (Figure 3-29).

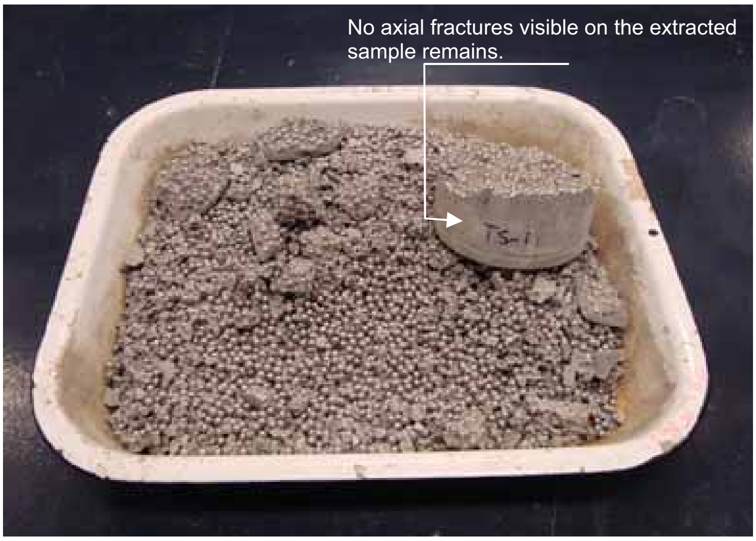

Figure 3-27: Triaxial synthetic rock specimen extracted from Hoek's cell.

Figure 3-28: Modes of Failure in Brazilian test samples after testing. Uniaxial samples are also present in the background.

Figure 3-29: Failure surface of the lower half of the shear box test synthetic rock specimen.

3.5 Mechanical Behaviour of Cement Paste and Derivation of Micro Parameters

An adequate number of tests were repeated for cement samples across each testing method. The test results yielded meaningful and representative parameters in each test indicating sufficient rigour and reliability in laboratory testing (Table 3-4). As discussed earlier, testing on cement paste samples was undertaken to acquire micro parameters for the numerical simulation of synthetic conglomerates. Cement paste is the interparticle cementing material in synthetic conglomerates. To simulate an equivalent synthetic conglomerate in a numerical simulation, micro mechanical parameters, such as shear and normal (tensile) strength and the shear and normal stiffness of the cement particle, are required.

Micro shear and normal strengths of the interparticle cement in numerical simulations are assumed to represent the macroscopic shear and tensile strength of the cement paste. Normal and shear stiffness is a function of the Young's modulus of the cement paste. Hence, laboratory data on cement samples was analysed to obtain the strength and elastic parameters of the cementing materials which would be the direct inputs of the micro parameters for onward numerical simulations in PFC3D. The steel ball parameters (density, shear modulus and Poisson's ratio) to be used for numerical simulation were also discussed.

Initially, the mechanical response of the cement paste was analysed by applying Mohr-Coulomb and Hoek-Brown criteria to determine the strength parameters, such as the cohesion and angle of friction of the cement paste.

3.5.1 Strength Criteria for Cement Paste

Mohr-Coulomb and Hoek-Brown criteria were applied, to obtain the strength parameters, on the test results of cement samples that characterise the strength and failure of Portland cement with a water-cement ratio (w/c) of 0.6.

Mohr's circles were plotted for mean values of uniaxial, triaxial and Brazilian test results in shear strength-normal stress space and strength parameters were obtained as c= 3.98 MPa and ϕ = 30.4°. The plot is shown in Figure 3-30.

Hoek-Brown criteria (Hoek et al. 2002) was also applied on the uniaxial, triaxial and Brazilian testing data of the cement paste using computer program RocLab 1.0 (Rocscience 2008). The material constant (m_i) of 9.15 was selected by Roclab to suit the laboratory data. At this value, Hoek-Brown parameters were determined together with the fitted Mohr-Coulomb parameters.

The results are given in Table 3-12 and curves are plotted in Figure 3-31a & b. In Figure 3-31a & b, both Mohr-Coulomb criterion curves, that is, direct and fitted on Hoek-Brown curves, are shown together with the laboratory data. The values of cohesion, angle of friction and tensile strength are 3.49 MPa, 34.04° and 1.37 MPa respectively. Although these values are comparable to the measured tensile strength, and Mohr-Coulomb parameters determined with Mohr-Coulomb criterion by drawing Mohr's circles, the values of cohesion and angle of friction were not close to the directly determined values. Therefore, a value 3.98 MPa of cohesion and a 30.4° angle of friction were selected, as they are the output from the direct application of the Mohr-Coulomb criterion on the laboratory data.

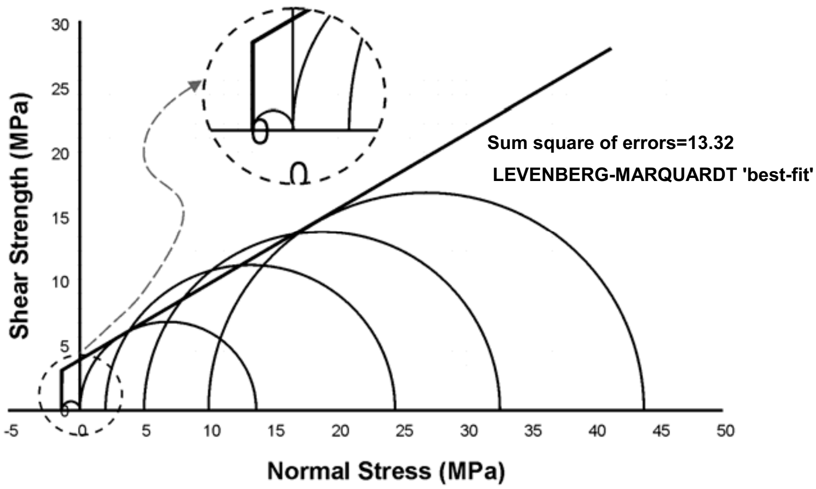

Figure 3-30: Plotting of uniaxial, triaxial and Brazilian results in shear strength-normal stress field to yield Mohr-Coulomb strength parameters (i.e., angle of internal friction of 30.4°, cohesion of 3.98 MPa and tensile cut-off at 1.36 MPa).

Table 3-12: Summary of Hoek-Brown and fitted Mohr-Coulomb parameters determined by applying Hoek-Brown criterion at m_i=9.15.

Hoek-Brown classification	**Parameters**	**Lab Data (m_i =9.15)**	**Units**
Uniaxial compressive strength	σ_c	12.55	MPa
Geological strength index	*GSI*	100	
Material constant	m_i	9.15	
Disturbance factor	D	0	
Intact rock Young's modulus	E_i	3180	MPa
Hoek-Brown criterion			
Material constant	m_b	9.15	
HB constant	*s*	1	
HB constant	*a*	0.50	
Failure envelope range			
	Application	General	
Maximum minor principal stress	σ_3^{Max}	10	MPa

Mohr-Coulomb fit			
Cohesion	c	3.49	MPa
Angle of friction	ϕ	34.04	degrees
Rock mass parameters			
Tensile strength	σ_t	-1.37	MPa
Compressive strength	σ_c	12.55	MPa
Rock mass compressive strength	σ_{cm}	11.60	MPa
Rock mass modulus	E_{rm}	3180	MPa
	Sum square of errors	14.96 (LEVENBERG-MARQUARDT 'best-fit' curve)	

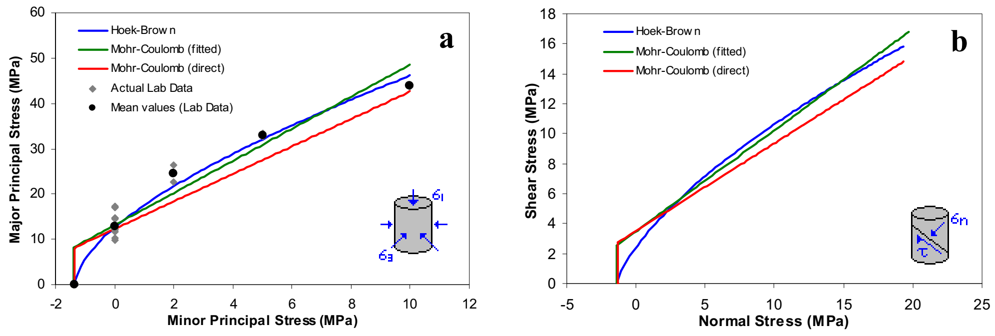

Figure 3-31: Plots showing Hoek-Brown and Mohr-Coulomb (both fitted and direct) criteria curves derived directly based on laboratory data (m_i =9.15); a) in major and principal stress space, b) in normal and shear stress field.

3.5.2 Derivation of Micro Parameters for Numerical Simulation

Micro-parameters required for numerical simulations are given in Table 3-13 and illustrated in Figure 3-32. A detailed discussion of these parameters is provided in Chapter 4.

Table 3-13: Summary of micro-parameters required for the numerical simulation of a synthetic conglomerate in PFC3D.

Type	Micro parameters
Parallel bond representing interparticle cement	Normal strength (MPa) of Parallel bond (cementing material)
	Shear strength (MPa) of Parallel bond (cementing material)
	Normal stiffness of Parallel bond (cementing material)
	Shear stiffness of Parallel bond (cementing material)
	Extent of cementing material (radius of Parallel bond)
Particles	Normal and shear stiffness (defined by Hertz-Mindlin contact law in terms of Poisson's ratio and shear modulus)
	Interparticle Friction
	Ball diameter (mm)
	Ball density (Kg/m^3)
	Poisson's ratio of balls
	Shear modulus of balls (MPa)
	Initial friction of balls

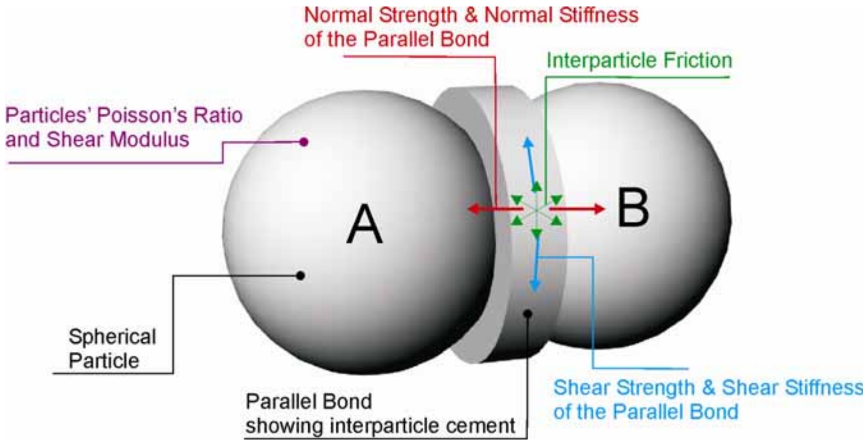

Figure 3-32: Schematic illustration of micro-parameters for a parallel bonded assembly i.e. an assembly whose grains are bonded with cementing material.

3.5.2.1 Cement based Parameters

- **Strengths of Parallel Bond (Interparticle Cement)**

The interparticle strengths of a parallel bond include the shear and normal strengths that interparticle cement can carry to hold the particles in shear and normal directions (Figure 3-32).

In the normal direction, a bond can be broken by applying force to separate the balls in opposite directions which refers to the tensile strength of the bond or cement and hence can be referred to as tensile strength of Portland cement paste. The tensile strength of the cement was obtained as 1.35 MPa in Brazilian testing. This much strength is required to break the cemented particles. But obviously the cross-sectional area of the Brazilian cement disc and Brazilian cemented granular disc would be different when incorporating the spherical surfaces of the particles embedded in the Brazilian disc.

Hence, to overcome this discrepancy, the number of particles that could fit into a Brazilian disc of the same dimensions (diameter and thickness) were counted, and half the surface areas of the counted balls were added to compute the actual cross-section of the Brazilian disc of cemented particles. The strength computed in the Brazilian disc was then divided by this area to achieve the tensile (normal) strength required to break the interparticle cement bond (Figure 3-33).

The adjusted value of normal strength was obtained as 1.5 MPa (Table 3-14). The shear strength of the Parallel bond was calculated from cohesion determined from Mohr-Coulomb parameters obtained by analysing the uniaxial and triaxial test results on cement. The adopted value of 3.98~4.0 MPa is given in Table 3-14.

Figure 3-33: Number of balls that can fit in a failure cross-sectional area of Brazilian cement specimens for the calculation of the inter-particle tensile strength of cementing material.

- **Stiffness of the Parallel Bond (Interparticle Cement)**

The normal and shear stiffnesses of the parallel bond are the elastic stiffness of cement in tension and shear and are specified in stress per unit displacement dimensions, that is, N/m^2.m. Normal stiffness is related to Young's modulus of the parallel bond as per the following relation (Itasca 2005);

$$\bar{k}^n = \frac{\bar{E}_c}{L} \qquad (3\text{-}13)$$

Where

$\bar{k}^n$ - normal stiffness of the parallel bond or cementing material.

$\bar{E}_c$ - modulus of the cementing material at particle contact (normally assumed to be the modulus of the cementing material).

L - length of the beam representing the parallel bond (equal to two times the radius of the particles for uniformly sized particles).

Both normal and shear stiffness were calculated from the Young's modulus of the cementing material for different size of particles using Equation (3-13) and are summarised in Table 3-14.. Shear stiffness was assumed to be equal to normal stiffness as there is no direct means to calculate the normal to shear stiffness ratio.

Table 3-14: Summary of cement based micro-parameters derived from testing on cement samples.

Description of parameters for the Parallel Bond (Cementing material)	Values
Normal strength (MPa)	1.50
Shear strength (MPa)	3.98
Normal stiffness of cement (Pa/m) (bond diameter = 4.75mm)	6.69e11
Shear stiffness of cement (Pa/m) (bond diameter = 4.75mm)	6.69e11
Normal stiffness of cement (Pa/m) (bond diameter = 6.34mm)	5.01e11
Shear stiffness of cement (Pa/m) (bond diameter = 6.34mm)	5.01e11
Normal stiffness of cement (Pa/m) (bond diameter = 6.34mm)	8.92e11
Shear stiffness of cement (Pa/m) (bond diameter = 6.34mm)	8.92e11

- **Radius of Parallel Bond (Extent of Inter-particle cement)**

The radius of the parallel bond refers to the extent of cementing material among the particles. In PFC, the extent of the cement is expressed by the radius of the parallel bond relative to particle radius. Figure 3-34a shows a real case with a certain extent of interparticle cement relative to the particle radius. This extent is simulated in PFC by the radius of the parallel bond, illustrated in Figure 3-34b. In the synthetic conglomerate with uniform sized particles, interparticle cement filled all the interparticle gaps among the particles, suggesting its extension is comparable to the particle size in a single bonded contact (Figure 3-34c). Therefore, the parallel bond's radius was kept equal to the radius of the particle (Figure 3-34c).

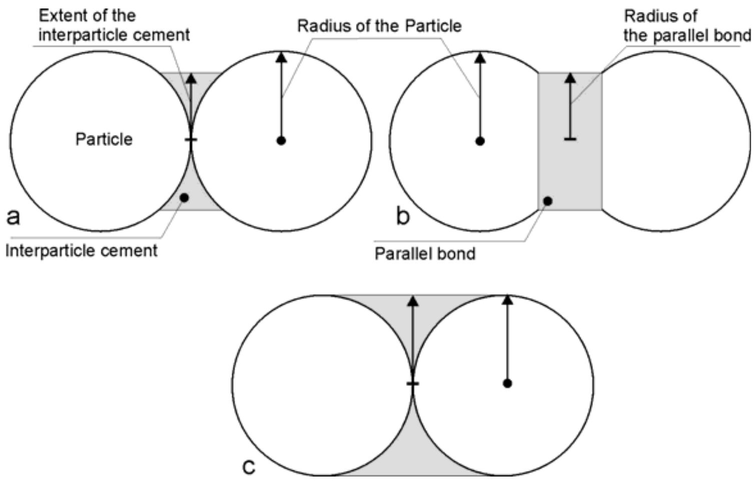

Figure 3-34: The conceptual illustration of the extent of the parallel bond in representing the interparticle cement: a) extent of interparticle in a real physical situation, b) representation of (a) in PFC, and c) the interparticle cement's extent comparable to the particle diameter in synthetic conglomerate (present research).

3.5.2.2 Particle Parameters

Particle parameters include physical parameters, such as density, radius, friction and elastic parameters, such as shear modulus and Poisson's ratio. Two sizes of steel balls 4.75 mm and 6.34 mm were used in the preparation of the conglomerates samples. The density of the balls was calculated 7800 kg/m^3. Initial particle friction was assumed to be 5.5° (after O' Sullivan & Bray 2002; O' Sullivan et al. 2004).

Shear modulus and Poisson's ratio were supplied by the ball supplier (Hooper Bearings Pty, Australia) and were used in the numerical simulations. In the numerical simulations, the Hertz-Mindlin contact stiffness model (Mindlin 1949; Mindlin & Deresiewicz 1953) was used to specify the non-linear stiffness of the particles. In Hertz-Mindlin contact model, the particles' normal and shear stiffness is specified with the shear modulus and Poisson's ratio of the particle materials. The relations of the particle stiffnesses and elastic parameters are described in detail in chapter 4.

All the particle based parameters are provided in Table 3-15.

Table 3-15: Summary of ball based parameters for numerical simulation.

Description of ball parameters	Values
Ball diameter (mm)	4.75 & 6.34
Ball density (Kg/m^3)	7800
Poisson's ratio of balls	0.30
Shear modulus of balls (GPa)	74.5
Initial friction of balls	5.5°

3.5.2.3 Specimen Properties

The specimen properties are the physical properties of the specimens prepared for a specific test and include the specimen dimensions and the porosity or number of balls. The main objective of the physical modelling was to prepare specimens with geometric properties that could be modelled numerically, with acceptable geometric similitude.

The numbers of balls were counted to fill the mould for a specific testing specimen and sample porosity was calculated by the total volume of all balls and the mould volume. Since uniformly sized particles were used in all the specimens; almost identical porosity (39.7%) was achieved. The number of balls, porosity and the specimen dimensions for uniaxial/ triaxial, Brazilian and shear box testing specimens are summarised in Table 3-16.

Table 3-16: Summary of physical properties of testing specimens.

Description of properties	Uniaxial/ triaxial	Brazilian test	Shear box test
Sample diameter/ length (mm)	94	94	100
Sample width (mm)	-	-	100
Sample height/ thickness (mm)	188	47	36
Sample porosity (%)	39.7	39.7	39.7
Number of balls	14000~14020	3500~3515	3840~3865
Number of balls (diameter 6.34 mm)	5890~5905	-	-

3.6 Summary and Conclusions

Synthetic conglomerate samples were prepared with steel balls (diameter 4.75mm and 6.34mm) as clasts and Portland cement paste as the cement matrix. The sample diameter (or least dimension) to steel ball diameter ratio of 15~21 was maintained in meeting the ISRM testing requirements. A consistent water cement ratio (w/c) of 0.6 was adopted in the preparation of synthetic conglomeratic and cement samples. All the samples were prepared and cured carefully to obtain the reproducibility of the test results. Cement samples were tested in uniaxial, triaxial and Brazilian tensile testing to determine the strength and elastic parameters of the cementing material (cement paste). Synthetic conglomerate samples were tested in uniaxial, triaxial, Brazilian and shear box testing to record the response of synthetic material under various loading conditions.

The synthetic conglomerate samples showed a good reproducibility of the test results in uniaxial, triaxial and shear box testing. However, in the Brazilian tensile testing results variability was observed with standard deviation of about 30% which was considered to be associated mainly with the composite nature of the samples with a very weak cement matrix. In addition, a thin layer of cement paste at the top of the Brazilian samples was also considered to be a possible factor inducing variability in the determined tensile strength.

The mechanical response of the synthetic conglomerate showed a sufficient behavioural similitude and a good correspondence with that of natural conglomerates.

In uniaxial loading, the response of the synthetic conglomerate in all samples was observed as ductile and strain softening, exhibiting an axial splitting mode of failure. The ductile behaviour of uniaxial samples was considered because of high dilation induced by the steel balls, which are rigid and all deformation is occurring at their contact points. A careful observation was made on the failure surfaces of the uniaxial samples. It was noted that the predominant failure in all the samples was along the particle-cement interface, that is, along particle boundaries. This observation indicated that the particle-cement interface strength was lower than that of the cement matrix in the synthetic conglomerates. This suggests that the interface strength is an important parameter that controls the behaviour of coarse grained rocks, such as conglomerates, and is generally lower than the strength of cement matrix. This is also consistent with the findings of Savanick and Johnson (1974) on natural conglomerates. Additional discussion regarding the damage observation of the synthetic conglomerate samples and role of interface strength is included in the Chapter 7.

The Young's modulus of the synthetic conglomerate was found to be approximately one third of that of cement matrix. It seems that the modulus of the assembly is a function of the elasticity of the cement matrix and the micro structure, that is, particle size and fibre. By changing the particle size from 4.75 mm to 6.34 mm, a decrease in the Young's modulus was noted. This decrease in modulus was considered because of the change in the micro structure, as cement and particle properties were same in both conglomerates.

The acoustic emission monitoring helped to understand and identify the stages of the progressive damage in the synthetic conglomerate in relation to axial stress and strains (axial, radial and volumetric). These stages were found similar to that of fine grained natural rocks (e.g., Martin 1993; Diederichs 2000; Diederichs et al. 2004). AE monitoring on synthetic conglomerate samples proved to be a very useful technique to characterise progressive damage and could be used in the research of natural conglomerates rocks.

Similar to natural rocks, an increase in the strength and modulus of the synthetic conglomerate was noted with the increase of confining pressure. However, a gradual transition of the failure mechanism from strain softening to strain hardening was noted with the increase of confining pressure, that is, from uniaxial conditions to triaxial conditions. This strain hardening effect was considered to be because of the high strength steel particles glued with very weak cement matrix. In the initial stage of triaxial loading, applied load was carried by both particles and interparticle cement. However, when the applied load exceeded the strength of synthetic conglomerate resulting into failure, the particles were stressed additionally by crushing the cement matrix. At this stage, the applied load was carried mostly by the particles resulting in strain hardening behaviour.

The crushing of cement matrix among the steel particles was observed in triaxial as well as shear box test specimens. It was hypothesised that this cement crushing might have significant effect on the elastic response of the synthetic conglomerates. Thus the presence of cement matrix is not only important in controlling the strength and elasticity of the synthetic conglomerate in the pre-peak region but also contribute to the post peak mechanism of deformation.

In the Brazilian tests, a distinct crack through the samples was obtained indicating a perfect tensile failure. In shear box testing, the vertical dilation was found greater than the angle of internal friction owing to presence of steel balls along the shearing surface. The angle of friction calculated in the shear box was found to be the same as observed in the analysis of uniaxial and triaxial shear box tests indicating a very good correspondence between the uniaxial and triaxial, and shear box tests. The shear box test specimens also clearly indicated the phenomenon of cement crushing along the shearing similar to triaxial testing. This phenomenon was anticipated in natural clast-supported conglomerates, where clastic materials had high strength and elasticity compared to the cement matrix. Hence, in a natural conglomerate material, cement matrix not only affects the strength and deformation but also has significance in controlling the mode of deformation.

The laboratory tests' results were also analysed for the macroscopic response of synthetic conglomerate. Mohr-coulomb and Hoek-Brown strength criteria were applied to uniaxial, triaxial and Brazilian tests to determine the strength and elastic parameters. Hoek-Brown criterion was observed to be more suitable in predicting the strength of the synthetic conglomerate. The material's constant of synthetic conglomerate was found to resemble those of the natural conglomerates.

Laboratory test results on cement paste samples were analysed to derive the strengths and stiffnesses of the cementing material to be input as micro parameters for a parallel bond in PFC3D simulation. Bond normal (tensile) strength was obtained from Brazilian tests on cement and adjusted to incorporate the effect of the balls' surface areas that could fit in the cross-sectional area of the sample disc. Bond shear strength was considered to be the cohesion of the cement obtained from the analysis of the uniaxial and triaxial test results on cement. Normal and shear stiffnesses were determined from Young's modulus of the cement.

Besides the cement parameters, a summary of the particle properties supplied by the ball supplier was also provided which includes ball diameters, density, friction, shear modulus and Poisson's ratio. A summary of specimen dimensions, porosity and number of balls used in each specimen, was also provided.

All the known and derived parameters are to be used in numerical simulation using PFC3D computer code. The details of numerical simulations are discussed in Chapter 4.

Numerical Simulation: Diagenesis, Testing and Analyses

4.1 Introduction

Numerical simulation is a central part of the present research and a vital tool for investigating the mechanics of conglomerates coupled with physical modelling. Numerical simulations were aimed at addressing two main objectives: firstly, to correlate the response of a numerical conglomerate to that of a synthetic conglomerate in order to examine the capability of the parallel bond to represent real life interstices cement, and secondly, to study the macroscopic behaviour of the idealised conglomeratic rock for the sensitivity of various factors – a study which is impossible in physical tests on natural conglomerates.

Numerical modelling was conducted to simulate and test conglomeratic samples using “Particle Flow Code” commonly known as PFC (Itasca 1987). PFC is available in 2D (PFC2D) and 3D (PFC3D) (Itasca 2004; 2005). Alternative discrete particle formulations published by several researchers are discussed in Chapter-2. PFC was selected due to its previous applications in rock mechanics (e.g., Konietzky 2002; Shimizu et al. 2004) and its flexibility in writing algorithms (in FISH language) for modelling complex geometries and problems. PFC has also been used in the past for the simulation of laboratory testing on various natural and synthetic rocks (e.g., Gil et al. 2005; Holt et al. 2005)

Numerical simulations to represent and test conglomerate samples were performed using PFC3D, inputting micro parameters and sample geometries derived from physical experiments (Chapter 3) for uniaxial, triaxial, Brazilian and shear box testing. The macroscopic response was monitored in all the numerical tests together with the sensitivity of various micro and macro parameters. The test results were then analysed to develop correlations with the synthetic conglomerate and to test the applicability of the investigated responses of the idealised conglomerate into a coherent conclusion, applicable to a natural conglomerate.

This chapter presents the numerical simulation techniques, numerical testing and analyses of the test results, while the comparison of and a detailed discussion on the macroscopic response of the numerical conglomerates are in the following chapter (Chapter 5).

This chapter firstly provides an introduction to PFC and then discusses the standard procedures adopted for specimen diagenesis and numerical testing for various test environments. Parametric sensitivity studies conducted during numerical simulations are presented together with the analyses of the test results, for their onward correlation with the synthetic conglomerates.

4.2 Formulation of Particle Flow Code (PFC)

In PFC a material can be simulated by circular discs (PFC2D) and spheres (PFC3D) bonded at their contacts with a defined set of parameters. In general, three main types of objects are used in PFC; the primary material constituent that occupies volume and has mass is represented as “particles”. The particles can be cemented together with “bonds”. Finally, “walls” provide a boundary for sample generation or for applying surface stresses on the specimen. By using microscopic input parameters for particle geometries in PFC, the macroscopic behaviour of physical specimens is represented.

In PFC, contacts are formed and broken automatically during the course of a simulation, and micromechanical rules are repeatedly updated by a time-stepping algorithm. At the start of each time-step, contacts are updated from the known particle and wall positions. The force-displacement law updates contact forces according to the relative motion between particles and the contact constitutive model. Particle accelerations are computed according to the resultant force and the moment acting on the particle.

Some of the basic assumptions in PFC are (Potyondy & Cundall 2004):

- The particles are circular (2D) or spherical (3D) rigid bodies with a finite mass.
- The particles interact only at contacts, which, because the particles are circular or spherical, are exactly between two particles.

- The particles are allowed to overlap and the force is given by this overlap. This overlap is much smaller in relation to the sizes of the interacting particles, that is, maximum allowed overlap is 10% of the mean particle diameter of the two contacting particles.
- Bonds can exist at contacts, carry a load and can break. The bonds representing interstices cement, that is, the parallel bonds establish an elastic interaction between particles that acts in parallel with the particle-based portion of the force-displacement behaviour. The particles at a bonded contact need not overlap.
- Generalized force-displacement laws at each contact relate relative particle motion to force and moment at contact.

The deformation of a frictional granular assembly such as sand is described well by the assumption of particle rigidity, because deformation results primarily from the sliding and rotation of particles as rigid bodies and the opening and interlocking at interfaces rather than from individual particle deformation. The addition of parallel bonds between the particles in the assembly corresponds to the cementation between the grains of a sedimentary rock, such as conglomerate or sandstone. Hence, conglomeratic rocks can be well represented by rigid particles and parallel bonds where cement strength is much lower than the strength of the particles. However, this assumption is not valid when modelling conglomerates with particles whose properties are comparable to that of cement, as deformation is likely in both particles and interparticle cement. Therefore, the deformation characteristics of the particles need to be specified (such as by the Hertzian model for elastic deformation) in modelling such rocks.

In PFC, the deformation of a bonded particle assembly exhibits damage formation processes (induced by contact forces) that are similar to granular rock under an increasing load where the bonds are broken and gradually evolve toward a granular state (Potyondy & Cundall 2004).

4.2.1 Particle-Particle Behaviour

There are two ways to treat contact deformation in PFC, namely linear and Hertzian.

4.2.1.1 Linear Contact Theory

In linear contact theory the contacts between the particles are represented by springs with prescribed normal and shear stiffnesses (Figure 4-1)

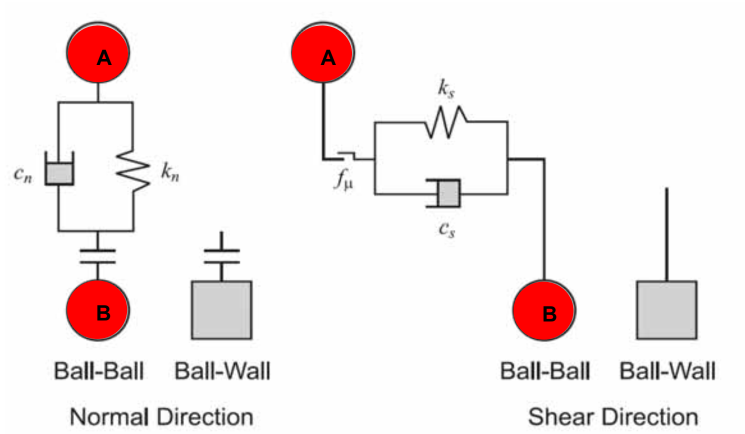

Figure 4-1: A conceptual representation of a linear spring contact model between ball-ball and ball- wall in normal and shear direction (Itasca 2005).

In the linear contact model, contact forces are described by a force-displacement law between two objects (particle-particle or particle-wall). For a particle-particle contact, the total force and moment acting at each contact is comprised of a force, $\vec{F}_i$, that arises from the particle-particle overlap (Figure 4-2). When two particles have a finite overlap (U_i^n in Figure 4-2), a contact is formed at the centre of the overlap region along the line joining the particle centres (x_i^c in Figure 4-2), and two linear springs are inserted that act in series.

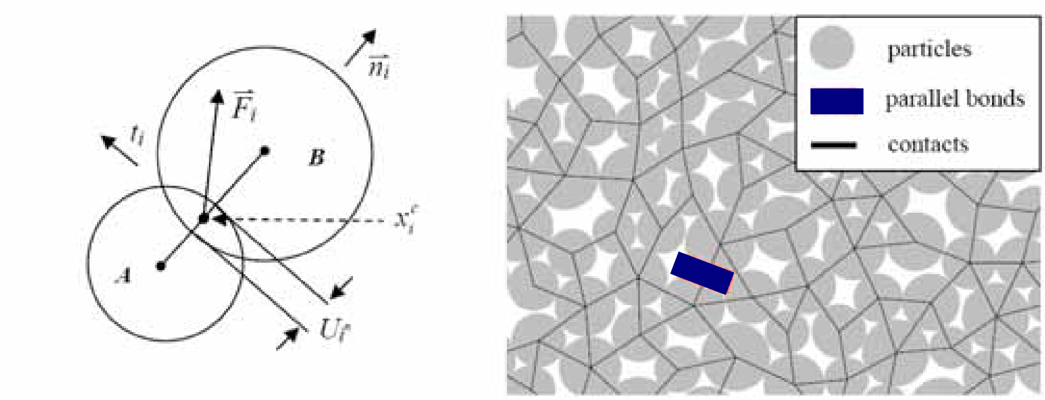

Figure 4-2: Force- displacement law in particle-particle contact (after Potyondy & Cundall 2004)

The spring stiffnesses correspond to the stiffness assigned to the given particles. The contact force vector $\vec{F}_i$, that represents the action of particle A on particle B, can be resolved into normal and shear components with respect to the contact plane as:

$$\vec{F}_i = \vec{F}_i^n + \vec{F}_i^s \qquad (4.1)$$

Where

$\vec{F}_i^n$ - normal force component

$\vec{F}_i^s$ - shear force components, and subscript "i" denotes the i[th] particle.

The normal force is given by:

$$\vec{F}_i^n = K_i^n U_i^n \vec{n}_i \qquad (4.2)$$

Where

K_i^n - normal stiffness [force/displacement] at the contact, and

$\vec{n}_i$ - unit normal vector.

The shear force is computed in an incremental fashion. When the contact is formed, the total shear contact force $\vec{F}_i^s$, is initialized to zero. Each subsequent relative shear-displacement increment ΔU_i^s, results in an increment of elastic shear force $\Delta\vec{F}_i^s$, that is added to the total shear contact force. The increment of elastic shear force is given by:

$$\Delta\vec{F}_i^s = -K_i^s \Delta U_i^s = -K_i^s \vec{V}_i^s \Delta t \qquad (4.3)$$

Where

K_i^s - shear stiffness [force/displacement] at the contact,

$\vec{V}_i^s$ - shear component of the contact velocity vector, and

Δt - an increment of time.

The contact stiffnesses relate to the contact forces and relative displacements in normal and shear directions, as represented by equations (4.2) and (4.3). The contact stiffnesses for the linear contact model are computed assuming that the stiffnesses of the two contacting entities act in series. The contact normal stiffness is given by

$$K^n = \frac{k_n^{[A]} k_n^{[B]}}{k_n^{[A]} + k_n^{[B]}} \qquad (4.4)$$

Similarly, the contact shear stiffness is given by:

$$k^s = \frac{k_s^{[A]} k_s^{[B]}}{k_s^{[A]} + k_s^{[B]}} \qquad (4.5)$$

Contact normal stiffness is the secant stiffness while contact shear stiffness is the tangent stiffness.

4.2.1.2 Hertz-Mindlin Contact Theory

Hertz Mindlin contact theory (after Mindlin 1949) derived from the elastic deformation of contacting deformable spheres, specifies the non-linearity of the stiffness of the deformable entities. Since, in the present study, original steel spheres bonded with cement were tested, it was appropriate to use Hertz-Mindlin contact theory in the PFC simulations to define the contacts between the particles.

In this theory, normal stiffness is defined by:

$$K^n = \left(\frac{2\langle G \rangle \sqrt{2\widetilde{R}}}{3\left(1 - \langle \nu \rangle\right)} \right) \sqrt{U^n} \qquad (4.6)$$

Where

G - shear modulus

ν - is the Poisson's ratio of the two entities, and

$\widetilde{R}$ - geometric constant related to particles' radii, as per Equation (4.8).

Contact normal stiffness is the secant stiffness while contact shear stiffness is the tangent stiffness and is given by:

$$k^s = \left(\frac{2\langle G \rangle^2 3\left(1 - \langle \nu \rangle\right)\widetilde{R}}{2 - \langle \nu \rangle} \right)^{1/3} \left| F_i^n \right|^{1/3} \qquad (4.7)$$

Where

U^n - ball overlap, and

F_i^n - magnitude of the normal contact force.

The multipliers in both equations above are geometric and the properties of the materials of the two contacting bodies (i.e., ball-ball, and ball-wall) are given by:

$$\widetilde{R} = \frac{2R^{[A]}R^{[B]}}{R^{[A]} + R^{[B]}}$$

$$\langle G \rangle = \frac{1}{2}\left(G^{[A]} + G^{[B]}\right) \qquad \text{(ball to ball)} \qquad (4.8)$$

$$\langle \nu \rangle = \frac{1}{2}\left(\nu^{[A]} + \nu^{[B]}\right)$$

Subscripts A and B denote the two balls or particles in contact.

$$\widetilde{R} = R^{[ball]}$$
$$\langle G \rangle = \langle G \rangle^{[ball]} \qquad \text{(ball to wall)} \qquad (4.9)$$
$$\langle \nu \rangle = \langle \nu \rangle^{[ball]}$$

For the Hertz model, the normal-secant stiffness K^n is related to the normal-tangent stiffness k^n by the following relation, while K^n can be determined by Equation (4.6):

$$k^n \equiv \frac{dF^n}{dU^n} = \frac{3}{2} K^n \qquad (4.10)$$

4.2.1.3 Slip Model and Interparticle Friction

A value of interparticle friction in terms of a frictional coefficient is specified to define the slip along unbonded particles (after the breakage of bonds). The slip on contacts occurs when the magnitude of the resolved shear force exceeds the frictional strength. The slip model, acting in parallel with granular behaviour, provides no normal strength in tension and allows slip to occur by limiting the shear force. If the overlap is less than or equal to zero ($U^n \le 0$, i.e. a gap exists), both normal and shear forces are set to zero, otherwise, slip is accommodated by computing the contact friction coefficient:

$$\mu = \min\left(\mu^{[A]}, \mu^{[B]}\right) \qquad (4.11)$$

The contact is checked for slip conditions by calculating the maximum allowable shear contact force:

$$F^s_{\max} = \mu \left| F^n_i \right| \qquad (4.12)$$

If $F^s_i > \left| F^s_{\max} \right|$, slip is allowed to occur during the next calculation cycle by setting:

$$F^s_i = \mu F^n_i \qquad (4.13)$$

4.2.2 Particle-Cement Behaviour

There are two bonding models, the Contact Bond Model and the Parallel Bond Model, in PFC that can be applied by specifying definite values of strengths to simulate a cemented assembly. These models display different characteristics when transferring forces and moments among the particles. A brief discussion on these models is given in the following sections.

4.2.2.1 Contact Bond Model

The contact bond reproduces the effect of adhesion acting over the vanishingly small area of the contact point. It can be envisioned as a pair of elastic springs (or a point of glue) with definite values of normal and shear stiffnesses and specified strengths (Itasca 2005). The existence of a contact bond precludes the possibility of slip, that is, the magnitude of the shear contact force is not adjusted to remain less than the allowable maximum of Equation (4.12). Instead, the magnitude of the shear contact force is limited by the shear contact bond strength. Contact bonds also allow tensile forces to develop at a contact. These forces arise from the application of Equation (4.2) when there is no overlap (i.e., $U^n < 0$). In this case, the contact bond acts to bind the balls together (Itasca 2005).

The magnitude of the tensile normal contact force is limited by the normal contact bond strength. If the magnitude of the tensile normal contact force equals or exceeds the normal contact bond strength, the bond breaks, and both the normal and shear contact forces are set to zero. If the magnitude of the shear contact force equals or exceeds the shear contact bond strength, the bond breaks, but the contact forces are not altered, provided that the shear force does not exceed the friction limit and provided that the normal force is compressive (Itasca 2005).

The constitutive behaviour relating the normal and shear components of the contact force and the relative displacement for particle contact occurring at a point is shown in Figure 4-3. Since, the contact bond was not used to bond the assembly in the present research, it will not be discussed further.

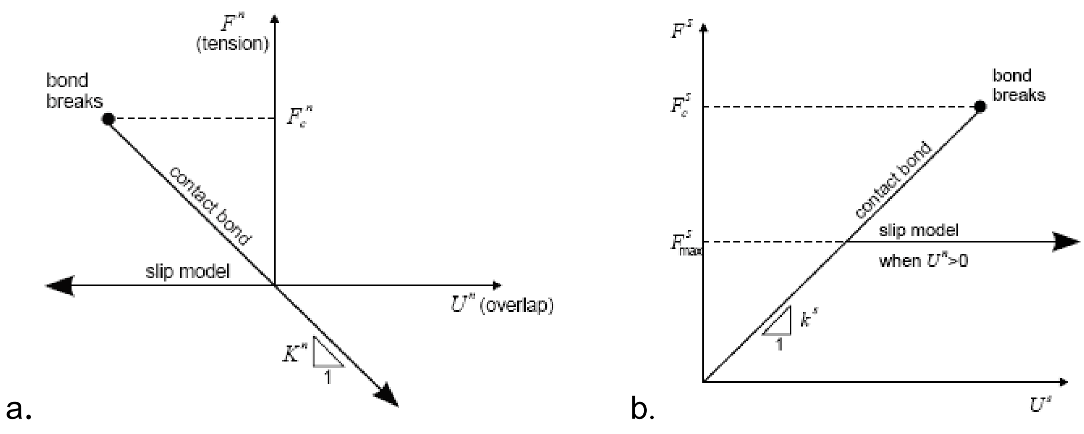

Figure 4-3: Constitutive behaviour for contact occurring at a point; a) Normal component of contact force; b) Shear component of contact force (after Itasca 2004; 2005).

4.2.2.2 Parallel Bond Model

The parallel bond reproduces the effect of additional material (e.g., cementation) deposited when particles are in contact. The parallel bond model was considered appropriate and is of particular interest in the present study, and is described here.

Parallel bonds approximate the mechanical behaviour of brittle elastic cement joining two bonded particles. Parallel bonds establish an elastic interaction between these particles that act in parallel with the particle-based portion of the force-displacement behaviour. Thus, the existence of a parallel bond does not prevent slip. Parallel bonds can transmit both force and moment between particles, while particles can transmit only force. A parallel bond can be envisioned as a set of elastic springs uniformly distributed over a rectangular cross-section in PFC2D, and a circular cross-section in PFC3D lying on the contact plane and centred at the contact point.

Relative motion at a contact causes a force and a moment to develop within the bond material as a result of the parallel bond stiffnesses. These forces and moments acting on the two bonded particles are related to the maximum normal and shear stresses acting within the bond material. If either of these maximum stresses exceeds its corresponding bond strength, the parallel bond breaks, representing the development of a crack. The following five microscopic input parameters are used to describe the cement-like behaviour of parallel bonds: normal and shear stiffness per unit area, $\bar{k}_n$ and $\bar{k}_s$; tensile and shear strengths, $\bar{\sigma}_c$ and $\bar{\tau}_c$; and a parallel bond radius multiplier, $\bar{\lambda}_c$, such that the parallel bond radius is:

$$\bar{R} = \bar{\lambda}_c \min(R^{[A]}, R^{[B]}) \qquad (4.14)$$

Where,

$R^{[A]}$ - radius of particle “A”.

The total force and moment associated by the parallel bond are denoted by $\bar{\vec{F}}_i$ and $\bar{\vec{M}}_i$, respectively, which represent the action of the bond on particle B of Figure 4-4. Each of these vectors can be resolved into normal and shear components with respect to the contact plane as;

$$\begin{aligned} \bar{\vec{F}}_i &= \bar{\vec{F}}_i^n + \bar{\vec{F}}_i^s \\ \bar{\vec{M}}_i &= \bar{\vec{M}}_i^n + \bar{\vec{M}}_i^s \end{aligned} \qquad (4.15)$$

Where

$\bar{\vec{F}}_i^n$ - normal force

$\bar{\vec{F}}_i^s$ - shear force

$\bar{\vec{M}}_i^n$ - normal moments

$\bar{\vec{M}}_i^s$ - shear moments.

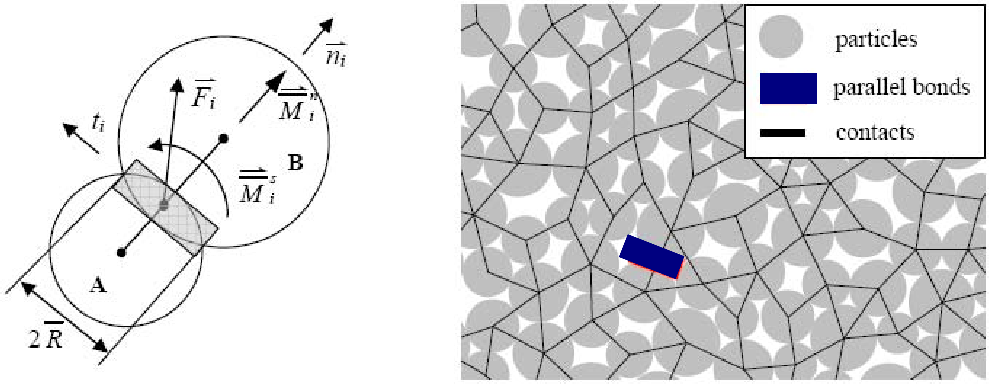

Figure 4-4: Force-displacement law in a particle-cement system (after Potyondy & Cundall 2004)

When a parallel bond is formed, $\bar{\vec{F}}_i$ and $\bar{\vec{M}}_i$ are initialized to zero. Each subsequent relative displacement or rotation increment at the contact produces an increment of elastic force and moment that is added to the current values.

The increments of the elastic force and moment over a time-step of Δt are given by:

$$\begin{aligned}
\Delta\bar{\vec{F}}_i^n &= (-\bar{k}_n A \Delta U_i^n)\vec{n}_i \\
\Delta\bar{\vec{F}}_i^s &= -\bar{k}_s A \Delta U_i^s = -\bar{k}^s A \vec{V}_i^s \Delta t \\
\Delta\bar{\vec{M}}_i^n &= (-\bar{k}_s J \Delta\theta_i^n)\vec{n}_i \\
\Delta\bar{\vec{M}}_i^s &= -\bar{k}_n I \Delta\theta_i^s = -\bar{k}_s I(\varpi_i^{[A]} - \varpi_i^{[B]})\Delta t
\end{aligned} \qquad (4.16)$$

Where

A - bond cross-section area

J - polar moment of inertia of parallel bond

I - moment of inertia of parallel bond

θ - increment of rotation, and

ϖ - rotational velocity.

These quantities are given by:

$$
\begin{aligned}
&A = 2\overline{R}t \\
&J = N / A \qquad \text{(PFC2D)} \qquad\qquad (4.17) \\
&I = \frac{2}{3}\overline{R}^3 t
\end{aligned}
$$

Where

t - thickness of the disc.

$$
\begin{aligned}
&A = \pi\overline{R}^2 \\
&J = \frac{1}{2}\pi\overline{R}^4 \qquad \text{(PFC3D)} \qquad\qquad (4.18) \\
&I = \frac{1}{2}\overline{R}^4
\end{aligned}
$$

The maximum tensile and shear stresses acting on the parallel bond are calculated by the beam theory to be:

$$
\begin{aligned}
&\overline{\sigma}_{\max} = \frac{-\overline{\overline{F}}^n}{A} + \frac{\left|\overline{\overline{M}}_i^s\right|}{I}\overline{R} \\
&\overline{\tau}_{\max} = \frac{\left|\overline{\overline{F}}_i^s\right|}{A} + \frac{\left|\overline{\overline{M}}_i^n\right|}{J}\overline{R}
\end{aligned}
\qquad\qquad (4.19)
$$

If the maximum tensile stress exceeds the tensile strength $(\overline{\sigma}_{\max} \geq \overline{\sigma}_c)$ or the maximum shear stress exceeds the shear strength $(\overline{\tau}_{\max} \geq \overline{\tau}_c)$, the parallel bond breaks and its contributions to force and moment are no longer considered.

4.3 Preparation of Numerical Conglomerate Samples

PFC can be used to represent the rock or cohesive-frictional material by generating dense particles and installing parallel bonds among the particles' contacts. In PFC2D, circular discs and in PFC3D, spherical particles can be used to represent rock or rock like materials. Since in this study, the synthetic conglomerate was formed using uniformly sized steel balls and Portland cement, it was deemed appropriate to use PFC3D to generate identical particles to produce a similar numerical conglomerate. In PFC3D, conglomeratic samples were prepared for uniaxial, triaxial, Brazilian tensile and shear box testing at the same porosity obtained from the corresponding synthetic conglomeratic specimens.

The standard specimen procedures (Potyondy & Cundall 2004; Itasca 2005) were followed with some modifications (as per the process followed in the physical laboratory to the fabricate the synthetic conglomerate) to generate numerical conglomeratic samples. The procedural steps in the generation of the specimen are described below:

4.3.1 Particle Generation

A uniformly sized array of elastic particles, initially at half of their final sizes were generated inside rectangular or cylindrical containers bounded by frictionless walls (Figure 4-5a). The sizes of the created particles were then increased to their final sizes and the required porosity was obtained as per the synthetic conglomerate. Subsequently, the initial friction coefficient for interparticle friction, and the density of the particles were specified. The particles were then provided with the shear modulus and Poisson's ratio to implement a Hertz-Mindlin contact model representing the physical laboratory. The program was run for a definite number of cycles to minimize any unbalanced force. Finally, standard gravity was specified to represent the physical laboratory process for particle packing.

4.3.2 Isotropic Stress Installation and Elimination of Free Floating Particles

In the present study, particles were generated with a uniform diameter of 4.75mm and 6.34mm, so that the possibility of free floating particles would be greatly reduced, in contrast to an assembly with variable size distribution (Potyondy & Cundall 2004; Itasca 2005). In the creation of the particles with various size distributions, however, free floaters were eliminated by running gravity compaction for additional cycles in order to obtain a well-connected conglomeratic assembly. Further, to ensure that all particles are well connected and to generate isotropic stress installation throughout the specimen, assemblies were subjected to calculation cycles between 400,000~450,000, for the uniform distribution of particles (equal sized particles), and 850,000~900,000 for the normal distribution of the particles (unequal sized particles). This step helped to reduce the locked-in forces and bring the assembly to an equilibrium state (Figure 4-5b).

4.3.3 Parallel Bond Installation

Parallel bonds were installed at the contact points between particles to mimic cementation. Micro mechanical parameters (Table 4-1) for the parallel bond, determined from physical testing on cement samples (Chapter 3), were specified and the system was allowed to stabilise (Figure 4-5d).

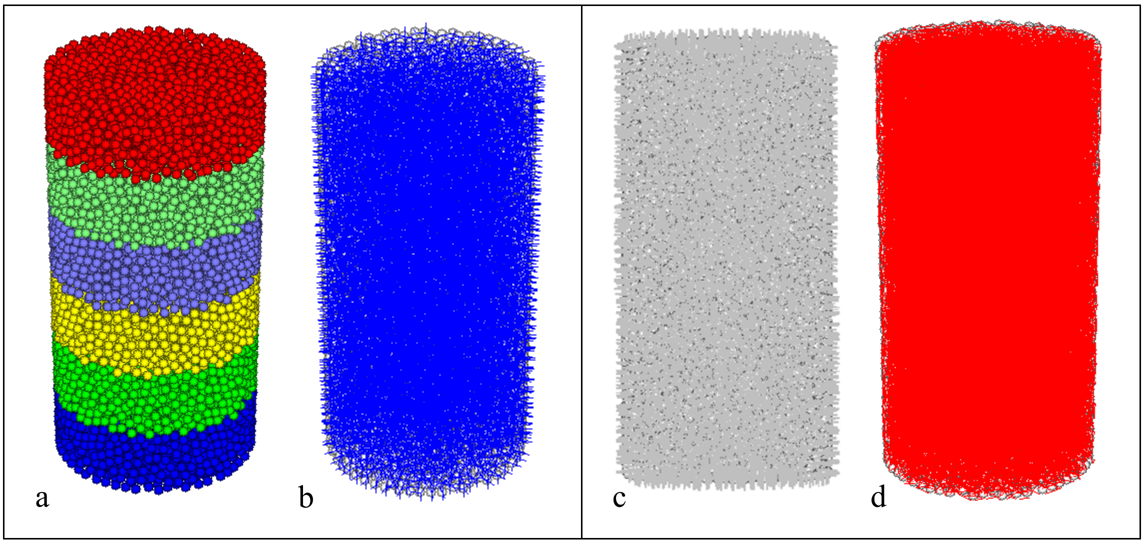

Figure 4-5: Specimen diagenesis procedure' a) creation of particles to final size, b) getting well- connected assembly by gravity packing, c) Isotropic stress installation, d) installation of parallel bonds.

Table 4-1: Summary of Parameters for Numerical Simulations

Strength parameters of cementing material (Parallel bond)			**Values**
Normal strength (MPa) [$\bar{\sigma}_c$]			1.50
Shear strength (MPa) [$\bar{\tau}_c$]			3.98
Normal stiffness of cement (Pa/m) (bond diameter = 4.75mm) [$\bar{k}_n$]			6.69e11
Shear stiffness of cement (Pa/m) (bond diameter = 4.75mm) [$\bar{k}_s$]			6.69e11
Normal stiffness of cement (Pa/m) (bond diameter = 6.34mm) [$\bar{k}_n$]			5.01e11
Shear stiffness of cement (Pa/m) (bond diameter = 6.34mm) [$\bar{k}_s$]			5.01e11
Normal stiffness of cement (Pa/m) (bond diameter = 3.56mm) [$\bar{k}_n$]			8.92e11
Shear stiffness of cement (Pa/m) (bond diameter = 3.56mm) [$\bar{k}_s$]			8.92e11
Ball properties		**Sample dimensions**	**Shear box test**
Ball diameter (mm) [$R^{[A]} = R^{[B]}$]	4.75 & 6.34	Length (mm)	100
Ball density (Kg/m^3)	7800	Width (mm)	100
Poisson's ratio of balls [ν]	0.30	Thickness (mm)	36
Shear modulus of balls [G]	74.5 GPa	Porosity (%)	39.7%
Initial friction of balls [$\mu^{[A]} = \mu^{[B]}$]	5.5°	Number of balls	3840~3865
Sample dimensions		**Uniaxial/ Triaxial**	**Brazilian test**
Sample diameter (mm)		94	94
Sample height/ thickness (mm)		188	47
Sample porosity (%)		39.7	39.7
Number of balls		14000~14020	3500~3515
Number of balls (diameter 6.34 mm)		5890~5905	-

4.4 Numerical Testing Technique

Numerical testing was conducted to simulate the physical laboratory testing on the specimens. Efforts were made to establish numerical simulations equivalent to physical conditions so as to obtain numerical test results representative of the physical test results. The dimensions and porosities of the numerical specimens were kept the same as those of the physical specimens. Important mechanisms and the procedural steps followed to obtain a representative numerical testing environment are discussed below.

4.4.1 Computing and Installing Stress States

In numerical testing, stress states around the prepared specimens can be implemented by specifying the velocities of the boundary walls. The stress and strain states are determined by the FISH function that averages all the forces on the walls by dividing by appropriate wall areas (Itasca 2005). The strains are computed by the following general relation;

$$\varepsilon = \frac{L - L_0}{\frac{1}{2}\left(L_0 + L\right)} \tag{4.20}$$

Where

L - current specimen dimension (length, height, or radius), and

L_0 - original dimension.

Throughout the loading process, the confining stress is kept constant by adjusting the confining wall velocity (the radial wall in uniaxial and triaxial testing, and the top and bottom walls in shear box testing), using a numerical servo-mechanism that is implemented by the servo-mechanism (FISH Function) which is called once per cycle. The servo-mechanism calls another FISH function to compute the current stresses on the specimen and adjust the velocities of the confining walls to reduce the difference (as per specified tolerance) between the current and requested stresses on the walls. A switch is provided to make the servo-mechanism functional throughout the test (Itasca 2005).

4.4.2 Computing Initial Testing Conditions

The initial testing environment for the uniaxial, triaxial, shear box and Brazilian tests was implemented using the above-mentioned logic (section 4.4.1) and FISH functions (Itasca 2005). Testing conditions the same as the physical laboratory were implemented in all the numerical tests by the servo-mechanism gaining suitable stresses on the relevant walls. In the PFC standard procedure of preparation, stress conditions are applied before the application of cementation (parallel bond) (Itasca 2005), however, in doing so the interparticle cement does not carry the installed stress and the numerical assembly does not reflect actual laboratory conditions. Therefore, bonds were installed before the initial stress conditions so that the cementation would also take the load of initial test conditions, as well as the balls.

To achieve an unconfined stress state around the specimen, boundary walls were applied with 1.0 atmospheric pressure (similar to the physical laboratory) which is equal to 0.1 MPa. Hence, in all unconfined tests, a value of 0.1 MPa stress was maintained around the specimen. Similarly, for triaxial or shear box testing where the confining pressure or normal stress is greater than 0.1MPa, the required stresses on the boundary walls was achieved by the servo-mechanism.

4.4.3 Loading of the Specimen

After establishing the initial testing conditions, the specimens were ready for loading. Tests began with the application of loading at a uniform displacement rate. The velocities for the loading platen were specified through a FISH function which applies velocities (in turn stresses) to the platens in such a way that the final required velocity is achieved in definite chunks containing a finite number of steps. This approach was adopted to avoid any initial damage to the specimens because of the application of sudden high velocity at the start of the test (Itasca 2005). Appropriate numbers of cycles (time-steps) were specified for each test to execute and record peak and post peak behaviour.

4.4.4 Monitoring the Parameters during Testing

Stresses and strains were monitored and recorded throughout the tests as history variables for onward test analyses. PFC's standard algorithms (Itasca 2005) for crack tracing were used, with some modification, to trace the shear, normal (tensile) and total number of cracks that developed as a result of parallel bond failure in shear or normal directions. The number of cracks were also monitored and recorded as history variables.

4.4.5 Parameter Determination: Interparticle to Assembly (Bulk) Friction

All the micro parameters used in the present studies were determined in physical testing (Chapter 3), except the coefficient of interparticle friction (μ). The micro friction (interparticle friction) normally adopted in the PFC (Figure 4-6a) is a point friction at the ball-ball contact ($\mu_{b\text{-}b}$) and does not represent the bulk (assembly) friction.

The analysis of uniaxial, triaxial and shear box tests on synthetic conglomerates yielded a bulk friction angle of 37.3°~37.8°, which is a function of the interparticle friction. At present no rigorous relation is available to estimate interparticle friction from bulk friction. Although a few attempts (e.g., Skinner 1969; Sallam et al. 2004) were made to investigate the effect of interparticle friction on bulk friction, none were found sufficiently conclusive to relate to these parameters.

Notably, in physical samples, the balls were glued together with interstitial cement. The failure through cement or along cement-ball contact will yield slip along points and surfaces of balls and cementing material; that is, ball-ball point friction (μ_{b-b}), ball-cement surface friction (μ_{b-c}) and cement-cement surface friction (μ_{c-c}) (Figure 4-6b &c). In addition, the effect of cement crushing and dilation or the overriding of the particles is also a considerable factor affecting the relative slip of the particles. As a result, the slip of the particles is a complex combination of ball-ball, ball-cement and cement-cement frictions along with the effect of cement crushing, dilation and the rotation of individual particles.

By contrast, in PFC, after the failure of parallel bonds, the spheres are free to move according to the specified friction coefficient which necessarily depicts slip along the contact point of the spheres. Hence, the specified interparticle friction (μ) represent the slip (μ_{b-b}) through the contact points of the balls.

Consequently, for a definite value of interparticle friction between balls (μ_{b-b}) which is normally taken as (μ) in PFC, the resultant interparticle slip will not produce results similar to a physical sample with identical parameters unless other contributing frictions (i.e., μ_{c-c} & μ_{b-c}) and factors such as dilation, cement crushing and restricted particle rotations are incorporated. Thus, interparticle friction (μ) for the simulation of a physical cemented assembly should be higher than that of the friction between two contacting balls (i.e., μ_{b-b}).

Alternatively, it was considered appropriate to adopt an interparticle friction that yields the same bulk friction as obtained for the physical assembly (i.e., 37.3°). To obtain this, a sequence of numerical testing (uniaxial and triaxial) was run with interparticle friction varying from 5.5° to 85° to obtain an interparticle-bulk friction curve.

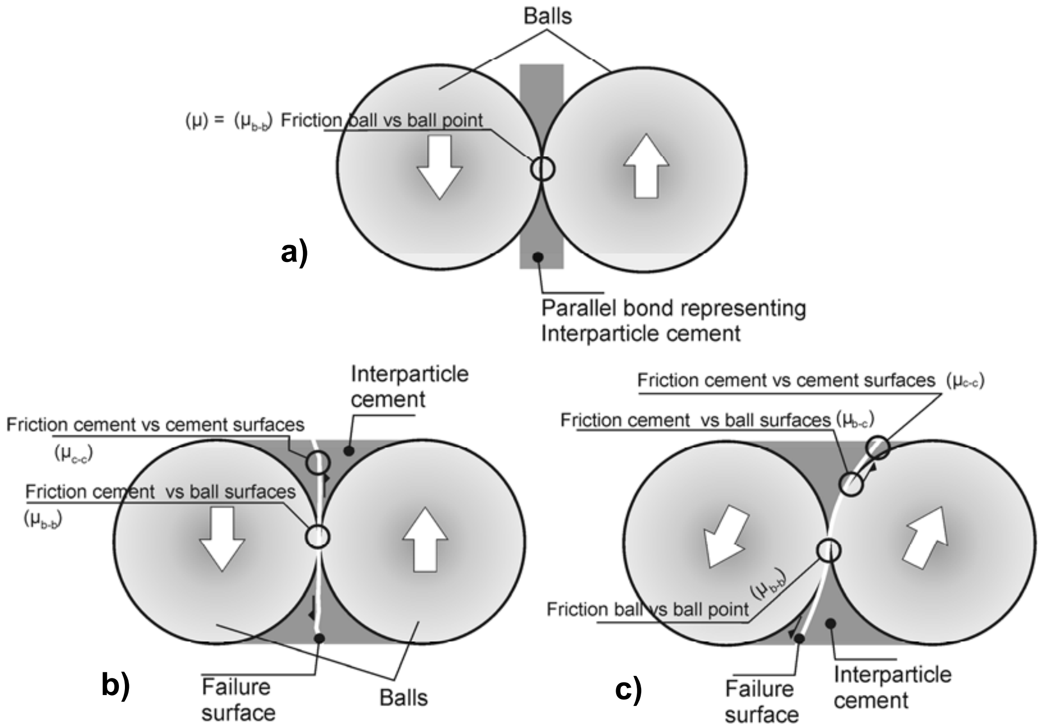

Figure 4-6: Illustration of interparticle friction components in a real life situation and PFC: a) PFC assembly, b) Physical assembly with failure surface through cement, c) Failure surface through cement-ball contact (modified after Akram & Sharrock 2009; 2010).

4.5 Numerical Test Results

After specimen diagenesis and with the required testing conditions, numerical conglomerate specimens were ready for testing. All the algorithms written for the specimens' preparation and testing are provided in Appendix B. The details of the testing and results are given in the following sections.

4.5.1 Uniaxial Testing

In the uniaxial test simulation, a cylindrical specimen similar to a physical specimen was created within a cylindrical container bounded by two rectangular (planar) walls at top and bottom, and one cylindrical wall. Initial confinement was applied on the cylindrical wall and also to the top and bottom walls. Suitable values of velocity to top and bottom walls were specified in such a way that the final required velocity was achieved in definite chunks containing a finite number of steps. A parametric sensitivity study was performed to adopt a suitable displacement rate which is detailed in Section 4.6.

After the adoption of a suitable displacement rate (i.e., 0.001 m/s), a sequence of numerical modelling was run to obtain the interparticle to bulk friction curve (Figure 4-7a) to adopt a suitable value for the friction coefficient for the final run of testing.

Interparticle fiction was varied, keeping the other parameters constant and, stresses and strains were recorded as history variables. The variation of peak strength and Young's modulus versus interparticle friction is shown in Figure 4-7b.

This investigation demonstrated (Figure 4-7) that an interparticle friction angle of 78°, with a corresponding bulk friction angle of 37.3° with the given set of micro-mechanical parameters. The adopted interparticle friction of 78° seems unrealistic, but it should be noted that this value incorporates the effect of base and internal friction which includes the effects of particle packing, cement crushing and friction similar to the physical sample.

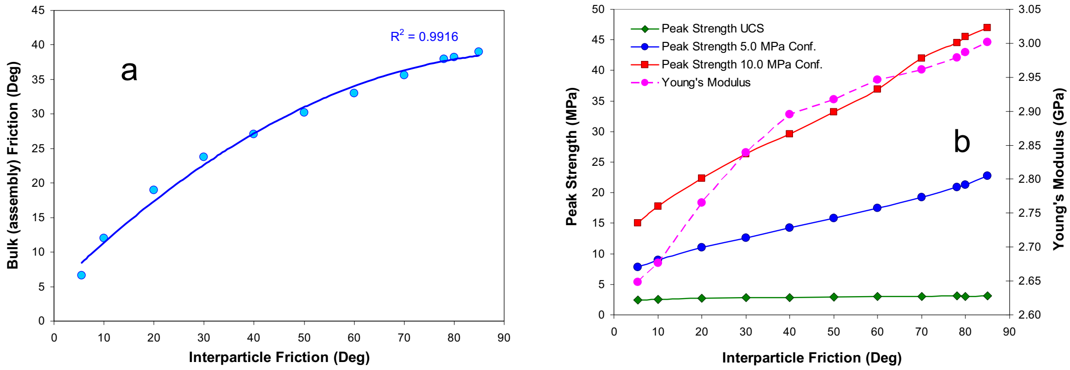

Figure 4-7: Interparticle friction in relation to; a) bulk (assembly) friction, b) peak strengths and Young's modulus (modified after Akram & Sharrock 2009; 2010).

After adopting 78° of interparticle friction, a final test was run to generate a macroscopic response in uniaxial test conditions. The test result, in terms of the stress-strain curve is given in Figure 4-8. It should be noted that the angle of interparticle friction of 78° and a loading displacement rate of 0.001 m/s was adopted for all uniaxial and triaxial testing in parametric sensitive studies, detailed in Section 4.6.

4.5.2 Triaxial Testing

Triaxial testing was undertaken following the same methodology as that of uniaxial testing by changing the confinement from 0.1 MPa to 2.5, 5.0, 7.5 and 10.0 MPa. A parametric sensitivity study, like uniaxial testing, was also conducted for the loading rate (displacement) and finally a suitable value (i.e. 0.001 m/s) was adopted. A sequence of triaxial testing was performed by varying interparticle friction from 5.5° to 85° to obtain the interparticle-bulk friction curve (see Figure 4-7b). Peak strengths plotted against interparticle friction are given in Figure 4-7b.

A final set of triaxial testing was conducted at the above mentioned confining pressures to record the macroscopic response of the numerical conglomerate.

Stresses and strains were monitored throughout the tests. The test results in terms of deviatoric stress-strain curves are given in Figure 4-8.

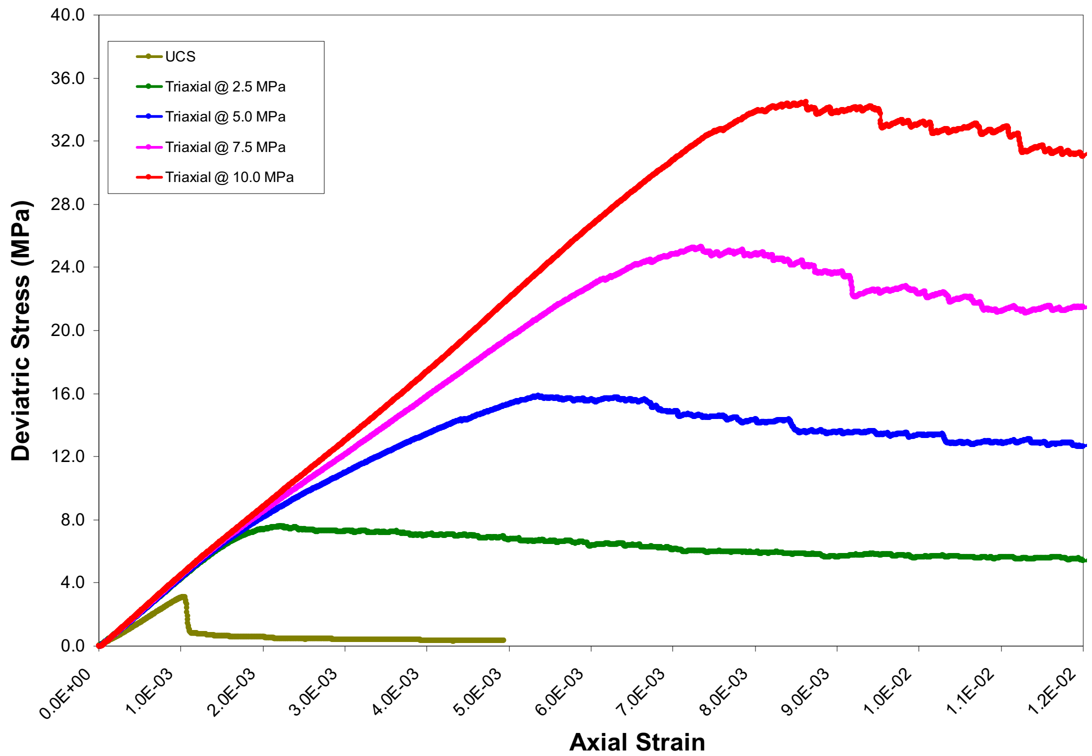

Figure 4-8: Plots of uniaxial and triaxial tests at confining pressure 0.1, 2.5, 5.0, 7.5 and 10.0 MPa in deviatoric stress-strain space (modified after Akram & Sharrock 2009; 2010).

4.5.3 Brazilian Testing

Brazilian tensile tests were conducted on a circular disc created within two rectangular walls and one cylindrical wall (Figure 4-9a). The thickness of the disc was kept equal to its radius (Figure 4-9b). After specimen creation and obtaining the initial condition, the cylindrical wall was removed and the top and bottom platens were loaded by applying a suitable velocity. The loading rate (displacement rate) was adopted as 0.005 m/s, corresponding to 0.005 mm/s in physical testing. The peak load (force) was extracted from the load-displacement curve and tensile strength was determined using the following equation (Goodman 1980):

$$\sigma_t = \frac{F_f}{\pi R t_B} \tag{4.21}$$

Where

σ_t - Brazilian tensile strength

F_f - peak force acting on the platens

R - radius of the sample and,

t_B - thickness of the sample

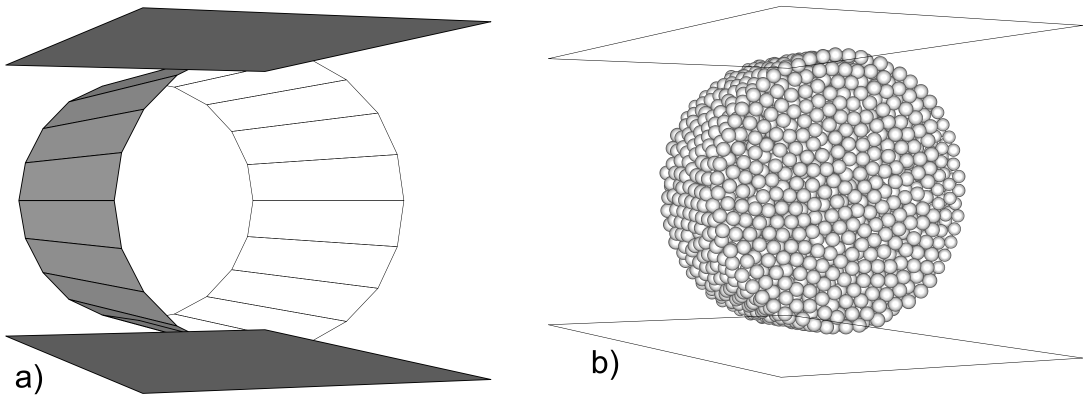

Figure 4-9: a) A cylindrical wall and two rectangular walls (top and bottom) for creation of the Brazilian disc, b) Brazilian disc with top and bottom walls and ready for testing.

A displacement rate sensitivity study was also conducted as part of the Brazilian testing sequence to observe the failure of disc. The failure pattern was estimated tracing the location and type of cracks.

4.5.4 Shear Box Testing

A shear box was simulated by creating a specimen in a two part rectangular box, that is, upper and lower box, each of which is bounded by five rectangular walls with a gap of 1.0 mm between top and bottom boxes (Figure 4-10). The specimen was created within the shear box and initial testing was obtained (Figure 4-10a). The test was conducted by loading the side walls of the top and bottom halves of the box in opposite directions at various values of normal loads (as shown in Figure 4-10a). Normal loads were applied on the top and bottom walls by specifying the velocities of the walls, and were maintained as constant throughout the test using the servo-mechanism.

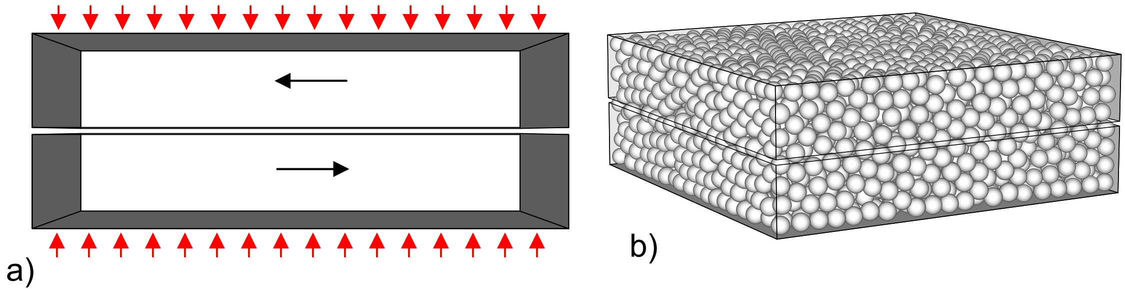

Figure 4-10: a) Shear box consisting of upper and lower boxes bounded by rectangular walls, b) Created shear box specimen and ready for testing.

Shear box tests were conducted at a normal load of 0.0, 0.5, 1.0, and 2.0 MPa corresponding to physical shear box tests at a normal stress of 0.5, 1.0 and 2.0 MPa.

Shear stress, normal stress, shear displacement and vertical dilation were monitored during tests as history variables.

Parametric sensitivity studies were also conducted for displacement rate and for thickness of a layer of unbonded particles along the shearing surface. The outcome of the sensitivity studies will be discussed in the following sections.

The test results for the adopted horizontal or shearing displacement rate (i.e., 0.001 m/s) are shown in Figure 4-11 in shear stress-shear displacement space and in vertical dilation (displacement)–horizontal (shear) displacement space.

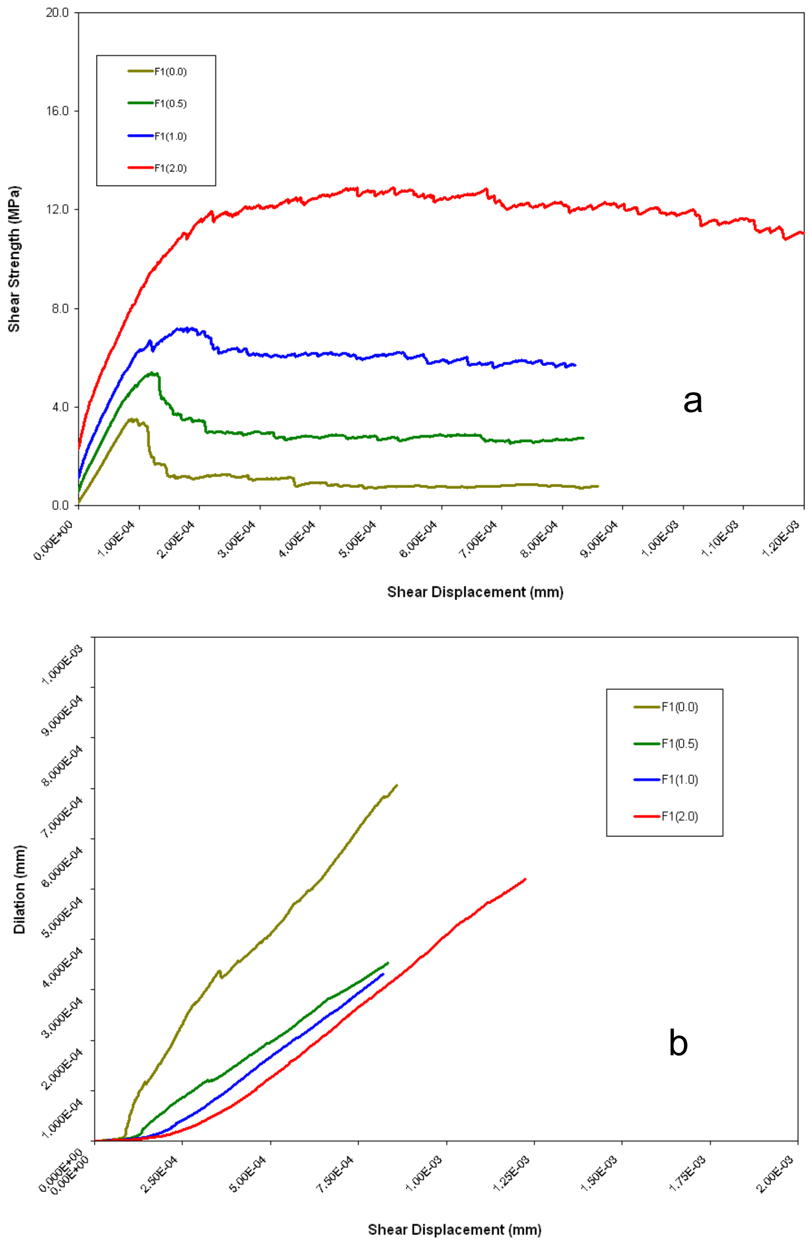

Figure 4-11: Results of PFC shear box testing at normal stresses 0.0, 0.5, 1.0 and 2.0 MPa : a) shear stress vs shear displacement, b) vertical dilation versus shear displacement (modified after Akram & Sharrock 2009; 2010).

4.6 Parametric Sensitivity Studies

Parametric sensitivity studies in numerical simulation provide an understanding of the dependence and interaction of various parameters on the mechanical response of an assembly. It was anticipated that by varying the parameters a deep insight into the behaviour of numerical conglomerates could be generated, which is very difficult if not impossible in real life. In real life, the influence of a specific parameter can not be gained discretely as any mechanical response is a composite phenomenon of the various parameters which can not be kept constant. Hence, a parametric sensitivity study is an important aid in exploring the response of materials whose mechanics are not well known.

In the present study, the parametric studies conducted had two aims:

Firstly, studies of the parameters which control the testing set-up in numerical simulation were undertaken. The purpose of these studies was to achieve numerical testing conditions close to physical laboratory conditions. These studies are predominantly connect with the influence of the loading or displacement rate in relation to the mechanical responses. Therefore, displacement rates were examined in all testing to adopt a particular displacement rate which is equivalent to physical testing. In addition, the effect of parameters which can not be determined from experiments or do not have a one to one relation with physical parameters was also investigated and is presented in this section.

Secondly, studies of those parameters whose effect is not known or not fully understood in real life in relation to conglomeratic rocks were made. These studies are not discussed here but are provided in Chapter 6 with reference to investigating the response of numerical conglomerates.

A summary of parametric sensitivity studies conducted in numerical testing is given in Table 4-2 .

Table 4-2: Summary of parametric sensitivity studies conducted in each test.

Sensitivity studies	Numerical tests
Displacement rate (loading rate)	Uniaxial, triaxial, Brazilian tensile and shear box
Particle size	Uniaxial and triaxial
Normal to shear stiffness of Parallel bond (interparticle cement)	Uniaxial and triaxial
A layer of unbonded particles along shearing	Shear box

A detailed description of the sensitivity studies is discussed in the following sections under the respective numerical tests.

4.6.1 Uniaxial and Triaxial Testing

In numerical uniaxial and triaxial testing, the sensitivity of the mechanical response of numerical conglomerates was analysed towards the sensitivity of the loading or displacement rate, particle size and stiffness ratio of the cementing material.

4.6.1.1 Loading Rate (Displacement Rate)

In physical testing on synthetic conglomerate, a displacement rate of 0.001 mm/s was adopted to reduce vibration in the system because of the presence of steel balls in the specimens. However, this rate is too slow if it were to be adopted for numerical simulations. In order to explore the material's sensitivity to displacement rate, a study was conducted with displacement rates of 0.0001 to 0.1 m/s. The outcome of this study was found to be consistent with the response of natural rocks (Peng 1973), that is, the peak strengths of the material in uniaxial and triaxial loading increase with the increase of displacement rate and vice-versa. The results are shown in Figure 4-12 for uniaxial testing and Figure 4-13 for triaxial testing at confining pressures of 5 MPa and 10 MPa.

The modulus remains almost constant under various displacement rates. The stress-strain curves (Figure 4-12 & Figure 4-13) of various displacement rates show that the post peak response is brittle at a lower displacement rate (0.0001-0.001 m/s) and becomes more ductile in uniaxial, and strain hardening in triaxial conditions towards higher displacement rate (0.05-0.1 m/s). These observations are consistent with the behaviour of natural rocks, as explored by Peng (1973). In view of the findings of this study, a displacement rate of 0.001m/s was adopted in numerical simulations for uniaxial and triaxial testing.

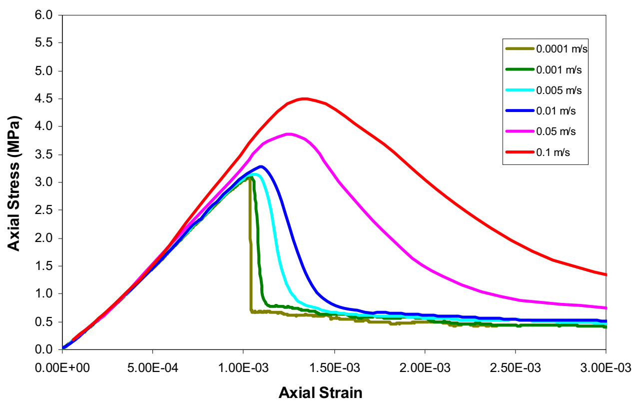

Figure 4-12: Displacement rate sensitivity of stress-strain curves in uniaxial compression (modified after Akram & Sharrock 2009; 2010).

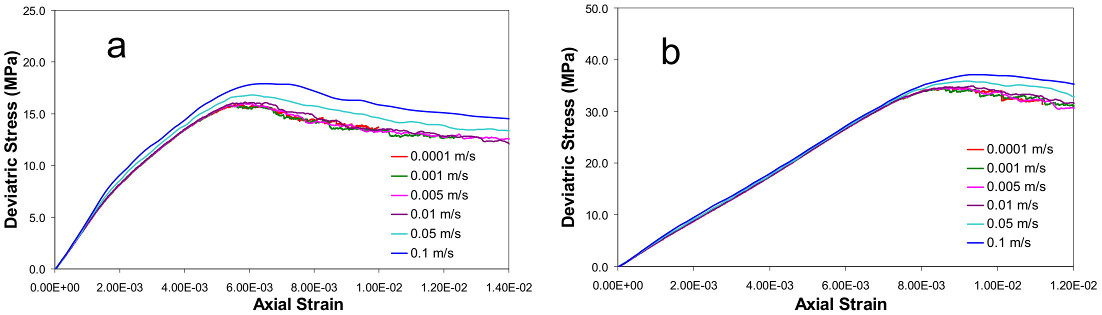

Figure 4-13: Displacement rate sensitivity of stress-strain curves in triaxial compression; a) at 5MPa, and b) at 10MPa confining pressure.

4.6.1.2 Stiffness Ratio of the Parallel bond

The normal and shear stiffness of parallel bonds were determined from Young's modulus of the cement. The shear to normal stiffness ratio of 1.0 was adopted assuming both stiffnesses are equal (i.e., $\bar{k}^s / \bar{k}^n = 1$) as no direct means are available to measure the stiffness ratio directly from experiments. However, in contrast, the material's response was investigated numerically with shear to normal stiffness ratios of 0.25, 0.50, 0.75 and 1.0 to observe the sensitivity of shear stiffness on the macroscopic behaviour of the assembly.

The outcome of this study is demonstrated in Figure 4-14. It is noted that the UCS decreases significantly with the decrease in the stiffness ratio when compared to the peak strength in triaxial conditions (Figure 4-14a). Young's modulus in uniaxial condition decreases with the decrease in the stiffness ratio, while it shows an increasing trend with the increase of confining pressures. Poisson's ratio increases with the decrease in the stiffness ratio in both uniaxial and triaxial compressions (Figure 4-14b).

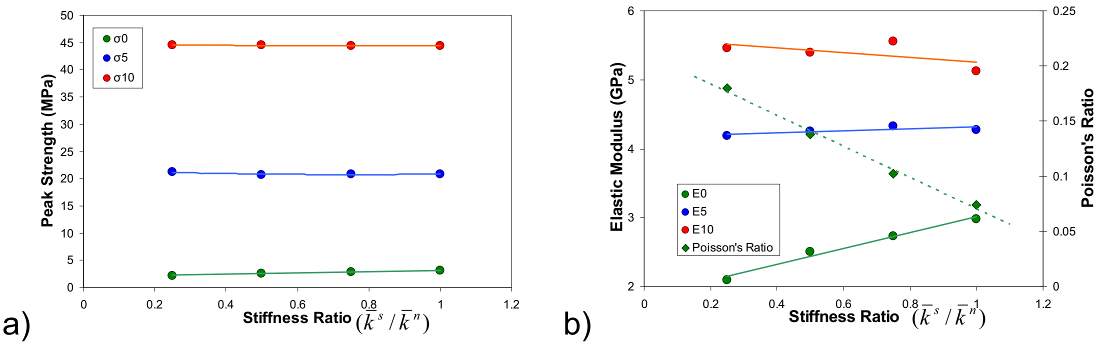

Figure 4-14: Effect of stiffness ratio (shear to normal) in uniaxial and triaxial test; a) on peak strength, b) on Young's modulus and Poisson's ratio of the numerical conglomerate (modified after Akram & Sharrock 2009; 2010).

4.6.1.3 Particle Size

The sensitivity of the response of numerical conglomerates was investigated with the variation of particle size in uniaxial compression. The purpose of this study was to examine the response of numerical conglomerate with respect to the synthetic conglomerate. In the synthetic conglomerate, particle sizes of 4.75 mm and 6.34 mm were used to create specimens with a uniform size distribution, which resembles natural well-graded conglomerates. Hence, this study was considered important in predicting the response of the natural well-graded conglomerates that vary in particle size.

Additional specimens of the numerical conglomerate were prepared with a uniform size distribution, with particles of 6.34 mm and 3.56 mm, and underwent uniaxial testing. The test results in terms of peak strengths, Young's modulus and Poisson's ratio are given in Figure 4-15. It was observed that the peak strength and Young's modulus both increase whereas Poisson's ratio decreases with an increase of particle size. These observations clearly indicate the dependence of the mechanical response of a conglomerate on particle size.

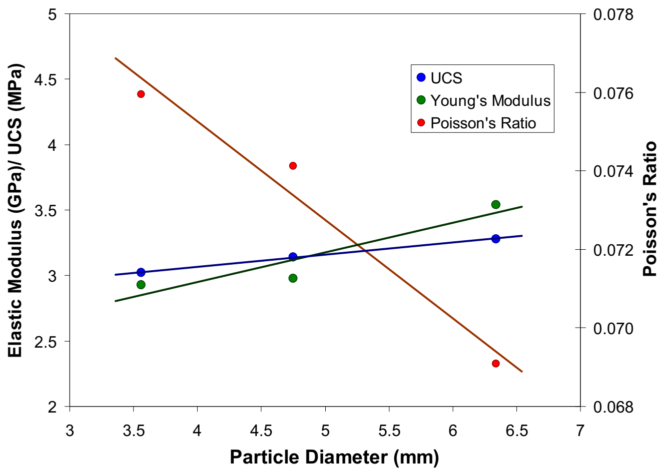

Figure 4-15: Variation of peak strength (UCS), Young's modulus and Poisson's ratio of numerical conglomerate assembly with particle size (modified after Akram & Sharrock 2010).

4.6.2 Brazilian Testing

4.6.2.1 Loading Rate (Displacement Rate)

In the Brazilian test simulation, the indirect tensile strength of the numerical conglomerate was studied under various displacement rates to find an appropriate displacement rate to compare test results to the output of the corresponding physical tests. It was noted in this study that the tensile strength increases with the loading rate (Figure 4-16). It increased from 0.092 MPa to 1.11 MPa with the increase of the platens' velocity from 0.001 m/s to 1.0 m/s respectively. This increase in tensile strength is less pronounced, that is, less than 20% between the platens' velocity of 0.001 m/s to 0.01 m/s. However, with the increase of platens' velocity from 0.01 m/s to 1.0 m/s, there is abrupt increase in tensile strength reaching a maximum of 1.11 MPa at 1.0 m/s producing damage progressively along the loading axis. A loading rate of 0.005 m/s was adopted for the final simulation of the Brazilian test compared to the physical test at 0.005 mm/s.

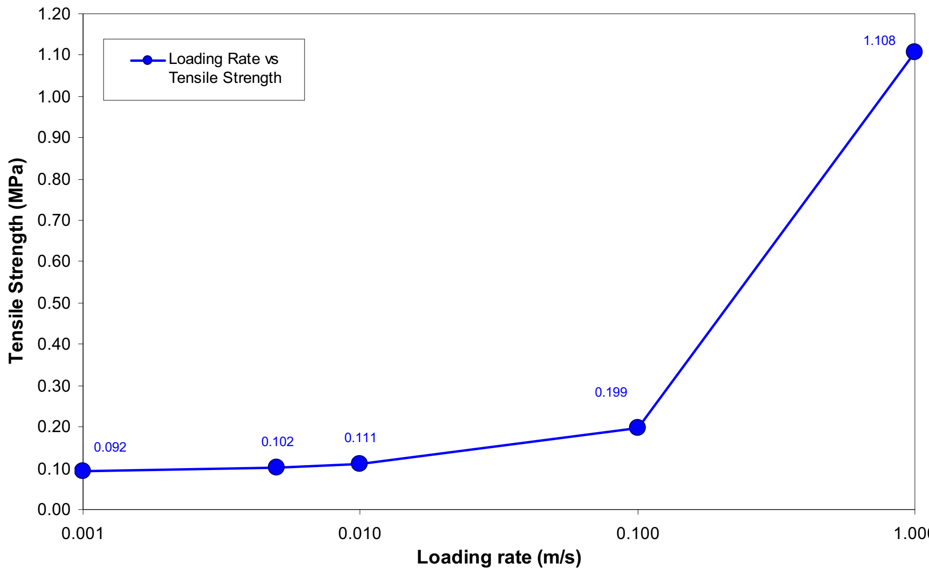

Figure 4-16: Sensitivity of the tensile strength with loading rate in Brazilian Tensile Testing on the numerical conglomerate.

4.6.3 Shear Box Testing

4.6.3.1 Loading Rate (Displacement Rate)

Similar to the uniaxial and Brazilian test simulation, a parametric sensitivity study of the shear displacement rate from 0.01 m/s to 0.0001 m/s in the shear box test was conducted to look into its effect on the macroscopic response of the numerical conglomerates. The results are plotted in Figure 4-17.

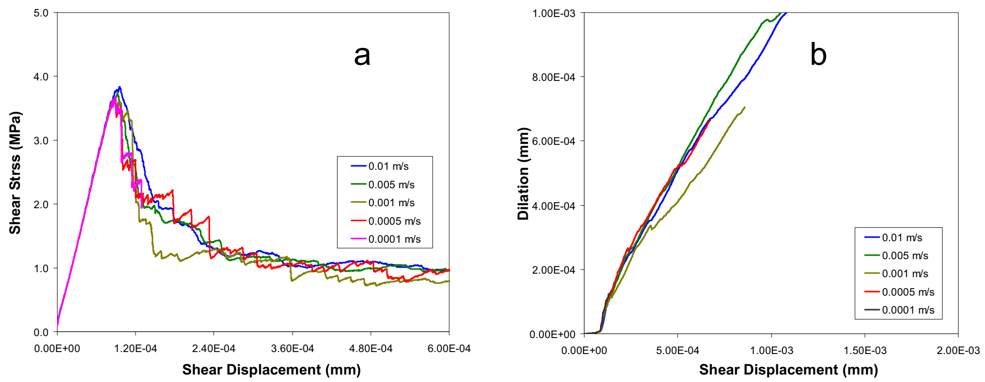

Figure 4-17: Sensitivity of numerical conglomerate towards shear displacement rate; a) Shear strength vs. shear displacement rate, b) Vertical dilation vs. shear displacement rate (modified after Akram & Sharrock 2010).

These results indicated that the shear strength is proportional to the loading rate (Figure 4-17a), the same as was observed in uniaxial and triaxial compression (Peng 1973), while the vertical dilation did not produce conclusive results against shear displacement (Figure 4-17b). However, the variation of the shear strength is less pronounced as it was in uniaxial and triaxial compression. Hence in view of this study a displacement rate of 0.001m/s was adopted for the shear box simulation in PFC3D.

4.6.3.2 Unbonded Particles along Shearing

A numerical study was also undertaken to examine the micro mechanisms governing the macroscopic response of the assembly that occur along the shearing, for example, the rotation and sliding of unbonded particles, microscopic dilation etc. For this reason, the shear box test was run by incorporating a layer of unbonded particles along the shear plane which were allowed to rotate and slide freely during shearing. The thickness of the layer varied from 0.0 mm to 5.0 mm (almost the diameter of the particle). The shear strengths in each shear box test corresponding to specific normal stresses were recorded (Figure 4-18).

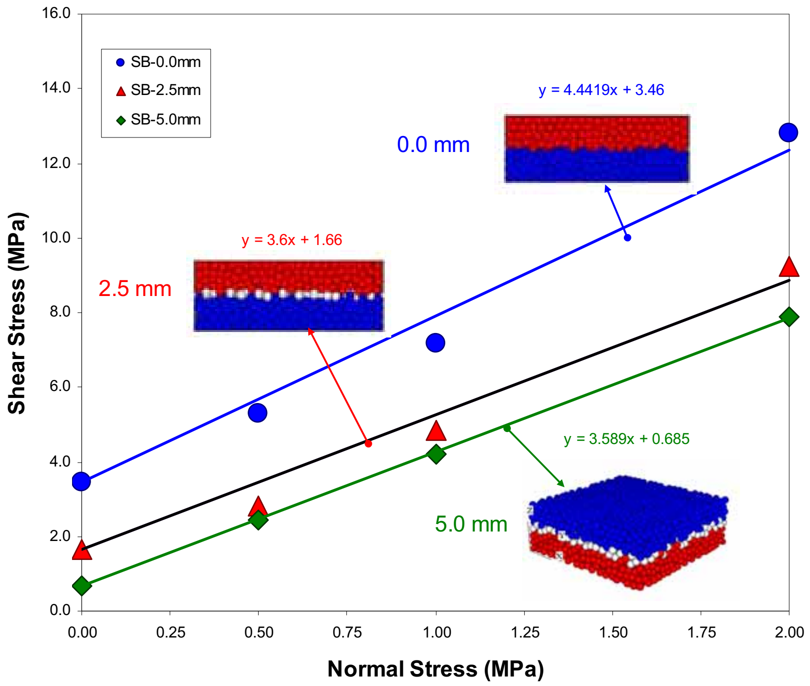

Figure 4-18: Variation of peak shear strength at various normal stresses in shear box test with the layer of unbonded particles along shearing (modified after Akram & Sharrock 2010).

This study showed that the cohesion intercept is much more sensitive towards the number of unbonded particles (Figure 4-19). It reduces from 3.46 MPa to 0.69 MPa with the thickness of the unbonded particles' layers from 0.0 mm to 5.0 mm (one particle diameter) respectively along the shear plane. The dilation angle also reduces with the increase in the number of free rotating particles (thickness of the layer of the unbonded particles). This, in turn, suggests that during shearing particles with broken bonds undergo excessive rotation and yield less dilation in contrast to experiments where the particle rotation is restricted because of interparticle cement.

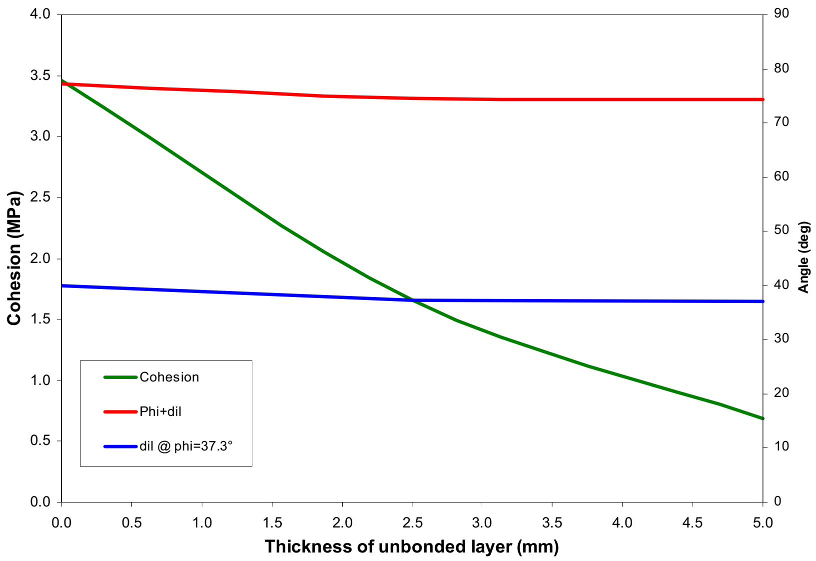

Figure 4-19: Variation of cohesion, apparent angle of friction and angle of dilation with the thickness of the layer of unbonded particles along shearing (modified after Akram & Sharrock 2010).

4.7 Analyses of Numerical Test Results

This section presents the analyses conducted on the laboratory test results of numerical conglomerates. All the numerical tests were undertaken in a testing environment as close as possible to physical conditions. The purpose of the numerical testing was to examine the DEM's simulation in representing physical laboratory testing and to further explore the mechanics of conglomeratic rocks for the sensitivity of various parameters. In this section, the macroscopic response of the numerical conglomerate is analysed in terms of strength and elastic parameters for comparison with synthetic conglomerate. It was hypothesised that if the numerical conglomerates were microstructurally equivalent to the synthetic conglomerates and tested under similar conditions, their macroscopic responses should be comparable to that of synthetic conglomerates.

The following sections present the test results and analyses conducted to determine the quantitative and qualitative response of the numerical conglomerate in uniaxial, triaxial, shear box and Brazilian testing.

4.7.1 Uniaxial Testing

Numerical uniaxial testing was conducted on conglomerates having particle diameters of 3.56 mm, 4.75 mm and 6.34 mm. A summary of the test results is given in Table 4-3. During uniaxial testing on a granular assembly with a particle diameter 4.75mm the formation of cracks as a result of bond breakage were monitored simulating the acoustic emissions in physical samples. Both normal or tensile (i.e., when parallel bonds break in tension) and shear (i.e., when parallel bonds break in shear) cracks were also separately monitored throughout the tests to identify the mode of failure in the sample. The uniaxial test plot with tensile and shear crack monitoring is given in Figure 4-20.

Table 4-3: Summary of numerical test results (modified after Akram & Sharrock 2010)..

Particle diameter (mm)	Test	Peak strength (MPa)	Y. modulus (GPa)	Poisson's ratio
3.56	UCS	3.02	2.93	0.076
6.34	UCS	3.28	3.54	0.074
4.75	UCS	3.14	2.98	0.069
	Triaxial (2.5 MPa)	10.10	4.09	-
	Triaxial (5.0 MPa)	20.82	4.25	-
	Triaxial (7.5 MPa)	32.71	4.21	-
	Triaxial (10.0 MPa)	44.43	4.39	-
	Brazilian Tensile	0.102	-	-

Besides the monitoring of cracks, circumferential and volumetric strains were also monitored. In physical uniaxial testing, the stress-strain curve was characterised into various damage thresholds corresponding to stress states. These damage thresholds were discussed in Chapter 3 and further explanation can be found in the references (e.g., Eberhardt et al. 1998; Diederichs 2000; 2003; Diederichs et al. 2004).

The damage thresholds ($\sigma_{ci,}$ σ_{cd} and σ_{Peak}) were identified in the numerical PFC models (Figure 4-20) by tracing cracks and with circumferential and volumetric strains. The crack initiation stress was estimated from tracing the cracks (a point on stress-strain curve where ~10 cracks were recorded, comparable to physical tests).

Crack initiation is normally followed by the random distribution of cracks (Diederichs et al. 2004), but in our case, most of the cracks seemed to be localised along the sample edges. The crack damage (σ_{cd}) stage was identified as a point where stress-axial strain curve changes to exhibit non-linear behaviour and random cracks interact. This point was not clearly indicated by the reversal of the volumetric strain of the numerical model as compared to the corresponding strain of the synthetic conglomerate (Figure 4-20). However, the slope of the radial strain reflected a slight change in curve at this point.

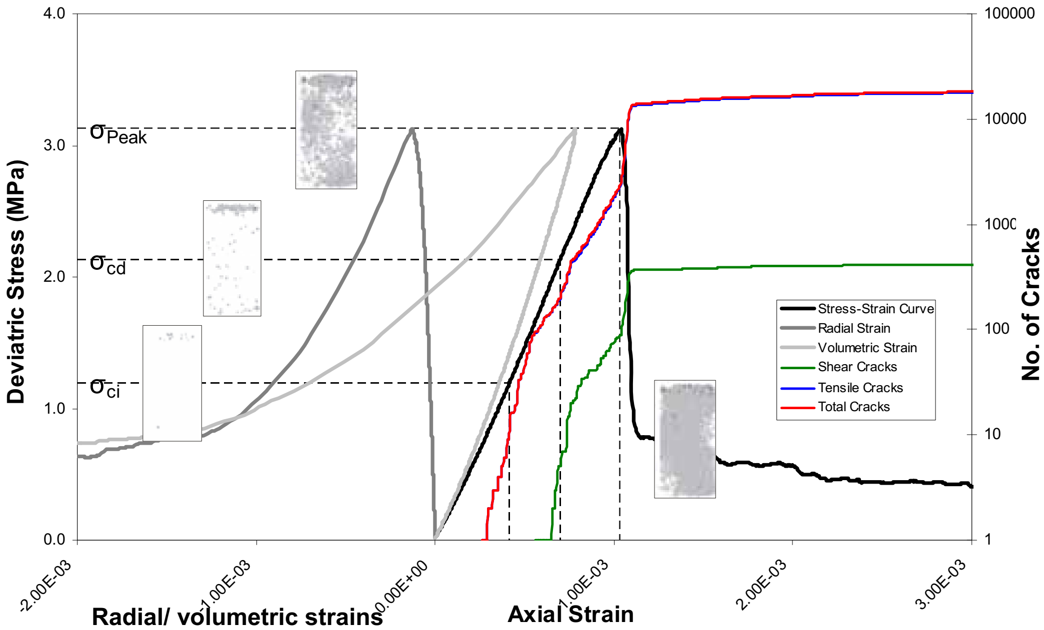

Figure 4-20: A plot of the strains (axial, circumferential and volumetric) and the growth of tensile (normal) and shear cracks versus vertical stress to identify stress stages corresponding to damage thresholds in the uniaxial test on numerical conglomerate (modified after Akram & Sharrock 2010).

Systematic crack growth followed the crack damage stage due to the localisation of contact stresses which led towards the sample failure after exhibiting a maximum strength of the material (i.e. σ_{Peak}). Distributions of cracks corresponding to damage thresholds are presented in Figure 4-21. The values of stress states corresponding to the damage threshold in the uniaxial test simulation are summarised in Table 4-4.

The post peak behaviour of the conglomeratic samples was observed as brittle followed by a sudden stress-drop in axial splitting with no strain softening. This is a characteristic failure mechanism for hard crystalline rocks. However, pre-peak dilation and post peak ductility are usually associated with conglomeratic rocks and were also observed in the synthetic conglomerates. These mechanisms, however, were not observed in the numerical conglomerates. One reason can be the absence of the interparticle cement after the breakage of the parallel bonds as the particles' rotation is not restricted which in turn, suppresses the dilation in the pre-peak regime and yields brittleness in post-peak behaviour (Figure 4-22).

Table 4-4: Damage stress states in uniaxial compression of numerical models.

Stress states corresponding to damage thresholds	σ_{cc}	σ_{ci}	σ_{cd}	σ_{Peak}
PFC3D Model (MPa)	-	1.19	2.13	3.14
% of Peak	-	38.14	68.27	100

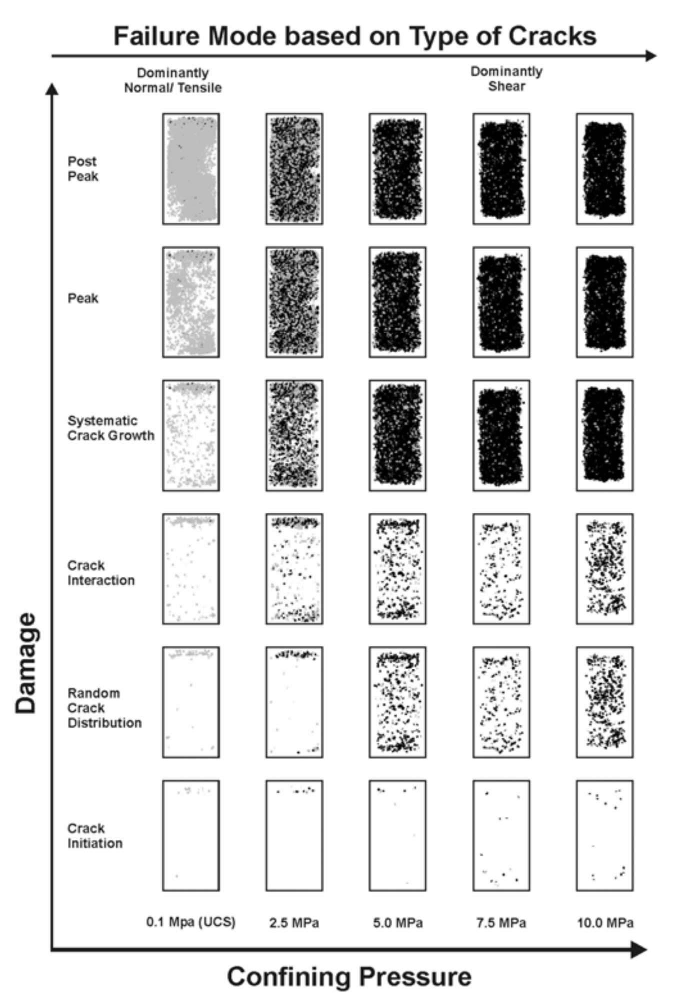

Figure 4-21: Stages of damage in numerical models indicated by tensile (grey) and shear (black) cracks in uniaxial and triaxial loading (modified after Akram & Sharrock 2010).

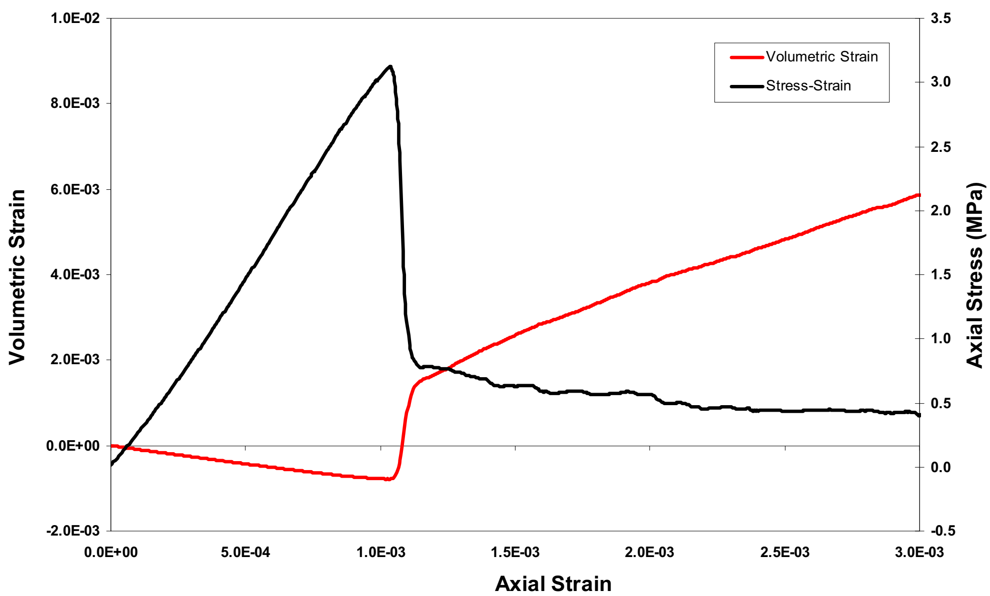

Figure 4-22: Variation of volumetric strain in uniaxial testing on the numerical conglomerate.

4.7.2 Triaxial Testing

Triaxial testing in PFC3D was conducted at four confinement pressures (i.e., 2.5, 5.0, 7.5 and 10.0 MPa). The test results are summarised in Table 4-3 and presented in Figure 4-8. Similar to uniaxial testing, circumferential and volumetric strains were recorded as history variables in triaxial testing. The recorded strains were plotted against corresponding deviatoric stresses to analyse the macroscopic response of the numerical specimens in triaxial testing. These curves are shown in Figure 4-23. Both shear and normal cracks were monitored separately to observe the effect of confining pressure on the mode of failure in the samples (Figure 4-24).

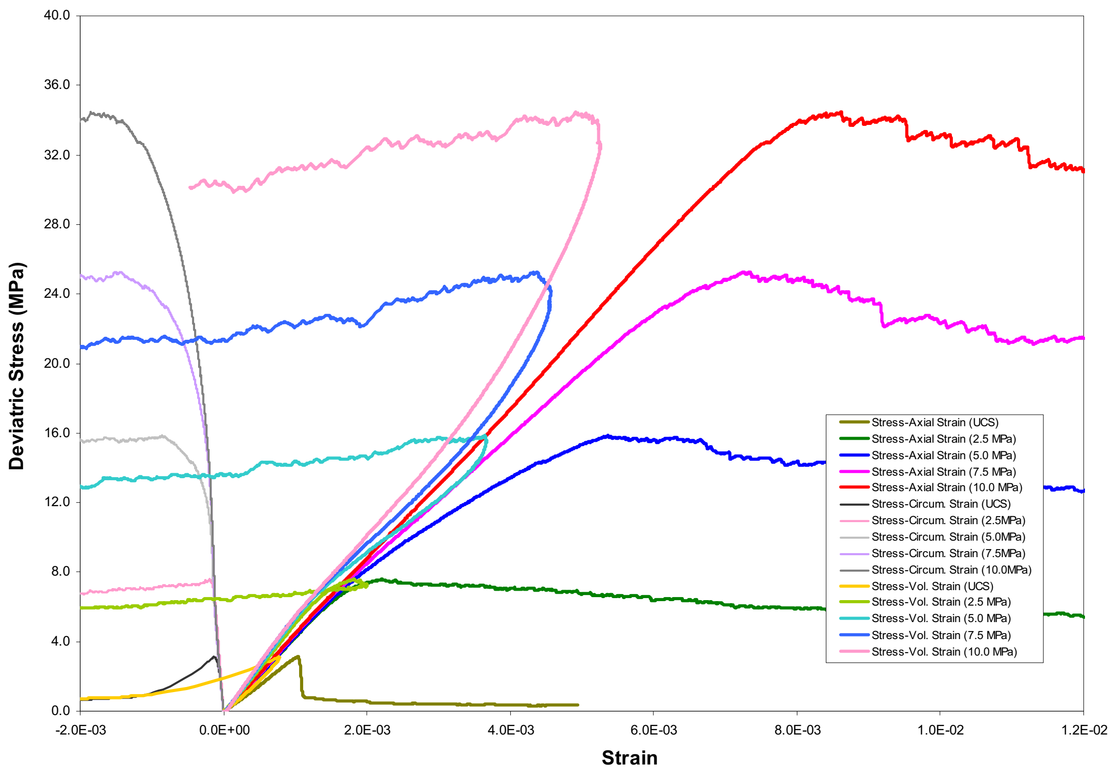

Figure 4-23: Plots of deviatoric stress versus axial, radial and volumetric strains for uniaxial and triaxial testing at confining pressures of 2.5, 5.0, 7.5 and 10.0 MPa.

Figure 4-24 suggests that the formation of interparticle cracks is greatly influenced by the confining pressure that defines the macroscopic failure pattern of the numerical specimen. At lower confinement conditions, between 0 and 2.5 MPa, samples mainly fail because of the formation of tensile cracks (normal), as shown in Figure 4-20, Figure 4-21 and Figure 4-24a, while shear cracks are limited by comparison. However, with an increase in the confining pressure, the formation of shear cracks increases in comparison to tensile cracks and contributes to the failure of the numerical specimen (Figure 4-21 and Figure 4-24). The normal to shear crack ratio was also plotted for the numerical uniaxial and triaxial tests to observe the mechanism of failure (Figure 4-25).

The numerical tests showed a change in failure mechanism from tensile to shear with the increase of confinement from 0.1 MPa (at UCS) to 10.0 MPa. At peak strength, the decrease in the normal to shear crack ratio from 150 to 0.1, suggests that shear failure at a micro level dominates tensile failure with an increase of confining pressure from 0.1 (UCS) to 10 MPa (Figure 4-24 & Figure 4-25). This can also be traced with the formation and concentration of crack type through the course of the test at various confining pressures (Figure 4-21).

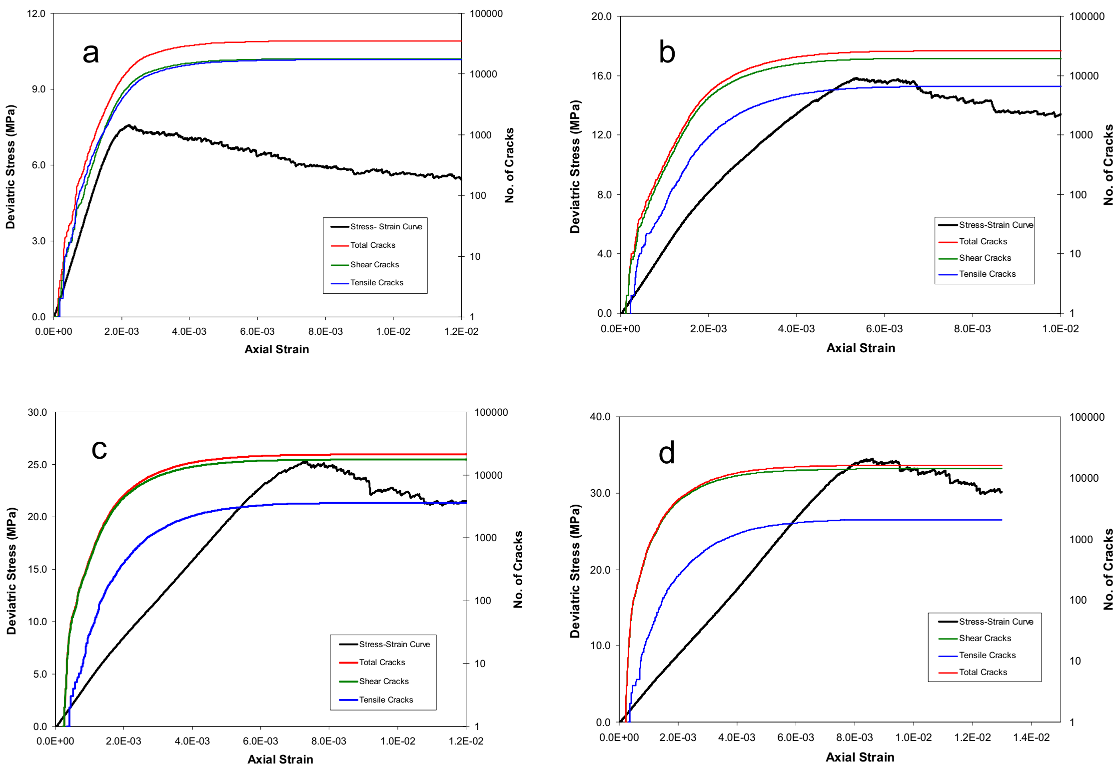

Figure 4-24: Plots of crack monitoring, i.e., shear cracks, tensile cracks and the total number of both cracks, in stress-strain space for triaxial tests at confinement: a) 2.5 MPa, b) 5.0 MPa, c) 7.5 MPa, and d) 10.0 MPa.

However, no dominant shear direction was observed in numerical samples in triaxial testing as cracks were distributed uniformly throughout the sample. This was attributed to high dilation along the possible shearing direction induced by the uniform size distribution of the particles and particle size to specimen size. Mostly well-defined shear failures were obtained using PFC simulations in random particle size distribution (dense packing) and usually in two dimensions (e.g., Diederichs et al. 2004; Potyondy & Cundall 2004).

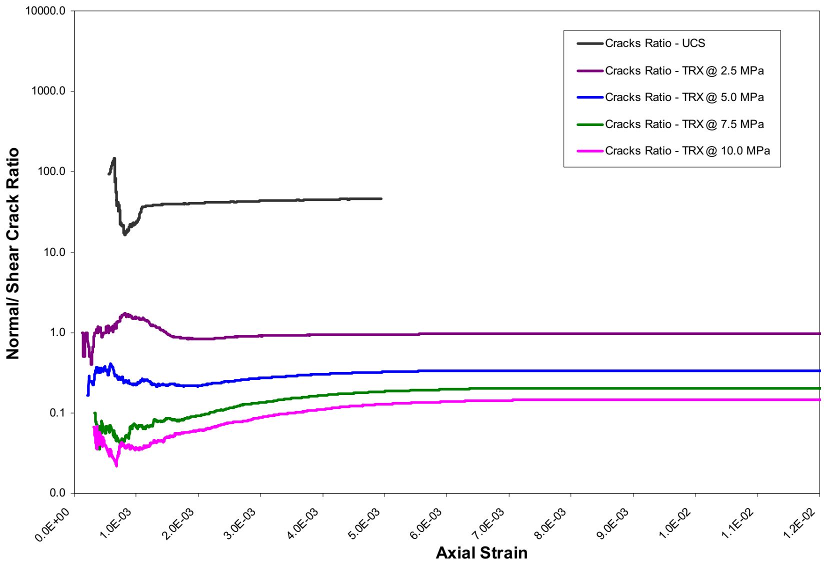

Figure 4-25: Normal to shear crack ratio plotted in the stress-strain field for uniaxial and triaxial compression (modified after Akram & Sharrock 2009; 2010).

Young's modulus and Poisson's ratio, measured at 50% of peak strengths for each confining pressure are summarised in Table 4-3. The stress states corresponding to the damage thresholds (i.e., σ_{ci}, σ_{cd} and σ_{Peak}) were identified in the numerical samples in triaxial testing with the tracing of cracks (Figure 4-21) and circumferential and volumetric strains (Figure 4-23). The observed damage thresholds and corresponding deviatoric axial stresses are summarised in Table 4-5 and shown graphically in Figure 4-26.

Table 4-5: Damage stress states in triaxial compression of numerical models.

Stress states corresponding to damage thresholds (deviatoric stresses)	σ_{ci}	σ_{cd}	σ_{Peak}
Triaxial (2.5 MPa)	1.16	4.9	7.58
Triaxial (5.0 MPa)	1.14	8.5	15.84
Triaxial (7.5 MPa)	1.44	5.94	25.29
Triaxial (10.0 MPa)	1.34	6.78	34.74

It was observed that under deviatoric stress conditions, the magnitude of stress corresponding to damage increases with the increase in confining pressure. However, this increase in crack initiation stress is insignificant between uniaxial and triaxial loading (Figure 4-26). But other damage stress states (Figure 4-21) are sensitive to the confining pressure and increase with the corresponding increase in confinement, as shown in Figure 4-26.

The post peak behaviour of the conglomeratic samples was observed sensitive to the confining pressure and shifts from brittle axial splitting in uniaxial to ductile with the increase of the confining pressures. At low confining pressure, that is, in a uniaxial condition, brittle failure with significant stress-drop was observed accompanied by high volumetric dilation (Figure 4-22). However, with the increase of confining pressure, brittle behaviour transforms to ductile with a systematic reduction in volumetric dilation and a drop in stress (Figure 4-27).

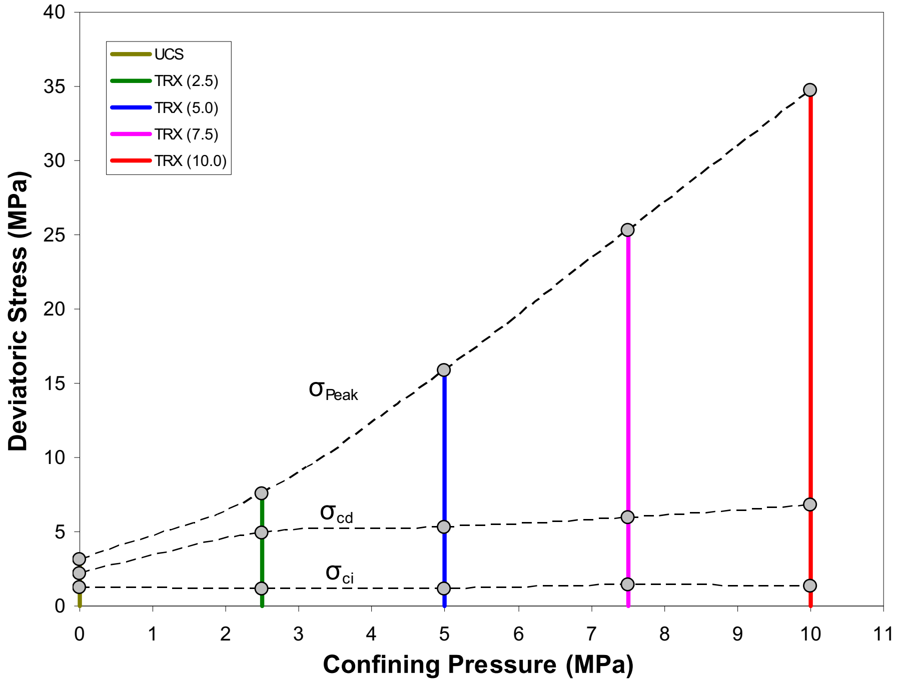

Figure 4-26: Deviatoric stress corresponding to damage thresholds in uniaxial and triaxial testing.

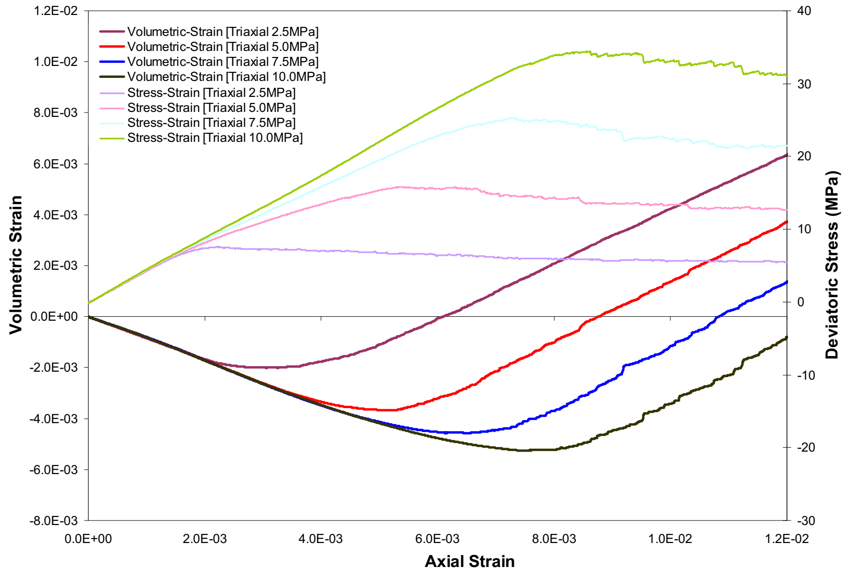

Figure 4-27: Variation of volumetric strain in triaxial testing on the numerical conglomerate at confining pressures of 2.5, 5.0, 7.5 and 10.0 MPa.

4.7.3 Peak Strength Criteria for Numerical Conglomerate

A peak strength criterion can be defined as a relation between stress components that permits the peak strengths developed under various stress conditions to be predicted (Brady & Brown 2005). Since the rocks and rock-like materials show non-linearity under varying stress conditions, classical strength criteria applied in other disciplines to quantify the materials can not be used straightforwardly in rock mechanics. In view of these implications, two well documented strength criteria, Mohr-Coulomb and Hoek-Brown, were applied on the numerical test results to examine the extent of the criteria in capturing the response of the numerical conglomerate.

Mohr's circles were plotted for uniaxial, triaxial and Brazilian test results in shear strength-normal stress space to obtain strength parameters (i.e., c, ϕ). The plot is shown in Figure 3-18.

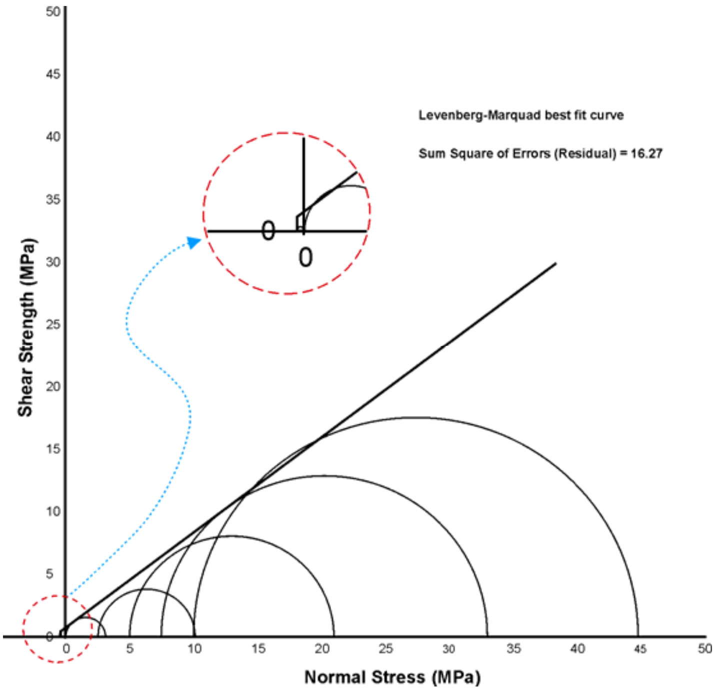

Figure 4-28: Plotting of uniaxial, triaxial and Brazilian results in the shear strength-normal stress field to yield Mohr-Coulomb strength parameters i.e., angle of internal friction of 37.3°, cohesion of 0.70 MPa and tensile cut-off at 0.102 MPa, (modified after Akram & Sharrock 2010).

The Hoek-Brown criterion was applied to a material equivalent to intact rock, that is, laboratory specimen of the numerical conglomerate; a GSI value of 100 was adopted along with material's peak strengths and intact Young's modulus E_i. RocLab1.0 (Rocscience 2008) was used to apply the Hoek-Brown criterion using uniaxial, triaxial and Brazilian tensile testing data (Table 4-3) which selected a value of 27.97 for the material constant (m_i) to suite the results. At this value of material constant, Hoek-Brown parameters with the fitted Mohr-Coulomb parameters are given in Table 4-6 and curves are plotted in Figure 4-29a & b. Mohr-Coulomb envelopes determined directly (given in Figure 4-28) and testing data are also overlaid on the plots (Figure 4-29a & b).

Table 4-6: Summary of Hoek-Brown and fitted Mohr-Coulomb parameters determined applying the Hoek-Brown criterion to numerical test results.

Hoek-Brown classification	**Parameters**	**Values**	**Units**
Uniaxial compressive strength	σ_c	2.86	MPa
Geological strength index	*GSI*	100	
Material constant	m_i	27.97	
Disturbance factor	D	0	
Intact rock Young's modulus	E_i	2980	MPa
Hoek-Brown criterion			
Material constant	m_b	27.97	
HB constant	*s*	1	
HB constant	*a*	0.5	
Failure envelope range			
	Application	Custom	
Maximum minor principal stress	σ_3^{Max}	10.0	MPa
Mohr-Coulomb fit			
Cohesion	c	2.16	MPa
Angle of friction	ϕ	31.95	degrees
Rock mass parameters			
Tensile strength	σ_t	-0.102	MPa
Compressive strength	σ_c	2.86	MPa
Rock mass compressive strength	σ_{cm}	2.96	MPa
Rock mass modulus	E_{rm}	2963	MPa

From the plot, it is clear that the Hoek-Brown criterion and fitted Mohr-Coulomb curves do not match the testing data. Instead, the Mohr-Coulomb (direct) curve shows the promise of matching the test data, with a sum square of errors of 16.27 in contrast to the corresponding value of 100.23 for Hoek-Brown. This observation suggests that the response of a numerical conglomerate is more predictable with the Mohr-Coulomb than the Hoek-Brown criterion. However, the response of numerical conglomerates needs to be further explored in view of strength criteria.

4.7.4 Brazilian Testing

In PFC, Brazilian samples were prepared equivalent to physical ones with parallel bonds and tested under the equivalent conditions. The peak compressive load was noted in the test and used to calculate the indirect tensile strength of the sample. The calculated tensile strength is given in Table 4-3. To find an appropriate loading rate and to investigate the sensitivity of loading (displacement) rates with tensile strength, a sensitivity study was conducted by varying the velocities of the loading platens from 0.001 m/s to 1.0 m/s.

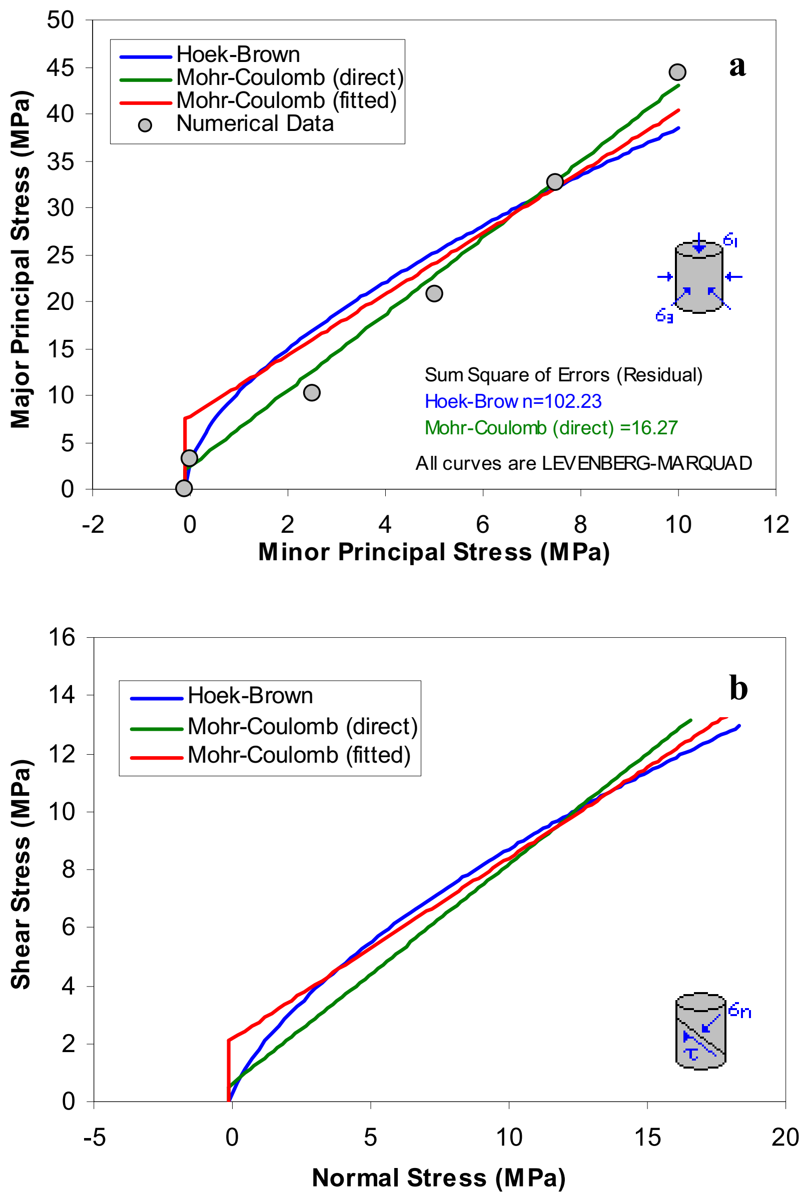

Figure 4-29: Plots showing Hoek-Brown and fitted Mohr-Coulomb criteria curves derived directly based on numerical test data: a) in major and principal stress space, b) in normal and shear stress field.

It was observed in the sensitivity study that the tensile strength is sensitive to the loading rate (Figure 4-31). The values of the tensile strength determined are 0.092, 0.101, 0.111, 0.199 and 1.08 MPa at loading rates 0.001, 0.005, 0.01, 0.1 and 1.0 m/s respectively. The adopted value was taken as 0.101 MPa corresponding to a loading rate of 0.005 m/s as per the following correlation of loading rates between experimental and numerical testing (after Akram & Sharrock 2010):

$$\text{Exp. Loading rate (mm/s)} \cong \text{PFC3D Loading rate (m/s)} \qquad (4.22)$$

Tensile strength variation (from 0.092 to 0.111MPa) has little significance at loading rates of 0.001 to 0.01 m/s; however at loading rates of 0.01 to 1.0m/s, it increases from 0.111MPa to 1.108m/s, showing a significant variation. A similar trend in variation was also observed in the uniaxial and triaxial testing in the loading rate sensitivity study. This observation is consistent with that of natural rocks (Peng 1973).

The reason for the increase of tensile strength with the increase of the loading rate could be due to the higher loading rate than of the rate of fracture propagation. Generally, in cemented granular assemblies, failure in Brazilian testing occurs because of the notches (wedges) near the loading platen which are responsible for propagating the discrete fracture though the disc which bisects it (Potyondy & Cundall 2004), as shown in Figure 4-30.

It was assumed that the length of the wedge (*a*) is constant for the definite size of particles and its development is also the function of time or the loading rate, that is, the size of the wedge is inversely proportional to the loading rate. It was also found that a smaller wedge induced by a higher displacement rate could more easily trigger the development of discrete cracks through the sample disc than a larger wedge (result of lower loading rate). Moreover at lower loading rates, fractures find more time to propagate and result in early failure showing less peak load and vice versa.

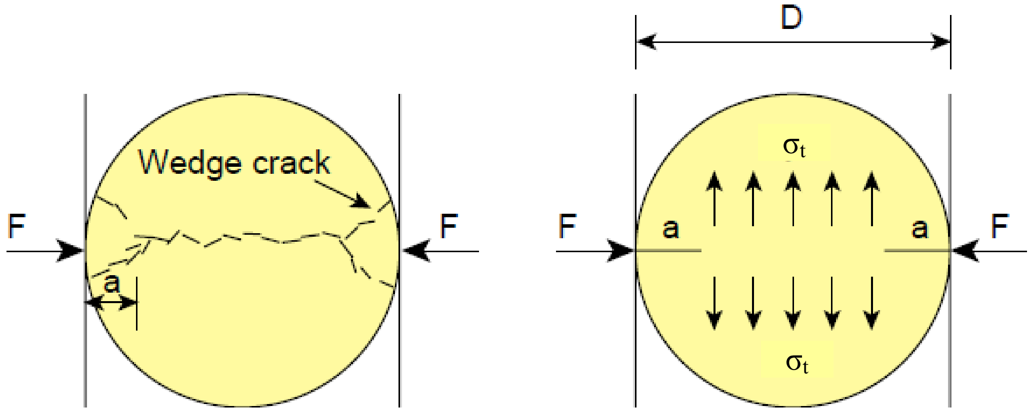

Figure 4-30: Relating Brazilian strength to fracture toughness (after Potyondy & Cundall 2004; Cho et al. 2007).

In numerical tests, at a displacement rate of 0.005 m/s, the sample did not yield a distinct failure plane parallel to the loading direction, but instead the sample collapsed showing localised damage (notches) near the loading platens (Figure 4-31). This failure is consistent with the previous findings of numerical Brazilian tests (Potyondy & Cundall 2004; Itasca 2005). Perhaps, the reason for the development of localised distribution of cracks near the top and bottom platens is the empty spaces between the balls and parallel bonds (if, for example the parallel bond are transmitting load and moments).

It is understood that a force chain or fibre is developed through point contacts and bonded region of the particles, that is, the forces and moments are transferred through the ball contact points and parallel bonds. Hence, the empty spaces between the balls do not contribute either to load or moment transfer, which in turn, relaxes the vertical load by breaking the bond in a random direction along the distribution of balls and parallel bonds. Although the fibre developed through the top and bottom platens clearly indicates the loading direction, this force-chain diminishes and is distributed throughout the disc as it gets away from the platens, with out giving a pronounced trend along the load axis.

Consequently, the increase in the applied load contributes to bond breakage in the stressed region near the top and bottom platen as is evident in Figure 4-31 rather than concentrating along the load axis. However, with continuous loading or at higher loading rates, damage progressively becomes parallel to the loading axis allowing the development of macroscopic tensile cracks through the sample disc.

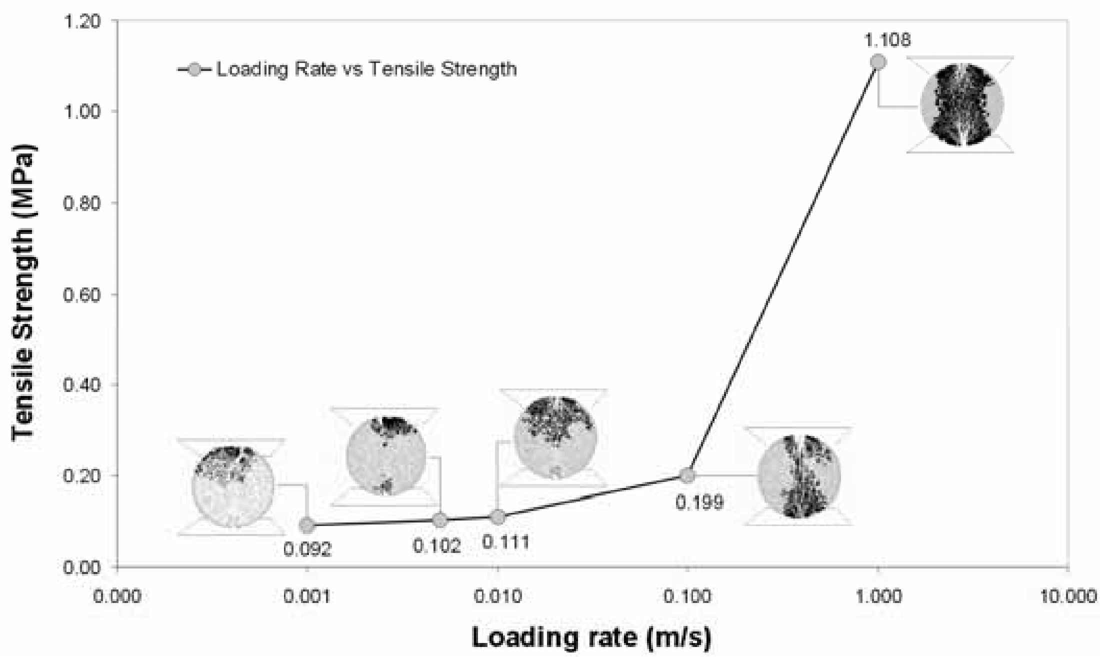

Figure 4-31: Sensitivity of Brazilian tensile strength and distribution of damage with loading rate (modified after Akram & Sharrock 2010).

4.7.5 Shear Box Testing

Shear box test results were analysed for cohesion (c) and angle of friction (ϕ). The analysis output is summarised in Table 4-7 and plotted in Figure 4-32. The analyses of the numerical modelling results identified a cohesion of 3.46 MPa and an apparent angle of friction (i.e. angle of friction + angle of dilation ($\phi + i$)) of 77.25°.

Table 4-7: Summary of numerical shear box test results.

Normal load (MPa)	Shear strength (MPa)
0.0	3.46
0.5	5.3
1.0	7.18
2.0	12.8

Cohesion (MPa)	3.46
Apparent angle of friction (deg)	77.25
Mean Angle of dilation (deg)	39.98
Angle of friction (deg)	37.3

The variation of dilation versus shear displacement was plotted for all values of normal stresses to determine the dilatation angle. A decrease in the dilation angle was noted with the increase of normal stress (Figure 4-11). This observation was found consistent with the uniaxial and triaxial test results on the numerical conglomerates, which showed a decrease in volumetric dilation with the increase of the confining pressure (Figure 4-22).

The determined dilation angles are plotted corresponding to normal stresses in Figure 4-32. An average angle of dilation was calculated as 31.5° at a maximum shear displacement of 1.25 mm which yielded an angle of friction of 46°. This value of friction angle was found to be greater than that determined in uniaxial and triaxial compression (37.3°). It is understood that for most geomaterials, the angle of friction measured in uniaxial and triaxial compression is similar to that measured in the shear box test.

However, the angle of dilation in shear box test could vary with the characteristics of the shearing plane. Therefore, the angle of friction was kept the same (37.3°) for the numerical conglomerate and the angle of dilation was calculated from the apparent angle of friction (i.e., $\phi + i$). The dilation angle (i) was determined as 39.98° which seems reasonable considering the excessive rotation of the spherical particles along shearing. The data points corresponding to the apparent angle of friction ($\phi + i$) were adjusted for true value of angle of friction, that is, 37.3°, keeping the cohesion same (i.e., 3.46 MPa). These points were then plotted in the shear-normal stress field (Figure 4-32).

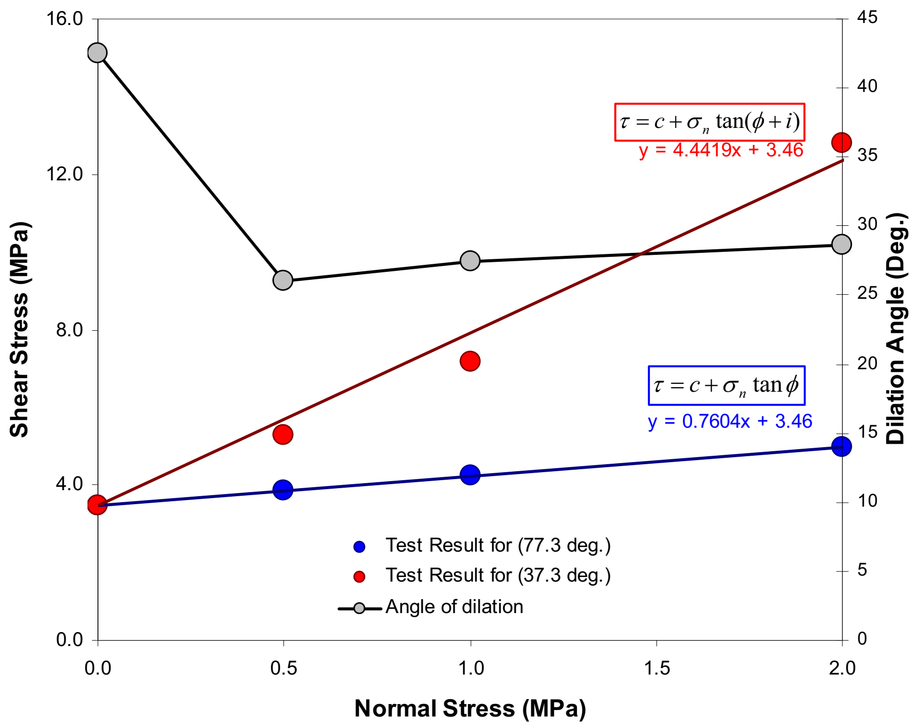

Figure 4-32: Shear box test results for the apparent angle of friction ($\phi + i$) of 77.25° with angle of dilation (i) of 39.98°, and the angle of friction (ϕ) of 37.3°. The value of the dilation angle (i) determined (for all values of normal stresses) at a shear displacement of 1.25 mm has also been plotted against normal stresses (modified after Akram & Sharrock 2010).

4.8 Summary and Conclusion

Numerical tests similar to standard laboratory tests were conducted using PFC3D. Test specimens of numerical conglomerates were created using standard and modified FISH algorithms. Numerical testing was executed as close as possible to represent physical laboratory conditions. To create interparticle cement, parallel bonds were installed and micro parameters for parallel bonds were derived in the physical laboratory by testing on the cement paste samples. Interparticle to bulk friction was determined using the inverse modelling approach as no direct method is available to relate these parameters. Numerical testing was completed using the numerical servo-control mechanism which maintains the specified stress and strain conditions around the specimens. The loading was applied, in terms of a constant displacement rate, to the loading platens. Numerical conglomerate specimens were found sensitive to the loading rate and, therefore, appropriate loading rates were determined in parametric sensitivity studies and adopted in each testing environment.

In uniaxial and triaxial testings, appropriate confining pressures were applied to obtain the required testing conditions. The peak strengths were observed as 3.14, 10.10, 20.82, 32.71 and 44.74 MPa in uniaxial and triaxial testing at 2.5, 5.0, 7.5 and

10 MPa confining pressures respectively. The elastic response of the conglomerate was observed in terms of Young's modulus and Poisson's ratio at 50% of peak strength. The Young's modulus and Poisson's ratio were found as 2.98 GPa and 0.074 respectively. An increase in the modulus similar to natural rocks was observed with the increase of confining pressure. However, the value of Poisson's ratio was found to be much lower than what was anticipated for conglomeratic material (i.e., 0.25~0.35).

In uniaxial and triaxial testing, a sensitivity study was conducted to record the response of numerical conglomerates with different particle sizes. This study showed that both the peak strength and Young's modulus of the numerical conglomerate increase with the increase of particle size at fixed porosity. However, Poisson's ratio decreases with the increase of particle size. These findings indicate that a conglomerate sample with large clasts will yield higher strength and stiffness compared to those with small particles.

In the numerical conglomerate, shear to normal stiffness ratio of 1.0 was assumed for interparticle cement as no experimental data is available to validate this ratio. However, a sensitivity study was conducted to examine the response of numerical conglomerates with varying stiffness ratios. It was observed that both strength and Young's modulus increase and Poisson's ratio decreases with the increase of the shear to normal stiffness ratio, and vice versa. Currently, the understanding of the physical and numerical meaning of the input parameters stands on existing knowledge which is insufficient to address this issue. Therefore, it is anticipated that more detailed and quantitative work is required in future to relate DEM's parameters to that of the physical system.

The failure mechanisms of the conglomerate specimens in uniaxial and triaxial testing were observed to vary with confining pressure. In uniaxial tests, samples failed in axial splitting with a sudden stress-drop indicating a brittle failure mechanism, while a transition from axial splitting to strain softening was observed in triaxial testing with the increase of confining pressures. The failure mechanism was estimated by the ratio of tensile to shear crack so that for uniaxial testing the ratio is very high and decreases with the increase of confinement. In triaxial testing, a random distribution of cracks was noted with no well defined shear surface through the specimen. This was considered to be the effect of high dilation because of the particles along the possible shear. However, the mode of micro crack failure gradually becomes shear with an increase in the confining pressure. Both in uniaxial and triaxial testing, progressive damage in the specimens was characterised into corresponding stress states based on axial, radial and volumetric strains together with the monitored number of cracks representing a phenomenon of acoustic emission (AE) in physical testing. These stress states were observed to increase with the increase in confining pressure.

In Brazilian tensile testing, the numerical conglomerates showed a tensile strength of 0.106 MPa. The tensile strength is sensitive to the loading rate and increases with that loading rate. However, no discrete crack, that is, axial splitting of the specimen was observed, which is a typical mechanism of failure in Brazilian testing. Instead, localised damage was seen in the specimen near the top and bottom platens, which is consistent with the early findings of the studies involving PFC. This could be because of the empty spaces among the balls, which do not contribute either to load or moment transfer.

In shear box testing, cohesion and the apparent angle of friction ($\phi + i$) were determined as 3.46 MPa and 77.25° respectively. The angle of dilation was determined as 39.98°. The sensitivity of the unbonded particles along the shear direction was determined by incorporating a layer of unbonded particles. The thickness of the layer was varied and it was observed that both the angle of apparent friction and cohesion decrease with the increase of the layer's thickness.

The uniaxial, triaxial and Brazilian tensile strengths were analysed for Mohr-Coulomb and Hoek-Brown criteria. It was observed that a Mohr-Coulomb criterion has a higher level agreement with the testing data than a Hoek-Brown criterion. A contrast in the direct Mohr-Coulomb and fitted Mohr-Coulomb (on Hoek-Brown) parameters was noted.

It should be noted that in the digenesis of the numerical conglomerate, averaged micro parameters (e.g., strengths and stiffnesses of interparticle cements) were used and, as a result, the observed mechanical response of numerical conglomerate should be considered averaged, which may change with the variation of the micro parameters. However, in the present research, all the discussions on the numerical conglomerates are based on the averaged results of the tests.

In addition to micro parameters, other factors may also induce variation in the mechanical response of numerical conglomerates, such as particle packing and boundary conditions. In the current numerical simulations, efforts were made to prepare the specimen by gravity induced packing similar to synthetic conglomerates. For this purpose, all the numerical specimens (during packing) were computed for almost the same number of cycles to obtain similar packing of particles. However, it is anticipated that particle packing by other means than gravity might induce variation in the mechanical response of the numerical conglomerates in all tests.

Likewise, boundary conditions may also affect the numerical test results and failure mechanisms of the numerical specimens. The simulations of numerical tests were conducted in relation to physical experiments and based on the current understanding and knowledge of boundary conditions being applied in PFC. However, in future, boundary conditions might be improved to obtain rigorous and well defined failure mechanisms in the numerical specimens, particularly in Brazilian tensile testing.

In summary, the observed mechanical behaviour of numerical conglomerates in various tests is based on averaged parameters, gravity induced packing and the current understanding of the boundary conditions which may vary as these factors and parameters change. This variation was not investigated as part of the present research; however, a variation of 5-10% could be applied to the obtained test results.

A comparison of the test results of the synthetic and numerical conglomerates was made in Chapter 5 to undertake correlations in understanding and further investigating the mechanics of conglomerates.

Comparison of Synthetic and Numerical Conglomerates

5.1 Introduction

This chapter presents a comparison of the responses of synthetic and numerical conglomerates in laboratory testing. The objective of this comparison was to validate the response of numerical conglomerate against a physical system (synthetic conglomerate) to make DEM simulation a rigorous tool for onward investigation into natural conglomerates. It was hypothesised that this comparison will give important insights into DEM simulation with reference to modelling the behaviour of a physical system, that is, synthetic conglomerates, and will highlight the strengths and weaknesses of DEM for research into conglomeratic rocks.

The test results of synthetic and numerical conglomerates in uniaxial, triaxial, shear box and Brazilian testing were compared for strength, elastic and physical parameters to develop a numerical versus physical correlation. The analyses of the physical test results were discussed in Chapter 3 together with the derivation of micro parameters for numerical simulations, whereas a discussion on the equivalent numerical testing was given in Chapter 4.

5.2 Comparison of Physical and Numerical Test Results

Physical and numerical test results were analysed to develop correlations between the macroscopic response of physical assemblies and numerical (PFC3D) simulations performed using known micro-parameters. This comparison includes both quantitative and qualitative correlations. The quantitative comparison addresses the correlation of strength and elastic parameters whereas the qualitative comparison describes the failure modes and mechanisms observed both in numerical and physical samples. These correlations have been detailed in the following sections under headings of respective testing.

5.2.1 Uniaxial and Triaxial Testing

Numerical simulations of uniaxial and triaxial tests were conducted in PFC3D following the specimen diagenesis and testing procedures equivalent to physical testing. Hence, it was hypothesised that the numerical test results should have strong correlations with the corresponding results of the synthetic conglomerate. A summary of numerical and physical uniaxial and triaxial test results is provided in Table 5-1. The details of the number of samples tested experimentally and the loading conditions were discussed in Chapter 3.

Table 5-1: Summary of numerical and physical test results.

Particle diameter (mm)	Test	Peak strength (MPa)			Y. mod. (GPa)			Poisson’s ratio		
		Num.	Physical		Num.	Physical		Num.	Physical	
			Mean	Stdev (%)		Mean	Stdev (%)		Mean	Stdev (%)
3.56	Uniaxial	3.02	-	-	2.93	-	-	0.076	-	-
	Triaxial (5.0 MPa)	20.5	-	-	-	-	-	-	-	-
	Triaxial (10.0 MPa)	44.0	-	-	-	-	-	-	-	-
6.34	Uniaxial	3.28	1.98	24.4	3.54	0.96	10.4	0.074	-	-
	Triaxial (5.0 MPa)	21.2	-	-	-	-	-	-	-	-
	Triaxial (10.0 MPa)	45.3	-	-	-	-	-	-	-	-
4.75	Uniaxial	3.14	2.98	18.3	2.98	1.08	19.6	0.069	0.32	33
	Triaxial (2.5 MPa)	10.10	-	-	4.09	-	-	-	-	-
	Triaxial (5.0 MPa)	20.82	25.48	1.7	4.25	2.63	5.8	-	-	-
	Triaxial (7.5 MPa)	32.71	-	-	4.21	-	-	-	-	-
	Triaxial (10.0 MPa)	44.43	42.70	0.62	4.39	3.23	1.1	-	-	-
	Brazilian Tensile	0.102	0.16	34	-	-	-	-	-	-

A detailed discussion on numerical and physical comparison in uniaxial and triaxial testing is given in the following sub-sections. It should be noted that all correlations of the results are based on a ball diameter of 4.75mm, unless otherwise mentioned.

5.2.1.1 Peak Strengths

The peak strengths determined in experimental and numerical uniaxial and triaxial testing are summarised in Table 5-1. In uniaxial testing, experimental results showed a mean value of 2.98 MPa with a standard deviation of 18.3%. This variability yields a value of 3.52 MPa and 2.43 MPa as upper and lower values respectively. Correspondingly, numerical UCS test yielded a value of 3.14 MPa which lies within the variability range and shows good agreement with the experimental results.

Experimental triaxial testing at confining pressures of 5.0 MPa and 10.0 MPa yielded mean values of 25.48 MPa and 42.70 MPa with a standard deviation of 1.7% and 0.62% respectively. The peak strengths in physical triaxial testing showed less variability, that is, less than 2% at 5 MPa confinement and less than 1% at 10 MPa confinement, which demonstrates a very good reproducibility and repeatability of the testing and curing conditions. Correspondingly, numerical triaxial tests were conducted at 2.5, 5.0, 7.5 and 10.0 MPa confining pressures. The peak strengths determined at these confining pressures are also summarised in Table 5-1. Numerical test results at 5.0 MPa confinement produced a peak strength of 20.82 MPa corresponding to experimental value of 25.48 MPa and 44.43 MPa in comparison to 42.7 MPa at 10.0 MPa of confining pressure. These numerical and physical peak strengths also show good correlation (i.e., variability less than 20%) similar to uniaxial testing. Additionally, numerical triaxial tests were conducted on intermittent confining pressures of 2.5 MPa and 7.5 MPa to increase confidence and introduce improved rigor in the numerical test results.

All the values of the numerical and experimental peak strengths were plotted in a peak strength-confining pressure space (i.e., $\sigma_1 - \sigma_3$). Fitting trend lines were plotted through numerical and experimental data and intercepted at mean UCS values corresponding to 0 MPA confining pressure (Figure 5-1). The linear curves of the upperbound and lowerbound were drawn for synthetic conglomerates as per the variation observed in test results. It was observed that the fitting curve of the numerical conglomerate lies within the scatter of the physical test results (Figure 5-1).

The slopes of both lines showed a linear relation between peak strength and confining pressure, for 0 to 10 MPa confining pressure range. The angle of the trend lines (ψ) were calculated as 75.8° and 76.2° for numerical and experimental data respectively which can related to the angle of internal friction (ϕ) by the following relation (after Brady & Brown 2005):

$$\tan\psi = \frac{1+\sin\phi}{1-\sin\phi} \qquad (5\text{-}1)$$

In summary, the peak strengths in numerical uniaxial and triaxial testing showed a good correlation with that of experimental tests as per the measured micro mechanical parameters input in PFC3D.

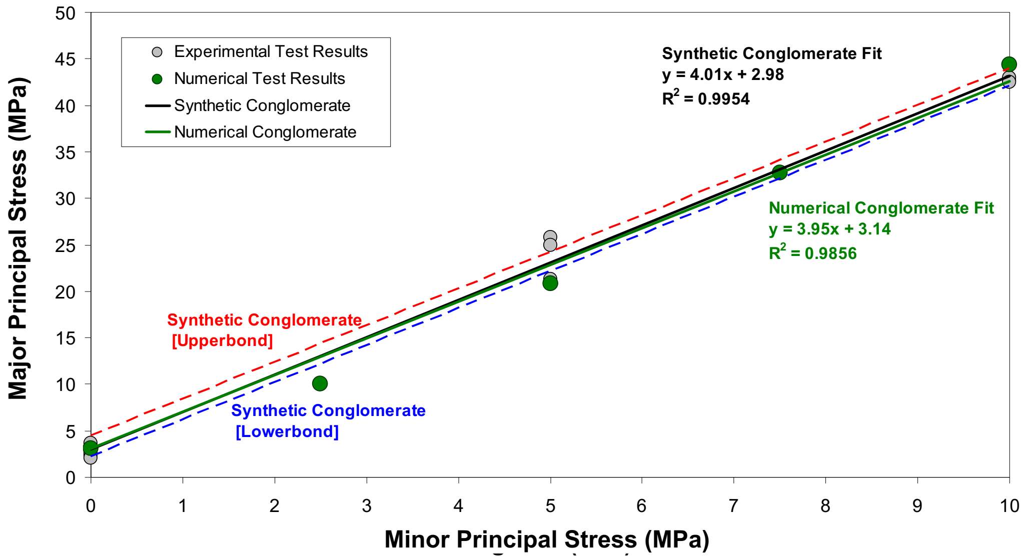

Figure 5-1: Comparison of peak strengths determined in uniaxial and triaxial testing on synthetic and numerical conglomerates.

5.2.1.2 Damage Thresholds

Experimental uniaxial testing was monitored for acoustic emissions and axial and circumferential strain measurements. The main objective of this exercise was to examine the progressive damage in the synthetic conglomerate, which can be traced in numerical assemblies in PFC (Diederichs 2003; Diederichs et al. 2004). A detailed discussion about experimental setup and analyses of the test results has been provided in Chapter 3. A comparison of stages of damage, observed in experimental and numerical uniaxial testing is given in Table 5-2 and shown in Figure 5-2. Both test results show a standard deviation of 15.3% and 3.3% for crack initiation (σ_{ci}) and crack damage (σ_{cd}) stages respectively, hence showing a good agreement in uniaxial testing when experimental test results themselves display a variability of 10.16% and 7.47% respectively.

In numerical conglomerates, damage stages were also determined in triaxial testing (Table 5-2 & Figure 5-2). It was observed that both the crack initiation and crack damage stages (in terms of the percentage of peak strengths) generally decrease with the increase of confining pressure. This decrease is less pronounced in the crack initiation stage (i.e., from 38.3% in UCS to 25.4% at 10.0 MPa confining pressure) and more pronounced in crack damage stage (i.e., from 68.3% in UCS to 37.5% at confinement of 10.0 MPa). The mean values of these stages in terms of percentages of peak strengths were calculated as 31.9% and 56.9% for crack initiation and crack damage thresholds respectively (Figure 5-2). A standard deviation of 16.9% and 24.1% were observed for these stages.

Table 5-2: Comparison of damage stress states in uniaxial compression between the synthetic and numerical conglomerates.

Stress states corresponding to damage thresholds			σ_{cc}	σ_{ci}	σ_{cd}	σ_{Peak}
Uniaxial	Experimental Test Results	Mean	0.31	1.05	2.03	2.98
		Stdev %	32.50	10.16	7.47	15.41
		Mean % of Peak	11.07	32.84	68.31	100
	Numerical Test Results	PFC3D Model	-	1.19	2.13	3.14
		% of Peak	-	38.14	68.27	100
	Comparison	Stdev %		15.28	3.28	3.32
Triaxial	Triaxial (2.5 MPa)	PFC3D Model	-	3.66	7.4	10.08
		% of Peak	-	36.31	73.41	100
	Triaxial (5.0 MPa)	PFC3D Model	-	6.14	13.5	20.84
		% of Peak	-	29.46	64.78	100
	Triaxial (7.5 MPa)	PFC3D Model	-	8.94	13.44	32.79
		% of Peak	-	27.26	40.99	100
	Triaxial (10.0 MPa)	PFC3D Model	-	11.34	16.78	44.74
		% of Peak	-	25.35	37.51	100
	Uniaxial & Triaxial	Mean % of Peak	-	31.26	56.90	100
		Stdev. (%)	-	16.93	24.09	0

In general it was observed that the systematic damage of the numerical conglomerate is equivalent to the synthetic conglomerate and they have a strong correspondence with each other.

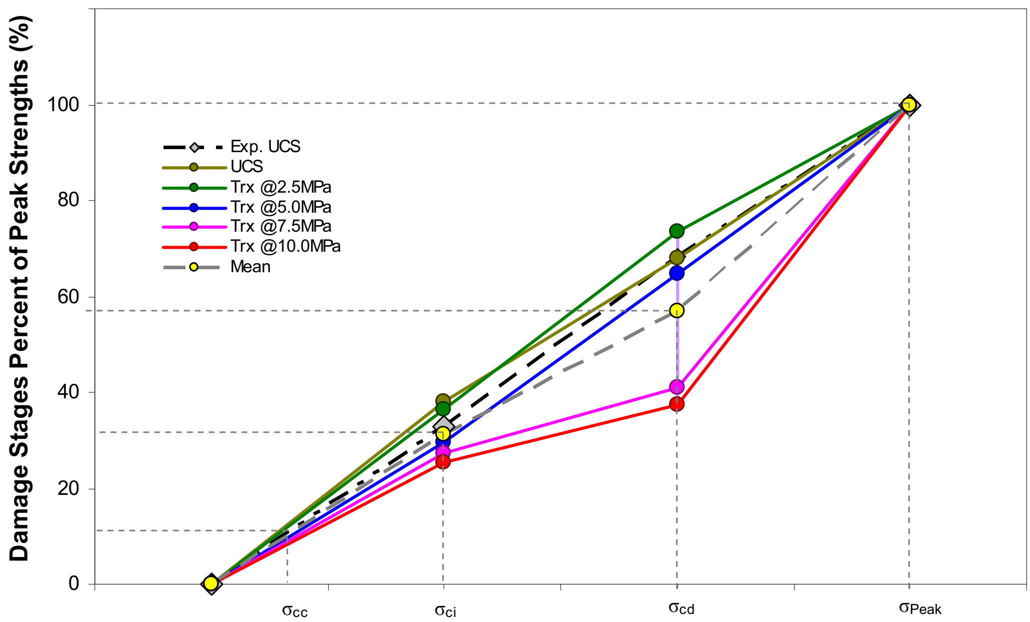

Figure 5-2: Plot showing progressive stages of damage (in terms of percent of peak strengths) observed in physical uniaxial testing and numerical uniaxial and triaxial testing. Mean curves for the damage threshold in numerical uniaxial and triaxial test results are also plotted.

Moreover, numerical triaxial investigations revealed that the crack initiation starts at 25-35% of the peak strengths and systematic crack growth starts at 45-65% of peak strengths. However, at low confining pressures these hold at upper bound values while at higher confining pressures they remain at lower bound values (Figure 5-2).

The crack closure stage (σ_{cc}) was not investigated in numerical testing as fixed porosity was used in specimen diagenesis, however, this can be investigated by assigning a high value of porosity and then creating more particles to reduce the porosity after the crack closure stage. Such a study was considered beyond the scope of the present research.

5.2.1.3 Elastic Parameters

The elastic parameters (i.e., Young's modulus and Poisson's ratio) of the physical and numerical conglomerates are summarised in Table 5-1. Both Young's modulus and Poisson's ratio of the numerical assemblies showed poor agreement with the experimental test results. Physical samples exhibited a Young's modulus of 1.02 GPa and Poisson's ratio of 0.32, while, in contrast, the numerical model yielded 3.0 GPa and 0.074 respectively, demonstrating a stiffer response in relation to the synthetic conglomerates. The elastic response of the numerical conglomerate is governed by the microscopic elastic parameters, that is, the elastic modulus of the contact and of the parallel bond (Itasca 2005). Since the Hertz-Mindlin contact model (Mindlin 1949) defines the elastic modulus of the interparticle contact, the only parameter that can contribute to the elastic response of the assembly is the elastic modulus of the parallel bond, which is defined by the normal and shear stiffnesses of the cementing material (i.e., parallel bond). The stiffnesses of the parallel bond were derived from the Young's modulus of the cementing material (cement paste). The ratio of the normal to shear stiffnesses was kept at 1.0 in all numerical simulations in this research as no direct method is available to determine this ratio. The values of Young's modulus of the numerical and physical test results are plotted in Figure 5-3 along with the value of the cementing material (cement paste). The plot indicates that the Young's modulus values of the numerical conglomerate are about three times the Young's modulii of the synthetic conglomerate. Interestingly, Instead of demonstrating a correlation with the synthetic conglomerate, these correspond to the modulii of the cement paste (Figure 5-3).

This observation suggests that the assembly's modulus is governed by the modulus of the parallel bond and in turn by the normal and shear stiffnesses and their ratio. In order to investigate the sensitivity of the stiffness ratio, a parametric sensitivity study was conducted to investigate the elastic response of the numerical model with shear/normal stiffness ratios of 0.75, 0.5 and 0.25. The results suggest that a lower stiffness ratio results in the macroscopic elastic parameters being closer to that of the physical system. However, reducing the stiffness ratio results in a reduction in peak strength to 2.1 MPa, compared to 2.98 MPa in the physical experiments. To understand the relation between normal and shear stiffness, a detailed micro-mechanical investigation including the explicit representation of the cement and particle contacts, is required in future work.

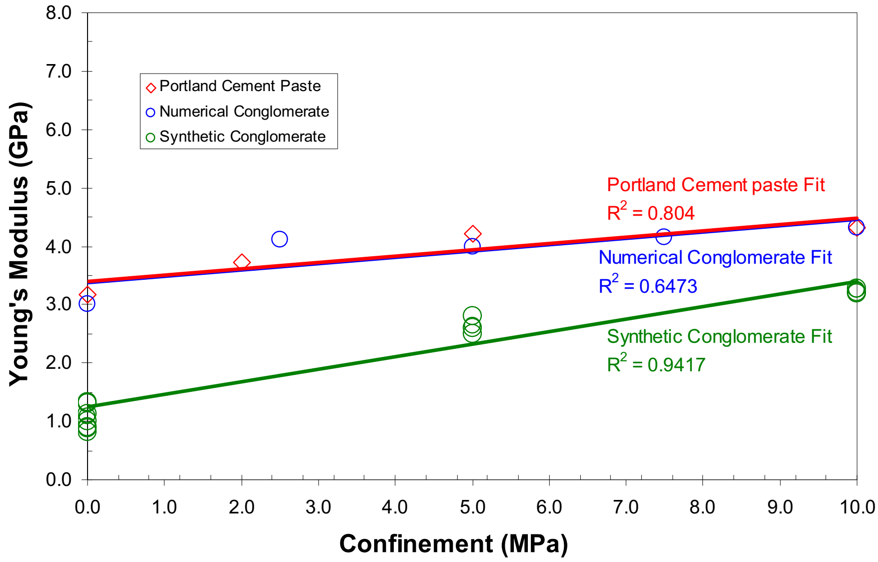

Figure 5-3: Variation of Young's modulii of cement paste, synthetic conglomerate and numerical conglomerate with the confining pressure.

Besides the stiffness ratio, another factor that could be responsible for obtaining lower values of Young's modulus in physical experiments is the friction and the presence of interparticle cement. The presence of interparticle cement offers the strain softening behaviour due to the friction and the crushing of cementing material. Whereas in the numerical simulation, after the parallel bond breaks, the load is carried by the interparticle contacts only as no interparticle cement is present between the particles. This could be one of the reasons for high values of the modulus and the lower values of Poisson's ratio in the numerical conglomerate. However, in future studies, the effect of high stiffness should be dealt either by measuring the exact stiffness ratio of the parallel bond or by replacing the parallel bond by an assembly of the fine particles to induce true interlocking of the interparticle cement.

5.2.1.4 Strength Envelopes

Mohr-Coulomb and Hoek-Brown criteria were compared between the synthetic and numerical conglomerates. The aim was to examine the suitability of failure criterion for synthetic and numerical conglomerates. The strength envelopes determined, are discussed in the following sections under the respective criteria headings.

- **Mohr- Coulomb Criterion**

The Mohr-Coulomb criterion for strength parameters was applied to both experimental and numerical test results (uniaxial, triaxial and Brazilian testing) and discussed in Chapter 3 and 4. Tension cut-offs were drawn on a negative shear strength axis based on the results of Brazilian tensile testing. The best fitted linear lines were drawn through the tangents of the Mohr's circles to yield cohesion (where the line intercepts on y-axis at 0 normal stress) and the angle of friction (being the slope of the line) by using Rocdata 4.0 (www.rocscience.com). A summary of Mohr-Coulomb parameters with tensile strength is given in Table 5-3 and plotted in Figure 5-4.

Table 5-3: Comparison of Mohr-Coulomb parameters for synthetic and numerical conglomerate.

Parameters	Physical	Numerical
Cohesion (MPa)	0.75	0.70
Angle of friction (Deg.)	37.3	37.0
Tensile strength (MPa)	0.16	0.10
Sum square of errors	10.21	16.27

Both the synthetic and numerical conglomerates produced the Mohr-Coulomb parameters with very good correspondence.

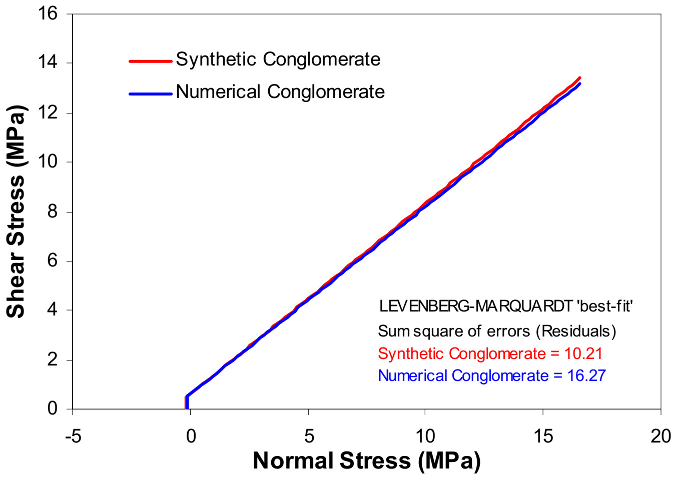

Figure 5-4: Comparison of Mohr-Coulomb best-fit curves for synthetic and numerical conglomerates.

The plot (Figure 5-4) demonstrates a good correspondence between the responses of the numerical and synthetic conglomerates. The Mohr-Coulomb ‘best-fit’ curves show a sum square of errors (residual) of 10.21 for synthetic conglomerate and 16.27 for numerical conglomerate. This comparison shows that the behaviour of the numerical and synthetic conglomerate can be predicted with a reasonable accuracy using Mohr-Coulomb criterion.

- **Hoek- Brown Criterion**

Hoek-Brown criterion was also applied on the physical and numerical test results. Hoek-Brown parameters were determined based on the testing data at a minor principal stress (σ_3) of 10.0 MPa. The summary of numerical and experimental parameters representing the strength envelopes is shown in Table 5-4 and curves are plotted in Figure 5-5. Synthetic conglomerate test data was observed to follow Hoek-Brown criterion with a sum square of errors of 6.33 and a value of 24.14 as the material’s constant (m_i). This shows that the synthetic conglomerate fits more rigorously with Hoek-Brown than with Mohr-Coulomb with a sum square of errors of 10.21. Moreover, the value of m_i =24.14 of the synthetic conglomerate lies within the range of the material’s constant of the natural conglomerate i.e., m_i =21±4 (Rocscience 2008).

Table 5-4: Summary showing the comparison of Hoek-Brown and fitted Mohr-Coulomb parameters determined by applying Hoek-Brown criteria on numerical and physical test data.

Hoek-Brown classification	Parameters	Comparison		Units
		Numerical	Physical	
Uniaxial compressive strength	σ_c	2.86	3.98	MPa
Geological strength index	*GSI*	100	100	
Material constant	m_i	27.99	24.14	
Disturbance factor	*D*	0	0	
Intact rock Young’s modulus	E_i	2980	1080	MPa
Hoek Brown criterion				
Material constant	m_b	27.99	24.14	
HB constant	s	1.0	1.0	
HB constant	a	0.5	0.5	
Failure envelope range				
	Application	Custom	Custom	
Maximum minor principal stress	σ_3^{Max}	10	10	MPa
Mohr-Coulomb fit				
Cohesion	*c*	2.16	2.35	MPa
Angle of friction	ϕ	31.96	33.48	degrees

Rock mass parameters				
Tensile strength	σ_t	-0.102	-0.16	MPa
Compressive strength	σ_c	2.86	3.98	MPa
Rock mass compressive strength	σ_{cm}	2.96	4.02	MPa
Rock mass modulus	E_{rm}	2963	1074	MPa
Sum square of Errors (Hoek-Brown fit)		100.23	6.33	

However, in contrast, numerical conglomerate data fitted the Hoek-Brown criterion curve with a sum square of errors of 100.23 yielding m_i of 27.99. The difference in the fitting parameters clearly indicates the contrasts between the behaviours of numerical and synthetic conglomerates. The response of numerical conglomerate is, therefore, best represented by Mohr-Coulomb criterion than Hoek-Brown.

Yet, as Table 5-4 demonstrates, the Hoek-Brown parameters (i.e. m_b, m_i, a and s) of both synthetic and numerical conglomerates, show reasonable correspondence. The material's constants (m_b, m_i) of synthetic conglomerate yield a value of 24.14 while the numerical conglomerate gives 27.99 in comparison. The difference in material's constant was considered to be because of the number of tests and corresponding confinements. A sensitivity study was conducted to vary the results of the triaxial test data to match the m_b and m_i values. It was noted that if both numerical and experimental tests had been conducted under the same confining pressure, the difference in the values could have been reduced.

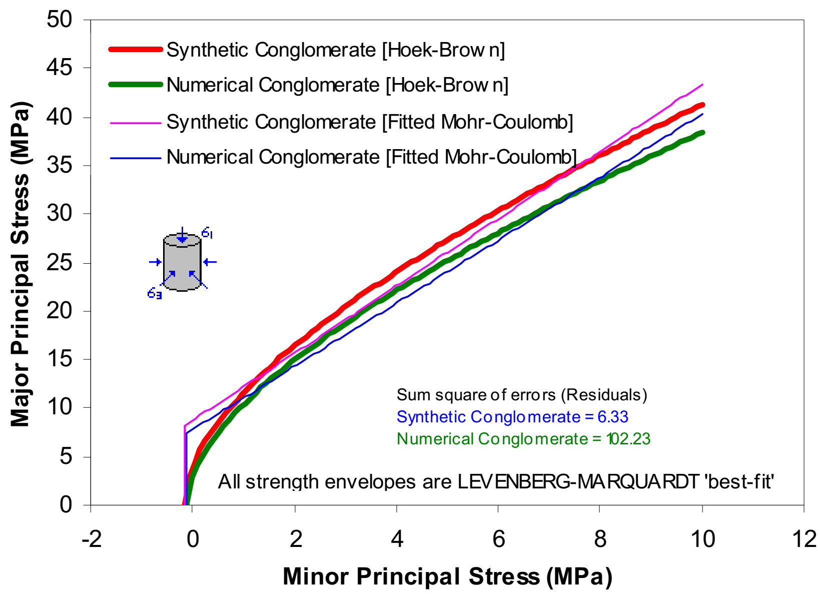

Figure 5-5: Comparison curves of Hoek-Brown criteria applied to results of synthetic and numerical conglomerates in major and principal stress space.

5.2.1.5 Modes of Failure

As well as a quantitative comparison (i.e., strength and elastic parameters) of the responses of the synthetic and numerical conglomerates, a qualitative comparison of the failure modes or mechanisms was necessary. It was even considered to be of greater importance as it reflects the stress distribution and assembly's response to a particular loading. Therefore, in uniaxial and triaxial testing, care was taken to observe the modes of failure in the experiments. In uniaxial testing, all the samples were observed to fail in the axial direction, that is, tensile fractures were observed parallel to the loading axis.

In triaxial compression, synthetic conglomeratic samples lost cohesion during extraction from the Hoek's cell and therefore, the failure mode was not precisely observed. However, no axial cracks were observed from the recovered remains of the specimen in contrast to uniaxial testing. Hence, it is hypothesised that the failure mode of the specimen in triaxial testing was not axial splitting.

In PFC, the failure mode of a specimen can be traced by the bond breakage, that is, the development of cracks. The breakage of every bonded contact can be traced as a normal or tensile crack if bond breaks because of tensile forces acting on the bond, and as a shear crack, if the bond breaks because of shear forces exceeding the shear strength of the bond. The tracing of the cracks in numerical uniaxial and triaxial was detailed in Chapter 4.

From the analysis of uniaxial testing, the failure mode of the numerical specimen was also observed as axial splitting comparable to the synthetic conglomerate. The dominant types of micro cracks developed in uniaxial testing were tensile or normal cracks which were considered to be a function of the development of the tensile forces in the specimen. This suggested that the mode of failure is tensile or axial splitting. This was also evident from the high normal to shear crack ratio. Hence, in summary, numerical and synthetic conglomerates showed agreement in the mode of failure in uniaxial testing which, in turn, suggests an equivalent load distribution and damage in both systems.

In numerical triaxial testing, it was observed that the development of micro cracks progressively changes from tensile to shear with an increase in the confining pressure. This was observed by the normal to shear crack ratio. In uniaxial testing, this ratio is greater than 50, while is less than 0.1 in the triaxial test at 10.0 MPa confinement, reflecting the dominance of shear cracks over tensile cracks. The concentration of the cracks was observed throughout the specimen and the failure mode could not be traced. This is because, in PFC3D, cracks on a cross-section plan cannot be transferred to delineate a macroscopic fracture. However, micro fracture development suggests shearing in the specimen at higher confinements, which leads to shear failure. This is in line with the experimental observations in the triaxial testing and therefore, shows reasonable agreement.

In uniaxial testing, the post peak behaviour of the synthetic conglomerate was observed as ductile, or strain softening and strain hardening, in triaxial testing probably due to interparticle dilation and crushing of interparticle cement. But in numerical conglomeratic specimens, post peak behaviour was observed as brittle with a sudden stress-drop in uniaxial testing. However, this response was found sensitive to the confining pressure and shifted from brittle axial splitting towards progressive ductile (strain softening) when the confining pressure was increases.

5.2.1.6 Sensitivity of Particle size

The macroscopic response of a granular assembly such as a conglomerate is influenced by the size of particles (Itasca 2004; Potyondy & Cundall 2004; Itasca 2005). To investigate and compare this effect in both numerical and synthetic conglomerate, various particle sized specimens were tested in uniaxial and triaxial testing.

In the experimental study, uniaxial testing was undertaken using particles size of 4.75 mm and 6.34 mm. Correspondingly, numerical uniaxial testing was performed on assemblies with particle diameters of 3.56 mm, 4.75 mm and 6.34 mm. The observed macroscopic responses of both numerical and physical assemblies are compared in Figure 5-6.

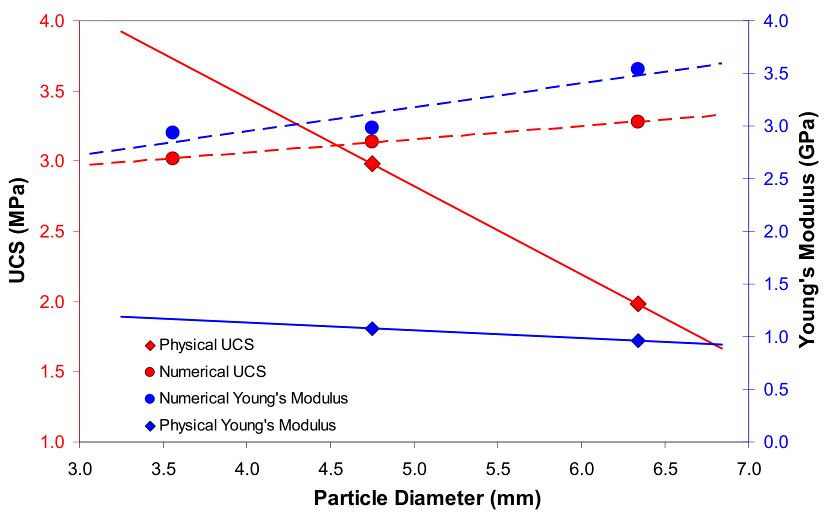

Figure 5-6: Comparison of particle size sensitivity on peak uniaxial strength and Young's modulus of synthetic and numerical conglomerates (modified after Akram & Sharrock 2010).

It was noted that the peak strength and Young's modulus both decrease in experimental studies. The UCS decreases from 2.98 to 1.98 MPa, and the modulus from 1.08 to 0.96 GPa with the increase of particle size from 4.75 mm to 6.34 mm. However, in contrast, numerical conglomeratic specimens showed an increase in both peak strength and Young's modulus. The UCS increased from 3.02 to 3.3 MPa and modulus from 2.9 to 3.5 GPa with the increase of particle size from 3.56 mm to 6.34 mm (Figure 5-6). These results are consistent with that of the parametric sensitivity study, discussed in Section 3.5.4.3 of FISH volume,(Itasca 2005). One reason for the decrease of peak strength and modulus observed in the synthetic conglomerate may be the use of the same normal strength (for the parallel bond) as was used when the particle diameter was 4.75mm. Another reason could be the development of micro cracks during the curing of physical samples and/ or the presence of residual moisture at the time of testing, which resulted in early failure and more strain softening behaviour. Further work on the sensitivity of particle size is required to make the numerical and physical correlations more conclusive.

The sensitivity of particle size within the numerical simulation of triaxial testing was also studied. The triaxial tests were conducted with particle's size of 3.56 mm, 4.75 mm and 6.34 mm. The test results were then subjected to Mohr-Coulomb and Hoek-Brown criteria at a minor principal stress (σ_3) of 10.0 MPa using Rocdata. The summary and comparison of the input and output parameters for all three responses are given in Table 5-5 and the curves are shown in Figure 5-7 for Hoek-Brown and in Figure 5-8 for Mohr-Coulomb criteria. The parameters for Mohr-Coulomb fit corresponding to Hoek-Brown criterion were also determined.

Table 5-5: Summary showing comparison of the Hoek-Brown and Mohr-Coulomb parameters determined by applying Hoek-Brown and Mohr-Coulomb criteria on numerical test data for particle diameters 3.56, 4.75 and 6.34 mm.

Hoek-Brown classification	Parameters	Comparison of numerical models with different diameters			Units
		3.56mm	4.75mm	6.34mm	
Uniaxial compressive strength	σ_c	2.91	2.86	2.95	MPa
Geological strength index	*GSI*	100	100	100	
Material constant	m_i	26.41	27.97	29.47	
Disturbance factor	*D*	0	0	0	
Intact rock Young's modulus	E_i	2930	2980	3530	MPa
Hoek-Brown criterion					
Material constant	m_b	26.41	27.97	29.47	
HB constant	*s*	1	1.0	1	
HB constant	*a*	0.5	0.5	0.5	
Failure envelope range					

	Application	Custom	Custom	Custom	
Maximum minor principal stress	σ_3^{Max}	10	10	10	MPa
Mohr-Coulomb fit to Hoek-Brown criterion					
Cohesion	c	2.14	2.16	2.22	MPa
Angle of friction	ϕ	31.62	31.96	32.68	degrees
Mohr-Coulomb criterion (Directly applied on numerical data)					
Cohesion	c	0.50	0.53	0.55	MPa
Angle of friction	ϕ	37.42	37.59	38.00	degrees

The analysis demonstrated that Hoek-Brown parameters (m_i, m_b) and Mohr-Coulomb parameters (c, ϕ) both increase with the increase of the particle diameters, from 3.56mm to 6.34mm (Figure 5-9).

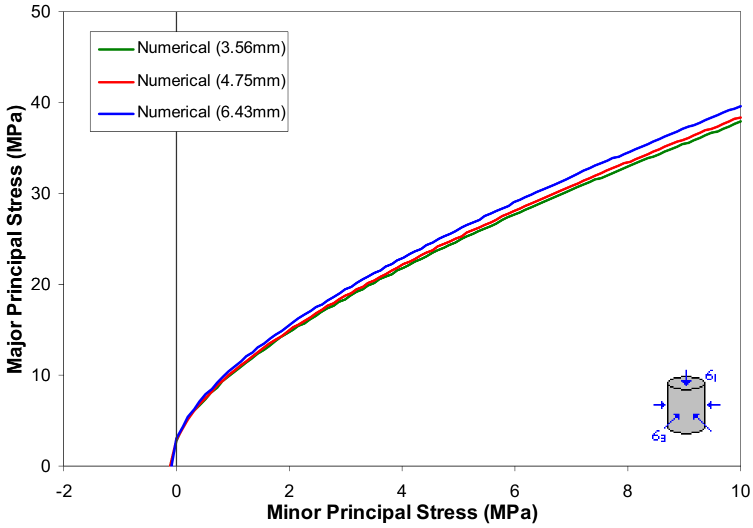

Figure 5-7: Comparison curves of Hoek-Brown criteria applied to numerical and experimental test results based on test data in major and principal stress space.

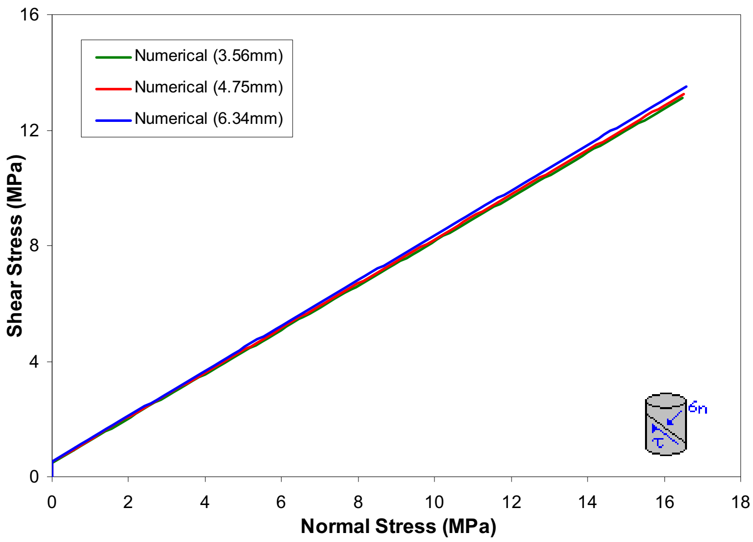

Figure 5-8: Comparison curves of Mohr-Coulomb criterion applied to numerical test results (direct) in normal and shear stress space.

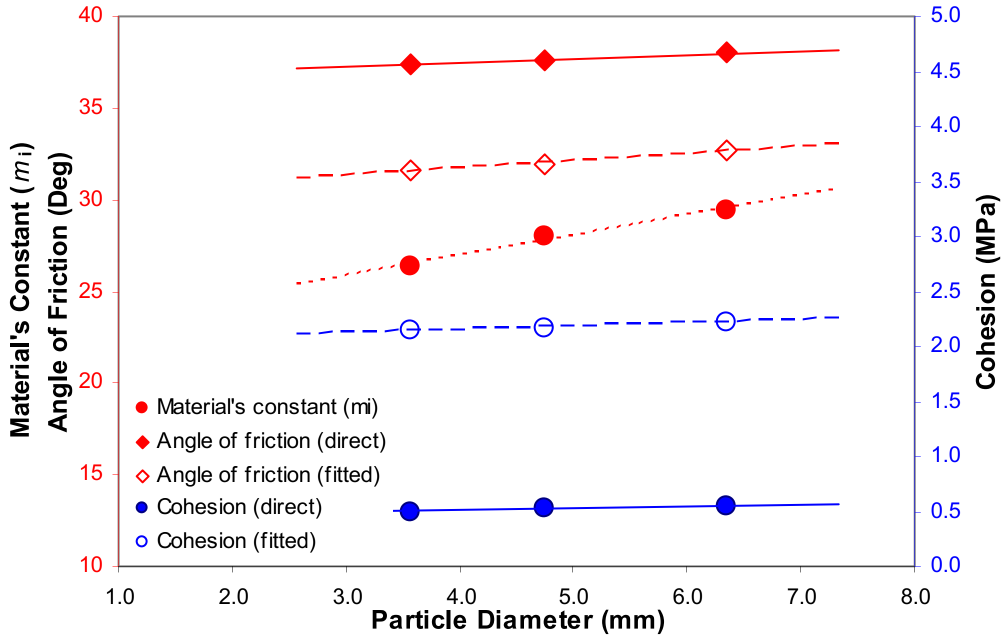

Figure 5-9: Sensitivity of Hoek-Brown and Mohr-Coulomb parameters (i.e., m_i & c,ϕ), with particle size. Mohr-Coulomb parameters (c,ϕ) shown here comprise both determined directly by applying criterion on the test data and those obtained by fitting curves on Hoek-Brown criterion.

5.2.2 Brazilian Testing

The results of the experimental and numerical Brazilian tensile strength tests were compared for tensile strength and mode of failure. These are discussed below under respective headings.

5.2.2.1 Tensile Strength

The analysis of the experimental Brazilian test results yielded a value of 0.16 MPa (Table 5-1) at the loading rate of 0.005 mm/s. In PFC, a sample was prepared corresponding to the physical specimen, with parallel bonds, and tested under equivalent conditions. The numerical test produced a tensile strength of 0.1 MPa with a standard deviation of 32% from the experimental value. This variability further reduced to approximately 25% at a displacement rate of 0.01m/s. The comparison (Table 5-1) was considered reasonable, as experimental test results had 35% variability.

5.2.2.2 Failure mode

Besides the tensile strength, the mode of failure of the Brazilian specimen is very important, as a well developed discrete crack through the sample depicts the necessary tensile stress conditions.

In all physical Brazilian tests, a well defined crack along the loading axis was obtained in synthetic conglomerate specimens, which, necessarily, depicts the tensile failure of the sample disc into two halves (Figure 5-10).

Figure 5-10: Failure modes obtained in physical discs in Brazilian testing.

The damage in the numerical Brazilian disc at various loading rates is illustrated in Figure 5-11. At the adopted loading rate (i.e. 0.005 m/s), the numerical Brazilian sample did not fail in tension properly parallel to the loading direction, but instead it collapsed showing localised damage (notches) near the loading platens (Figure 5-11). This failure is consistent with previous findings of numerical Brazilian tests (Potyondy & Cundall 2004; Itasca 2005).

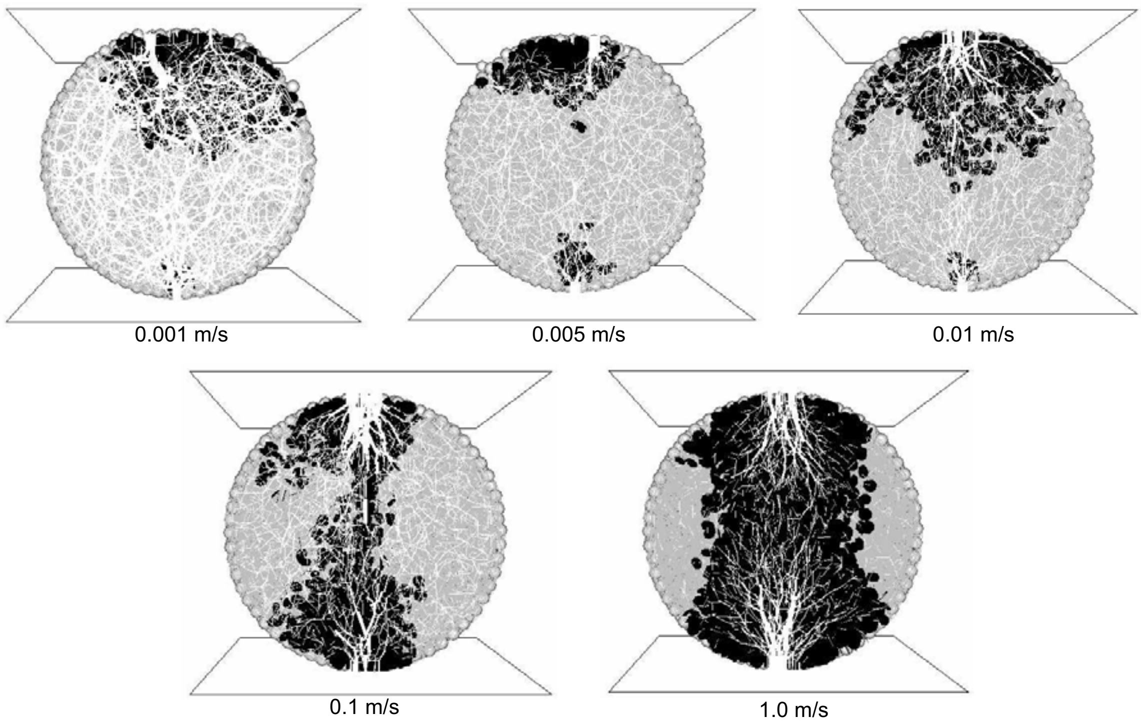

Figure 5-11: Failure modes observed at various loading rates in numerical Brazilian testing: grey lines indicate the locations of parallel bonds, black colour denotes the cracks, and white lines show the stress distribution in the discs.

However, at high loading rates (i.e., 0.1 - 1.0 m/s), the location of damage in the sample becomes progressively parallel to the loading axes (Figure 5-11).

Perhaps, the reason for the development of localised distribution of cracks near the top and bottom platens is the empty spaces between the balls and parallel bonds (if for example, the parallel bonds are transmitting load and moments).

It is understood that a force chain or fibre is developed through point contacts and bonded region of the particles, that is, the forces and moments are transferred through the ball contact points and parallel bonds. Hence, the empty spaces between the balls do not contribute either to load or moment transfer, which in turn, relaxes the vertical load by breaking the bond in a random direction along the distribution of balls and parallel bonds. Although the fibre developed throughout the top and bottom platens clearly indicates the loading direction, this force-chain diminishes and is distributed throughout the disc as it gets away from the platens, without giving a pronounced trend along the load axis.

Consequently, the increase in the applied load contributes to bond breakage in the stressed region near the top and bottom platen as is evident in Figure 5-11 rather than concentrating along the load axis.

The contrast in the observed failure mechanisms of synthetic and numerical conglomerates, again highlights the significance of the presence of the interparticle cement similar to its effect on the failure mechanism in triaxial specimens. This suggests that presence of the interparticle cement even after the bond breakage has significant implication in controlling the mechanisms and behaviour of a conglomerate.

5.2.3 Shear Box Testing

The comparison of the shear box test results of synthetic and numerical conglomerates is presented in Table 5-6 and shown in Figure 5-12.

The analyses of the numerical modelling produced a cohesion of 3.46 MPa comparable to corresponding experimental value of 3.56 MPa, whereas the apparent angle of friction (i.e., $\phi + i$) was 77.25°, in comparison to 83.90° of the experimental apparent angle of friction.

Both physical and numerical test results showed that maximum dilation occurred at the post peak deformation stage. The onset of dilation was found sensitive to the normal load. An increase in normal stress delays the onset of dilation by increasing the peak strength. These observations were found consistent with the numerical uniaxial and triaxial test results and were also in agreement with tests on natural rocks (Zhao & Cai 2010).

Table 5-6: Comparison of physical and numerical shear box test results (modified after Akram & Sharrock 2010).

Normal load (MPa)	Shear strength (MPa)	
	Physical	Numerical
0.0	-	3.46
0.5	7.88	5.3
1.0	12.57	7.18
2.0	21.20	12.8
Cohesion (MPa)	3.56	3.46
Apparent angle of friction (deg)	83.90	77.25
Mean angle of dilation (deg)	46.08	39.98
Angle of friction (deg)	37.82	37.3

The angle of dilation calculated in the experiments was 46.1 which yielded an angle of friction of 37.8° comparable to 37.3° in numerical uniaxial and triaxial testing. Correspondingly, an angle of friction of 37.3 and angle of dilation of 40° were calculated in the numerical test results. The lower value of the dilation angle in numerical simulation (40°) compared to the experimental value (46.1°), suggests that the vertical dilation in shear is the function of interparticle friction and particle rotation only. However, in physical tests, the high value of the dilation angle is a function of all the components of the interparticle friction between the balls and the cement matrix along with complex phenomena such as the crushing of the cement matrix, and the overriding and restricted rotation of particles because of the interstices cement. Moreover, the specified friction (interparticle friction in PFC) can be mobilised as long as particles stay in contact with each other. But in the case when bonds are broken and there is gap between the particles simulating a crack, no material is present between the particles that can offer friction along the crack plane. This would contribute to the lower angle of dilation.

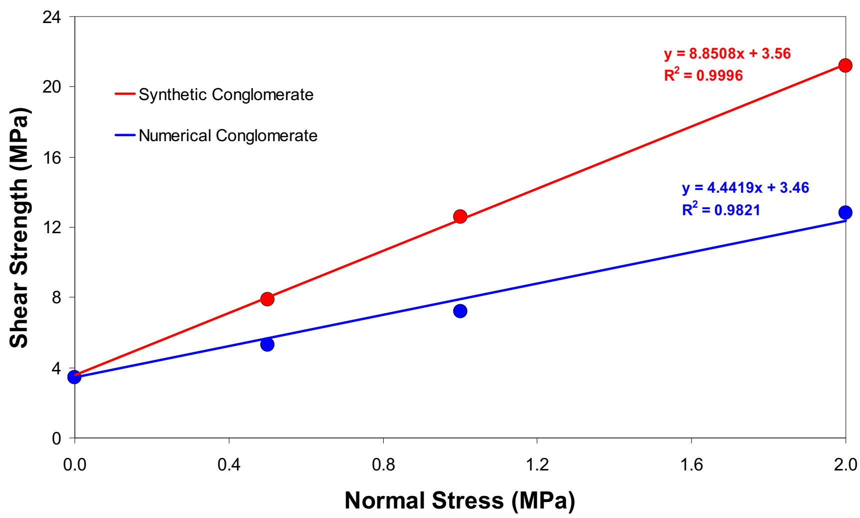

Figure 5-12: Comparisons of peak strengths determined in shear box testing on synthetic and numerical conglomerates (modified after Akram & Sharrock 2010).

According to the findings of Lajtai (1969) in his study of the shear strength of intact material, the shear strength at low confinements should be equal to the tensile strength of the intact material, as per Equation (5-2). This hypothesis was also demonstrated by Cho et al. (2008) in PFC2D simulation of a shear box test in their investigation of shear zones.

$$\tau = \sqrt{\sigma_t(\sigma_t - \sigma_n)} \tag{5-2}$$

But in our case at zero confining pressure, the cohesion intercept was obtained as 3.56 MPa in synthetic conglomerates, and 3.46 MPa, in numerical simulations, which is significantly higher than the tensile strengths (0.1 MPa and 0.16 MPa of the numerical and physical respectively). This suggests that the PFC2D model used by these researchers perhaps may not represent a real life situation, due to constraint of the third dimension. Another reason could be the discrete nature and behaviour of the numerical conglomerate which was simulated with steel particles and Portland cement matrix.

In view of Figure 5-12 and Table 5-6, a poor correlation was observed in the responses of numerical and synthetic conglomerates in shear box testing. However, at 0 MPa normal stress, a reasonable agreement of both conglomerates was noted, but, with an increase of normal stress, the contrast of the results increased. This was induced by the difference in the dilation angle. The angle of dilation of the synthetic conglomerate was not reproduced in the numerical conglomerates because of high micro frictions and complex mechanisms such as cement crushing, overriding and restricted rotations of particles owing to cement matrix. These mechanisms, that offer high interlocking in synthetic conglomerate, can not be induced in PFC simulation with parallel bonds.

A numerical study was also undertaken to examine the role of particle rotation during shear box testing by incorporating a layer of unbonded particles so that the particles could rotate freely during shearing. The thickness of the layer varied from 0.0 mm to 5.0 mm (almost the diameter of the particle). This study showed that the cohesion and dilation angle decrease with an increase in the number of free rotating particles (the thickness of the layer of the unbonded particles). This, in turn, suggests that during shearing particles with broken bonds undergo excessive rotation and yield less dilation incontrast to experiments where particle rotation is restricted because of interparticle cement. This finding is consistent with the low value of dilation angle (40°) obtained in shear box simulation.

5.3 Summary and Conclusions

A comparison of synthetic and numerical conglomerate was presented in ISRM recommended tests. Synthetic conglomerate specimens were created by Portland cement and steel balls of uniform size. Equivalent numerical conglomerate specimens were constructed in PFC3D using parallel bonds. The parallel bond represents the cementing material between the spheres; hence the micro-mechanical parameters measured through physical testing on Portland cement paste were specified in order to construct microstructurally equivalent numerical specimens. Interparticle friction was determined using inverse modelling to recover the bulk friction of synthetic conglomerates.

The numerical simulation reproduced many of the important features of the macroscopic response of the synthetic conglomerate in laboratory testing. In uniaxial compression, the numerical tests had good agreement with the physical tests for peak strengths, damage thresholds and failure mechanisms. Similarly, a good comparison of the same results was obtained in triaxial testing, except for the failure mechanism which was not observed in synthetic conglomerate as specimens collapsed during their extraction from the confinement cell. The post peak behaviour of the synthetic conglomerate was not produced by the numerical simulation as when the parallel bonds representing the cementing material fail, the particles are free to move and rotate. Therefore, the post peak effect of actual cementing material as was observed in the synthetic conglomerates cannot be gained using the parallel bond model. For this purpose, the presence of the cementing material is required to restrict the particle rotation and the interparticle transfer of the load after the breakage of parallel bonds.

In uniaxial and triaxial laboratory tests, the numerical conglomerate produced a relatively stiffer elastic response (i.e. higher Young's modulus and lower Poisson's ratio) than that of the synthetic conglomerate which is more comparable to cement paste than the synthetic conglomerate. This indicates that in the numerical model, the interparticle friction yields bulk friction (equal to that of the physical assembly) based on the stiffness of cement only without taking into account the presence of interparticle cement. Whereas in the physical model, interparticle friction is a complex interaction of ball-ball, ball-cement and cement-cement frictions as well as cement crushing, which makes the overall elastic response more strain softening.

The parametric study of the bond stiffness ratio in uniaxial tests showed that the elastic response of the numerical conglomerate is sensitive to the shear to normal stiffness ratio of the cementing material. Young's modulus decreases and Poisson's ratio increases with the reduction of the stiffness ratio. Hence, an appropriate stiffness ratio comparable to the physical model along with measured interparticle friction needs to be incorporated in the simulation of all laboratory testings to validate the elastic parameters of the numerical assembly. This is a topic for future research.

In uniaxial and triaxial tests, the particle size sensitivity of numerical and synthetic conglomerates did not show any correspondence between their responses. More work is required to precisely account for the effect of particle size on assembly behaviour.

In Brazilian tests, the tensile strength of the numerical simulation depends upon the loading condition and increases with an increase in the loading rate. The adopted tensile strength was found within the variation range of the physical test results. However, a well developed distinct crack through the sample could not be obtained at the adopted loading rate. This seems to be the function of the loading fibre through the particles and interparticle cement. After breakage of the parallel bond near the relative high stressed regions (e.g., near top and bottom platens), forces are transferred through the interparticle contacts only (as interparticle cement is not present) which induce damage in random directions rather than its concentration along a definite failure surface.

Further, load is transferred through the platens and through the boundary particles which are in contact with platens. If the boundary particles do not make a uniform geometry of the boundary, during loading some particles in contact with platens will experience high forces while others, having no direct contact with the platens, will experience reduced forces. This non-uniform load distribution transferred to the specimen may not induce a framework of tensile forces leading to a discrete crack.

In the shear box tests, a relatively poor correlation between the overall responses of the synthetic and numerical conglomerates was observed. At low normal stresses, the correlation between the both conglomerates was found reasonable, while at high normal stresses, a poor correlation, induced by the difference in the dilation angle, was noted. The angle of dilation of the synthetic conglomerate was not reproduced in the numerical conglomerate, even with the use of high interparticle friction.

The contrasts in the responses and failure mechanisms of numerical and synthetic conglomerates in all tests highlight the significance of the existence of the cement matrix. The presence of the cement was found to be responsible for inducing high interlocking and dilation at a micro level and resulting high bulk friction at assembly level in synthetic conglomerates. Cement matrix also affects the failure mechanism of the specimens in all tests due to high micro frictions between the particles and the cement matrix as well as complex mechanisms, such as cement crushing, overriding and the restricted rotation of particles. Hence, cement matrix has an important role in controlling the responses and failure mechanisms of conglomerates in various loading.

Conversely, the parallel bonds simulate the cement matrix as long as bonds are intact; however, after the bond breakage when no cement is present, the mechanisms of cement crushing and micro frictions among the particles and cement can not be induced to affect the macroscopic response of numerical conglomerates. However, this problem can be solved either revising the contact and/ or bonding models or replacing the cement (parallel bond) with fine particles, which definitely will involve greater computation cost using normal computing machines.

It should be noted that in the present research, no sensitivity study was conducted to investigate the effect of different boundary conditions. In all numerical simulations, wall based boundary condition were applied for specimen diagenesis and testing in an attempt to obtain numerical testing conditions as equivalent as possible to physical testing conditions. However, it was considered that the adopted boundary conditions may have impact on the mechanical response of the numerical conglomerates and implication on the failure mechanisms especially in Brazilian tests. Therefore, in future research, boundary conditions need to be investigated for modelling the response of conglomerates in all tests.

In spite of observed behavioural contrasts in the synthetic and numerical conglomerates, the overall response of the numerical conglomerate was considered reasonably good and in agreement with that of the synthetic conglomerate, and can be used to investigate the mechanics of natural conglomerates, which is impossible in physical experiments. The comparison of the numerical and synthetic conglomerates provides a baseline understanding of the capability of the DEM and highlights its strengths and weaknesses in simulating the behaviour of a natural conglomerate.

The influence of the particle and interparticle cementing materials, scaling and particle size distributions have been investigated for natural conglomerates using PFC3D simulations. These investigations are discussed in Chapter 6.

Similarly, using PFC2D, a micro investigation was conducted to explore and investigate the particle-cement interaction of synthetic as well as numerical conglomerates. This study is detailed in chapter 7.

Numerical Investigation of Idealised Natural Conglomerates

6.1 Introduction

This chapter presents the investigations undertaken on numerical conglomerates that represent idealised natural conglomerates with spherical clasts. The investigations were conducted to examine the sensitivity of the mechanical behaviour of an idealised conglomerate with reference to particle material, the properties of the interstices cement, scaling and particle size distribution. These factors are commonly believed to influence the mechanical response of a conglomeratic rock; however, the relative significance of these factors is not well-understood as the mechanical response is mutual interplay of these factors. Therefore, the main objective of these studies was to observe the relative significance of a particular parameter in controlling the response of a numerical conglomerate and apply the findings to understand the response of natural conglomeratic rocks.

The correlations in the responses of synthetic and numerical conglomerates in various tests detailed in Chapter 5, showed that DEM simulations can model the behaviour of physical material. Despite the contrasts observed in these correlations, numerical simulation was hypothesised to capture the sensitivity of the parameters that were kept constant in the comparison study.

Firstly, the effect of particle size distribution was studied. In previous numerical simulations, uniform sized particles were modelled (Chapter 4) to create the numerical conglomerate so that the maximum to minimum particle size (diameter) ratio was one (1). But here, in the sensitivity study, a non-uniform particle size distribution with a particle ratio greater than one was used and the relative variation of the assembly response was analysed.

Scaling, or the effect of specimen size, is an important parameter in rock mechanics and influences the test results. In natural rocks, the effect of specimen size has been investigated by various researchers (e.g., Hoek & Brown 1980b) and, generally, the strength of a rock was observed to decrease when increasing the specimen size. In order to examine the effect of specimen size in a conglomeratic rock, an investigation was undertaken on a numerical conglomerate. In this study two aspects of scaling were investigated; namely proportional and non-proportional scaling.

In proportional scaling, specimen dimensions and particle sizes were varied proportionally so that number of particles in a specimen, and the particle size to specimen size ratio, remained the same in all scaled models. While in non-proportional, scaling specimen dimensions were varied, keeping the particle size constant so that both the number of particles and the particle to specimen ratio were different for each scaled model. The results of non-proportional scaling were compared with that of natural rocks.

In the sensitivity study of the particle material, the steel balls used in the previous numerical simulations (Chapter 4) were replaced with low strength rock materials and the variation in the mechanical response was studied. Similarly, Portland cement paste, the interparticle cement in numerical conglomerate (Chapter 4) was also replaced by natural interparticle cementing agents. The effect of the stiffness and strengths of both clast and interparticle cement in controlling the mechanical response of idealised natural conglomerate was investigated.

6.2 Effect of Particle Size Distribution

In natural conglomerates, particle distribution is primarily related to the depositional environment. Uniformly grained conglomerates are considered to be the result of constant flow conditions while poorly graded conglomerates are believed to be the result of changing flow conditions. In synthetic conglomerates, uniform sized steel balls were used which resulted in a uniformly grained conglomerate (Chapter 3) and correspondingly, the same texture was reproduced in the numerical simulations (the numerical conglomerate, Chapter 4). Hence, in both synthetic and numerical conglomerates, the maximum to minimum particle size ratio (R_{max}/R_{min}) was one (1).

To investigate the effect of particle size distribution, numerical conglomerates were prepared with two particle size distributions. In the first conglomerate test specimens, a maximum to minimum particle radii ratio of 1.25 was used while in second set of specimens, this ratio was changed to 1.5 (Figure 6-1).

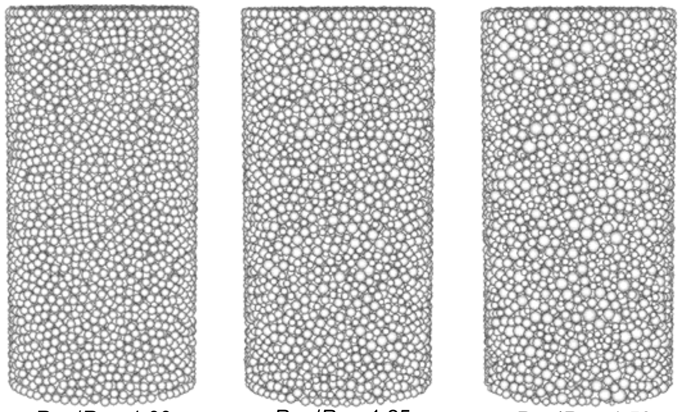

Figure 6-1: Prepared specimen of numerical conglomerates for uniaxial and triaxial testing at particle ratio (R_{max}/R_{min}) of 1.0, 1.25 and 1.50.

To eliminate the effect of porosity on the mechanical response, the initial porosity of both conglomerates was constant (39.7%), equivalent to the synthetic conglomerate. The sequence of specimen preparation and testing was kept the same, as discussed in Chapter 4, for uniaxial, triaxial and Brazilian testing. During the specimen preparation, the properties of particles and interparticle cements (parallel bonds) were kept constant as for the previous numerical simulation of the same, so that the only variable was the particle size distribution. Similarly, numerical testing conditions were also kept constant in all tests on both conglomerates. Uniaxial, triaxial (at 5 MPa and 10 MPa confining pressures) and Brazilian tensile strength tests were conducted to record mechanical responses in terms of peak strengths, Young's modulii and Poisson's ratios. The results were then plotted against the particle size ratios to observe the sensitivity of particle size distribution (Figure 6-2 & Figure 6-3).

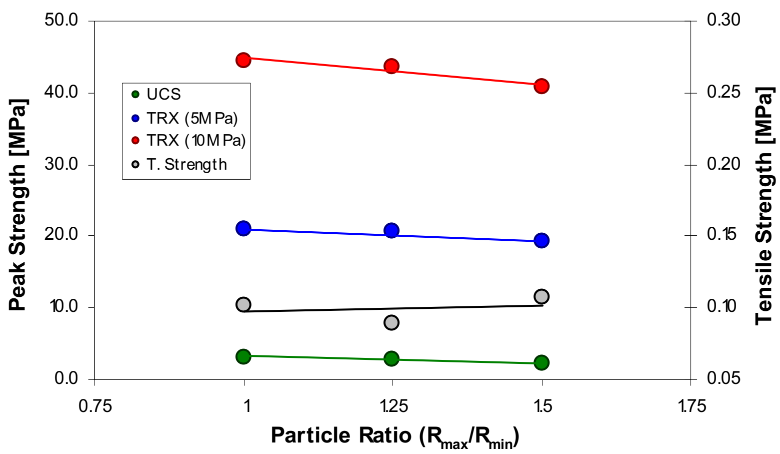

Figure 6-2: Variation of the peak strengths in uniaxial, triaxial and Brazilian tensile tests with particle radii ratio (R_{max}/ R_{min}).

The peak strengths both in uniaxial and triaxial testing, were observed to decrease with the increase of the particle size ratio from 1.0 to 1.5 at the same porosity. The damage in the conglomeratic specimens in uniaxial testing is shown in Figure 6-4 with particle radii ratios of 1.0, 1.25 and 1.50. The contrast in the damage reflects the different stress distributions (fibre effect) in the specimen induced by the distribution of different particle size ratios. Hence, changing the particle size distribution not only affects the peak strengths but also the evolution of damage in the specimen, and the variability in the test results.

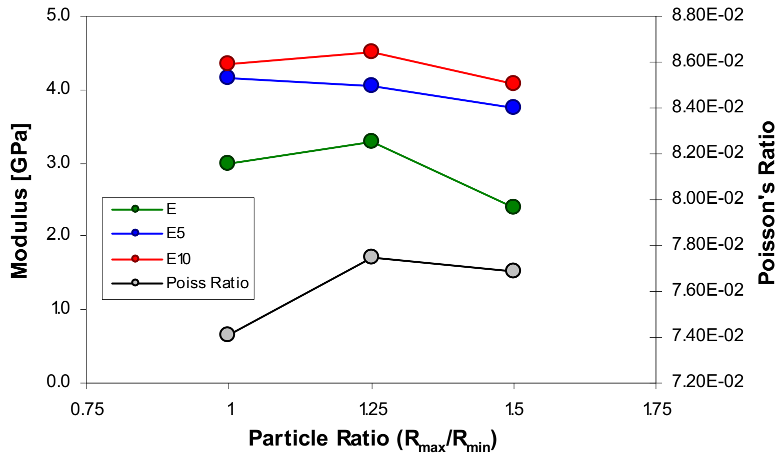

Figure 6-3: Variation of Young's modulii and Poisson's ratio with particle ratio.

The tensile strength in Brazilian tensile tests, however, did not show any definite trend with the particle size ratio. It decreased at a particle ratio of 1.25 and increased at a particle ratio of 1.50 (Figure 6-2). Similarly, the damage in the specimen also changes with the variation of particle size distribution (Figure 6-5). However, no discrete fracture through the specimen was obtained with either size distribution.

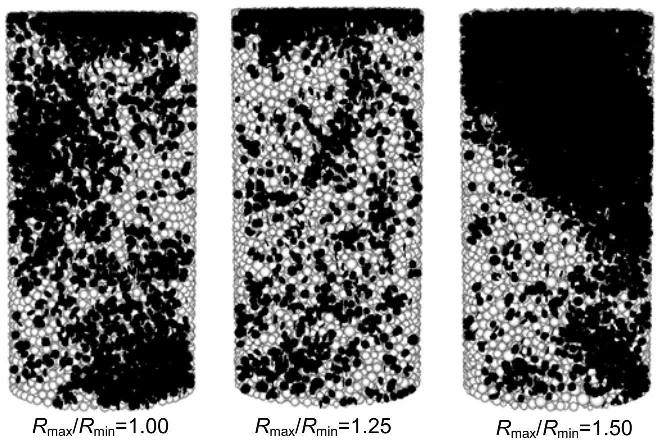

Figure 6-4: Failure mechanisms of numerical conglomerates in uniaxial testing at particle ratio (R_{max}/R_{min}) of 1.0, 1.25 and 1.50. Black dots represent the cracks (interparticle bond breakage).

The change in elastic response (Young's modulus and Poisson's ratio), was also observed to vary with the particle size ratio. Generally, a decrease in Young's modulii was observed with an increase in particle radii ratio (Figure 6-3). However, an increase in Poisson's ratio was noted with an increase of the particle ratio from 1.0 to 1.50 (Figure 6-3).

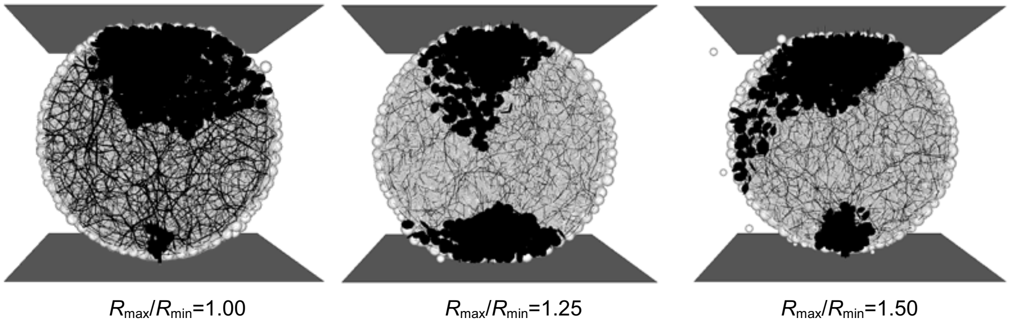

Figure 6-5: Failure mechanisms of numerical conglomerates in Brazilian tensile testing at particle ratio (R_{max}/R_{min}) of 1.0, 1.25 and 1.50. Black dots represent the cracks (interparticle bond breakage).

The results of uniaxial, triaxial and Brazilian tensile tests were analysed for Hoek-Brown and Mohr-Coulomb criteria. The plots of Hoek-Brown and Mohr-Coulomb criteria are shown in Figure 6-6 and Figure 6-7 along with the respective test data.

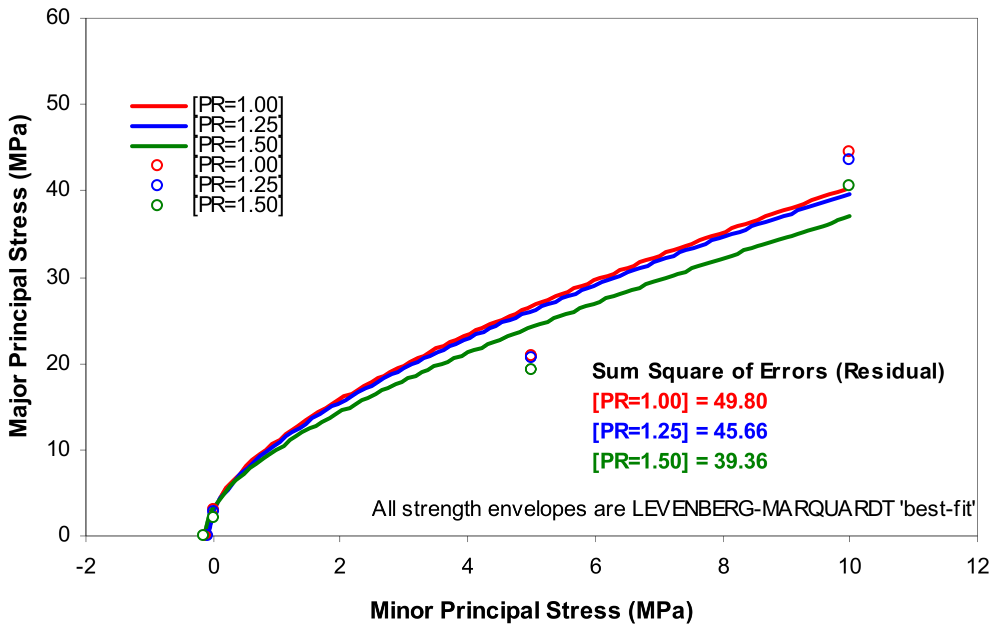

Figure 6-6: Hoek-Brown criteria applied to results of uniaxial, triaxial and Brazilian tensile tests on numerical conglomerates with particle ratio (R_{max}/R_{min}) of 1.0, 1.25 and 1.50.

On the one hand, the behaviour of numerical conglomerates with varying particle distribution seems less predictable using Hoek-Brown criterion, as the fitting curves give a sum square of errors from 39 to 50. However, these values reduce with an increase in the particle radii ratio (Figure 6-6). On the other hand, Mohr-Coulomb criterion results in a reasonable fit, with a sum square of errors from 3.08 to 5.82, based on the uniaxial and triaxial test data (Figure 6-7). The sum square of errors of Mohr-Coulomb criterion curves decreases with the increase of particle radii ratio, similar to the corresponding values of the Hoek-Brown criterion curves.

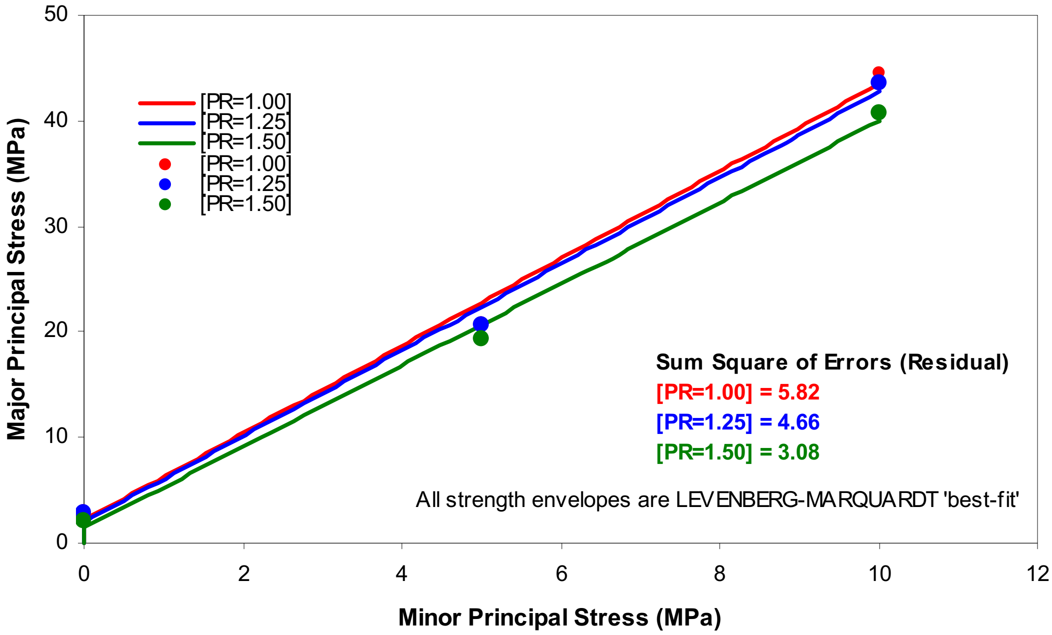

Figure 6-7: Mohr-Coulomb criteria applied to results of uniaxial and triaxial tests on numerical conglomerates with particle ratio (R_{max}/R_{min}) of 1.0, 1.25 and 1.50.

Based on these analyses, it is suggested that the response of numerical conglomerates is more rigorously predictable using Mohr-Coulomb criterion than Hoek-Brown criterion. It was observed that the material constant (m_i) of Hoek-Brown criteria generally decreases with the increase of the particle radii ratio from 1 to 1.50 (Figure 6-8a).Similarly, Mohr-Coulomb parameters (cohesion and angle of friction) were also found to decrease with the increase of particle radii ratio (Figure 6-8b).

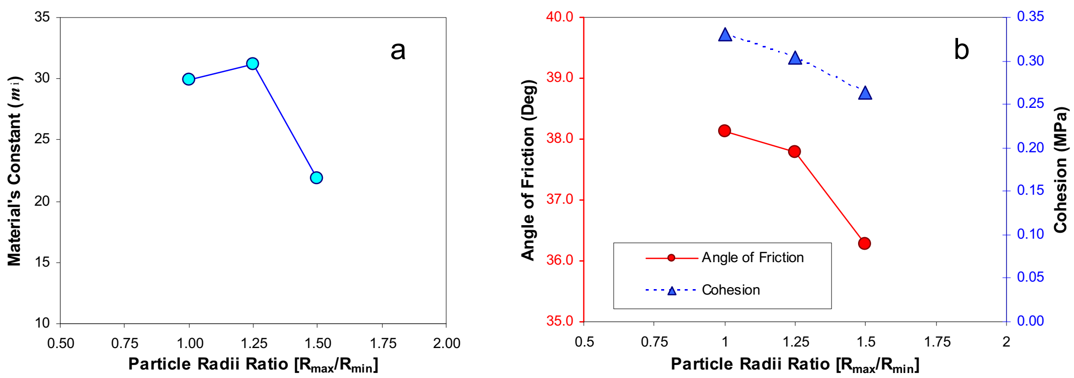

Figure 6-8: Variation of; a) Hoek-Brown parameter, i.e., material constant (m_i), b) Mohr-Coulomb parameters i.e., cohesion, angle of friction of numerical conglomerates with a particle radii ratio (R_{max}/R_{min}) of 1.0, 1.25 and 1.50.

6.3 Effect of Scaling

Scaling effects relating to specimen size are important factors in rock mechanics that significantly influence the rock strength and deformation. The natural rocks are inhomogeneous materials and contain discontinuities at all scales, from micro fractures to large tectonic slips. Consequently, the mechanical response of a particular rock is different on a laboratory scale (intact rock) from that of a field scale (rock mass). However, in this study scaling refers to the laboratory scale response of a conglomeratic rock with respect to its micro structure (i.e., its particle size and interstices cement), and the dimensions of the specimen to be tested. In the sensitivity study, both factors were investigated by proportional and non-proportional scaling. In proportional scaling, the model dimensions and the structure of the conglomerate (particle sizes) were varied proportionally so that the particle diameter to specimen diameter ratio remained the same. In non-proportional scaling, only the model dimensions were varied while the micro structure remained the same.

In addition, the scale effect has also important implications in numerical simulations. PFC can compute a model with a finite number of particles, that is, a maximum of 1~2 million at normal PC with minimum particle stiffness. With a decrease in particle size, contact stiffness increases, as it is a function of particle size, which further slows down the computation. Therefore, for a large scale simulation, the number of particles can be reduced by using bigger particles provided the mechanical response of bigger particles is representative of the laboratory scale response. Therefore, the mechanical response of the numerical assembly was investigated for both proportional and non-proportional scaling.

6.3.1 Proportional Scaling

In proportional scaling, the model dimensions and ball sizes were varied proportionally with a scaling factor of 0.1, 0.2, 1, 5 and 10 and scale dependent micro parameters, that is, the normal and shear stiffness of parallel bonds, were determined for each ball size. A summary of the model details and the corresponding determined parameters are given in Table 6-1. The loading/ displacement rate was also determined for each scaled model so they would have the same proportion in loading. Non-scale dependent parameters, such as normal and shear bond strengths, the bond radius multiplier, coefficient of friction, density and porosity were kept the same for all the scaled models. Uniaxial and triaxial tests (σ_3 = 5 MPa & 10 MPa) were carried out to record the macroscopic response of the assemblies at different scales. The results are shown in Figure 6-9.

Table 6-1: Summary of model dimension and corresponding particles sizes and parallel bond parameters.

Model	Scaling factor	Model dimensions		Particle diameter	Loading rate	Parallel bond parameters	
						Normal stiffness	Shear stiffness
		Diameter (m)	Length (m)	(m)	(m/s)	(Pa/m)	(Pa/m)
M-1	0.1	9.4e-3	1.88e-3	4.75e-4	1e-4	6.69e12	6.69e12
M-2	0.2	1.88e-2	3.76e-2	9.50e-4	5e-4	3.34e12	3.34e12
M-3	1	9.4e-2	1.88e-2	4.75e-3	1e-3	6.69e11	6.69e11
M-4	5	4.7e-1	9.4e-1	2.375e-2	5e-3	1.34e11	1.34e11
M-5	10	9.4e-1	1.88	4.75e-2	1e-2	6.69e10	6.69e10

The results of this investigation show an increase in the peak strengths in both uniaxial and triaxial testing with a scaling factor of 0.1 to 10, which seems insignificant (less than 5%). Young's modulus was more sensitive as it decreased with the increase of the scaling factor. Poisson's ratio, however, does not show any specific trend, as it first decreased with a scaling factor from 0.1 to 1.0 and then increased to a scaling factor of 10.

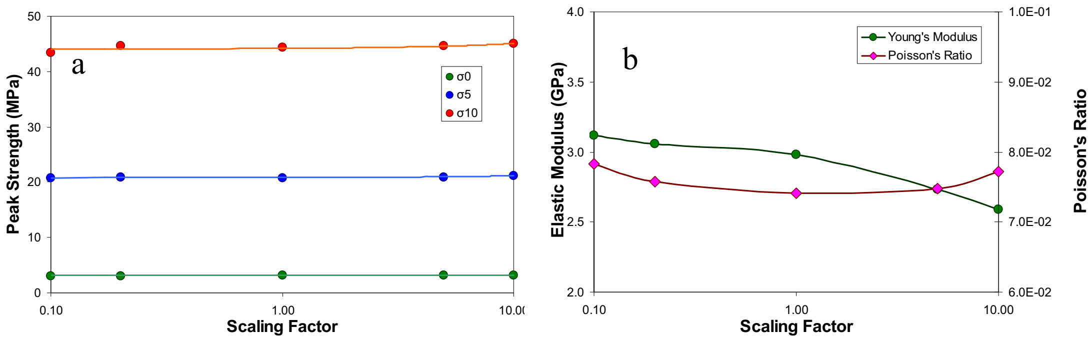

Figure 6-9: Uniaxial and triaxial test results of proportionally scaled model; a) peak strengths versus scaling factor, b) variation of Young's Modulus and Poisson's ration with scaling factor.

6.3.2 Non-Proportional Scaling

Non-proportional scaling refers to increasing the model dimensions while keeping the micro structure of the assembly the same. In this investigation, three numerical models were prepared, keeping the porosity and the parallel bond parameters constant. The dimensions of the already tested conglomeratic specimen were doubled and halved, so that the prepared model had scaling factors of 0.5, 1 and 2 (i.e., X/2, X and 2X). The length to diameter ratio was equal to 2 in all three models. The details of the non-proportionally scaled models are given in Table 6-2, and the models are shown in Figure 6-10. The results of the non-proportional scaling are shown in Figure 6-11, in terms of the variation of uniaxial peak strength, Young's modulus and Poisson's ratio.

Table 6-2: Summary of model dimensions for non-proportionally scaled models.

Model	Scaling factor	Model dimensions		Particle diameter (m)	Loading rate (m/s)
		Diameter (m)	Length (m)		
M-1	0.5	4.70e-2	9.40e-2	4.75e-3	5e-4
M-2	1.0	9.40e-2	1.88e-2	4.75e-3	1e-3
M-3	2.0	1.88e-1	3.76e-1	4.75e-3	5e-3

Hoek and Brown (1980b) proposed the following relation to address the influence of scaling on the uniaxial strengths of natural rocks based on extensive laboratory testing:

$$\sigma_{cD} = \sigma_{c50}\left(\frac{50}{D}\right)^{0.18} \qquad (6.1)$$

Where

σ_{c50} - UCS of a rock with specimen diameter of 50 mm, and

σ_{cD} - UCS of a rock with specimen diameter of D mm.

A similar decreasing trend of uniaxial strength was observed in the results of numerical conglomerates. In order to quantify the scaling induced strength variation, ratios of peak strengths at diameters *D* (i.e., σ_{cD}) and 94 mm (i.e., σ_{c94}) were plotted against the specimen diameters. The plot was then overlaid on the graph of natural rocks (after Hoek & Brown 1980b) for the corresponding uniaxial strength ratio of σ_{cD} and σ_{c50} at diameters *D* and 50 mm, respectively against the specimen dimensions (Figure 6-12). The plotted trend line through the conglomerate data yielded the following relation:

$$\sigma_{cD} = \sigma_{c94}\left(\frac{94}{D}\right)^{0.22} \qquad (6.2)$$

Where

σ_{c94} - UCS of a rock with specimen diameter of 94mm, and

σ_{cD} - UCS of a rock with specimen diameter of D mm.

Clearly, Equation (6.2) resembles Equation (6.1). This is also evident from the plots of the both equations in Figure 6-12. This comparison illustrates a reasonable agreement and is a rigorous representation of the scale effect similar to natural rock in numerical conglomerates.

Young's modulus was observed to decrease with an increase in specimen size. This decrease is sharp, from a 0.5 to 1.0 scaling factor, and becomes gentle from a scaling factor of 1.0 to 2.0 (Figure 6-11). Poisson's ratio was found to increase with the increase of specimen size.

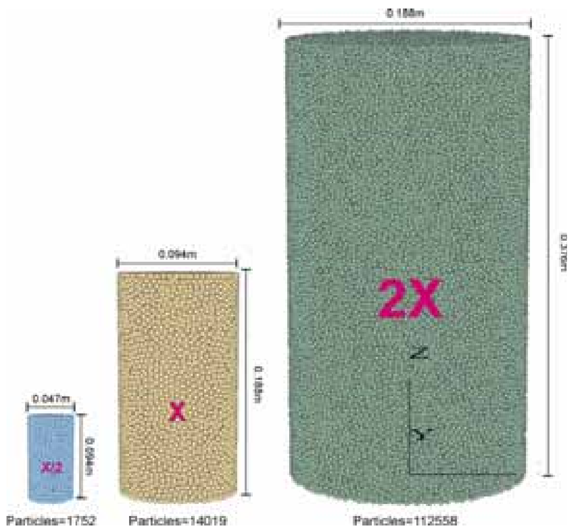

Figure 6-10: Non-proportionally scaled models with scaling factors of 0.5, 1.0 and 2.0 (i.e., X/2, X and 2X).

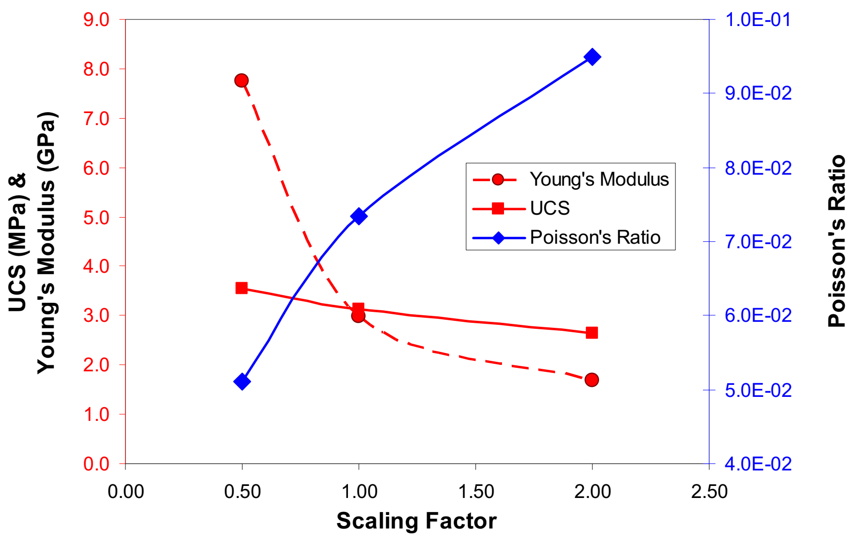

Figure 6-11: Variation of peak strength, Young's modulus and Poisson's ratio with scaling factors.

6.4 Effect of Particle and Interparticle Cementing Materials

This section presents the sensitivity of the particle (clast) material and interparticle cement on the mechanical response of numerical conglomerates. In synthetic conglomerates, steel balls and Portland cement were used as clasts and interstices cement and numerical simulations were performed using the properties of both materials. Sufficient correspondence in the responses of both synthetic and numerical conglomerates was observed (Chapter 5). This comparison motivated us to investigate the sensitivity of both the particle material and interstices cement.

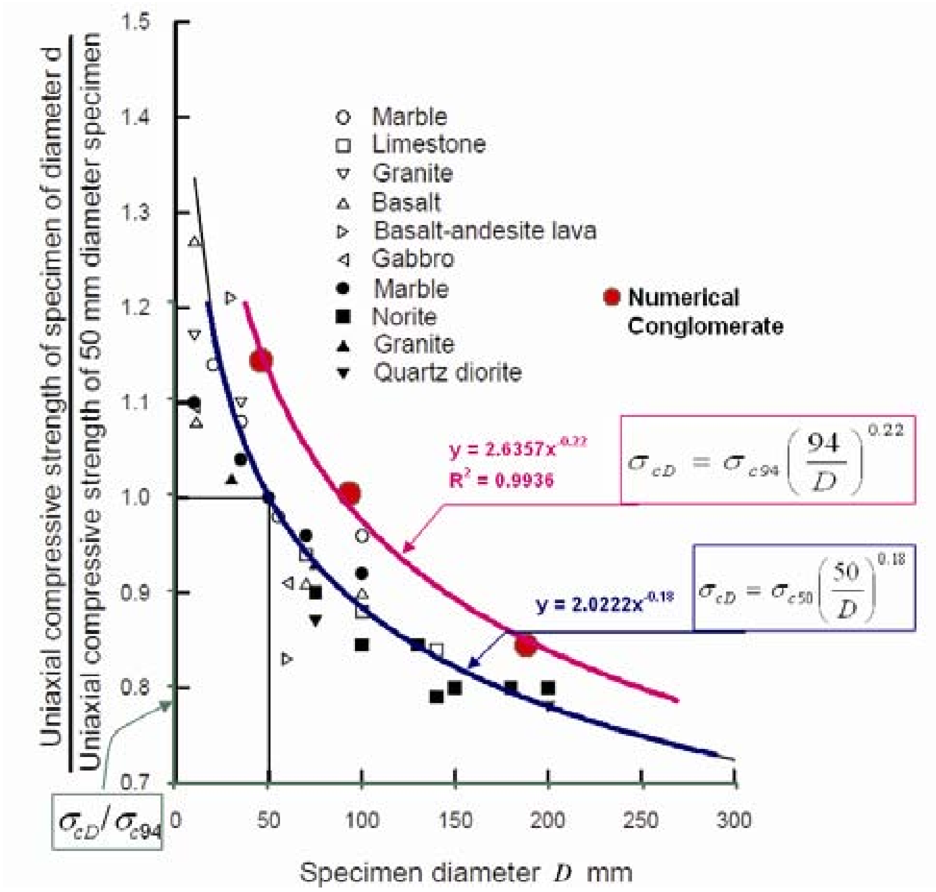

Figure 6-12: Influence of specimen size on the strength of numerical conglomerates. The plot is overlaid on the plot of natural rocks (after Hoek & Brown 1980b). Both plots show a similar trend of the strength variation with the change of specimen diameters.

The sensitivity study involves two particle materials, granite and sandstones, in addition to steel. The properties of these materials were used to simulate the particles in the numerical conglomerates. The properties of these materials were outsourced from literature and are summarised in Table 6-3, together with the source references. Similarly, the properties of two interparticle materials, argillaceous and arrenaceous cements, in addition to Portland cement, were used to derive the micro parameters of the parallel bonds in the simulation of conglomerates. The types of interparticle cementing material and their properties are given in Table 6-4, together with the source references. The numerical conglomerate specimens were prepared using all particle and cementing materials (Table 6-3 and Table 6-4). Each particle material assembly was glued with three different cementing materials and, in total; nine (9) conglomerates were prepared for uniaxial, triaxial and Brazilian tensile testing. The details of the prepared conglomerates and the nomenclature used to denote them are summarised in Table 6-5.

Table 6-3: Summary of particle materials and their properties used to create numerical conglomerates.

Particle materials		Density (ρ) Kg/m^3	Young's modulus (E) GPa	Shear modulus (G) GPa	Poisson's ratio (ν)
Steel	STL	7800	200	74.5	0.313
Granite[1]	GR	2600	73	30	0.21
Sandstone[2]	SST	2300	33	13	0.25

[1]Properties outsourced from pink Lac du Bonnet granite (after Duevel & Haimson 1997)

[2]Properties outsourced from Fell sandstone, Northamberland, UK. (after Bell 2007)

All the parameters, that is, normal and shear stiffnesses and strengths defining the parallel bond (interparticle cement) were calculated from Table 6-4.

Table 6-4: Summary of interparticle cements and their properties used for parallel bonds to create numerical conglomerates.

Cementing materials		UCS (σ_c) MPa	Shear strength (τ) MPa	Tensile strength (σ_t) MPa	Young's modulus (E) GPa
Portland cement	PC	12.7	4.0	1.5	3.18
Argillaceous cement[1]	ARG	27.4	4.9	2.0	4.2
Arrenaceous cement[2]	ARN	70	12.5	6.0	30

[1]Properties outsourced from Hawkesbury sandstone, Sydney, Australia (after Sharrock et al. 2009).

[2]Properties outsourced from Fell sandstone, Northamberland, UK. (after Bell 2007)

However, interparticle friction was kept the same in all numerical conglomerates to rule out its dependence on the mechanical responses.

Table 6-5: Nomenclature and details of the conglomerates prepared by using different particle and cementing materials.

		Cementing Materials		
		Portland Cement (PC)	Argillaceous Cement (ARG)	Arrenaceous Cement (ARN)
Particle Material	Steel (STL)	[STL+PC]	[STL+ARG]	[STL+ARN]
	Granite (GR)	[GR+PC]	[GR+ARG]	[GR+ARN]
	Sandstone (SST)	[SST+PC]	[SST+ARG]	[SST+ARN]

It should be noted that in the sensitivity study of particle and cementing materials, the strengths and stiffness of real (physical) materials were used (Table 6-3 and Table 6-4). Any particle or interparticle cement inducing a variation in the mechanical response of a conglomerate will be the function of both the strength and stiffness of the particles or the cement. No separate sensitivity of only the stiffness or the strength of a particular material has been conducted. However, the relations between the strength (*UCS*) and stiffness (*E*) of particle and cementing materials are shown in Figure 6-13. The relation between *UCS* and *E* is generally linear, and is named modulus ratio in rock mechanics literature (e.g., Rocscience 2008; 2010). The modulus ratios for selected particle and interparticle cements lie between 300 and 400.

However, mechanical behaviour of the investigated conglomerates was analysed for both the strength ratio (UCS_{cem} / UCS_{part}) and the stiffness ratio (E_{cem} / E_{part}) of interparticle cement to particle material.

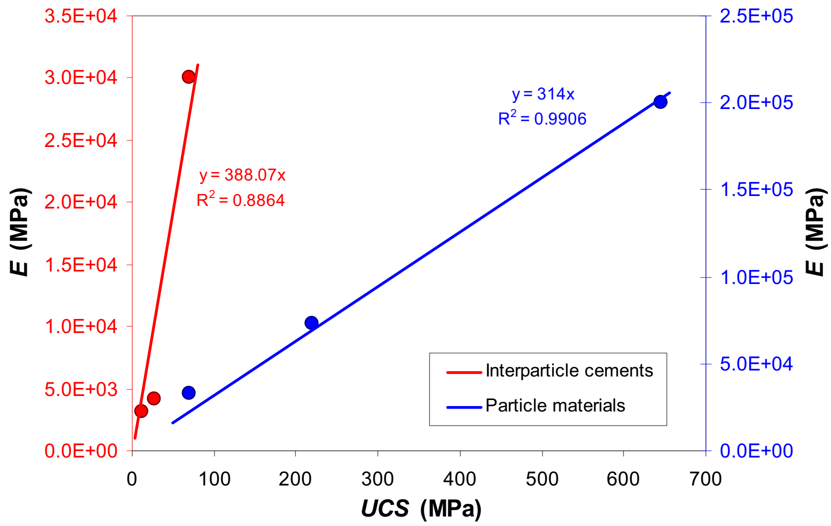

Figure 6-13: Relation of the strength (*UCS*) and stiffness (*E*) of the particle materials and cements.

The preparation of numerical conglomerates and laboratory testing was conducted following the steps already discussed in Chapter 4. Uniaxial and triaxial tests (at 5 MPa and 10 MPa confining pressures), and Brazilian tensile tests, were conducted on all conglomerates to record their mechanical responses. A summary of the test results of all the numerical conglomerates is shown in Table 6-6. A discussion of the test results is given in the following sections.

Table 6-6: Summary of test results on conglomerates.

Composition of conglomerates	Peak strength (MPa)			Young's modulus (GPa)			Poisson's ratio	Tensile strength (MPa)
	Uniaxial (UCS)	Triaxial (5 MPa)	Triaxial (10 MPa)	E_0	E_5	E_{10}		
[STL+PC]	3.122	20.843	44.467	2.98	4.17	4.34	0.074	0.102
[STL+ARG]	3.870	20.888	44.670	3.55	4.76	4.23	0.067	0.176
[STL+ARN]	7.377	20.194	44.573	14.88	2.59	3.19	0.043	0.431
[GR+PC]	2.871	23.329	50.642	2.30	1.72	2.40	0.054	0.134
[GR+ARG]	3.542	23.324	50.435	2.84	1.58	2.35	0.052	0.184
[GR+ARN]	6.772	22.544	50.439	12.20	1.07	2.55	0.035	0.485
[SST+PC]	2.645	25.159	55.194	1.98	0.94	1.56	0.047	0.131
[SST+ARG]	3.267	25.201	55.701	2.49	0.78	1.57	0.046	0.199
[SST+ARN]	6.457	27.377	55.815	9.58	0.72	1.64	0.027	0.744

6.4.1 Peak Strengths

The tests results of uniaxial and triaxial testing are shown in Figure 6-14 for peak strengths. These results were analysed for the dependence of the particle materials and interparticle cements. In uniaxial testing, the interparticle material was observed to influence the peak strength significantly, irrespective of the particulate material. The peak strengths of the numerical conglomerates were observed to increase with the increase of cement strength, as shown in Figure 6-14a for steel particles, Figure 6-14b for granitic particles, and Figure 6-14c for sandstone particles. However, interestingly, this influence gradually decreased with the increase of confining pressures, again irrespective of the particle material (Figure 6-14a, b & c).

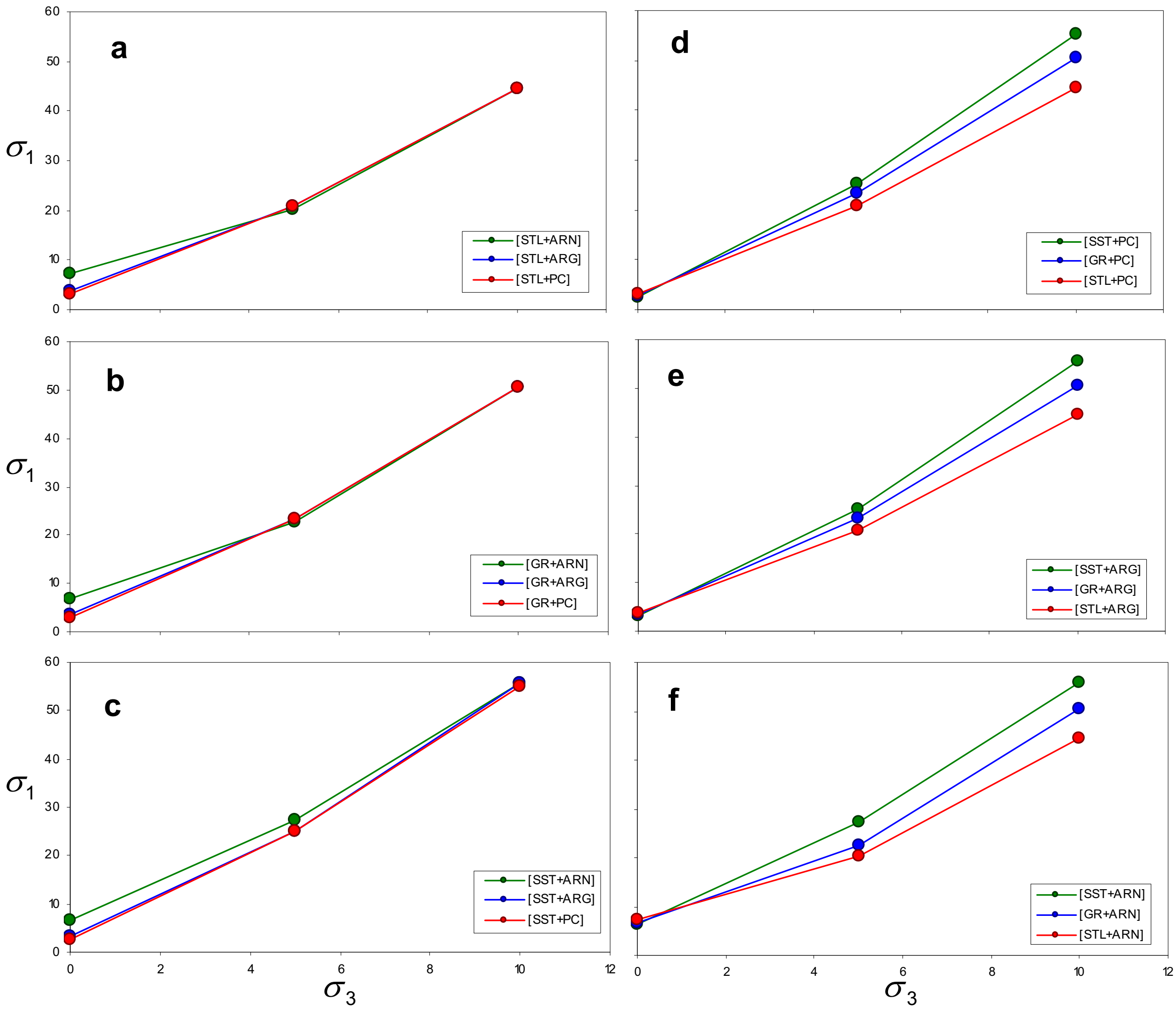

Figure 6-14: Sensitivity of the peak strengths of various conglomerates with particle and cementing materials in $\sigma_1 - \sigma_3$ space. Plots a, b and c show a relative variation of peak strengths with the variation of cementing material for: a) steel particles, b) granitic particles and c) sandstone particles. Plots d, e and f show a relative variation of peak strengths with the variation of particle materials with: d) Portland cement, e) argillaceous cement and f) arrenaceous cement.

On the other hand, the particle material was found to have negligible effect on the uniaxial strengths for all given cementing materials. However, this effect became pronounced with the increase of confining pressure irrespective of the cementing materials; that is, the peak strengths increased with a decrease in the stiffness and strengths of the particles. This is shown for Portland cement in Figure 6-14d, for argillaceous cement in Figure 6-14e and for arrenaceous cement in Figure 6-14f.

These observations suggest that the properties of interparticle cement mainly influence the peak strengths in uniaxial, or close to uniaxial, conditions, while they have a negligible effect in confined conditions. While in contrast, the properties of the particle material have a significant effect in confined conditions and a negligible effect in uniaxial conditions.

The variation of the peak strengths of all numerical conglomerates were also observed with a contrast in the strength properties of the particles and the cementing materials. The strength contrast was determined in terms of the ratio of *UCS* of the cementing material to the *UCS* of the particle material. Peak strengths plotted against the *UCS* ratio of particles and the cement is shown in Figure 6-15. The peak strengths of the conglomerates were found to generally increase with the decrease of the strength contrast; that is, with the increase of UCS_{cem}/ UCS_{part} ratio (Figure 6-15).

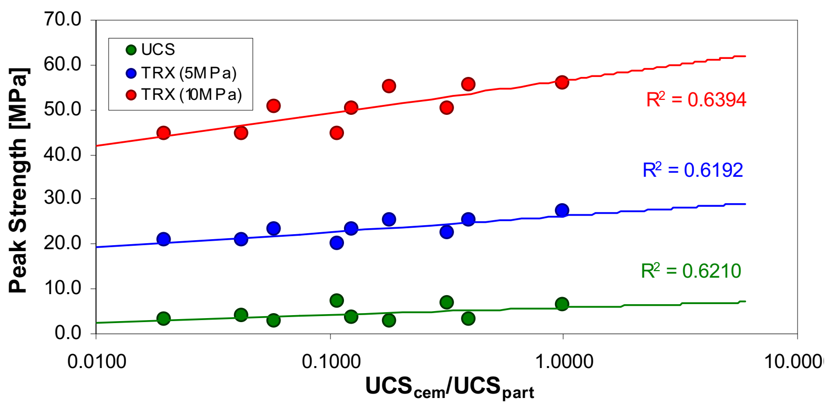

Figure 6-15: Variation of peak strengths of various conglomerates against the ratio of the uniaxial strengths of the cement to particle material.

The tensile strengths of the conglomerates determined in Brazilian tensile testing are also plotted against the *UCS* ratio of the particle material and the cement is shown in Figure 6-16. Generally, an increasing trend of tensile strengths was noted with the increase in UCS_{cem}/ UCS_{part}, from 0.01 to 1.0, similar to peak strengths in uniaxial and triaxial tests (Figure 6-15). The sensitivity of the tensile strengths was also analysed for particular cementing material and particle material (Figure 6-17). It was noted that with Portland and argillaceous cements, tensile strengths increased with almost the same trend, with the change of particle material from steel to sandstone. However, a relatively sharp increasing trend was observed with arrenaceous cement (Figure 6-17a). The difference in the increasing trends was thought to be mainly because of the strengths of the cementing materials.

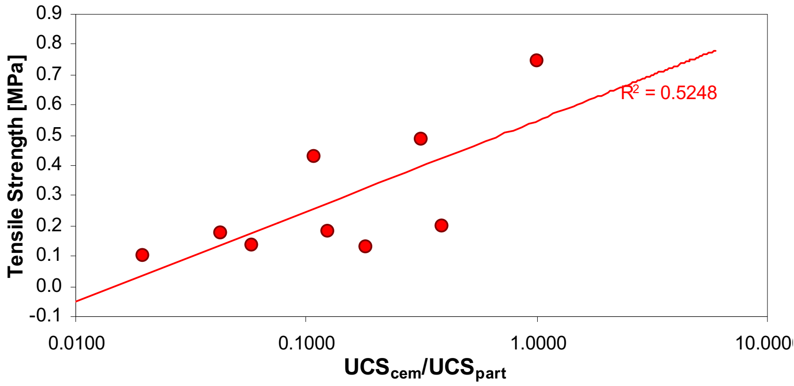

Figure 6-16: Tensile strengths of various conglomerates against the ratio of the uniaxial strengths of the cement to particle material.

The effect of the particle material on the tensile strength is shown in Figure 6-17b, for different interparticle cements. An increasing trend in tensile strength was observed with all particle materials; however, this trend was relatively sharper with the use of sandstone particles which show less contrast in the strengths of the particle and interparticle cement, that is, a high value of UCS_{cem}/ UCS_{part} ratio (Figure 6-17b).

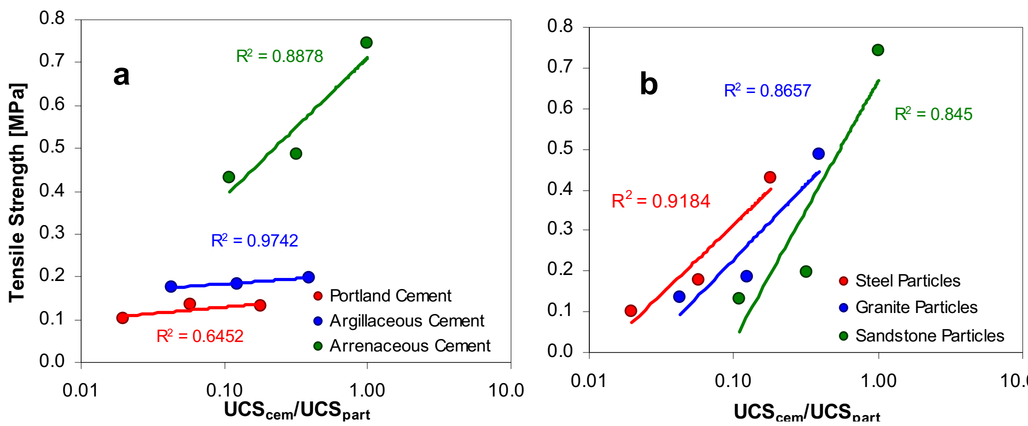

Figure 6-17: Variation of tensile strength versus the ratio of the uniaxial strengths of the cement to particle material; a) with the change of cementing material, b) with the change of particle material.

In general, the variation of tensile strength with particle and interparticle cementing materials is similar to that of the peak strengths in uniaxial and triaxial testing.

The compressive to tensile strength ratio is an important mechanical characteristics of any particular material. Based on uniaxial and Brazilian tensile test results, the uniaxial compressive to tensile strength ratios (*UCS/T*) of all conglomerates were determined and plotted against the uniaxial strength and the stiffness ratios of the cement to particle material (i.e., the UCS_{cem}/ UCS_{part}, and E_{cem}/ E_{part}). Generally, a decreasing trend of UCS/T was observed with the increase of the UCS_{cem}/ UCS_{part} ratio (Figure 6-18a). A similar decrease in *UCS/T* was noted with the increase of the E_{cem}/ E_{part} ratio (Figure 6-18b). These observations conclude that the compressive to tensile strength ratio of a conglomerate decreases with the decrease of the contrast in the stiffness and strength of the particle and cementing materials.

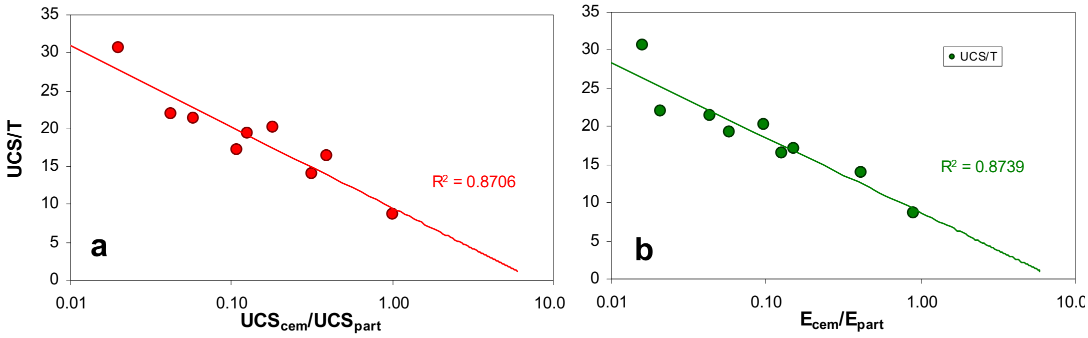

Figure 6-18: Variation of uniaxial compressive strength to tensile strength ratio: a) with uniaxial strength ratio of cement to particle materials (UCS_{cem}/ UCS_{part}) and, b) with Young's modulii ratio of cement to particle materials (E_{cem}/ E_{part}).

The variation of *UCS/T* with the cementing materials is shown in Figure 6-19a, and with the particle material in Figure 6-19b. It is observed that the *UCS/T* ratio is highest for Portland cement and lowest for arrenaceous cement (Figure 6-19a). Similarly, *UCS/T* is highest for steel particles and lowest for sandstone particles (Figure 6-19b). In combining the effect of particle and cementing materials, it is clear that the *UCS/T* ratio is highest for a conglomerate [STL+PC] consisting of steel particles glued together with Portland cement (corresponding to UCS_{cem}/ UCS_{part} of about 0.02) and is lowest for conglomerates [SST+ARN] having sandstone particles and arrenaceous interparticle cement (corresponding to UCS_{cem}/ UCS_{part} of about 1.0).

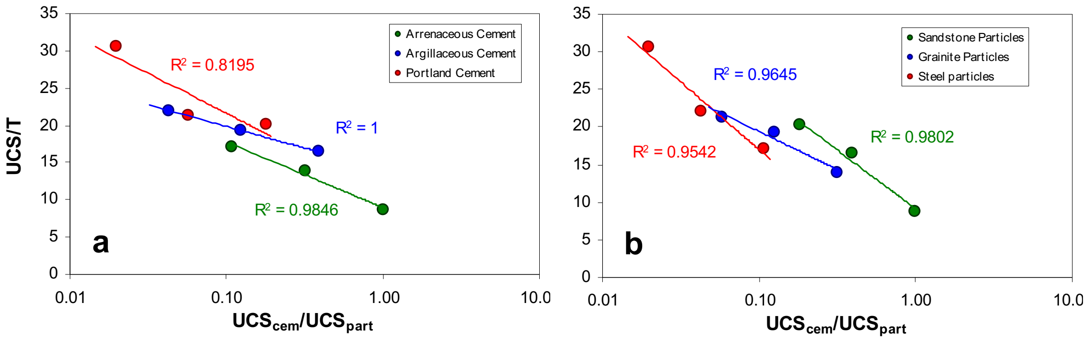

Figure 6-19: Variation of uniaxial compressive strength to tensile strength ratio (UCS/T) with uniaxial strength ratio of cement to particle materials (UCS_{cem}/ UCS_{part}); a) for interparticle cements and, b) with particle materials.

Another factor that is believed to control the *UCS/T* ratio is the ratio of the shear to normal (tensile) strength (i.e., $\bar{\tau}\ /\bar{\sigma}_n$) of the interparticle cement (parallel bond). The shear and tensile strengths of the cementing materials used for numerical simulations are summarised in Table 6-4. The *UCS/T* ratio was plotted against the shear to tensile strength ratio of the interparticle cement in Figure 6-20. It was observed that the *UCS/T* ratio increases with the increase of the shear to normal strength ratio ($\bar{\tau}\ /\bar{\sigma}_n$) of the interparticle cement, irrespective of the particle material.

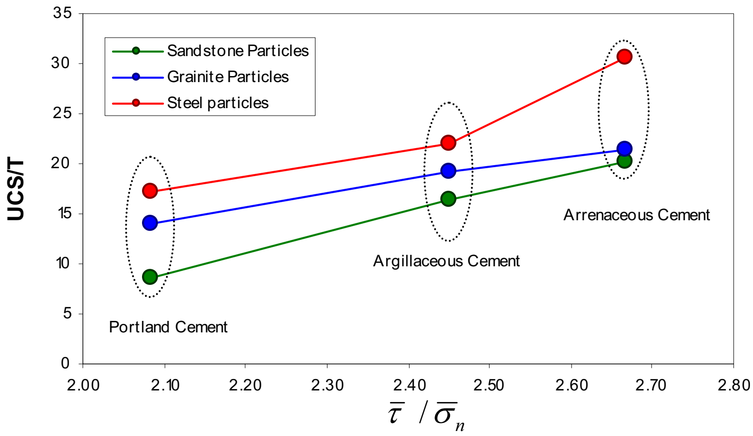

Figure 6-20: Variation of uniaxial compressive strength to tensile strength ratio (*UCS/T*) with shear to normal strength ratio ($\bar{\tau}\ /\bar{\sigma}_n$) of the interparticle cement (parallel bond) for steel, granitic and sandstone particles.

6.4.2 Young's Modulii and Poisson's Ratios

Elastic response of the tested conglomerates was determined to examine its sensitivity with the particle and cementing materials. Although the response of the numerical conglomerates was stiffer in comparison to the synthetic conglomerates (discussed in Chapter 5), this section presents the relative variation of the elastic response of the numerical assemblies with a variation in the particle and cementing materials.

Young's modulus and Poisson's ratio were determined at 50% of the peak strength in uniaxial testing. The recorded values were plotted against the modulus ratio of cementing material to particle material (E_{cem}/ E_{part}). The plot of the Young's modulii versus E_{cem}/ E_{part} ratio is shown in Figure 6-21.

Young's modulus was found to increase when increasing the stiffness of particles or interparticle cement. With a particular particle material, the modulus increases by E_{cem}/ E_{part} ratio, that is, by increasing the stiffness of the cementing material. The increasing trend is steep with steel particles (*E*= 200 GPa) and relatively gentle with sandstone particles (*E*= 33 GPa) corresponding to the same cementing materials.

The granitic particles (E= 73 GPa) show an intermediate increasing trend. Similarly, with a particular cementing material, modulii decrease with an increase of the E_{cem}/E_{part} ratio; that is, by decreasing the stiffness of the particles (Figure 6-21). This decreasing trend is sharper for arrenaceous cement (E= 30 GPa) than for argillaceous (E= 4.8 GPa) or Portland cement (E= 3.18 GPa).

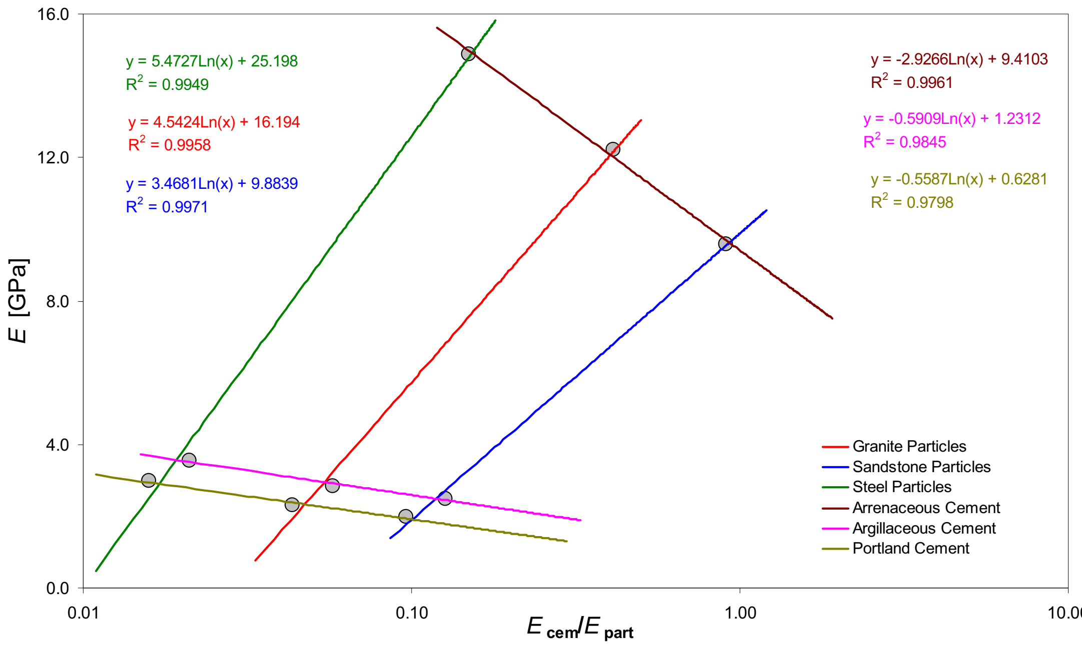

Figure 6-21: Variation of Young's moduli (E) of conglomerates with particle and cementing materials corresponding to the modulus ratio of cementing material to particle material (E_{cem}/E_{part}).

The Young's modulii of all conglomerates were found to have a linear relation with the respective uniaxial compressive strengths (*UCS*). A linear increasing trend in the modulii was noted with the increase of peak strengths (*UCS*) in uniaxial testing (Figure 6-22).

The modulii of all conglomerates were also determined in triaxial tests at confining pressures of 5 MPa and 10 MPa at 50% of peak strengths. These values have been plotted against the confining pressures for all conglomerates (Figure 6-23).

In contrast to the uniaxial testing, an unexpected elastic response of the conglomerates was observed in confined loading. The Young's modulii were found to decrease with the confining pressures, except for the steel particles bonded with Portland or argillaceous cement (Figure 6-23).

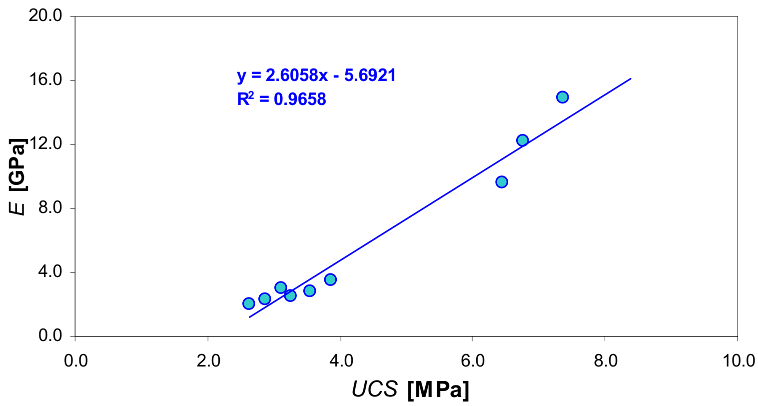

Figure 6-22: Plot showing the relation of Young's modulus (*E*) and the uniaxial compressive strength (*UCS*) of the conglomerates.

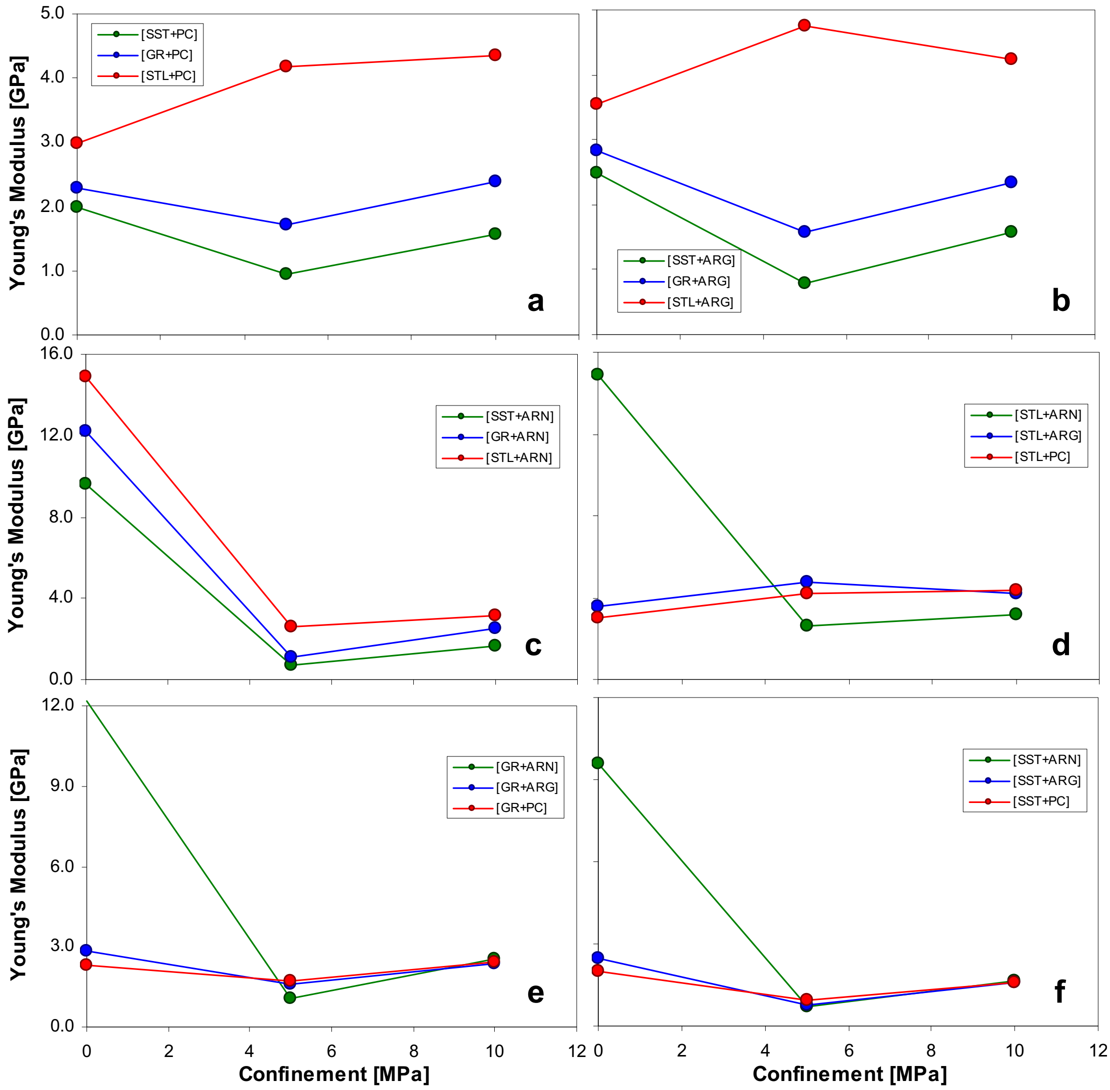

Figure 6-23: Sensitivity of Young's modulii (*E*) of various conglomerates with particle and cementing materials versus confining pressure (σ_3). Plots a, b and c show the relative variation of modulii with the variation of interparticle cement for: a) Portland cement, b) argillaceous cement and c) arrenaceous cement. Plots d, e and f show the relative variation of modulii with the variation of particle materials with: d) steel particles, e) granitic particles and f) sandstone particles.

These unusual results indicate the unrealistic behaviour of the numerical conglomerates. This behaviour becomes more unrealistic when elasticity of the cement is comparable to the elasticity of the particles; specifically, arrenaceous cement (E= 30 GPa) and sandstone particles (E= 33 GPa). This strange phenomenon was thought to be because of the elastic deformation of the particles (Hertzian contact models) due to less stiffness contrast. With the use of steel particles, the stiffness contrast between the particles and interparticle cement is high and hence deformation occurs only because of the bond breakage. With the decrease of stiffness contrast between the particles and cement, the possibility of particle deformation increases, in addition to bond breakage. However, more work is required to address this problem.

The Poisson's ratios of all the conglomerate assemblies were determined in uniaxial testing at 50% of the peak strengths. Although the Poisson's ratios in the numerical simulations are lower compared to the synthetic conglomerates (Chapter 5), here a relative variation was demonstrated with respect to particle and cementing materials. The variation of the Poisson's ratio was assessed with the stiffness ratio of cement to particle material (E_{cem}/ E_{part}) and is shown in Figure 6-24.

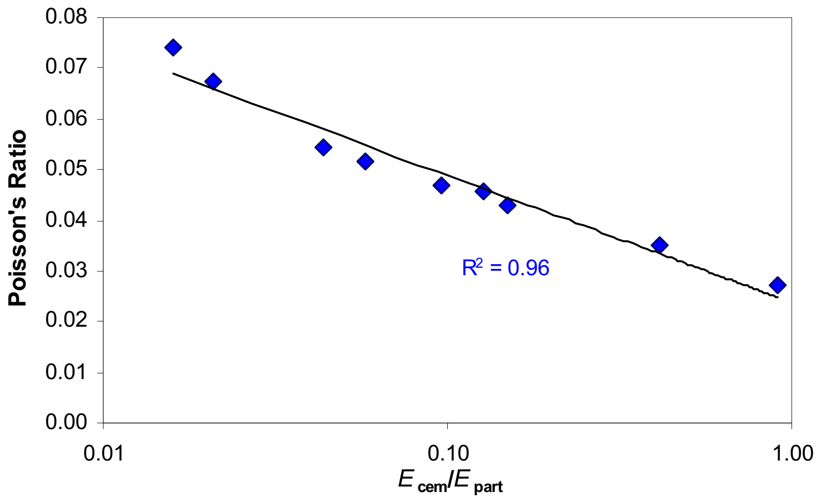

Figure 6-24: Variation of Young's modulii (E) of conglomerates with particle and cementing materials corresponding to the modulus ratio of cementing material to particle material (E_{cem}/ E_{part}).

Poisson's ratio was found to decrease with the increase of (E_{cem}/ E_{part}) ratio, irrespective of the particle or cementing material.

6.4.3 Strength Criteria of Conglomerates

The test results of all numerical conglomerates were subjected to strength criteria to observe the effect of particle and cementing materials. Mohr-Coulomb and Hoek-

Brown criteria were applied on the test results using Rocdata 4.0 (Rocscience 2010). Mohr-Coulomb criterion was applied to uniaxial and triaxial test results, while Hoek-Brown criterion was applied to uniaxial, triaxial and Brazilian tensile test results. The analyses of the Mohr-Coulomb and Hoek-Brown criteria are discussed in the following sections.

6.4.3.1 Mohr-Coulomb Criterion

Mohr-Coulomb criterion depicts the behaviour of a material as a linear function of normal and shear strengths acting on a failure plane. It was observed that the numerical conglomerate shows a linear behaviour in contrast to that of synthetic conglomerate (Chapter 3, 4 and 5). Hence, Mohr-Coulomb criterion was applied to the uniaxial and triaxial test results on all conglomerate assemblies (Table 6-6) using RocData 4.0. The Mohr-Coulomb fitting curves for all conglomerates are shown in major-minor principal stress field (Figure 6-25a) and shear-normal stress space (Figure 6-25b). The curve fitting parameters are also given in Figure 6-25a. Generally, the sum square of errors (residuals) (SSE[R]) is less than 10 for most of the conglomerates, demonstrating a reasonable fit. A summary of the Mohr-Coulomb parameters for all conglomerates is provided in Appendix C.

It was noted that conglomerates with the same particle materials show a similar trend of curves, irrespective of the cementing material. The slope of the curves is steep for low strength particles (i.e., sandstone particles) and is gentle for high strength particles (i.e., steel particles) yielding high and low internal friction angles respectively. The cohesion of numerical conglomerates was found to decrease corresponding to an increase in internal friction angles; that is, high for high strength particles and low for low strength particles.

The variation of the friction angle and the cohesion of the conglomerates is shown in Figure 6-26 against the uniaxial strength ratio of cement to particle material (i.e., UCS_{cem}/ UCS_{part}). Irrespective of the particle material, friction angle decreases and cohesion increases with the increase in the UCS_{cem}/ UCS_{part} ratio induced by the increase in the strength of the cementing material. Similarly, for a particular cementing material, the friction angle increases and cohesion decreases with the increase of the UCS_{cem}/ UCS_{part} ratio induced by the increase in the strength of the particle material.

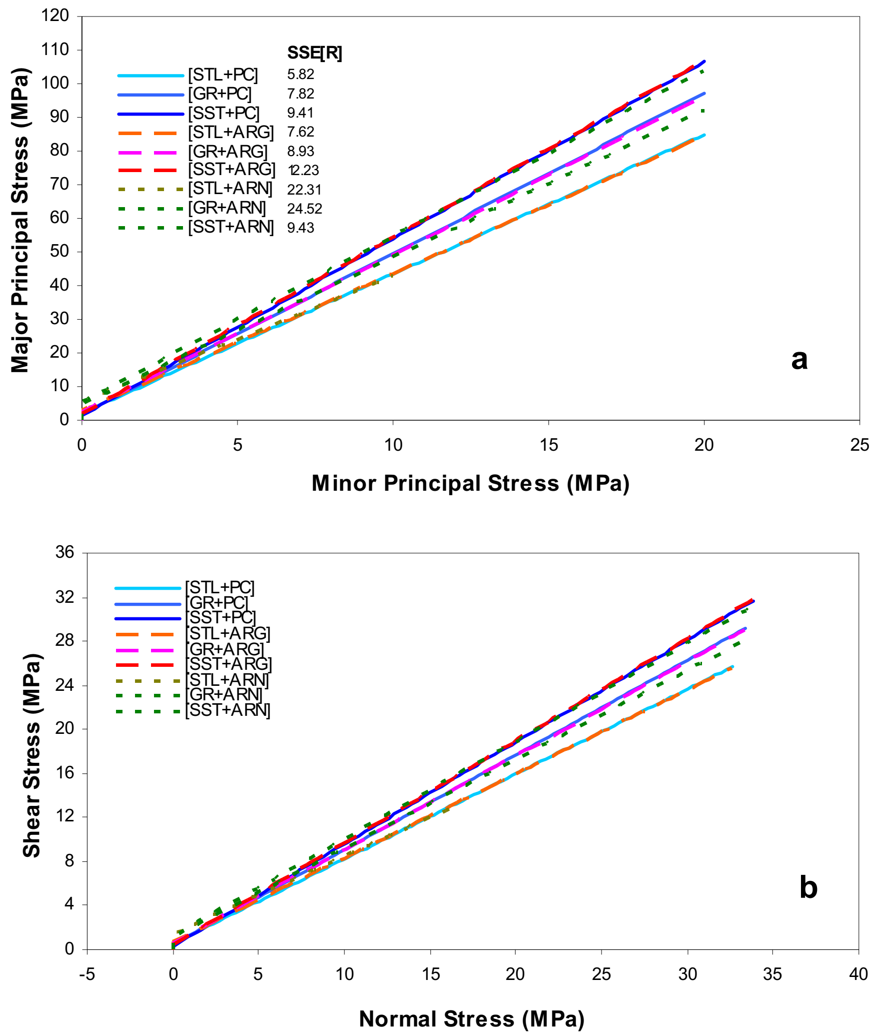

Figure 6-25: Mohr-Coulomb criterion curves for various conglomerates: a) in major-minor principal stress space and, b) in shear-normal stress space.

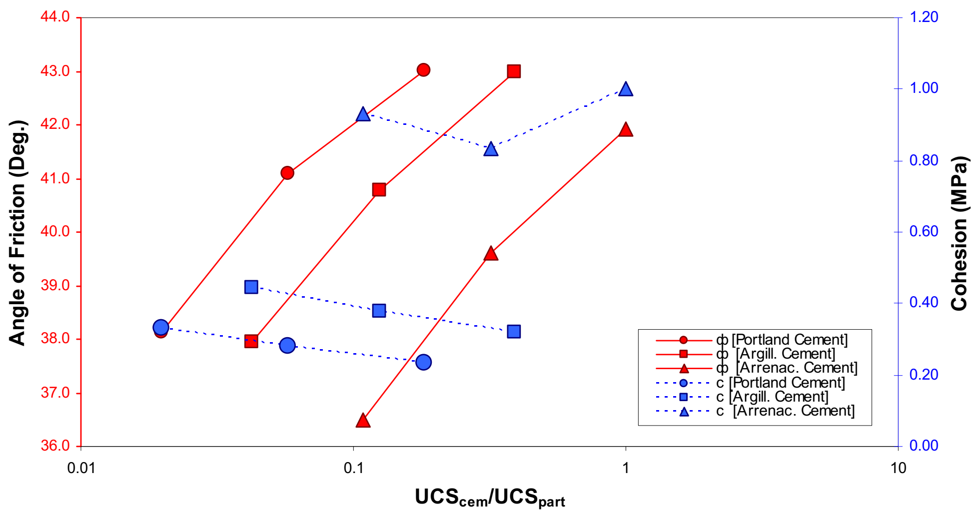

Figure 6-26: Variation of Mohr-Coulomb parameters (angle of friction and cohesion) of conglomerates comprising different particle and cementing materials corresponding to the uniaxial strength ratio of cementing to particle material (UCS_{cem}/ UCS_{part}).

Hence, from Figure 6-26, it may be suggested that cohesion is directly proportional to the strength of the cementing material or inversely proportional to the strength of the particle material. Likewise, the angle of friction is directly proportional to the strength of the particle material and inversely proportional to the strength of the cementing material.

6.4.3.2 Hoek-Brown Criterion

Hoek-Brown criterion was applied to the results of uniaxial, triaxial and Brazilian tensile tests (Table 6-6) using RocData 4.0. As discussed above (Chapter 4 and 5), the behaviour of numerical conglomerates is more predictable using Mohr-Coulomb than the Hoek-Brown owing to the linearity in peak strengths corresponding to confining pressure. The purpose of the application of Hoek-Brown criterion was to observe the relative variation of Hoek-Brown parameters with respect to particle and cementing materials; that is, the material constant (m_i). The Hoek-Brown curves for all conglomerates are shown in Figure 6-27a in major-minor principal stress field and as Figure 6-27b in shear-normal stress space. A detailed summary of Hoek-Brown parameters and fitted Mohr-Coulomb parameters for all conglomerates is provided in Appendix C. The curve fitting parameters; that is, the sum square of errors (residuals) (SSE[R]) and material constant (m_i), are also shown in Figure 6-27a. The relative variation of the material constant (m_i) induced by the properties of the particle and cementing materials can be clearly observed in Figure 6-27a. As per literature (e.g., Rocscience 2008; 2010), the typical value of the material constant (m_i) for natural conglomerates is 21±3 with lower and upper values of 18 and 24 respectively. It should be noted that these values are based on the results of a limited number of tests on specific types of conglomerates documented in literature and can vary as per the characteristics of conglomerates (Rocscience 2008; 2010). However, to compare the variation of material constant (m_i) in numerical conglomerates with that of natural conglomerates, 18, 21 and 24 were considered as the lower, mean and upper values of the material constant (m_i) for natural conglomerates (Figure 6-28).

On one hand, the material constant (m_i) was observed to particularly increase with week cementing materials (i.e., Portland or argillaceous cements), with a decrease in the strength and stiffness of the particles. It increased from 29.92 to 45.25 with Portland cement and from 22.76 to 36.66 with argillaceous cements corresponding to steel and sandstone particles respectively. However, with arrenaceous cements, it increased from 14.8 to 15.40 corresponding to steel and granitic particles, and decreased to 13.98 for sandstone particles (Figure 6-27a and Figure 6-28).

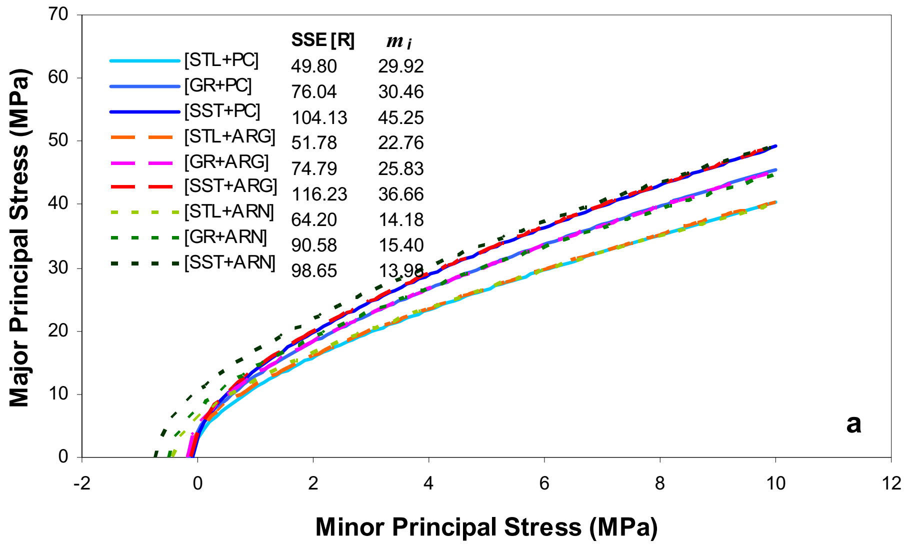

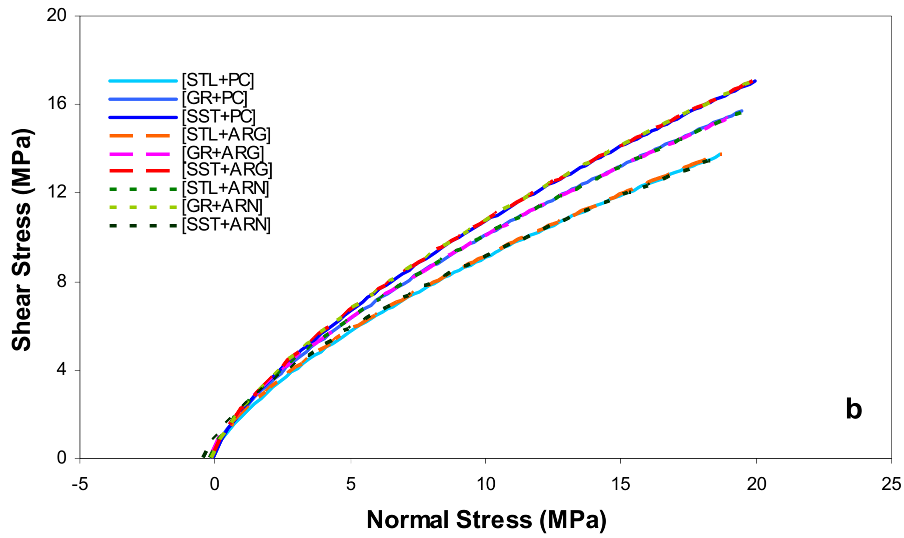

Figure 6-27: Hoek-Brown criterion curves for various conglomerates; a) in major-minor principal stress space and, b) in shear-normal stress space.

On the other hand, for a particular particle material, the values of the material constant were found to decrease with the increase of the strength of the cementing material; for example, it decreased from 29.92 to 14.18 for steel particles, from 30.46 to 15.40 for granitic particles and 45.25 to 13.98 for sandstone particles, corresponding to Portland and arrenaceous cements respectively (Figure 6-27a and Figure 6-28).

These observations suggest that the value of the material constant (m_i) for conglomerates is quite sensitive to the particle and interparticle cementing materials. Generally, for a particular cementing material, m_i increases with the increase of the

UCS_{cem}/UCS_{part} ratio, however this increase is more pronounced for argillaceous cementing materials (Figure 6-28). Likewise, for a particular particle material, m_i generally decreases with the increase of the UCS_{cem}/UCS_{part} ratio which is induced by the increase in the cement strength. This observation is consistent with the relationships obtained between the strength and petrographic characteristics of the sandstones and limestones. Notably, a high quartz content in sandstones and increase of sparitic material in limestones, generally result in higher UCS and in a lower material constant (Sabatakakis et al. 2008).

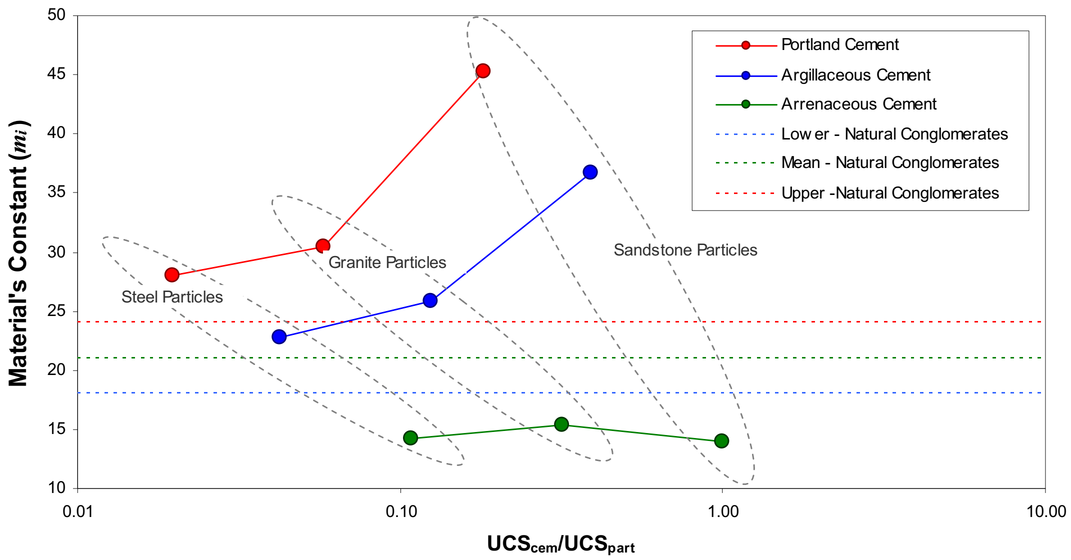

Figure 6-28: The sensitivity of the Hoek-Brown parameter, i.e., material constant (m_i) with particle and cementing materials of various conglomerates, corresponding to a uniaxial strength ratio of cementing material to particle material (UCS_{cem}/ UCS_{part}). Upper, lower and mean values of the material constant (m_i) based on the literature (e.g., Rocscience 2008; 2010) are also plotted.

6.5 Summary and Conclusions

The mechanical behaviour of an idealised conglomerate was examined with reference to particle size distribution, scaling, particle material and interparticle cement. The dependence on these factors was studied keeping the rest of the parameters that can influence the mechanical behaviour of a conglomerate, the same. The effect of particle size distribution was studied in relation to uniform particle size distribution. In this study three particle size distributions were considered with maximum to minimum particle radii ratio (R_{max}/R_{min}) of 1.00, 1.25 and 1.5 at the same porosity. The relative variation of the assembly response was analysed in uniaxial, triaxial and Brazilian tensile tests. The peak strengths, both in uniaxial and triaxial testing, were observed to decrease with the increase of the particle size ratio from 1.0 to 1.5. The tensile strength in Brazilian tensile tests, however, did not show any definite trend with the change of particle size ratio. Young's modulii were found to decrease, while Poisson's ratio was observed to increase with the increase in particle size ratio from 1.0 to 1.50. The damage in the conglomeratic specimens was also observed to be sensitive to particle size distribution being the result of a change in the contact force chains.

Scaling or the effect of specimen size was examined in uniaxial testing in two ways: proportional and non-proportional scaling. In proportional scaling, in which the whole model, including the specimen size and microstructure (particle size), was varied proportionally, no significant variation of peak strength was noted with the scaling factor. Only slight variation for the Young's modulus and Poisson's ratio was noted.

In non-proportional scaling, however, interesting observations were noted. Keeping the particle size the same, the model dimensions were varied in non-proportional scaling. It was noted that both peak strength and Young's modulus decreased and Poisson's ratio increased with the increase of the specimen's dimensions. This response was found consistent with the testing on natural rocks, although the actual magnitude of test results is less in comparison to the tests on natural rocks. Only the results of three scaled models were plotted, which produced a strength variation of conglomerates similar to that of natural rocks. However, this relation needs to be examined for further scaled models and also by incorporating different particle materials and cements. The analysis of non-proportional scaling indicates the capability of DEM simulation to induce the effect of the specimen's dimensions for a conglomeratic rock.

In the sensitivity study of particle and interparticle cementing materials three particle materials and three interparticle cements were considered to create and test numerical conglomerates in uniaxial, triaxial and Brazilian tensile testing. The particle materials considered were steel, granite and sandstone which represent the clasts of natural conglomerates. Similarly, the strength and stiffness of three interparticle cementing materials were considered namely; Portland cement, argillaceous cement and arrenaceous cement. The properties of all particle and interparticle cementing materials were obtained from literature. Using all particle and cementing materials, a total of nine conglomerate assemblies were prepared to record the variation in their mechanical responses.

In uniaxial testing, the interparticle cement was observed to influence peak strength significantly, irrespective of the particle material. On the one hand, the peak strengths of the numerical conglomerates were observed to increase with the increase of the cement strength. However, this influence gradually decreased with the increase of confining pressures, irrespective of the particle materials. On the other hand, the particle material was found to have a negligible effect on the uniaxial strengths of all given cementing materials. However, this effect became pronounced with the increase of confining pressures, irrespective of cementing materials. That is, the peak strengths increased with the decrease of the stiffness and strengths of the particles. These observations suggest that the properties of interparticle cement mainly influence the peak strengths in uniaxial, or close to, uniaxial conditions and have a negligible effect in confined conditions. In contrast, the properties of the particle material have a significant effect in triaxial conditions and a negligible effect in uniaxial conditions.

The variation of the peak strengths was also examined with the contrast of the strength properties of particles and cementing materials; that is, the $UCS_{\mathrm{cem}}/ UCS_{\mathrm{part}}$ ratio. The peak strengths of the conglomerates were found to increase with the decrease of the strength contrast; that is, with an increase of the $UCS_{\mathrm{cem}}/ UCS_{\mathrm{part}}$ ratio. The tensile strengths of the conglomerates determined in Brazilian tensile testing were also found to increase with the increase of the $UCS_{\mathrm{cem}}/ UCS_{\mathrm{part}}$ ratio similar to the peak strengths in uniaxial and triaxial tests. The effect of the particle and interparticle cementing materials was also analysed for the non-dimensional ratio of uniaxial compressive strength to tensile strength (*UCS/T*). The UCS/T ratio was found to decrease with the increase of $UCS_{\mathrm{cem}}/ UCS_{\mathrm{part}}$. However, the decreasing trend depends on the particular particle and cementing material.

Young's modulii and Poisson's ratios were determined at 50% of the peak strengths in uniaxial testing. Young's modulii were found to increase with the increase of the stiffness of both the particles and the interparticle cement. With a particular particle material, the modulii increase with an increase of the $E_{\mathrm{cem}}/ E_{\mathrm{part}}$ ratio; that is, by increasing the stiffness of the cementing material. The increasing trend depends on the stiffness of the particles; that is, high stiffness particles demonstrate a steeper trend, while low stiffness particles show a gentler trend. Similarly, with a particular cementing material, the modulii decrease with the increase of the $E_{\mathrm{cem}}/ E_{\mathrm{part}}$ ratio; that is, by decreasing the stiffness of the particles. This decreasing trend is steeper for high stiffness cement and gentler for low stiffness cement. Poisson's ratio was found to decrease with the increase of the $E_{\mathrm{cem}}/ E_{\mathrm{part}}$ ratio, irrespective of the particle or cementing materials.

Mohr-Coulomb and Hoek-Brown criteria were applied to the test results of all the numerical conglomerates. Mohr-Coulomb criterion was found to show more promise with the test data of numerical conglomerates than Hoek-Brown criterion. Both Mohr-Coulomb and Hoek-Brown criteria showed similar trends of the fitting curves for the same particle materials. Steep slopes of the fitting curves were obtained for low strength particles (i.e., sandstone particles) and gentle slopes were obtained for high strength particles (i.e., steel particles), which yielded high and low internal friction angles (Mohr-Coulomb criterion) and, low and high values of the material constant (Hoek-Brown criterion) respectively.

The variation of Mohr-Coulomb parameters (angle of friction and cohesion) of the conglomerates was examined corresponding to the UCS_{cem}/ UCS_{part} ratio. Irrespective of the particle material, the angle of friction decreased and cohesion increased with the increase in the UCS_{cem}/ UCS_{part} ratio, induced by the increase in the strength of the cementing material. Similarly, for a particular cementing material, the angle of friction increased and cohesion decreased with the increase of the UCS_{cem}/ UCS_{part} ratio, induced by the increase in the strength of the particle material. This suggests that cohesion is directly proportional to the strength of the cementing material or inversely proportional to the strength of the particle material. Likewise, the angle of friction is directly proportional to the strength of the particle material and inversely proportional to the strength of the cementing material.

The Hoek-Brown parameter, material constant (m_i), was also found to be sensitive to the particle and interparticle cementing materials. Generally, for a particular cementing material, it increased with the increase of the $UCS_{\text{cem}}/UCS_{\text{part}}$ ratio, however this increase was more pronounced for the argillaceous cementing materials. Likewise, for a particular particle material, m_i generally decreased with the increase of the $UCS_{\text{cem}}/UCS_{\text{part}}$ ratio, which is induced by the increase in the cement strength. This observation was found consistent with the existing understanding of the dependence of the material constant on the strength of the cementing material.

Micro-mechanical Investigation of Particle-Cement Interaction

7.1 Introduction

This chapter discusses the numerical study conducted on a micro level to investigate the particle-cement interaction and the role of interparticle cement on the mechanical response of a bonded pair of particles. The comparison of the responses of synthetic and numerical conglomerates (Chapter 5) showed both similarities and contrasts between the behaviour of physical models and numerical conglomerates. For example, in uniaxial compression, the numerical tests had good agreement with physical tests for peak strengths, damage thresholds and failure mechanisms. Similarly, a good comparison of the results was obtained in triaxial testing. The tensile strength was also found within the variation range of physical test results showing a reasonable agreement. Similarly, in the shear box tests, a good agreement of synthetic and numerical conglomerates was observed in terms of cohesion and angle of friction.

However, numerical conglomerates did not reproduce the elastic response of synthetic conglomerates in uniaxial and triaxial testing. Similarly, the post peak behaviour of the numerical conglomerates was also different to what was observed in tests on synthetic conglomerates. Likewise, a well developed distinct crack through the numerical conglomerate was not obtained in the Brazilian tensile test. In shear box tests, the vertical dilation in the numerical conglomerate was also lower than that of the synthetic conglomerate. These contrasts highlight significant differences in the responses of the interparticle cement (in synthetic conglomerate) and its corresponding parallel bond (in numerical conglomerate), as well as other factors, such as loading rates. In the numerical conglomerate, after the bond breakage, no cement matrix exists and they are free to rotate as per the specified interparticle friction. Any additional forces and moments are transferred only by the interparticle contacts; while in synthetic conglomerates, even after failure of the interparticle contact, cement is present and affects the overall mechanical response of the model by restricting particle rotation, and transferring the forces and moments. Hence, the influence of cement is considered an important factor controlling the elastic response, post peak behaviour, high dilation and failure mechanisms.

All these factors necessitate the need to explore the difference of particle-cement interaction and the presence of the cement in a conglomeratic rock which causes the mechanical response of an equivalent numerical conglomerate to deviate from that of a synthetic conglomerate. Therefore, the micromechanical investigation aimed to answer the following questions:

- Firstly, to what extent, can the strength and stiffness of the interparticle cement be approximated by a parallel bond? In particular, the impact of the normal and shear interparticle strengths and stiffnesses on the bulk behaviour.

  Additionally, in PFC, a parallel bond simulates the interparticle cement with a uniform strength in the cement and along the particle-cement interface. The uniform strength of the cement and interface leads to the equal possibility of failure through the cement and along the interface. This assumption may hold for the simulation of fine-grained rocks, such as siltstones or sandstones where failure through the cement or along the interface may not significantly affect the overall mechanical response. However, the particle-cement interface strength is an important parameter in modelling the response of a conglomeratic rock where the interface and cement matrix strengths are not necessarily the same (Savanick & Johnson 1974). Therefore at a micro level, the influence of the interface strength on the response and failure mechanism of bonded contacts, needs to be studied.

- Secondly, the significance of existence of the interparticle cement in controlling the macro-mechanical response of a conglomerate? This explores the post failure strain hardening response of the synthetic conglomerate with the presence of interparticle cement and, corresponding strain softening behaviour of the numerical conglomerate with parallel bonds. This will also help answer the causes of the strange failure mechanism in Brazilian tests.

To investigate these questions, a 3D study was, initially, considered but due to the requirement of the high computational cost for the cement sized particles, and to gain approximation of the governing mechanics, micro investigation was undertaken in 2D. Therefore, the findings of the study cannot be directly compared with the physical tests but aim to identify and describe the mechanisms and explore the relations between the key parameters.

In micro mechanical investigation, firstly, a calibration study was conducted to acquire the micro mechanical parameters by the inverse modelling approach, to reproduce the response of cement paste. Then a bond model using two steel balls (as in the synthetic conglomerate) glued together with the cement particles (micro particles) was simulated. The sensitivity of the interface properties was investigated together with the corresponding failure mechanism in tension, shear and rotation modes. The sensitivity of the cement particle size was also investigated. The modes of failures were also observed by changing the particle material from steel to granite and sandstone. Finally, the effect of the cementing material was examined in a simple three ball test to extrapolate its mechanical response from a micro to macro level.

7.2 Calibration - Cement Paste

In the synthetic conglomerate, interparticle cement was Portland cement, that is, cement paste whose behaviour was investigated experimentally in laboratory testing. The strengths and stiffnesses of the cement paste were measured (Chapter 3) from laboratory tests and used to estimate micro input parameters for parallel bonds in PFC3D (Chapter 4).

In the simulation of the numerical conglomerates, elastic particles were modelled using the Hertzian contact model in PFC3D. Therefore, as per the limitation of PFC in simulating Hertzian and linear stiffness models together, we also decided to use Hertzian contact models for the cement particles, that is, the elastic particles that make up the cement particles in PFC2D. Hence, in the calibration of the mechanical response of the cement paste, Hertzian stiffness model was used instead of linear stiffness model which is used in PFC2D for the calibration process (Itasca 2004; Potyondy & Cundall 2004). The size range of the cement paste particles was kept same as per actual cement particle sizes (equivalent diameter) of 40-70 μm in synthetic conglomerate. In the calibration process, this particle size range was adopted at 15% porosity. Parallel bonds were used in the calibration of the cement paste properties in PFC2D. In the beginning, the stiffness of cement particles and parallel bonds were derived from the laboratory test results on the cement paste. However, these models produced a mechanical response based on the elastic deformation of the particles (excessive overlap of the particles) rather than the bond breakage, that is, the models showed failure with out any bond breakage. To overcome this problem, the stiffness of the cement particles (Shear modulus) was increased to allow deformation along the particles' bonded contacts. Approximately 150 iterations were run to reproduce the cement paste response in uniaxial, triaxial and Brazilian tests. In the calibration, suggested methodology (Itasca 2004; Potyondy & Cundall 2004) was adopted for the specimen diagenesis and testing.

A summary of the input micro mechanical parameters and calibrated parameters is given in Table 7-1.

Table 7-1: Summary of micro-mechanical parameters selected in the PFC2D calibration process together with a comparison of the macroscopic parameters of cement paste determined in experiments and the calibration process.

Micro mechanical Input parameters				
Parallel bond parameters	Normal strength (MPa)		$\bar{\sigma}_c$	8.53
	Shear strength (MPa)		$\bar{\tau}_c$	12.8
	Shear of normal strength ratio		$\bar{\tau}_c / \bar{\sigma}_c$	1.50
	Normal stiffness (MPa/m)		$\bar{k}^n$	1.0e09
	Shear stiffness (MPa/m)		$\bar{k}^s$	5.0e07
	Normal to shear stiffness ratio		$\bar{k}^n / \bar{k}^s$	20
	Bond radius multiplier		λ	1
Ball parameters	Minimum ball radius (m)		r_{min}	2.00e-05
	Maximum ball radius (m)		r_{max}	3.50e-05
	Ball radii ratio		r_{max} / r_{min}	1.75
	Average ball radius (m)		$r_{avg.}$	2.75e-05
Contact parameters	Angle of Friction (0.839)		ϕ	40°
	Hertz- Mindlin contact model	*Shear modulus (GPa)*	G	7.81
		Poisson's ratio	ν	0.28
Calibrated output parameters			**Experimental**	**Calibrated**
Young modulus (secant - GPa)			3.18	3.16
Peak compressive strength (MPa)			12.76	12.70
Angle of internal friction (0-10 MPa Fit - deg.)			30.4	30.8
Tensile strength (MPa)			-1.36	-1.83
Poisson's ratio			0.2	0.05

7.3 Two-Ball Test

The two-ball test is a simulation of two macro balls bonded together with interparticle cement. The cement is simulated with tiny (micro) particles whose micro mechanical properties have been determined by calibrating the macroscopic response of the cement paste. Both the macro particles and cement particles have Hertzian contacts. The macro particles are then subjected to various modes of deformation, that is, tension, shearing and rotation, where one particle is fixed and other is given translational or rotational velocity in a specified direction as illustrated in Figure 7-1. The forces and displacement of both particles are monitored.

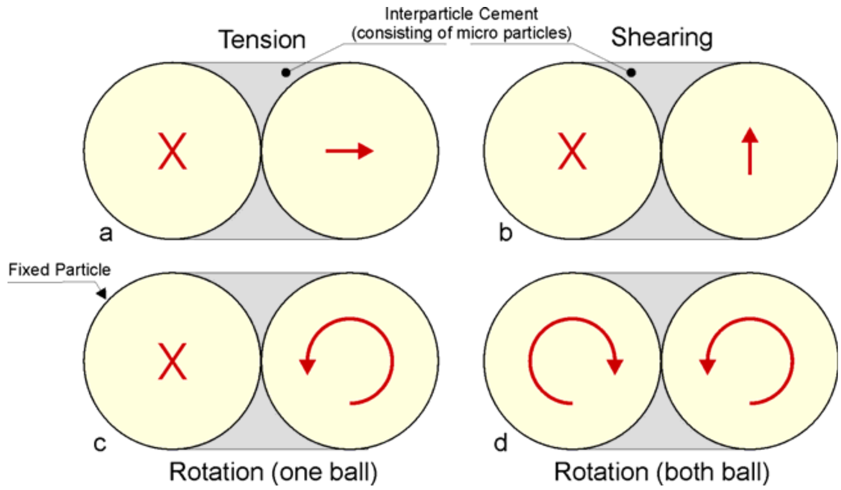

Figure 7-1: Various modes of deformation of cemented particles in the two-ball test: a) Tension, b) Shear, c) Rotation of one ball, d) Rotation of both balls. The symbol "X" denotes the fixed position of the balls while the arrows represent the translation or rotational movements of the balls.

7.3.1 Test Objectives

The two-ball test is an investigation into the mechanics of the particle-cement interaction at a micro level, and a validation of the capability of the PFC's parallel bond in representing real life cemented particles. Through studies (e.g., Dvorkin et al. 1991; 1994; Dvorkin & Yin 1995; Dvorkin 1996; Itasca 2004; Potyondy & Cundall 2004; Itasca 2005), it is known that the macroscopic response in DEM is controlled by the properties and interaction of the particles and interparticle cement.

In PFC, the parallel bond behaves like a beam of certain dimensions and strength properties, placed at the centre of two particles (Itasca 2004; 2005). This beam is capable of transmitting forces and moments across the bond. When forces or moments exceed the strength of the beam, the parallel bond breaks. The parallel bond also contributes stiffness to the system of bonded particles. The parallel bond can be envisioned as two particles cemented together in such a way that the strength of the cement and cement-particle interface is the same and has an equal possibility of breaking the bond either along the cement-particle interface or through the cement, that is, both the cement and the interface have the same strength.

However, in physical experiments, different mechanisms were observed. Most of the particle-cement contacts were noted to have failed along the cement-particle interface or the particle boundaries (Figure 7-2a). Some indicated the crack surface through the cement and particle-cement interface (Figure 7-2b, c & e). Very few were observed to have failed through the cement (Figure 7-2d). These observations highlight the significance of particle-cement interface properties on failure mechanisms.

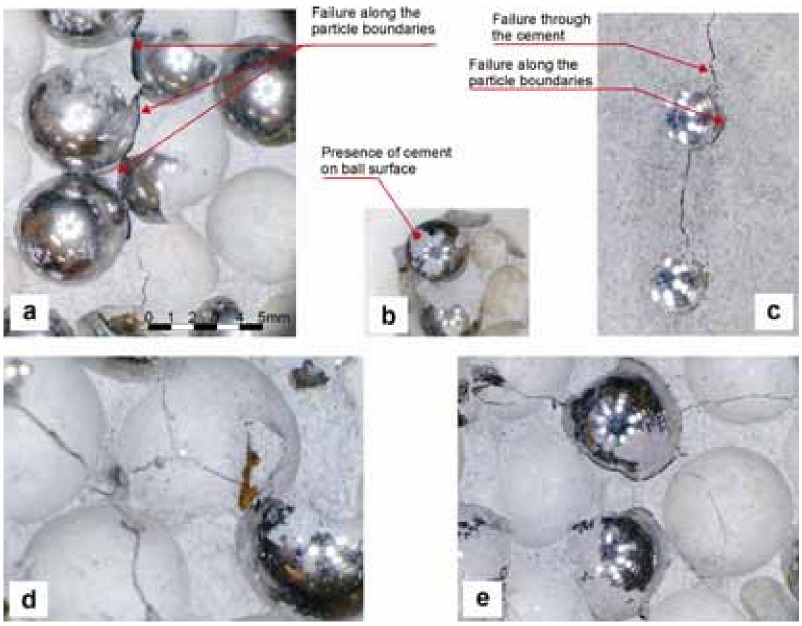

Figure 7-2: Microscopic damage observations in synthetic conglomerate samples consisting of steel balls and cement paste; a) well developed crack along the steel ball- cement interface, b) presence of the cement layer on the steel ball surface indicates that the failure occurred through the cement and along ball boundary, c) macroscopic crack through the cement and ball boundaries on the sample surface, d) complex framework of the cracks through the cement, and e) distribution of cracks in the cement and ball-cement interface.

The observations are summarised as follow:

- The failure in the synthetic conglomerate samples is mainly associated with micro cracking along the particle-cement interface which, in turn, suggests that the strength of the particle-cement interface is lower compared to the cement itself. This observation is consistent with the findings of a study on natural conglomerate (Savanick & Johnson 1974). This study showed that the interface cohesive strength could be half that of the cement matrix.
- The strength of the interface is variable and can be higher, at some points, than the strength of the cement to allow the failure to occur through the cement rather than along the interface (Figure 7-2b).

- Crack development is a function of the localised stress concentration (fibre) and the overall distribution of the cement and interface strengths in the sample.

Besides the effect of interface properties on a cemented contact, it is more reasonable to validate the parallel bond's capability of simulating the response of the real life interparticle cement which controls the overall mechanical response of a bonded contact. Moreover, as proposed by Wawersik (2000), the mechanical response of the contact and bonding models should be investigated in simple testing with a few particles to convert DEM into a quantitative tool for simulation.

Therefore, the objective of the two-ball test is to study and investigate the response of a parallel bond by simulating the interparticle cement as an aggregate of micro particles.

7.3.2 Test Configuration

In two-ball testing, firstly particles representing the cement were created with 15% porosity in a confined rectangular container and given initial parameters (shear modulus, Poisson's ratio and density). The cement particles were then deleted from the circular regions where steel (macro) balls were planned to be inserted. Afterwards, steel balls were created in the circular regions (Figure 7-3a) and their initial micro parameters were specified. The cement particles (micro particles) in contact with the bigger particles (representing clasts) were identified as an interface layer (Figure 7-3b). Subsequently, parallel bonds were installed as per the micro parameters given in Table 7-1 (Figure 7-3c). The particle assembly was then brought to equilibrium to minimise the locked-in stresses by fixing the positions of the steel balls. Initially, the interface properties were defined as for the cement properties, except interparticle friction. Interparticle friction for the cement particles was defined as 40°, while for the steel balls it was 5.5°. This model comprised of two balls bonded together with the calibrated interparticle cement was termed as *Composite Bond Model* [7] (CBM).

The next step was to monitor the forces and displacement in tension, shear and rotations. The forces acting on the steel balls were uncoupled into X (tensile) and Y (Shear) forces and were measured by monitoring unbalanced forces along the X and Y axes, where the forces along the X-axis represent tensile forces and the Y-axis mainly represents shear forces.

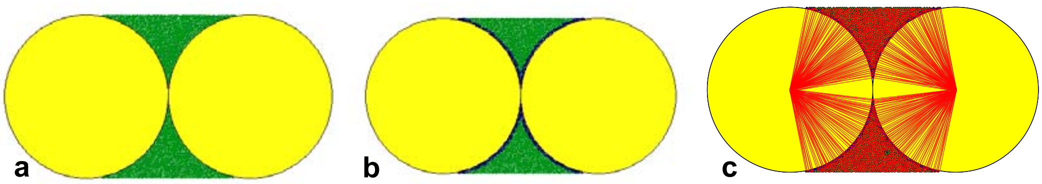

Figure 7-3: The Composite Bond Model's (CBM) diagenesis steps; a) creation of cement and steel particles, b) defining concentric layer of cement particles around steel particles, and c) installation of bonds in cement and cement and steel particles.

The position of one cemented ball was fixed (left balls in Figure 7-1a, b & c), while fixed translation or rotational velocities were specified to the other balls (right balls) as in the deformation modes (i.e., tension, shear and rotation). The translation velocities were kept at 0.02 m/s in shear and tension modes to maintain quasistatic conditions throughout the tests (Figure 7-1a & b). For the rotation mode, two mechanisms of testing were considered: a one ball rotation and a rotation of both balls. In the one ball rotation test, a rotational velocity of 10 rad/s was specified in an anti clockwise direction to the right ball (Figure 7-1c) by fixing the position of the left ball. In two ball rotation test, the same velocity was given to the right ball in anti clockwise direction and to the left ball in the clockwise direction (Figure 7-1d).

To observe the failure mechanism in two-ball testing, positions of cracks (breakage of bonds) were traced by using the available crack tracing algorithm (after Itasca 2004). The cracks were monitored as history variables. Forces acting on both balls in X and Y directions were also monitored separately as history variables against translational and angular displacements.

The FISH algorithms written for two-ball testing are provided in Appendix B.

7.3.3 Tension Mode of Deformation

The two-ball test was conducted to find the peak normal or tensile strength of the CBM represented by the cement and steel particles. Both X and Y forces acting on ball 1 (left ball) and ball 2 (right ball) were monitored as unbalanced forces. The forces were then plotted against the horizontal displacement. Firstly, interface strengths (normal and shear) were kept the same as the cement. The results are shown in Figure 7-4.

The plots clearly show the contribution of the x-forces experienced by both balls along the tension (Figure 7-4a) while the y-forces acting normal to the tension are generally close to zero. After the peak, the x-forces decrease gradually with the formation of an increased number of cracks (Figure 7-4b).

The mechanism of failure and the position of the macro crack obtained during the test is also shown in Figure 7-4. The position of failure was located along the particle-cement interface in the centre and shifts into the cement towards the edges. This suggests that, in tension mode, failure through the cemented balls with the same interface and cement strength occurs partially along the particle boundary and partially through the cement matrix.

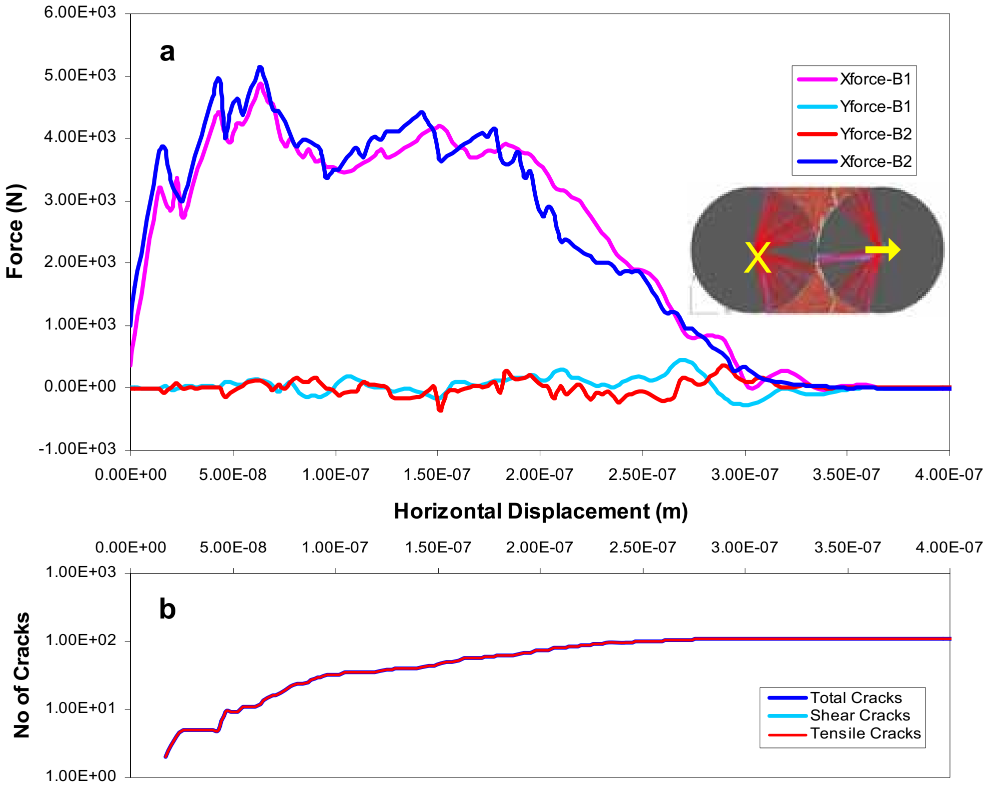

Figure 7-4: Tensile mode of failure of CBM having an interface strength equivalent to the cement strength; a) Plot of out of balance forces acting on balls 1 & 2 in the X (horizontal) and Y (vertical) directions, b) monitored number of cracks versus horizontal displacement. The mechanism of failure in tension is also shown on the plot.

7.3.4 Shear Mode of Deformation

The two-ball test was conducted to find the peak strength of the CBM in shearing. Both X and Y forces acting on the steel balls were monitored as out of balance forces. The forces were then plotted against the vertical (shear) displacement. The results are shown in Figure 7-5.

The plots indicate the bond's shear strength with the dominant contribution of the y-forces. In shearing up to peak strength, the x-forces were close to zero, but after the peak strength (failure) their contributions increased. This suggests that in CBM, the rupture is not exactly perpendicular to the shear direction and consequently any obliquity may raise the contribution of the x-forces. This is also consistent with the observed failure mechanism. The failure is along the particle-cement interface (Figure 7-5). The stiffness of the contact, pre and post peak, is also evident from the plots (Figure 7-5a). Post peak stiffness is slightly lower than pre peak stiffness and is an indication of the post peak strain softening behaviour. The formation of cracks increases immediately after reaching the peak strength of the CBM (Figure 7-5b).

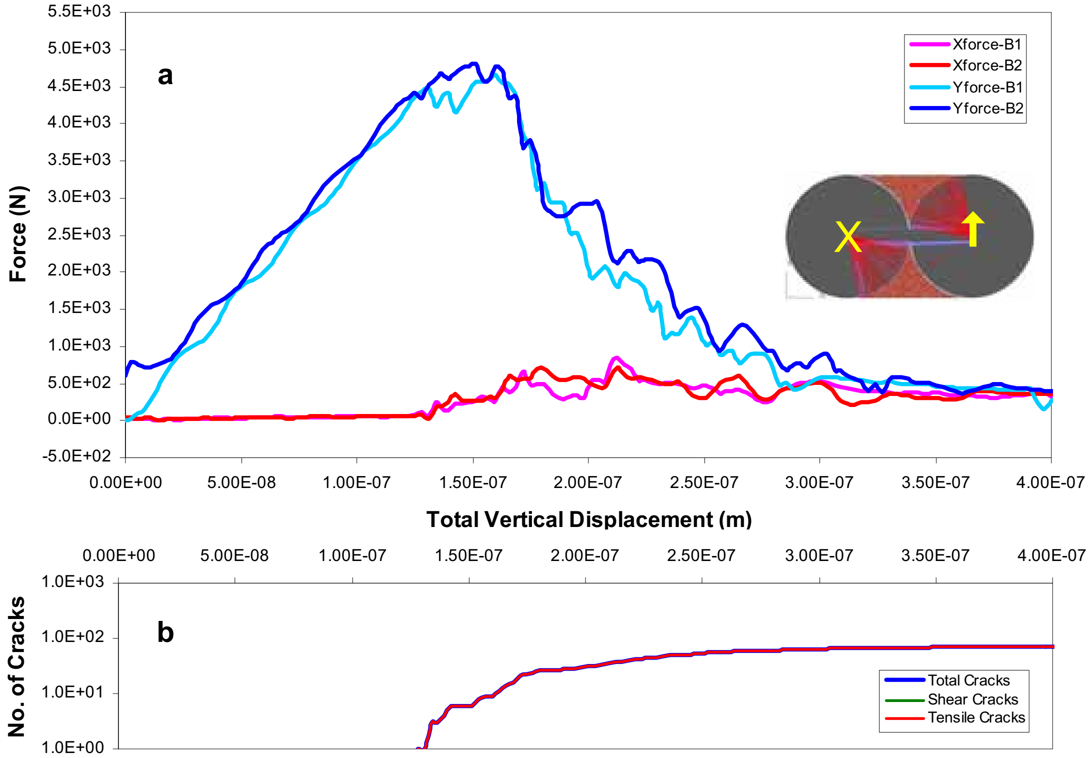

Figure 7-5: Shear mode of failure of the CBM having an interface strength equivalent to the cement strength: a) Plot of out of balance forces acting on balls 1 & 2 in the X (horizontal) and Y (vertical) directions , b) monitored number of cracks versus horizontal displacement. The mechanism of failure in shear is also shown on the plot.

7.3.5 Rotation Mode of Deformation

The strength of the bond was also tested for rotation in two-ball test. Two types of rotation were tested and in both cases, the X and Y translational movement were constrained: a one ball rotation test that involved the rotation of one particle, and a two ball rotation test involving the rotation of both particles. Both X and Y forces were monitored in the both tests. The forces plotted against the rotations of the one and two ball rotation modes are shown in Figure 7-6 and Figure 7-7 respectively. The number of cracks monitored and the obtained failure mechanisms are also shown in Figure 7-6 and Figure 7-7.

In the rotation of one ball, X and Y forces were induced in the CBM (Figure 7-6a). This observation suggests that the net failure mechanism of the bond is neither a perfect tensile (as observed in Figure 7-4a) nor a perfect shear (as observed in

Figure 7-5a) but is the combination of both. Initially, the Y forces increase while X forces remain close to zero, suggesting resistance to shearing. However, later, the increase in X forces implies the contribution of tensile forces in the model. In the one ball rotation, peak X forces were found to correlate with those observed in tension mode (Figure 7-4a). Similarly, Y forces correspond to those seen in shear mode (Figure 7-5a). It is interesting to note that all the cracks observed are tension induced (Figure 7-6b) with no shear cracks.

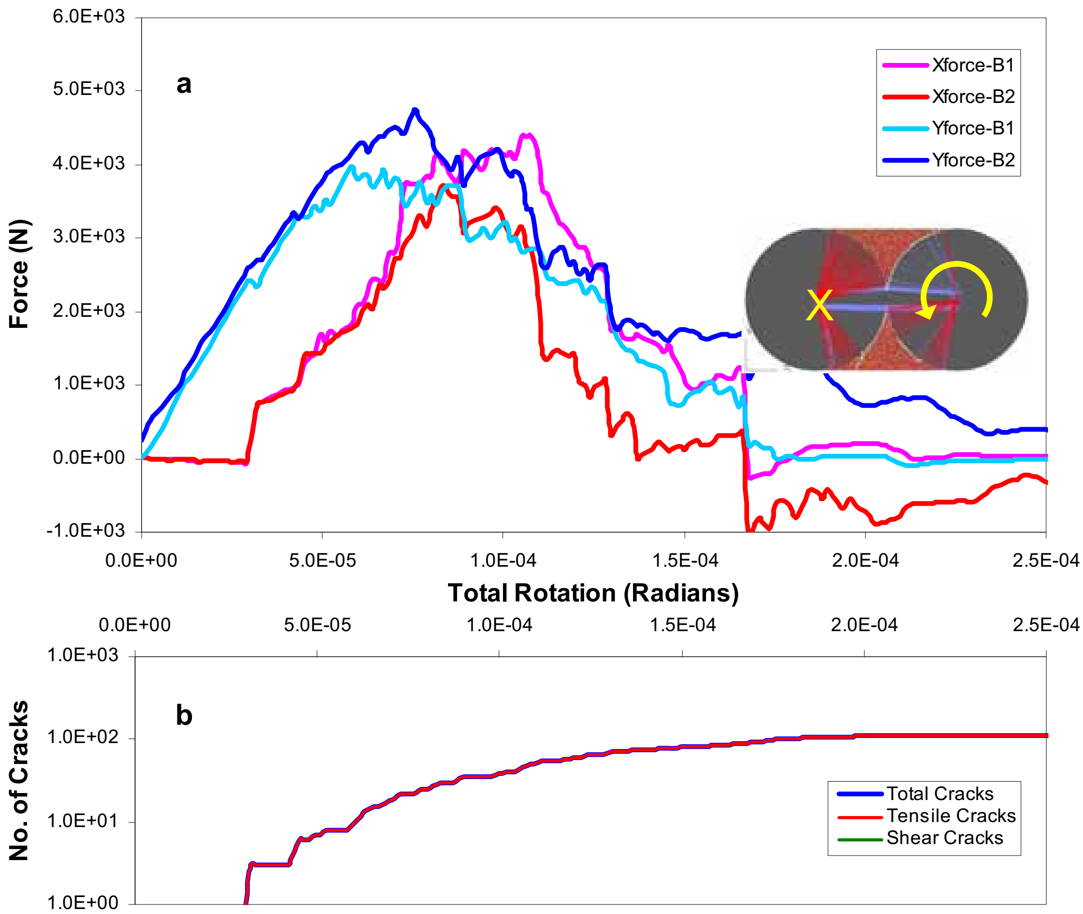

Figure 7-6: One ball rotation in CBM having an interface strength equivalent to the cement strength: a) Plot of out of balance forces acting on balls 1 & 2 in the X (horizontal) and Y (vertical) directions, b) monitored number of cracks versus particle rotation. The mechanism of failure is also overlaid on the plot.

In the two-ball test with the rotation of both balls, a clear contribution of X forces was observed (Figure 7-7), indicating a tensile mechanism of failure (as observed in Figure 7-4a in tension mode). However, the development and position of the cracks were different to those observed in pure tension mode (Figure 7-4a). Furthermore, the peak strength of the bond in the two-ball rotation was two times the magnitude of the tension results. These findings are attributed to the failure along the interfaces of both steel balls and also to the cement crushing between the steel balls near their contact joints (Figure 7-7a).

The development of shear cracks in the bond model is an indication of cement crushing (Figure 7-7) induced in the cement matrix.

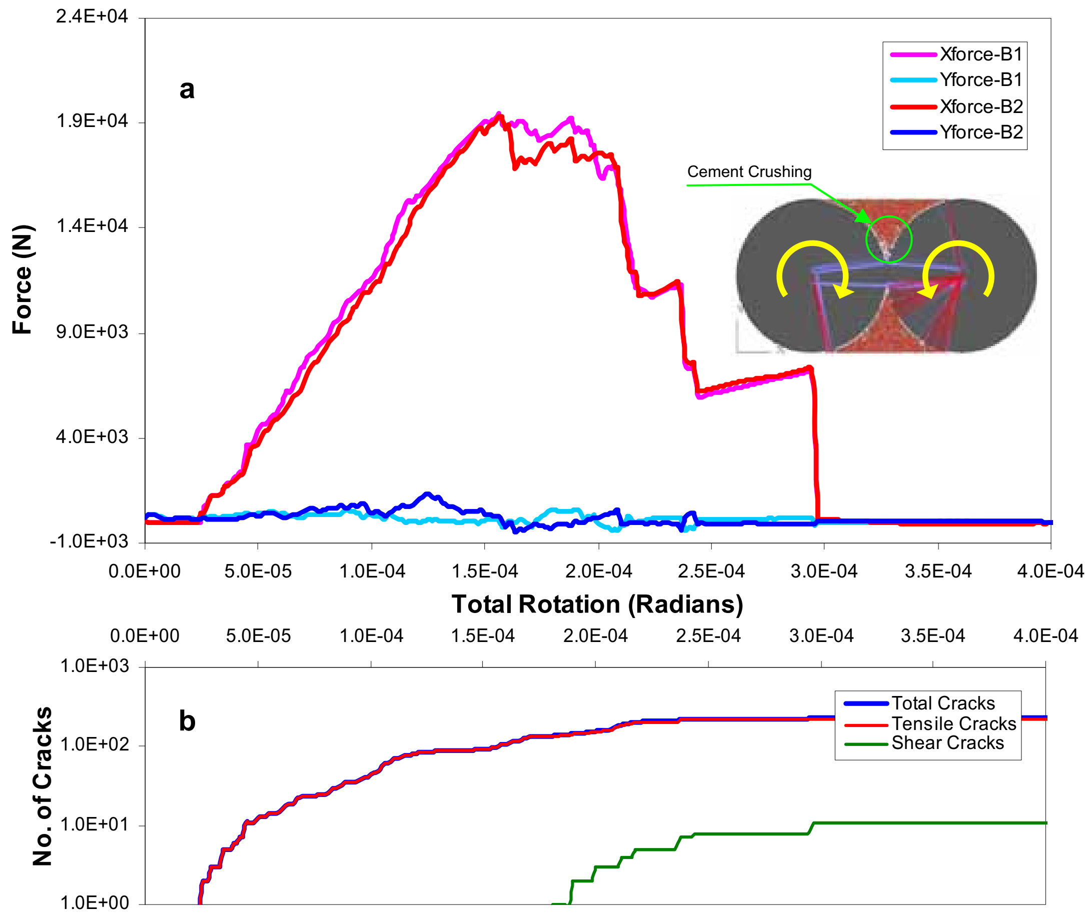

Figure 7-7: Two ball rotation in CBM having an interface strength equivalent to the cement strength: a) Plot of out of balance forces acting on balls 1 & 2 in X (horizontal) and Y (vertical) directions , b) monitored number of cracks versus rotation of both balls. The rotation of both balls was considered in a clock wise direction for plotting purpose. The mechanism of failure is also overlaid, showing the important mechanism of cement crushing.

7.3.6 Comparison with Equivalent Parallel Bond

The two-ball model was then re-created with parallel bond replacing the interparticle cement. The term *Parallel Bond Model* [8](PBM) is used to differentiate it from the CBM. The properties of the interparticle cement (from Chapter 4) were used as the properties of the parallel bond in the PBM. The response of the PBM was then compared to that of the CBM in tension, shear and rotation modes. The objective of this comparison was to investigate the extent to which the parallel bond can simulate the response of a pair of balls cemented together with equivalent cement, that is, the CBM in this study. Although the response of the parallel bond was validated earlier with that of cylindrical disc (Cundall 2004), its capability of simulating interstitial cement in conglomeritic rocks has not yet been examined.

The response of the PBM was investigated and plotted along with the equivalent CBM in tension (Figure 7-8), shear (Figure 7-9) and rotation (Figure 7-10) modes. It should be noted that the rotation of both balls could not be achieved in the PBM and only the response of a one ball rotation is presented here. In two ball rotation mode, the PBM shows all peak forces equal to zero even at a very low rotational velocity. Therefore, its response was not determined.

In tension and shear modes of testing, peak forces (strengths of PBM) were found very sensitive to the displacement rate of balls in normal and shear directions. However, in contrast, no sensitivity of the angular displacement rate was observed in rotation mode. The response of the PBM was investigated in tension, shear and rotation modes in relation to the sensitivity of the displacement rates. The results are shown in Figure 7-11, Figure 7-12 and Figure 7-13 for tension, shear and rotation respectively. Finally, as in sensitivity studies, the adopted displacement rates were 0.002 mm/s, 0.001 mm/s and 1e6 radian/s for tension, shear and rotation respectively. Afterwards, the mechanical response of PBM was compared to the equivalent response of the CBM in tension mode (Figure 7-8). A significant difference was observed in the stiffness and peak strength of the PBM and CBM. The peak strength of the CBM is approximately 73% of the PBM. The stiffness of the PBM was found to be about 250 times the stiffness of the CBM.

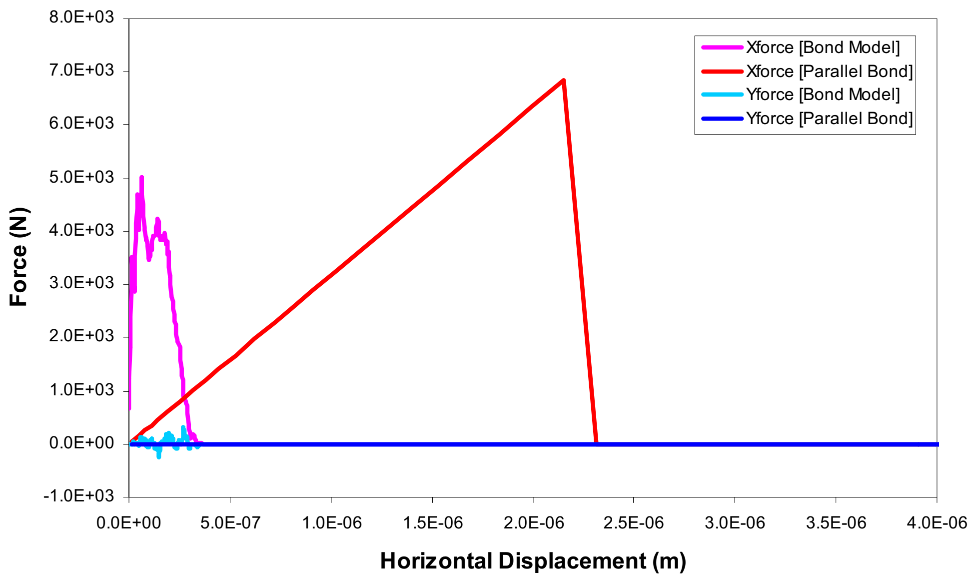

Figure 7-8: Comparison of the responses of the Composite Bond Model (CBM) and Parallel Bond Model (PBM) in the tension mode of deformation.

Similar observations were made when comparing the CBM and PBM in the shear mode (Figure 7-9). Here the strength of CBM is just 25% of the PBM's strength. The stiffness of the PBM is about 10 times that of the CBM. The stiffness ratio normal (in tension mode) to shear (in shear mode) of the CBM is approximately 25 whereas this is 1.0 in the PBM. It should be noted that the stiffness of the steel balls in both models is constant, the only difference arising is due to the cement and parallel bond.

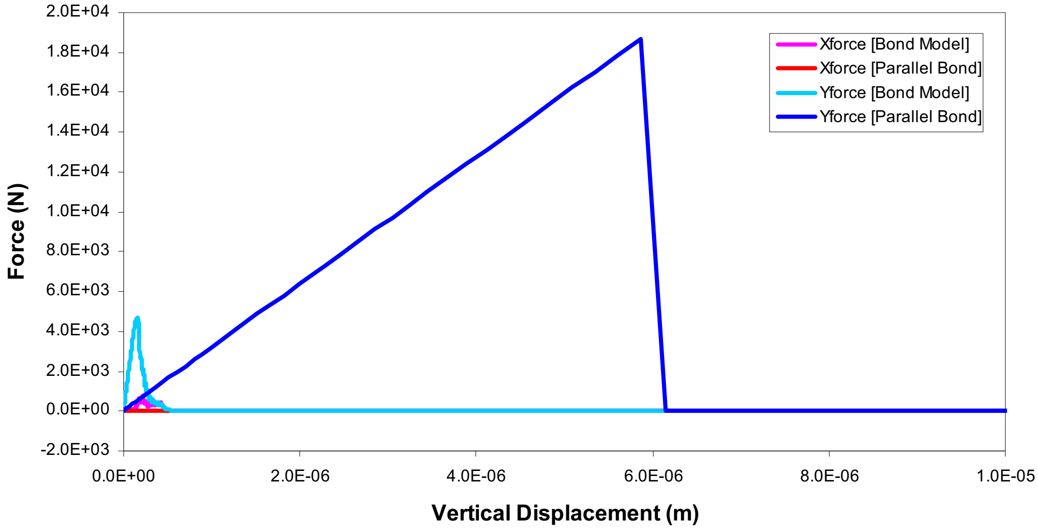

Figure 7-9: Comparison of the responses of the Composite Bond Model (CBM) and Parallel Bond Model (PBM) in the shear mode of deformation.

The comparison of the peak strengths and stiffnesses of the CBM and PBM in the one ball rotation mode is shown in Figure 7-10. In CBM, the failure is observed to be controlled by both tensile and shear strengths, whereas in the PBM, the failure is solely controlled by the shear strength. This is a big contrast and indicates the assumption behind the simulation of the parallel bond. Further, the peak strength of the PBM is close to tensile strength of the PBM (in tension mode) rather it should be close to the shear strength (in shear mode). The peak strengths (tensile and shear) of the CBM are 50~60% of the PBM, which is shear strength in rotation mode. The stiffness of the PBM is 5~7 times the stiffnesses of the CBM, indicating a normal to shear stiffness ratio of 0.66 in the CBM. This is in contrast with the stiffness ratio of the CBM determined in the tensile and shear modes, which was approximately 25. This observation suggests that the stiffnesses are not independent variables but also depend on the mode of deformation. Alone, shear or tensile stiffnesses are not enough to depict the stiffnesses of a bonded contact in the rotation mode of deformation. This is important in modelling the response of conglomerates comprised of macro particles (clasts) embedded in cement matrix. However, this may not be applicable to the simulation of brittle or fine grained rocks which are normally modelled by a densely packed bonded assembly of the particles with no dominant structure (Potyondy & Cundall 2004).

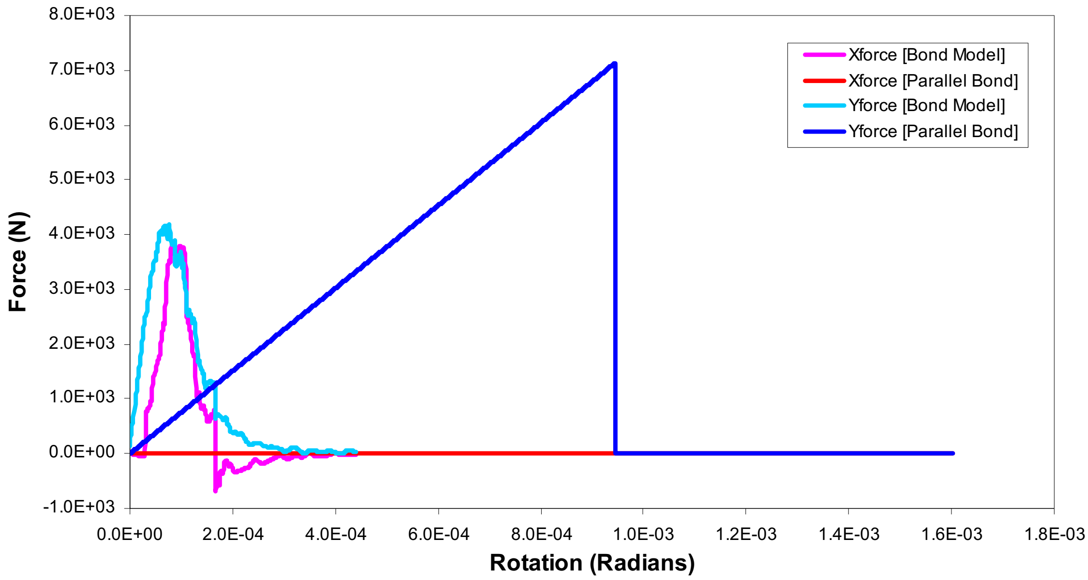

Figure 7-10: Comparison of the responses of the Composite Bond Model (CBM) and Parallel Bond Model (PBM) in a one ball rotation.

7.3.7 Sensitivity Studies

In a two-ball test, the response of the CBM was further investigated for the sensitivity of various parameters. Since, when comparing the peak strengths of the CBM and PBM in various modes of deformation, reasonable differences were noted, it was considered reasonable to examine the effect of the interface properties in matching the peak strengths of the CBM and PBM. Similarly, the effect of particle size in simulating the interparticle cement was also studied in the two-ball test. The dependency of the particles' material on the mechanical response of the CBM was also examined by replacing the steel balls of the CBM with granitic and sandstone particles.

The details of these sensitivity studies are discussed in the following sections under respective hearings.

7.3.7.1 Interface Properties

The strengths of the cement particles were determined from the calibration process (refer to Section 4.7). These are the normal and shear strength of the parallel bond between the cement particles. The interface strengths are the strengths of the parallel bonds installed between the cement balls and steel balls along the steel ball boundaries, that is, the interface. In the PFC, parallel bonds between two balls shows the same strength of the cement and the particle-cement interface. However, in reality, the strength of the interface varies with the cohesion of the cement and the adhesion characteristics of the cement and particles, and consequently, this influences the macroscopic response. In the present interface strength sensitivity study, the normal and shear strengths of the interface were changed in terms of the interface to cement strength ratio. The studied range of this ratio was from 0.25, where interface strength was one quarter of the cement strengths, to 2.0, corresponding to double the strength of the cement. The details of the interface strengths corresponding to strength ratios is provided in Table 7-2.

Table 7-2: Summary of the normal and shear interface strengths corresponding to various interface to cement strength ratios used in the sensitivity study.

Cement strengths (MPa)		Interface to cement strength ratio	Interface strengths (MPa)	
Normal	Shear		Normal	Shear
8.53	12.8	0.25	2.13	3.20
		0.50	4.27	6.40
		1.00	8.53	12.8
		1.25	10.7	16.0
		1.50	12.8	19.2
		1.75	14.9	22.4
		2.00	17.1	25.6

The response of the composite bond model (CBM) was investigated using the above mentioned values of interface strengths in tension, shear and, two ball and one ball rotation. The peak strengths (X and Y forces) were determined and plotted against translation and rotational displacement. The failure mechanisms were also examined in all the tests and pasted on the plots corresponding to the specific interface strength ratio.

In tension mode, the results of the peak X and Y forces are shown in Figure 7-11, together with the overlaid mechanisms of failure. The variation of peak strength (in terms of X and Y forces) of the PBM is also shown in Figure 7-11. It was noted that the tensile strength of the CBM increases with the increase of the interface to cement strength ratio. This increase is sharp (linear) up to the strength ratio of 1.25. It is interesting to note that the peak strength of the CBM at interface strength ratio of 1.5 resembles the corresponding strength of the PBM (i.e. at strength ratio of 1.0).

The failure mechanisms of the CBM were observed to be sensitive to the interface to cement strength ratio. At lower interface strengths than that of cement, these are along the interfaces, while with the gradual increase in interface strengths, these shift away from the interface to the cement (Figure 7-11). At an interface to cement strength ratio of 1.0, the failure mechanism obtained was partially along the interface and partially through the cement.

In shear mode, the results of the peak X and Y forces are shown in Figure 7-12 together with the superimposed mechanisms of failure. The variation of the peak strength (in terms of X and Y forces) of the PBM is also shown in Figure 7-12. It was noted that the shear strength of the CBM increases with the increase of the interface to cement strength ratio. In shear mode, the peak strength of the CBM corresponding to a strength ratio of 1.5~1.75 was found to resemble that of the PBM.

The failure mechanisms of the CBM in the mode shear remained almost insensitive to the interface-cement strength ratio. At lower interface strengths than that of cement, the failure surface was strictly along the interface, while with the increase of the interface strength, it shifted slightly towards the cement matrix (Figure 7-12).

In the one ball rotation, the results of the peak X and Y forces are shown in Figure 7-13 together with the superimposed mechanisms of failure. The variation of the peak strength (in terms of X and Y forces) of the PBM is also shown in Figure 7-13. It is interesting that in rotation, the peak shear strength of the PBM is insensitive to the rate of ball rotation (Figure 7-13). It was observed that both the tensile and shear strengths of the CBM increased with the increase of the interface to cement strength ratio. The peak strength of the CBM corresponding to 1.5~1.75 of the strength ratio, was found to resemble that of the PBM.

The failure mechanism of the CBM varied with the interface to cement strength ratio. At low interface strengths, the failure surface was strictly along the interface, while with the increase of interface strength, it shifted towards the cement. At an interface to cement strength ratio of 2, a reasonable shearing was observed through the cement (Figure 7-13).

The results of the peak X and Y forces in the two ball rotation mode are shown in Figure 7-14, together with the overlaid mechanisms of failure. The failure in the two ball rotation was controlled by mainly the tensile strength of the bond model which was observed to increase with the increase of the interface to cement strength ratio. The failure surface was along the steel ball boundaries. In the failure mechanism, an interesting phenomenon of cement crushing was observed by tracing the formation and positions of the cracks near the contact point of the steel balls. This mechanism became more pronounced with the increase of the interface strength and extended gradually outward from the contact point of the steel balls (Figure 7-14).

All the mechanisms of failures in two-ball tests are also provided in Appendix C.

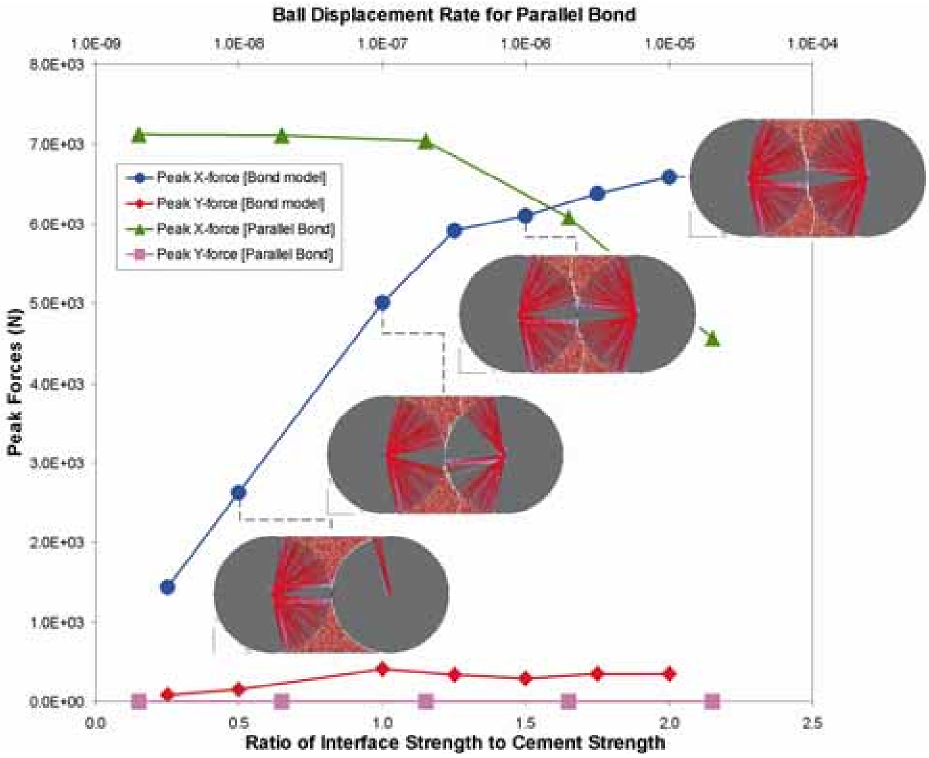

Figure 7-11: Composite Bond Model (CBM) in tensile mode of deformation; peak out of balanced forces (mean) acting on the balls along X (Tensile) and Y (shear) directions at an interface to cement strength ratio of 0.25 to 2.0 together with the corresponding (selective) failure mechanisms. Displacement rate sensitivity of the peak forces of Parallel Bond Model (PBM) at an interface to cement strength ratio of 1.0 is also presented.

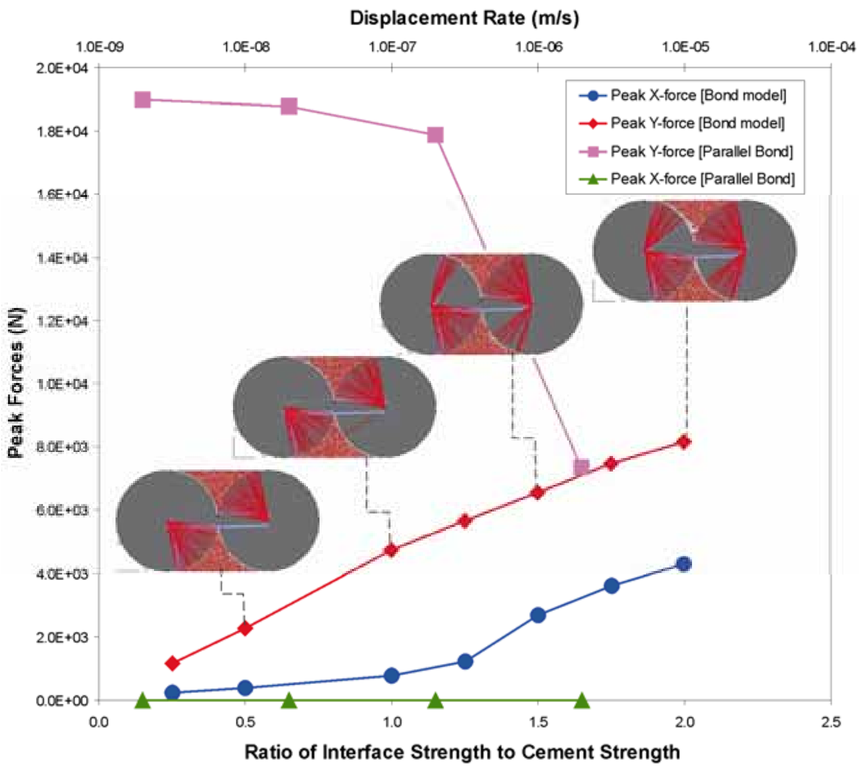

Figure 7-12: CBM in shear mode, peak forces (mean) acting on the balls along X (Tensile) and Y (shear) directions at an interface to cement strength ratio of 0.25 to 2.0 together with the corresponding (selective) failure mechanism. Displacement rate sensitivity of the peak forces of the PBM at an interface to cement strength ratio of 1.0 is also presented.

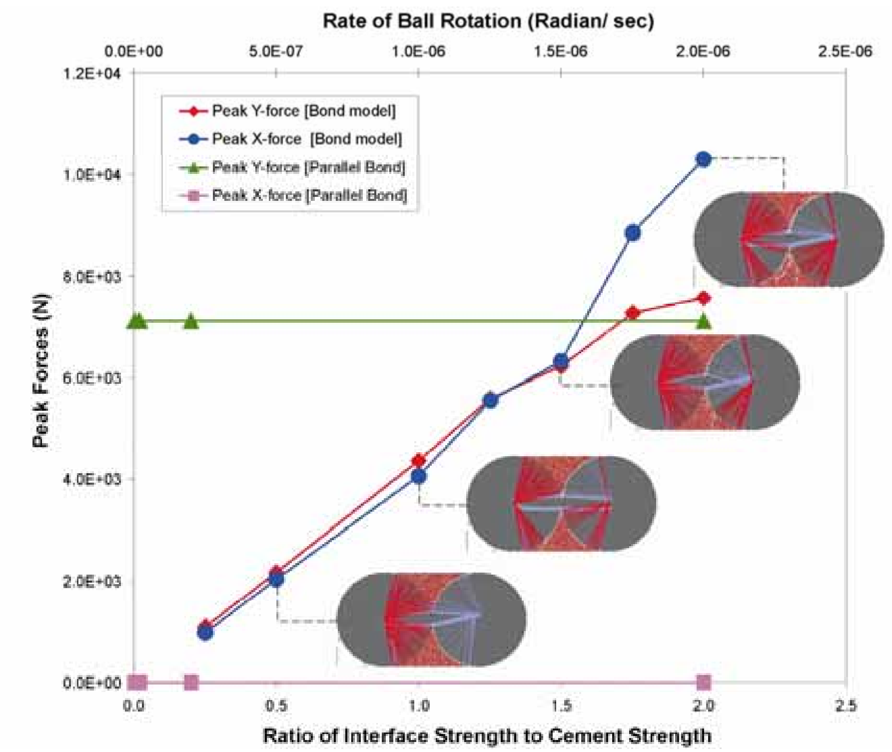

Figure 7-13: Composite Bond Model (CBM) in one ball rotation; peak forces (mean) acting on the balls along X (Tensile) and Y (shear) directions at an interface to cement strength ratio of 0.25 to 2.0 together with the corresponding (selective) failure mechanism. Displacement rate sensitivity of the peak forces of Parallel Bond Model (PBM) at an interface to cement strength ratio of 1.0 is also presented.

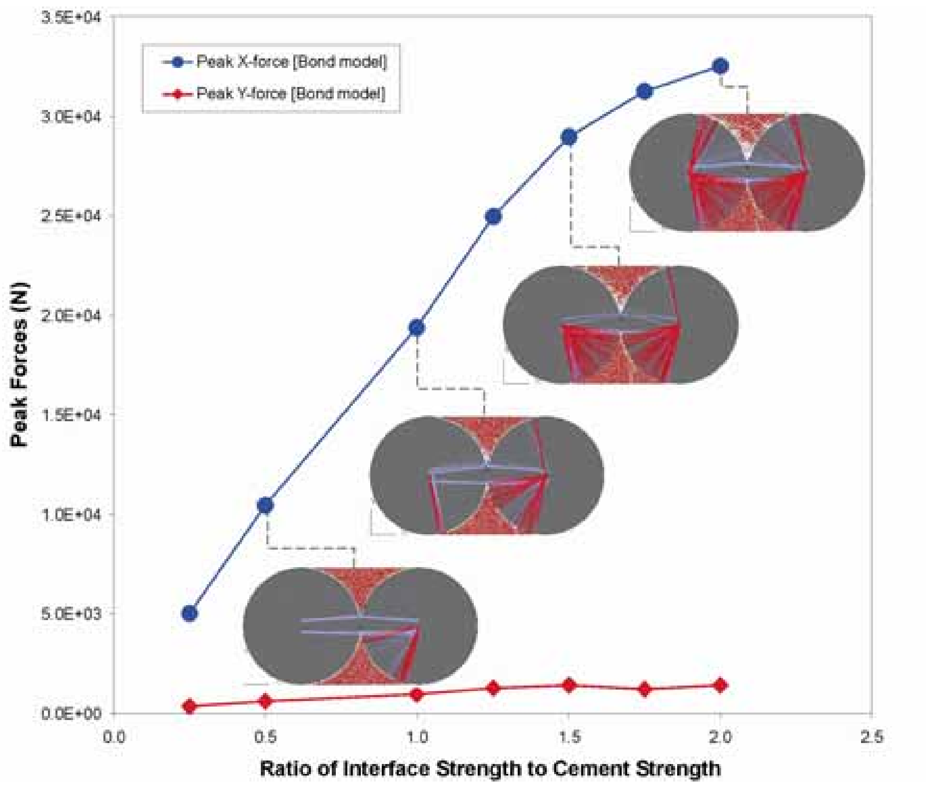

Figure 7-14: CBM in two ball rotation; peak forces (mean) acting on the balls along X (Tensile) and Y (shear) directions at an interface to cement strength ratio of 0.25 to 2.0 together with the corresponding (selective) failure mechanism.

7.3.7.2 Size of Cement Particles

The sensitivity of the size of the cement particles with respect to strengths of the composite bond model (CBM) and the failure mechanisms was also assessed. The cement particles' size (average) was increased from 2.75e-5 m to 5.5e-5 m. The mechanical parameters derived for sensitivity studies are summarised in Table 7-3.

Table 7-3: Summary of micro mechanical parameters for particle radius (mean) of 5.5e-5 m used in sensitivity studies.

Micro mechanical Input parameters				
Parallel bond parameters	Normal strength (MPa)		$\bar{\sigma}_c$	8.53
	Shear strength (MPa)		$\bar{\tau}_c$	12.8
	Shear of normal strength ratio		$\bar{\tau}_c / \bar{\sigma}_c$	1.50
	Normal stiffness (MPa/m)		$\bar{k}^n$	5.0e08
	Shear stiffness (MPa/m)		$\bar{k}^s$	2.5e07
	Normal to shear stiffness ratio		$\bar{k}^n / \bar{k}^s$	20
	Bond radius multiplier		λ	1.0
Ball parameters	Minimum ball radius (m)		r_{min}	4.0e-05
	Maximum ball radius (m)		r_{max}	7.0e-05
	Ball radii ratio		r_{max} / r_{min}	1.75
	Average ball radius (m)		$r_{avg.}$	5.5e-05
Contact parameters	Angle of friction (0.839)		ϕ	40°
	Hertz- Mindlin contact model	*Shear modulus (GPa)*	G	7.81
		Poisson's ratio	ν	0.28

The two-ball test was conducted for tension, shear and rotation (one ball rotation only) modes and the peak X and Y forces were monitored. The interface to cement strength ratios of 0.5, 1.0, 1.5 and 2.0 were kept constant in each mode of deformation. The forces were compared with that of CBM with the average radius (of cement particles) of 2.75e-5. The results are presented as Figure 7-15, Figure 7-16 and Figure 7-17 for tension, shear and one ball rotation respectively. A comparison of the failure mechanisms of the CBM with an average radius of 5.5e-5 and 2.75e-5 m is attached in Appendix-C.

In tension mode, an increase in the particle size resulted in the increase of both tensile and shear strengths (Figure 7-15). The observed failure mechanisms with bigger cement particles were slightly different from those with smaller cement particle radius. This suggests that the size of the cement particles not only affects the peak strengths but also controls the mechanism of failure.

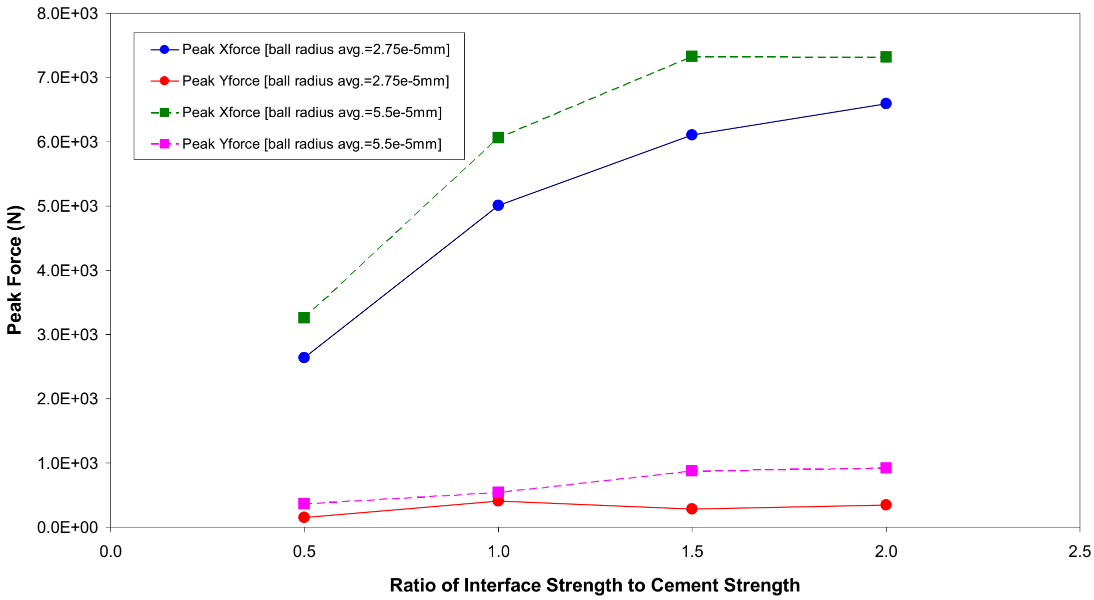

Figure 7-15: Particle size sensitivity in tension mode; peak X and Y forces at interface to cement strength ratio of 0.5 to 2.0 for particle radii (mean) 2.75e5 and 5.5e-5m.

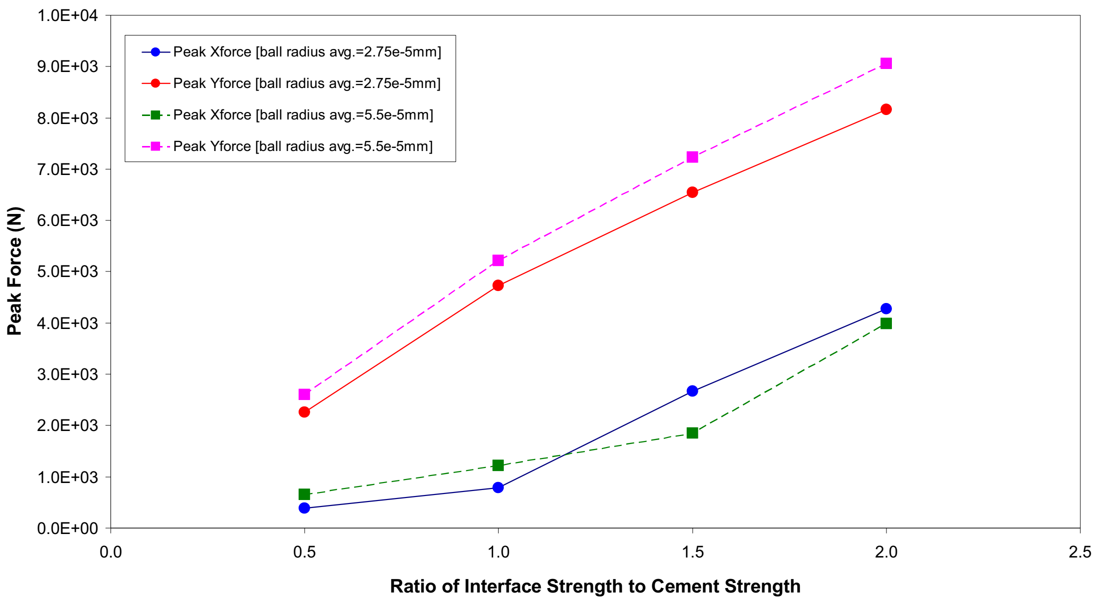

Figure 7-16: Particle size sensitivity in shear mode; peak X and Y forces at interface to cement strength ratio of 0.5 to 2.0 for particle radii (mean) 2.75e5 and 5.5e-5m.

In shear mode, the CBM showed an increase of peak Y forces (shear strength) while the X forces did not show any conclusive trend (Figure 7-16). These were higher, corresponding to the interface to cement strength ratio of 0.5 and 2, and lower, at ratio of 1.5 and 2.0. The cement particle size was also observed to influence the failure mechanism in shear mode. However, the trend of the failure mechanism was more or less same as was observed in fine grained cement (average radius of 2.75e-5 m).

In the one ball rotation mode, the contribution of both shear and tensile forces was observed to be similar to that of fine grained cement CBMs. However, both tensile (Peak X forces) and shear (Peak Y forces) strengths were found to decrease with the increase of particle size (Figure 7-17). In rotation mode, particle size was also observed to influence the resolution of the failure surface. However, the trend of the failures is the same as was observed in fine grained cement (average radius of 2.75e-5 m).

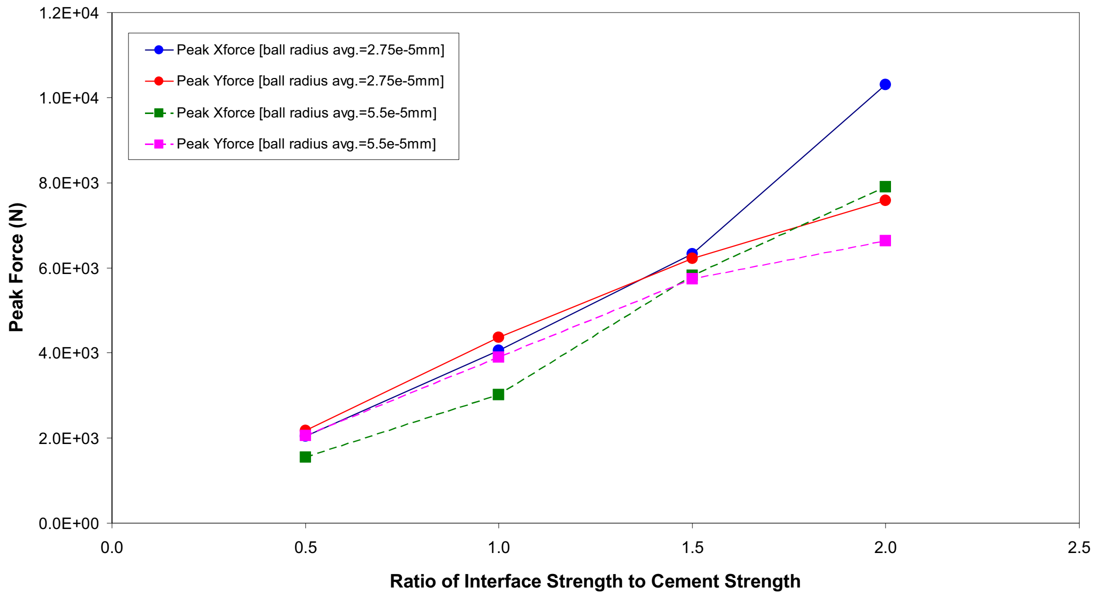

Figure 7-17: Particle size sensitivity in one ball rotation mode; peak X and Y forces at interface to cement strength ratios of 0.5 to 2.0 for particle radii (mean) 2.75e5 and 5.5e-5 m.

7.3.7.3 Stiffness of the Particles

A sensitivity study of the particle materials was conducted, keeping the cement properties constant. A two-ball test was previously conducted using steel particles with high elastic parameters. However, instead of steel balls, granitic and sandstone particles were used to record the mechanical response of the CBM in tension, shear and rotation modes of deformation. The properties of the granite and sandstone particles used in the sensitivity study are summarised in Table 7-4.

The CBM with granitic and sandstone particles was tested for various interface to cement strength ratio; from 0.25 to 2.0. The peak strengths (Peak X and Y forces) of CBM versus the interface to strength ratios are shown as Figure 7-18, Figure 7-19, Figure 7-20 and Figure 7-21 in tension, shear, one ball rotation and two ball rotation modes respectively. The peak strengths of the CBM with steel particles are also plotted in order to compare them with the granite and sandstone particles.

Table 7-4: Summary of the particle's material and their properties used in the sensitivity study.

Particle materials and parameters				
Parameters		Steel	Granite	Sandstone
Shear modulus (GPa)	G	74.5	30	13
Young's modulus (GPa)	E	200	73	33
Poisson's ratio	ν	0.313	0.21	0.25
Density (Kg/m^3)	ρ	7800	2600	2300

In tension mode (Figure 7-18), the model with granite and sandstone particles generally showed an increase in the tensile strength (Peak X forces) with respect to the steel particles. Similarly, in shear mode (Figure 7-19), an increase in shear strength (Peak Y forces) was also noted with a decrease in the stiffness of the particles.

The same increasing trend was observed in the peak strengths with the decrease in the stiffness of the particles in both one ball (Figure 7-20) and two ball rotation (Figure 7-21) modes.

On the basis of these results, it may be concluded that the peak strength of a CBM generally increases with the decrease in the stiffness of the particles in all modes of deformation. No significant changes in the failure mechanisms of the CBM with granitic or sandstone particles were observed compared to that of steel particles. The failure mechanisms of granitic particles and sandstone particles in tension, shear and rotation modes are attached in Appendix C.

The elastic responses of the CBM with granite and sandstone particles were determined in tension and shear modes of deformation and compared with the corresponding responses of the CBM with steel particles. The determined normal (tensile) and shear stiffnesses were plotted against the Young's modulii ratio of cement (E_{cem}) to particle (E_{part}), and are shown in Figure 7-22.

The plot shows that both the normal and shear stiffnesses of the bond model decreases with an increase in modulii ratio (E_{cem} / E_{part}) or with a decrease in particle stiffness.

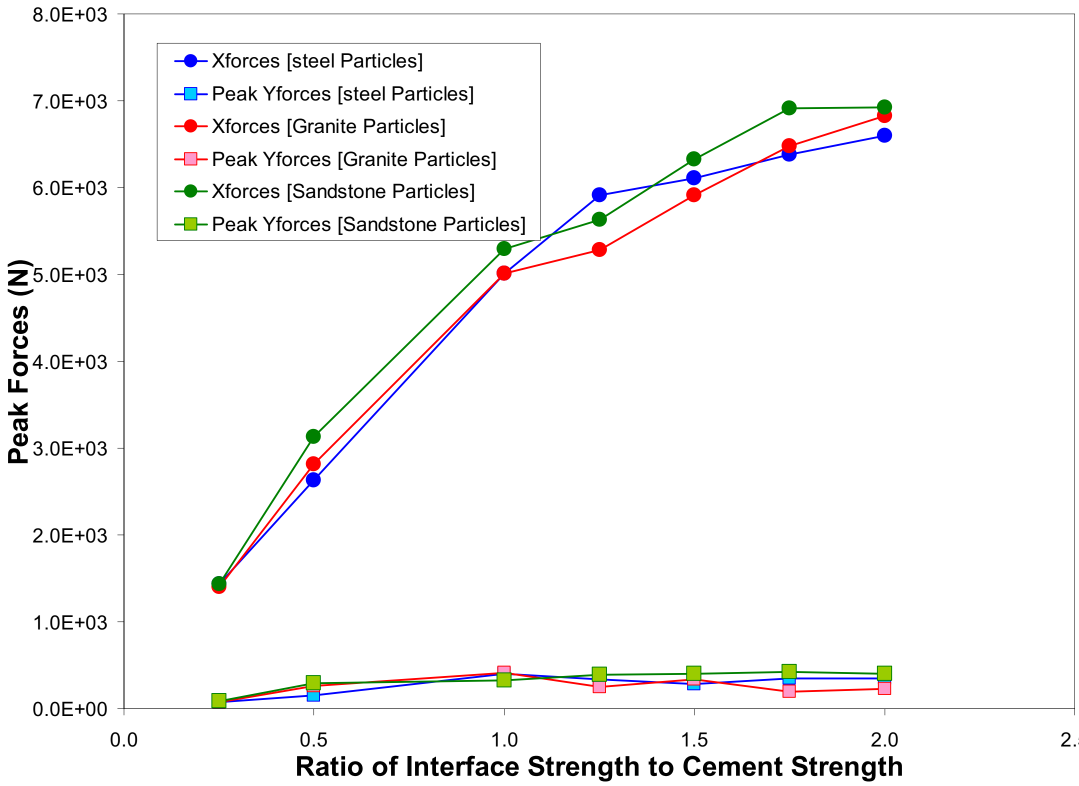

Figure 7-18: Sensitivity of particle material in tension mode; peak X and Y forces for steel, granite and sandstone particles at interface to cement strength ratio of 0.25 to 2.0.

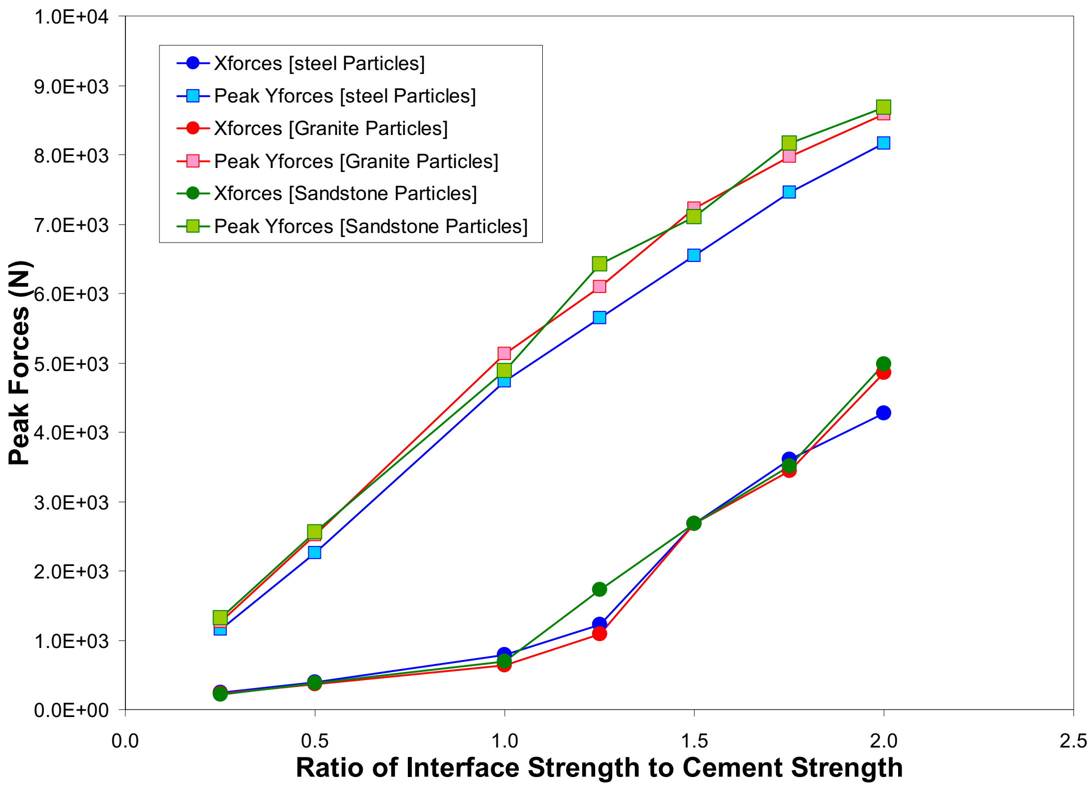

Figure 7-19: Sensitivity of particle material in shear mode; peak X and Y forces for steel, granite and sandstone particles at interface to cement strength ratio of 0.25 to 2.0.

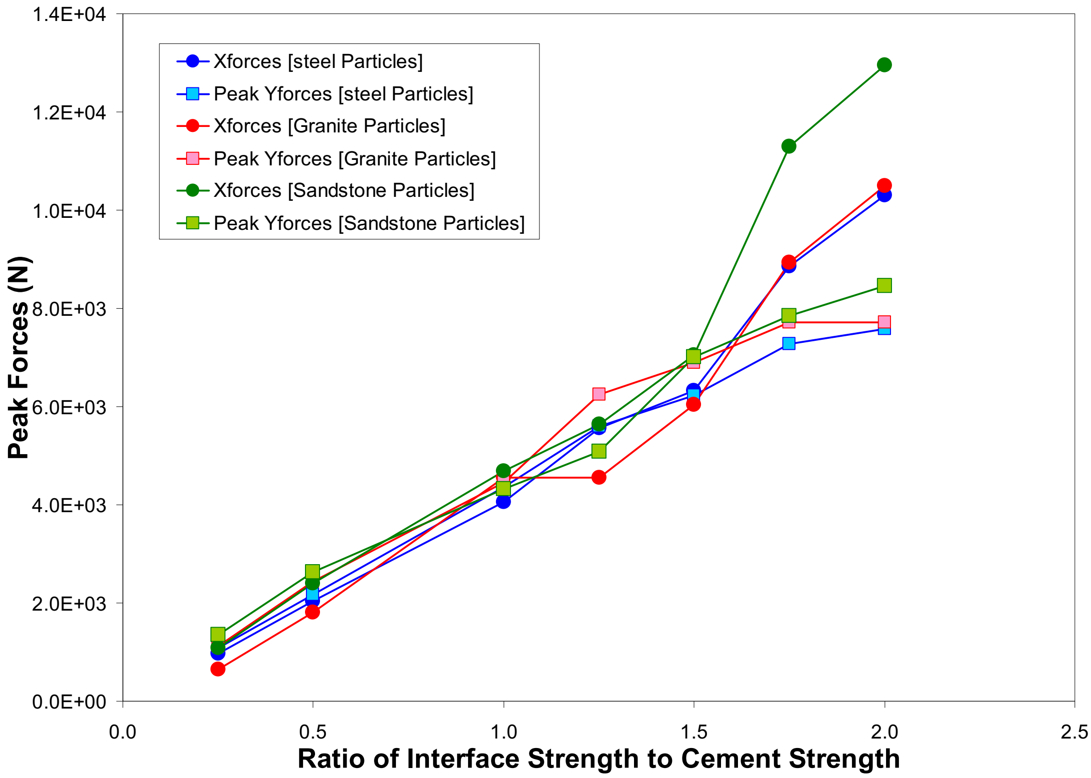

Figure 7-20: Sensitivity of particle material in one ball rotation; peak X and Y forces for steel, granite and sandstone particles at interface to cement strength ratio of 0.25 to 2.0.

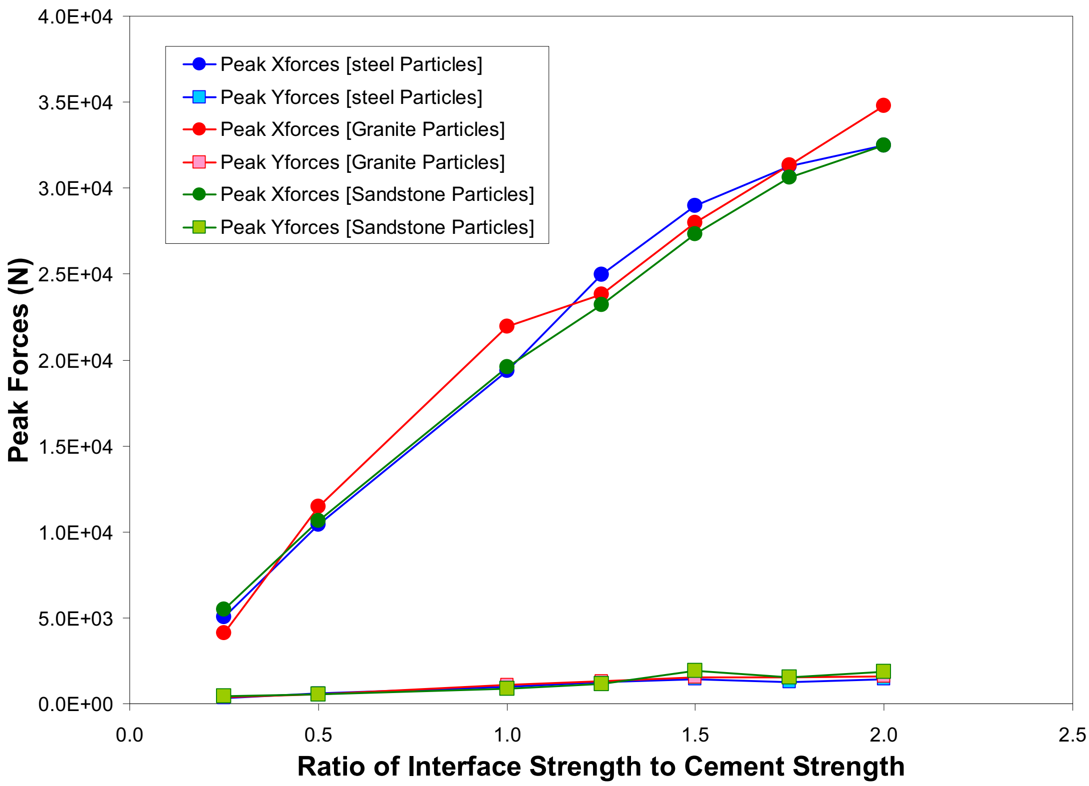

Figure 7-21: Sensitivity of particle material in two ball rotation mode; peak X and Y forces for steel, granite and sandstone particles at interface to cement strength ratio of 0.25 to 2.0.

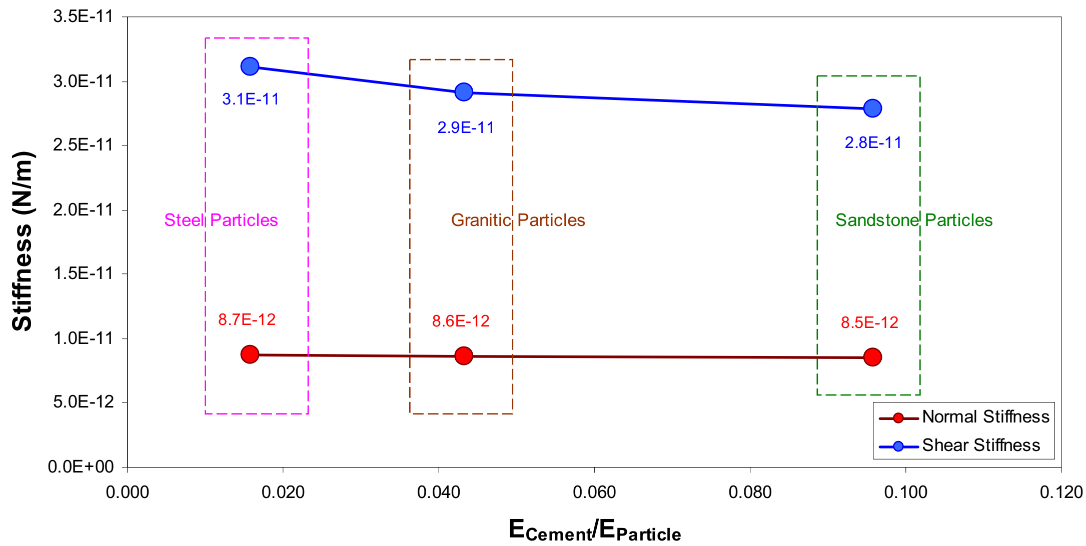

Figure 7-22: A comparison of the normal and shear stiffnesses of the CBM in tension and shear mode for steel particles, granitic particles and sandstone particles. The Young's modulii of steel, granite and sandstone particles, and cement matrix (from calibration) are 200, 73, 33 and 3.16 GPa respectively.

7.4 Three-Ball Test

A three-ball test was devised to observe the role of a piece of interparticle cement placed in between the contacting particles. The objective of the test was to investigate the presence of the cement in controlling the mechanics of the bond and generalise these findings to understand the macroscopic behaviour of an assembly having interparticle cement among the particles, as in the synthetic conglomerate (discussed in Chapter 3). The methodology adopted to investigate the role of the cement wedge was comprised of two three-ball tests with and without a cement wedge, together with a comparison of their mechanical responses. The methodology is shown in Figure 7-23. It was anticipated that the differences in failure mechanism in Brazilian test of the synthetic and numerical conglomerates could be clearly understood by this simple three-ball test.

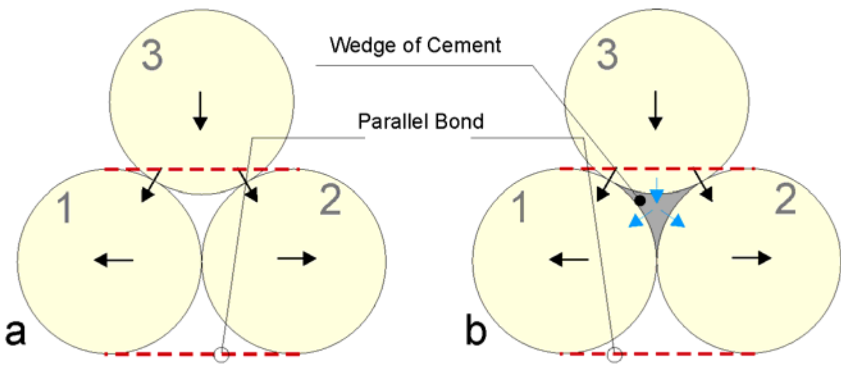

Figure 7-23: Conceptual illustration of the three-ball test; a) balls 1 and 2 bonded with a parallel bond and ball 3 (top ball) is exerting force through the particle contacts to break the parallel bond in tension, b) presence of the cement wedge among the three balls is also contributing, along with particle contact forces, to break the bond.

7.4.1 Test Configuration

The testing configuration consisted of three balls in contact with each other, as shown in Figure 7-23. Balls 1 and 2 were placed horizontally on a frictionless base, while ball 3 rested unconstrained on top. A parallel bond was installed between balls 1 and 2 with the properties of cement paste (from Chapter 4). A cement wedge consisting of cement particles was created among the three balls, using calibrated properties of cement (as in Table 7-1). The cement particles were bonded with parallel bonds as per cement calibrated properties. However, the interface between the cement wedge and the particles was frictional, with cohesion set to zero.

Two modelling permutations were planned in the three ball testing. The first model with a cement wedge (Model-1), as shown in Figure 7-23b and the second model (Model-2) without a cement wedge, as shown in Figure 7-23a.

In the both models, the top ball (ball 3) was given a constant downward (in z direction) velocity and the axial force on ball 3 was monitored as an unbalance force in axial direction. This force was recorded as a history variable up to the failure of the parallel bond (in tension) between the two horizontally lying balls, 1 and 2.

In both the micro models, rotations of balls 1 and 2 were also monitored as history variables. The Fish algorithms written for three-ball testing are attached in Appendix B.

7.4.2 Discussion of Test Results

The out of balance axial forces on the top ball in both Model-1 (with a cement wedge) and Model-2 (without a cement wedge) were plotted against the vertical displacement of the top ball (Figure 7-25a). Similarly, the rotations of ball 1 and ball 2 were also plotted against the vertical displacement of the top ball (Figure 7-25b).

In Model-1, the peak out of balance axial force was recorded as 1.42e4 N, while in Model-2, it was 1.80e4 N (Figure 7-25a). The comparison of the peak axial forces experience by the top ball in both models shows that the model with a cement wedge has approximately 21% less peak force than that of the model without a cement wedge. The only difference between two models was the presence of the cement wedge which caused the breaking of the parallel bond at low axial forces and hence yielded the low tensile strength of the parallel bond. This means that the presence of the cement wedge among the particles also contributes to the transmission of forces (Figure 7-24b), although this transmission is low compared to the transmission of forces through the particle contacts.

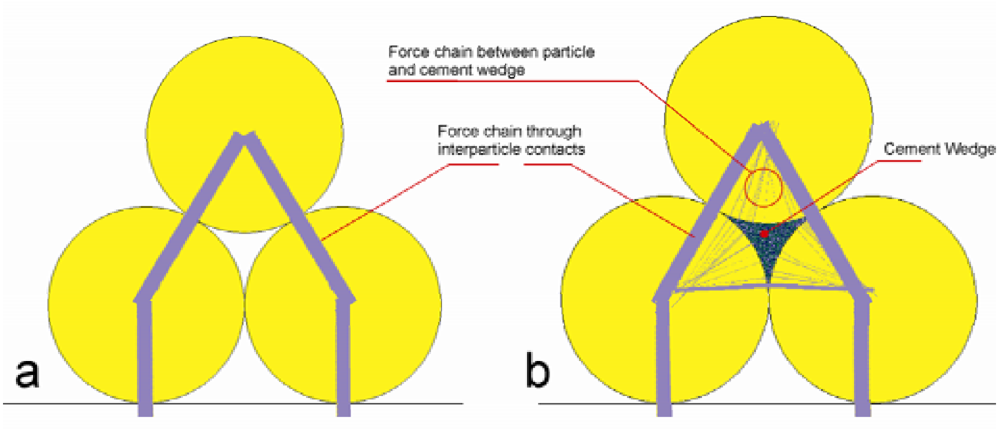

Figure 7-24: Illustration of contact forces during the three-ball test; a) Force chain through interparticle contact (Model-2) and, b) Force chain through interparticle contacts and through the cement wedge (Model-1).

This transmission of forces by the cement wedge affecting the strength of the parallel bond was named the *Cement Wedge Effect*. To quantify this effect, the following relation was proposed;

$$CWE = \frac{\left(f^{peak} - f_{cw}^{peak}\right)}{f^{peak}} * 100 \qquad (7\text{-}1)$$

Where

CWE - cement wedge effect in percent.

f^{peak} - peak axial force in Model-2 (with out cement wedge)

f_{cw}^{peak} - peak axial force in Model-1 (with cement wedge), and

$$f_{cw}^{Peak} = f^{peak} - f_{cw} \qquad (7\text{-}2)$$

Where

f_{cw} - force transmitted through the cement wedge.

The graphical representation of these forces is shown in Figure 7-26.

Thus the CWE can be defined as *the percent ratio of the difference of the peak strength of the models with and without the cement wedge to the peak strength of the model without the cement wedge*.

The CWE calculated using Equation (7-1) was 21%. This is the difference between the peak forces required to break the same bond with and without cement wedge. This suggests that the presence of the cement wedge increases the applied stress on the parallel bond (in a three ball test) acting as a stress raiser.

It should be noted that the particles or balls simulated in the test are of steel having very high stiffness in comparison to cement wedge material.

In Figure 7-25a, the response of Model-1 (with the cement wedge) was found slightly stiffer than that of Model-2 (without the cement wedge). This increase in stiffness could be attributed to the cement's stiffness. This effect was further investigated in sensitivity studies by using low stiffness particles - granite and sandstone. The results of the sensitivity studies are discussed in the following section.

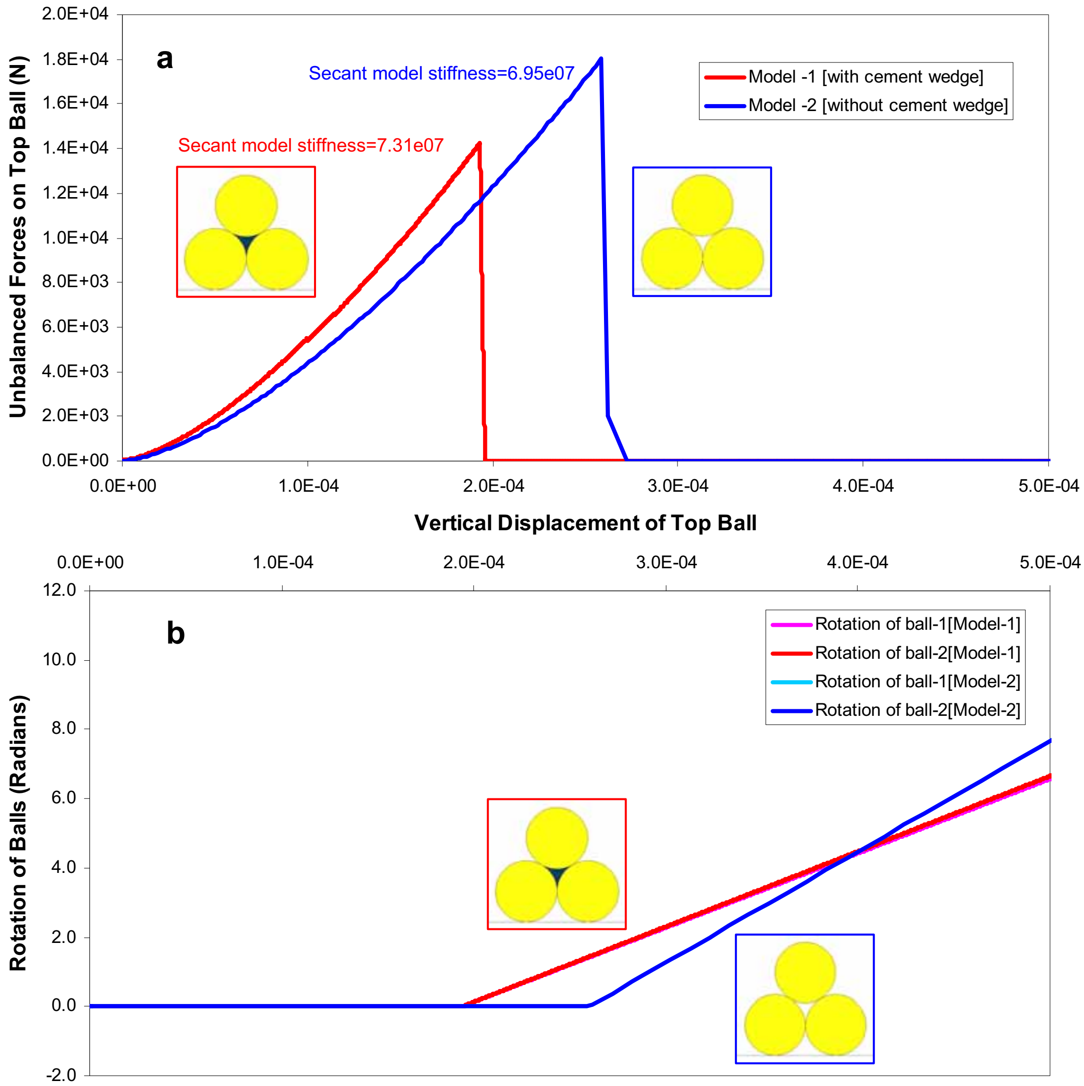

Figure 7-25: Plots of: a) axial forces experienced by ball 3 (top ball), and b) rotations of balls 1 and 2 in model-1 (with the cement wedge) and model-2 (without the cement wedge) against the axial displacement of ball 3.

Another significant effect relating to the cement wedge was observed when comparing the rotation of the horizontal balls (ball 1 & 2) of Model-1 and Model-2. The plots (Figure 7-25b) show that the post failure magnitude of rotation of both horizontal balls (in contact with the cement wedge) was influenced by the presence of the cement wedge. The balls with the cement wedge (Model-1) showed less rotation compared to the balls without the cement wedge (Model-2). Restricted particle rotation (induced by the presence of interparticle cement as in synthetic conglomerates) results in more dilation along the shearing surfaces compared to unrestricted rotation (as in numerical conglomerates with parallel bonds). This finding helps to explain the differences observed in the shear box tests on synthetic and numerical conglomerates (Chapter 5). Numerical conglomerates showed less dilation compared to synthetic conglomerates due to unrestricted particle rotation after bond breakage, except the specified interparticle friction which acts only at the particle contact points. However, the physical tests on the synthetic conglomerate showed higher dilation because of the presence of the cement material even after micro cracking along the particle boundaries and through the cement.

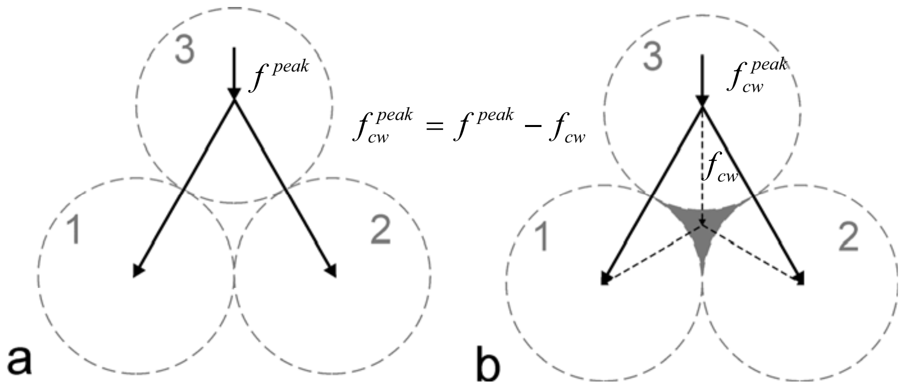

Figure 7-26: Illustration of the forces in the three ball test; a) peak axial force (f^{peak}) required (on ball 3) to break the bond in tension between the underlying balls (Model-2), b) Peak axial force (f_{cw}^{peak}) required (on ball 3) to break the bond in tension between the underlying balls with the cement wedge among the three balls (Model-1). The cement wedge is also contributing force (f_{cw}), along with particle contact forces, in breaking the bond.

7.4.3 Sensitivity of the Particles' Material

The sensitivity study was aimed to examine the cement wedge effect with respect to a change of particles' material. Two types of particle materials were considered: granite and sandstone. The properties of both materials (given in Table 7-4) were used to define the stiffness of the particles in the three-ball test. The tests were conducted on particles with a cement wedge (Model-1) and without a cement wedge (Model-2). Axial out of balance forces experienced by the top ball were monitored to break the bond between the underlying balls. The rotations of the underlying balls were monitored in each test. The monitored forces and rotations were plotted against the vertical displacement of the top ball and are shown in Figure 7-27 for granite particles and Figure 7-28 for sandstone particles.

The results of the models with and with out the cement wedge for granitic and sandstone particles were found to be similar to those of the models with steel particles. The peak axial forces experienced by the top ball in both models with and without the cement wedge, were observed to decrease with the decrease in the stiffness of the particles (Figure 7-27a & Figure 7-28a). Similarly, a decreasing trend was also observed in the stiffnesses of the models with the decrease in the stiffness of the particles.

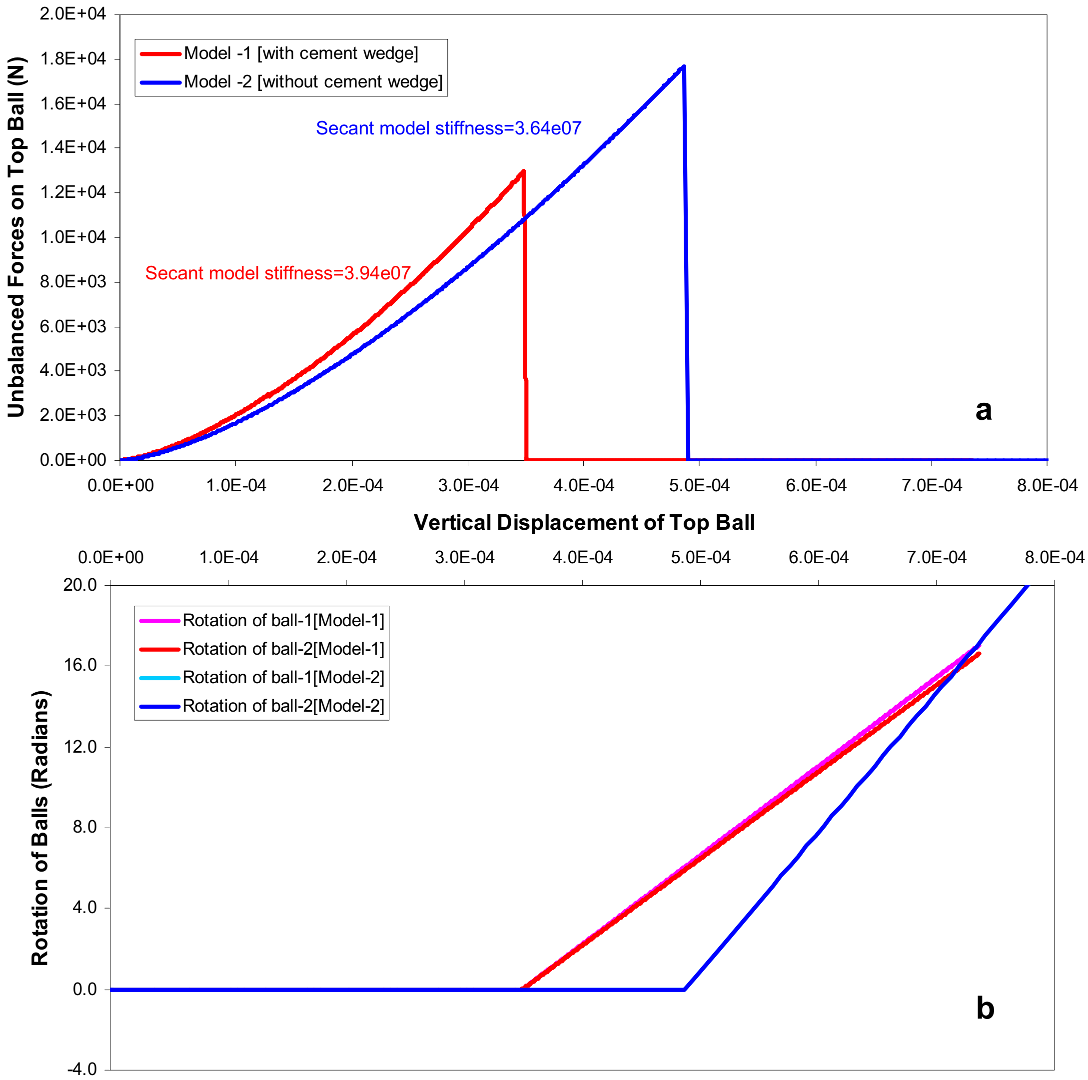

Figure 7-27: Plots of: a) axial forces experienced by ball 3 (top ball), and b) rotations of balls 1 and 2 in model-1 (with the cement wedge) and model-2 (without the cement wedge) against the axial displacement of ball 3. the balls' material in both models is granite.

The CWE was found to increase from 21%, corresponding to the steel particles to 27% for the granite particles and 30% for the sandstone particles. This increasing trend suggests that the reduction in the contrast of the stiffnesses between the particles and cement wedge increases the cement wedge effect, that is, the difference of the peak forces. The contrast of the stiffness was measured as ratio of Young's modulus of cement to Young's modulus of the particle (E_{cem}/ E_{part}). Young's modulus of the cement was taken as 3.16 GPa from the cement calibration (Table

7-1), while Young's modulii of steel, granite and sandstone particles were taken as 200 GPa, 73 GPa and 33 GPa respectively (Table 7-4).

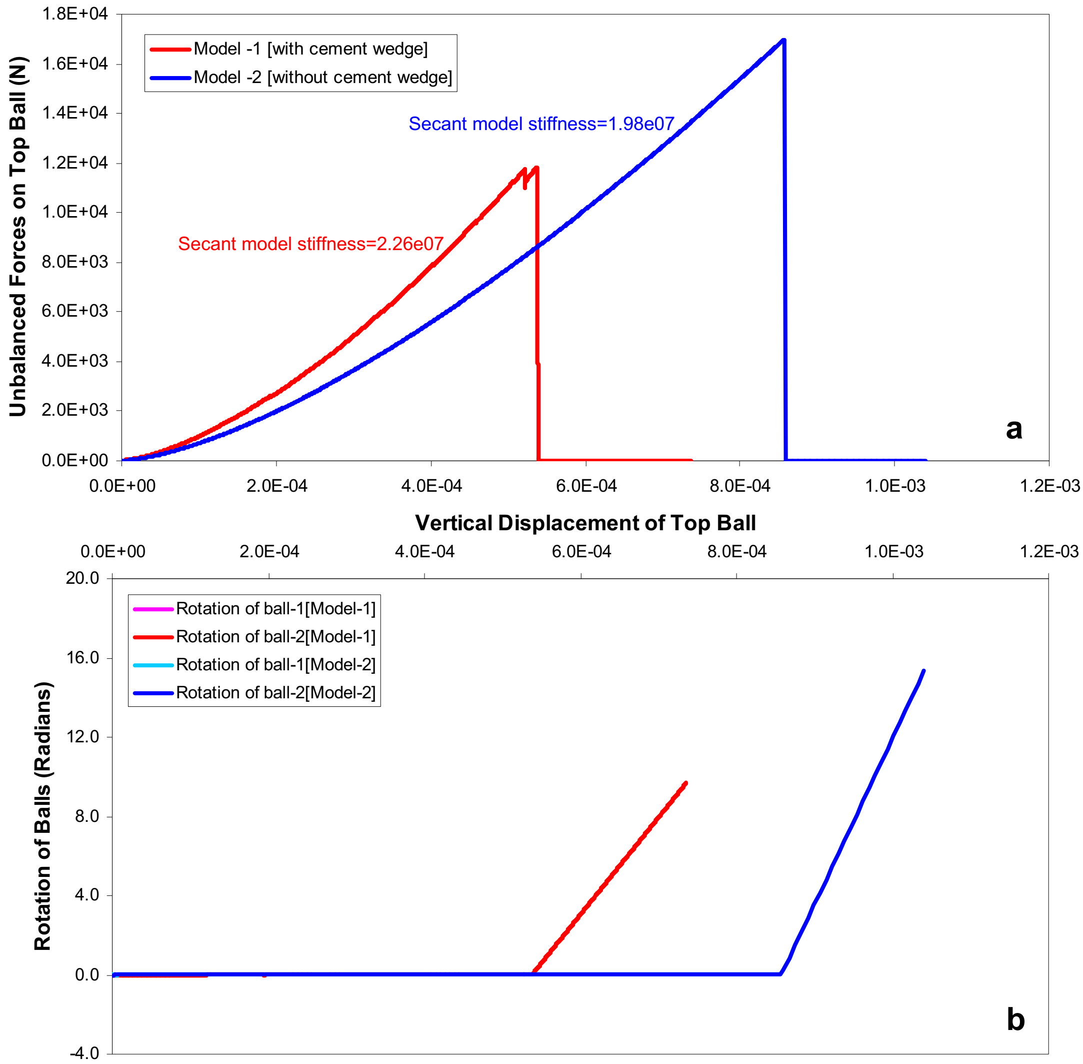

Figure 7-28: Plots of: a) axial forces experienced by ball 3 (top ball), and b) rotations of balls 1 and 2 in model-1 (with the cement wedge) and model-2 (without the cement wedge) against axial displacement of ball 3. The balls' material in both models is sandstone.

The variation of the peak forces obtained from Figure 7-25a, Figure 7-27a and Figure 7-28a and corresponding CWE values are plotted against the Young's modulus ratio of the cement to the particle in Figure 7-29. Similarly, the variation of the stiffnesses (secant) of the models was also determined from Figure 7-25a, Figure 7-27a and Figure 7-28a, and plotted against the cement to particle modulii ratio (Figure 7-30).

It is interesting to note that the difference of the stiffnesses induced by the cement wedge remains insensitive towards the decrease of particle stiffnesses (Figure 7-30) and this may be associated with the stiffness of the cement wedge only. Hence, the granular assemblies with the same interparticle cement matrix will show the same difference of stiffnesses with different particle stiffnesses.

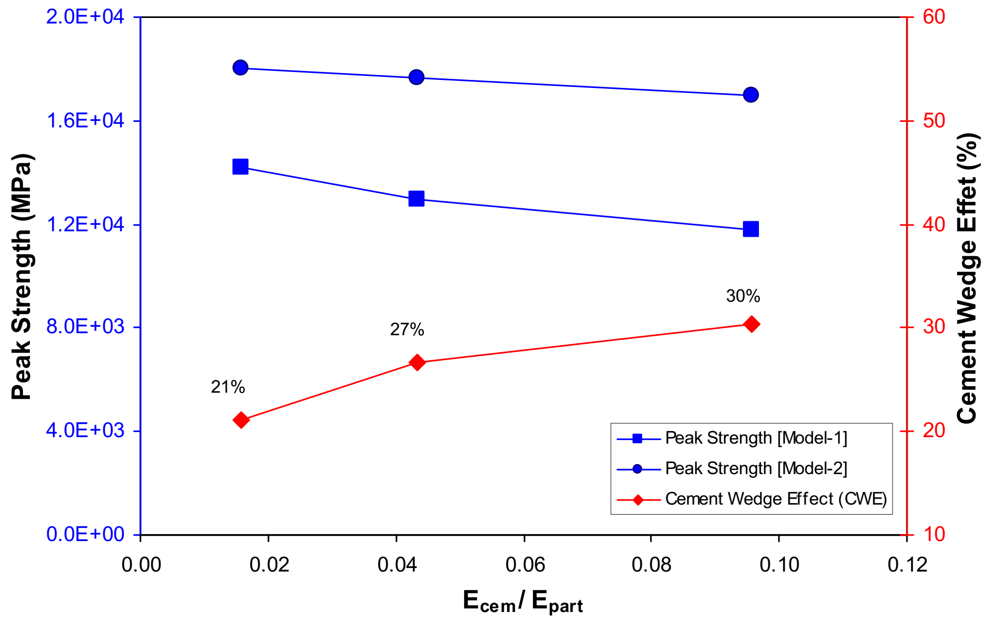

Figure 7-29: Peak strengths of model-1 (with the cement wedge) and model-2 (without the cement wedge) and corresponding cement wedge effect (*CWE*) values plotted against the ratio of Young's modulii of the cement and particle materials; steel, granite and sandstone.

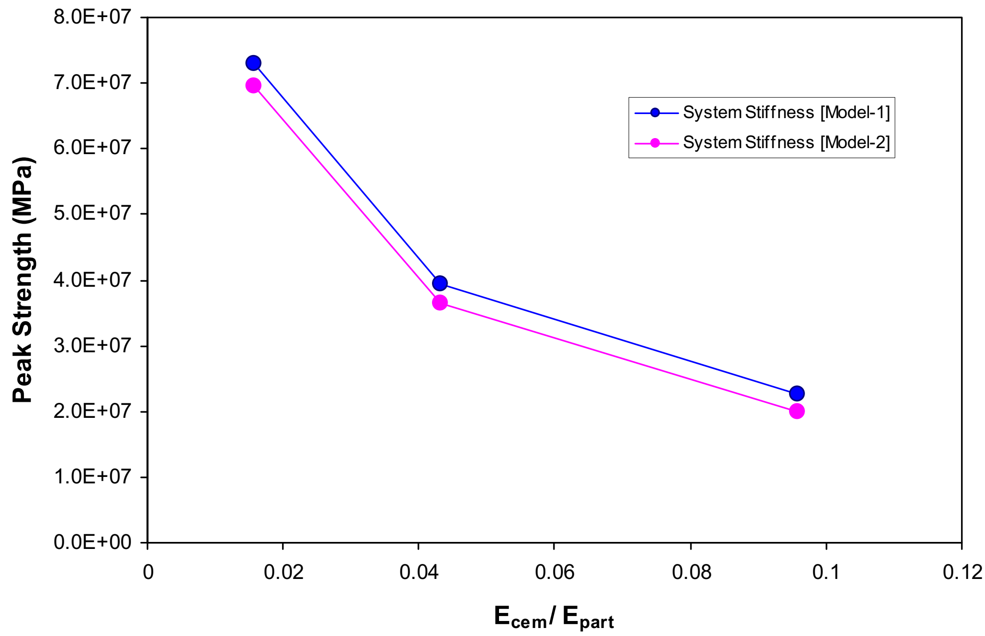

Figure 7-30: Stiffness of model-1 (with the cement wedge) and model-2 (without the cement wedge) plotted against the ratio of Young's modulii of cement and particle materials; steel, granite and sandstone.

7.5 Summary and Conclusions

An investigation was conducted to explore the significance of interstitial cement on the mechanical response of synthetic and numerical conglomerates at a particle scale. On a micro scale, synthetic conglomerate was composed of particles bonded with interstitial cement (Portland cement paste), while the numerical conglomerate was comprised of particles bonded with a parallel bond so that the properties (strengths and stiffness) of the parallel bond were the same as those of the interstices cement in the synthetic conglomerate. Any difference in macroscopic responses of both conglomerates, necessitates the calibration of a parallel bond in relation to the physical interparticle cement. Therefore, the objectives of this investigation were to determine the extent to which strength and stiffness of the interparticle cement could be gained by a parallel bond in a cemented contact, and to analyse the significance of the presence of the interparticle cement among the bonded or unbonded particle contacts in controlling the overall mechanical response of a conglomerate assembly.

In order to meet these objectives, the particle-cement interaction of synthetic conglomerates was studied numerically by simulating interparticle cement as an aggregate of micro particles. However, the simulation of parallel bond representing the micro structure of numerical conglomerate was quite easy and straightforward at particle scale. Hence, the investigation aimed to examine the mechanical response of the particles bonded with cement particles with reference to the simulation of a parallel bond so that the parallel bond simulates the interparticle cement. It was also planned to investigate the impact of the deposited interstices cement on the mechanical response of the synthetic conglomerate in relation to the numerical conglomerate.

Two types of tests were planned: a two-ball test and a three-ball test. In the two-ball test, two models, the Cement Bond Model (CBM) and the Parallel Bond Model (PBM) were tested in tension, shear and rotation modes. The CBM has two particles bonded to each other with the interparticle cement simulated by micro particles. The micro mechanical parameters of the interparticle cement were obtained by reproducing the macroscopic response of Portland cement paste in the calibration process. The PBM consists of two particles glued together with a parallel bond with the same properties as that of the cement paste.

The sensitivity of the various parameters, such as the particle-cement interface properties, the size of the particle cement and the type of particle material were examined in the CBM together with its comparison to the corresponding PBM. Firstly, a significant difference in the mechanical responses of the CBM and PBM was noted in all modes of deformation, suggesting a poor correlation between the two models. However, the peak strengths of the CBM corresponding to high interface to cement strength ratios, 1.5~1.75 were found to agree with the corresponding PBM result at an interface to cement strength ratio of 1.0. Further, the response of the CBM was found to be much stiffer than that of PBM in all modes of deformation. This contrast was considered to be related to the use of parallel bonds in simulating the cement matrix. A variation of the interface to cement strength ratio in the CBM produced the similar failure mechanisms as were observed in synthetic conglomerates, that is, at lower interface to cement strength ratio, failure occurs along the particle-cement interface while at high ratio, sample splits through the cement. The synthetic conglomerate samples generally failed along the particle-cement interface, suggesting low values of the interface strength than the cement strength. However, a few particles were also observed to fail through the cement. Therefore, the interface strength in the synthetic conglomerate varies in relation to the cement strength. This observation is consistent with the previous findings on natural conglomerates by Savanick and Johnson (1974).

In the one ball rotation mode, the peak strength of the PBM was found to be close to the tensile strength (tension mode) of the PBM, however, it should be close to shear strength (in shear mode) as the bond breaks in shear. The peak strengths (tensile and shear) of the CBM were 50~60% as that of the PBM which was close to the shear strength in rotation mode. The stiffness of the PBM was 5~7 times the stiffnesses of the CBM indicating a normal to shear stiffness ratio of 0.66 in the CBM. This was in contrast with the stiffness ratio of the CBM determined in the tension and shear modes, which was approximately 25. This observation leads us to suggest that the stiffnesses are not independent variables but also depend on the mode of deformation. Alone, shear or tensile stiffness is not enough to depict the stiffness of a bonded contact in the rotation mode of deformation. This is important in modelling the response of conglomerates comprised of macro particles (clasts) embedded in a cement matrix. However, this may not be applicable to the simulation of brittle or fine grained rocks which are normally modelled by a densely packed bonded assembly of particles with no dominant structure (Potyondy & Cundall 2004).

In the two ball rotation mode, the CBM showed mechanisms of cement crushing near the ball contacts which are consistent with, and help explain, the physical tests on synthetic conglomerates presented in Chapter 3.

In the three-ball testing, the main objective was to investigate the sensitivity of the interparticle cement on the mechanical response of the models. The three-ball test consisted of three balls, two of which were bonded with a pralllel bond and lay horizontally, with the third ball lying over the top so that a wedge shaped void was present among the three contacting balls. This void was filled with cement particles (Model-1) and particle-cement interface strengths were set to zero; that is, there was no bond between the cement and the particles. The second model (Model-2) was constructed with a parallel bond only without a cement wedge. Both models were tested by giving a constant downward velocity to the top ball to break the parallel bond between the underlying particles. It was found that Model-1 (with the cement wedge) and Model-2 (without the cement wedge) showed significant differences in the mechanical responses. The mechanical response of the three ball test was analysed in terms of peak axial force which was defined as "the force experienced by top ball in vertical direction to break the bond in tension between the underlying balls". The peak axial force in Model-1 (with the cement wedge) was found to be lower than the corresponding force in Model-2 (without the cement wedge). This difference in peak forces was named the "Cement Wedge Effect" (CWE) and was defined as a percent ratio of the difference of the peak forces of both models (with and without cement wedge) to the peak force of the model without cement wedge. The elastic response of Model-1 was found to be slightly stiffer than Model-2 due to the contribution of the stiffness of the cement wedge. An important effect of the cement wedge was the restriction on the ball rotation after bond breakage. This restricted rotation causes an increase in the dilation in the granular assembly as was observed in the actual physical shear box tests on the synthetic conglomerate, shown in Chapter 3. By contrast, granular assemblies with parallel bonds showed less dilation induced by the excessive rotation of the particles as was observed in shear box testing on numerical conglomerates, shown in Chapter 4.

A sensitivity study was conducted to explore the significance of the Cement Wedge Effect. The stiffnesses of the particles were varied according to the particle materials (i.e., from steel to granite and sandstone) in order to examine the variation of the CWE. It was observed that the CWE increased with the decrease of the particle-cement stiffnesses contrast induced by the increase in the E_{cem}/ E_{part} ratio. However, interestingly, the stiffness contrast of Model-1 and Model-2 was found consistent with the change of particle stiffnesses (i.e., Young's modulus). It is therefore concluded that the stiffness contrast of both models is primarily controlled by the stiffness of the cement wedge and is largely independent of particle stiffness. However, the sensitivity of cement stiffness on the CWE was not explored here and is left to future studies.

Summary, Conclusions and Recommendations for Future Research

8.1 Objectives and Hypothesis

The present research was based on the premise that by using an *idealised*[9] synthetic conglomerate (with spherical and uniformly sized clasts, and homogeneous cement matrix) and DEM simulations, the role of the cement matrix in controlling the strength, deformation and the failure mechanisms of natural clast supported conglomerates can be understood. An added premise was to use the DEM simulations in investigating the sensitivity of an idealised conglomerate for the clast size and size distribution (packing), the strength and stiffness of the clasts and cement matrix, and the clast-cement interface properties in controlling mechanical behaviour.

The broad aim was to use physical and numerical ISRM tests to explore the factors controlling the failure mechanisms, and the intact strength and deformation properties of clast-supported conglomerates. In addition, the extension of this work is to investigate the impact of clast and cement properties of commonly occurring natural conglomerates.

The objectives set to obtain the research aim are given below:

1. To prepare and test an idealised synthetic conglomerate (by physical modelling) comprised of spherical uniformly sized clasts having sufficient *similitude credibility* with a natural conglomerate in ISRM recommended laboratory tests.
2. Use DEM simulation to prepare and test an equivalent numerical conglomerate similar to the synthetic conglomerate.

3. To determine correlations between the macroscopic responses of both the synthetic and numerical conglomerates to validate the response of DEM simulations.
4. To investigate the sensitivity of the clasts and matrix properties on the mechanical behaviour of commonly occurring natural conglomerates in DEM simulation.
5. To conduct a micro-mechanical investigation to explore the clast-cement interaction and the role of the cement matrix on the macroscopic response in conglomerate rocks.

In this chapter, the outcome of the present research corresponding to the research aims, together with a brief discussion of their applications in modelling the behaviour of conglomeratic rocks are given. The key findings are framed as the conclusions of the present research. Subsequently, directions for future research are suggested.

8.2 Summary and Discussions

The present research was focused on investigating the mechanics of clast supported idealised conglomerates having spherical clasts. Spherical casts were selected to eliminate the variation induced by the clast shape. Two approaches were adopted in this regard: Physical modelling and numerical simulation using PFC3D. The results of both approaches were compared to validate the response of numerical simulations with physical modelling. Using DEM simulations, the mechanical response of an idealised conglomerate was investigated for various factors and the particle-cement interaction was explored in a micro-mechanical investigation. A summary and a discussion of the key observations in these investigations are brought forward from Chapters 3, 4, 5, 6, and 7 and presented in the following sections for completeness.

8.2.1 Physical Modelling and Numerical Simulation

Physical modelling involved the preparation and testing of synthetic conglomerates comprising uniformly sized steel balls as clasts and Portland cement as a cement matrix. The synthetic conglomerate specimens were tested in compression (uniaxial and triaxial), indirect tension (Brazilian tensile) and direct shear (shear box) testing. Uniaxial testing was monitored for acoustic emissions to characterise progressive damage in the specimens. The mechanical response of the idealised synthetic conglomerate showed sufficient credibility of behavioural similitude with natural conglomerates. Hoek-Brown criterion was observed more suitable to predict the strength of the synthetic conglomerate than Mohr-Coulomb criterion.

DEM simulations (using PFC3D) were performed to create and test numerical conglomerate specimens in the same laboratory tests. The properties of the steel balls and Portland cement were used to construct equivalent numerical conglomerates. To create interparticle cement, parallel bonds were installed and the micro parameters for parallel bonds were measured in physical laboratory testing on cement paste specimens. The particles (clasts) of numerical conglomerates were treated as elastic bodies with Hertzian contacts. A high interparticle friction was adopted to match the bulk friction of the numerical conglomerate with that of the synthetic conglomerate. In numerical conglomerates, Mohr-Coulomb criterion was observed more suitable than the Hoek-Brown criterion in predicting their mechanical responses.

The mechanical responses of the numerical conglomerate were compared to the corresponding responses of the synthetic conglomerate to validate the numerical simulations. The following observations were made from these comparisons:

In uniaxial and triaxial tests, peak strengths of numerical conglomerates were found to have a good agreement with that of the synthetic conglomerates. Similarly, the progressive damage of the numerical conglomerates (in uniaxial testing) also had good agreement with the synthetic conglomerates. In uniaxial testing, the failure mechanism of the numerical conglomerate was found to be tensile or axial splitting, which was consistent with that of the synthetic conglomerate specimens. However, in the numerical conglomerates, the failure mechanisms in uniaxial and triaxial testing were observed to vary with the confining pressures. In uniaxial testing, samples failed in axial splitting with a sudden stress-drop indicating a brittle failure mechanism, while a transition from axial splitting to strain softening was observed in triaxial testing with an increase in the confining pressure. In triaxial testing, random distribution of cracks was noted with no well-defined shear surface though the specimen. This was considered to be the effect of high dilation because of the particles along the possible shear. At a micro level, the mode of failure gradually became shear with increasing confining pressure.

In uniaxial and triaxial testing, the elastic response of the numerical conglomerate was stiffer than that of the synthetic conglomerate. In the numerical conglomerate, the shear to normal stiffness ratio of 1.0 was assumed for interparticle cement as no experimental mean was available to find this ratio. However, a sensitivity study was conducted to examine the response of the numerical conglomerate with varying stiffness ratios. It was observed that both the uniaxial strength and Young's modulus increase and Poisson's ratio decreases with the increase of the shear to normal stiffness ratio and vice versa. At the moment, understanding about the physical and numerical meanings of the input parameters stands on existing knowledge which is perhaps not sufficient enough to address this issue. Therefore, it is anticipated that much more detailed and quantitative work is required in future to validate the elastic parameters of the numerical conglomerates.

The post peak behaviour of numerical conglomerates was found brittle in uniaxial testing while the synthetic conglomerates showed ductile behaviour. In triaxial testing, numerical conglomerates showed a strain softening behaviour in contrast to the strain hardening behaviour observed in the synthetic conglomerates. The differences of the post peak behaviours in uniaxial and triaxial testing were attributed mainly to the presence of interparticle cement in synthetic conglomerates which does not exist in numerical conglomerates. In the synthetic conglomerate, interparticle cement results in a complex interaction of ball-ball, ball-cement and cement-cement frictions, and cement crushing, which restricts particle movements and rotation, and makes the overall elastic response strain softening in uniaxial testing and strain hardening in triaxial testing. In the numerical conglomerates, after the failure of parallel bonds (representing the interparticle cement), particles are free to move and rotate (as per interparticle friction) producing low interlocking, and consequently, low dilation. This was in contrast to synthetic conglomerates in which restricted particle rotation, even after failure, produced high dilation. Hence, the post peak effect of interparticle cement in the synthetic conglomerate can not be gained using a parallel bond model. It is anticipated that in the simulation of conglomeratic rocks, this problem can be solved either by revising the interparticle contact laws and/ or bonding models, or by replacing the cement (parallel bonds) with an aggregate of fine particles. However, such models will involve greater computation cost than is current available on normal desktop computers.

The sensitivity of the peak strength and deformation with the particle size did not show any correspondence between the synthetic and numerical conglomerates. The uniaxial compressive strength increases in the numerical conglomerate and decreases in the synthetic conglomerate as particle size is increased. However, more work is required to precisely account for the effect of particle size on assembly behaviour.

The average tensile strength of the numerical conglomerate was found to fall within the range of the tensile strength of the synthetic conglomerate. In Brazilian tests, the tensile strength of the numerical simulation depends upon the loading condition and increases with loading rate. The tensile strength was found within the variation range of physical test results. However, well developed distinct cracks through the samples were not observed. The failure mechanism in the Brazilian test seems to be strongly influenced by the loading fibre through the particles' contacts and interparticle cement. After breakage of the parallel bond near high stressed regions (e.g., near the top and bottom platens), forces were observed to redistribute through the interparticle contacts (as interparticle cement was not present) which induced damage in random directions rather than concentrating along a definite failure surface. Further, the load was transferred through the platens and boundary particles which were in contact with the platens. It was hypothesised that the boundary particles in contact with platens experience high forces while others which have no direct contact with platens experience low forces. This non-uniform load distribution, transferred to the specimen, may not induce a framework of tensile forces leading to a discrete crack through the specimen. This hypothesis was also supported by the observed failure mechanism of the numerical conglomerate in Brazilian testing at a high displacement rate resulting in a discrete fracture through the specimen. But the use of high platens velocity yielded high values of tensile strength.

In the shear box tests, a good agreement in the results of synthetic and numerical conglomerate was observed in terms of cohesion and angle of friction. However, the vertical dilation in the numerical conglomerate was found lower in comparison to the synthetic conglomerate possibly because of the excessive rotation of unbonded particles along shearing in former, whereas in the later particle rotation is restricted by the cement matrix and a mechanism of cement crushing at high normal loads.

A comparison of synthetic and numerical conglomerates clearly showed that interparticle cement has a significant effect on the macroscopic response, especially deformability and failure mechanism. For synthetic conglomerates, in triaxial and shear box tests, a mechanism of cement crushing was observed, which significantly influenced the pre and post peak responses. However, such a mechanism was not observed and can not be induced, in numerical simulations using a parallel bond even at higher interparticle friction. Therefore, in the numerical conglomerates, high stiffness in the pre peak response was observed, together with the brittle failure in uniaxial testing, and strain softening post peak behaviour in triaxial testing.

8.2.2 Parametric Sensitivity Studies - Idealised Natural Conglomerate

Based on the reasonable agreement found between the mechanical responses of the synthetic and numerical conglomerates, PFC3D was used to investigate the sensitivity of the mechanical behaviour of selected idealised conglomerate with particle size distribution, scaling, particle material and interparticle cementing materials. The dependence of these factors was studied, keeping the all other parameters that could influence the mechanical behaviour constant.

The effect of particle size distribution was studied in relation to uniform particle size distribution. Three particle size distributions were considered with maximum to minimum particle radii ratio (R_{max}/R_{min}) of 1.0, 1.25 and 1.50 at the same porosity. In this study, the peak strengths both in uniaxial and triaxial testing were observed to decrease with the increase of particle radii ratio from 1.0 to 1.5. The Young's modulii were found to decrease, while Poisson's ratio was observed to increase with the increase in the particle ratio from 1.0 to 1.5. The damage in the conglomeratic specimens was also observed to be sensitive to the particle size distribution which was the result of a change in the fibre (contact force chains).

Scaling, or the effect of specimen size, was examined in uniaxial testing in two ways: proportional and non-proportional scaling. In proportional scaling, the whole model, including the specimen size and microstructure (particle size), was varied proportionally, and no significant variation in peak strength was noted with the scaling factor. Only a slight variation for the Young's modulus and Poisson's ratio was noted.

In non-proportional scaling, keeping the particle size the same, specimen sizes were varied and it was noted that both *UCS* and Young's modulus decreased and Poisson's ratio increased with the specimen size. The dimensionless strength variation with the specimen size was observed to be similar to that of natural rocks. However, this relation needs to be examined for more scaled models and also by incorporating different particle materials and cements. The analysis of non-proportional scaling indicates the capability of DEM simulation to induce the effect of the specimen's dimensions for a conglomeratic rock.

In the sensitivity study on particle and interparticle cementing materials, three particle materials and three interparticle cements were considered to create and test numerical conglomerates in uniaxial, triaxial and Brazilian tensile testing. The particle materials considered were steel, granite and sandstone which represent the clasts of natural conglomerates. Similarly, three interparticle cement matrices, Portland cement, argillaceous cement and arrenaceous cement, were used to bind the clasts together. With these clast and cementing materials, a total of nine different conglomeratic rocks were fabricated, and tested. The test results are discussed in the following paragraphs.

In uniaxial testing, the interparticle cement was observed to influence peak strength significantly, irrespective of the particle material. The peak strengths of the numerical conglomerates were observed to increase with the increase of the cement strength. However, this influence gradually decreased with the increase of confining pressure, irrespective of the particle materials. In addition, the particle material was found to have a negligible effect on the uniaxial strengths for all cementing materials. However, with the increase of confinement, this effect became pronounced, that is, the peak strengths increased with the decrease of the stiffness and strengths of the particles.

These observations suggest that the behaviour of a conglomerate is significantly influenced by the properties of the cement matrix in unconfined conditions, while the properties of the clasts have more influence in confined conditions.

In all nine conglomerates, the variation of the uniaxial and triaxial strengths was examined with the strength contrast of the particles and cementing materials; that is, the UCS_{cem}/ UCS_{part} ratio. The strengths of the conglomerates were found to increase with the decrease of the strength contrast; that is, with an increase of the UCS_{cem}/ UCS_{part} ratio. The same trend was also noted in the tensile strengths of the conglomerates. The effect of the particle and interparticle cementing materials was also analysed for the non-dimensional ratio of uniaxial compressive strength to tensile strength (*UCS/T*) of the conglomerates. The *UCS/T* ratio was found to decrease with the increase of UCS_{cem}/ UCS_{part}. However, the decreasing trend was observed to depend on a particular particle or a cementing material.

Young's modulii were found to increase with the increase in the stiffness of the particles as well as the interparticle cement. The stiffness of the conglomerates were analysed in terms of the interparticle cement to particle stiffness ratio. With a particular particle material, the modulii increase with an increase of the E_{cem}/ E_{part} ratio; that is, by increasing the stiffness of the interparticle cement. The increasing trend depends on the stiffness of the particles; that is, high stiffness particles demonstrate a steeper trend, while low stiffness particles show a gentler trend. Similarly, for particular interparticle cement, modulii decrease with the increase of the E_{cem}/ E_{part} ratio; that is, by decreasing the stiffness of the particles. This decreasing trend is steeper for high stiffness interparticle cement and gentler for low stiffness cement. Poisson's ratio was found to decrease with the increase of the E_{cem}/ E_{part} ratio, irrespective of the particle or cementing materials.

The test results of all numerical conglomerates were modelled with Mohr-Coulomb and Hoek-Brown criteria. Mohr-Coulomb criterion was found to better represent the test data of numerical conglomerates than Hoek-Brown criterion. Hoek-Brown criteria were, however, fitted to each sample data set, to gain an appreciation of the indicative m_i values.

The variation of Mohr-Coulomb parameters (angle of friction and cohesion) of the conglomerates was examined corresponding to the UCS_{cem}/ UCS_{part} ratio. Irrespective of the particle material, the angle of friction decreased and cohesion increased with the increase in the UCS_{cem}/ UCS_{part} ratio (i.e., by increasing the strength of the interparticle cement). Similarly, for a particular cementing material, the angle of friction increased and cohesion decreased with the increase of the UCS_{cem}/ UCS_{part} ratio (i.e., by increasing the strength of the particle material). This suggests that cohesion is directly proportional to the strength of the cementing material or inversely proportional to the strength of the particle material. Likewise, the angle of friction is directly proportional to the strength of the particle material and inversely proportional to the strength of the cementing material.

The Hoek-Brown parameter, material constant (m_i), was also found to be sensitive to the particle material and interparticle cement. Generally, m_i was found to increase with the $UCS_{\text{cem}}/UCS_{\text{part}}$ ratio. This increase was observed more pronounced for weak cements, that is, Portland cement and argillaceous cement. Likewise, for a particular particle material, m_i, generally, decreased with the increase of the $UCS_{\text{cem}}/UCS_{\text{part}}$ ratio (i.e., by increasing the strength of the interparticle cement). This observation was found consistent with the existing understanding of the dependence of the strength of the interparticle cement on the material constant.

8.2.3 Micromechanical Investigations

An investigation was conducted to explore the significance of interstitial cement on the mechanical response of synthetic and numerical conglomerates at clast scale. On a micro scale, the synthetic conglomerate is composed of particles bonded with interparticle cement (Portland cement paste) while the numerical conglomerate is comprised of the particles bonded with a parallel bond, such that the properties (strengths and stiffness) of the parallel bond are the same as the interparticle cement in the synthetic conglomerate. Any difference in the macroscopic responses of both conglomerates necessitates the calibration of the parallel bond in relation to the physical interparticle cement.

Therefore, the objectives of this investigation were to determine the extent to which the strength and stiffness of the interparticle cement can be approximated by a parallel bond, and to analyse the significance of the interparticle cement in controlling the overall mechanical response of a conglomerate assembly. For this purpose, the particle-cement interaction of synthetic conglomerates was studied numerically by simulating interparticle cement as an aggregate of micro particles.

Two types of tests were conducted: a two-ball test and a three-ball test. In the two-ball test, two models, a Cement Bond Model (CBM) and a Parallel Bond Model (PBM) were tested in tension, shear and rotation modes. The CBM has two particles or clasts bonded with each other with interparticle cement simulated by micro particles. The micro mechanical parameters of the interparticle cement were determined from the calibration of the Portland cement paste. The PBM consists of two particles (clasts) cemented together with a parallel bond that has the same properties as that of cement paste.

A significant difference in the mechanical responses of the CBM and PBM was noted in all modes of deformation, suggesting a poor correlation between the two models. However, the peak strengths of CBM, at high interface to cement strength ratios (i.e., 1.5~1.75), were found to agree with the corresponding PBM results at an interface to cement strength ratio of 1.0. Furthermore, the CBM's response was much stiffer than the PBM is in all modes of deformation. This contrast is related to the use of parallel bonds in simulating the cement matrix. The variation of the interface to cement strength ratio in CBM produced similar failure mechanisms as observed in synthetic conglomerates. That is, at a lower interface to cement strength ratio, failure occurs along the particle-cement interface, while at a high ratio, the sample splits through the cement. In the synthetic conglomerate samples, the failure was observed, generally, along the particle-cement interface suggesting lower values of the interface strength than the cement strength. However, a few particles were also observed to fail through the cement. Hence, the interface strength in the synthetic conglomerate varies in relation to the cement strength. This observation is consistent with the previous findings on natural conglomerates by Savanick and Johnson (1974).

In the one ball rotation mode, the peak strength of the PBM was found to be close to the tensile strength (in tension mode) of the PBM, however, it should be close to shear strength (in shear mode) as the bond breaks in shear. The peak strengths (tensile and shear) of the CBM were 50~60% of those of the PBM, which was close to the shear strength in rotation mode. The stiffness of the PBM was 5~7 times the stiffness of the CBM indicating a normal to shear stiffness ratio of 0.66 in the CBM. This was in contrast with the stiffness ratio of the CBM, determined in the tension and shear modes, which was approximately 25.

This observation indicates that the stiffness of a bonded contact is function of the normal and shear stiffness of the contact (including the stiffness of the particles and interparticle cement), and the mode of deformation. Alone, shear or tensile stiffness is not enough to represent the stiffness of a bonded contact in the rotation mode of deformation. This is important in modelling the response of conglomerates comprised of macro particles (clasts) embedded in a cement matrix. However, this may not be applicable to the simulation of brittle or fine grained rocks which are normally modelled by a densely packed bonded assembly of particles with no dominant structure (Potyondy & Cundall 2004).

In the two ball rotation mode, the CBM showed a mechanism of cement crushing near the ball contacts which is consistent with, and helps explain the physical tests on synthetic conglomerates.

In the three-ball tests, the main objective was to investigate the sensitivity of the interparticle cement on the mechanical response (peak strength and stiffness) of the assembly. In the three-ball test two balls were bonded with a parallel bond (resting horizontally) and the third ball positioned on top so that a wedge shaped void was present among the three contacting balls. This void was filled with cement particles (Model-1) and the particle-cement interface cohesive strengths were set to zero; that is, there was no bond between the cement and the particles. The second model (Model-2) was constructed with a parallel bond only, without a cement wedge. Both models were tested by giving a constant downward velocity to the top ball to break the parallel bond between the underlying particles.

Model-1 (with cement wedge) and Model-2 (without cement wedge) showed significant differences in mechanical responses in terms of peak axial force, defined as “the force experienced by the top ball in the vertical direction to break the bond in tension between the underlying balls”, and the bulk stiffness. The peak axial force in Model-1 (with cement wedge) was found to be lower than the corresponding force in Model-2 (without cement wedge). This difference in peak forces was named the Cement Wedge Effect (*CWE*) and was defined as “the percent ratio of the difference of the peak forces of the both models (with and with out cement wedge) to the peak force of the model with out a wedge”. Mathematically, *CWE* was defined as;

$$CWE = \frac{\left(f^{peak} - f_{cw}^{peak}\right)}{f^{peak}} * 100$$

Where

CWE - cement wedge effect in percent.

f^{peak} - peak axial force in three ball model without cement wedge

f_{cw}^{peak} - peak axial force in three ball model with cement wedge,

Such that

$$f_{cw}^{Peak} = f^{peak} - f_{cw}$$

Where

f_{cw} - Force transmitted through the cement wedge.

The elastic response of Model-1 was found to be slightly stiffer than that of Model-2 due to the contribution of the cement wedge stiffness to the model. Another important effect of the cement wedge was the restriction on ball rotation after bond breakage. This restricted rotation increases dilation in a granular assembly, as observed in actual physical shear box tests on the synthetic conglomerate. By contrast, granular assemblies with parallel bonds show less dilation induced by the excessive rotation of the particles, as observed in shear box testing on numerical conglomerates.

The observations in the three-ball test suggest that interparticle cement acts as a stress riser, inducing the *CWE* in a granular assembly, and also inducing high dilation by restricting particle rotation.

A sensitivity study was conducted to explore the significance of the *CWE* with the change of particle material. The particle material was changed from steel to granite and sandstone to examine the variation of the *CWE*. It was observed that the *CWE* increases with the decrease of the particle-cement stiffness contrast, that is, by increasing the E_{cem}/ E_{part} ratio. However, interestingly, the stiffness contrast of the Model-1 and Model-2 was found constant with the change of particle stiffness (i.e., Young's modulus).

It is therefore concluded that the stiffness contrast of both models is primarily controlled by the stiffness of the cement wedge and is largely independent of particle stiffness. However, the sensitivity of cement stiffness on the *CWE* was not explored here and is left to future studies.

8.3 Conclusions

The key findings of the present research are presented below under respective headings:

8.3.1 Mechanics of Clast Supported Conglomerates

The present research was conducted on idealised clast-supported conglomerates comprised of high strength and stiffness spherical clasts, cemented with weak cement matrices. Physical and numerical modelling techniques were applied to understand the mechanics of these conglomerates. The key findings derived from both techniques are summarised as follows:

The peak uniaxial strength, Young’s modulus and mechanism of failure of clast supported conglomerates are largely controlled by the strength and stiffness of the cement matrix. The interparticle cement affects the strength and stiffness of a clast supported conglomerate in two ways. First, the cement matrix strength and stiffness controls the peak strength, as observed in synthetic conglomerates and numerical simulations. Second, the presence of the cement matrix acts as a stress riser by transmitting forces and moments and induces high interlocking by restricting the clast rotations, as observed in synthetic conglomerates and micro-mechanical investigation. These mechanisms affect the bulk stiffness and the failure mechanisms, and induce non-linearity in the mechanical response of the conglomerates. Therefore, the Hoek-Brown criterion seems more appropriate to predict the non-linear response of clast supported conglomerates.

The stiffness of clast supported conglomerates is a complex combination of the stiffness of the cement matrix and the clast material, and the packing of the clasts. For the range of parameters tested, the conglomerate stiffness is lower than the stiffness of the cement matrix (and the clasts), and increases as the stiffness of the cement or clasts or both is increased.

On an intact specimen scale (i.e., sample diameter to clast diameter ratio ≥ 10), the failure mode of conglomerates is generally ductile due to the high dilation offered by the clasts and cement matrix, while it shifts to strain hardening with the increase of confinement, exhibiting a mechanism of cement crushing. Generally, the specimens’ failure mechanism is axial splitting in uniaxial conditions due to high dilation. The failure mechanism in triaxial loading was not observed in synthetic conglomerate specimens; however, a shift from tensile to shear failure of the interparticle contacts was noted in numerical simulations, which supports the hypothesis of shear failure in the synthetic conglomerate under confining pressures.

In natural conglomerates, the clast-cement interface strength specifies the failure through the cement matrix or along the clast boundaries. For many conglomerates the interface strength is lower than the strength of the cement matrix and this allows failure to occur along clast-cement interfaces. However, with the increase of interface strength, failure progressively occurs through the cement. These failure surfaces induce high interparticle frictions and, in turn high interlocking on a particle scale which results in high dilation on a specimen scale. On an intact specimen scale, the angle of dilation is comparable and even greater than the angle of friction of the conglomerates and seems to be related to the clast size.

The stiffness and strength of the cement matrix significantly influences the peak strength and elasticity of the conglomerate in uniaxial conditions, while a negligible effect was observed in triaxial conditions. However, in contrast, the strength and stiffness of the clasts has a negligible effect on the strength of the conglomerates in uniaxial conditions and significant influence in triaxial conditions.

The clast size distribution affects the peak strength, stiffness and failure mechanism of conglomerates. The peak strength and Poisson's ratio increase while Young's modulus decreases, with the increase of the clast size ratio (i.e., R_{max}/R_{min}) at fixed porosity.

The specimen size of the conglomerate significantly affects the strength and deformation parameters. An increase in the specimen size results in a decrease in the strength and stiffness, and an increase in the Poisson's ratio of the conglomerates, similar to fine grained natural rocks. However, keeping the specimen to clast size ratio constant, an increase in the specimen size has a negligible effect on the strength and elastic parameters (Young's modulus and Poisson's ratio) of conglomerates.

The findings on the effect of specimen size are important in estimating the intact and large scale strength and deformation using DEM simulations. In natural conglomerates, where the clast size, with respect to the sample size, does not meet the ISRM testing requirements, a numerical simulation can be used to fabricate and test a large specimen, corresponding to clast size, which meets the testing requirements. For such samples, the sample geometry and mechanical properties of the clasts and the cement matrix should be extracted from the natural conglomerates. In the same way, the estimation of in situ strength can be made by increasing the specimen size and keeping the clast size constant.

8.3.2 Towards Validation of DEM Simulation

In the present research, an important element was to study and compare the responses of the numerical and synthetic conglomerates, in order to understand the behaviour of an idealised conglomerate.

DEM simulation reproduced many important features of the synthetic conglomerates including, peak strengths, progressive damage and failure mechanisms in uniaxial tests. However, the stiffness of the numerical conglomerate was higher than the synthetic conglomerates.

In triaxial and Brazilian tensile tests, the peak strength was in reasonable agreement with the synthetic conglomerates; however, no distinct crack through the specimen, similar to the corresponding failure in the synthetic conglomerates was observed.

In shear box testing, dilation was lower than that of the synthetic conglomerates even at higher interparticle friction due to excessive rotations of the particles.

These contrasts in the behaviour of numerical and synthetic conglomerates were attributed to the representation of the cement paste by the parallel bonds in the numerical conglomerates when compared to the Portland cement paste in the synthetic conglomerates. It was observed that the representation of the cement at post failure stage of the bonded contacts has a significant effect on the assembly response, especially in controlling the assembly stiffness, interlocking and dilation. Micro mechanical investigations also showed that the response of a cement paste can not be obtained using a parallel bond, especially when modelling the coarse grained rocks such as conglomerates. Besides, the shear to stiffness ratio of the parallel bonds also affects the assembly stiffness and needs to be investigated in relation to the physical system.

These findings lead to the need to redefine the contact or bonding models or to simulate the interparticle cement with an aggregate of micro particles in the simulation of conglomerates or coarse grained rocks. However, more than one million particles would be required to simulate the cement in 3D intact rock models. One alternative is to construct a simplified model by determining the optimum number of cement particles that can induce the cement wedge effect presented in this thesis at the post failure stage of the bonded contacts.

8.4 Recommendations for Future Research

The present research provides an improved understanding of the behaviour of an idealised clast supported conglomeratic rock with spherical clasts. However, future research should focus on the following aspects of the clast supported conglomerates, both in experiments and numerical simulations:

- Effect of clast shape
- Clast size sensitivity
- Effect of clast size distribution
- Effect of porosity of Clasts

In addition, the obtained mechanical response of the conglomerates was based on micro parameters derived from the mean values of the strength and elastic parameters of interparticle cement (Portland cement paste). These mean values of micro parameters were used to install parallel bonds in all conglomeratic specimens. However, in future research, these micro parameters should be varied and distributed throughout the specimens based on the variation in strength and elastic response of Portland cement paste.

A thorough investigation is required to examine the mechanics of cement matrix supported conglomerates both in physical experiments and numerical simulations. In this case, numerical simulation may include the use of revised bond models that can be implemented on two particles having no contact or by simulating the interparticle cement with micro cement particles. The use of cement particles involves a much higher computational cost, which means 3D specimens meeting ISRM specifications can not be modelled on personal desktop computers.

DEM simulations, although capable of investigating the response of granular rocks, require an investigation of the facets for a true representation of physical conditions:

- The boundary condition's equivalence in relation to physical experiments for the calculation of a mechanical response, especially an elastic response (i.e., Young's modulus and Poisson's ratio).
- Interparticle friction to assembly friction.
- The Cement Wedge Effect (CWE) observed in micro mechanical investigations needs to be investigated in uniaxial, triaxial, Brazilian tensile and shear box tests to examine its effect on the peak strengths, elastic response and failure mechanisms of the specimens. It is anticipated that this effect will induce high interlocking in conjunction with interparticle cement and consequently will yield high assembly or bulk friction and high dilation in the shear box test, and a discrete fracture in the Brazilian specimen.

References

Akram, M. S. and Sharrock, G. (2009). Physical and numerical investigation of a cemented granular assembly under uniaxial and triaxial compression. *The 43rd US Rock Mechanics Symposium and 4th U.S.-Canada Rock Mechanics Symposium June 28 – July 1, 2009*, Asheville, American Rock Mechanics Association (ARMA), (CD-ROM) 09-024.

Akram, M. S. and Sharrock, G. (2010). Physical and numerical investigation of a cemented granular assembly of steel spheres. *Int. J. Numer. Anal. Meth. Geomech.* Published online in Wiley InterScience (www.interscience.wiley.com). DOI: 10.1002/nag.885.

Almossawi, H. I. H. (1988). Physical properties of synthetic sandstone rocks. *Geophysical Prospecting*. 36: 689-699.

Alonso, E., Alejano, L. R., Manfin, G. F. and Bastante, F. G. (2008). Influence of post-peak properties in the application of the convergence-confinement method for designing underground excavations. *5th International Conference and Exibition on Mass Mining*, Luled, Sweden.

Andriani, G. F. and Walsh, N. (2002). Physical properties and textural parameters of calcarenitic rocks: Qualitative and quantitative evaluations. *Engineering Geology*. 67 (1): 5-15.

AS (1993). Geotechnical site investigations. *Australian Standards*. AS 1726-1993.

Ashmawy, A. K., Sukumaran, B., Hoang, A. V., Sukumaran, B. and Hoang, A. V. (2003). Evaluating the influence of particle shape on liquefaction behavior using discrete element methods. *Thirteenth International Offshore and Polar Engineering Conference (ISOPE 2003)*, Honolulu, Hawaii.

ASTM (2005). Mechanical mixing of hydraulic cement pastes and mortars of plastic consistency. *Annual Book of ASTM standards, American Society of Testing Materials, Philadelphia*. ASTM C305-99.

Bagster, D. F. and Kirk, R. (1985). Computer generation of a model to simulate granular material behavior. *Journal of Powder Bulk Solids Tech.* 9 (3): 19-24.

Bathurst, R. J. and Rothenburg, L. (1989). Analytical study of induced anisotropy in idealized granular materials. *Geotechnique*. 39 (4): 601-614.

Bell, F. G. (1978). Physical and mechanical properties of the Fell sandstones, Northumberland, England. *Engineering Geology*. 12 (1): 1-29.

Bell, F. G. (2007). *Engineering Geology*. Butterworth-Heinemann, ELSEVIER, Oxford.

Bell, F. G. and Lindsay, P. (1999). The petrographic and geomechanical properties of sandstones from the Newspaper member of the Natal Group near Durban, South Africa. *Engineering Geology*. 53 (1): 57–81.

Benito, C. (1960). Scales, materials and manufacturing processes. *Proceedings of the Symposium on Models of Structures, Madrid 1959, R.I.L.E.M. Bull. No. 8*. 5-14.

Berkman, D. A., Ed. (2001). *Field Geologist's Manual*. The Australian Institute of Mining and Metallurgy, Carlton, Victoria.

Bernabe, Y., Fryer, D. T. and Hayes, J. A. (1992). The effect of cement on the strength of granular rocks. *Geophysical Research Letters*. 19 (14): 1511-1514.

Beshir, B. A. C. (1967). Model materials for structural concrete analysis. MSc Thesis. *Imperial College of Science and Technology,* London.

Bishop, A. W. (1954). Correspondence on shear characteristics of a saturated silt measured in triaxial compression. *Geotechnique*. 4 (1): 43-45.

Blatt, H., Middleton, G. and Murray, R. (1980). *Origin of Sedimentary Rocks*. Prentice-hall, New Jersey.

Bobet, A., Fakhimi, A., Johnson, S., Morris, J., Tonon, F. and Yeung, M. R. (2009). Numerical models in discontinuous media: Review of advances for rock mechanics applications. *J. Geotech. Geoenvirn. Eng.* 135 (11): 1547-1561.

Bodonyi, J. and Szabo, A. (1962). Examining the rock movements caused by caving in using models. Hungarian Research Institute in Mining, (6): 73-82.

Boyum, B. H. (1961). Subsidence case studies in Michigan mines. *Symposium on Rock Mechanics*, University Park, Penn., USA. 19-57.

Brace, W. F., Paulding, B. W. and Scholz, C. (1966). Dilatancy in the fracture of crystalline rocks. *J. Geophys. Res.* 71: 3939-3953.

Brady, B. H. G. and Brown, E. T. (2005). *Rock Mechanics for Underground Mining*. Kluwer Academic Publisher, Dordrecht.

Bratton, J. L. and Pratt, H. R. (1968). Two dimensional finite difference calculations of dynamic insitu response of layered geologic media to a large explosive load. *Symposium on Rock Mechanics*, Univ. Texas, Austin. 149-198.

Brown, E. T., Ed. (1981). *Rock Characterization, Testing and Monitoring - ISRM Suggested Methods*. Pergamon Press.

Bruno, M. S. and Nelson, R. B. (1991). Microstructural analysis of the inelastic behavior of sedimentary rock. *Mechanics of Materials*. 12: 95-18.

Burman, B. C. (1971). A numerical approach to the mechanics of discontinua. PhD Thesis. *James Cook University of North Queensland,* Townsville, Australia.

Byrne, R. J. (1974). Physical and numerical models in rock and soil-slope stability. PhD Thesis. *James Cook University of North Queensland,* Townsville, Australia.

Cambou, B., Dubuiet, P., Emeriault, F. and Sidoroff, F. (1995). Homogenization for granular materials. *Eur. J. Mech. A/Solids*. 14 (2).

Cecconi, M., Viggiani, G. and Rampello, S. (1998). An experimental investigation of the mechanical behaviour of a pyroclastic soft rock. *The Geotechnics of Hard Soils–Soft Rocks.* Evangelista, A. and Picarelli, L., (Eds). Balkema, Rotterdam: 473–482.

Chang, C. S., Shi, S. Q. and Zhu, H. (1999). Microstructural modeling for elastic moduli of bonded granules. *J. Eng. Mech.* 125 (6): 648-653.

Chang, C. S., Sundaram, S. S. and Misra, A. (1989). Initial moduli of particulated mass with frictional contacts. *Int. J. Numer. Anal. Meth. Geomech.* 13 (6): 626–641.

Chappel, B. A. (1972). The mechanics of blocky material. PhD Thesis. *Australia National University,* Canberra, Australia.

Chen, H. and Wan, J. P. (2004). The effect of orientation and shape distribution of gravel on slope angles in central Taiwan. *Engineering Geology*. 72 (2004): 19-31.

Cho, N., Martin, C. D. and Sego, D. C. (2007). A clumped particle model for rock. *Int. J. Rock Mech. Min. Sci.* 44: 997–1010.

Cho, N., Martin, C. D. and Sego, D. C. (2008). Development of a shear zone in brittle rock subjected to direct shear. *Int. J. Rock Mech. Min. Sci.* 45: 1335-1346.

Clark, A. R. and Walker, B. F. (1977). A proposed scheme for the classification and nomenclature for use in the engineering description of Middle Eastern sedimentary rocks. *Geotechnique*. 27 (1): 93-99.

Cleary, P. W. (1993). Design and loading of dragline bucket. *Mathematics in Industry Study Group (MISG 1993)*, Melbourne. 39-67.

Clegg, B. (1965). A weakly cemented sand and its behaviour in a model pavement structure. *Sixth International Conference on Soil Mechanics and Foundation Engineering*. 27-31.

Clough, G. W., Sitar, N. and Bachus, R. C. (1981). Cemented sands under static loading. *J. Geotech. Eng. Div. ASCE*. 107 (799-817).

Coates, D. F. and Parson, R. C. (1966). Experimental criteria for classification of rock substances. *Int. J. Rock Mech. Min. Sci. Geomech. Abstr.* 3: 181-189.

Cox, S. J. D. and Meredith, P. G. (1993). Microcrack formation and material softening in rock measured by monitoring acoustic emissions. *Int. J. Rock Mech. Min. Sci. Geomech. Abstr.* 30 (1): 11-24.

Cundall, P. A. (1971). A computer model for simulation of progressive, large scale movements in blocky rock systems. *International Society of Rock Mechanics Symposium*, Nancy. Article 8.

Cundall, P. A. (1974). Rational design of tunnel support: A computer model for rock mass behavior using interactive graphics for the input and out put of geometric data. *Report AD/A-001.602* U.S. National Technical Information Service.

Cundall, P. A. (1978). BALL-A Program to model granular media using the distinct element method. *Technical Note TN-LN-13.* Advanced Technology Group, Dames & Moore, London.

Cundall, P. A. (1980). UDEC- A generalized distinct element program for modeling jointed rock. U.S. Army, European Research Office, London. (Report PCAR- 1-80, Contract DAJA 37-79-0548).

Cundall, P. A. (1988). Formulation of three dimensional distinct element model Part-I. A scheme to detect and represent in a system composed of many polyhedral blocks. *Int. J. Rock Mech. Min. Sci. Geomech. Abstr.* 25 (3): 107-116.

Cundall, P. A. (2004). A self-similar bond model for PFC2D. *Numerical Modeling in Micromechanics via Particle Methods: 2nd International PFC Symposium*, Kyoto, Japan. Shimizu, Y., Hart, R. D. and Cundall, P. A., (Eds). A. A. Balkema: 217-223.

Cundall, P. A. and Hart, R. D. (1992). Numerical modeling of discontinua. *J. Eng. Comp.* 9: 101-113.

Cundall, P. A. and Hart, R. D. (1993). Numerical modeling of discontinua. *Comprehensive Rock Engineering: Principles, Practice & Projects.* Hudson, J. A., (Ed.). Pergamon Press. 2: 231-243.

Cundall, P. A. and Strack, O. D. L. (1978). The distinct element method as a tool for research in granular media, Part I. (NSF Report, Grant ENG76-20711).

Cundall, P. A. and Strack, O. D. L. (1979a). The development of constitutive laws for soil using distinct element method. *Numerical Methods in Geomechanics: Third International Conference on Numerical Methods in Geomechanics*, Aachen. Wittke, W., (Ed.). A. A. Balkema: 289-298.

Cundall, P. A. and Strack, O. D. L. (1979b). The distinct element method as a tool for research in granular media, Part II. (NSF Report, Grant ENG76-20711).

D.E.H. (1966). Deformabilite de la roche de fondation dans le cas de quelques barrages Italliens (Deformability of solid rock in the case of some Italian stoppings). *1st Cong. Int. Soc. Rock mech.*, Lisbon. 603-615.

David, C., Menrndes, B. and Bernabr, Y. (1998). The mechanical behaviour of synthetic sandstone with varying brittle cement content. *Int. J. Rock Mech. Min. Sci.* 35: 759-770.

Deflandre, J. P., Vincke, O. and Rebut, E. (1995). Contribution of the acoustic emission analysis to the interpretation of the uniaxial compressive test. *35th U.S. Symposium on Rock Mechanics, June 5–7*, Reno, Nevada. Daemen, J. J. K. and Schultz, R. A., (Eds). A. A. Balkema, Neitherland: 867–872.

Deluzarche, R., Cambou, B. and Fry, J. J. (2002). Modeling of rock fill behavior with crushable particles. *Numerical Modeling in Micromechanics via Particle Methods: 1st International PFC Symposium* Gelsenkirchen, Germany. Konietzky, H., (Ed.). A.A. Balkema: 219-224.

Dhakal, G., Yoneda, T., Kato, M. and Kaneko, K. (1993). Slake durability and minerlogical properties of some pyro clastic and sedimentary rocks. *Engineering Geology*. 65 (1): 31-45.

Diederichs, M. S. (2000). Instability of hard rock masses: The role of tensile damage and relaxation. PhD Thesis. *University of Waterloo,* Ontario.

Diederichs, M. S. (2003). Rock fracture and collapse under low confinement conditions. *Rock Mech. Rock Eng.* 36 (5): 339-381.

Diederichs, M. S., Kaiser, P. K. and Eberhardt, E. (2004). Damage initiation and propagation in hard rock during tunnelling and influence of near-face stress rotation. *Int. J. Rock Mech. Min. Sci.* 41: 785-812.

Digby, P. J. (1981). The effective moduli of porous granular rocks. *Journal of Applied Mechanics*. 48: 803-808.

Dobereiner, L. and De Freitas, M. H. (1986). Geotechnical properties of weak sandstone. *Geotechnique*. 36 (1): 79–94.

Dodds, R. K. (1965). Measurement and analysis of rock physical properties on the Dez Project, Iran. *Symp. Tesing Techniques for Rock Mech.*, Seattle, Wash. 52-72.

Duevel, B. and Haimson, B. (1997). Mechanical characterization of pink lac du Bonnet granite: Evidence of nonlinearity and anisotropy. *Int. J. Rock Mech. Min. Sci.* 34 (3-4): 117.e1-117.e18.

Dvorkin, J. (1996). Cement among grains. *11th Conference on Engineering Mechanics*, Fort Lauderdale, FL, USA. ASCE, New York, NY, USA.

Dvorkin, J., Mavko, G. and Nur, A. (1991). The effect of cementation on the elastic properties of granular material. *Mechanics of Materials*. 12: 207-217.

Dvorkin, J., Nur, A. and Yin, H. (1994). Effective properties of cemented granular materials. *Mechanics of Materials*. 18: 351-366.

Dvorkin, J. and Yin, H. (1995). Contact laws for cemented grains: Implication for grain and cement failure. *Int. J. Solids Structures*. 32 (17): 2497-2510.

Eberhardt, E., Stead, D., Stimpson, B. and Read, R. S. (1998). Identifying crack initiation and propagation thresholds in brittle rock. *Canadian Geotech Journal*. 35 (2): 222-233.

Esmaieli, K., Hadjigeorgiou, J. and Grenon, M. (2009). Estimation of synthetic rock mass strength accounting for sample size. *International Conference on Rock Joints and Jointed Rock Masses*, Tucson, Arizona, USA, January 7-8, 2009.

Esmaieli, K., Hadjigeorgiou, J. and Grenon, M. (2010). Estimating geometrical and mechanical REV based on synthetic rock mass models at Brunswick Mine. *Int. J. Rock Mech. Min. Sci.* doi: 10.1016/J.ijrmms.2010.05.010.

Farmer, I. W. (1983). *Engineering Behaviour of Rocks*. Chapman & Hall, London.

Favier, J. F., Abbaspour, F. M. H. and Kremmer, M. (1999). Modeling non-spherical particles using multi-sphere discrete element. *J. Eng. Mech.* 127 (10): 971-976.

Ferrez, J. A. (2001). Dynamic triangulations for efficient 3D simulation of granular materials. PhD Thesis. *Department of Mathematics, Ecole Ploytechnique Federale de Lausanne,* Lausanne.

Fredrich, J. T., Menendez, B. and Wong, T. (1995). Imaging the pore structure of geomaterials. *Science*. 268: 276-279.

Fu, Y. (2005). Experimental quantification and DEM simulation of micro-macro behaviors of granular materials using x-ray tomography imaging. PhD Thesis. *Department of Civil and Environmental Engineering, Louisiana State University and Agricultural and Mechanical College,* Baton Rouge.

Garner, E. and Gatun, C. (1963). Experimental study of crater formation in plastically deforming synthetic rocks. *J. Petrol. Technol.* : 1025-1030.

Ghaboussi, J. (1990). Three dimensional discrete method for granular materials. *Int. J. Numer. Anal. Meth. Geomech.* 14: 451-472.

Gil, I., Roegiers, J. C., Hart, R. and Shimizu, Y. (2005). Modeling the mechanical properties of Antler sandstone using a discrete element model. *The 40th U.S. Symposium on Rock Mechanics (USRMS)*, Anchorage, Alaska, USA.

Goodman, R. E. (1980). *Introduction to Rock Mechanics*. John Wiley & Sons, New York.

Goodman, R. E. and Blake, W. (1965). An investigation of rock noise in landslides and cut slopes. *Rock Mech. Eng. Geol.* Suppl. II: 88–93.

Habimana, J., Labiouse, V. and Descoeudres, F. (2002). Geomechanical characterization of cataclastic rocks: Experience from Cleuson-Dixence project. *Int. J. Rock Mech. Min. Sci.* 39: 677-693.

Hajiabdolmajid, V. and Kaiser, P. (2003). Brittleness of rock and stability assessment in hard rock tunneling. *Tunnelling and Underground Space Technology*. 18: 35-40.

Hakuno, M. and Tarumi, Y. (1988). A granular assembly simulation for the seismic liquefaction of sands. *Str. Eng./ Earthquake Eng., Japan Society of Civil Engineers*. 5 (2): 333-342.

Hakuno, M. and Yamamoto, T. (1991). Simulation analysis of dynamic nonlinear behavior of underground structures by the extended distinct element method. *Computer Methods and Advances in Geomechanics.* Beer, G., (Ed.). Balkema: 481-486.

Hardy, H. R. (2003). *Acoustic Emission/ Microseismic Activity: Principles, Techniques and Geotechnical Applications*. A. A. Balkema, Lisse.

Hart, R., Cundall, P. A. and Lemos, J. (1988). Formulation of three dimensional distinct element model Part-II: Mechanical calculations for motion and interaction of a system composed of many polyhedral blocks. *Int. J. Rock Mech. Min. Sci. Geomech. Abstr.* 25 (3): 117-125.

Hart, R. D. (1993). An introduction to distinct element modeling for rock engineering. *Comprehensive Rock Engineering: Principles, Practice & Projects.* Hudson, J. A., (Ed.). Pergamon Press. 2: 245-261.

Hawkes, I. and Mellor, M. (1970). Uniaxial testing in rock mechanics laboratories. *Engineering Geology*. 4 (3): 177-288.

Hayashi, M., Fuziwara, Y. and Komoda, H. (1974). Dynamic deformability and viscosity of rock mass and rock fill material under repeated loadings in situ and triaxial test. *Rock Mech.*, Japan. 84-86.

Hertz, H. (1882). Uber die beruhrung fester elastischer korper (On the contact of elastic solid). *Mathematik*. 92: 156-171.

Hill, J. M. and Zheng, X. M. (1994). Dynamic Modelling of flowing granular materials: Post doctoral report No. 1/94. Department of Mthematics, University of Woolongong, Ontario.

Hobbs, D. W. (1967). Behaviour and simulation of sedimentary rocks. *J. Strain Anal.* 2: 307-316.

Hoek, E. (1977). Rock mechanics laboratory testing in the context of a consulting engineering organization. *Int. J. Rock Mech. Min. Sci. Geomech. Abstr.* 14: 93-101.

Hoek, E. and Brown, E. T. (1980a). Empirical strength criterion for rock masses. *J. Geotech. Eng. Div, ASCE* 106 (GT9): 1013–1035.

Hoek, E. and Brown, E. T. (1980b). *Underground Excavations in Rock*. Institute of Mining and Metallurgy, London, UK.

Hoek, E. and Brown, E. T. (1997). Practical rock estimates of rock mass strength. *Int. J. Rock Mech. Min. Sci. Geomech. Abstr.* 34 (8): 1165-1186.

Hoek, E., Carranza, T. and Corkum, B. (2002). Hoek-Brown failure criterion—2002 edition. *5th North American Symposium—NARMS-TAC*, Toronto.

Hoek, E. and Diederichs, M. S. (2006). Empirical estimation of rock mass modulus. *Int. J. Rock Mech. Min. Sci. Geomech. Abstr.* 43: 203-215.

Hoek, E. and Marinos, P. (2007). A brief history of the development of the Hoek-Brown failure criterion. *Soils and Rocks*. 2: 1-13.

Holcomb, D. J. (1993). General theory of the Kaiser effect. *Int. J. Rock Mech. Min. Sci. Geomech. Abstr.* 30 (7): 929–935.

Holt, R. M. (2001). Particle vs laboratory modelling of in-situ compaction. *Physics Chem. Earth (A)*. 26 (1-2): 89-93.

Holt, R. M., Kjolaas, J., Larsen, I., Li, L., Pillitteri, A. G. and Sonstebo, E. F. (2005). Comparison between controlled laboratory experiments and discrete particle simulations of the mechanical behvior of rock. *Int. J. Rock Mech. Min. Sci.* 42: 985-995.

Hustrulid, A. I. and Brown, H. (1997). Parallel implementation of the discrete element method. (Acessed on 3/9/1998). *Colrado School of Mines*, from http://ppl.mines.colorado.edu:/ppl.html

ISRM (1983). Suggested methods for determining the strength of rock materials in triaxial compression: Revised version. *Int. J. Rock Mech. Min. Sci. Geomech. Abstr.* 20 (6): 285-290.

Itasca, C. G. I. (1987). Particle Flow Code (PFC). Minneapolis, Minnesota, USA.

Itasca, C. G. I. (2004). PFC2D (Particle Flow Code in Two Dimensions). Minneapolis, Minnesota, USA.

Itasca, C. G. I. (2005). PFC3D (Particle Flow Code in Three Dimensions). Minneapolis, Minnesota, USA.

J.N.C.L.D. (1958). Present status of measurement of structural behavior of dams in Japan. *Trans 6th Cong. large Dams*, New York. Vol. 2. R. 25, Q. 22: 301-357.

Jackson, R., Gorski, B. and Gyenge, M. (1995). Geotechnical properties of rock. *A Database of Physical Properties of Canadian Rock Including both Intact and Residual Strengths.* Canada Communication Group: 15-91.

Jensen, R. P., Bosscher, P. J., Plesha, M. E. and Edil, T. B. (1999). DEM simulation of granular media - structure interface: Effects of surface roughness and particle shape. *Int. J. Numer. Anal. Meth. Geomech.* 23: 531-547.

Jiang, M. J., Yu, H. S. and Harris, D. (2006). Bond rolling resistance and its effect on yielding of bonded granulates by DEM analyses. *Int. J. Numer. Anal. Meth. Geomech.* 30: 723–761.

Jing, L. (2003). A review of techniques, advances and outstanding issues in numerical modelling for rock mechanics and rock engineering. *Int. J. Rock Mech. Min. Sci.* 40 (3): 283-353.

Jing, L. and Hudson, J. A. (2002). Numerical Methods in Rock Mechanics. *Int. J. Rock Mech. Min. Sci.* 39: 19.

Johansson, C. E. (1976). Structural studies of frictional sediments. *Geogr. Ann. Ser. A. Phys. Geogr.* 58 (4): 201-301.

Kobayashi, T., Mimuro, T. and Yoshinaka, R. (1995). Mechanical properties and failure mechanism of gravelly soft rocks. *Rock Foundation*, Rotterdam. Yoshinaka, R. and Kikuchi, K., (Eds). Balkema: 91-98.

Kobayashi, T. and Yoshinaka, R. (1994). Mechanical properties of gravelly soft rocks. *Jpn. Soc. Civ. Eng. 487 III-26* Japan, Jpn. Soc. Civ. Eng.

Kobayashi, T., Yoshinaka, R. and Mimuro, T. (1994). Strength and deformation behavior of gravelly soft rock. *IV CSMR Integr. Approach Appl. Rock Mech.*, Japan, CSMR.

Konietzky, H., Ed. (2002). *Numerical Modeling in Micromechanics via Particle MMethods:1st International PFC Symposium*. A.A. Balkema, Gelsenkirchen, Germany.

Koster, E. H. and Steel, R. J., Eds. (1984). *Sedimentology of Gravels and Conglomerates*. Can.Soc. Pet. Geol, Calgary.

Koyama, T. and Jing, L. (2007). Effects of model scale and particle size on micro-mechanical properties and failure processes of rocks:A particle mechanics approach. *Engineering Analysis with Boundary Elements*. 31: 458-472.

Krsmanovic, D. (1967). Initial and residual shear strength of hard rocks. *Geotechnique*. 17: 145-160.

Kulatilake, P. H. S. W., Liang, J. and Gao, H. (2001a). Experimental and numerical simulations of jointed rock block strength under uniaxial loading. *J. Eng. Mech.* 127 (12): 1240-1247.

Kulatilake, P. H. S. W., Malama, B. and Wang, J. (2001b). Physical and particle flow modeling of joined rock block behavior under uniaxial loading. *Int. J. Rock Mech. Min. Sci. Geomech. Abstr.* 38: 641-657.

Lajtai, E. Z. (1969). Strength of discontinuous rocks in direct shear. *Geotechnique*. 19: 218-33.

Lajtai, E. Z. (1998). Microscopic fracture processes in a granite. *Rock Mech. Rock Eng.* 31 (4): 237-250.

Lama, R. D. and Vutukuri, V. S. (1978). *Handbook on Mechanical Properties of Rocks: Testing Techniques and Results*. Trans Tech publications, Clausthal, Germany.

Lavroc, A. (2003). The Kaiser effect in rocks: principles and stress estimation techniques. *Int. J. Rock Mech. Min. Sci.* 40 (2): 151-171.

Lemos, J., Hart, R. D. and Cundall, P. A. (1985). A generalized distinct element program for modeling jointed rock mass (a key note lecture). *Int. Symp. Fundamentals of Rock Joints*, Bjorkliden, Sweden. Stephansson, O., (Ed.). Centek, Lulea, Sweden: 335-343.

Leverett, M. C., Lewis, W. B. and True, M. E. (1942). Dimensional model studies of oil field behaviour. *Trans. A.I.M.E*. 146.

Lin, X. and Ng, T. T. (1995). Numerical simulation of fabric anisotropy of gravitationally deposited soils using random arrays of ellipsoidal particles. *Proceedings of the 1995 Joint ASME Applied Mechanics and Materials Summer Meeting*, Los Angeles, CA, USA. American Society of Mechanical Engineers, Applied Mechanics Division, AMD 201: 83-89.

Lin, X. and Ng, T. T. (1997). A three dimensional discrete element model using arrays of ellipsoids. *Geotechnique*. 47 (2): 319-329.

Lindquist, E. S. (1994). Mechanical properties of a physical model melange. *7th Congress of Int. Ass. Eng. Geol.*, Lisbon, Portugal. Balkema.

Link, H. (1964). Evaluation of elasticity moduli of dam foundation rock determined seismically in comparison to those arrived at statistically. *Trans 8th Cong. Large Dams*, Edinburgh. Vol. 1, R. 45, Q. 28, 833-858.

Lisle, R. J. (1985). The effect of composition and strain on quartz-fabric intensity in pebbles from a deformed conglomerate. *Int. J. Earth Sci.*: 657–663.

Lockner, D. (1993). The role of acoustic emission in the study of rock fracture. *Int. J. Rock Mech. Min. Sci. Geomech. Abstr.* 30 (7): 883-899.

Lotti, C. and Beamonte (1964). Execution and controls of consolidation works carried out in the foundation rock of an arch gravity dam. *Trans 8th Cong. Large Dams*, Edinburgh. Vol. 1, R. 37, Q. 28, 671-698.

Martin, C. D. (1993). The strength of massive lac du Bonnet Granite around underground Opening. PhD Thesis. *Department of Civil and Geological Engineering, University of Manitoba,* Winnipeg.

Martin, C. D. (1994). The strength of massive lac du Bonnet Granite around underground Opening. Ph.D Thesis. *University of Manitoba,* Winnipeg, Manitoba, Canada.

Massimilla, L., Astarita, G. and Gambino, A. (1958). Thermal Study of a Dam by means of a Model. *Sixth International Congress on Large Dams*, New York. 771-784.

Matsushima, T. (2004). 3D Image-based discrete element modeling for irregularly-shaped grains. *Numerical Modeling in micromechanics via particle methods: 2nd International PFC Symposium* Kyoto, Japan. Shimizu, Y., Hart, R. D. and Cundall, P. A., (Eds). Balkema: 421-427.

Matsushima, T. and Konagai, K. (2001). Grain-shape effect on peak strength of granular materials. *10th International Conference on Computer methods and Advances in Geomechanics* Tucson, Arizona, USA. Shimizu, Y., Hart, R. D. and Cundall, P. A., (Eds). Balkema: 361-366.

McLane, M. (1995). *Sedimentology*. Oxford University Press, New York.

Meng, J. and Pan, J. (2007). Correlation between petrographic characteristics and failure duration in clastic rocks. *Engineering Geology*. 89: 258-265.

Mindlin, R. D. (1949). Compliance of elastic bodies in contact. *Journal of Applied Mechanics*: 259-268.

Mindlin, R. D. and Deresiewicz, H. (1953). Elastic spheres in contact under varying oblique forces. *Journal of Applied Mechanics*. 20 (3): 327-344.

Mishra, B. K. and Rajmani, R. K. (1992). Discrete element method in modelling ball mills. *Journal of Applied Math. Modelling*. 16, Nov: 598-604.

Mogi, K. (1962). Magnitude-frequency relation for elastic shocks accompanying fractures of various materials and some related problems in earthquakes. *Bull. Earthq. Res. Inst. Tokyo Univ.* 40: 831-853.

Mogi, K. (1963). The fracture of a semi-infinite body caused by an inner stress origin and its relation to the earthquake phenomena. *Bull. Earthq. Res. Inst. Tokyo Univ.* 41: 595-614.

Montoto, M., Suarezdel, L. M., Khair, A. W. and Hardy, H. R. (1981). Acoustic emission behaviour of sound to weak granites: Petrographic interpretation. *International Symposium on Weak Rock: Soft, Fractured, and Weathered Rock* Tokyo, Japan. 285–290.

Moon, V. G. (1993). Geotechnical characteristics of ignimbrite: A soft pyroclastic rock type. *Engineering Geology*. 35: 33-48.

Morrison, R. G. K. (1970). *A Philophy of Ground Control*. Ontario Dept. Mines, Ontario.

Muller, D. (1996). Techniques informatiques efficaces pour la simulation de milieux granulaires par des methods d`elements distincts (Effective data processing techniques for the simulation of granular mediums by distinct elements methods) 1545. PhD Thesis. *Depatment of Mathematics, Ecoloe Polytechnique,* Palaiseau Cedex.

Muller, L. (1960). Der felsbau, band i, stuttgart. *Ferdinand Enke Verlag*: 624.

Nakata, Y., Bolton, M. D. and Cheng, Y. P. (2004). Macro-mechanical behavior for an assembly of grains modelled by bonding spheres. *Numerical Modeling in Micromechanics via Particle Methods: 2nd International PFC Symposium*, Kyoto, Japan. Shimizu, Y., Hart, R. D. and Cundall, P. A., (Eds). A.A. Balkema: 407-413.

Narayanasamy, R. (2004). Numerical behavior of weak sand. *Numerical Modeling in Micromechanics via Particle Methods: 2nd International PFC Symposium* Kyoto, Japan. Shimizu, Y., Hart, R. D. and Cundall, P. A., (Eds). A.A. Balkema: 397-406.

Neville, P. M. (1966). Energy and stress distribution in impacted solid cylinders. DIC Thesis. *Mining and Mineral Technology Department, Imperical Colledge of London,* London.

Newland, P. L. and Allely, B. H. (1957). Volume changes in drained triaxial tests on granular materials. *Geotechnique*. 7 (1): 13-34.

Ng, T. T. (1989). Numerical simulation of granular soil under monotonic and cyclic loading: A particulate mechanics approach. PhD Thesis. *Department of Civil Engineering, Renssler Ploytechnic Institute,* Troy, New York.

Ng, T. T. (1994). Numerical simulation of granular soil using elliptical particles. *Comput. Geotech.* 16 (2): 153-170.

Ng, T. T. and Dobry, R. (1991). CONBAL- simulated granular material using quartz sphere with the discrete element method. *Report to NSF* Rensseler Polytechnic Institute, Troy, New York.

Ng, T. T. and Lin, X. (1993a). Numerical Simulation of naturally deposited granular soil with ellipsoidal elements. *2nd Conference on Discrete Element Methods, MIT*, Cambridge, MA. MIT: 557-567.

Ng, T. T. and Lin, X. (1993b). Numerical simulation of inherent fabric anisotropy of gravitational deposited arrays of elliptical particles. *9th International Conference on Mathematical and Computer Modeling*, University of California, Berkeley.

O' Sullivan, C. and Bray, J. D. (2002). Relating the response of idealized analogue particles and real sands. *Numerical Modeling in Micromechanics via Particle Methods: 1st International PFC Symposium*, Gelsenkirchen, Germany. Konietzky, H., (Ed.). A.A. Balkema: 157-164.

O' Sullivan, C., Cui, L. and Bray, J. D. (2004). Three-dimensional discrete element simulations of direct shear tests *Numerical Modeling in Micromechanics via Particle Methods: 2nd International PFC Symposium* Kyoto, Japan. Shimizu, Y., Hart, R. D. and Cundall, P. A., (Eds). A.A. Balkema: 373-382.

Oberti, G. and Fumagalli, E. (1964). Propretés physico-mécaniques des roches d'appui aux grands barrages et leur influence statique documentée par les modèles (Physicomechanical properties of the rocks for support to dam and their static influence documented by the models). *Trans 8th Cong. Large Dams*, Edinburgh. Vol. 1, R. 35, Q. 28: 637-657.

Oda, M. and Konishi, J. (1974). Microscopic deformation of granular material in simple shear. *Soils & Foundations (Japanese Society of Soil Mech. & Found. Eng.)*. 14 (4): 25-38.

Olsson, W. A. (1974). Grain size dependence of yield stress in marble. *J. Geophys. Res.* 79 (32): 4859–4862.

Onodera, T. F. and Kumara, H. M. (1980). Relation between texture and mechanical properties of crystalline rocks. *Bull Assoc Eng Geol*. 22: 173-177.

Ozbek, A. (2009). Variation of Schmidt hammer values with imbrication direction in clastic rocks. *Int. J. Rock Mech. Min. Sci.* 46: 548-554.

Patton, F. D. (1966). Multiple modes of shear failure in rock and related materials. PhD Thesis. *University of Illinois,* Illinois.

Peng, S. S. (1973). Time-dependent aspects of rock behavior as measured by a servo-controlled hydraulic testing machine. *Int. J. Rock Mech. Min. Sci. Geomech. Abstr.* 10: 235-246.

Pollard, D. D. and Aydin, A. (1988). Progress in understanding jointing over the past century. *Geol. Soc. Am. Bull*. 100: 1181-1204.

Potapov, A. and Campbell, C. (1998). A fast model for the simulation of non-round particles. *Granular Matter*. 1: 9-14.

Potyondy, D. (2008). Technical Memorandum on Smooth Joint - Model Version 3 for PFC2D/ PFC3D 4.0. Itasca Consulting Group, Minneapolis. 1-23.

Potyondy, D. O. and Cundall, P. A. (2004). A bonded-particle model for rock. *Int. J. Rock Mech. Min. Sci.* 41: 1329-1364.

Pradhan, T. B. S. and Swada, S. (1992). Distinct element analysis of sand under cyclic loading using oval elements. *10th Conference on Earthquake Engineering*, Rotterdam. Balkema.

Prikryl, R. (2001). Some microstructural aspects of strength variation in rocks. *Int. J. Rock Mech. Min. Sci.* 38: 671–682.

Prikryl, R., Lokajıcek, T., Li, C. and Rudajev, V. (2003). Acoustic emission characteristics and failure of uniaxially stressed granitic rocks: The effect of rock fabric. *Rock Mech. Rock Eng.* 36 (4): 255-270.

Radosavljevic, Z., Colic, B. and Lokin, P. (1970). Stabilité des talus des excavations a ciel ouvert des mines de Cuivre à Bor (Stability of the excavation slopes of Bor copper open pit mines). *2nd Cong. Int. Soc. Rock Mech.*, Belgrade. Vol. III: 403-410.

Rao, M. V. M. S. and Kusunose, K. (1995). Failure zone development in andesite as observed from acoustic emission locations and velocity changes. *Phys. Earth Planet. Interior.* 88 (2): 131–143.

Rao, M. V. M. S. and Ramana, Y. V. (1992). A study of progressive failure of rock under cyclic loading by ultrasonic and AE monitoring techniques. *Rock Mech. Rock Eng.* 25: 237-251.

Read, M. D., Ayling, M. R., Meredith, P. G. and Murrell, S. A. F. (1995). Microcracking during triaxial deformation of porous rocks monitored by changes in rock physical properties, II. Pore volumometry and acoustic emission measurements on water-saturated rocks. *Tectonophysics*. 245: 223-235.

Reynolds, O. (1885). On the dilatancy of media composed of rigid particles in contact. *Phil. Mag. 5th Series*. 20 (127): 469-481.

Richard, C. S. (2000). *Applied Sedimentology*. Academic Press, London, UK.

Roberts, A. (1966). A model study of rock foundation problems underneath a concrete gravity dam. *Engineering Geology*. 1 (349-372).

Rocscience (2008). RocLab1.0. *Rocscience (www.rocscience.com)*, Toronto.

Rocscience (2010). RocData 4.0. *Rocscience (www.rocscience.com)*, Toronto.

Rothenburg, L. and Bathurst, R. J. (1991). Numerical simulation of idealized granular assemblies with plane elliptical particles. *Comput. Geotech.* (11): 315-329.

Rothenburg, L. and Bathurst, R. J. (1992). Micromechanical features of granular assemblies with planar elliptical particles. *Geotechnique*. 42 (1): 79-95.

Ruffolo, R. M. and Shakoor, A. (2009). Variability of unconfined compressive strength in relation to number of test samples. *Engineering Geology*. 108: 16-23.

Sabatakakis, N., Koukisa, G., Tsiambaos, G. and Papanakli, S. (2008). Index properties and strength variation controlled by microstructure for sedimentary rocks *Engineering Geology*. 97: 80-90.

Sallam, A. M., Ashmawy, A. K. and Runkles, B. D. (2004). Experimental validation of modeling irregular particle shapes using DEM. *Numerical Modeling in Micromechanics via Particle Methods: 2nd International PFC Symposium* Kyoto, Japan. Shimizu, Y., Hart, R. D. and Cundall, P. A., (Eds). Balkema: 363-372.

Saotomea, A., Yoshinaka, R., Osada, M. and Sugiyama, H. (2002). Constituent material properties and clast-size distribution of volcanic breccia. *Engineering Geology*. 64 (1): 1-17.

Sargent, R. G. (2004). Validation and verification of simulation models. *Winter Simulation Conference*. Ingalls, R. G., Rossetti, M. D., Smith, J. S. and Peters, B. A., (Eds).

Savanick, G. A. and Johnson, D. I. (1974). Measurements of the strength of grain boundaries in rock. *Int. J. Rock Mech. Min. Sci. Geomech. Abstr.* 11: 173-180.

Sebastianus, W. J., Brok, D., David, C. and Bernabe, Y. (1997). Preparation of synthetic sandstones with variable cementation for studying the physical properties of granular rocks. *C.R. Acad. Sci. Paris/ Earth & Planetary Sciences*. 325: 487-492.

Shafiei, A. and Dusseault, M. B. (2008). Geomechanical properties of a conglomerate from Iran. *The 42nd US Rock Mechanics Symposium and 2nd U.S.-Canada Rock Mechanics Symposium June 29 – July 2, 2008*, San Francisco, ARMA 08-053.

Shah, K. R. and Labuz, J. F. (1995). Damage mechanisms in stressed rock from acoustic emission. *J. Geophys. Res. Solid Earth* 100 (B8): 15527–15539.

Sharrock, G., Akram, M. S. and Mitra, R. (2009). Application of synthetic rock mass modeling to estimate the strength of jointed sandstone. *The 43rd US Rock Mechanics Symposium and 4th U.S.-Canada Rock Mechanics Symposium June 28 – July 1, 2009*, Asheville, American Rock Mechanics Association (ARMA), (CD-ROM) 09-59.

Sharrock, G. B. (2003). Tool shearing of granular media. PhD Thesis. *The Division of Mining and Minerals Process Engineering, University of Queensland,* St Lucia.

Shi, G. (1988). Discontinuous deformation analysis: A numerical model for for the statics and dynamics of block systems. PhD Thesis. *Department of Civil Engineering, University of California,* Berkeley.

Shi, L. P., Huang, T. H. and Hung, J. J. (1995). A study on the uniaxial compression behaviors and acoustic emission characteristics of rocks in Taiwan. *8th ISRM Congress on Rock Mechanics*, Tokyo, Japan. Fuji, T., (Ed.). Balkema, Rotterdam: Vol. I, Theme 2: 211–214.

Shimizu, Y., Hart, R. D. and Cundall, P. A., Eds. (2004). *Numerical Modeling in Micromechanics via Particle Methods: 2nd International PFC Symposium* Balkema, Kyoto, Japan.

Sitharam, T. G. (1999). Micromechanical modeling of granular media: The power of discrete element modeling. *Distinct Element Modeling in Geomechanics.* Sharma, V. M., Saxena, K. R. and Woods, R. D., (Eds). A. A. Balkema: 47-88.

Skinner, A. E. (1969). A note on the influence of interparticle friction on the shearing strength of a random assembly of sphere particles. *Geotechnique*. 19 (1): 150-157.

Stimpson, B. (1970). Modelling materials for engineering rock mechanics. *Int. J. Rock Mech. Min. Sci. Geomech. Abstr.* 7: 77-121.

Strack, O. D. L. and Cundall, P. A. (1979). A discrete numerical model for granular assemblies. *Geotechnique*. 29 (1): 47-65.

Swada, S. and Pradhan, T. B. S. (1994). Analysis of anisotropy and particle shape by distinct element method. *8th International Conference for Computer Methods and Advances in Geomechanics*, West Virginia University, Morgatown. 665-670.

Szucs, E. (1980). *Similitude and Modelling*. Elsevier, Budapest.

Taylor, L. M. and Preece, D. S. (1989). DMC- a rigid body motion code for determining the interaction of multiple spherical particles, Part-1. Sandia National Laboratories, New Mexico. (Report SAND-88-3482).

Thill, R. E. (1972). Acoustic methods for monitoring failure in rock. *14th Symposium on Rock Mechanics, University Park, Pennsylvania*, University Park, Pennsylvania. Hardy, H. R. and Stefanko, R., (Eds). American Society of Civil Engineers: 649–687.

Thomas, R. and Bray, J. D. (1999). Capturing non-spherical shape of granular media with disk clusters. *J. Geotech. Geoenvirn. Eng.* 125 (3): 169-178.

Ting, J. M. (1991). An ellipse-based micromechanical model for angular materials. *ASCE Engineering Mechanics Speciality Conference*, Columbus, Ohio. 1214-1218.

Ting, J. M. (1993). A robust algorithm for ellipse-based discrete element modeling of granular materials. *Comput. Geotech.*

Ting, J. M. and Corkum, B. T. (1992). Computational laboratory for discrete element geomechanics. *J. Comp. Civil Eng.* ASCE 6 (2): 129-146.

Ting, J. M., Corkum, B. T., Kauffman, C. R. and Greco, C. (1989). Discrete numerical model for soil mechanics. *J. Geotech. Eng.* ASCE 115 (3): 379-398.

Ting, J. M., Rowell, J. D. and Meachum, L. (1993). Influence of particle shape on the strength of ellipse-shaped granular assemblies. *2nd Conference on Discrete Element methods, MIT*, Cambridge, MA. MIT: 215-225.

Tobita, Y. and Oda, M. (1999). Friction based deformation and strength behaviors of granular soils. *Mechanics of Granular Materials: An Introduction.* Oda, M. and Iwashita, K., (Eds). A.A. Balkema, Rotterdam: 50-55.

Tomiczek, K. (2002). Modelling of sandstone rock samples using PFC2D. *Numerical Modeling in Micromechanics via Particle Methods: 1st International PFC Symposium* Gelsenkirchen, Germany. Konietzky, H., (Ed.). A.A. Balkema: 223-239.

Trent, B. C. (1989). Numerical simulation of wave propagation through cemented granular material. *Wave Propagation in Granular Media.* Karamanlidis, D. and Stout, R. B., (Eds). AMD. 1: 9-15.

Trent, B. C. and Margolin, L. G. (1992). A numerical laboratory for granular solids. *Engineering Computations*. 9: 191-197.

Walker, R. G. (1975). Gerlized facies models for resedimented conglomerates of turbidite association. *GSA Bull*. 86: 737-748.

Walker, R. G. (1978). Deep-water limestone facies and ancient submarine fans: Models for exploration for stratigraphic traps. *AAPG Bull*. 62: 932-966.

Walton, K. (1987). The effective elastic moduli of a random packing of spheres. *Journal of Mech. Physics of Solids.* 35 (2): 213-226.

Walton, O. R., Braun, R. G., Mallon, D. M. and Cervelli, D. M. (1988). *Micromechanics of Granular Media*. Elsevier Science Publishers, Amsterdam.

Wang, H., Khrishnan, G. R., Zaman, M. and Roegiers, J. C. (1995). Behavior of natural and remolded Antler sandstone: Sample preparation and grain crushing aspects. *The 35th U.S. Rock Mechanics Symposium*, Reno, Nevada. Damen and Schultz, (Eds). 127-133.

Wanne, T. (2002). PFC3D simulation procedure for compressive strength testing of anisotropic hard rock. *Numerical Modeling in Micromechanics via Particle Methods: 1st International PFC Symposium*, Gelsenkirchen, Germany. Konietzky, H., (Ed.). A.A. Balkema: 241-249.

Wawersik, W. R. (2000). The value of laboratory experiments for code validations. *Int. J. Rock Mech. Min. Sci.* 37: 307-316.

Weatherley, D. (2009). https://launchpad.net/esys-particle. Retrieved 01/01, 2009.

Wei, Q., Cheng, X. and Lui, G. (1991). The elliptic discrete element method as a new approach to simulating granular media. *Asian pacific Conference on Computational Mechanics*, Hong Kong.

West, G., Carter, P. G., Dumbleton, M. J. and Lakes, L. M. (1981). Rock mechanics review: Site investigations for tunnels. *Int. J. Rock Mech. Min. Sci. Geomech. Abstr.* 18: 345-367.

Wiles, T. D. (2005). Reliability of numerical modelling predictions. *Int. J. Rock Mech. Min. Sci.* 43: 454-472.

Williams, J. R. and Pentland, A. P. (1989). Superquadratics and model dynamics for discrete elements in concurrent design. *1st US Conference on Discrete Element Methods*. Mustoe, G. G. W., Henrikson, H. P. and Huttelmair, (Eds). CSM Press, Colorado.

Willian, J. R. and Mustoe, G. G. W. (1987). Modal methods for the analysis of discrete systems. *Comput. Geotech*. 4: 1-19.

Winkler, K. W. (1983). Frequency dependent ultrasonic properties of high porosity sandstones. *J. Geophys. Res.* 88 (B11): 9493-9499.

Wisecarver, D. W., Merrill, R. H. and Stateham, R. M. (1969). The microseismic technique applied to slope stability. *Trans. AIME* 244: 378–385.

Wong, T. and Wu, L. C. (1995). Tensile stress concentration and compressive failure in cemented granular material. *Geophysical Research Letters*. 22 (13): 1649-1652.

Xu, B. H. and YU, A. B. (1997). Numerical simulation of the gas-solid flow in a fluidised bed by combining discrete particles method with computational fluid dynamics. *J. Chem. Eng. Sci.* 52 (16): 2785.

Yasir, E. and Tolgay, A. (2010). Industrial use of conglomerate from the Kayranlik Mountains, Turkey. *Bull Eng Geol Environ*. Published online: DOI 10.1007/s10064-010-0280-4.

Yun, H. H. and Quan, S. L. (2008). Experimental study on mechanical properties of granite under repeated loading and unloading. *Int. J. Modern Phys. B*. 22 (9, 10 & 11): 1634-1639.

Zang, A., Wagner, C. F. and Dresen, G. (1996). Acoustic emission, microstructure and damage model of dry and wet sandstone stressed to failure. *J. Geophys Res.* 101 (B8): 17507-17521.

Zhang, A. and Wong, T. F. (1995). Elastic stiffness and stress concentration in cemented granular material. *Int. J. Rock Mech. Min. Sci. Geomech. Abstr.* 32 (6): 563-574.

Zhang, J., Wong, T., Yanagidani, T. and David, D. M. (1990). Pressure-induced microcracking and grain crushing in Berea and Bois sandstones: Acoustic emission and quantitative microscopy measurements. *Mechanics of Materials*. 9: 1-15.

Zhao, X. G. and Cai, M. (2010). A mobilized dilation angle model for rocks. *Int. J. Rock Mech. Min. Sci.* Published online in ELSEVIER (www.elsevier.com), doi 10.1016/j.ijrmms.2009.12.007.

Zhu, W. and Wong, T. (1997). Shear-enhanced compaction in sandstone under nominally dry and water-saturated conditions. *Int. J. Rock Mech. Min. Sci.* 34 (3-4): Paper No. 364.

APPENDICES

APPENDIX A

A1. Literature Review - Acoustic Emission (AE) Monitoring

A2. Figures of Strain Measurement and Acoustic Emission (AE) Monitoring

APPENDIX B

B1. Uniaxial, Triaxial, Brazilian tensile and Shear Box Testing (PFC3D)

B2. Micro Investigations: 2Ball and 3Ball Testing (PFC2D)

APPENDIX C

C1. Hoek-Brown and Mohr-Coulomb Parameters (Numerical Conglomerates)

C2. Additional Figures for 2-Ball Testing

APPENDIX A

Appendix A1 (Literature Review - Acoustic Emission Monitoring)

A1-1 Introduction

Acoustic emissions (AE) or micro-seismicity are the characteristics of any material under stress and deformation. This is an indication and function of the material's internal damage/ dislocation or failure and is related to the initiation, propagation and coalescence of pre-existing cracks (Yun & Quan 2008). During the process of micro crack propagation, the stored energy is released in the form of waves generating AEs (Lavroc 2003). This characteristic feature of rocks was discovered in the 1930s in the USA (Hardy 2003). Since that time, this technique has been promoted, advanced and applied to various fields in science and engineering.

In rock mechanics, AE has been considered a vital tool for identifying the mechanism of the deformation of various rocks at both the laboratory and field scale. In geotechnical engineering, AE has been used for the stability monitoring of underground structures, such as mines, tunnels, storage caverns for gas and petroleum, and radioactive waste depositaries, as well as monitoring surface structures, such as foundations, soil and rock slopes, bridge piers, abutments and dams (Hardy 2003).

A detailed description of the historical development and applications of AE in rock mechanics can be found in the literature (e.g., Hardy 2003). Lockner (1993) has also presented a review of AE's applications and their limitations in understanding the growth and propagation of rock fractures. The AE studies broadly can be categorise d into two groups: one involving the recording of self generated signals, also named the passive AE technique, and the other group involving the recording of artificially triggered AE using vibrators, named Tomography. By definition, a true AE study is a passive technique that involves only the recording of self-generated events as a result of the material's failure (Hardy 2003).

A1-2 AE Applications to Natural Rocks

Since the early applications of AE monitoring were motivated by a desire to predict mine failures or slope stability (Goodman & Blake 1965; Wisecarver et al. 1969), later developments lead to the frequent use of AE as a passive method sensitive to the growth of defects during laboratory deformational tests of different rocks, for example, sandstones (Zhang et al. 1990; Deflandre et al. 1995; Read et al. 1995; Zang et al. 1996; Zhu & Wong 1997), granite (Eberhardt et al. 1998; Prikryl et al. 2003; Yun & Quan 2008), granitoids (Thill 1972; Montoto et al. 1981; Rao & Ramana 1992; Shah & Labuz 1995), andezites (Rao & Kusunose 1995) or tuffs (Shi et al. 1995). Further, the application of AE as an indicator of prior stress conditions was studied based on the so called Kaiser effect (Holcomb 1993) and the amplitude of AE was related to geometric properties like crack size (Cox & Meredith 1993).

In natural rocks the origin of AE activity is not well understood and is considered to be related to the process of deformation and failure which are accompanied by the sudden release of strain energy (Hardy 2003). In such microcrystalline materials, AE activity may be induced due to micro movements, or the initiation and propagation of fractures through or among the mineral grains, and at a mega level by fracturing and the failure of large areas of materials or the relative movement between structural units (Hardy 2003). Hence, AE activity is primarily linked to the deformation characteristics of a rock. In brittle rocks such as granite, strain is produced by two mechanisms; elastic deformation and axial micro-cracking (Lajtai 1998; Hajiabdolmajid & Kaiser 2003).

Another mechanism also considered responsible for strain is compaction which is not an elastic process but permanent damage (Yun & Quan 2008). Besides these mechanisms, there are also minor contributions from the closure of pre-existing cracks at low stresses, occasionally, some non-linear behaviour close to the peak stress and also the unloading of the samples (Yun & Quan 2008). All these mechanisms are responsible for AE activity in a rock. However, micro crack examinations have showed that the shearing along the micro cracks occurs after the peak is passed and hence more activity is observed near the peak and post peak stress.

The AE activity has also been used to characterise the stages of damage along the stress-strain curve in uniaxial or confined testing on rock specimens (e.g., Eberhardt et al. 1998). The study of the initiation and growth of cracks with AE monitoring in a laboratory sample can delineate the progressive damage into definite stages, whereby every stage corresponds to a definite damage threshold characterised by a specific trend in AE activity. Eberhardt et al. (1998) explained the methodology to identify these stages by the analysis of axial, radial and volumetric strains and acoustic emission monitoring. Later Diederichs et al. (2004) further explored this area using numerical modelling and provided a typical framework (Figure A-1) of crack damage thresholds in uniaxial testing being the function of axial, radial and volumetric strains and acoustic emissions. The study showed that AE activity is quite sensitive to different stages of rock disintegration during laboratory deformation, regardless of the type of rock and intensity of its fabric.

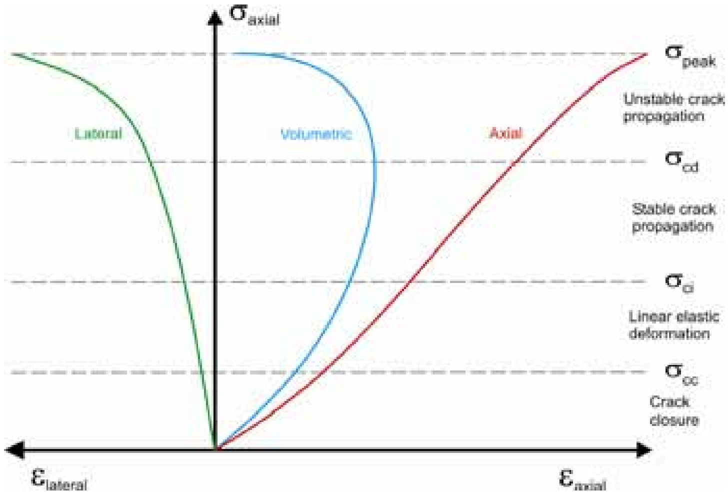

Figure A-1: Damage thresholds corresponding to stages of stress-strains and acoustic response in uniaxial testing (modified after Diederichs et al. 2004).

Looking into the definite characteristic features of AE in relation to axial, lateral and volumetric strains, Diederichs et al. (2004) identified four principal stages of damage namely crack closure (σ_{cc}), a level of stress corresponding to which all pre-existing cracks close, crack initiation (σ_{ci}), where cracks initiate followed by linear elastic deformation, crack damage (σ_{cd}) followed by the unstable crack propagation and then is peak stress (σ_{Peak}). A detailed description of these damage thresholds has been provided in Chapter 3 together with their identification criteria in uniaxial testing.

Looking into benefits of AE monitoring on natural rocks, this technique can also be used for rock like materials i.e. synthetic rock to characterise the progressive damage at micro and macro level in particular laboratory testing.

A1-3 AE Monitoring for Laboratory Testing

The laboratory studies involving AE comprise recording and processing of acoustic signals in a rock specimen under specific loading conditions. In the previous studies, laboratory testing with AE monitoring has been a successful tool in determining the progressive damage in the rock specimen in various loading conditions such as uniaxial, triaxial, bending etc. An essential set up for AE monitoring for laboratory testing consists of following three basic components (Figure A-2).

- Sensor/ Transducer (to record the activity)
- Filter (to filter the signals and transmit to read out device)

- Recorder (Readout device)

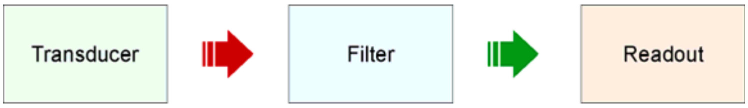

Figure A-2: Basic components of a AE monitoring set-up.

The function of the sensor is to detect those AE signals with a defined frequency range, while the filter identifies AE signals from the background noise. This is normally done by setting the sensors' input to a higher frequency range above the background noise or by amplifying the AE signals. Modern types of digital filters not only amplify the signals but also can separate the AE activity from the noise. This section of AE set up has been greatly improved by the advances in technology.

Readout devices include all the post filtration processes, such as the recording and visualization of the AE signals and number of events being recorded. A number of read out-put devices are available, including magnetic tape recording devices to digital devices. Most of the modern devices are digital which are configured by a computer using specific software and filter-computer interface devices which record the input from the filter in mV. The signals can be viewed on a computer screen and recorded as a number of events in time. The recorded data can then be analysed together with the stress-strain behaviour of the sample.

The modern AE laboratory set, as described by Hardy (2003), is a parametric system that consists of many components within the main three components of the AE set up (Figure A-2). A typical parametric system is shown in Figure A-3. A detailed description of its elements was considered outside the scope of present research and can be found elsewhere (e.g., Hardy 2003).

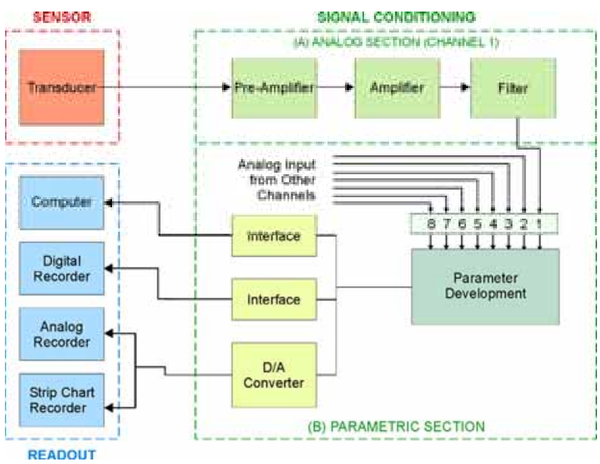

Figure A-3: General form of a parametric laboratory set up for AE monitoring (modified after Hardy 2003) .

A1-3 References for Appendix A1

All bibliographic refrecnes to Appendix A1 are provided in “References”.

Appendix A2 (Figures of Strain Measurement and Acoustic Emission Monitoring)

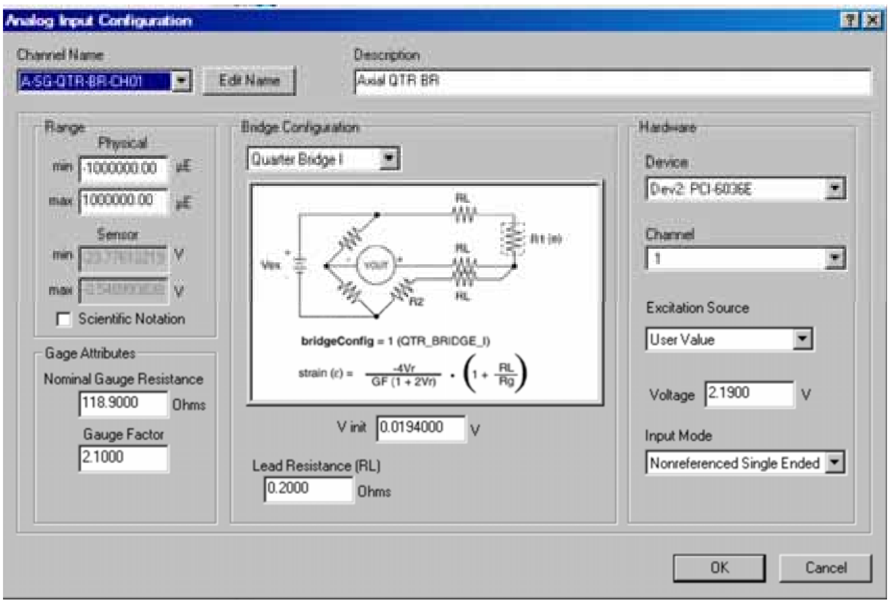

Figure A-4:Notational Instruments (NI) DAQ set up window for Quarter Wheatstone Bridge for strain measurement

Figure A-5:National Instruments (NI) data acquisition system (SC-2043-SG)

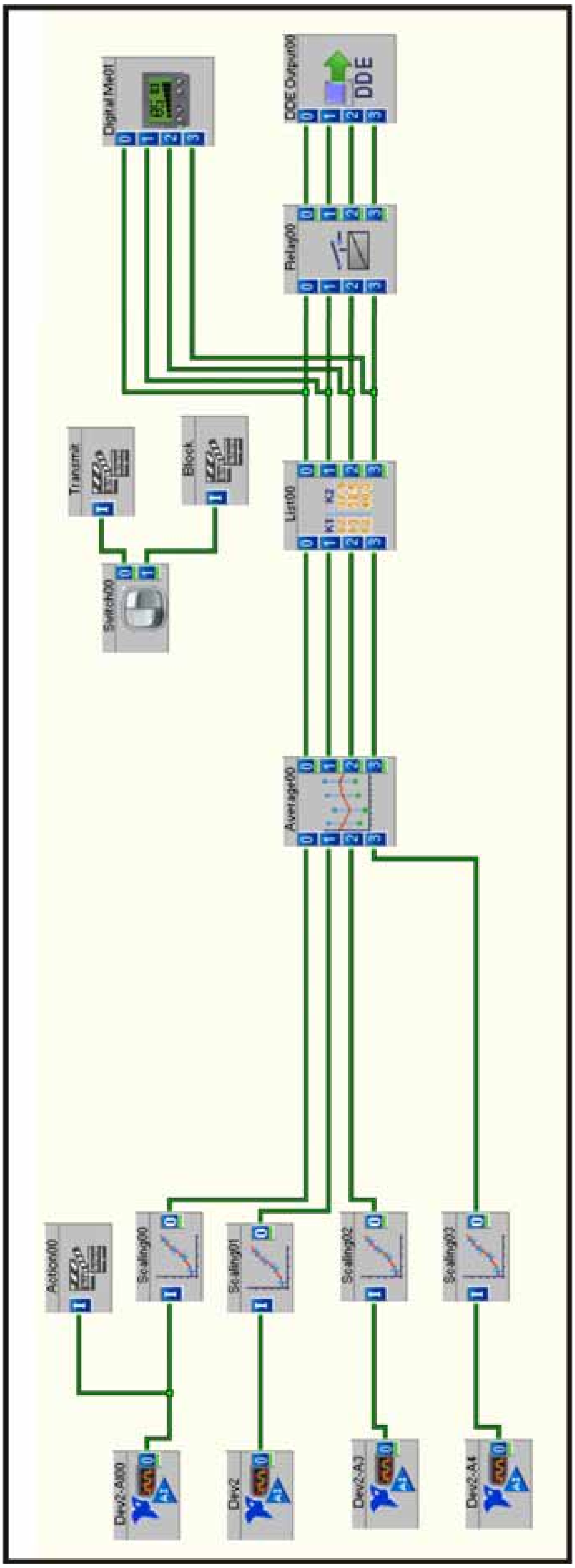

Figure A-6: Circuit diagram configured in Daisylab 6.0 for acquiring and logging of strain data.

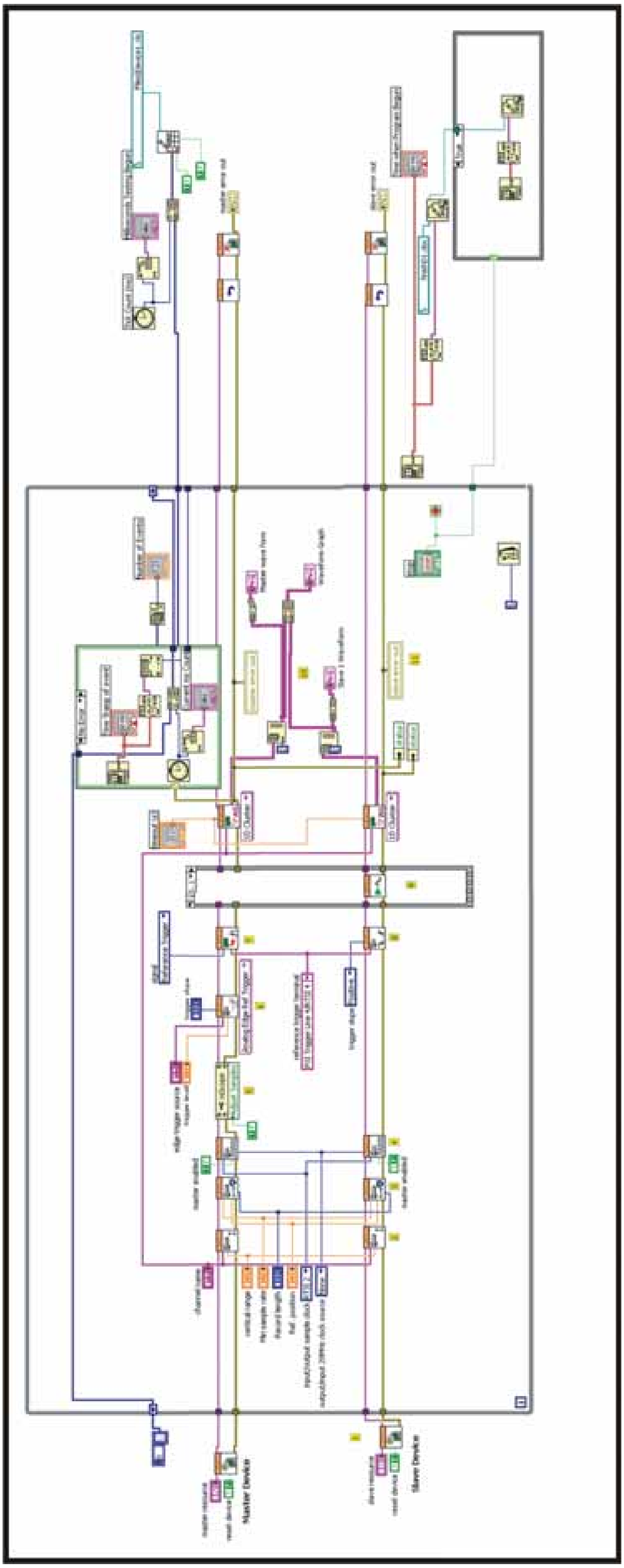

Figure A-7: Circuit diagram of the Acoustic Emission (AE) monitoring setup configured in Labview 8.0.

APPENDIX B

FISH ALGORITHMS

Appendix B summarises all the FISH algorithms used in the present research. The FISH algorithms are presented as;

B1 FISH algorithms for PFC3D

FISH algorithms for PFC3D were extracted from User's Guide of PFC3D manual (Itasca 2005) and modified as per requirements. These algorithms were used for numerical simulation of uniaxial, triaxial, Brazilian tensile and shear box tests in 3D. The algorithms were also used for parametric sensitivity studies by changing definite variables. In all the algorithms, embedded notes specify the variables that were modified for parametric sensitivity studies.

B2 FISH algorithms for PFC2D

FISH algorithms for PFC2D were written for micromechanical investigations conducted as part of the present research. These algorithms were used for numerical simulations of 2 ball and 3 ball tests. The algorithms were also used for parametric sensitivity studies by changing definite variables highlighted in the embedded notes.

The detail of the FISH algorithms both for PFC3D and PFC2D are given below.

Appendix B1
FISH ALGORITHMS FOR PFC3D

B1A. FISH ALORITHMS FOR UNIAXIAL & TRIAXIAL TESTS

B1B. FISH ALORITHMS FOR BRAZILIAN TENSILE TESTS

B1C. FISH ALORITHMS FOR SHEAR BOX TESTS

B1D. FISH ALORITHMS FOR CRACK TRACING

Appendix B1 (FISH Alogrithms for PFC3D)

B1A. FISH ALORITHMS FOR UNIAXIAL & TRIAXIAL TESTS

B1B. FISH ALORITHMS FOR BRAZILIAN TENSILE TESTS

B1C. FISH ALORITHMS FOR SHEAR BOX TESTS

B1D. FISH ALORITHMS FOR CRACK TRACING

```
=========================================================
        B1A UNIAXIAL AND TRIAXIAL TESTING
=========================================================
;===============================================================================
; STEP-1 CREATION AND PACKING OF PARTICLES
;===============================================================================
; Refer to User's Guide of PFC3D manual (Itasca 2005)
; M_UCS_1.DAT
new
SET random   ; reset random-number generator
;===============================================================================
def make_walls  ; create walls: a cylinder and two rectangular at top and bottom
  extend = 0.1
  rad_cy = 0.5*width
  w_stiff= 1.4e8
  _z0 = -extend
  _z1 = height*(1.0 + extend)
  command
    wall type cylinder id=1 kn=w_stiff end1 0.0 0.0 _z0 end2 0.0 0.0 _z1 &
    rad rad_cy rad_cy ; cylindrical wall
  end_command

  _x0 = -rad_cy*(1.0 + extend)
  _y0 = -rad_cy*(1.0 + extend)
  _z0 = 0.0
  _x1 =  rad_cy*(1.0 + extend)
  _y1 = -rad_cy*(1.0 + extend)
  _z1 = 0.0
  _x2 =  rad_cy*(1.0 + extend)
  _y2 =  rad_cy*(1.0 + extend)
  _z2 = 0.0
  _x3 = -rad_cy*(1.0 + extend)
  _y3 =  rad_cy*(1.0 + extend)
  _z3 = 0.0
  command
    wall id=5 kn=w_stiff face (_x0,_y0,_z0) (_x1,_y1,_z1) (_x2,_y2,_z2) &
     (_x3,_y3,_z3) ; bottom wall
  end_command

  _x0 = -rad_cy*(1.0 + extend)
  _y0 = -rad_cy*(1.0 + extend)
  _z0 = height
  _x1 = -rad_cy*(1.0 + extend)
  _y1 =  rad_cy*(1.0 + extend)
  _z1 = height
  _x2 =  rad_cy*(1.0 + extend)
  _y2 =  rad_cy*(1.0 + extend)
  _z2 = height
  _x3 =  rad_cy*(1.0 + extend)
  _y3 = -rad_cy*(1.0 + extend)
  _z3 = height
  command
    wall id=6 kn=w_stiff face (_x0,_y0,_z0) (_x1,_y1,_z1) (_x2,_y2,_z2) &
     (_x3,_y3,_z3) ; bottom wall
  end_command
end
;===============================================================================
def assemble  ; assemble sample
  s_stiff=0.0 ; initial stiffnesses
  n_stiff=1.4e8
  tot_vol = height * pi * rad_cy^2.0

  rbar    = 0.5 * (rlo + rhi); average radius
  num     = int((1.0 - poros) * tot_vol / (4.0 / 3.0 * pi * rbar^3))

  mult    = 2.9  ; initial radius multiplication factor
  rlo_0   = rlo / mult
```

```
  rhi_0   = rhi / mult
  ;
   command
    gen id=1,num rad=rlo_0,rhi_0 x=-0.047,0.047 y=-0.047,0.047 z=0.0,height hertz &
    filter ff_cylinder   ; Hertzian contact model was invoked
    prop dens=7800 shear 74.5e9 poiss 0.313 ; properties of steel balls
  end_command
;=====================================================================================
;NOTE:  Particle properties i.e. shear & poiss were varied as per type of material
;       i.e. steel, granite and sandstone in uniaxial and triaxial tests in
;       sensitivity study of particle material.
;=====================================================================================

  ii = out(string(num)+' particles were created')
  sum = 0.0 ; get actual porosity
  bp  = ball_head
  loop while bp # null
    sum = sum + 4.0 / 3.0 * pi * b_rad(bp)^3
    bp  = b_next(bp)
  end_loop
  pmeas = 1.0 - sum / tot_vol
  mult = ((1.0 - poros) / (1.0 - pmeas))^(1.0/3.0)
  command
    ini rad mul mult ; to get targeted radii of the balls
    cycle 10000
    hist diag muf
    prop fric 0.0963 ; friction of steel balls
    cycle 20000
  end_command
end
;=====================================================================================
def cws ;  change lateral wall stiffnesses to incorporate the effect of membrane of
;           Hoek Cell
  command
  range name sample cylinder end1 0 0 0 end2 0 0 0.2 radius 0.047
  range name extra_balls sample not
  delete ball range extra_balls ; remove extra ball created outside the walls
    wall type cylinder id 1 kn=w_stiff
  end_command
end
;=====================================================================================
def ff_cylinder ; filter to create the particles within a cylindrical region
  ff_cylinder = 0
  _brad = fc_arg(0)
  _bx   = fc_arg(1)
  _by   = fc_arg(2)
  _bz   = fc_arg(3)
  _rad  = sqrt(_bx^2 + _by^2)
  if _rad + _brad > rad_cy then
    ff_cylinder = 1
  end_if
end
;=====================================================================================
macro zero 'ini xvel 0 yvel 0 zvel 0 xspin 0 yspin 0 zspin 0'
 SET height=0.188 width=0.094 rlo=0.002375 rhi=0.002375 poros=0.397
;=====================================================================================
;NOTE:  In particle sensitivity study, variables rlo & rhi were modified to required
        radii such that the ratio rhi/rlo is always 1.0 (for uniform size
;       distribution). However, in particle size distribution sensitivity the ratio
;       rhi/rlo was set to 1.25 and 1.50.
;
;       In scaling studies, variables width and height were modified to required
;       dimensions of the specimen.
;=====================================================================================

make_walls
assemble
hist diag muf
plot create assembly
plot set cap size 25
plot set mag 20
plot set rot 30 0 40
plot add ball red wall white
plot show
set grav 0 0 -9.81
cyc 450000 ; Gravity induced packing as per physical experiments
SET w_stiff= 1.4e7 ;
cws
cyc 8000
zero
save M_UCS_1.sav ; creation and packing of specimen is complete
;=====================================================================================
; STEP-2 COMPUTING AND CONTROLLING STRESS STATE BY SERVO CONTROL: INITIAL STRESS STATE
;=====================================================================================
res M_UCS_1.sav ; restore packed assembly of particle
;=====================================================================================
prop fric=4.7; corresponding to assembly friction angle of 37.3°.
```

```
prop pb_kn=6.69e11 pb_ks=6.69e11 pb_rad=1.0
prop pb_nstren=1.5e6 pb_sstren=4.0e6
;=====================================================================================
;NOTE: Installing parallel bonds by specifying micro parameters. This step is
;      consistent with the physical experiments.
;
;      Parallel bond stiffnesses i.e. pb_kn & pb_ks and strengths
;      i.e. pb_nstren & pb_sstren are corresponding to Portland cement here
;      and were changed corresponding to argillaceous and
;      arrenaceous cements in interparticle cement sensitivity study.
;
;      In particle sensitivity studies, the stiffness of the parallel bonds were
;      changed corresponding to radii of the particles.
;=====================================================================================

def get_ss ; determine average stress and strain at walls
  new_rad = w_radend1(wadd1)
  rdif  = new_rad - rad_cy
  zdif  = w_z(wadd6) - w_z(wadd5)
  new_height = height + zdif
  wsrr  = -w_radfob(wadd1) / (new_height * 2.0 * pi * new_rad)
  wszz  = 0.5*(w_zfob(wadd5) - w_zfob(wadd6)) / (pi * new_rad^2.0)
  werr  = 2.0 * rdif / (rad_cy + new_rad)
  wezz  = 2.0 * zdif / (height + new_height)
  wevol = wezz + 2.0 * werr
end
;=====================================================================================
def get_gain  ; determine servo gain parameters for axial and lateral motion
  alpha = 0.5 ; relaxation factor
  count = 0
  avg_stiff = 0
  cp    = contact_head  ; find avg. number of contacts on lateral walls
  loop while cp # null
    if c_gobj2(cp) = wadd1
      count = count + 1
      avg_stiff = avg_stiff + c_kn(cp)
    end_if
    cp = c_next(cp)
  end_loop
  avg_stiff = avg_stiff / count
  gr = alpha * height * pi * rad_cy * 2.0 / (avg_stiff * count * tdel)
  count = 0
  avg_stiff = 0
  cp = contact_head      ; find avg. number of contacts on top/bottom walls
  loop while cp # null
    if c_gobj2(cp) = wadd5
      count = count + 1
      avg_stiff = avg_stiff + c_kn(cp)
    end_if
    if c_gobj2(cp) = wadd6
      count = count + 1
      avg_stiff = avg_stiff + c_kn(cp)
    end_if
    cp = c_next(cp)
  end_loop
  ncount = count / 2.0
  avg_stiff = avg_stiff / count
  gz = alpha * pi * rad_cy^2.0/ (avg_stiff * ncount * tdel)
end
;=====================================================================================
def servo
  while_stepping
  get_ss                 ; compute stresses & strains
  udr = gr * (wsrr - srrreq)
  w_radvel(wadd1) = -udr
  if z_servo = 1         ; switch stress servo on or off
    udz = gz  * (wszz - szzreq)
    w_zvel(wadd5) = udz
    w_zvel(wadd6) = -udz
  end_if
end
;=====================================================================================
def iterate
  loop while 1 # 0
    get_gain
    if abs((wsrr - srrreq)/srrreq) < sig_tol then
      if abs((wszz - szzreq)/szzreq) < sig_tol then
        exit
      end_if
    end_if
    command
      cycle 100
    end_command
  end_loop
end
;=====================================================================================
def wall_addr
```

```
  wadd1 = find_wall(1)
  wadd5 = find_wall(5)
  wadd6 = find_wall(6)
end
wall_addr
zero
 SET srrreq=-1e5 szzreq=-1e5 sig_tol=0.005 z_servo=1
;=====================================================================================
;NOTE: Triaxial testing was done by putting the variables srrreq &
;       szzreq values equal to required confining pressure i.e. 2.5 -
;       10 MPa
;=====================================================================================
iterate  ; get all stresses to requested state
sav M_UCS_2.sav
;=====================================================================================
; STEP-3 PREPARATION FOR UPCOMING TESTS
;=====================================================================================
res M_UCS_2.sav
;=====================================================================================
def set_ini ; set initial strains
  wezz_0  = wezz
  wevol_0 = wevol
   werr_0 = werr
end
;=====================================================================================
def conf                      ; variables for histories
  axlst = wszz                ; Axial stress
  devi  = wszz - wsrr         ; deviatoric stress
  deax  = wezz - wezz_0       ; axial strain
  devol = wevol - wevol_0     ; volumetric strain
  conf  = wsrr                ; confining stress
  rstrn = werr - werr_0      ; Radial Strain
end
;=====================================================================================
def accel_platens
; ----- Accelerates the platens to achieve vel of _vfinal in _nsteps,
;       using _nchunks
  _niter = _nsteps / _nchunks
  loop _chnk (1,_nchunks)
    if _close = 1 then
      _vel = _chnk*(_vfinal/_nchunks)
    else
      _vel = -_chnk*(_vfinal/_nchunks)
    end_if
    _mvel = -_vel
    command
      wall id 5 zvel= _vel
      wall id 6 zvel= _mvel
      cycle _niter
    end_command
  end_loop
end
;=====================================================================================
Call crk.FIS ;  algorithm to monitor and record crack development in the
;               sample, given in FISH TANK.
;=====================================================================================
set_ini
history id=3 axlst
history id=4 conf
history id=5 devi
history id=6 deax
history id=7 devol
history id=8 rstrn
history id=9 wezz
history id=10 crk_num
history id=11 crk_num_pnf ;crack formed due to tensile failure of
;                          parallel bond
history id=12 crk_num_psf ;crack formed due to shear failure of
;                          parallel bond
;=====================================================================================

SET hist_rep=500; recording of history variables after 500 steps
SET z_servo=0
Zero
;=====================================================================================
; Separation of specimen into discrete colour layers
property c_index 1 range x -0.095 0.095 y -0.095 0.095 z 0.000 0.031
property c_index 2 range x -0.095 0.095 y -0.095 0.095 z 0.031 0.062
property c_index 3 range x -0.095 0.095 y -0.095 0.095 z 0.062 0.093
property c_index 4 range x -0.095 0.095 y -0.095 0.095 z 0.093 0.124
property c_index 5 range x -0.095 0.095 y -0.095 0.095 z 0.124 0.155
property c_index 6 range x -0.095 0.095 y -0.095 0.095 z 0.155 0.188
;=====================================================================================
plot add ball red blue green yellow lblue lgreen
plot set background white
plot set foreground black
plot set mag 1.5
```

```
plot set center 0 1.023e-2 5.802e-2
plot set rot 10 0 0
plot show
;=====================================================================================
sav M_UCS_3.SAV ; ready for testing.
;=====================================================================================
; STEP-4 UNIAXIAL AND TRIAXIAL TESTING
;=====================================================================================
res M_UCS_3.SAV

set _vfinal= 1e-3  _nsteps= 800  _nchunks= 30; velocity of top and bottom walls
;=====================================================================================
;NOTE: In loading rate sensitivity study and in scaling, variable -vfinal was varied
;      as per requirements.
;=====================================================================================
set plot avi size 640 480 ; to make a movie of the model of required resolution
movie avi_open file movie_ M_UCS_4.avi
movie step 1000 1 file movie_ M_UCS_4.avi
;=====================================================================================
set _close= 1  ; load
;=====================================================================================
; call of crack tracking functions
crk_init
crk_chk_crkdata
crk_makeview
_crk_formpb
_crk_num_mark
_crk_draw3d_polygon
;=====================================================================================
accel_platens ; start of test.
;=====================================================================================
cyc 48000
save M_UCS_4ci.SAV           ; crack initiation stage
cyc 16000
save M_UCS_4rancrk.SAV       ; random crack growth stage
cyc 17000
save M_UCS_4cd.SAV           ; crack damage stage
cyc 20000
save M_UCS_4syscrk.SAV       ; systematic crack growth stage
cyc 20000
save M_UCS_4peak.SAV         ; peak failure stage
cyc 10000
save M_UCS_4psp.SAV          ; post peak stage 1
cyc 127000
save M_UCS_4psp2.SAV         ; post peak stage 2
cyc 292000
;=====================================================================================
;NOTE: The specified cycles are for uniaxial test corresponding to given loading
;      (displacement rate). These were modified in triaxial testing and in load
;      sensitivity studies.
;=====================================================================================
movie avi_close file movie_ M_UCS_4.avi
hist  write -4 vs -6 file M_UCS_4axl
hist  write -5 vs -6 file M_UCS_4devi
hist  write 10 11 12 vs -6 file M_UCS_4crk
hist  write 8 vs -6 file M_UCS_4anrs
;=====================================================================================
;NOTE: stresses, strains and cracks were saved as separate history variable for
;      subsequent analyses.
;=====================================================================================
save M_UCS_4.SAV
return ; test complete.
```

```
==================================================================
                B1B. BRAZILIAN TENSILE TESTING
==================================================================
```

```
; STEP-1 CREATION AND PACKING OF PARTICLES
; Refer to User's Guide of PFC3D manual (Itasca 2005) for detailed description
; M_BZ_1.DAT
new
SET random   ; reset random-number generator
;==============================================================================
def make_walls  ; create walls: a cylinder and two rectangular at top and bottom
  extend = 0.1
  rad_cy = 0.5*width
  w_stiff= 1.4e8

  _z0 = -extend
  _z1 = height*(1.0 + extend)
  command
    wall type cylinder id=1 kn=w_stiff end1 0.0 0.0 _z0 end2 0.0 0.0 _z1 &
    rad rad_cy rad_cy ; cylindrical wall
  end_command
  _x0 = -rad_cy*(1.0 + extend)
  _y0 = -rad_cy*(1.0 + extend)
  _z0 = 0.0
  _x1 =  rad_cy*(1.0 + extend)
  _y1 = -rad_cy*(1.0 + extend)
  _z1 = 0.0
  _x2 =  rad_cy*(1.0 + extend)
  _y2 =  rad_cy*(1.0 + extend)
  _z2 = 0.0
  _x3 = -rad_cy*(1.0 + extend)
  _y3 =  rad_cy*(1.0 + extend)
  _z3 = 0.0
  command
    wall id=5 kn=w_stiff face (_x0,_y0,_z0) (_x1,_y1,_z1) (_x2,_y2,_z2) &
    (_x3,_y3,_z3) ; bottom wall
  end_command

  _x0 = -rad_cy*(1.0 + extend)
  _y0 = -rad_cy*(1.0 + extend)
  _z0 = height
  _x1 = -rad_cy*(1.0 + extend)
  _y1 =  rad_cy*(1.0 + extend)
  _z1 = height
  _x2 =  rad_cy*(1.0 + extend)
  _y2 =  rad_cy*(1.0 + extend)
  _z2 = height
  _x3 =  rad_cy*(1.0 + extend)
  _y3 = -rad_cy*(1.0 + extend)
  _z3 = height
  command
    wall id=6 kn=w_stiff face (_x0,_y0,_z0) (_x1,_y1,_z1) (_x2,_y2,_z2) &
     (_x3,_y3,_z3) ; top wall
  end_command
end
;===============================================================================
def assemble  ; assemble sample
  s_stiff=0.0 ; initial stiffnesses
  n_stiff=1.4e8
  tot_vol = height * pi * rad_cy^2.0
  rbar    = 0.5 * (rlo + rhi)
  num     = int((1.0 - poros) * tot_vol / (4.0 / 3.0 * pi * rbar^3))
  mult    = 2.9  ; initial radius multiplication factor
  rlo_0   = rlo / mult
  rhi_0   = rhi / mult
  command
    gen id=1,num rad=rlo_0,rhi_0 x=-0.047,0.047 y=-0.047,0.047 z=0.0,height hertz &
     filter ff_cylinder
    prop dens=7800 shear 74.5e9 poiss 0.313
  end_command
;===============================================================================
;NOTE:  Particle properties i.e. shear & poiss were varied as per type of material
;       i.e. steel, granite and sandstone in sensitivity study of particle material.
;===============================================================================
  ii = out(string(num)+' particles were created')
  sum = 0.0 ; get actual porosity
  bp  = ball_head
  loop while bp # null
    sum = sum + 4.0 / 3.0 * pi * b_rad(bp)^3
    bp  = b_next(bp)
  end_loop
  pmeas = 1.0 - sum / tot_vol
  mult = ((1.0 - poros) / (1.0 - pmeas))^(1.0/3.0)
  command
    ini rad mul mult
```

```
    cycle 10000
    hist diag muf
    prop fric 0.0963
    cycle 20000
  end_command
end
;=====================================================================================
def ff_cylinder ; filter to create the particles within a cylindrical region
  ff_cylinder = 0
  _brad = fc_arg(0)
  _bx   = fc_arg(1)
  _by   = fc_arg(2)
  _bz   = fc_arg(3)
  _rad  = sqrt(_bx^2 + _by^2)
  if _rad + _brad > rad_cy then
    ff_cylinder = 1
  end_if
end
;=====================================================================================
macro zero 'ini xvel 0 yvel 0 zvel 0 xspin 0 yspin 0 zspin 0'
 SET height=0.047 width=0.094 rlo=0.002375 rhi=0.002375 poros=0.397
;=====================================================================================
;NOTE:  In particle sensitivity study, variables rlo & rhi were modified to required
        radii such that the ratio rhi/rlo is always 1.0 (for uniform size
;       distribution). However in particle size distribution sensitivity, the ratio
;       rhi/rlo was set to 1.25 and 1.50.
;=====================================================================================
make_walls
assemble
hist diag muf
plot create assembly
plot set cap size 25
plot set mag 1.5
plot set rot 30 0 40
plot add ball red wall white
plot show
set grav 0 0 -9.81
cyc 450000 ; Gravity induced packing as per physical experiments
zero
save M_BZ_1.sav ; creation and packing of specimen is complete
;=====================================================================================
; STEP-2 COMPUTING AND CONTROLLING STRESS STATE BY SERVO CONTROL: INITIAL STRESS STATE
;=====================================================================================
res M_BZ_1.sav ; restore packed assembly of particle
;=====================================================================================
prop fric=4.7; corresponding to assembly friction angle of 37.3°.
prop pb_kn=6.69e11 pb_ks=6.69e11 pb_rad=1.0
prop pb_nstren=1.5e6 pb_sstren=4.0e6
;=====================================================================================
;NOTE: Installing parallel bonds by specifying micro parameters. This step is
;       consistent with the physical experiments.
;
;       Parallel bond stiffnesses i.e. pb_kn & pb_ks and strengths
;       i.e. pb_nstren & pb_sstren are corresponding to Portland cement here
;       and were changed corresponding to argillaceous and
;       arrenaceous cements in interparticle cement sensitivity study.
;
;       In particle sensitivity studies, the stiffness of the parallel bonds were
;       changed corresponding to radii of the particles.
;=====================================================================================

def get_ss ; determine average stress and strain at walls
  new_rad = w_radend1(wadd1)
  rdif  = new_rad - rad_cy
  zdif  = w_z(wadd6) - w_z(wadd5)
  new_height = height + zdif
  wsrr  = -w_radfob(wadd1) / (new_height * 2.0 * pi * new_rad)
  wszz  = 0.5*(w_zfob(wadd5) - w_zfob(wadd6)) / (pi * new_rad^2.0)
  werr  = 2.0 * rdif / (rad_cy + new_rad)
  wezz  = 2.0 * zdif / (height + new_height)
  wevol = wezz + 2.0 * werr
end
;=====================================================================================
def get_gain ; determine servo gain parameters for axial and lateral motion
  alpha = 0.5 ; relaxation factor
  count = 0
  avg_stiff = 0
  cp    = contact_head  ; find avg. number of contacts on lateral walls
  loop while cp # null
    if c_gobj2(cp) = wadd1
      count = count + 1
      avg_stiff = avg_stiff + c_kn(cp)
    end_if
    cp = c_next(cp)
  end_loop
  avg_stiff = avg_stiff / count
  gr = alpha * height * pi * rad_cy * 2.0 / (avg_stiff * count * tdel)
```

```
  count = 0
  avg_stiff = 0
  cp = contact_head      ; find avg. number of contacts on top/bottom walls
  loop while cp # null
    if c_gobj2(cp) = wadd5
      count = count + 1
      avg_stiff = avg_stiff + c_kn(cp)
    end_if
    if c_gobj2(cp) = wadd6
      count = count + 1
      avg_stiff = avg_stiff + c_kn(cp)
    end_if
    cp = c_next(cp)
  end_loop
  ncount = count / 2.0
  avg_stiff = avg_stiff / count
  gz = alpha * pi * rad_cy^2.0/ (avg_stiff * ncount * tdel)
end
;=====================================================================================
def servo
  while_stepping
  get_ss                 ; compute stresses & strains
  if r_servo = 1
    udr = gr * (wsrr - srrreq)
    w_radvel(wadd1) = -udr
   else
   exit
  end_if
;
  if z_servo = 1         ; switch stress servo on or off
    udz = gz  * (wszz - szzreq)
    w_zvel(wadd5) = udz
    w_zvel(wadd6) = -udz
   else
   exist
  end_if
end
;=====================================================================================
def iterate
  loop while 1 # 0
    get_gain
    if abs((wsrr - srrreq)/srrreq) < sig_tol then
      if abs((wszz - szzreq)/szzreq) < sig_tol then
        exit
      end_if
    end_if
    command
      cycle 100
    end_command
  end_loop
end
;=====================================================================================
def wall_addr
  wadd1 = find_wall(1)
  wadd5 = find_wall(5)
  wadd6 = find_wall(6)
end
wall_addr
zero
 SET srrreq=-1e5 szzreq=-1e5 sig_tol=0.005 z_servo=1 r_servo=1
; to get same initial stress condition on Brazilian disc
;=====================================================================================
iterate  ; get all stresses to requested state
sav M_BZ_2.sav
;=====================================================================================
; STEP-3 PREPARATION FOR UPCOMING TESTS
;=====================================================================================
res M_BZ_2.sav

set z_servo=0
delete wall 5 6 ;delete top and bottom walls after compacting the assembly.
;=====================================================================================
def make_xwalls  ; create walls for Brazilian Testing in YZ planes normal to X-axis.
  extend = 0.1
  n_hthk = 0.5*thick
  w_stiff= 1.4e8
  _x0 = n_hthk*(1.0 + extend)
  _y0 = -n_hthk*(1.0 + extend)
  _z0 = -extend
  _x1 =  n_hthk*(1.0 + extend)
  _y1 = -n_hthk*(1.0 + extend)
  _z1 = thick*(1.0 + extend)
  _x2 =  n_hthk*(1.0 + extend)
  _y2 =  n_hthk*(1.0 + extend)
  _z2 = thick*(1.0 + extend)
  _x3 =  n_hthk*(1.0 + extend)
  _y3 =  n_hthk*(1.0 + extend)
```

```
  _z3 = -extend
  command
    wall id=7 kn=w_stiff face (_x0,_y0,_z0) (_x1,_y1,_z1) (_x2,_y2,_z2) &
    (_x3,_y3,_z3) ;(positve x-axis - right hand wall)
  end_command

  _x0 = -n_hthk*(1.0 + extend)
  _y0 = -n_hthk*(1.0 + extend)
  _z0 = -extend
  _x1 = -n_hthk*(1.0 + extend)
  _y1 =  n_hthk*(1.0 + extend)
  _z1 = -extend
  _x2 =  -n_hthk*(1.0 + extend)
  _y2 =  n_hthk*(1.0 + extend)
  _z2 = thick*(1.0 + extend)
  _x3 = -n_hthk*(1.0 + extend)
  _y3 = -n_hthk*(1.0 + extend)
  _z3 = thick*(1.0 + extend)
  command
    wall id=8 kn=w_stiff face (_x0,_y0,_z0) (_x1,_y1,_z1) (_x2,_y2,_z2) &
    (_x3,_y3,_z3) ;(Negative x-axis - left hand wall)
  end_command
end
set thick 9.4504e-2; diameter of the specimen
make_xwalls
;=================================================================================
def get_forces ; determine average force and strain at x walls
  xdif  = w_x(wadd7) - w_x(wadd8); difference between x walls
  new_thick = thick + xdif
  wfxx  = 0.5*(w_xfob(wadd8) - w_xfob(wadd7)); axial force on x walls
  wexx  = 2.0 * xdif / (thick + new_thick)
end
;=================================================================================
def set_ini ; set initial strains
  wexx_0  = wexx
   end
;=================================================================================
def deax                      ; variables for histories
  axlfr = wfxx                ; axial force on x walls
  deax  = wexx - wexx_0       ; axial strain
 end
;=================================================================================
def accel_platens
; ----- Accelerates the platens to achieve vel of _vfinal in _nsteps,
;       using _nchunks
  _niter = _nsteps / _nchunks
  loop _chnk (1,_nchunks)
    if _close = 1 then
      _vel = _chnk*(_vfinal/_nchunks)
    else
      _vel = -_chnk*(_vfinal/_nchunks)
    end_if
    _mvel = -_vel
   if p_isvt=1 then ; to remove the cover of radial wall for Brazilian test
     w_radvel(wadd1) = 100*_vel
      command
       cycle _niter
      end_command
  else
   command
     wall id 8 xvel= @_vel
     wall id 7 xvel= @_mvel
     cycle _niter
    end_command
  end_if
 end_loop
end
;=================================================================================
Call crk.FIS ;  algorithm to monitor and record crack development in the
;               sample, given in FISH TANK.
;=================================================================================
def servo_x ; servo to compute the axial forces and strain during Brazilian test.
   while_stepping
   if x_servo = 1             ; switch stress servo on or off
    get_forces                ; compute forces & strains
   end_if
end
;=================================================================================
def wall_2addr                ; addresses of the x walls
  wadd7 = find_wall(7)
  wadd8 = find_wall(8)
end
;=================================================================================
wall_2addr
set_ini
deax
;=================================================================================
```

```
history id=3 wfxx
history id=4 deax
history id=5 wexx
history id=6 crk_num
history id=7 crk_num_pnf ;crack formed due to tensile failure of
;                          parallel bond

history id=8 crk_num_psf ;crack formed due to shear failure of
;                          parallel bond
;=====================================================================================
SET hist_rep=10; recording of history variables after 10 steps
Set r_servo=0
Set x_servo=0
;=====================================================================================
Zero
;=====================================================================================
plot add ball red
plot set background white
plot set foreground black
plot set mag 1.5
plot set cen 0 1.023e-2 5.802e-2
plot set rot 90 0 180
plot show
;=====================================================================================
sav M_BZ_3.SAV ; ready for testing.
;=====================================================================================
; STEP-4 BRAZILIAN TENSILE TESTING
;=====================================================================================
res M_BZ_3.SAV

set _vfinal= 1.0 _nsteps= 500  _nchunks= 50 ; velocity to remove radial wall
set x_servo=1
set _close=1
set p_isvt=1
;=====================================================================================
accel_platens; removal of radial wall
;=====================================================================================
; calling crack tracking functions
crk_init
crk_chk_crkdata
crk_makeview
_crk_formpb
_crk_num_mark
_crk_draw3d_polygon
;=====================================================================================
Plot create 5
plot hist -3 vs -4
plot set rot 90 0 90
plot add wall black
plot add ball red
plot add cforce yellow
plot add pbond cyan
plot set background white
plot set foreground black
plot add fish crk_item black blue
plot set mag 1.5
plot set cent 0 1.023e-2 5.802e-2
plot show
;=====================================================================================
cyc 2000
save M_BZ_4_rr.SAV
;=====================================================================================
set x_servo=1
set _close=1  ; load
set p_isvt=0
;=====================================================================================
accel_platens; to get x walls in contact with the specimen.
cyc 5500
save M_BZ_4tr.SAV
set_ini
deax
;=====================================================================================
set _vfinal= 5.0e-3 _nsteps= 500  _nchunks= 50; displacement rate to perform the test
set x_servo=1
set _close=1  ; load
set p_isvt=0
;=====================================================================================
;NOTE: In loading rate sensitivity study, variable “-vfinal” was varied
;      as per required loading rate.
;=====================================================================================
set plot avi size 640 480; to make movie of the test
movie avi_open file movie_M_BZ_4.avi
movie step 100 1 file movie_M_BZ_4.avi
;=====================================================================================
accel_platens
cyc 500000
save M_BZ_4a.SAV
```

```
cyc 500000
save M_BZ_4b.SAV
cyc 500000
;==================================================================================
;NOTE: The specified cycles are corresponding to displacement rate of 5e-3m/s. These
;      were modified in load sensitivity study, and in particle and interparticle
       cementing material sensitivity studies.
;==================================================================================
movie avi_close file movie_M_BZ_4.avi
hist  write -3 vs -4 file M_BZ_4axl
hist  write 6 7 8 vs -4 file M_BZ_4crk
hist  write 6 vs -3 file M_BZ_4fc-crk
save M_BZ_4.SAV
return ; test complete.
```

===
B1C. SHEAR BOX TESTING
===

```
; STEP-1 CREATION AND PACKING OF PARTICLES
; Refer to User's Guide of PFC3D manual (Itasca 2005) for detailed description
; M_SB_1.DAT
new
SET random   ; reset random-number generator
;==================================================================================
; making a shear box with two halves; top and bottom each of bounded by five
; frictionless walls.
;
wall id=1 face (0,0,0) (0,0,0.0175) (0.1,0,0.0175) (0.1,0,0)
wall id=2 face (0,0,0.0185,) (0,0,0.036) (0.1,0,0.036) (0.1,0,0.0185)
wall id=3 face (0.1,0,0) (0.1,0,0.0175) (0.1,0.1,0.0175) (0.1,0.1,0)
wall id=4 face (0.1,0,0.0185) (0.1,0,0.036) (0.1,0.1,0.036) (0.1,0.1,0.0185)
wall id=5 face (0.1,0.1,0) (0.1,0.1,0.0175) (0,0.1,0.0175) (0,0.1,0)
wall id=6 face (0.1,0.1,0.0185) (0.1,0.1,0.036) (0,0.1,0.036) (0,0.1,0.0185)
wall id=7 face (0,0.1,0) (0,0.1,0.0175) (0,0,0.0175) (0,0,0)
wall id=8 face (0,0.1,0.0185) (0,0.1,0.036) (0,0,0.036) (0,0,0.0185)
wall id=9 face (0,0,0) (0.1,0,0) (0.1,0.1,0) (0,0.1,0)
wall id=10 face (0,0,0.036) (0,0.1,0.036) (0.1,0.1,0.036) (0.1,0,0.036)
;
wall id=1 kn=1.4e8 ks=1.4e8 f 0.01
wall id=2 kn=1.4e8 ks=1.4e8 f 0.01
wall id=3 kn=1.4e8 ks=1.4e8 f 0.01
wall id=4 kn=1.4e8 ks=1.4e8 f 0.01
wall id=5 kn=1.4e8 ks=1.4e8 f 0.01
wall id=6 kn=1.4e8 ks=1.4e8 f 0.01
wall id=7 kn=1.4e8 ks=1.4e8 f 0.01
wall id=8 kn=1.4e8 ks=1.4e8 f 0.01
wall id=9 kn=1.4e8 ks=1.4e8 f 0.01
wall id=10 kn=1.4e8 ks=1.4e8 f 0.01
;==================================================================================
def assemble  ; assemble sample
   s_stiff=0.0 ; initial stiffnesses
   n_stiff=1.4e8
   tot_vol = 0.036 * 0.1 * 0.1; dimensions of shear box specimen
   rbar    = 0.5 * (rlo + rhi)
   num     = int((1.0 - poros) * tot_vol / (4.0 / 3.0 * pi * rbar^3))
   mult    = 2.9  ; initial radius multiplication factor
   rlo_0   = rlo / mult
   rhi_0   = rhi / mult
;
command
    gen id=1,num rad=rlo_0,rhi_0 x=0.0 0.1 y=0.0 0.1 z=0.0,0.036 hertz
    prop dens=7800 shear 74.5e9 poiss 0.313
end_command
;
   ii = out(string(num)+' particles were created')
   sum = 0.0 ; get actual porosity
   bp  = ball_head
  loop while bp # null
    sum = sum + 4.0 / 3.0 * pi * b_rad(bp)^3
    bp  = b_next(bp)
  end_loop
   pmeas = 1.0 - sum / tot_vol
   mult = ((1.0 - poros) / (1.0 - pmeas))^(1.0/3.0)
 command
    hist diag muf
    ini rad mul mult
    cycle 10000
    prop fric 0.0963
    cycle 20000
 end_command
end
;==================================================================================
macro zero 'ini xvel 0 yvel 0 zvel 0 xspin 0 yspin 0 zspin 0'

SET rlo=0.002375 rhi=0.002375 poros=0.397
;==================================================================================
assemble
set grav 0 0 -9.8
cyc 450000 ;gravity induced packing similar to uniaxial, triaxial & Brazilian specimens
zero
;==================================================================================
range name top x=0.0 0.1 y=0.0 0.1 z=0.018, 0.036 ;top box
range name bot x=0.0 0.1 y=0.0 0.1 z=0.0,0.018    ;bottom box
range name sample x=0.0 0.1 y=0.0 0.1 z=0.0,0.036
range name osiders sample not
delete ball range osiders                         ;deleting ball outside the walls.
;==================================================================================
plot create assembly
plot set cap size 25
```

```
plot set mag 1.25
plot set rot 30 0 40
plot add ball red range top
plot add ball blue range bot
plot add wall white
plot show
;
save M_SB_1.sav
;==================================================================================
; STEP-2 COMPUTING AND CONTROLLING STRESS STATE BY SERVO CONTROL: INITIAL STRESS STATE
;==================================================================================
res M_SB_1.sav
;==================================================================================
def get_ss ; determine average stresses and strains at walls
  x_not = w_x(wadd3)
  x_vble = w_x(wadd4)
  xdif  = x_not - x_vble              ; horizontal or shear displacement
  zdif  = w_z(wadd10) - w_z(wadd9)     ; vertical displacement i.e. dilation
  new_length = length - xdif
  new_height = height + zdif
  wsxx  = (w_xfob(wadd4)) / (0.5*height*width)                 ; shear stress
  wszz  = 0.5*(w_zfob(wadd9) - w_zfob(wadd10)) / (length*width) ; normal stress
  wexx  = 2.0 * xdif / (length + new_length)
  wezz  = 2.0 * zdif / (height + new_height)
  z_disp = zdif
  x_disp = xdif
  devi = wsxx - wszz
end
;==================================================================================
def get_gain                ; determine servo gain parameters for top and bottom walls
  alpha = 0.5               ; relaxation factor
  count = 0
  avg_stiff = 0
  cp = contact_head         ; find avg. number of contacts on bottom walls
  loop while cp # null
    if c_gobj2(cp) = wadd9
      count = count + 1
      avg_stiff = avg_stiff + c_kn(cp)
    end_if
;
    if c_gobj2(cp) = wadd10 ; find avg. number of contacts on top walls
      count = count + 1
      avg_stiff = avg_stiff + c_kn(cp)
    end_if
    cp = c_next(cp)
  end_loop
  ncount = count / 2.0
  avg_stiff = avg_stiff / count
  gz = alpha * length*width / (avg_stiff * ncount * tdel)
end
;==================================================================================
Call crk.FIS ; algorithm to monitor and record crack development in the
;              sample, given in FISH TANK.
;==================================================================================
def servo
  while_stepping
  get_ss                 ; compute stresses & strains

if abs((wszz - szzreq)/szzreq) < sig_tol then
    get_gain
end_if

if z_servo = 1           ; switch stress servo on or off
    udz = gz * 2 * (wszz - szzreq)
    w_zvel(wadd9) = udz ;BOTTOM BOX ;(ONLY BOTTOM BOX DILATING)
    w_zvel(wadd1) = udz ;BOTTOM BOX
    w_zvel(wadd3) = udz ;BOTTOM BOX
    w_zvel(wadd5) = udz ;BOTTOM BOX
    w_zvel(wadd7) = udz ;BOTTOM BOX
  end_if
end
;==================================================================================
def iterate
  loop while 1 # 0
    get_gain
      if abs((wszz - szzreq)/szzreq) < sig_tol then
      exit
      end_if
     command
       print wszz szzreq
       cycle 10
     end_command
  end_loop
end
;==================================================================================
def wall_addr
  wadd1 = find_wall(1)
```

```
  wadd2 = find_wall(2)
  wadd3 = find_wall(3)
  wadd4 = find_wall(4)
  wadd5 = find_wall(5)
  wadd6 = find_wall(6)
  wadd7 = find_wall(7)
  wadd8 = find_wall(8)
  wadd9 = find_wall(9)
  wadd10 = find_wall(10)
end
wall_addr
;=========================================================================
SET  length 0.1 width 0.1 height  0.036 szzreq=-1e5 sig_tol=0.003 z_servo=1
iterate  ; get all stresses to requested state
;=========================================================================
;NOTE: Shear box tests at various normal stresses were conducted by changing the
;       variable "szzreq" to required normal stresses i.e. 0.0-2.0MPa.
;=========================================================================
save M_SB_2.sav
;
;=========================================================================
; STEP-3 PREPARATION FOR UPCOMING TESTS
;=========================================================================
res M_UCS_2.sav
;
;=========================================================================
def accel_platens
; ----- Accelerates the platens to achieve vel of _vfinal in _nsteps,
;       using _nchunks
  _niter = _nsteps / _nchunks
  loop _chnk (1,_nchunks)
    if _close = 1 then
      _vel = _chnk*(_vfinal/_nchunks)
    else
      _vel = -_chnk*(_vfinal/_nchunks)
    end_if
    _mvel = -_vel
    command
      wall id 2 xvel= _mvel   ;top half of shear box to move in positive X direction.
      wall id 4 xvel= _mvel
      wall id 6 xvel= _mvel
      wall id 8 xvel= _mvel
      wall id 10 xvel= _mvel
      cycle _niter
    end_command
  end_loop
end
;=========================================================================
history id=3 z_disp
history id=4 wszz
history id=5 wsxx
history id=6 xdif
history id=7 wexx
history id=8 devi
history id=9 wezz
history id=10 crk_num
SET hist_rep=500
SET z_servo=1
zero
;=========================================================================
plot create 10
plot hist 5 -4 vs 6
plot add ball blue range top
plot add ball red range bot
plot add axes black
;=========================================================================
range name topp x=0.0 0.1 y=0.0 0.1 z=0.0185, 0.036
range name bott x=0.0 0.1 y=0.0 0.1 z=0.0,0.0175
;=========================================================================
prop fric=4.7 ;range topp
prop pb_kn=6.69e11 pb_ks=6.69e11 pb_rad=1.0 ;range topp
prop pb_nstren=1.5e6 pb_sstren=4.0e6 ;range topp

;=========================================================================
save M_SB_3.sav
;
;=========================================================================
; STEP-4 SHEAR BOX TESTING
;=========================================================================
res M_SB_3.SAV
;
set _vfinal= 1e-3  _nsteps= 800  _nchunks= 80; adopted shear displacement
;=========================================================================
;NOTE: In shear displacement rate sensitivity study, variable "-vfinal" was varied
;       as per required displacement rates.
;=========================================================================
set plot avi size 640 480 ;  making movie of the test
```

```
movie avi_open file movie_6_1_4.avi
movie step 1000 1 file movie_6_1_4.avi
;=====================================================================================
set _close= 1  ; load
;=====================================================================================
; calling crack tracking functions
crk_init
crk_chk_crkdata
crk_makeview
_crk_formpb
_crk_num_mark
_crk_draw3d_polygon
;=====================================================================================
accel_platens
cyc 1000000
;=====================================================================================
movie avi_close file movie_6_1_4.avi
hist  write 5 vs 6 file 6-1-4sh-disp
hist  write 8 vs 6 file 6-1-4devi-sdisp
hist  write 10 vs 6 file 6-1-4crk-sdisp
hist  write 3 vs 6 file 6-1-4dil-sdip
hist  write -4 vs 6 file 6-1-4n-sdip
;=====================================================================================
save M_SB_4.SAV
return ; test complete
```

Appendix B2 (FISH Alogrithms for PFC2D)

[MICRO-MECHANICAL INVESTIGATIONS]

B2A. FISH ALORITHMS FOR 2BALL TEST

B2B. FISH ALORITHMS FOR 3BALL TEST

==

B2A. FISH ALORITHMS FOR TWO-BALL TEST

==

Two-ball test was conducted in tension, shear, one ball rotation and two ball rotation modes. Two models were prepared; Composite Bond Model (CMB) (with two macro balls cemented with micro cement particles) and parallel Bond Model (PBM) in which macro particles were bonded with a parallel bond with micro parameters derived from the cement paste.

The algorithms presented here only for CBM, as PBM is straightforward to prepared and test by deleting the cement particles and applying the parallel bond between the macro particles.

The algorithms used to record the mechanical response of two-ball tests in each mode of deformation are provided here. It should be noted that the specimen diagenesis is same for a definite set of micro parameters for all deformation modes. The properties used for cement matrix (simulated by micro particles) have been obtained from calibration process involving uniaxial, triaxial and Brazilian tensile testing using PFC2D standard algorithms incorporating Hertzian Contact Model.

==

```
;      Two ball Test was conducted in three steps for each mode of deformation
;==============================================================================
; STEP-1 SPECIMEN DIAGENSIS FOR TENSION, SHEAR, ONE BALL ROTATION AND TWO BALL
;        ROTATION MODES OF DEFORMATION
;==============================================================================
; file name: 2D_2M1.dat
new
SET random   ; reset random-number generator
SET disk on  ; treat balls as disks of unit thickness
set logfile 2D_2M.log
set log on
;==============================================================================
def make_walls  ; to create a container for the generation of cement particles
  extend = 1.0
  w_stiff = 1.4e10
  _x0 = -extend*width
  _y0 = 0.0
  _x1 = width*(1.0 + extend)
  _y1 = 0.0
   command
    wall id=1 kn=w_stiff nodes (_x0,_y0) (_x1,_y1)
   end_command
  ;
  _x0 = width
  _y0 = -extend*height
  _x1 = width
  _y1 = height*(1.0 + extend)
   command
    wall id=2 kn=w_stiff nodes (_x0,_y0) (_x1,_y1)
   end_command
  ;
  _x0 = width*(1.0 + extend)
  _y0 = height
  _x1 = -extend*width
  _y1 = height
   command
    wall id=3 kn=w_stiff nodes (_x0,_y0) (_x1,_y1)
   end_command
 ;
  _x0 = 0.0
  _y0 = height*(1.0 + extend)
  _x1 = 0.0
  _y1 = -extend*height
```

```
   command
    wall id=4 kn=w_stiff nodes (_x0,_y0) (_x1,_y1)
   end_command
end
;==============================================================================
def assemble  ; assemble sample
  s_stiff = 0.0 ; initial stiffnesses
  n_stiff = 1.4e8
  w_stiff = 1.4e8
  tot_vol = height * width * 1.0
  rbar    = 0.5 * (rlo + rhi)
  num     = int((1.0 - poros) * tot_vol / (pi * rbar^2))
  mult    = 2.9   ; initial radius multiplication factor
  rlo_0   = rlo / mult
  rhi_0   = rhi / mult
  make_walls
   command
    gen id=1,num rad=rlo_0,rhi_0 x=0,width y=0,height hertz t=1000000
    prop dens=1650 pois= 0.28 shear=7.81e9
   end_command
;
  ii = out(string(num)+' particles were created')
  sum = 0.0 ; get actual porosity
  bp  = ball_head
  loop while bp # null
    sum = sum + pi * b_rad(bp)^2
    bp  = b_next(bp)
  end_loop
;
  pmeas = 1.0 - sum / tot_vol
  mult = sqrt((1.0 - poros) / (1.0 - pmeas))
   command
    ini rad mul mult
    cycle 1000
    prop fric 0.25
    cycle 2000
   end_command
end
;==============================================================================
SET height=0.00475 width=0.0095 rlo=2.0e-5 rhi=3.5e-5 poros=0.15
;==============================================================================
call flt.FIS; PFC standard algorithm to eliminate the floaters, present in FISH Tank
make_walls
assemble
pc_zap_floaters; eliminate floaters
save 2D_2M1a.SAV
;==============================================================================
macro zero 'ini xvel 0 yvel 0 spin 0'
;==============================================================================
def assembst_ball; creating steel balls
command
ball id=200001 rad 0.002375 x=0.002375 y=0.002375 hertz; left steel ball
ball id=200002 rad 0.002375 x=0.007125 y=0.002375 hertz; right steel ball
end_command
end
;==============================================================================
def del_balls; Deleting cement particles to insert steel particles
 command
 range name circl_1 circle centre 0.002375 0.002375 rad 0.002375
 range name circl_2 circle centre 0.007125 0.002375 rad 0.002375
 range name circl_3 circle centre 0.00475 0.006488620668 rad 0.002375
 range name circl_4 circle centre 0 0.006488620668 rad 0.002375
 range name circl_5 circle centre 0.0095 0.006488620668 rad 0.002375
 range name circl_6 circle centre 0.00475 -0.001738620668 rad 0.002375

 del ball range circl_1
 del ball range circl_2
 del ball range circl_4
 del ball range circl_5
 delete ball range x=0 0.002375 y=0 0.00475 ; bottom left balls
 delete ball range x=0.007125 0.0095 y=0 0.00475 ; bottom right balls
 delete ball range x=0 0.00950  y=0.006488620668 0.00950 ; top left and right balls
 end_command
end
;==============================================================================
group cement_ball range id 1 500000
plot add  wall white axes black cfor lbl
plot add ball green range group cement_ball
plot show
;==============================================================================
save 2D_M1b.SAV
;==============================================================================
del_balls ; deleting cement balls except between the steel balls
assembst_ball; inserting steel balls
group steel_ball range id 200000 200005
plot add ball yellow range group steel_ball
;==============================================================================
```

```
macro ini_prop_cem 'dens= 1650, shear=7.81e9 pois= 0.28 fric 0.25'
; initial cement properties
macro ini_prop_steel 'dens= 7800, shear=74.5e9 pois= 0.313 fric 0.0963'
;initial steel ball properties
macro cement_bond 'fric=0.839 pb_kn=1.0e15 pb_ks=5.0e13  pb_rad=1.0 pb_nstren=8.53e6 &
pb_sstren=12.8e6';Properites of cement from calibration
macro interface_bond 'pb_kn=1.0e15 pb_ks=5.0e13  pb_rad=1.0 pb_nstren=8.53e6 &
pb_sstren=12.8e6'; Properties of steel particle-cement interface
;[here both properties are same i.e. (interface_bond/ cement_bond) ratio = 1]
;=====================================================================================
;NOTE: In interface strength sensitivity study, normal and shear strength of the
;      interface properties were varied in terms of interface to cement strength
;      ratio. This ratio was varied from 0.25 to 2.0 to observe the interface strength
;      sensitivity.
;      In the sensitivity study of the cement particle size, the normal and shear
;      stiffness of the cement particles were adjusted accordingly.
;      In the sensitivity of the particle material, the properties of steel were
;      replaced with granite and sandstone.
;=====================================================================================
prop ini_prop_cem range group cement_ball
; cement properties specified to cement particles
prop ini_prop_steel range group steel_ball
; steel ball properties were specified.
;=====================================================================================
fix x y spin range group steel_ball
property xvel 0 yvel 0 spin 0 range group steel_ball

cyc 1000; cycle to adjust cement particles by fixing the position of steel balls
;=====================================================================================
delete ball range x 0 0.0095 y 0.00475 0.0095; extra cement particles were deleted
delete ball range x 0 0.0095 y -0.00475 0; ; extra cement particles were deleted
;=====================================================================================
plot hist 1 blue
plot add  wall white axes black cfor lbl pbond red
plot add ball yellow range group steel_ball
plot add ball green range group cement_ball
plot show
;=====================================================================================
Prop interface_bond range circle center 0.002375 0.002375 rad 0.002403
; (bit bigger than L=2.4025e-3 i.e. 0.002375m, 2.75e-5)
Prop interface_bond range circle center 0.007125 0.002375 rad 0.002403
Prop interface_bond range circle center 0.00475 0.006488620668 rad 0.002403
;=====================================================================================
prop cement_bond range group cement_ball
prop pb_nstren=0 pb_sstren=0 range group steel_ball; no bond between steel balls
;=====================================================================================
delete wall 1 2 3 4
zero
;=====================================================================================
save 2D_2M1.SAV
return
;
;=====================================================================================
; STEP-2 SPECIFYING TEST CONFIGURATION (TENSION)
;=====================================================================================

res 2D_2M1.SAV  ; restore compacted assembly
;=====================================================================================
def get_ss ; determine displacements and forces on steel balls during test
  xpos1  = b_x(bad200001)
  ypos1  = b_y(bad200001)
  xpos2  = b_x(bad200002)
  ypos2  = b_y(bad200002)
  xdif1 = 0.002375 + xpos1
  xdif2 = xpos2 - 0.007125
  bfxx1 = b_xfob(bad200001)
  bfyy1 = b_yfob(bad200001)
  bfxx2 = b_xfob(bad200002)
  bfyy2 = b_yfob(bad200002)
end
;=====================================================================================
def servo
  while_stepping
  if x_servo = 1
  get_ss                 ; compute forces and displacement of balls
  end_if
end
;=====================================================================================
free x y spin range id 200002 ; right ball is freed
;=====================================================================================
def accel_ball
;   Accelerates the particle to achieve vel of _vfinal in _nsteps using _nchunks
  _niter = _nsteps / _nchunks
  loop _chnk (1,_nchunks)
    if _close = 1 then
      _vel = _chnk*(_vfinal/_nchunks)
```

```
    else
     _vel = -_chnk*(_vfinal/_nchunks)
    end_if
    _mvel = -_vel
      command
       fix x y spin range id 200002
       prop xvel= _vel yvel= 0 spin=0 range id 200002; only translation movement
       cycle _niter
      end_command
  end_loop
end
;==============================================================================
call crk.FIS; PFC2D standard algorithm for crack tracing present in FISH Tank (Itasca,
;             2004)
;==============================================================================
def ball_addr
  bad200001 = find_ball(200001)
  bad200002 = find_ball(200002)
end
;==============================================================================
ball_addr
;==============================================================================
history id=7 xpos1
history id=8 ypos1
history id=9 xpos2
history id=10 ypos2
history id=11 xdif1
history id=12 xdif2
history id=13 bfxx1
history id=14 bfyy1
history id=15 bfxx2
history id=16 bfyy2
history id=17 crk_num
history id=18 crk_num_pnf
history id=19 crk_num_psf
;==============================================================================
SET hist_rep=50
SET x_servo=0
;==============================================================================
sav 2D_MT2.SAV
return
;
;==============================================================================
; STEP-3 TESTING (TENSION MODE OF DEFORMATION)
;==============================================================================

;fname: 2D_MT3.DAT
res 2D_MT2.SAV
;==============================================================================
set _vfinal= 2e-2 _nsteps= 100  _nchunks= 10
set _close= 1  ; load
SET x_servo=1  ; compute forces and displacements
;==============================================================================
; calling crack tracking functions
crk_init
crk_chk_crkdata
crk_makeview
_crk_formpb
_crk_num_mark
_crk_draw2d_line
;==============================================================================
; plot configuration for movie file
plot set background white
plot hist 15 vs 12  blue
plot add  wall black; axes black
plot add ball yellow range group steel_ball
plot add ball lgreen range group cement_ball
plot add cfor lbl pbond red
plot add fish crk_item white blue
;==============================================================================
set plot avi size 1280 960
movie avi_open file movie_2D_T3.avi
movie step 100 1 file movie_2D_T3.avi
;==============================================================================
accel_ball; giving a constant velocity to right ball
;==============================================================================
cyc 155000
;==============================================================================
movie avi_close file movie_2D_T3.avi
hist  write -15 13 file MT3-Xforces
hist  write -16 14 vs 12 file MT3-yforces
hist  write 17 18 vs 19 file MT3-cracks
;==============================================================================
set plot jpg;         plot configuration to get the test image
plot creat Final_Print
plot set background white
plot add  axes black
```

```
plot add ball dgray range group steel_ball
plot add ball lgreen range group cement_ball
plot add cfor lbl pbond red
plot add fish crk_item white blue
set plot jpg
plot hardcopy file MT3.jpg
;==================================================================================
save 2D_2MT3.SAV
return
;
;==================================================================================
; STEP-2 SPECIFYING TEST CONFIGURATION (SHEAR)
;==================================================================================
;
res 2D_2M1.SAV  ; restore compacted assembly
;==================================================================================
def get_ss ; determine average stress and strain at walls
  xpos1  = b_x(bad200001)
  ypos1  = b_y(bad200001)
  xpos2  = b_x(bad200002)
  ypos2  = b_y(bad200002)
  ydif1 = 0.002375 + ypos1
  ydif2 = ypos2 - 0.002375
  bfxx1 = b_xfob(bad200001)
  bfyy1 = b_yfob(bad200001)
  bfxx2 = b_xfob(bad200002)
  bfyy2 = b_yfob(bad200002)
end
;==================================================================================
def servo
  while_stepping
  if y_servo = 1
  get_ss                ; compute forces and displacement of balls
  end_if
end
;==================================================================================
free x y spin range id 200002 ; ; right ball is freed
;==================================================================================
def accel_ball
; ----- Accelerates the particle to achieve vel of _vfinal in _nsteps,
;       using _nchunks
  _niter = _nsteps / _nchunks
  loop _chnk (1,_nchunks)
    if _close = 1 then
      _vel = _chnk*(_vfinal/_nchunks)
    else
     _vel = -_chnk*(_vfinal/_nchunks)
    end_if
    _mvel = -_vel
      command
      fix x y spin range id 200002
      prop xvel= 0 yvel= _vel spin=0 range id 200002
      cycle _niter
    end_command
  end_loop
end
;==================================================================================
call crk.FIS; PFC2D standard algorithm for crack tracing present in FISH Tank (Itasca,
;             2004)
;==================================================================================
def ball_addr
  bad200001 = find_ball(200001)
  bad200002 = find_ball(200002)
end
;==================================================================================
ball_addr
;==================================================================================
history id=7 xpos1
history id=8 ypos1
history id=9 xpos2
history id=10 ypos2
history id=11 ydif1
history id=12 ydif2
history id=13 bfxx1
history id=14 bfyy1
history id=15 bfxx2
history id=16 bfyy2
history id=17 crk_num
history id=18 crk_num_pnf
history id=19 crk_num_psf
;==================================================================================
SET hist_rep=50
SET y_servo=0
;==================================================================================
sav 2D_MS2.SAV
return
;
```

```
;================================================================================
;STEP-3 TESTING (SHEAR MODE OF DEFORMATION)
;================================================================================
;
res 2D_MS2.SAV
;================================================================================
set _vfinal= 2e-2 _nsteps= 100  _nchunks= 10
set _close= 1  ; load
set y_servo=1  ; compute forces and displacements
;================================================================================
; calling crack tracking functions
crk_init
crk_chk_crkdata
crk_makeview
_crk_formpb
_crk_num_mark
_crk_draw2d_line
;================================================================================
; plot configuration for movie file
plot set background white
plot hist 16 vs 12  blue
plot add  wall black; axes black
plot add ball yellow range group steel_ball
plot add ball lgreen range group cement_ball
plot add cfor lbl pbond red
plot add fish crk_item white blue
;================================================================================
set plot avi size 1280 960
movie avi_open file movie_2D_S3.avi
movie step 100 1 file movie_2D_S3.avi
;================================================================================
accel_ball; giving a constant velocity to right ball
;================================================================================
cyc 255000
;================================================================================
movie avi_close file movie_2D_S3.avi
hist  write 15 -13 file MS3-Xforces
hist  write -16 14 vs 12 file MS3-yforces
hist  write 17 18 vs 19 file MS3-cracks
;================================================================================
set plot jpg
plot creat Final_Print
plot set background white
plot add  axes black
plot add ball dgray range group steel_ball
plot add ball lgreen range group cement_ball
plot add cfor lbl pbond red
plot add fish crk_item white blue
set plot jpg
plot hardcopy file MS3.jpg
;================================================================================
save 2D_MS3.SAV
return
;
;================================================================================
; STEP-2 SPECIFYING TEST CONFIGURATION (ONE BALL ROTATION)
;================================================================================
;
res 2D_2M1.SAV  ; restore compacted assembly
;================================================================================
def get_ss ; determine average stress and strain at walls
  xpos1  = b_x(bad200001)
  ypos1  = b_y(bad200001)
  xpos2  = b_x(bad200002)
  ypos2  = b_y(bad200002)
  bfxx1 = b_xfob(bad200001)
  bfyy1 = b_yfob(bad200001)
  bfxx2 = b_xfob(bad200002)
  bfyy2 = b_yfob(bad200002)
  brot1 = b_rot(bad200001)
  brot2 = b_rot(bad200002)
end
;================================================================================
def servo
  while_stepping
  if r_servo = 1
  get_ss                ; compute forces and angular displacement of balls
  end_if
end
;================================================================================
free x y spin range id 200001 200002
;================================================================================
def accel_ball
; ----- Accelerates the particle to achieve vel of _vfinal in _nsteps,
;       using _nchunks
  _niter = _nsteps / _nchunks
  loop _chnk (1,_nchunks)
```

```
    if _close = 1 then
      _vel = _chnk*(_vfinal/_nchunks)
    else
     _vel = -_chnk*(_vfinal/_nchunks)
    end_if
    _mvel = -_vel
      command
      fix x y spin range id 200002
      prop xvel=0  yvel= 0 spin=_vel range id 200002 ; right ball is allowed to rotate
      fix x y spin range id 200001
      prop xvel=0  yvel= 0 spin=0 range id 200001 ; ; left ball is fixed
      cycle _niter
    end_command
  end_loop
end
;==============================================================================
call crk.FIS; PFC2D standard algorithm for crack tracing present in FISH Tank (Itasca,
;              2004)
;==============================================================================
def ball_addr
  bad200001 = find_ball(200001)
  bad200002 = find_ball(200002)
end
;==============================================================================
ball_addr
;==============================================================================
history id=7 xpos1
history id=8 ypos1
history id=9 xpos2
history id=10 ypos2
history id=11 bfxx1
history id=12 bfyy1
history id=13 bfxx2
history id=14 bfyy2
history id=15 brot1
history id=16 brot2
history id=17 crk_num
history id=18 crk_num_pnf
history id=19 crk_num_psf
;==============================================================================
SET hist_rep=50
SET r_servo=0
;==============================================================================
sav 2D_MR2.SAV
return
;
;==============================================================================
; STEP-3 TESTING (ONE BALL ROTATION)
;==============================================================================
;
res 2D_MR2.SAV
;==============================================================================
set _vfinal= 10 _nsteps= 100  _nchunks= 10
set _close= 1  ; load
set r_servo=1  ; compute forces and displacements
;==============================================================================
; calling crack tracking functions
crk_init
crk_chk_crkdata
crk_makeview
_crk_formpb
_crk_num_mark
_crk_draw2d_line
;==============================================================================
; plot configuration for movie file
plot set background white
plot hist 13 vs 16  blue
plot add  wall black; axes black
plot add ball yellow range group steel_ball
plot add ball lgreen range group cement_ball
plot add cfor lbl pbond red
plot add fish crk_item white blue
;==============================================================================
set plot avi size 1280 960
movie avi_open file movie_2D_R3.avi
movie step 100 1 file movie_2D_R3.avi
;==============================================================================
accel_ball
;==============================================================================
cyc 15000
;==============================================================================
movie avi_close file movie_2D_R3.avi
hist  write 13 -11 file MR3-Xforces
hist  write 14 -12 vs 16 file MR3-yforces
hist  write 21 22 vs 20 file MR3-cracks
;==============================================================================
set plot jpg
```

```
plot creat Final_Print
plot set background white
plot add  axes black
plot add ball dgray range group steel_ball
plot add ball lgreen range group cement_ball
plot add cfor lbl pbond red
plot add fish crk_item white blue
plot hardcopy file MR3.jpg
;===================================================================================
save 2D_MR3.SAV
;
;===================================================================================
; STEP-2 SPECIFYING TEST CONFIGURATION (TWO BALL ROTATION MODE)
;===================================================================================

res 2D_2M1.SAV  ; restore compacted assembly
;===================================================================================
def get_ss ; determine average stress and strain at walls
  xpos1  = b_x(bad200001)
  ypos1  = b_y(bad200001)
  xpos2  = b_x(bad200002)
  ypos2  = b_y(bad200002)
  bfxx1 = b_xfob(bad200001)
  bfyy1 = b_yfob(bad200001)
  bfxx2 = b_xfob(bad200002)
  bfyy2 = b_yfob(bad200002)
  brot1 = b_rot(bad200001)
  brot2 = b_rot(bad200002)
end
;===================================================================================
def servo
  while_stepping
  if r_servo = 1
  get_ss                 ; compute stresses & strains
  end_if
end
;===================================================================================
free x y spin range id 200001 200002 ; both balls are freed
;===================================================================================
def accel_ball
; ----- Accelerates the particle to achieve vel of _vfinal in _nsteps,
;       using _nchunks
  _niter = _nsteps / _nchunks
  loop _chnk (1,_nchunks)
    if _close = 1 then
      _vel = _chnk*(_vfinal/_nchunks)
    else
     _vel = -_chnk*(_vfinal/_nchunks)
    end_if
    _mvel = -_vel
      command
      fix x y spin range id 200002
      prop xvel=0  yvel= 0 spin=_vel range id 200002 ; anticlockwise rotation
      fix x y spin range id 200001
      prop xvel=0  yvel= 0 spin=_mvel range id 200001 ; clockwise rotation
      cycle _niter
    end_command
  end_loop
end
;===================================================================================
call crk.FIS; PFC2D standard algorithm for crack tracing present in FISH Tank (Itasca,
;             2004)
;===================================================================================
def ball_addr
  bad200001 = find_ball(200001)
  bad200002 = find_ball(200002)
end
;===================================================================================
ball_addr
;===================================================================================
history id=7 xpos1
history id=8 ypos1
history id=9 xpos2
history id=10 ypos2
history id=11 bfxx1
history id=12 bfyy1
history id=13 bfxx2
history id=14 bfyy2
history id=15 brot1
history id=16 brot2
history id=17 crk_num
history id=18 crk_num_pnf
history id=19 crk_num_psf
;===================================================================================
SET hist_rep=50
SET r_servo=0
;===================================================================================
```

```
sav 2D_MR2.SAV
return
;
;=====================================================================================
; STEP-3 TESTING (TWO BALL ROTATION MODE)
;=====================================================================================
;
res 2D_MR2.SAV
;=====================================================================================
set _vfinal= 10 _nsteps= 100  _nchunks= 10
set _close= 1  ; load
SET r_servo=1  ; compute forces and displacements
;=====================================================================================
; calling crack tracking functions
crk_init
crk_chk_crkdata
crk_makeview
_crk_formpb
_crk_num_mark
_crk_draw2d_line
;=====================================================================================
; plot configuration for movie file
plot set background white
plot hist 13 14 vs 16  blue
plot add  wall black; axes black
plot add ball yellow range group steel_ball
plot add ball lgreen range group cement_ball
plot add cfor lbl pbond red
plot add fish crk_item white blue
;=====================================================================================
set plot avi size 1280 960
movie avi_open file movie_2D_R3.avi
movie step 100 1 file movie_2D_R3.avi
;=====================================================================================
accel_ball; giving a constant angular velocity to both balls
;=====================================================================================
cyc 115000
;=====================================================================================
movie avi_close file movie_2D_R3.avi
hist  write 13 -11 file MR3-Xforces
hist  write 14 -12 file MR3-yforces
hist  write 16 -15 file MR3-rotations
hist  write 18 19 vs 17 file MR3-cracks
;=====================================================================================
set plot jpg
plot creat Final_Print
plot set background white
plot add  axes black
plot add ball dgray range group steel_ball
plot add ball lgreen range group cement_ball
plot add cfor lbl pbond red
plot add fish crk_item white blue
plot hardcopy file MR3.jpg
;=====================================================================================
save 2D_MR3.SAV
return
```

===

B2B. FISH ALORITHMS FOR THREE-BALL TEST

===

Three-ball test consists of three macro balls (two balls lying horizontally and third ball at top between the two to make a wedge shaped void among three balls. Two types of models were conducted: Model-1, with empty void and Model-2, in which wedge was filled with cement consisting of micro particles. The properties of the cement were obtained from calibration of cement paste, same as used in two-ball test.

In both models, a vertical downward velocity was given to top ball and forces on the top balls were monitored as history variable in both models. The rotations of horizontally lying balls were also monitored.

Here, algorithms are given for the three-ball test with cement wedge only (i.e. Model-2). The Model-1 can be simulated without cement or deleting the cement wedge from provided algorithms.

===

```
;                    Three-ball Test was completed in four steps

;==========================================================================
; STEP-1 CREATION OF CEMENT PARTICLES IN A CONTAINER BOUND BY FOUR WALLS
;==========================================================================

new
SET random   ; reset random-number generator
SET disk on  ; treat balls as disks of unit thickness
set logfile 2D_3M1.log
set log on
;==========================================================================
def make_walls  ; create walls with overhang of extend to create cement particles
  extend = 1.0
  w_stiff = 1.4e10
  _x0 = -extend*width
  _y0 = 0.0
  _x1 = width*(1.0 + extend)
  _y1 = 0.0
  command
    wall id=1 kn=w_stiff nodes (_x0,_y0) (_x1,_y1)
  end_command
  _x0 = width
  _y0 = -extend*height
  _x1 = width
  _y1 = height*(1.0 + extend)
  command
    wall id=2 kn=w_stiff nodes (_x0,_y0) (_x1,_y1)
  end_command
  _x0 = width*(1.0 + extend)
  _y0 = height
  _x1 = -extend*width
  _y1 = height
  command
    wall id=3 kn=w_stiff nodes (_x0,_y0) (_x1,_y1)
  end_command
  _x0 = 0.0
  _y0 = height*(1.0 + extend)
  _x1 = 0.0
  _y1 = -extend*height
  command
    wall id=4 kn=w_stiff nodes (_x0,_y0) (_x1,_y1)
  end_command
end
;==========================================================================
def assemble  ; assemble sample
  s_stiff = 0.0 ; initial stiffnesses
  n_stiff = 1.4e8
  w_stiff = 1.4e8
  tot_vol = height * width * 1.0
  rbar    = 0.5 * (rlo + rhi)
  num     = int((1.0 - poros) * tot_vol / (pi * rbar^2))
  mult    = 2.9   ; initial radius multiplication factor
  rlo_0   = rlo / mult
  rhi_0   = rhi / mult
  ;make_walls
  command
    gen id=1,num rad=rlo_0,rhi_0 x=0,width y=0,height hertz t=1000000
    prop dens=1650 pois= 0.28 shear=7.81e9
  end_command
  ii = out(string(num)+' particles were created')
  sum = 0.0 ; get actual porosity
  bp  = ball_head
```

```
  loop while bp # null
    sum = sum + pi * b_rad(bp)^2
    bp  = b_next(bp)
  end_loop
  pmeas = 1.0 - sum / tot_vol
  mult = sqrt((1.0 - poros) / (1.0 - pmeas))
  command
    ini rad mul mult
    hist diag muf
    cycle 1000
    prop fric 0.25
    cycle 2000
  end_command
end
;=====================================================================================
SET height=0.008863620668 width=0.0095 rlo=2.0e-5 rhi=3.5e-5 poros=0.15
;=====================================================================================
macro zero 'ini xvel 0 yvel 0 spin 0'
;=====================================================================================
call flt.FIS; PFC standard algorithm to eliminate the floaters, present in FISH Tank
make_walls
assemble
pc_zap_floaters; eliminate floaters
save 2D_3M1a.SAV
;=====================================================================================
def assembst_ball; to insert macro steel particles
command
ball id=600001 rad 0.002375 x=0.002375 y=0.002375 hertz
ball id=600002 rad 0.002375 x=0.007125 y=0.002375 hertz
ball id=600003 rad 0.002375 x=0.00475 y=0.006488620668 hertz
end_command
end
;=====================================================================================
group cement_ball range id 1 500000
plot add  wall white axes black cfor lbl
plot add ball green range group cement_ball
plot show
;=====================================================================================
save 2D_M1a.SAV ; cement particles have been created in the container
return;
;=====================================================================================
; STEP-2 SPECIMEN DIAGENSIS FOR THREE-BALL TEST
;=====================================================================================
;
restore 2D_3M1a.SAV
;=====================================================================================
def del_balls; deleting all cement balls except those created in the wedge among three
;              balls
command
 range name circl_10 circle centre 0.002375, 0.002375 rad 0.002375
 range name circl_20 circle centre 0.007125, 0.002375 rad 0.002375
 range name circl_30 circle centre 0.00475, 0.00648862 rad 0.002375
 range name circl_40 circle centre 0.0, 0.00648862 rad 0.002375
 range name circl_50 circle centre 0.0095, 0.00648862 rad 0.002375
 ;
 del ball range circl_10
 del ball range circl_20
 del ball range circl_30
 del ball range circl_40
 del ball range circl_50
 ;
 delete ball range x=0 0.002375 y=0 0.002375 ; bottom left balls
 delete ball range x=0.007125 0.02 y=0 0.002375 ; bottom right balls
 delete ball range x=0 0.02  y=0.006488620668 0.02 ; top left and right balls
 delete ball range x=0 0.0011875  y=0 0.02 ; top left corner
 delete ball range x=0.008.3125 0.02  y=0 0.02 ; top left corner
 delete ball range x=0 3.5625e-3  y=4.4318e-3 9.5e-3 ;left top wedge
 delete ball range x=5.9375e-3 9.5e-3 y=4.4318e-3 9.5e-3 ;right top wedge
 delete ball range x=2.3988e-3 7.1013e-3 y=0 2.375e-3 ;bottom central wedge
end_command
end
;=====================================================================================
del_balls;
assembst_ball
delete wall 2 3 4; deleting left, right and top walls
group cement_ball range id 1 500000
group steel_ball range id 600000 600005
plot add ball yellow range group steel_ball
;=====================================================================================
group extra range x= 0.009498 0.02 y=0 0.01
delete ball range group extra
;=====================================================================================
macro ini_prop_cem 'dens= 1650, shear=7.81e9 pois= 0.28 fric 0.25'
macro ini_prop_steel 'dens= 7800, shear=74.5e9 pois= 0.313 fric 0.0963'
macro steel_bond 'fric=0.0963 pb_kn=6.69e11 pb_ks=6.69e11 pb_rad=1.0 pb_nstren=1.5e6 &
pb_sstren=4.0e6'
```

```
macro cement_bond 'fric=0.839 pb_kn=1.0e16 pb_ks=5.0e14  pb_rad=1.0 pb_nstren=8.53e6 &
pb_sstren=12.8e6';(pb_kn=ks for L=5.5e-5m)
prop ini_prop_cem range group cement_ball
prop ini_prop_steel range group steel_ball
;=====================================================================================
;NOTE: In the sensitivity of the particle material for macro particles, the properties
;      of steel were replaced with granite and sandstone.
;=====================================================================================
fix x y spin range group steel_ball
property xvel 0 yvel 0 spin 0 range group steel_ball
;=====================================================================================
plot hist 1 blue
plot add  wall white axes black
plot add ball yellow range group steel_ball
plot add ball green range group cement_ball
plot add cfor lbl pbond red
plot show
;=====================================================================================
cyc 1000; cycle to adjust cement particles by fixing the position of steel balls
;=====================================================================================
delete ball range circle centre 0 0.006488620668 rad 0.002375
delete ball range circle centre 0.0095 0.006488620668 rad 0.002375
delete ball range x=0 0.02  y= -0.02 0 ; bottom scattered balls
;=====================================================================================
prop cement_bond range group cement_ball
prop pb_nstren=0 pb_sstren=0 range group steel_ball; no bond between steel balls
;=====================================================================================
meas id=1 x=0.00475 y=0.0041135 rad= 3e-4
; adding measurement circle to monitor stress in the cement wedge
;=====================================================================================
save 2D_3M1.SAV
return
;
;=====================================================================================
; STEP-3 SPECIFYING TEST CONFIGURATION
;=====================================================================================
;
res 2D_3M1.SAV  ; restore compacted assembly
;=====================================================================================
prop steel_bond range id 600001 600002
; installing parallel bonds between the horizontally lying macro particles
;=====================================================================================
def get_ss ; determine average stress and strain at walls
  xpos1  = b_x(bad600001)
  ypos1  = b_y(bad600001)
  xpos2  = b_x(bad600002)
  ypos2  = b_y(bad600002)
  xpos3  = b_x(bad600003)
  ypos3  = b_y(bad600003)
  xdif1 = 0.002375 + xpos1
  xdif2 = xpos2 - 0.007125
  ydif3 = 0.006488620668 - ypos3
  bfxx1 = b_xfob(bad600001)
  bfyy1 = b_yfob(bad600001)
  bfxx2 = b_xfob(bad600002)
  bfyy2 = b_yfob(bad600002)
  bfxx3 = b_xfob(bad600003)
  bfyy3 = b_yfob(bad600003)
  brot1 = b_rot(bad600001)
  brot2 = b_rot(bad600002)
  brot3 = b_rot(bad600003)
end
;=====================================================================================
def servo
  while_stepping
  if y_servo = 1
  get_ss                 ; compute forces and displacements
  end_if
end
;=====================================================================================
free x y spin range id 600001 600003; all balls released from fixed positions
;=====================================================================================
def accel_ball
; ----- Accelerates the particle to achieve vel of _vfinal in _nsteps,
;       using _nchunks
  _niter = _nsteps / _nchunks
  loop _chnk (1,_nchunks)
    if _close = 1 then
      _vel = _chnk*(_vfinal/_nchunks)
    else
     _vel = -_chnk*(_vfinal/_nchunks)
    end_if
     _mvel = -_vel
    command
      fix x y spin range id 600003
      prop xvel= 0 yvel= _mvel spin=0 range id 600003
      cycle _niter
```

```
    end_command
  end_loop
end
;=====================================================================================
call crk.FIS; PFC2D standard algorithm for crack tracing present in FISH Tank (Itasca,
;             2004)
;=====================================================================================
def ball_addr
  bad600001 = find_ball(600001)
  bad600002 = find_ball(600002)
  bad600003 = find_ball(600003)
end
;=====================================================================================
ball_addr
;=====================================================================================
history id=7 xpos1
history id=8 ypos1
history id=9 xpos2
history id=10 ypos2
history id=11 xpos3
history id=12 ypos3
history id=13 xdif1
history id=14 xdif2
history id=15 ydif3
history id=16 bfxx1
history id=17 bfyy1
history id=18 bfxx2
history id=19 bfyy2
history id=20 bfxx3
history id=21 bfyy3
history id=22 brot1
history id=23 brot2
history id=24 brot3
history id=25 crk_num
history id=26 crk_num_pnf
history id=27 crk_num_psf
history id=28 meas ed11 id=1
history id=29 meas ed12 id=1
history id=30 meas ed21 id=1
history id=31 meas ed22 id=1
history id=32 meas s11 id=1
history id=33 meas s12 id=1
history id=34 meas s21 id=1
history id=35 meas s22 id=1
;=====================================================================================
SET hist_rep=1000
SET y_servo=0
;=====================================================================================
sav 2D_M2.SAV
return
;=====================================================================================
; STEP-4 TESTING
;=====================================================================================
;
res 2D_3M2.SAV
;=====================================================================================
free x y spin range id 600001 600005
;=====================================================================================
set _vfinal= 1e-2 _nsteps= 400  _nchunks= 40
set _close= 1  ; load
set y_servo=0
;=====================================================================================
; calling crack tracking functions
crk_init
crk_chk_crkdata
crk_makeview
_crk_formpb
_crk_num_mark
_crk_draw2d_line
;=====================================================================================
plot set background white
plot hist 21 vs 15  blue
plot add  wall black; axes black
plot add ball yellow range group steel_ball
plot add ball lgreen range group cement_ball
plot add cfor lbl pbond red
plot add fish crk_item white blue
;=====================================================================================
set plot avi size 1280 960
movie avi_open file movie_2D_3.avi
movie step 10000 1 file movie_2D_3.avi
;=====================================================================================
accel_ball
;=====================================================================================
cyc 5000000
save 2D_3M3_1.SAV
;-------------------------------------------------------------------------------------
```

```
cyc 5000000
save 2D_3M3_2.SAV
;-------------------------------------------------------------------------------------
cyc 5000000
save 2D_3M3_3.SAV
;-------------------------------------------------------------------------------------
cyc 5000000
save 2D_3M3_4.SAV
;-------------------------------------------------------------------------------------
cyc 5000000
save 2D_3M3.SAV
;=====================================================================================
movie avi_close file movie_2D_3.avi
return; test complete
```

APPENDIX C

Appendix C1 (Summary of Hoek-Brown and Mohr-Coulomb Parameters for Numerical Conglomerates)

Summary of Hoek-Brown and fitted Mohr-Coulomb parameters for numerical conglomerates of different particle (clast) and interparticle cementing materials, determined using computer program Roclab1.0.

Hoek Brown Classification	**Numerical conglomerates of different particle and interparticle cementing materials**								
	[STL+PC]	[GR+PC]	[SST+PC]	[STL+ARG]	[GR+ARG]	[SST+ARG]	[STL+ARN]	[GR+ARN]	[SST+ARN]
σ_c (MPa)	3.055	4.092	3.367	4.011	4.748	4.157	6.129	7.49	10.335
GSI	100	100	100	100	100	100	100	100	100
m_i	29.92	30.46	45.25	22.76	25.83	36.67	14.18	15.40	13.98
D	0	0	0	0	0	0	0	0	0
E_i (MPa)	2980	2980	1982	3547	2841	2492			
Hoek Brown Criterion									
m_b	29.921	30.456	45.248	22.759	25.827	36.665	14.176	15.4	13.979
s	1	1	1	1	1	1	1	1	1
a	0.5	0.5	0.5	0.5	0.5	0.5	0.5	0.5	0.5
Failure Envelope Range									
Application	Custom	Custom	Custom	Custom	Custom	Custom	Custom	Custom	Custom
σ_3^{Max} (MPa)	10	10	10	10	10	10	10	10	10
Mohr-Coulomb Fit									
c (MPa)	2.26	2.53	2.63	2.32	2.56	2.67	2.48	2.76	3.19
ϕ (Deg.)	33.10	35.72	37.49	33.03	35.54	37.47	32.40	34.76	36.49
Rock Mass Parameters									
σ_t (MPa)	-0.10	-0.13	-0.07	-0.18	-0.18	-0.11	-0.43	-0.49	-0.74
σ_c (MPa)	3.06	4.09	3.37	4.01	4.75	4.16	6.13	7.49	10.34
σ_{cm} (MPa)	3.21	4.32	3.92	4.01	4.85	4.58	5.78	7.12	9.74
E_{rm} (MPa)	2963	2963	1971	3527	2825	2478	3527	3527	3527
Lab Data									
No. of Tests	4	4	4	4	4	4	4	4	4
σ_3 (MPa)	σ_1 (MPa)								
0	3.12	2.87	2.64	3.87	3.54	3.27	7.38	6.77	6.46
5	20.84	23.33	25.16	20.89	23.32	25.20	20.19	22.54	27.38
10	44.47	50.64	55.19	44.67	50.42	55.70	44.57	50.44	55.82

Explanations:

STL- Steel
GR- Granite
SST- Sandstone
PC- Portland Cement
ARG- Argillaceous Cement
ARN- Arrenaceous Cement

Summary of Hoek-Brown and fitted Mohr-Coulomb parameters for numerical conglomerates of different particle (clast) and interparticle cementing materials, determined using computer program Rocdata 4.0.

Mohr-Coulomb Criterion	**Numerical conglomerates of different particle and interparticle cementing materials**								
	[STL+PC]	[GR+PC]	[SST+PC]	[STL+ARG]	[GR+ARG]	[SST+ARG]	[STL+ARN]	[GR+ARN]	[SST+ARN]
c (MPa)	0.53	0.40	0.30	0.68	0.54	0.40	1.41	1.14	1.17
ϕ (Deg.)	37.63	40.83	42.87	37.32	40.42	42.82	35.18	38.86	41.54
σ_t (MPa)	0	0	0	0	0	0	0	0	0
σ_c (MPa)	2.14	1.72666	1.39	2.74	2.32	1.84	5.45	4.75	5.21
α (Deg.)	76.40	78.1768	79.23	76.23	77.96	79.20	74.95	77.10	78.55
Failure Envelope Range									
Application	Custom	Custom	Custom	Custom	Custom	Custom	Custom	Custom	Custom
σ_3^{Max} (MPa)	20	20	20	20	20	20	10	20	20
Lab Data									
No. of Tests	3	3	3	3	3	3	3	3	3
Sum square of errors (Residuals)	5.82	7.82	9.41	7.62	8.93	12.23	22.31	24.52	9.43
All strength envelopes are *LEVENBERG-MARQUARDT* 'best-fit'									
σ_3 (MPa)	σ_1 (MPa)								
0	3.12	2.87	2.64	3.87	3.54	3.267	7.38	6.77	6.46
5	20.84	23.33	25.16	20.89	23.32	25.2	20.19	22.54	27.38
10	44.47	50.64	55.194	44.67	50.42	55.7	44.57	50.44	55.82

Explanations:

STL- Steel
GR- Granite
SST- Sandstone
PC- Portland Cement
ARG- Argillaceous Cement
ARN- Arrenaceous Cement

Appendix C2 (Failure Mechanisms in Two-Ball Tests)

Failure Mechanisms in Two-Ball Tests (Cement & Steel balls)

Strength Ratio*	Modes of Deformation			
	One ball Rotation	Two ball Rotation	Shear	Tension
0.25	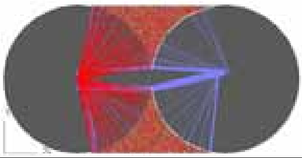	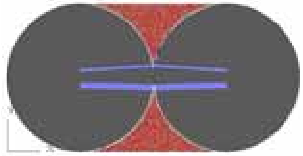	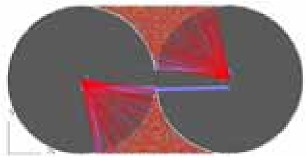	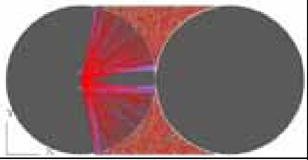
0.50	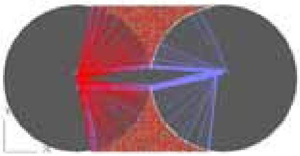	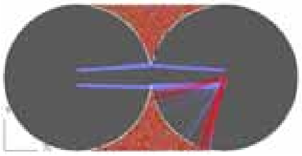	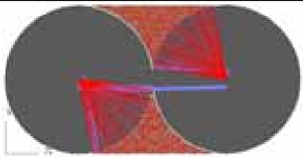	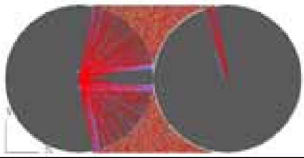
1.00	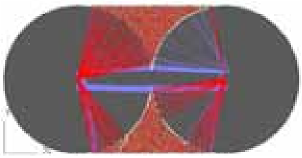	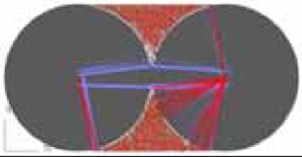	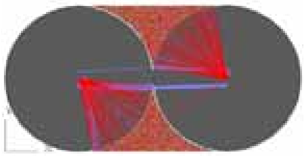	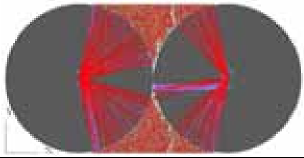
1.25	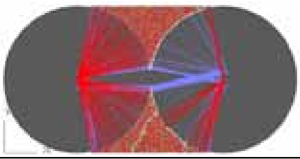	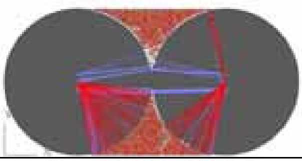	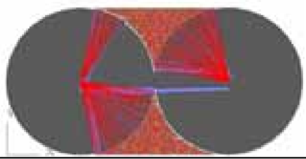	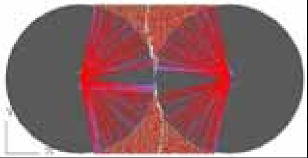
1.50	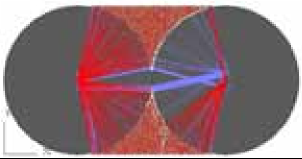	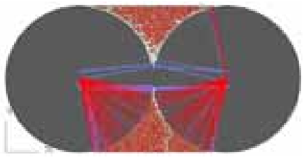	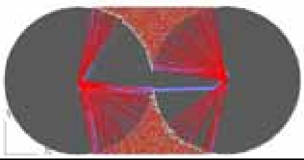	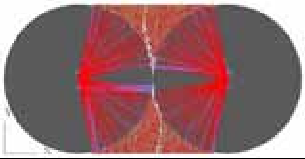
1.75	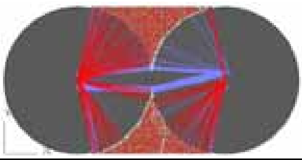	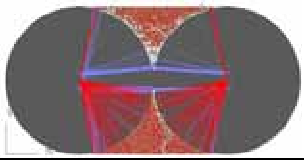	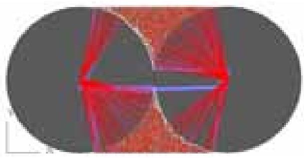	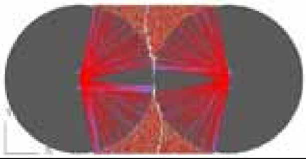
2.00	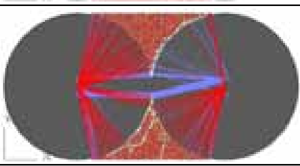	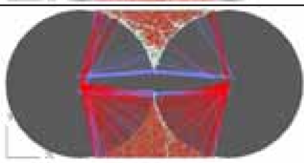	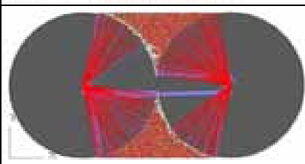	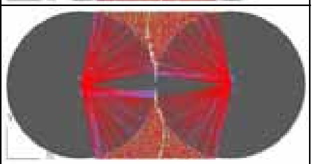

* Interface Strength to Cement Strength Ratio

Failure Mechanisms in Two-Ball Tests (Cement & Granitic Balls)

Strength Ratio*	Modes of Deformation			
	One ball Rotation	Two ball Rotation	Shear	Tension
0.25	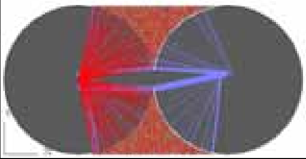	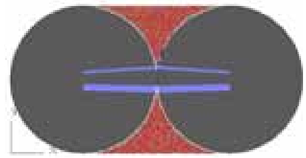	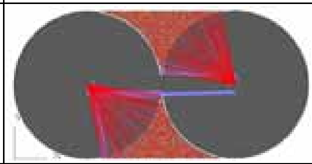	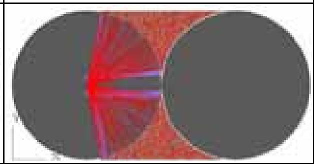
0.50	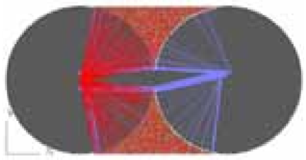	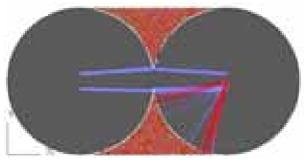	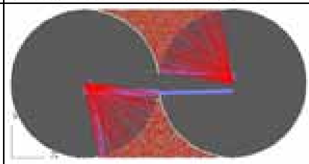	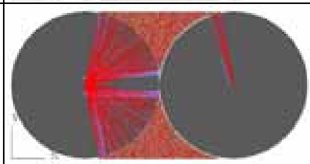
1.00	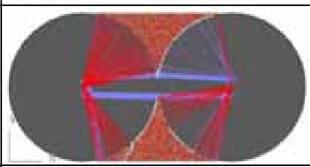	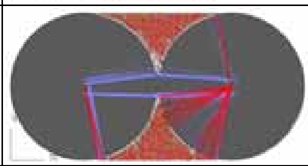	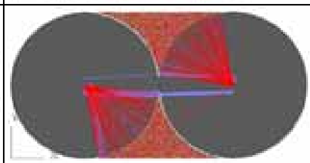	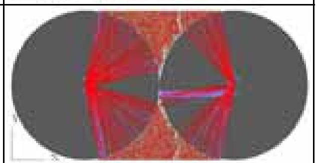
1.25	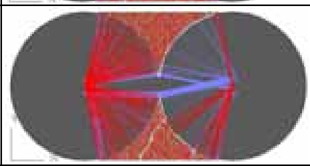	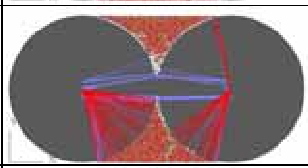	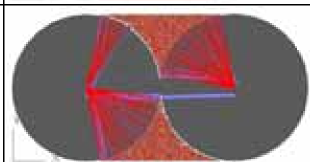	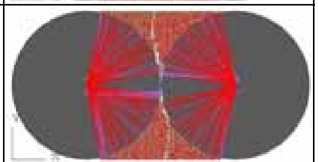
1.50	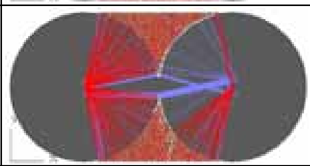	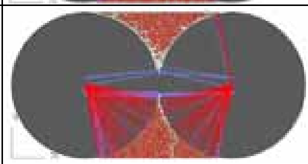	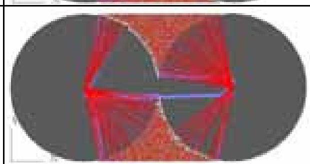	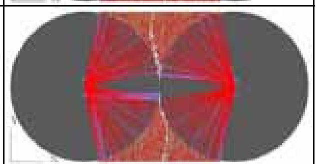
1.75	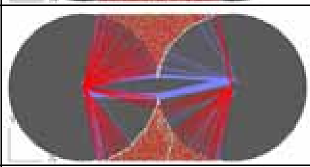	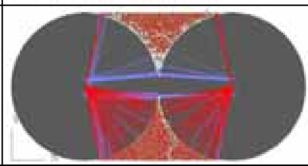	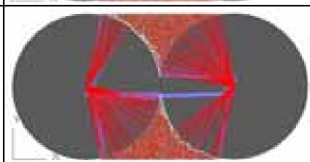	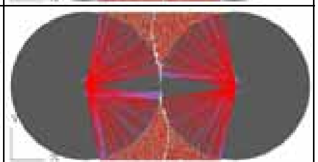
2.00	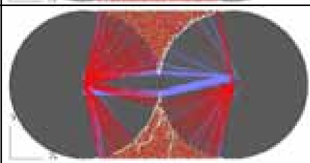	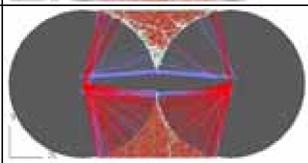	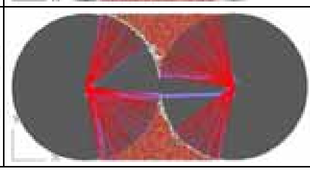	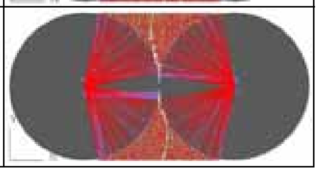

* Interface Strength to Cement Strength Ratio

Failure Mechanisms in Two-Ball Tests (Cement & Sandstone Balls)

Strength Ratio*	Modes of Deformation			
	One ball Rotation	Two ball Rotation	Shear	Tension
0.25	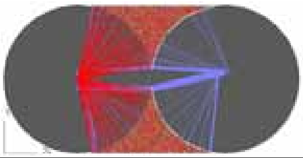	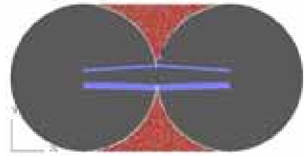	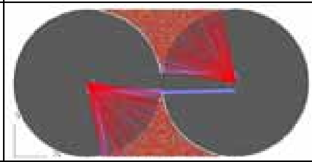	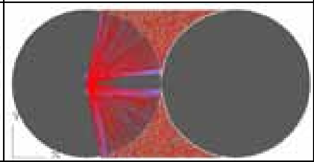
0.50	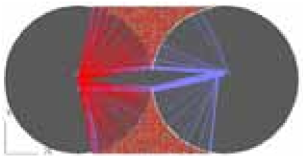	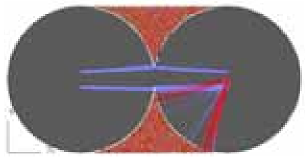	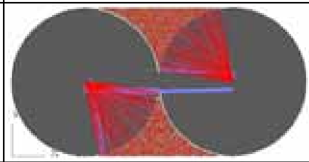	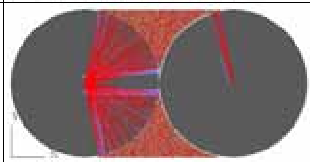
1.00	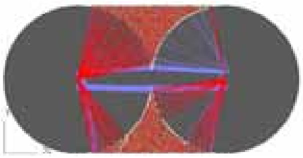	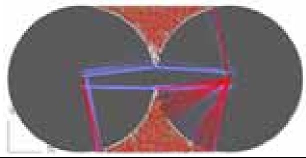	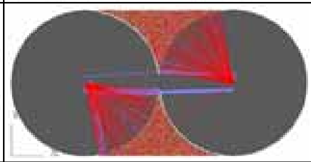	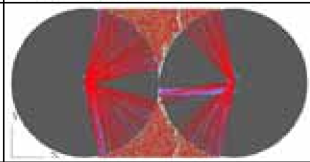
1.25	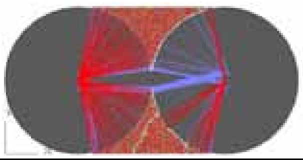	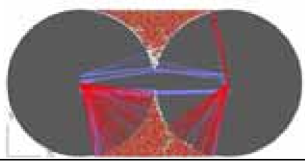	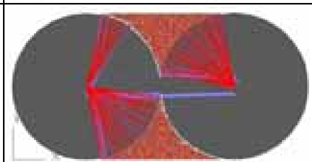	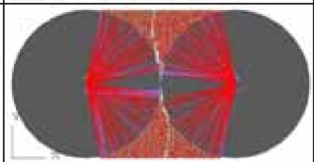
1.50	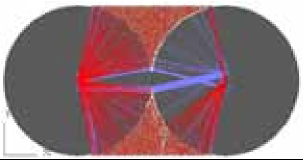	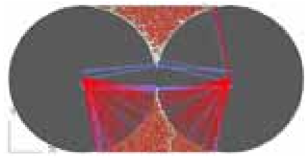	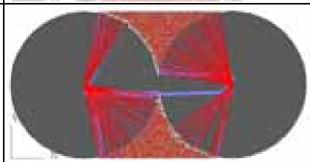	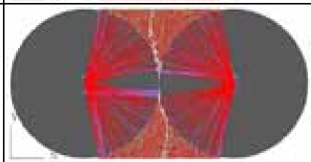
1.75	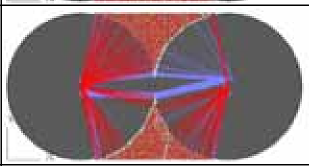	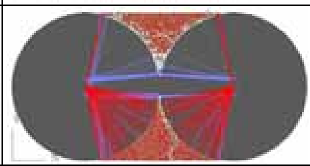	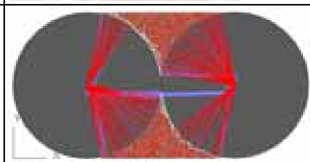	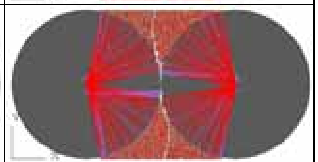
2.00	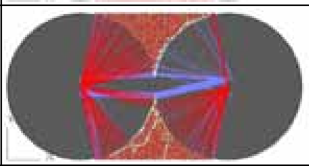	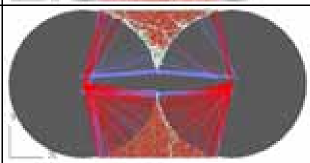	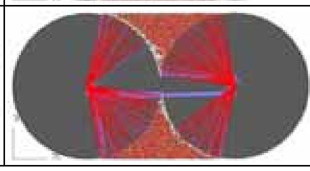	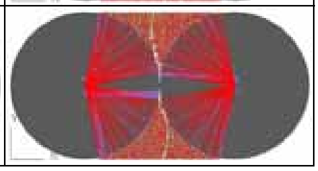

* Interface Strength to Cement Strength Ratio

Comparison of Failure Mechanisms in Two-Ball Tests (Cement & Steel Balls) for Fine# and Coarse## Grained Cement

Strength Ratio*	Modes of Deformation			
	One ball Rotation		Shear	
	Fine grained cement	Coarse grained cement	Fine grained cement	Coarse grained cement
0.50	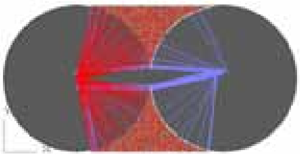	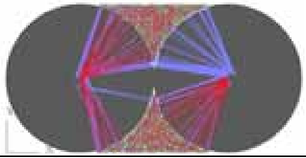	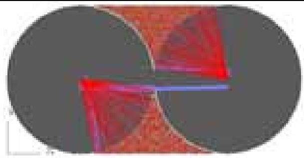	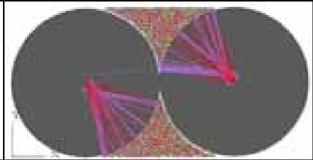
1.00	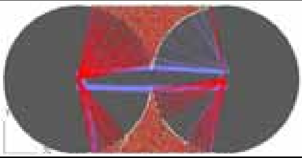	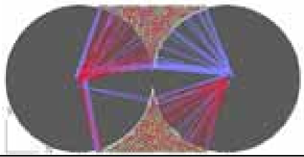	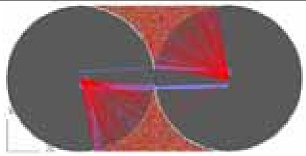	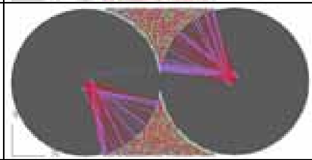
1.50	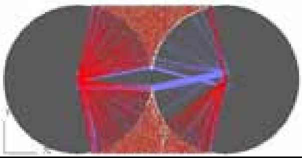	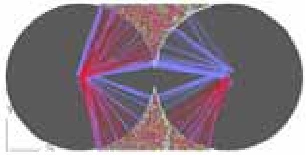	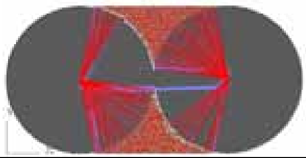	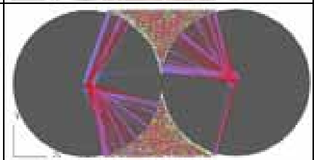
2.00	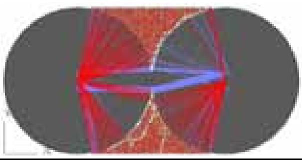	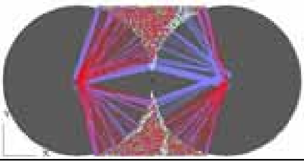	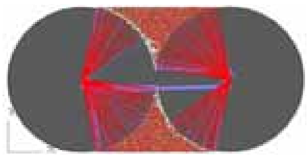	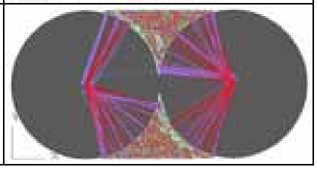

Strength Ratio*	Tension	
	Fine grained cement	Coarse grained cement
0.50	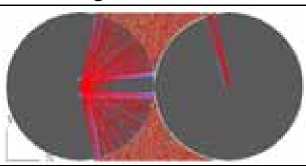	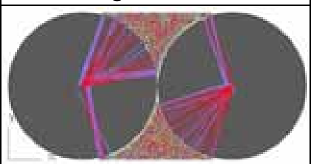
1.00	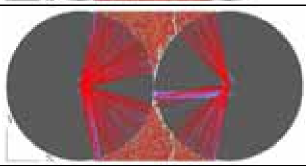	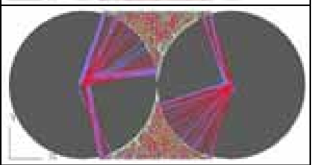
1.50	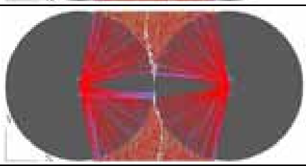	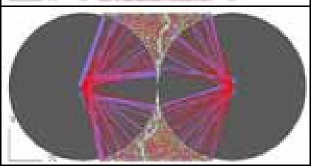
2.00	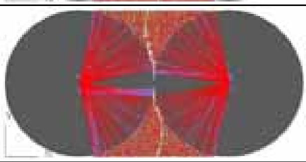	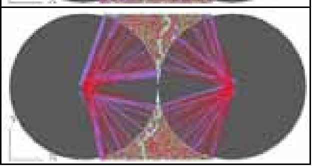

* Interface Strength to Cement Strength Ratio
# Average radius of cement particles = 2.75e-5 m
Average radius of cement particles = 5.50e-5m